Development of Failure Frequency, Shelter and Escape Models for Dense Phase Carbon Dioxide Pipelines

Christopher John Lyons

Thesis Submitted for the Qualification of
Doctor of Philosophy

Newcastle University, School of Marine Science and Technology
November 2015

Abstract

Carbon Capture and Storage (CCS) is recognised as one of a suite of solutions required to reduce carbon dioxide (CO_2) emissions into the atmosphere and prevent catastrophic global climate change. In CCS schemes, CO_2 is captured from large scale industrial emitters and transported, predominantly by pipeline, to geological sites, such as depleted oil or gas fields or saline aquifers, where it is injected into the rock formation for storage.

The requirement to develop a robust Quantitative Risk Assessment (QRA) methodology for high pressure CO_2 pipelines has been recognised as critical to the implementation of CCS. Consequently, failure frequency and consequence models are required that are appropriate for high pressure CO_2 pipelines. This thesis addresses key components from both the failure frequency and consequence parts of the QRA methodology development.

On the failure frequency side, a predictive model to estimate the failure frequency of a high pressure CO_2 pipeline due to third party external interference has been developed. The model has been validated for the design requirements of high pressure CO_2 pipelines by showing that it is applicable to thick wall linepipe. Additional validation has been provided through comparison between model predictions, historical data and the existing industry standard failure frequency model, FFREQ.

On the consequences side, models have been developed to describe the impact of CO_2 on people sheltering inside buildings and those attempting to escape on foot, during a pipeline release event. The models have been coupled to the results of a dispersion analysis from a pipeline release under different environmental conditions to demonstrate how the consequence data required for input into the QRA can be determined. In each model both constant and changing external concentrations of CO_2 have been considered and the toxic effects on people predicted. It has been shown that the models can be used to calculate safe distances in the event of a CO_2 pipeline release.

Acknowledgements

The Don Valley Power Project is co-financed by the European Union's European Energy Programme for Recovery
The sole responsibility of this publication lies with the author.
The European Union is not responsible for any use that may be made of the information contained therein.

The author would like to thank National Grid for their financial support and the advisory team of:

Harry Hopkins
Jane Haswell
Andrew Cosham
Dave Jones
Phil Cleaver
Julia Race

Contents

List of Figures

Chapter 2.

Chapter 3.

Chapter 4.

Chapter 5.

Chapter 6.

Chapter 7.

Chapter 8.

Chapter 9.

Chapter 10.

Appendix A.

Appendix C.

Appendix D.

List of Tables

Chapter 2.

Chapter 3.

Chapter 4.

Chapter 5.

Chapter 6.

Chapter 7.

Chapter 8.

Chapter 9.

Chapter 10.

Appendix B.

Nomenclature

A - Fracture area of a 2/3 Charpy specimen

A_h - Normalised hole area

A_1 - Area of rectangle which demarcates flaw

A_2 - Full load bearing area containing flaw

a - Weibull distribution parameter (Hazard Analysis/FFREQ)

a_m - Depth of micro-crack

b - Weibull distribution parameter (Hazard Analysis/FFREQ)

C - Constant in micro-crack determined from fit to experimental data

C_d - Discharge coefficient of opening in building envelope

C_p - Surface pressure coefficient

C_{pb} - Surface pressure coefficient back face of building

C_{pf} - Surface pressure coefficient front face of building

C_v - 2/3 Charpy v-notch upper shelf impact energy

C_{vfull} - Lower bound Charpy v-notch impact energy, full size specimen

c - Half axial defect length

$2c$ - Axial defect length

$c_{external}$ - External volume concentration of CO_2

$c_{internal}$ - Internal volume concentration of CO_2

c_o - Concentration (non-specific)

D - Pipeline external diameter

D_o - Toxic dose

DOC - Depth of cover factor

d - Depth of gouge

d_{crit} - Critical gouge depth

$d_{critBGDGFM}$ - Critical gouge depth based upon an infinitely long gouge

df - Pipeline design factor

$dose$ - CO_2 toxic dose

E - Young's modulus

F - Cumulative density function

F_{crit} - Critical dent force

F_{dent} - Dent force

f - Probability density function

f_d - Combined gouge depth probability density function

$f_{F_{dent}}$ - Dent force probability density function

f_{gdd} - Gouged dent gouge depth probability density function

f_{gd2c} - Gouged dent gouge length probability density function

f_{g2c} - Gouge length probability density function

f_H - Dent depth probability density function

f_w - Area correction term for a defect in a curved shell

f_{2c} - Combined gouge length probability density function

f_θ - Correction term in stress intensity factor for elliptical flaws

ff_{HDleak} - Historical data component leak failure frequency

$ff_{HDleakchain}$ - Chain trencher leak failure frequency

$ff_{HDrupture}$ - Historical data component rupture failure frequency

$ff_{HDrupturechain}$ - Chain trencher rupture failure frequency

ff_{leak} - Leak failure frequency

$ff_{rupture}$ - Rupture failure frequency

ff_{SRleak} - Structural reliability component leak failure frequency

$ff_{SRrupture}$ - Structural reliability component rupture failure frequency

$ff_{SRtotal}$ - Structural reliability component total failure frequency

ff_{total} - Total failure frequency

G_1 - Function in the bending stress intensity factor

G_2 - Function in the bending stress intensity factor

g - Correction term in stress intensity factor for elliptical flaws

g_a - Acceleration due to gravity

H - Depth of dent in an unpressurised pipeline

H_b - Function in the bending stress intensity factor

H_{crit} - Critical dent depth in an unpressurised pipeline

H_P - Depth of dent in a pressurised pipeline

H_{Pcrit} - Critical dent depth in a pressurised pipeline

H_1 - Function in the bending stress intensity factor

H_2 - Function in the bending stress intensity factor

h_b - Height of building in shelter model

$IncidentRate$ - Overall Incident-Rate for third party external interference

$IncidentRate_{gouge}$ - Incident-Rate for gouges

$IncidentRate_{gougeddent}$ - Incident-Rate for gouged dents

i - Counting index

j - Yield criterion constant

K_I - Stress intensity factor

K_{IC} - Material fracture toughness

K_{Ip} - Primary stress intensity factor

K_{Is} - Secondary stress intensity factor

K_r - Fracture ratio

K_t - Notch stress concentration factor

K_1 - Empirical constant (British Gas Dent Gouge Fracture Model)

K_2 - Empirical constant (British Gas Dent Gouge Fracture Model)

k - Integration limit

k_m - Stress magnification factor due to misalignment

k_t - Stress concentration factor

k_{tb}, - Bending stress concentration factor

k_{tm}, - Membrane stress concentration factor

L - Excavator tooth length

L_{crit} - Critical defect length for rupture

L_r - Load ratio

L_{rmax} - Cut off point for load ratio

l - Integration limit

l_b - Length of building in shelter model

M - Folias factor / Bulging Correction Factor

M_b - Bending stress magnification factor

$M_{internal}$ - Mass of air/CO_2 within the building

M_{kb}, - Stress intensity magnification factor

M_{km}, - Stress intensity magnification factor

M_m - Membrane stress magnification factor

M_P - Function used in the part-wall NG-18 equation

M_{Si} - Function in the reference stress for a part-wall defect

M_T - Stress magnification factor

M_{Ti} - Function in the reference stress for a through-wall defect

M_1 - Function in the membrane stress intensity factor

M_2 - Function in the membrane stress intensity factor

M_3 - Function in the membrane stress intensity factor

m_{air} - Molar mass of air

m_{CO_2} - Molar mass of CO_2

m_{in} - Mass of air/CO_2 entering the building

n - Hardening index

n_o - Toxic Index

P - Internal operating pressure

P_{atmos} - Atmospheric pressure

$P_{external}$ - External pressure on building face

$P_{gdrupture}$ - Probability of a gouged dent rupture (Monte Carlo method)

P_{gouge} - Probability of failure for gouges

$P_{gougedamage}$ - Probability that mechanical damage will be a gouge

$P_{gougeddent}$ - Probability of failure for gouged dents

$P_{gougeddentdamage}$ - Probability that mechanical damage will be a gouged dent

$P_{gougeddentleak}$ - Leak probability of failure for a gouged dent

$P_{gougeddentrupture}$ - Rupture probability of failure for a gouged dent

$P_{gougeddenttotal}$ - Total probability of failure for a gouged dent

$P_{gougeleak}$ - Leak probability of failure for a gouge

$P_{gougerupture}$ - Rupture probability of failure for a gouge

$P_{gougetotal}$ - Total probability of failure for a gouge

$P_{grupture}$ - Probability of a gouge rupture (Monte Carlo method)

$P_{internal}$ - Internal pressure on building face

P_{leak} - Overall probability of failure for leaks

$P_{reference}$ - Atmospheric pressure at top of building

$P_{rupture}$ - Overall probability of failure for ruptures

P_{total} - Overall total probability of failure

P_{wind} - Dynamic pressure due to wind flow

P_x - Probability

P' - Unknown pressure

ΔP - Pressure difference across and opening in building envelope

$probit$ - Probit value

Q - Ventilation flow rate

Q_{in} - Ventilation flow rate into the building

Q_{out} - Ventilation flow rate out of the building

q - Function in the bending stress intensity factor

R - External pipeline radius

R_d - Combined gouge depth reliability function

R_F - Dent force reliability function

R_{gd} - Gouge depth reliability function

R_{gdd} - Gouged dent gouge depth reliability function

R_H - Dent depth reliability function

R_I - Ideal gas constant

R_x - Reliability function

Res - Function in definition of dent force

r - Radius at point of interest

r_i - Internal shell radius

r_m - Average pipe radius

r_0 - External shell radius

r_r - Radius of root of gouge

S_r - Plastic collapse ratio

SCF - Stress concentration factor for micro-crack

s - Distance travelled by escaping person

T - Temperature (non-specific)

$T_{external}$ - External temperature

$T_{internal}$ - Internal temperature

t - Pipeline wall thickness (Chapters 2 to 8); time (Chapters 9 to 10)

U_{wind} - Wind Speed

u - Integration variable

$V_{building}$ - Total volume of building

$\Delta V_{CO_2 in}$ - Volume of CO_2 flowing in to the building in *dt*

$\Delta V_{CO_2\,out}$ - Volume of CO_2 flowing out of the building in *dt*

ν - Flow stress constant

v_p - Velocity of escaping person

W - Length of a typical pipe spool

W_o - Width of opening in building envelope

w_b - Width of building in shelter model

wg_{hr} - Probability of a hole size range for gouges

$wg_{>110}$ - Probability of a hole size greater than 110 mm for gouges

wgd_{hr} - Probability of a hole size range for gouged dents

$wgd_{>110}$ - Probability of hole size greater than 110 mm for gouged dents

X - Parameter representing defect size in the stress intensity factor

X_Fpress - Uncertainty factor in PIPIN for plastic collapse leak / rupture

X_Ki_gdr - Uncertainty factor in PIPIN for brittle fracture leak / rupture

X_Ki_gid - Uncertainty factor in PIPIN for brittle fracture gouged dent

X_Krfail - Uncertainty factor in PIPIN for fracture assessment curve

X_Lrcut - Uncertainty factor upper limit plastic collapse of gouge (PIPIN)

X_Pcf - Uncertainty factor in PIPIN for brittle fracture gouged dent

X_Scoll - Uncertainty factor in PIPIN for plastic collapse gouged dent

X_Sfail - Uncertainty factor in PIPIN for plastic collapse gouge

x - Random variable

x_1 - Example value of random variable

Y - Stress intensity factor correction

Y_1 - Stress intensity magnification factor

Y_2 - Stress intensity magnification factor

$(Y\sigma)_P$ - Primary component of stress intensity factor

$(Y\sigma)_S$ - Secondary component of stress intensity factor

z - Function in definition of plasticity correction factor

z_h - Height above ground level subtracted from building height

z_0 - Height of neutral pressure level

α - Weibull distribution parameter

α'' - Function in the reference stress for a part-wall defect

β - Weibull distribution parameter

γ - Constant in micro-crack determined from fit to experimental data

δ_r - Fracture Ratio defined using CTOD parameters

ζ - Constant in the secondary stress components

θ - Parametric angle to identify position along an elliptic flaw front

μ - Constant in micro-crack determined from fit to experimental data

μ_d - Lognormal distribution parameter

ξ - Constant in the secondary stress components

ρ - Plasticity correction factor

ρ_{air} - Air density (non-specific)

$\rho_{external}$ - External density

$\rho_{reference}$ - Air density at top of building

ρ_1 - Function in definition of plasticity correction factor

$\rho_{internal}$ - Internal density

σ - Stress state in the pipe wall

σ_b - Primary bending stress

σ_b^P - Primary bending stress component

σ_b^S - Secondary bending stress component

σ_d - Lognormal distribution parameter

σ_H - Circumferential hoop stress in the pipe wall

σ_i - Hoop stress at internal pipe wall

σ_m - Primary membrane stress

σ_m^P - Primary membrane stress component

σ_m^S - Secondary membrane stress component

σ_0 - Hoop stress at external pipe wall

σ_{ref} - Reference stress

σ_U - Ultimate tensile strength

σ_Y - Yield strength of the pipe steel

$\overline{\sigma}$ - Flow Stress

$\tilde{\sigma}$ - Plastic collapse stress

Φ - Function in the secondary stress components

$\emptyset$ - Correction term in stress intensity factor for elliptical flaws

Chapter 1. Introduction

Research indicates that climate change is a serious and urgent issue (Stern, 2006; IPCC, 2014). An increase in global temperatures could have a devastating effect on the Earth's ecosystems, causing extreme weather events, sea levels to rise, an increase in disease and the extinction of many plant and animal species. The climate is changing as a result of the increasing production of greenhouse gases such as carbon dioxide (CO_2); a direct consequence of the reliance on fossil fuels by humans. The atmospheric concentration of these gases is slowly rising above the level at which they can be removed from the environment naturally through vegetation and porous rocks. At current estimates, the concentration of greenhouse gases in the atmosphere could treble over the next century (Race, 2007). The effect of this on the climate would be an increase in the average global temperature of over 5 degrees Celsius (Stern, 2006).

In order to prevent future negative effects of climate change, the concentration of CO_2 in the atmosphere needs to be stabilised to a level which can be naturally regulated. It is therefore imperative that the emission of greenhouse gases to the atmosphere is reduced. Unfortunately, the continued use of fossil fuels by developing nations to provide energy for growth and development is inevitable, due to their cost and flexibility (CCSA, 2015). There is a motivation therefore, to develop new technology which can provide a balance between the increasing use of fossil fuels and the required reduction in emissions. The use of Carbon Capture and Storage (CCS) schemes is one such possibility for this.

CCS can be applied to any large industrial sources of CO_2, including those associated with the steel and chemical industries; it is not exclusive to fossil fuel power plants. Furthermore, in some industries CCS is the only available option for reducing greenhouse gas emissions by the required amount. In a CCS scheme the CO_2 produced from the burning of fossil fuels is collected at its source. Following this, the gas is transported to an appropriate storage site such as a saline aquifer or depleted oil well. Finally, the CO_2 is injected into the rock formation at the storage site to contain it and prevent it from escaping to the atmosphere. Suitable storage sites are expected to retain the CO_2 either

indefinitely or for timescales which are geologically significant. Alternatively, the captured CO_2 can be used to assist in the extraction of further fossil fuels, for example as part of Enhanced Oil Recovery (EOR). In the UK, depleted oil and gas reservoirs located in the North Sea may represent potentially suitable storage sites.

Research in the CCS field has seen carbon capture technology mature to the point of viability and the potential storage sites accepted as fit for purpose (Downie, 2007). The successful implementation of CCS schemes as a means of reducing greenhouse gas emissions is therefore dependent upon a establishing a method for the safe and efficient transportation of CO_2 from its source to its storage point. An important point to note with regards to this is that CO_2 is both toxic and an asphyxiant and could therefore cause harm to people in the event of an accidental release.

Pure CO_2 is colourless, odourless and non-flammable. The triple point of CO_2 is at a temperature of -56°C and a pressure of 5 barg. In the vicinity of this point CO_2 can exist as either solid, liquid or a gas. The critical point of CO_2 is at a temperature of 31°C and a pressure of 74 barg. At temperature and pressure values higher than these CO_2 exists as a supercritical fluid. If the pressure is above the critical pressure but the temperature below the critical temperature, CO_2 exists as a liquid with the property of increasing density with decreasing temperature. This form of CO_2 is known as a dense phase liquid. The most efficient method for the transportation for CO_2 is via pipeline in the dense phase. This is because in the dense phase CO_2 has the density of a liquid but the viscosity and compressibility of a gas (Downie, 2007).

Before CO_2 is transported by pipeline a compressor station is used to transform the gas into the dense phase. An appropriate safety margin above the critical pressure must be applied in order to ensure that pipeline flow remains in the dense phase throughout transportation. For pure CO_2, the pressure required would therefore be approximately 100 barg. CO_2 captured from power plants or other sources however will not be pure and can contain impurities such as sulphur and nitrogen oxides or hydrogen. The presence of impurities in the captured CO_2 will affect critical temperature and pressure and may mean that a

transportation pipeline must have an operating pressure of up to 200 barg to ensure single phase flow.

In the UK the operation of high pressure pipelines is controlled according to the Pipeline Safety Regulations (PSR) (Anon., 1996). The PSRs state that the risks associated with a pipeline must be “as low as reasonably practicable” (ALARP). Pipeline operators generally demonstrate that risks are ALARP by ensuring that their pipeline complies with relevant design codes. The pipeline design codes used in the UK are TD/1 (Anon., 2009), for natural gas pipelines; and PD-8010 (Anon., 2015a) for all other high pressure pipelines. These codes contain design requirements which ensure pipeline integrity is maintained, thereby imposing a high level of safety. Alternatively, if the requirements given in the codes are not definitive or particular conditions apply which are not covered under code guidance the pipeline risks can be made ALARP through the use of a procedure known as a quantified risk assessment (QRA) (Race, 2007; Barnett, 2014; Cooper, 2014).

For a pipeline carrying dense phase CO_2 in the UK, the relevant design code to apply in order to ensure compliance with the PSRs should be PD-8010. However, in this code the maximum allowable operating stress in the pipeline and the minimum allowable distance between the pipeline and any occupied buildings near to the pipeline route must be defined by the product being transported. PD-8010 was originally written to be applied to products which pose a thermal hazard and therefore there is currently no hazard category included in the code for dense phase CO_2. The code can therefore not be currently applied to the design of dense phase CO_2 pipelines. In order to ensure the safe design, construction and operation of a dense phase CO_2 pipeline as part of a CCS scheme in the UK a QRA approach would therefore be required (Barnett, 2014; Cooper, 2014).

To address and resolve key issues relating to the transport of dense phase CO_2 by pipeline, National Grid, in collaboration with various UK universities and engineering companies, has completed a detailed research programme known as COOLTRANS (**CO2L**iquid pipeline **TRANS**portation). The programme included extensive experimental testing and the development of theoretical

models to describe dense phase CO_2 behaviour. One of the aims of the COOLTRANS programme was the development of a comprehensive QRA methodology for application to dense phase CO_2 pipelines (Barnett, 2014; Cooper, 2014).

The purpose of a pipeline QRA is to determine the risks posed by the failure of the pipeline to people located nearby. The procedure involves the identification of hazard scenarios and considers both the probability of failure and the consequences of failure in order to calculate values for the individual and societal risk due to the pipeline. In general a QRA procedure covers the following steps:

i) Identify hazards
ii) Identify failure causes
iii) Calculate the frequency of failure for each cause
iv) Evaluate the consequences of failure
v) Calculate the individual and societal risk a specific locations along the pipeline
vi) Assess the tolerability of the calculated risks by comparison with recognised criteria

Identifying hazards for a QRA involves consideration of the pipeline geometry, material and operating conditions; the surrounding infrastructure and environment along the potential pipeline route; and appropriate meteorological data such as wind speed, direction and atmospheric conditions. In terms of failure causes, pipeline failure can occur due to numerous different mechanisms including, third party external interference, corrosion, material or construction defects, natural events and operational error; all of which must be considered as part of the assessment (Goodfellow, 2006).

The calculation of failure frequency and evaluation of the consequences of failure in the QRA process generally involve the use of theoretical models which are tailored to each individual case. Failure frequency is determined by assessing the probability of failure for each failure cause. Values are obtained either from relevant operational data or models based on structural reliability

methods. For the consequences of failure, models describing the product outflow and dispersion within the environment are required. For oil and natural gas pipelines, the hazards following pipeline failure are largely thermal and therefore the consequence models must consider the probability of ignition and thermal radiation effects. The behaviour of humans in the event of a pipeline failure is also an important consideration to model as part of the failure consequences and must consider the potential for escape and shelter from hazards. For failure consequences the various possible scenarios are drawn out logically in the form of an event tree in order to determine overall probabilities.

Individual risk is the probability per year of an individual, who is present year round at a specific location along the pipeline route, becoming a casualty. The individual risk is calculated by applying a risk sum for the failure frequency and consequences over all potential incidents which could occur. This is applied over the total length of the pipeline which could cause harm to the individual, the “interaction length”. The individual risk is presented as the risk level along a transect perpendicular to the pipeline. Societal risk is the relationship between the frequency of an incident and the total number of potential casualties which could occur as a result of that incident. To calculate the societal risk of a pipeline at a specific location, the frequency of each incident along with the associated number of casualties for that incident is calculated. This is performed for all potential incidents which could occur producing a number of frequency-casualty pairs. Using the frequency-casualty pairs an “F-N” curve can be constructed showing the frequency of N or more casualties per year against N. This provides a measure of the societal risk. The calculated individual and societal risk levels are assessed against published risk criteria in order to determine if they are tolerable. Acceptable risk levels in the UK are set by the Health and Safety Executive (HSE) (Anon., 1992; Anon., 1993; Anon., 2001b; Goodfellow, 2006).

In terms of developing a QRA methodology for dense phase CO_2 pipelines, the basic structure of the above procedure was appropriate; however the individual models used to calculate risk values required revision. The hazards and behaviour of dense phase CO_2 differ from those of oil and natural gas which has implications for both the frequency and consequences aspects of a QRA.

New models had to be developed for the QRA process in order to address these differences and provide accurate measures of risk for a dense phase CO_2 pipeline.

This thesis considers the development of three individual models to be used as part of the QRA methodology for dense phase CO_2 pipelines. The models address different aspects from both the failure frequency and consequences side of the QRA process. More specifically the models relate to: the frequency of pipeline failure due to third party external interference; the shelter provided by buildings in the event of a dense phase CO_2 pipeline failure; and the potential for escape on foot in the event of a dense phase CO_2 pipeline failure.

As noted above, pipeline failure can occur due to numerous different mechanisms including third party external interference, corrosion, material or construction defects, natural events and operational error. For a dense phase CO_2 pipeline material and construction defects can be addressed through material specifications, quality assurance and inspection; natural events can be addressed by choosing a pipeline route to avoid problematic locations or through surveillance and operational response; and operational errors can be addressed through staff training and applying rigorous operational procedures. External corrosion can be addressed through a suitable external pipeline coating and an operational cathodic protection system; and internal corrosion can be addressed by the product specification of the CO_2. The most significant cause of failure influencing the residual risk posed by a dense phase CO_2 pipeline is therefore third party external interference. This damage cause may be random, and is typically outside the direct control of the operator (Barnett, 2014; Cooper, 2014).

For oil and natural gas pipelines, the frequency of pipeline failure due to third party external interference is calculated using models based upon structural reliability methods. These models combine semi-empirical pipeline failure models with historical operational damage data. The high pressure design requirement for a dense phase CO_2 pipeline however, may necessitate the use of thick wall linepipe in pipeline construction, potentially with wall thickness dimensions outside the limits of operational experience for oil and natural gas.

Consequently, the reliance of the current failure frequency models on empirical data and semi-empirical relations suggested their application to dense phase CO_2 pipelines may be inappropriate.

This thesis presents the development of an external interference failure frequency model which is appropriate for application to dense phase CO_2 pipelines. The development of the model has considered the applicability of semi-empirical failure models to thick wall linepipe, advancements in damage modelling and contemporary operational data. Validation of the model is provided through comparison between model predictions, historical operational data and the existing industry standard failure frequency model, FFREQ.

In terms of the consequences of failure, the behaviour of dense phase CO_2 in the event of a pipeline failure is significantly different to that of oil or natural gas. The CO_2 will decompress, expand to atmospheric pressure and then disperse as a gas which is heavier than air at atmospheric pressure, in accordance with the environmental conditions at the location. A change of phase from liquid to gas will occur as a result of the decompression and expansion; and the temperature of the CO_2 will decrease. New models were therefore required in order to describe the outflow and dispersion of the released CO_2 as part of a QRA methodology for dense phase CO_2 pipelines. The chances of finding shelter or escape in the event of a pipeline failure will also be affected by the different hazards and behaviour of CO_2 compared to oil or natural gas. The ingress of CO_2 into occupied buildings must be considered, in addition to the ability to escape from a released CO_2 cloud.

This thesis presents the development of models to describe the impact of CO_2 on people sheltering inside buildings and those attempting to escape on foot during a pipeline release event. The models have been coupled to the results of a dispersion analysis from a pipeline release under different environmental conditions to demonstrate how the consequence data required for input into the QRA can be determined. In each model both constant and changing external concentrations of CO_2 has been considered and the toxic effects on people predicted.

The structure of the thesis is as follows: Chapter 2 presents a review of external interference failure frequency models currently in use for oil and natural gas pipelines; Chapter 3 presents a review of the pipeline failure models and historical operational data sources which can potentially be used to construct failure frequency models; Chapter 4 details a study intended to provide a validation of the applicability of specific pipeline failure models, the NG-18 equations, to thick wall pipelines; Chapter 5 explains the first four stages in the development of the external interference failure frequency model for dense phase CO_2 pipelines; Chapter 6 provides an analysis of the historical operational damage data used in the failure frequency model; Chapter 7 explains the final two stages in the development of the failure frequency model; Chapter 8 provides validation of the failure frequency model and details an analysis of the trends observed when the model is applied to different pipeline scenarios; Chapter 9 explains the development of the “shelter” model, considering the ingress of CO_2 into a building surrounded by an environment with a high CO_2 concentration; Finally, Chapter 10 explains the development of the “escape” model, considering escape on foot from a moving cloud of CO_2. Conclusions and recommendations for further work are provided in Chapter 11.

Chapter 2. Review of Failure Frequency Models

Chapter 2 to Chapter 8 of this thesis present the development of a model which can be used to calculate the failure frequency due to third party external interference, for a dense phase CO_2 pipeline.

For oil and gas pipelines, the frequency of pipeline failure due to third party external interference has traditionally been calculated using models based upon probabilistic, structural reliability methods. Structural reliability methods are applied by combining the following:

- Limit state functions, the mathematical models which define the conditions for failure;
- Probability distributions based around selected random variables;
- A mathematical technique to calculate the probability of failure (e.g. Numerical Integration, Monte Carlo, First Order Reliability Methods).

For pipelines the limit state functions are based on semi-empirical fracture mechanics failure models; and the probability distributions are based on pipeline damage and derived from historical operational data. The failure probability is converted into a failure frequency to take into account the regularity of third party external interference damage. The various models currently in use within the oil and natural gas pipeline industry differ in their subtleties; however all are based upon a methodology originally developed by British Gas in the 1980s.

To calculate pipeline failure frequency for dense phase CO_2 pipelines it would be desirable to extend the use of the current pipeline failure frequency methodology. The methodology has been employed for over 25 years, and as a result is tried, tested and well understood.

The transport of dense phase CO_2 by pipeline however requires operational pressures in excess of the CO_2 triple point; potentially up to 200 barg when incorporating an appropriate margin to ensure single phase flow. This high design pressure requirement necessitates the use of thick wall linepipe in

pipeline construction, potentially with wall thickness dimensions outside of the limits of current operational experience. Consequently, the reliance of the failure frequency methodology on empirical data and semi-empirical relations suggests its application to dense phase CO_2 pipelines may be inappropriate.

Chapter 2 presents a review of the failure frequency methodology and the existing models derived from it to assess their applicability to dense phase CO_2 pipelines. An overview of the models is given in order to explain their structure and to highlight the similarities and differences between each model.

2.1 External Interference Damage

External interference of a pipeline by a third party can result in mechanical damage to that pipeline. Mechanical damage is caused by a foreign object, such as earth moving or farming equipment, striking a pipeline.

2.1.1 *Damage Forms and Pipeline Failure*

Mechanical damage to a pipeline can occur in the form of either:

- Dents;
- Gouges (including spalling and cracks);
- Combinations of dents and gouges (gouged dents);
- Punctures (and broken/severed pipes).

A dent is a deformation in the wall of the pipeline. The normal cylindrical shape of the pipe is permanently changed as a result of being plastically deformed. Dents can be described as smooth or kinked depending on the shape of the deformation. A dent which is not associated with a metal loss defect is known as a plain dent. A dent will cause an area of local stress concentration.

A gouge is a defect which is defined by a loss of metal from the pipe wall resulting in a local reduction of the wall thickness. The metal is typically scraped

away for example, by the tooth of an excavator bucket. Spalling is a form of gouging in which small fragments of metal are chipped away from the pipe. Gouges also cause an area of local stress concentration in the pipe wall. Gouges can be characterised by their orientation, which is determined by the angle with which their length (the largest dimension of the defect parallel to the surface of the pipe) makes with respect to the pipe axis. In assessment terms gouges in pipelines are treated as crack-like defects. Consequently, for the purposes of this work the definition of a gouge caused by external interference also includes cracking in the pipe wall.

Gouged dent is a term used to describe defects which are a combination of both a dent defect and a gouge defect. This form of mechanical damage is considered to be more severe than an equivalent dent or gouge occurring in isolation.

Gouges and gouged dents which do not completely penetrate the pipe wall are known as part-wall defects. If part-wall damage is severe enough then the affected section of pipe is no longer able to tolerate the stresses produced during normal pipeline operation and the pipe will fail. The severity of the part-wall damage can be determined using fracture mechanics failure equations.

If however, the pipe is struck with sufficient force in the initial incident; or subject to drilling operations in-error; there can be a direct breach of the pipe wall, which will also result in a failure. This type of damage is known as a puncture. A typical puncture is effectively a gouge or gouged dent with a depth equal to the pipe wall thickness.

It is important to make a distinction between the failure of severe part-wall defects and through-wall punctures. Both types of failure result from external interference damage and in both cases the failures are instantaneous. For part-wall damage however, the failure occurs as a result of a reduction in the load the pipe structure can tolerate; whereas for punctures the failure is due to a hole in the pipe wall created by the offending foreign object, limited simply by the pipe wall thickness. It should be noted that although “puncture” is used as defined as above in the context of this work, the term may also refer to incidents

in which a pipe has been completely severed, leaving two open pipe ends. The reason for this is that the historical operational data and the original documentation relating to the development of the failure frequency methodology are non-specific with regards to the definition of a puncture. This however, has been avoided where possible.

It should be noted that third party external interference can also result in damage to branches and fittings on the pipeline. Failure can occur if these attachments are severely damaged or completely severed from the pipe. Damage to fittings is only considered in two of the models based upon the pipeline failure frequency methodology, using values for failure frequency derived from historical operational data. The other models described in this review do not consider damage to fittings when calculating pipeline failure frequency.

2.1.2 *Leak / Rupture*

Regardless of method, the failure of a pipeline will result in what is known as a through-wall defect. From a risk assessment point of view, the most important factor in pipeline failure is whether the failure will occur as a leak or as a rupture. A leak is defined as a failure which is stable, (i.e. there is no increase in the size of the through-wall defect). A rupture is defined as a failure which is unstable (i.e. there is an increase in the size of the through-wall defect). It should be noted that a severed pipe is considered to be a rupture failure. A rupture is significantly worse than a leak in consequence terms.

2.1.3 *Model Considerations*

As noted above the majority of the failure frequency models detailed for this review do not consider pipeline failure from damage to branches and fittings. Further assumptions of note made by the models are as follows:

- The failure of part-wall defects is considered to occur only due to axially orientated defects. This is due to the choice of fracture mechanics failure models used to formulate limit states in the failure frequency models. The equations were selected due to the fact that axially orientated defects are more severe than equivalent defects with other orientations. In a pipeline the maximum operational stress acts in the circumferential “hoop” direction, which is exactly perpendicular to an axially orientated defect (Cosham, 2001a; Cosham, 2002). Conversely, through-wall puncture failures are limited by the pipeline wall thickness and therefore their orientation is irrelevant.
- The failure of part-wall defects is considered to occur only due to static internal pressure loading. Axial loading, in-plane bending loading and time-varying internal pressure loading are not considered by the models (Cosham, 2001a; Cosham, 2002).
- The failure of plain dent damage is not considered. Documentation relating to the development original British Gas methodology notes that the risk of failure for dents up to 24% of the pipeline diameter is negligible, justifying their exclusion from the model (Corder, 1986). Experimental data reviewed in the Pipeline Defect Assessment Manual (PDAM) showed that the burst strength, due to static internal pressure, of pipes with plain dents is not less than that of undented pipe provided the dent is smaller than 10% of the pipeline diameter. However, plain dents on welds and kinked dents could potentially have a lower burst strength than undented pipe (Cosham, 2001b).

2.2 The British Gas ERS Hazard Analysis Model

A model to calculate pipeline failure frequency due to third party external interference was developed at the British Gas Engineering Research Station (ERS) in the 1980s. The model uses a combination of structural reliability methods and trends derived from historical operational data in order to calculate a value for failure frequency. The model was originally implemented in the form of a computer program known as “Hazard Analysis”. In the Hazard Analysis model a failure frequency is calculated for a user defined pipeline based upon

its diameter, wall thickness, operating pressure, steel grade, fracture toughness and area type (Matthews, 1984; Corder, 1985b; Corder, 1985a; Corder, 1986).

2.2.1 *Structural Reliability Component*

The structural reliability based component of the Hazard Analysis model considers the failure of part-wall damage and through-wall punctures. In this part of the model, pipeline failure is considered to occur via one of three damage failure mechanisms:

- Failure of a gouge or
- Failure of a gouged dent
- Direct breach of the pipe wall

As noted by the general failure frequency model assumptions detailed in section 2.1.3, the Hazard Analysis model does not consider failure due to plain dents, dented welds and kinked dents. Given mechanical damage has occurred to the pipeline, it is assumed that this damage must take the form of either a gouge, or a gouged dent only. The pipeline failure frequency is therefore dependent on:

- The frequency with which a pipeline is subject to a gouge;
- The frequency with which a pipeline is subject to a gouged dent;
- The probability of failure of a gouge;
- The probability of failure of a gouged dent.

Additionally, the model considers that pipeline failure will result in either a leak or a rupture. Each failure mechanism is therefore subdivided into leak and rupture. As noted in section 2.1.2, the consequences of a rupture are more severe than those of a leak due to a larger and more rapid release of potentially harmful pipeline product. Failure consequences however, are not considered by the model.

2.2.1.1 *Incident-Rates*

The frequency with which a pipeline is subject to a gouge or gouged dent is known as an Incident-Rate. In the Hazard Analysis model the Incident-Rates for gouges and gouged dents are based upon an analysis of the ERS Fault Database.

The ERS Fault Database was a database maintained by British Gas encompassing all of the transmission pipelines in the onshore gas transmission system in the UK. The database recorded details of all known pipeline faults and failures which were subject to an excavation and on-site assessment, dating back to 1962. The database was eventually merged into the United Kingdom Onshore Pipeline Operators Association (UKOPA) Fault Database (Cosham, 2007). Both the ERS and UKOPA Fault Databases were/are subject to an annual update to include new data.

An Incident-Rate value is derived from the number of third party external interference mechanical damage incidents and a value for operational exposure. A pipeline's operational exposure (in km.yr) is calculated from its length (in km) and the amount of time it has been in operation (in years):

Operational Exposure = Length of Pipeline x Duration Pipeline has been in Operation

In order to calculate a value for Incident-Rate, the total number of mechanical damage incidents of a certain type recorded historically; and the total operational exposure of all pipelines affected by that type of mechanical damage are required. Incident-Rate (per km.yr) is given by:

Incident-Rate = Total Number of Incidents/Total Operational Exposure

In the Hazard Analysis model four different Incident-Rates are used. In addition to the different values required for gouges and gouged dents, the Incident-Rates are also split depending on whether the land through which a pipeline is routed is rural (R-type) or suburban (S-type). Documentation relating to the

development of the Hazard Analysis model notes that different machinery operating in different area types produced different damage profiles. This was the motivation for the use of separate values (Matthews, 1984).

Example: In the ERS Fault Database in 1985 the number of gouges in R-type areas was 148. The total operational exposure of pipelines in R-type areas up to that point in time was 196,676 km.yr (converted from 122,209 mile.yr). The Incident-Rate for gouges in R-type areas was therefore calculated to be:

$$148/196676 = 7.53 \times 10^{-4} \text{ per km.yr}$$

The Incident-Rates used in the Hazard Analysis model (converted from per mile.yr in the original documentation) are given in Table 2.1:

Area Type	Damage Type	Incident-Rate (per km.yr)
Rural	Gouge	7.53×10^{-4}
	Gouged Dent	1.38×10^{-4}
Suburban	Gouge	2.90×10^{-3}
	Gouged Dent	8.22×10^{-4}

Table 2.1: Hazard Analysis Model Incident-Rates

2.2.1.2 *Limit State Functions*

The probability of failure of gouge or gouged dent and whether a defect will fail as a leak or a rupture are determined by limit state functions and probability distributions of random variables.

The limit state functions used in the Hazard Analysis model define the conditions for failure in terms of the size of the defect, the pipeline geometry, and the material properties of the linepipe steel. They are based upon empirical or semi-empirical fracture mechanics failure models for the failure of defects in linepipe.

In order to determine whether damage will fail as a leak or rupture, a critical defect length is defined. The critical defect length is defined using the flow stress dependent form of the through-wall NG-18 equation, for an axially orientated through-wall slit subject to static internal pressure loading. Further details on the through-wall NG-18 equations are given in section 3.1.1.1. The flow stress dependent form is preferred over the toughness dependent form due to the high toughness of modern pipe steels. Failure is more likely to occur due to plastic collapse rather than brittle fracture:

$$\sigma_H = M^{-1}\overline{\sigma} \qquad (2.1)$$

σ_H is the circumferential hoop stress in the pipe wall at failure (in Nmm^{-2}). M is known as the Folias factor and this is introduced in order to take account of the bulging which occurs when a defect is present in a pressurised pipeline. $\overline{\sigma}$ is a quantity known as the flow stress, this is a measure of the stress at which unconstrained plastic flow occurs (in Nmm^{-2}).

In the Hazard Analysis model the Folias factor is defined as:

$$M = \sqrt{1 + 0.3125\left(\frac{2c}{\sqrt{Rt}}\right)^2} \quad \text{for} \quad \frac{2c}{\sqrt{Rt}} \leq 2 \qquad (2.2)$$

$$M = 0.6 + 0.45\left(\frac{2c}{\sqrt{Rt}}\right) \quad \text{for} \quad \frac{2c}{\sqrt{Rt}} > 2 \qquad (2.3)[1]$$

Where $2c$ is the axial defect length (in mm), R is the external pipeline radius (in mm) and t the pipeline wall thickness (in mm). Further details on the Folias factor are given in section 3.1.1.2.

The flow stress is an empirical term which can take many different values. In the Hazard Analysis model it is been defined as:

[1] Note this equation was rearranged from the original text written as: $L_{crit} = (M\text{-}0.6)\sqrt{Rt}/0.45$ on a typewriter and is therefore ambiguous as to whether the "$/0.45$" portion is included in the square root. It has been assumed here that the square root applies only to "Rt".

$$\bar{\sigma} = 1.15\sigma_Y \quad (2.4)$$

Where σ_Y is the yield strength (in Nmm^{-2}) of the pipe steel (often approximated to the specified minimum yield strength (SMYS), in the absence of material test data). The flow stress was defined in this way in order to be consistent with the British Gas Dent-Gouge Fracture Model (BGDGFM) (equation (2.10)). Further details on the flow stress are given in section 3.1.1.3.

The circumferential hoop stress (in Nmm^{-2}) in the pipeline is calculated from the internal operating pressure, P (in barg); the pipeline external diameter, D (in mm); and the pipeline wall thickness, t (in mm); using Barlow's formula:

$$\sigma_H = \frac{PD}{20t} \quad (2.5)$$

A critical defect length for rupture (in mm) is defined by rearranging equation (2.1) and substituting into equation (2.2) and (2.3), replacing $2c$ with L_{crit}:

$$L_{crit} = \sqrt{3.2Rt\left[\left(\frac{\bar{\sigma}}{\sigma_H}\right)^2 - 1\right]} \quad \text{for } M \leq 1.5 \quad (2.6)$$

$$L_{crit} = \frac{\left[\left(\frac{\bar{\sigma}}{\sigma_H}\right) - 0.6\right]\sqrt{Rt}}{0.45} \quad \text{for } M > 1.5 \quad (2.7)$$

Equations (2.6) and (2.7) are the limit state function for leak / rupture. Defects with an axial length longer than the critical length, for the specified operating conditions, are predicted to fail as a rupture. Defects with an axial length shorter or equal to the critical length are predicted to fail as a leak. Note that the limit state equation for leak / rupture is applied to both gouge and gouged dent defects, where $2c$ represents either the gouge length or the gouged dent gouge length, respectively. From equation (2.1) the information required to determine whether a pipeline defect will leak or rupture is the pipe geometry, operating and material parameters and the gouge length or gouged dent gouge length.

The failure stress (in Nmm^{-2}) of a part-wall gouge is given by the flow stress dependent form of the part-wall NG-18 equation, for an axially orientated gouge

subject to static internal pressure loading. Further details on the part-wall NG-18 equations are given in section 3.1.1.1 The flow stress dependent form is preferred over the toughness dependent form due to the high toughness of modern pipe steels. Failure is more likely to occur due to plastic collapse rather than brittle fracture:

$$\sigma_H = \bar{\sigma}\left[1 - \frac{d}{t}\right]\left[1 - \frac{d}{t}\left(\frac{1}{M}\right)\right]^{-1} \quad (2.8)$$

Where $\overline{\sigma}$, σ_H, M and t are defined as above and d is the depth of the gouge (in mm). By rearranging equation (2.8) a critical defect depth (in mm) can be defined as:

$$d_{crit} = t\left[1 - \frac{\sigma_H}{\bar{\sigma}}\right]\left[1 - \frac{\sigma_H}{\bar{\sigma}}\left(\frac{1}{M}\right)\right]^{-1} \quad (2.9)$$

Equation (2.9) is the limit state function for part-wall gouge failure. Gouges deeper than the critical depth, for the specified operating conditions, are predicted to fail. The information required to determine whether a gouge will fail is the pipe geometry, operating and material parameters and the gouge depth.

The failure stress of a part-wall gouged dent is given by the BGDGFM, for an axially orientated gouge at the base of a dent, subject to static internal pressure loading. The BGDGFM assumes that part-wall gouged dent failure occurs due to a combination of brittle fracture and plastic collapse. Further details on the BGDGFM are given in section 3.1.2.1:

$$\frac{\sigma_H}{\bar{\sigma}} = \frac{2}{\pi}\cos^{-1}\left[\exp - \left\{113\frac{1.5\pi E}{\bar{\sigma}^2 Ad}\left[Y_1\left(1 - \frac{1.8H}{2R}\right) + Y_2\left(10.2\frac{R}{t}\frac{H}{2R}\right)\right]^{-2}\exp\left[\frac{\ln(0.738C_v) - K_1}{K_2}\right]\right\}\right] \quad (2.10)$$

Where E is Young's modulus (in Nmm^{-2}), A is the fracture area of a 2/3 Charpy specimen (in mm^2), d is the depth of the gouge (in mm), H is the depth of the

dent (in mm) and C_V is the 2/3 Charpy v-notch upper shelf impact energy (in J). $\tilde{\sigma}$ (in Nmm^{-2}), Y_1, Y_2, K_1 and K_2[2], are defined as:

$$\tilde{\sigma} = 1.15\sigma_Y\left(1 - \frac{d}{t}\right) \quad (2.11)$$

$$Y_1 = 1.12 - 0.23\left(\frac{d}{t}\right) + 10.6\left(\frac{d}{t}\right)^2 - 21.7\left(\frac{d}{t}\right)^3 + 30.4\left(\frac{d}{t}\right)^4 \quad (2.12)$$

$$Y_2 = 1.12 - 1.39\left(\frac{d}{t}\right) + 7.32\left(\frac{d}{t}\right)^2 - 13.1\left(\frac{d}{t}\right)^3 + 14.0\left(\frac{d}{t}\right)^4 \quad (2.13)$$

$$K_1 = 1.9 \quad (2.14)$$

$$K_2 = 0.57 \quad (2.15)$$

By rearranging equation (2.10) a dent depth (in mm) which is predicted to cause failure can be defined as:

$$H_{crit} = \frac{2R\left(\sqrt{\frac{\exp\left[\frac{\ln(0.738C_v) - K_1}{K_2}\right]}{\ln\left(\sec\left[\frac{\pi\sigma_H}{2\tilde{\sigma}}\right]\right)\left(0.00885\frac{\tilde{\sigma}^2 Ad}{1.5\pi E}\right)Y_1^2}} - 1\right)}{10.2\left(\frac{Y_2}{Y_1}\right)\left(\frac{R}{t}\right) - 1.8} \quad (2.16)$$

Equation (2.16) is the limit state function for gouged dent failure. Documentation relating to the development of the Hazard Analysis model notes that values of 2.049 and 0.534 should be used for K_1 and K_2 respectively in equation (2.16). The reason given for this is that the BGDGFM is semi-empirical and based on a linear regression of the $\frac{\ln(0.733C_v - K_1)}{K_2}$ term. The subject of the equation is changed in going from (2.10) to (2.16) and this requires a new regression to be performed, resulting in new values for the constants. Note that equations (2.10) through (2.16) have been converted to SI units from imperial units which were used in the Hazard Analysis model and documentation.

[2] Note that K_1 and K_2 as given by equations (2.14) and (2.15) are not dimensionless and have dimensions of ftlbf. Further information is given in section 3.1.2.1.

From equation (2.16) a dent of depth H_{crit} is predicted to cause a failure when it occurs in conjunction with a gouge of depth d for the specified operating conditions. From equation (2.10) the information required to determine whether a gouged dent will fail is the pipe geometry, operating and material parameters, the gouged dent dent depth and the gouged dent gouge depth. It should be noted that the length of the gouge is not included in the BGDGFM.

Through-wall punctures do not require a definition of a failure stress since the failure occurs due to the creation of a hole in the pipe wall. In the structural reliability component of the Hazard Analysis model it is implied that a through-wall puncture has occurred if the gouge depth of a gouge or gouged dent defect, d, is in excess of the pipe wall thickness, t.

2.2.1.3 *Probability Distributions*

The Hazard Analysis model uses six random variables in calculation of the probability of failure of a gouge or a gouged dent. These are variables which appear in the limit state functions described in the previous section and whose values are random, based upon probability distributions. The random variables used in the Hazard Analysis model alongside the limit state functions in which they appear are shown in Table 2.2:

Random Variable	Limit State Function
Gouge Length	Leak / Rupture & Gouge Failure
Gouged Dent Gouge Length	Leak / Rupture
Gouge Depth in R-Type Areas	Gouge Failure
Gouge Depth in S-Type Areas	Gouge Failure
Gouged Dent Gouge Depth	Gouged Dent Failure
Gouged Dent Dent Depth	Gouged Dent Failure

Table 2.2: Hazard Analysis Model Random Variables

All of the other variables in the limit state functions were assumed to be deterministic quantities. Six separate Weibull cumulative probability distributions were derived to describe the six random variables. The Weibull distributions were fitted using the maximum likelihood method. Weibull distributions were

chosen due to their versatility, allowing a wide variety of physical quantities to be accurately represented (Matthews, 1984). The Weibull distributions were based upon an analysis of pipeline damage data for gouges and gouged dents, contained in the ERS Fault Database.

As for Incident-Rate, the intent was to split the probability distributions between R-type and S-type areas due to evidence suggesting different machinery operating in different area types produced different damage profiles (Matthews, 1984). Unfortunately, there was insufficient data available in the ERS database to allow useable R-type and S-type distributions to be derived for both damage forms. Only gouge defects provided enough data to enable the distinction to be made. Furthermore, it was observed on derivation that the Weibull distributions for gouge length in R-type and S-type areas were almost identical. A decision was therefore made to merge the gouge length data sets, leaving gouge depth as the only variable with separate probability distributions for R-type and S-type areas.

Documentation relating to the development of the Hazard Analysis model notes that data from puncture damage was included in the derivation of the Weibull distributions. The damage was classified as a gouge or gouged dent with a depth equal to the wall thickness of the pipeline and was treated as an extreme form of part-wall damage. Exceptions to this were punctures caused by drilling operations in-error, which were excluded as it was suggested that this type of puncture cannot be viewed as typical gouge or gouged dent damage (Corder, 1985b).

It should be noted that although separate random variables are used for R-type area gouge depth and S-type area gouge depth, the same limit state function, equation (2.9), is applied to both. Also note that although the limit state function for gouged dent failure does not include the length of the gouge a random variable for this quantity is still required in order to apply the limit state function for leak / rupture for the gouged dent case.

A Weibull probability density function describing a random variable x has the form:

$$f(x) = \frac{\alpha}{\beta^{\alpha}} x^{\alpha-1} \exp\left[-\left(\frac{x}{\beta}\right)^{\alpha}\right] \quad (2.17)$$

Where α and β are distribution parameters. Integrating the probability density function, with respect to the random variable between two limits, k and l, will give the probability that the value of a sample of the random variable x lies between k and l:

$$P_x(k \leq x \leq l) = \int_k^l f(x)dx \quad (2.18)$$

In general terms, the definition of a cumulative probability density function is given by:

$$F(x) = \int_{-\infty}^{x} f(u)du \quad (2.19)$$

Assuming that the value of x can be anything from $-\infty$ to $+\infty$. (note that the Weibull distribution in particular is not defined for $x < 0$). The value of the cumulative probability distribution at any specific value of x (for example, x_1) can therefore be interpreted as the probability that the value of a sample of x will be less than or equal to x_1. Given that:

$$P_x(-\infty \leq x \leq \infty) = 1 \quad (2.20)$$

Then the function:

$$R_x(x) = 1 - F(x) \quad (2.21)$$

Can be interpreted as the probability that the value of a sample of x will be greater than any specific value of x (for example x_1).

In terms of the Hazard Analysis model, the derivation of cumulative distribution functions for each of the six damage variables and the use of equation (2.21) allows the probability of gouge or gouged dent damage of a certain size or

greater to be calculated, in the incidence of a random occurrence of gouge or gouged dent damage.

The Weibull cumulative probability distribution has the form:

$$F(x) = 1 - \exp\left[-\left(\frac{x}{\beta}\right)^{\alpha}\right] \qquad (2.22)$$

The parameters defining the cumulative probability distributions derived for the Hazard Analysis model are summarised in Table 2.3 (Matthews, 1984). From equation (2.21), the gouge length distributions are shown in Figure 2.1, the gouge depth distributions in Figure 2.2 and the dent depth distribution in Figure 2.3.

Random Variable	Distribution Type	α	β (mm)
Gouge Length	Weibull	0.810	161.063
Gouge Dent Gouge Length	Weibull	0.952	103.059
Gouge Depth in R-Type Areas	Weibull	0.926	1.460
Gouge Depth in S-Type Areas	Weibull	0.869	1.184
Gouged Dent Gouge Depth	Weibull	0.790	1.078
Gouged Dent Dent Depth	Weibull	1.078	7.064

Table 2.3: Hazard Analysis Model Weibull Parameters[3]

[3] Note that the Weibull parameters have been converted from those originally reported using the relations $a = \frac{1}{\beta^{\alpha}}$ and $b = \alpha$ and converting the parameter β from inches to mm.

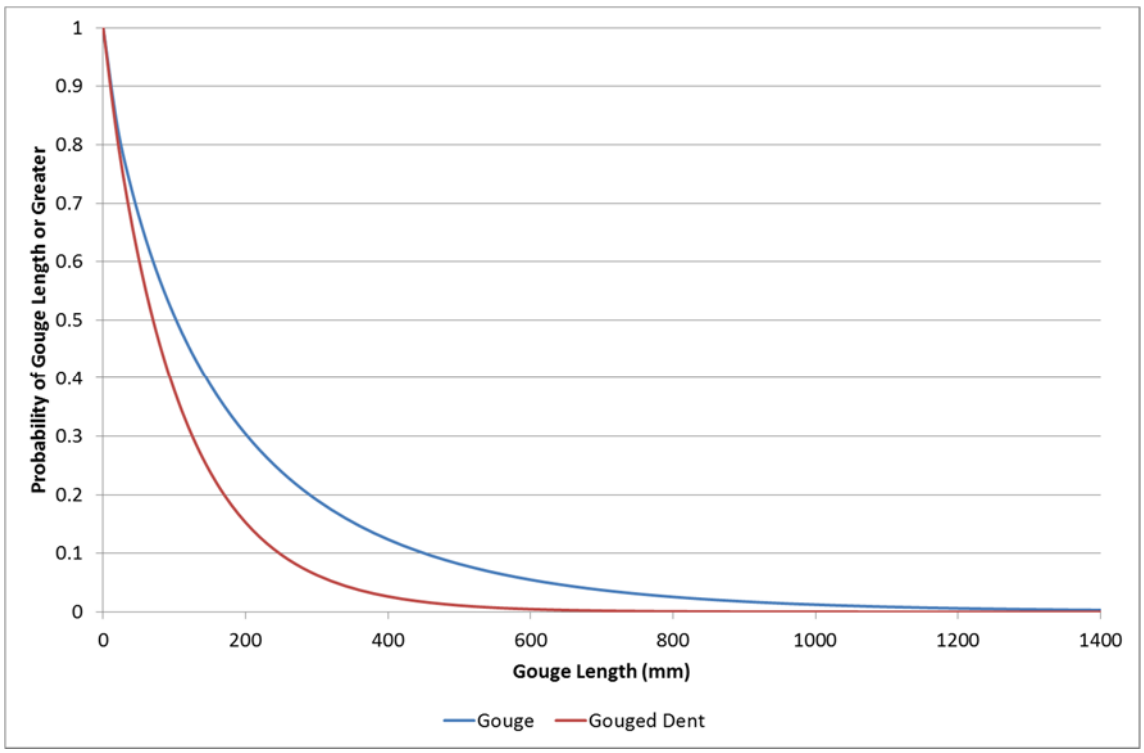

Figure 2.1: Hazard Analysis Model Gouge Length Distributions

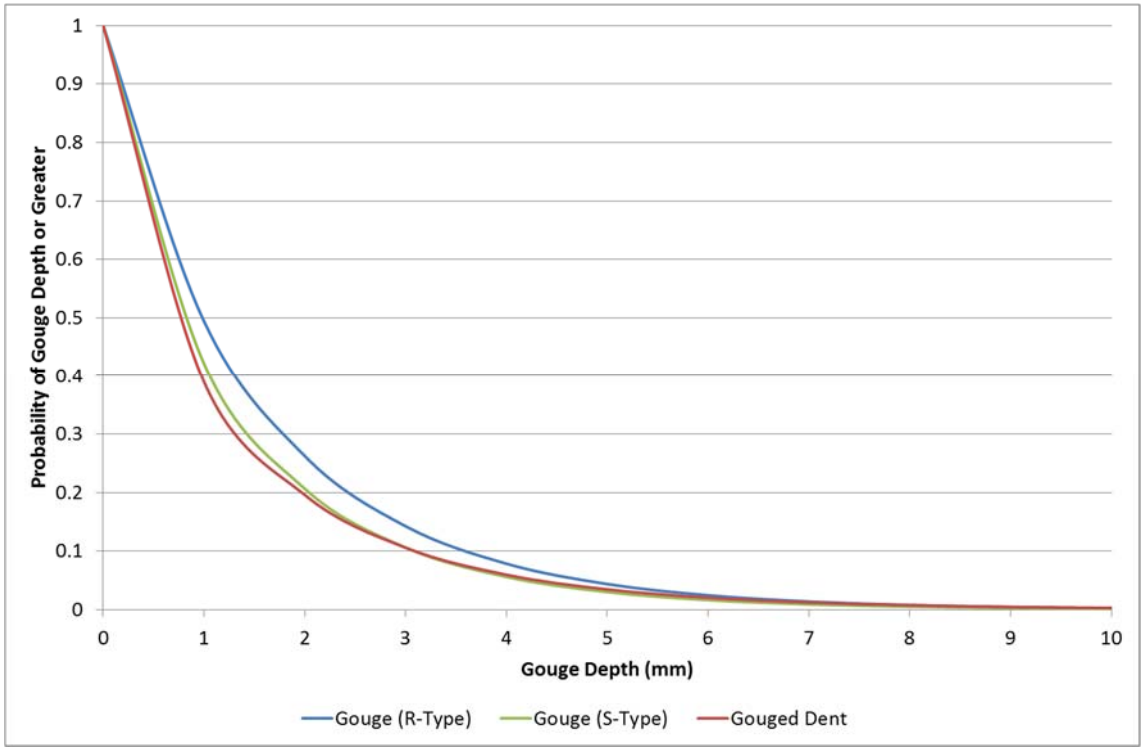

Figure 2.2: Hazard Analysis Model Gouge Depth Distributions

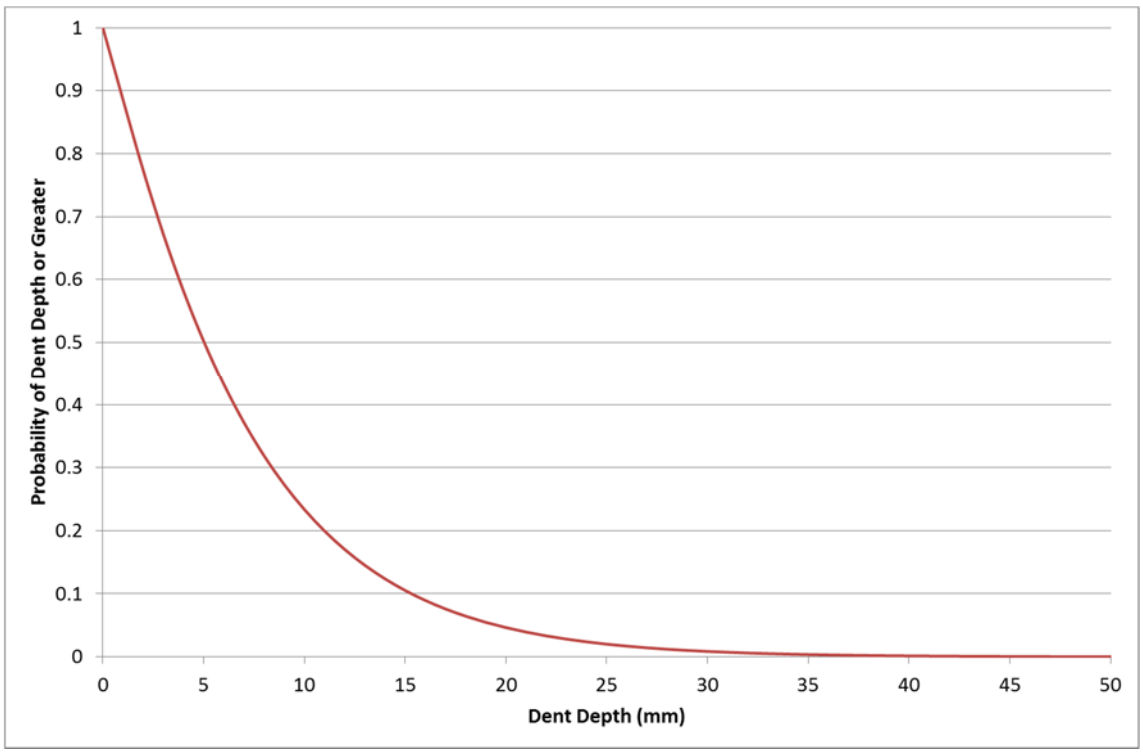

Figure 2.3: Hazard Analysis Model Dent Depth Distribution

2.2.1.4 *Probability of Failure of a Gouge and a Gouged Dent*

The probability and frequency of failure for gouge and gouged dent damage in the Hazard Analysis model are calculated using numerical integration with the trapezium rule (Matthews, 1984; Corder, 1985a).

From the limit state function for gouge failure (equation (2.9)), and section 2.2.1.3, the total probability of failure for gouges can be expressed as:

$$P_{gougetotal} = \int_0^{1397} f_{g2c}(2c) R_{gd}(d_{crit}) d2c \qquad (2.23)$$

Where the subscripts $g2c$ and gd denote the use of the gouge length and gouge depth Weibull parameters respectively. The use of R-type or S-type Weibull parameters for gouge depth is user-defined and depends upon the area type of the particular pipeline under consideration. The value of d_{crit} in equation (2.23) is dependent on the gouge length, $2c$ (from equation (2.9)). The gouge length Weibull distribution was truncated at 1397 mm (converted from 55” in the original documentation), fixing the upper limit of the integral. The reason for this

was to remain consistent with previous work, the details of which are unavailable.

Note that failures due to through-wall puncture are incorporated through the use of the function R_{dg} (equation (2.21)). Whilst d_{crit} corresponds to the critical depth for part-wall gouges, the function R_{dg} gives the probability of a gouge of depth d_{crit} and greater and therefore includes gouges of depth in excess of the pipe wall thickness, t.

Equation (2.23) can be split into a probability of a leak, $P_{gougeleak}$, and a probability of a rupture, $P_{gougerupture}$, using the critical length determined by the limit state function for leak / rupture (equations (2.6) and (2.7)):

$$P_{gougeleak} = \int_0^{L_{crit}} f_{g2c}(2c) R_{gd}(d_{crit}) d2c \qquad (2.24)$$

$$P_{gougerupture} = \int_{L_{crit}}^{1397} f_{g2c}(2c) R_{gd}(d_{crit}) d2c \qquad (2.25)$$

From the limit state function for gouged dent failure (equation (2.16)), and section 2.2.1.3, the total probability of failure for gouged dents, with a gouge of depth, d, and a dent of depth, H_{crit}, can be expressed as:

$$P_{gougeddenttotal} = \int_0^{1397} f_{gd2c}(2c) \left[\int_0^{d_{crit}} f_{gdd}(d) R_H(H_{crit}) dd \right] d2c \qquad (2.26)$$

Where the subscripts $gd2c$, gdd and H denote the use of the gouged dent gouge length, gouged dent gouge depth and gouged dent dent depth Weibull parameters respectively. The value of H_{crit} in equation (2.26) is dependent on d and calculated using equation (2.16). Note that despite the fact equation (2.26) describes gouged dent failure, the limit state function for gouge failure is used in the equation to calculate the value of d_{crit} in the second integral. Documentation relating to the development of the Hazard Analysis model indicates that d_{crit} was used as the integral limit as this would represent the depth at which a gouge would fail without the presence of a dent (Corder, 1985a). It is therefore implied that deeper gouge depths (including through-wall punctures) are covered by the

probability of failure for gouges, equation (2.23)[4]. The value of d_{crit} is dependent on the gouge length (taken to be the gouged dent gouge length in this case), $2c$. The upper limit of the second integral in equation (2.26) therefore changes depending on the value of $2c$ in the first integral. As with gouge damage, the gouged dent gouge length Weibull distribution was truncated at 1397 mm (converted from 55" in the original documentation), fixing the upper limit of the first integral.

In order to determine the probability of a gouged dent failing as a leak and a gouged dent failing as a rupture, equation (2.26) can be split in a similar way to equations (2.23), (2.24) and (2.25):

$$P_{gougeddentleak} = \int_0^{L_{crit}} f_{gd2c}(2c) \left[\int_0^{d_{crit}} f_{gdd}(d) R_H(H_{crit}) dd \right] d2c \qquad (2.27)$$

$$P_{gougeddentrupture} = \int_{L_{crit}}^{1397} f_{gd2c}(2c) \left[\int_0^{d_{crit}} f_{gdd}(d) R_H(H_{crit}) dd \right] d2c \qquad (2.28)$$

The critical length of the gouged dent gouge in equation (2.27) and (2.28) is the same as that for the gouge failures described by equations (2.24) and (2.25), as calculated by the limit state function for leak / rupture, equations (2.6) and (2.7).

2.2.1.5 *Failure Frequency*

The leak, rupture and total failure frequency (per km.yr), ff_{SRleak}, $ff_{SRrupture}$ and $ff_{SRtotal}$ respectively, of a pipeline due to gouge and gouged dent damage in the structural reliability component of the Hazard Analysis model are calculated by combining the results of Sections 2.2.1.1 and 2.2.1.4:

$$ff_{SRleak} = IncidentRate_{gouge} . P_{gougeleak} + IncidentRate_{gougeddent} . P_{gougeddentleak} \qquad (2.29)$$

$$ff_{SRrupture} = IncidentRate_{gouge} . P_{gougerupture} + IncidentRate_{gougeddent} . P_{gougeddentrupture} \qquad (2.30)$$

[4] In actuality, gouged dent gouges with depths deeper than d_{crit} must also be counted. The Cosham model described in section 2.6 addresses this oversight.

$$ff_{SRtotal} = ff_{SRleak} + ff_{SRrupture} \quad (2.31)$$

Where $IncidentRate_{gouge}$ and $IncidentRate_{gougeddent}$ are Incident-Rates for gouges and gouged dents from Table 2.1 respectively. The use of R-type or S-type Incident-Rates depends on the area type of the particular pipeline under consideration.

2.2.1.6 *Hole Size*

Documentation relating to the development of the Hazard Analysis model notes that the consequences of pipeline failure are strongly dependent upon the size of the breach in the pipeline wall (Corder, 1986). For this reason, a relationship to calculate hole size was incorporated into the structural reliability failure frequency calculation in the model.

The hole size relationship was based upon work performed by Baum and Butterfield (Butterfield, 1979) into the rates of pipeline depressurisation following the failure of subcritical damage. The area of the hole in the pipeline was found to be related to the initial length of the defect. In the Hazard Analysis model the Baum and Butterfield relationship can be used to split the failure frequency for leaks down further, into different hole size diameter ranges of (converted from inches in the original documentation):

- 0 – 25.4 mm;
- 25.4 – 76.2 mm;
- 76.2 – 152.4 mm.

Note that the hole size relationship is only used to split the leak failure frequency and not the rupture failure frequency. The exact form of the hole size relationship used in the Hazard Analysis model is not stated in the documentation.

2.2.2 *Historical Data Component*

The historical data component of the Hazard Analysis model considers through-wall damage only. In this part of the model a value for failure frequency is determined for failures resulting from damage to branches and fittings on the pipeline. The failure frequency is determined directly from historical operational data for failures of this type contained in the ERS Fault Database. It should be noted that through-wall damage from punctures, as described in section 2.1.1 are not addressed in the historical data component of the model. As explained in section 2.2.1.3, punctures are treated as an extreme form of part-wall damage in the Hazard Analysis model and the historical operational data relating to them is included in the derivation of Weibull distributions for the structural reliability component of the model only. Exceptions to this are punctures caused by drilling operations in-error (noted as hot tap in-error in the documentation). Having been excluded from the structural reliability component of the model, this type of puncture is included in the failure data used by the historical data component.

Documentation relating to the development of the Hazard Analysis model notes that failure resulting from damage to branches and fittings or hot tap in-error is strongly dependent on the pipeline wall thickness (Corder, 1986). Relationships giving failure frequency as a function of wall thickness were derived from the historical operational failure data for R-type and S-type areas. These relationships are used to determine the failure frequency due to the historical data component for the particular pipeline under consideration. Curves showing the relationships between failure frequency and wall thickness are presented in Figure 2.4 (converted from failures per mile.yr versus inches in the original documentation). It should be noted that no failure frequency values for the historical data component which resulted in a pipeline rupture are quoted in the documentation. The distributions derived are therefore assumed to give the failure frequency for leaks only.

In a similar way to the structural reliability component, a hole size relationship is also included in the historical data component of the model. This can be used to

split the leak failure frequency for the historical data component down into the same hole size ranges listed in section 2.2.1.6.

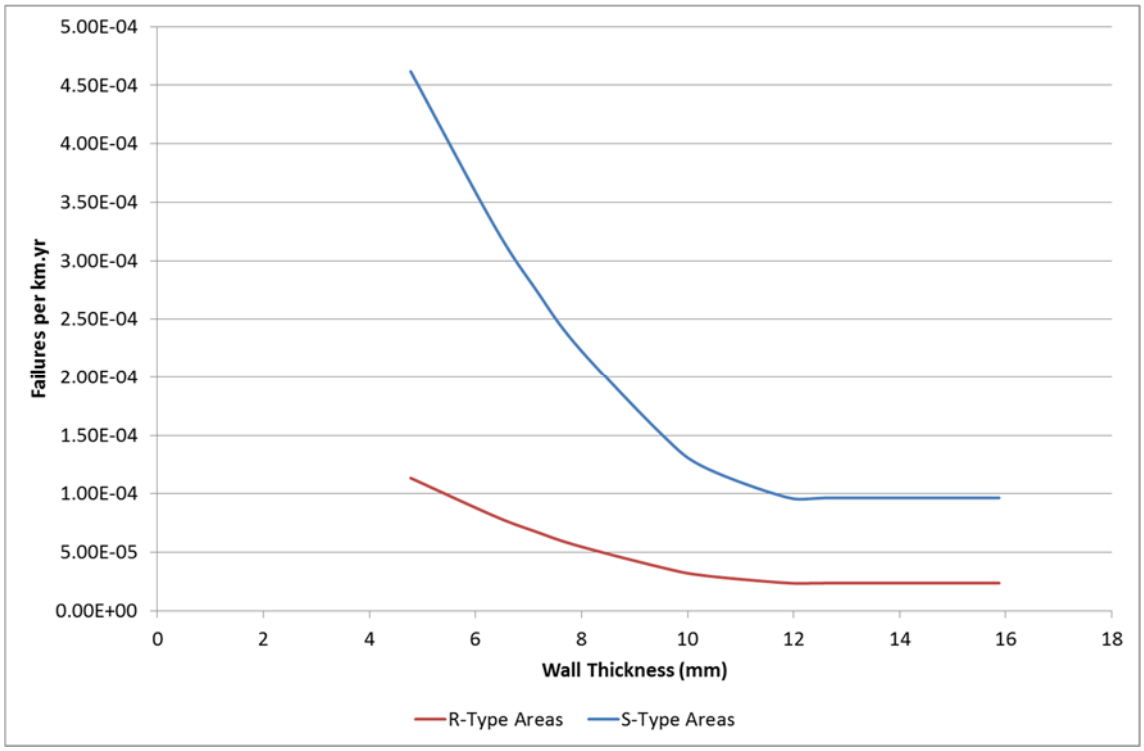

Figure 2.4: Leak Failure Frequency for Historical Data Component in R-Type and S-Type Areas in the Hazard Analysis Model

2.2.3 *Overall Failure Frequency*

In the Hazard Analysis model the overall leak, rupture and total failure frequency, ff_{leak}, $ff_{rupture}$ and ff_{total} respectively, for the particular pipeline under consideration are calculated by combining the results from the structural reliability component and the historical data component:

$$ff_{leak} = ff_{SRleak} + ff_{HDleak} \quad (2.32)$$

$$ff_{rupture} = ff_{SRrupture} \quad (2.33)$$

$$ff_{total} = ff_{leak} + ff_{rupture} \quad (2.34)$$

Where ff_{HDleak} is the failure frequency from the historical data component of the model, determined using the relationships described in section 2.2.2. The use of

the R-type or S-type relationship depends on the area type of the pipeline. Note that equation (2.33) is assumed on the basis that historical data component failure frequencies for ruptures were not quoted in the documentation.

2.3 The FFREQ Model

FFREQ is the current industry standard model to calculate pipeline failure frequency due to third party external interference and the model recommended for use by UKOPA. It exists in the form of a software package. The model was developed at the British Gas ERS sometime between August 1986 and April 1993, as an update to the Hazard Analysis model described in section 2.2 (Corder, 1993; Corder, 1995a). Access to the software can be obtained through UKOPA from DNV-GL, who are responsible for making updates to the model.

FFREQ is an updated version of the Hazard Analysis model and a summary paper published in 1995 (Corder, 1995a) indicates that the overall structure of the two models is identical. As with Hazard Analysis, FFREQ uses the combination of a structural reliability component and a historical data component in order to calculate a value for failure frequency. It is known however, that certain modifications and augmentations were made to the failure frequency calculation methodology used in Hazard Analysis in order to produce FFREQ. Indeed the FFREQ software offers a number of options to which no reference was made in documentation relating to Hazard Analysis. Unfortunately, documentation relating to the structure and development of FFREQ is sparse and the source code for the model is not available. It is therefore not possible to determine the exact changes made between Hazard Analysis and FFREQ; and to give a complete review of the FFREQ model.

This section will describe what is known about the differences between FFREQ and the Hazard Analysis model, based upon the available information.

2.3.1 *FFREQ Incident-Rates*

The Incident-Rates used in the structural reliability component of FFREQ are given in Table 2.4. The values are taken from the FFREQ.dat file used by the software (Wild, 1993). It is assumed that the units used in FFREQ.dat are per mile.yr, this is because some of the Weibull distribution parameter values which are also given in FFREQ.dat are retained from the Hazard Analysis model (see section 2.3.6), and the Hazard Analysis model uses imperial units. The values have therefore been converted to per km.yr in Table 2.4.

Table 2.4 shows that for each area type, FFREQ includes one Incident-Rate for gouges and four Incident-Rates for gouged dents. This is in contrast to the Hazard analysis model which uses a single Incident-Rate for each damage type. Multiple Incident-Rates for gouged dent damage are used in the FFREQ model as part of an additional algorithm to address dent resistance. Further details on the FFREQ dent resistance algorithm are given in section 2.3.5. A memo (Acton, 2011) from GLND regarding probability distributions and Incident-Rates in FFREQ indicates that the different gouged dent rates are applied to different wall thickness ranges[5]:

- 0 – 5 mm;
- 5 – 10 mm;
- 10 – 15 mm;
- >15 mm.

It should be noted that the Incident-Rates for gouges in FFREQ are slightly different to those used in the Hazard Analysis model. It is assumed that the rates are updated values, derived from a later version of the ERS Fault Database containing additional data.

[5] Note that certain wording in the FFREQ programmer's guide suggests the gouged dent Incident-Rates shown in Table 2.4 should in fact be applied to different crack length ranges, rather than wall thickness ranges. This implication is assumed to be incorrect due to a lack of supportive evidence.

Area Type	Damage Type	Incident-Rate (per km.yr)
Rural	Gouge	7.02×10^{-4}
	Gouged Dent (1)	6.41×10^{-4}
	Gouged Dent (2)	2.05×10^{-4}
	Gouged Dent (3)	9.51×10^{-5}
	Gouged Dent (4)	4.72×10^{-5}
Suburban	Gouge	2.70×10^{-3}
	Gouged Dent (1)	3.81×10^{-3}
	Gouged Dent (2)	1.22×10^{-3}
	Gouged Dent (3)	5.64×10^{-4}
	Gouged Dent (4)	2.79×10^{-4}

Table 2.4: FFREQ Model Incident-Rates

2.3.2 *Depth of Cover*

In addition to the updated values of Incident-Rate, FFREQ also includes an optional facility to take into account the pipeline depth of cover. The FFREQ user's guide (Corder, 1993) notes that historically, pipelines which are buried deeply are less prone to damage than those with less cover, justifying the introduction of a specific algorithm.

If the depth of cover analysis is chosen by the user, a depth of cover value (in m) must be entered as part of the model input data. The algorithm takes into account the depth of cover by applying a modifying factor to the appropriate Incident-Rates in the structural reliability component of FFREQ. The modifying factors were derived from historical operational data contained in the ERS Fault Database by relating the number of pipeline damage incidents to the depth of cover (Corder, 1993). The modifying factors for depth of cover used in FFREQ are shown graphically in Figure 2.5 (Wild, 1993).

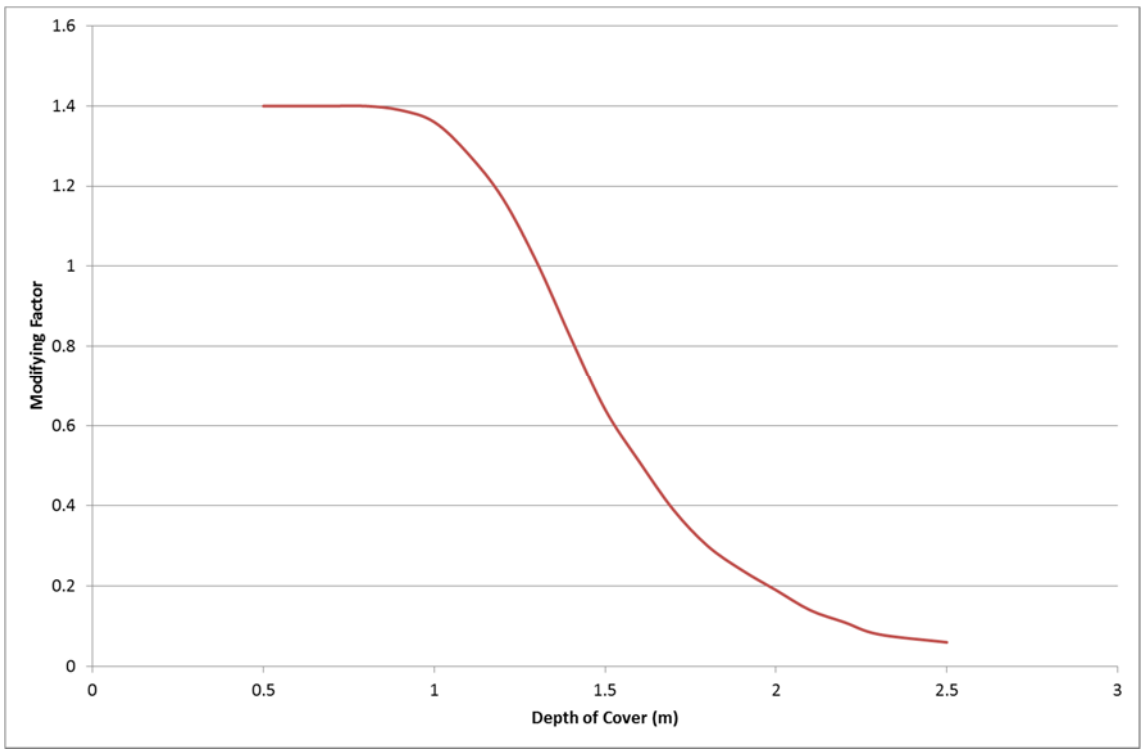

Figure 2.5: Depth of Cover Factors in FFREQ

Figure 2.5 shows that the modifying factor has a value of 1 when the depth of cover is 1.31 m. This represents the average depth of cover for all of the pipelines considered in the ERS Fault Database at the time FFREQ was developed. It follows logically that if the depth of cover analysis is omitted, the assumption is that the particular pipeline under consideration is buried with a depth of 1.31 m.

2.3.3 *Sleeve Analysis*

Another optional algorithm included in FFREQ is that of a sleeve analysis. Sleeves are used to provide an additional layer of protection for pipelines at road crossings, or to allow pipeline construction closer to areas of a high population density.

If a sleeve analysis is chosen by the user, a sleeve thickness value (in mm) must be entered as part of the input data. The algorithm takes into account the extra protection from the sleeve by using a value for wall thickness in the FFREQ structural reliability component of the pipe and the sleeve combined. Additionally a different Incident-Rate, specific to sleeves, is applied in place of

the standard Incident-Rates. The sleeve Incident-Rate was derived from historical operational data contained in the ERS Fault Database for damage incidents to sleeves (Corder, 1993). The sleeve Incident-Rate used in FFREQ is given in Table 2.5:

Damage Type	Incident-Rate (per km.yr)
Sleeve Damage	1.70×10^{-3}

Table 2.5: FFREQ Sleeve Analysis Incident-Rate

The FFREQ programmer's guide (Wild, 1994) indicates that a further calculation is performed using the sleeve's external diameter in order to determine the proportion of the circumference of the pipe which could be damaged if the sleeve was penetrated by third party external interference. However, the details of this calculation and its application are unknown.

2.3.4 *FFREQ Folias Factor*

In FFREQ a different expression for the Folias factor is used in the structural reliability component of the model. The alternative two term expression applicable to long defects is used in place of that given by equations (2.2) and (2.3) (Wild, 1994; Corder, 1995a):

$$M = \sqrt{1 + 0.26\left(\frac{2c}{\sqrt{Rt}}\right)^2} \qquad (2.35)$$

Further details on the Folias factor are given in section 3.1.1.2.

2.3.5 *FFREQ Dent Resistance*

The structural reliability component of FFREQ includes an algorithm to take into account the resistance of pipes to denting. The algorithm was implemented as it was acknowledged that different parameters would affect the susceptibility of a

pipeline to denting. For example, a thin pipeline can be dented more easily than a thick pipeline.

The FFREQ user's guide (Corder, 1993) indicates that the algorithm acts by:

- Relating the number of dent incidents to the wall thickness of the pipeline;
- Using a model to determine the probability that the machinery damaging the pipeline is capable of generating sufficient force to cause a dent which would lead to failure.

The first point above is addressed through the use of the multiple gouged dent Incident-Rates detailed in Table 2.4. The FFREQ programmer's guide (Wild, 1994) notes that the second point is addressed through the use of a relationship between dent depth and dent force; and a probability distribution for impact force of machines in use in the United Kingdom. A dent depth / dent force relationship derived by Spiekhout is used in the procedure, however this was modified by Corder and Fedorov. Unfortunately the form of the dent depth / dent force relationship is not stated. The FFREQ user's guide only references an internal ERS memo detailing a semi-empirical model for dent resistance in pipelines, from the 15th June 1992.

In the algorithm, the dent size required to cause a failure is calculated using the limit state function for gouged dent failure (equation (2.16)). Following this the force required to cause such a dent is calculated using the dent depth / dent force relationship. The machine force probability distribution is then used to calculate the probability of that force.

2.3.6 *FFREQ Probability Distributions*

The parameters defining the cumulative probability distributions used in FFREQ are summarised in Table 2.6. The values are taken from the FFREQ.dat file used by the software (Wild, 1993). As with the Hazard Analysis model, Weibull distributions were chosen to represent the necessary random variables.

Random Variable	Distribution Type	α	β (mm for non-highlighted cases)
Gouge Length	Weibull	0.810	161.063
“Length”	Weibull	0.905	117.866
Gouge Depth in R-Type Areas	Weibull	0.926	1.460
Gouge Depth in S-Type Areas	Weibull	0.869	1.184
“Gouge”	Weibull	1.216	21.339
“Dent”	Weibull	0.735	12.422

Table 2.6: FFREQ Model Weibull Parameters[6]

In Table 2.6 “Length”, “Gouge” and “Dent” refer to the Weibull distributions used to calculate the probability of failure for gouged dents. The “Length”, “Gouge” and “Dent” labels are taken directly as written in the FFREQ.dat file. In the Hazard Analysis model (Table 2.3), the gouged dent distributions represent gouged dent gouge length, gouged dent gouge depth and gouged dent dent depth. In FFREQ however, the specific definition and application of the distributions is not clear from the available documentation.

The memo from GLND on probability distributions and Incident-Rates (Acton, 2011) states that the distributions refer to gouged dent dent length (“Length”), gouged dent dent depth in S-type areas (“Gouge”) and gouged dent dent depth in R-type areas (“Dent”). These definitions are also implied by the FFREQ programmer’s guide (Wild, 1994) through labelling and variable names. In contradiction however, the available information regarding the FFREQ dent resistance algorithm (section 2.3.5) suggests that in FFREQ an impact force probability distribution is required, which would replace the gouged dent dent depth distribution. Furthermore, the limit state functions used in FFREQ are the same as those used in the Hazard Analysis model (Corder, 1993; Wild, 1994; Corder, 1995a) meaning the use of gouged dent gouge length and gouged dent gouge depth distributions is required; with the dent length distribution being redundant.

---

[6] Note that the Weibull parameters have been converted from those originally reported using the relations $a = \frac{1}{\beta^{\alpha}}$ and $b = \alpha$. The conversions are assumed to be the same as those in Table 2.3 due to the FFREQ’s similarity to the Hazard Analysis model. The parameter β has been converted from inches to mm apart from the highlighted cases, for which the units are not clear. In these cases the parameters are presented exactly as given in the FFREQ.dat file.

The equations used to calculate the probability of failure for gouged dents in FFREQ will be different to those used in the Hazard Analysis model (equations (2.26), (2.27) and (2.28)) due to the inclusion of the dent resistance algorithm. Unfortunately, it is not possible to state the equations due to the ambiguity surrounding the gouged dent Weibull distributions and their application.

It is noted that the Weibull parameters used for gouges are the same as those used in the Hazard Analysis model. This suggests that an updated analysis using a later version of the ERS Fault Database was not performed with regards to distribution fitting when FFREQ was developed, in contrast to the values of Incident-Rate.

2.3.7 *FFREQ Historical Data Component*

The historical data component of FFREQ is very similar to that of the Hazard Analysis model. Relationships giving the frequency of through-wall damage as a function of wall thickness were derived from historical operational data contained in the ERS Fault Database. The relationships consider only failures resulting from damage to branches and fittings; and from drilling operations in-error (Corder, 1993).

Unfortunately, the relationships and values for the historical data failure frequency used in FFREQ are not known. It is therefore unclear whether the relationships were updated from those used in the Hazard Analysis model (and illustrated in Figure 2.4) via analysis of a later version of the ERS Fault Database. The FFREQ programmer's guide (Wild, 1994) however, indicates the existence of a designated variable in the historical data component for pipeline rupture. As no such values are quoted in the documentation relating to the development of the Hazard Analysis model, it is therefore likely that updated relationships were derived for FFREQ.

In addition to through-wall failure frequencies for branches, fittings and drilling operations in-error, FFREQ also includes an optional algorithm to determine the through-wall failure frequency due to chain trencher machines. The FFREQ

user's guide (Corder, 1993) indicates that chain trenchers pose a serious threat to pipeline integrity as they are able to excavate trenches up to a depth of three metres and can cut through pipelines with a repeated gouging action. The algorithm was introduced due to the increasing use of chain trenchers in farming activity.

For the chain trencher algorithm, failure frequencies were also derived from historical operational data contained in the ERS Fault Database. This data was modified to take into account trench depth. In comparison with the Hazard Analysis model, it is not known if the chain trencher failure data from the ERS Fault Database was previously included in the analysis to derive Weibull probability distributions for the structural reliability component of the model; or in the historical data component failure frequencies. The damage description in the FFREQ user's guide as "repeated gouging"; and the fact that the damage affects the pipeline itself, rather than branches or fittings suggests the former. However, the Weibull probability distributions for gouge damage did not change between the Hazard Analysis model and FFREQ which perhaps suggests the latter.

In addition to a failure frequency value derived from historical operational data, the FFREQ programmer's guide indicates that separate calculations are performed in order to determine if the failure following impact with a chain trencher will occur as a leak or rupture. The calculations are based upon the chain trencher angle of attack; the pipeline geometry and operating conditions; and the extent of the damage. The details of the calculations are unknown.

It is therefore assumed that in calculating the overall leak and rupture failure frequency for FFREQ, equations (2.32) and (2.33) are replaced with:

$$ff_{leak} = ff_{SRleak} + ff_{HDleak} + (ff_{HDleakchain}) \quad (2.36)$$

$$ff_{rupture} = ff_{SRrupture} + ff_{HDrupture} + \left(ff_{HDrupturechain}\right) \quad (2.37)$$

Where $ff_{HDrupture}$ is the failure frequency for ruptures from the historical data component which does not appear in the Hazard Analysis model and $ff_{HDleakchain}$

and $ff_{HDrupturechain}$ are the optional chain trencher failure frequencies for leak and rupture respectively.

2.3.8 *FFREQ Other Considerations*

In addition to the elements described above FFREQ also includes two other considerations which are either of less significance or not directly relevant to this work. This section provides a brief description of each.

2.3.8.1 *Maximum and Minimum Wall Thickness*

FFREQ includes an optional facility to take into account the potential maximum and minimum wall thickness for the particular pipeline under consideration. If this option is chosen the type of welding (longitudinally submerged arc welded (LSAW), spiral, seamless or electric resistance welded (ERW)) used on the pipeline must be entered by the user as part of the input data. In the model, the weld type is used to select a particular set of over and under tolerances, which are then applied to the nominal pipeline wall thickness in order to calculate the potential maximum and minimum values. Separate failure frequencies are calculated using the maximum and minimum wall thickness in addition to those calculated using the nominal. In this way a failure frequency range is produced, which is dependent on the weld type. As this facility effectively amounts to simply a change in the wall thickness used to calculate failure frequency it is not considered to be a significant addition to the FFREQ model.

2.3.8.2 *Ground Movement*

FFREQ also includes an optional facility to determine the failure frequency due to ground movement. Upper and lower bound leak and rupture failure frequencies can be produced and depend on whether the pipeline is located in an R-type or an S-type area. The values were derived from historical operational data for ground movement failures. Although ground movement is a

potential failure mechanism for pipelines, it is not classed as third party external interference and therefore the algorithm is not relevant to this work.

2.4 The PIPIN Model

PIPIN is the model used by the HSE to determine failure frequencies for a user defined pipeline for the four largest causes of failure (construction defects, natural events, corrosion and third party external interference). The model was developed for the HSE by W.S. Atkins in the late 1990s (HSE, 2003). The PIPIN model exists in the form of a computer program which has been updated several times since its initial development, including a complete rewrite by the Health and Safety Laboratory (HSL) in 2009 to solve stability issues (Chaplin, 2012). The model is currently under revision for further reissue (Chaplin, 2013).

Certain elements of the PIPIN model are based upon the pipeline failure frequency methodology developed by British Gas and used in the Hazard Analysis model. However, due to differences in application; changes to the methodology; and updated statistics, the PIPIN and Hazard Analysis models appear notably different to each other. This section will outline the differences between PIPIN and the Hazard Analysis model, with emphasis on the aspects which are most relevant to this work. The version of PIPIN addressed here is the 2009 update, which is the most recent at the time of writing.

As with the Hazard Analysis model, PIPIN consists of a structural reliability component and a historical data component. In PIPIN however, these two components are completely distinct and produce failure frequency values relating to different causes. Failure frequencies for construction defects, natural events and corrosion are determined using the historical data component. The structural reliability component of PIPIN is directly analogous to the structural reliability component of the Hazard Analysis model and is used to calculate the failure frequencies for third party external interference.

2.4.1 *PIPIN Structural Reliability Component*

2.4.1.1 *PIPIN Incident-Rates*

The Incident-Rates used in the structural reliability component of PIPIN are given in Table 2.7 (Chaplin, 2013). The Incident-Rates have been inferred to be based upon an analysis of the 2000 UKOPA Fault Database, however this is not explicitly stated in the available documentation. The UKOPA Fault Database covers approximately 23,000 km of gas and liquid pipelines (both operating and decommissioned) in the UK. Details of all known pipeline faults and failures which were subject to an excavation and on-site assessment are included, dating back to 1962. The database includes records from various pipe operators, however over 85 percent of the pipelines are former British Gas pipelines (Cosham, 2007). Consequently, the database includes all of the data originally contained in the ERS Fault Database.

PIPIN was originally developed to provide failure frequencies for pipelines located in rural areas only. Consequently, the Incident-Rates specified in PIPIN are for R-type areas only. In 2003 the use of PIPIN was extended to include pipelines in suburban areas. To incorporate this change, an additional factor was added to the PIPIN model which allowed Incident-Rates for pipelines located in S-type areas to be derived from the rates for R-type areas. The factor was derived from a review carried out by W.S. Atkins, using data obtained from B.G. Transco (HSE, 2003).

If assessment of a pipeline located in an S-type area is required, the Incident-Rates given in Table 2.7 are multiplied by a factor approximately equal to 4[7] before being applied.

[7] The exact value was not available in the documentation.

Area Type	Damage Type	Incident-Rate (per km.yr)
Rural	Gouge	1.29×10^{-3}
	Gouged Dent	2.07×10^{-4}

Table 2.7: PIPIN Model Incident-Rates

2.4.1.2 *PIPIN Depth of Cover*

PIPIN includes an optional facility to take into account the pipeline depth of cover. The PIPIN depth of cover analysis works in exactly the same way as the equivalent analysis in the FFREQ model, by applying a modifying factor to the Incident-Rates in the structural reliability component. The modifying factors originate from a table supplied by B.G. Transco, which was extrapolated via regression analysis to include factors for low depth of cover (HSE, 2003). The modifying factors for depth of cover used in PIPIN are shown graphically in Figure 2.6. For comparison the equivalent factors from FFREQ are also shown.

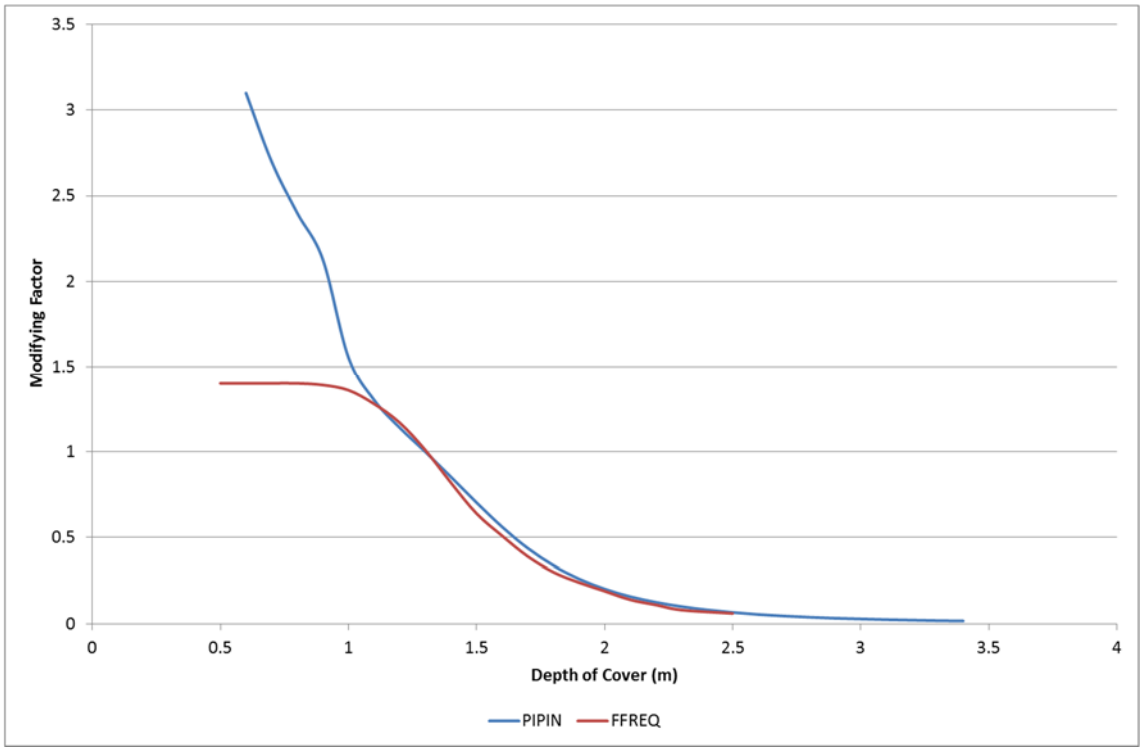

Figure 2.6: Depth of Cover Factors in PIPIN and FFREQ

Figure 2.6 shows that the depth of cover factors in PIPIN and FFREQ are very similar above 1.1 m depth of cover; below this point the factors diverge. A large

degree of similarity between the two data sets would be expected as both originate from the same source (B.G. Transco was a successor company to British Gas). Documentation relating to development of PIPIN notes that the table of factors was obtained from B.G. Transco in 1997 (HSE, 2003), whereas FFREQ was developed in 1993. The divergence between the two data sets below 1.1 m may suggest that further analysis was carried out in the intervening period. Note that the PIPIN factors below 0.9 m depth of cover are extrapolated values, derived from a regression on the other points.

2.4.1.3 *PIPIN Limit State Functions*

The structural reliability component of PIPIN is based upon the pipeline failure frequency methodology developed by British Gas and used in the Hazard Analysis model. In defining limit state equations for the model however, the methodology has been modified to incorporate elements of an British Energy R6 rev. 3 assessment procedure (Anon., 1986; Anon., 2001a; Chaplin, 2012). Supplementary uncertainty factors have also been introduced to each limit state function in order to represent the uncertainty in modelling pipeline failure. Each factor is assumed to be a random variable, with an associated probability distribution.

In the Hazard Analysis model, whether severe gouge or gouged dent damage will fail as a leak or rupture is assumed to be controlled by plastic collapse. This is implied by the use of the flow stress dependent through-wall NG-18 equation in the model (equation (2.1)). In PIPIN, the limit state function for leak / rupture is defined using the R6 rev. 3 assessment procedure; this introduces a brittle fracture component to the failure.

In order to determine whether severe gouge or gouged dent damage will fail as a leak or rupture, quantities for both plastic collapse and brittle fracture are defined. The plastic collapse quantity, the load ratio, L_r, is defined as:

$$L_r = \frac{M\sigma_H}{\sigma_Y.X\_Fpress} \tag{2.38}$$

Where X_Fpress is an uncertainty factor. In the structural reliability component of PIPIN the Folias factor is defined using the original two term expression only applicable to short defects:

$$M = \sqrt{1 + 0.40\left(\frac{2c}{\sqrt{Rt}}\right)^2} \quad (2.39)$$

Further details on the Folias factor are given in section 3.1.1.2. The brittle fracture quantity, the fracture ratio, K_r, is defined as:

$$K_r = \frac{K_I}{K_{IC}} \quad (2.40)$$

Where K_{IC} is the fracture toughness (in MPa√m) defined by:

$$K_{IC} = \sqrt{\frac{1000 C_v E}{A}} \quad (2.41)^8$$

And K_I is the stress intensity factor (in MPa√m):

$$K_I = \sigma_H M \sqrt{\frac{\pi c}{1000}} . X\_Ki\_gdr \quad (2.42)$$

Where c (in mm) is half the axial defect length (the full axial length is represented by $2c$, as in the Hazard Analysis model) and X_Ki_gdr is an uncertainty factor.

The defect is predicted to fail as a rupture if the values of the load ratio and fracture ratio are such that the R6 rev. 3 fracture assessment curve is exceeded:

$$K_r = (1 - 0.14L_r^2)\{0.3 + 0.7\exp(-0.65L_r^6)\}. X\_Krfail \quad (2.43)$$

[8] Note that in equation (2.41) E is measured in units of GPa.

Where X_Krfail is an uncertainty factor. Or if the value of load ratio exceeds the upper limit for plastic collapse:

$$L_r = \frac{\bar{\sigma}}{\sigma_Y}.X\_Lrcut \quad (2.44)$$

Where X_Lrcut is an uncertainty factor. In PIPIN the flow stress is defined as the average of the yield and tensile strength (in Nmm^{-2}) (often approximated to the specified minimum ultimate tensile strength (SMUTS), in the absence of material test data):

$$\bar{\sigma} = \frac{\sigma_Y + \sigma_U}{2} \quad (2.45)$$

It can be seen that if the brittle fracture component of the limit state function is ignored (i.e. failure occurs only by plastic collapse) then defect rupture is determined by equations (2.38) and (2.44) which can be combined to give:

$$\sigma_H = M^{-1}\overline{\sigma}.X\_Fpress.X\_Lrcut \quad (2.46)$$

Which is the flow stress dependent through-wall NG-18 equation (equation (2.1)), i.e. for a purely plastic collapse failure the limit state function for leak / rupture in PIPIN reduces to that of the Hazard Analysis model (allowing for the additional uncertainty factors and differences in the Folias factor and flow stress).

For part-wall gouge failure, PIPIN and the Hazard Analysis model are very similar. The failure of a gouge in PIPIN is assumed to be controlled entirely by plastic collapse, with the failure stress given by the flow stress dependent part-wall NG-18 equation. The limit state function for gouge failure in PIPIN is therefore almost identical to that used in the Hazard Analysis model[9]. The only differences lie in the definition of the Folias factor and flow stress (given by

[9] The limit state function in equation (2.47) is written in terms of a limiting stress. The limit state equation in the Hazard Analysis model is written in terms of a critical defect depth (equation (2.9)). The two equations however are essentially identical.

equations (2.39) and (2.45)) and the presence of uncertainty factors. The failure stress of a gouge in PIPIN is given by:

$$\sigma_H = \bar{\sigma}\left[1-\frac{d}{t}\right]\left[1-\frac{d}{t}\left(\frac{1}{M}\right)\right]^{-1}.X\_Sfail.X\_Lrcut \qquad (2.47)$$

Where X_Sfail and X_Lrcut are uncertainty factors. X_Lrcut is the same uncertainty factor used in equation (2.44).

For part-wall gouged dent failure, the limit state function in PIPIN is again defined using the R6 rev. 3 assessment procedure. Failure is therefore assumed to occur due to a combination of brittle fracture and plastic collapse. This is consistent with the Hazard Analysis model in which gouged dent failure is determined using the BGDGFM.

In this case the plastic collapse load ratio, L_r, is defined as:

$$L_r = \frac{\sigma_H}{\sigma_Y.\left(1-\frac{d}{t}\right).X\_Scoll} \qquad (2.48)$$

Where X_Scoll is an uncertainty factor. The brittle fracture ratio, K_r, is defined as:

$$K_r = \frac{K_{Ip}+K_{Is}}{K_{IC}} + \rho.X\_Pcf \qquad (2.49)$$

Where K_{Ip} and K_{Is} are the primary and secondary stress intensity factors (in MPa√m), ρ is the plasticity correction factor and X_Pcf is an uncertainty factor. The fracture toughness, K_{IC}, is defined by equation (2.41).

PIPIN assumes that a micro-crack exists at the base of the gouge in the gouged dent. The depth of the micro-crack, a_m (in mm), is calculated using an expression taken from a paper by Linkens (Linkens, 1997; Chaplin, 2012):

$$a_m = \frac{\sigma_H H+14806.4}{85470.0} \qquad (2.50)$$

Taking this into consideration, the primary and secondary stress intensity factors in equation (2.49) are defined as:

$$K_{Ip} = Y_1 SCF.\sigma_m \sqrt{\frac{\pi a_m}{1000}} \quad (2.51)$$

$$K_{Is} = Y_2 SCF.\sigma_b \sqrt{\frac{\pi a_m}{1000}} \quad (2.52)$$

In equations (2.51) and (2.52), SCF is a stress concentration factor for the micro-crack which is assumed to have a value of 3; Y_1 and Y_2 are given by:

$$Y_1 = \left(1.12 - 0.23\left(\frac{a_m}{t}\right) + 10.6\left(\frac{a_m}{t}\right)^2 - 21.7\left(\frac{a_m}{t}\right)^3 + 30.4\left(\frac{a_m}{t}\right)^4\right).X\_Ki\_gid \quad (2.53)$$

$$Y_2 = \left(1.12 - 1.39\left(\frac{a_m}{t}\right) + 7.32\left(\frac{a_m}{t}\right)^2 - 13.1\left(\frac{a_m}{t}\right)^3 + 14.0\left(\frac{a_m}{t}\right)^4\right).X\_Ki\_gid \quad (2.54)$$

Where X_Ki_gid is an uncertainty factor; σ_m and σ_b in equations (2.51) and (2.52) are the membrane and bending stress (in Nmm^{-2}) due to the dent respectively. σ_m and σ_b are given by:

$$\sigma_m = \sigma_H\left(1 - \frac{1.8H}{2R}\right) \quad (2.55)$$

$$\sigma_b = \sigma_H\left(10.2\frac{R}{t}\frac{H}{2R}\right) \quad (2.56)$$

The plasticity correction factor in equation (2.49) is calculated as follows:

If $L_r \leq 0.8$ $\quad \rho = \rho_1$ (2.57)

If $0.8 < L_r < 1.05$ $\quad \rho = 4\rho_1(1.05 - L_r)$ (2.58)

If $L_r \geq 1.05$ $\quad \rho = 0$ (2.59)

Where ρ_1 is defined:

If $z \leq 4.0$ $\rho_1(z) = 0.1z^{0.714} - 0.007z^2 + 0.00003z^5$ (2.60)

If $z > 4.0$ $\rho_1(4) = 0.188$ (2.61)

And z is defined:

$$z = \frac{K_{Is}}{K_{Ip}/L_r} \quad (2.62)$$

As with the leak / rupture limit state function, a gouged dent is predicted to fail if the values of the load ratio and fracture ratio are such that the R6 rev. 3 fracture assessment curve (equation (2.43)) is exceeded; or if the value of the load ratio exceeds the upper limit for plastic collapse (equation (2.44)).

A visual comparison between the equations used for the gouged dent limit state function in PIPIN and the BGDGFM reveals many similarities between the two. An assessment similar to that shown in section 4.2.2 can be used to show that both are based upon the Dugdale strip-yield model. Furthermore, the dent stress intensity factors are identical in both models. PIPIN differs from the BGDGFM in its use of additional variables such as the plasticity correction factor, which is taken directly from the R6 assessment code; and micro-cracking. In addition, different expressions for the flow stress and the Charpy fracture toughness correlation are used and uncertainty factors are included.

In a similar way to FFREQ, PIPIN includes additional functionality to take into account the resistance of pipes to denting. In PIPIN the probability of failure of a gouged dent is determined from the force required to cause the dent, rather than the dent depth. The dent force is incorporated into the limit state function defined by equations (2.48) to (2.62) through the use of an expression which relates it to dent depth:

$$H = \left(\frac{F_{dent}}{0.49\sqrt{Res}}\right)^{2.38} \quad (2.63)$$

Where F_{dent} is the dent force (in kN) and Res (in $N^{1/2}mm$) is defined as:

$$Res = \sqrt{80\sigma_Y t}\left(t + \frac{0.7PD}{10\sigma_U}\right) \quad (2.64)$$

Equations (2.63) and (2.64) represent the mean value of the semi-empirical, dynamic dent force relationship as reported by Corder and Chatain (Corder, 1995b) if an assumption of 80 mm for the excavator tooth length is made.

As with the Hazard Analysis model in the structural reliability component of PIPIN it is implied that a through-wall puncture has occurred if the gouge depth of a gouge or gouged dent defect, d, is in excess of the pipe wall thickness, t.

2.4.1.4 *PIPIN Probability Distributions*

In PIPIN all of the independent variables and uncertainty factors which appear in the limit state functions described in section 2.4.1.3 are represented as random variables. In total there are 16 random variables used in the calculation of the probability of failure of a gouge or a gouged dent. In this way, PIPIN differs from the Hazard Analysis model which uses random variables to describe only the dimensions of the damage, keeping all other quantities deterministic. The 16 random variables in PIPIN are described using Weibull, Normal or Lognormal probability distributions. Table 2.8 shows the distribution type for each variable in the model (Chaplin, 2012). The random variables used for the pipeline geometry and material properties of the linepipe steel represent the small amount of variation in these "fixed" quantities which would be observed in practice.

Random Variable	Distribution
Gouge Length	Weibull
Gouged Dent Gouge Length	Weibull
Gouge Depth	Weibull
Gouged Dent Gouge Depth	Weibull
Dent Force	Weibull
Pipe Radius	Normal
Pipe Wall Thickness	Normal
Operating Pressure	Normal
Yield Strength (SMYS)	Lognormal
Ultimate Tensile Strength (SMUTS)	Normal
2/3 Charpy V-Notch Impact Energy	Lognormal
X_Scoll	Lognormal
X_Lrcut	Lognormal
X_ki_gid	Lognormal
X_Krfail	Lognormal
X_Pcf	Normal

Table 2.8: PIPIN Model Random Variables

The probability distributions for damage dimensions were based upon an analysis of pipeline damage data for gouges and gouged dents, contained in the 2000 UKOPA Fault Database. The exact origin of the distributions for the pipe parameters and uncertainty factors is unknown. It is likely however that the pipe geometry and material property distributions were derived from mill certificate tolerances as published when failure frequency prediction models have been applied to specific projects (Espiner, 1996b; Owen, 1996; Edwards, 1998; Hay, 1998; Anon., 2005). It is noted that this data is pipeline specific, and varies with the pipe manufacturing method and age.

It is unclear how data regarding punctures and failure from damage to branches and fittings from the UKOPA Fault Database was treated in the derivation of the damage dimension distributions for PIPIN. In the Hazard Analysis model, conventional puncture data was included in distribution derivation, with failures due to damage to branches and fittings; and punctures due to drilling operations in-error being excluded. The Hazard Analysis model however includes a separate failure frequency for damaged braches and fittings; and drill punctures as part of its historical data component, an aspect which has no direct analogue in PIPIN. Given that gouges with a depth exceeding the pipe wall thickness are treated as punctures in PIPIN (section 2.4.1.3), it is reasonable to assume that

conventional puncture data was included in the derivations. A satisfactory conclusion regarding the branches and fittings failures; and drill puncture data however, cannot be made.

Note that only one distribution is used for gouge depth in PIPIN. As explained in section 2.4.1.1 PIPIN was originally developed to provide failure frequencies for pipelines located in rural areas only. The separate distributions for S-type and R-type areas used in the Hazard Analysis model were therefore not derived. This aspect of the model was not updated when PIPIN's use was extended to include pipelines located in suburban areas. It is not known whether data from both S-type and R-type areas in UKOPA Fault Database was included in the derivation of the PIPIN gouge depth distribution.

Table 2.9 summarises the parameters defining the probability distributions for the damage dimensions derived for PIPIN (Chaplin, 2013). The distribution parameters for the remaining variables and uncertainty factors are unknown.

Random Variable	Distribution Type	α	β (mm, or kN for Dent Force)
Gouge Length	Weibull	0.840	183.407
Gouge Dent Gouge Length	Weibull	0.902	236.991
Gouge Depth	Weibull	0.630	0.736
Gouged Dent Gouge Depth	Weibull	1.211	1.289
Dent Force	Weibull	2.125	110.203

Table 2.9: PIPIN Model Weibull Parameters

2.4.1.5 *PIPIN Probability of Failure of a Gouge and Gouged Dent*

The probability and frequency of failure for gouges and gouged dents in PIPIN are calculated using the Monte Carlo method (Chaplin, 2012). The Monte Carlo method is more appropriate for PIPIN than the numerical integration used in the Hazard Analysis model due to the increase in the number of random variables in the model.

The Monte Carlo method is used to calculate the probability of failure for gouges, P_{gouge}, by:

- Randomly sampling each of the variables stated in Table 2.8 relevant to gouge damage according to their respective probability distributions.
- Using the resulting combination of values as input to the gouge limit state equation defined in section 2.4.1.3 to determine if a failure would occur.

The above steps are iterated and a probability of failure value is calculated by dividing the number of iterations in which a failure is predicted by the total number of iterations. The process is continued until the probability of failure for a gouge converges to a single value. The probability of failure for gouged dents, $P_{gougeddent}$, using the gouged dent limit state equation, is calculated separately in the same way.

A similar process is also used to calculate values for the probability of a leak and the probability of a rupture based upon the leak / rupture limit state function. In the Hazard Analysis model, the probability of a leak or a rupture is determined entirely by the leak / rupture limit state function. In PIPIN however, an additional definition of rupture is imposed which is based upon hole size. PIPIN requires that all stable leaks with a hole size diameter greater than 110 mm are classified as ruptures.

In order to calculate overall leak and rupture probabilities an algorithm to calculate the probability of different hole sizes is required. PIPIN divides hole size diameter into ranges for which different probabilities are calculated:

- 0 – 25 mm;
- 25 – 75 mm;
- 75 – 110 mm;
- > 110 mm.

Values for the first three ranges correspond to leak probabilities with the last assumed to represent a rupture probability. By using an expression relating the area of the hole in the pipeline to the length of the defect the probabilities can be determined from the gouge length and gouged dent gouge length Weibull distributions in Table 2.9. The hole size relationship was based upon work

performed by Baum and Butterfield in a similar way to the hole size relationship in the Hazard Analysis model (Butterfield, 1979; Chaplin, 2012). The relationship is given by:

$$2c = \sqrt{Dt}\left(\frac{A_h}{7.548\ x\ 10^{-4}}\right)^{\frac{1}{3.706}} \quad (2.65)$$

Where A_h is the normalised hole area (the hole area divided by the pipeline's internal cross-sectional area, expressed as a percentage).

The overall probability for a gouge and a gouged dent failing as a rupture are therefore calculated from:

$$P_{gougerupture} = P_{gouge}.P_{grupture} + P_{gouge}.wg_{>110}.\left(1 - P_{grupture}\right) \quad (2.66)$$

$$P_{gougeddentrupture} = P_{gougeddent}.P_{gdrupture} + P_{gougeddent}.wgd_{>110}.\left(1 - P_{gdrupture}\right) \quad (2.67)$$

Where $P_{grupture}$ and $P_{gdrupture}$ are the probability of a gouge and gouged dent rupture calculated according to the Monte Carlo method for the leak / rupture limit state equation for gouge damage and gouged dent damage respectively; and $wg_{>110}$ and $wdg_{>110}$ are the probability of a hole size greater than 110 mm in diameter according to equation (2.65) and the gouge length and gouged dent gouge length Weibull distributions respectively.

In a similar way the probability for a gouge and gouged dent failing as a leak, with one of the three leak hole sizes are calculated from:

$$P_{gougeleak_i} = P_{gouge}.wg_{hr_i}.\left(1 - P_{grupture}\right) \quad (2.68)$$

$$P_{gougeddentleak_i} = P_{gougeddent}.wgd_{hr_i}.\left(1 - P_{gdrupture}\right) \quad (2.69)$$

$i = 1,2,3$

Where wg_{hr} and wgd_{hr} are the probabilities of a certain hole size range according to equation (2.65) and the gouge length and gouged dent gouge

length Weibull distributions respectively. The index i is used to represent the three different hole size ranges.

2.4.1.6 *PIPIN Failure Frequency*

In PIPIN separate failure frequencies are given for each of the three leak hole sizes from section 2.4.1.5, ff_{leak_i}, $i = 1,2,3$ and for ruptures, $ff_{rupture}$. The failure frequencies are calculated using:

$$ff_{leak_i} = DOC.IncidentRate_{gouge}.P_{gougeleak_i} + DOC.IncidentRate_{gougeddent}.P_{gougeddentleak_i} \quad (2.70)$$

$i = 1,2,3$

$$ff_{rupture} = DOC.IncidentRate_{gouge}.P_{gougerupture} + DOC.IncidentRate_{gougeddent}.P_{gougeddentrupture} \quad (2.71)$$

Where $IncidentRate_{gouge}$ and $IncidentRate_{gougeddent}$ are Incident-Rates for gouges and gouged dents from Table 2.7 respectively; and DOC is the optional depth of cover factor in accordance with section 2.4.1.2. Note that if the pipeline is located in an S-type area, the Incident-Rate values from Table 2.7 are multiplied by a factor of 4 before equations (2.70) and (2.71) are calculated.

Given that the historical data component of PIPIN does not consider third party external interference the failure frequencies calculated by equations (2.70) and (2.71) are considered to be the overall final failure frequencies values for that particular failure cause.

2.4.2 *PIPIN Historical Data Component*

As noted in section 2.4 the historical data component of PIPIN is used to determine failure frequencies from construction defects, natural events and corrosion (HSE, 2003). Although these are potential failure mechanisms for pipelines, this work is concerned only with third party external interference. The historical data component of PIPIN is therefore not relevant to the current study.

2.5 The PIE Model

The PIE model was developed by Pipeline Integrity Engineers (PIE) in 2006 (Lyons, 2006; Haswell, 2008; Lyons, 2008) as a reproduction of the failure frequency methodology from the Hazard Analysis model. The model was developed for UKOPA in order to investigate and understand the impact of pipeline parameters on failure frequency due to external interference, and to understand the significance of the damage data recorded in the UKOPA pipeline Fault Database. It exists in the form of a Microsoft Excel spreadsheet.

In the 20 year period since the development of the Hazard Analysis model, FFREQ had been widely adopted within the pipeline industry to calculate third party external interference failure frequencies for QRA. The reliance on FFREQ however raised concern, given the somewhat opaque nature of the model. Users did not have access to the FFREQ source code and could only enter input and receive output. This was compounded by the lack of definitive documentation as to the exact content of the model. Overall there was a need for greater transparency to the process. It was also felt that since FFREQ was developed in 1993, there now existed over 10 years of additional operational data, which could be used to provide an updated and more accurate probability distributions and Incident-Rates for the model.

The PIE model was developed using the original documentation relating to the development of the Hazard Analysis model in addition to the 2005 UKOPA Fault Database. Although the model was an attempt to directly reproduce the Hazard Analysis model with updated operational data, it is somewhat simplified in comparison. In particular, the model does not include an historical data component meaning the output failure frequencies are derived entirely from structural reliability methods. This section outlines other differences which exist between the PIE model and the structural reliability component of the Hazard Analysis model.

2.5.1 *PIE Model Incident-Rates*

Only one Incident-Rate is included in the PIE model and this is given in Table 2.10. The Incident-Rate in the PIE model makes no distinction between gouges and gouged dents, instead representing an overall frequency for which a pipeline is subject to mechanical damage.

The Incident-Rate is based upon an analysis of the 2005 UKOPA Fault Database. It should be noted that unlike the Hazard Analysis model, the PIE model does not take into account pipeline area type. Consequently the value for Incident-Rate includes damage to pipelines located in both R-type and S-type areas. In the 2005 database the total number of mechanical damage incidents was 556 and the total operational exposure up to that point in time was 654,732 km.yr (Lyons, 2006).

Incident-Rate (per km.yr)
8.49×10^{-4}

Table 2.10: PIE Model Incident-Rate

Given that the PIE model Incident-Rate represents only the overall frequency for which a pipeline is subject to mechanical damage, additional factors must be applied in order to provide appropriate damage specific rates for use in the failure frequency calculation. The factors give the probability that a mechanical damage incident will manifest as either a gouge or a gouged dent. The factors were also derived from the 2005 UKOPA Fault Database by considering the total number of mechanical damage incidents and the fractional split between gouge and gouged dent. The factors are given in Table 2.11.

Damage Type	Symbol	Probability
Gouge	$P_{gougedamage}$	0.82
Gouged Dent	$P_{gougeddentdamage}$	0.18

Table 2.11: Probability that Mechanical Damage will be a Gouge or a Gouged Dent

2.5.2 *PIE Model Folias Factor*

For the most part, the limit state functions used in the PIE model are identical to those used in the structural reliability component of the Hazard Analysis model. The only difference lies in the definition of the Folias factor. In a similar way to FFREQ, the PIE model uses the alternative two term expression, applicable to longer defects and given by equation (2.35). Further details on the Folias factor are given in section 3.1.1.2.

The use of a different Folias factor leads to a different expression for the critical defect length for rupture in the PIE model:

$$L_{crit} = \sqrt{\frac{Rt}{0.26}\left[\left(\frac{\bar{\sigma}}{\sigma_H}\right)^2 - 1\right]} \qquad (2.72)$$

Equation (2.72) replaces equations (2.6) and (2.7) as the limit state function for leak / rupture for the PIE model[10].

2.5.3 *PIE Model Probability Distributions*

In the PIE model the use of random variables is simplified in comparison to the Hazard Analysis model. As noted in section 2.5.1., the model does not take into account pipeline area type. The separation of gouge depth into separate random variables for R-type and S-type areas was therefore not performed for the PIE model. More significantly, the PIE model makes no distinction between gouge and gouged dent damage in terms of the gouge length and gouge depth. Only one variable is included for each dimension, ignoring the damage type. Overall, the PIE model uses only three random variables to calculate the probability of failure (Lyons, 2006; Lyons, 2008), compared to six in the Hazard Analysis model.

[10] Note that although the limit state function for part-wall gouge failure will also change, given that it contains the Folias factor, the form of the equation remains the same. All that is required is simply a substitution for the value of M.

For gouge depth and gouge length, the single variable included in the PIE model is used to represent each quantity for both damage types. One variable must therefore be used in different limit state functions. Table 2.12 shows the random variables included in the PIE model alongside the limit state functions in which they are used:

Random Variable	Limit State Function
Gouge Length	Leak / Rupture & Gouge Failure
Gouge Depth	Gouge Failure & Gouged Dent Failure
Dent Depth	Gouged Dent Failure

Table 2.12: PIE Model Random Variables

As with the Hazard Analysis model, Weibull distributions were chosen to represent the variables. The Weibull distributions were based upon an analysis of pipeline damage data for gouges and gouged dents contained in the 2005 UKOPA Fault Database. In line with the reduced number of variables, the distributions for gouge length and gouge depth were derived using data sets which incorporated both gouge and gouged dent data; and all three distributions included data from both R-type and S-type areas. The Weibull distributions were fitted using the maximum likelihood method. The variables used and the parameters defining their Weibull distributions are summarised in Table 2.13 (Lyons, 2006). The distributions are shown in Figure 2.7, Figure 2.8 and Figure 2.9:

Random Variable	Distribution Type	α	β (mm)
Gouge Length	Weibull	0.6	120.851
Gouge Depth	Weibull	0.889	1.442
Dent Depth	Weibull	0.69	6.202

Table 2.13: PIE Model Weibull Parameters

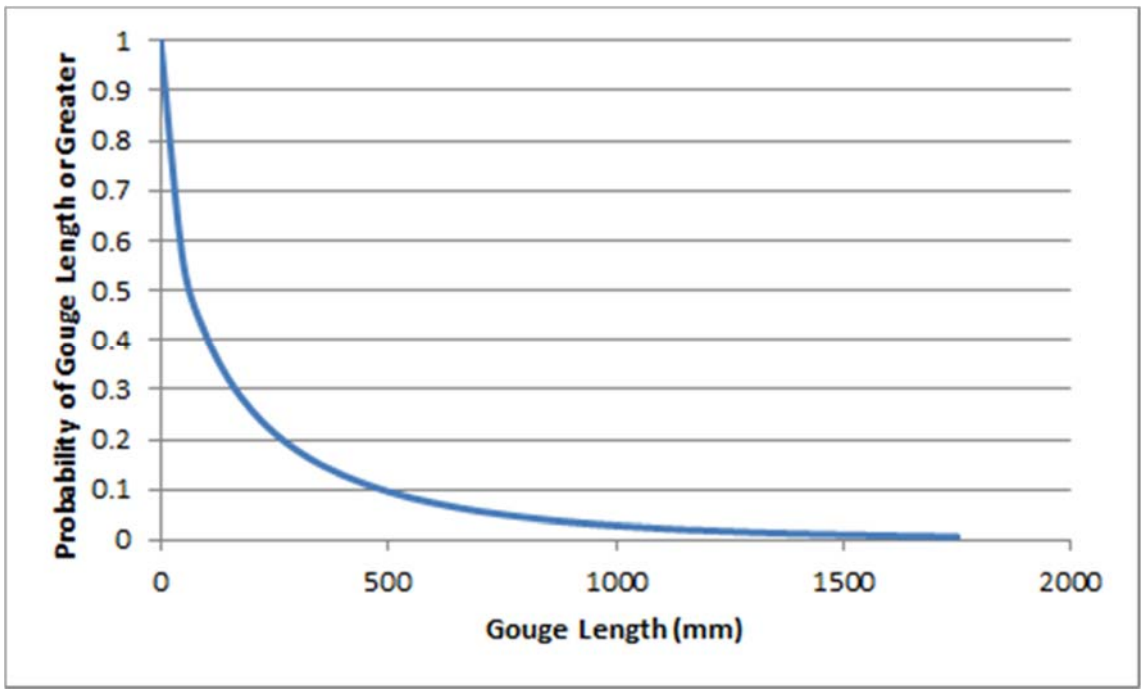

Figure 2.7: PIE Model Gouge Length Distribution

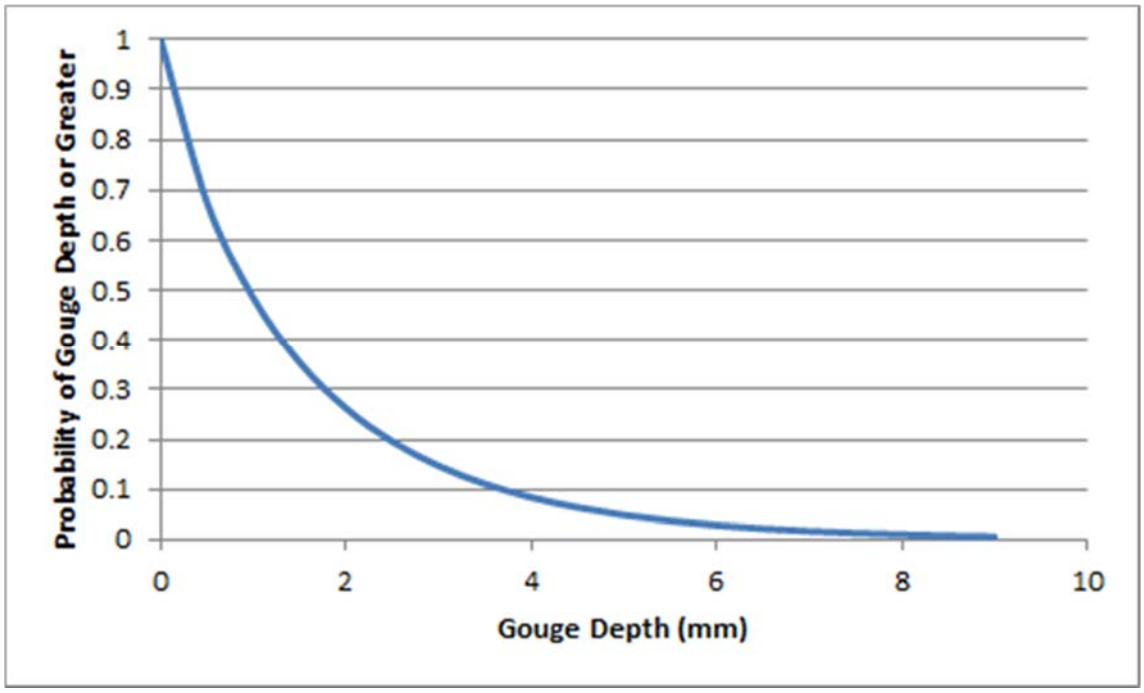

Figure 2.8: PIE Model Gouge Depth Distribution

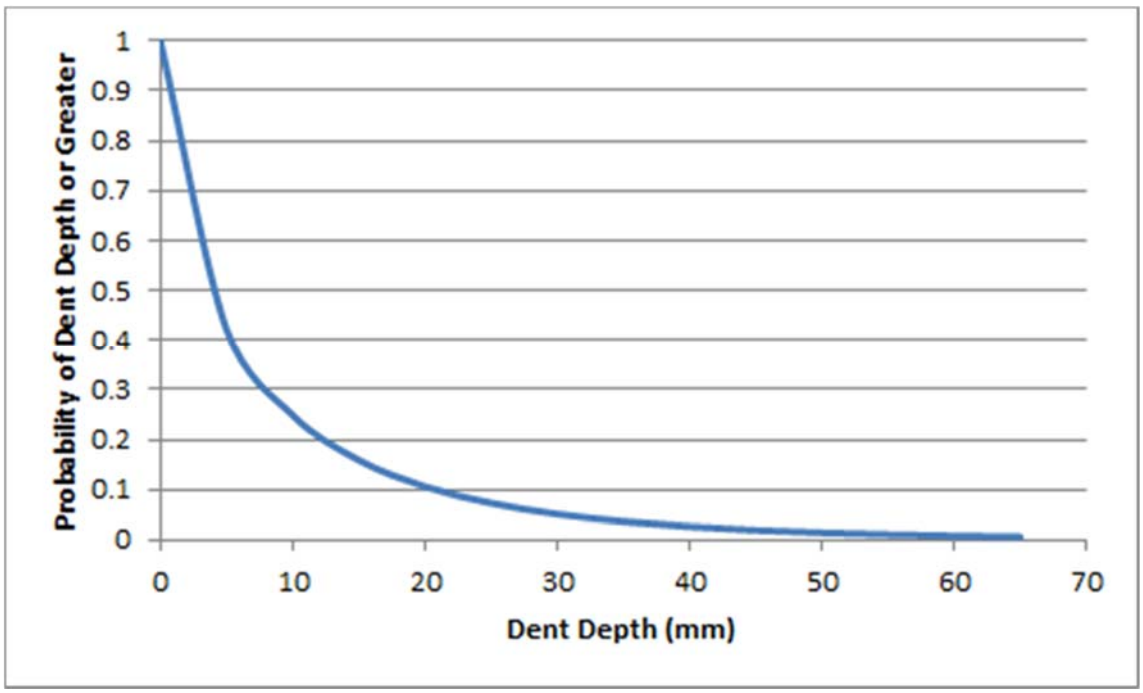

Figure 2.9: PIE Model Dent Depth Distribution

The data sets used to derive the Weibull distributions given in Table 2.13 included puncture data from the UKOPA Fault Database. It should be noted however, that this data also included punctures which were caused by drilling operations in-error and failures as a result of damage to branches and fittings. In the Hazard Analysis model, data from the latter two categories was acknowledged to be the result of a different failure mechanism and was only included in the historical data component of the model.

2.5.4 *PIE Model Probability of Failure of a Gouge and a Gouged Dent*

The probability and frequency of failure for gouge and gouged dent damage in the PIE model are calculated using numerical integration with the trapezium rule (Lyons, 2006). Due to the reduced number of random variables in the PIE model, the expressions for probability of failure are slightly different to those from the Hazard Analysis model.

The total probability of failure for gouges can be expressed as:

$$P_{gougetotal} = \int_0^{1397} f_{2c}(2c) R_d(d_{crit}) d2c \qquad (2.73)$$

Where the subscripts $2c$ and d denote the use of the gouge length and gouge depth Weibull parameters respectively. As with the Hazard Analysis model the value of d_{crit} in equation (2.73) is dependent on the gouge length, $2c$. The gouge length Weibull distribution was truncated at 1397 mm, fixing the upper limit of the integral in line with the Hazard Analysis model.

Equation (2.73) can be split into a probability of a leak, $P_{gougeleak}$, and a probability of a rupture, $P_{gougerupture}$, using the critical length determined by the limit state function for leak / rupture (equation (2.72)):

$$P_{gougeleak} = \int_0^{L_{crit}} f_{2c}(2c) R_d(d_{crit}) d2c \tag{2.74}$$

$$P_{gougerupture} = \int_{L_{crit}}^{1397} f_{2c}(2c) R_d(d_{crit}) d2c \tag{2.75}$$

The total probability of failure for gouged dents can be expressed as:

$$P_{gougeddenttotal} = \int_0^{1397} f_{2c}(2c) \left[\int_0^{d_{crit}} f_d(d) R_H(H_{crit}) dd \right] d2c \tag{2.76}$$

Where the subscripts $2c$ and d denote the use of the same gouge length and gouge depth Weibull parameters as those used in equations (2.73), (2.74) and (2.75); and H denotes the use of the dent depth parameters. The value of H_{crit} in equation (2.76) is again dependent on d and calculated using equation (2.16). The value of d_{crit} is dependent on the gouge length, $2c$. As with gouge damage, the gouge length Weibull distribution was truncated at 1397 mm, fixing the upper limit of the first integral.

In order to determine the probability of a gouged dent failing as a leak and a gouged dent failing as a rupture, equation (2.76) can be split in a similar way to equations (2.73), (2.74) and (2.75):

$$P_{gougeddentleak} = \int_0^{L_{crit}} f_{2c}(2c) \left[\int_0^{d_{crit}} f_d(d) R_H(H_{crit}) dd \right] d2c \tag{2.77}$$

$$P_{gougeddentrupture} = \int_{L_{crit}}^{1397} f_{2c}(2c) \left[\int_0^{d_{crit}} f_d(d) R_H(H_{crit}) dd \right] d2c \tag{2.78}$$

The critical length of the gouged dent gouge in equation (2.77) and (2.78) is the same as that for the gouge failures described by equations (2.74) and (2.75), as calculated by the limit state function for leak / rupture, equation (2.72).

2.5.5 *PIE Model Failure Frequency*

The leak, rupture and total failure frequency, ff_{leak}, $ff_{rupture}$ and ff_{total} respectively, of a pipeline due to gouge and gouged dent damage in the PIE model are calculated by combining the results of Sections 2.5.1 and 2.5.4:

$$ff_{leak} = IncidentRate \times \left(P_{gougedamage}P_{gougeleak} + P_{gougeddentdamage}P_{gougeddentleak}\right) \quad (2.79)$$

$$ff_{rupture} = IncidentRate \times \left(P_{gougedamage}P_{gougerupture} + P_{gougeddentdamage}P_{gougeddentrupture}\right) \quad (2.80)$$

$$ff_{total} = ff_{leak} + ff_{rupture} \quad (2.81)$$

Given that the PIE model does not include an historical data component the failure frequencies calculated by equations (2.79), (2.80) and (2.81) are considered to be the overall final failure frequencies values for third party external interference.

It is noted that unlike the structural reliability component of the Hazard Analysis model, the PIE model does not include a hole size relationship to separate the leak failure frequency into different hole diameter ranges.

2.6 The Andrew Cosham "Reduction Factors" Model

In 2007 UKOPA commissioned A. Cosham of WS Atkins to investigate "risk reduction factors" which were included in the pipeline integrity management code supplement PD 8010-3 (Anon., 2013). The purpose of the study was to determine if the factors, which had been derived from a deterministic parametric study, were suitable for use in "screening" risk assessments to estimate the pipeline failure frequency due to third party external interference. As part of this

study a probabilistic model was developed, hereafter referred to as the "Cosham model", which could be used to calculate the probability of failure of a pipeline due to mechanical damage. This model was used to determine probabilistic risk reduction factor values which could then be compared with the deterministic values included in the code (Cosham, 2007).

The Cosham model is based upon the Hazard Analysis model. The model however, does not calculate the pipeline failure frequency as with the other models from this review; instead it is concerned only with the probability of failure. Additionally, the model does not include an historical data component; its output is determined entirely using structural reliability methods. Although the Cosham model is based upon the Hazard Analysis model, structurally it is very similar to the PIE model. The purpose of this section is therefore to outline the differences which exist between the Cosham model and the PIE model, rather than with the Hazard Analysis model.

2.6.1 *Cosham Model Probability of a Gouge or a Gouged Dent*

As noted in section 2.6 the Cosham model does not calculate a failure frequency value for the user-defined pipeline; only an overall value for the probability of failure of mechanical damage is calculated. Consequently, a value for the Incident-Rate is not required in the Cosham model.

The Cosham model calculates an overall probability of failure value by considering the individual probabilities of failure of gouge and gouged dent damage, in the same way as the PIE model or Hazard Analysis model. An overall value is determined by including factors which give the probability that a mechanical damage incident will manifest as either a gouge or a gouged dent; and allow the individual probabilities to be summed.

The probability factors used in the Cosham model are the same as those used in the PIE model, given in Table 2.11 (Cosham, 2007). In the PIE model these values are used as multipliers to the Incident-Rate. The factors are based upon an analysis of the 2005 UKOPA Fault Database.

2.6.2 *Cosham Model Limit State Functions*

In the Cosham model the basic limit state functions used are almost identical to those used in the PIE model. The only difference lies in the values of the constants, K_1 and K_2, included in the limit state function for gouged dent failure. In the Cosham model, the limit state function itself is the rearranged form of the BGDGFM used in both the PIE and Hazard Analysis models and given by equation (2.16). For the PIE and Hazard Analysis models however, updated values derived from a linear regression analysis are used for K_1 and K_2 in equation (2.16). In the Cosham model however, the original values from the BGDGFM are retained. These are given by equations (2.14) and (2.15).

In a similar way to FFREQ and PIPIN, additional expressions have been included in the Cosham model to take into account the behaviour of pipes subject to denting. Firstly, the model considers the difference in dent depth between pressurised and unpressurised pipelines. When a dent is introduced into a pressurised pipeline, the internal pressure of the pipeline will cause a "re-rounding" effect, reducing the dent depth. Given a set denting force, a dent in an unpressurised pipeline would be deeper than a dent in the same pipeline if it were pressurised.

The dent depth used in the gouged dent limit state is defined as the dent depth in an unpressurised pipeline. The BGDGFM, which is used for the gouged dent limit state, is a semi-empirical model formulated using fracture mechanics theory and the results of experimental burst tests of gouged dent defects. In the burst tests used to calibrate the model, the dent damage was introduced and measured with the pipeline at zero pressure (Cosham, 2001a).

The dent depth recorded in the UKOPA Fault Database however, is (in most cases) the dent depth measured at pressure and therefore any probability distributions derived using dent data from the database will refer to dent characteristics at pressure.

The Cosham model acknowledges that the use of the BGDGFM may produce non-conservative predictions of the behaviour of damage recorded during

operation. In order to correct for this the model includes a relationship which was developed by the European Pipeline Research Group (EPRG) to account for the "re-rounding" effect of internal pressure (Corder, 1995b). The relationship was based upon the results of burst tests and damage resistance experiments. The dent depth in an unpressurised pipeline can be related to the dent depth in a pressurised pipeline by:

$$H = 1.43H_P \tag{2.82}$$

Where H is the dent depth in the unpressurised pipeline (in mm) and H_P is the dent depth in the pressurised pipeline (in mm). In the Cosham model a critical unpressurised dent depth predicted to cause failure is calculated using equation (2.16). This value is then transformed to an equivalent, critical pressurised dent depth, H_{Pcrit}, using equation (2.82).

Secondly, the Cosham model considers the resistance of pipes to denting[11]. The probability of failure of a gouged dent is determined from the force required to cause the dent, rather than the dent depth. The dent force is incorporated into the limit state function defined by equation (2.16) and (2.82) through the use of an expression which relates it to dent depth:

$$F_{dent} = 0.49\sqrt{Res}H_P^{0.42} \tag{2.83}$$

Where F_{dent} is the dent force (in kN) and Res (in $N^{1/2}mm$) is defined using equation (2.64):

$$Res = \sqrt{80\sigma_Y t}\left(t + \frac{0.7PD}{10\sigma_U}\right)$$

Equations (2.83) and (2.64) represent the mean value of the semi-empirical, dynamic dent force relationship as reported by Corder and Chatain (Corder, 1995b) if an assumption of 80 mm for the excavator tooth length is made. The

[11] Note that other than the use of the pressurised dent depth in equation (2.83), the dent force expressions in the Cosham model are identical to those used in PIPIN.

report on risk reduction factors indicates that the assumption of an 80 mm tooth length is made to be consistent with a paper by Linkens (Linkens, 1998; Cosham, 2007).

The critical pressurised dent depth calculated by equations (2.16) and (2.82) is transformed into a critical dent force, F_{crit}, using equations (2.83) and (2.64) before being used to calculate dent force probability.

2.6.3 *Cosham Model Probability Distributions*

Like the PIE model, the Cosham model includes only three random variables to calculate the probability of failure (Cosham, 2007). The model does not take into account pipeline area type and it makes no distinction between gouge and gouged dent damage in terms of the gouge length and gouge depth.
Unlike the PIE model however, the Cosham model considers the resistance of pipes to denting. A random variable for dent force is therefore included in place of the dent depth variable used in the PIE model. Table 2.14 shows the random variables included in the Cosham model alongside the limit state functions in which they are used:

Random Variable	Limit State Function
Gouge Length	Leak / Rupture & Gouge Failure
Gouge Depth	Gouge Failure & Gouged Dent Failure
Dent Force	Gouged Dent Failure

Table 2.14: Cosham Model Random Variables

In the development of the Cosham model an analysis to derive updated probability distributions was not performed. Instead, the model uses distributions from previous models. For the gouge length and gouge depth variables, the distributions from the PIE model are used. The dent force variable uses a Weibull distribution taken from the independent review of the QRA for the onshore Corrib Field Development Project conducted by Advantica (Cosham, 2007). The origin of the dent force distribution is not clear. It is known that it was derived using data from the ERS Fault Database from an unknown

year. It is also not known if the data used to derive the distribution included data from punctures, punctures which were caused by drilling operations in-error or failures as a result of damage to branches and fittings. In the Hazard Analysis model, data from the latter two categories was acknowledged to be the result of a different failure mechanism and was only included in the historical data component of the model. This issue was not addressed by the PIE model, which included data from all categories in its distributions. It is not known whether the distribution included data from both R-type and S-type areas. The variables used and the parameters defining their Weibull distributions are summarised in Table 2.15. The dent force distribution is shown in Figure 2.10.

Random Variable	Distribution Type	α	β (mm, or kN for Dent Force)
Gouge Length	Weibull	0.6	120.851
Gouge Depth	Weibull	0.889	1.442
Dent Force	Weibull	2.12	110.2

Table 2.15: Cosham Model Weibull Parameters

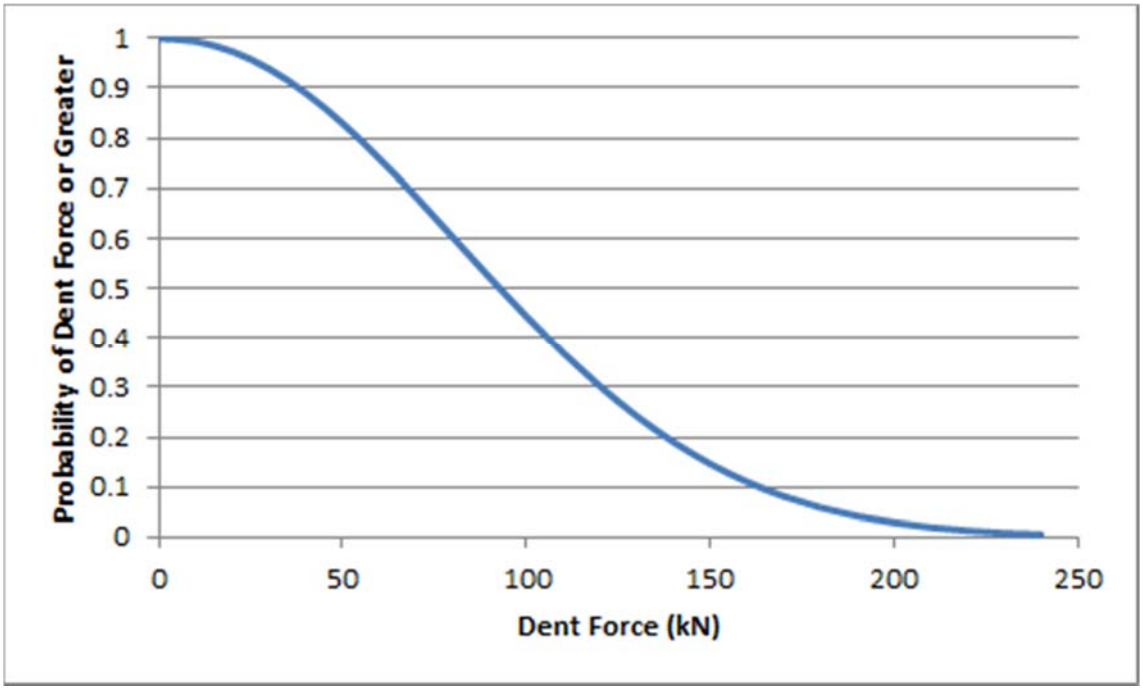

Figure 2.10: Cosham Model Dent Force Distribution

2.6.4 *Cosham Model Probability of Failure of Gouge and a Gouged Dent*

In the Cosham model the calculations for the probability of failure for gouge and gouged dent damage are very similar to those used in the PIE model. There are however certain subtle differences.

Firstly, the Cosham model uses direct integration rather than numerical integration to produce its output. Under this method, the truncation of the gouge length distribution which is applied in both the PIE and Hazard Analysis models is not required. Instead the entire curve can be considered.

Taking this into consideration the total probability of failure for gouges is therefore expressed as:

$$P_{gougetotal} = \int_0^{\infty} f_{2c}(2c) R_d(d_{crit}) d2c \qquad (2.84)$$

Where the subscripts are defined as they are for the PIE model.

Equation (2.84) can be split into a probability of a leak, $P_{gougeleak}$, and a probability of a rupture, $P_{gougerupture}$, using the critical length determined by the limit state function for leak / rupture (equation (2.72)). Note that for leaks, the equation is exactly the same as that used in the PIE model (equation (2.74)):

$$P_{gougeleak} = \int_0^{L_{crit}} f_{2c}(2c) R_d(d_{crit}) d2c$$

$$P_{gougerupture} = \int_{L_{crit}}^{\infty} f_{2c}(2c) R_d(d_{crit}) d2c \qquad (2.85)$$

In terms of gouged dent failure, the Cosham model uses a dent force distribution in place of the dent depth distribution in the PIE model. This however is implemented in exactly the same way as dent depth is for the PIE model and simply involves the substitution of one cumulative probability distribution for another. The Cosham model also makes a slight adjustment to the form of the probability of failure calculation. In the Hazard Analysis and PIE models the limit of the gouged dent gouge depth integral was set at the critical

gouge depth, d_{crit}. This implied that the probability of failure of gouges with a depth greater than the critical gouge depth (including through-wall punctures), were included in the calculation for the probability of failure for gouges, regardless of whether or not they were associated with a dent. In the Cosham model if a gouged dent contains a gouge which is deeper than the critical depth then it is counted separately in the gouged dent probability of failure calculation.

Taking the above points into consideration, the total probability of failure for gouged dents can be expressed as:

$$P_{gougeddenttotal} = \int_0^{\infty} f_{2c}(2c)d2c \,.\left[\int_0^{d_{critBGDGFM}} f_d(d)R_F(F_{crit})dd + R_d(d_{critBGDGFM})\right] \quad (2.86)$$

Where the subscript F denotes the use of the dent force Weibull parameters and the other subscripts are as equation (2.84). The value of F_{crit} is dependent on d and calculated using equations (2.16), (2.82), (2.64) and (2.83). In equation (2.86) the second term in the bracket represents the gouged dents with a gouge depth large enough to cause failure regardless of the size of the dent depth. The limit of the first integral is infinite, in line with equation (2.84). Note that the $d_{critBGDGFM}$ term in equation (2.86) is the critical gouge depth (in mm) based upon an infinitely long gouge. The Cosham model acknowledges that the BGDGFM, on which the gouged dent limit state function is based, was originally derived with the assumption that a gouge located within a dent is of infinite length (Cosham, 2001a). This assumption follows from the use of experimental ring test data from British Gas to calibrate the model. $d_{critBGDGFM}$ is determined from the gouge limit state function (equation (2.9)):

$$d_{crit} = t\left[1 - \frac{\sigma_H}{\bar{\sigma}}\right]\left[1 - \frac{\sigma_H}{\bar{\sigma}}\left(\frac{1}{M}\right)\right]^{-1}$$

Where from equation (2.35):

$$M = \sqrt{1 + 0.26\left(\frac{2c}{\sqrt{Rt}}\right)^2}$$

Assuming that the gouge length, $2c$, is infinite, equation (2.9) reduces to:

$$d_{critBGDGFM} = t\left(1 - \frac{\sigma_H}{\bar{\sigma}}\right) \quad (2.87)$$

It should be noted that as a consequence of defining $d_{critBGDGFM}$ in this way, its value is no longer dependent on $2c$ and therefore the bracketed terms in equation (2.86) do not take part in the length integral. This is contrary to both the PIE and Hazard Analysis models.

In order to determine the probability of a gouged dent failing as a leak and a gouged dent failing as a rupture, equation (2.86) can be split in a similar way to equations (2.84), (2.74) and (2.85):

$$P_{gougeddentleak} = \int_0^{L_{crit}} f_{2c}(2c)d2c \,.\left[\int_0^{d_{critBGDGFM}} f_d(d)R_F(F_{crit})dd + R_d(d_{critBGDGFM})\right] \quad (2.88)$$

$$P_{gougeddentrupture} = \int_{L_{crit}}^{\infty} f_{2c}(2c)d2c \,.\left[\int_0^{d_{critBGDGFM}} f_d(d)R_F(F_{crit})dd + R_d(d_{critBGDGFM})\right] \quad (2.89)$$

The critical length of the gouged dent gouge in equation (2.88) and (2.89) is the same as that for the gouge failures described by equations (2.74) and (2.85), as calculated by the limit state function for leak / rupture, equation (2.72).

2.6.5 *Cosham Model Failure Probability*

A pipeline failure frequency is not calculated by the Cosham model. The leak, rupture and total probability of failure, P_{leak}, $P_{rupture}$ and P_{total} respectively, of a pipeline due to gouge and gouged dent damage in the Cosham model are calculated by combining the results of Sections 2.6.1 and 2.6.4:

$$P_{leak} = P_{gougedamage}P_{gougeleak} + P_{gougeddentdamage}P_{gougeddentleak} \quad (2.90)$$

$$P_{rupture} = P_{gougedamage}P_{gougerupture} + P_{gougeddentdamage}P_{gougeddentrupture} \quad (2.91)$$

$$P_{total} = P_{leak} + P_{rupture} \quad (2.92)$$

Given that the Cosham model does not include an historical data component or calculate failure frequencies, the values calculated by equations (2.90), (2.91) and (2.92) are considered to be the overall final output from the model. Like the PIE model, a hole size relationship to separate the failure frequency into different hole diameter ranges is not included in the Cosham model.

2.7 Penspen Damage Distributions Update

The development and publication of the PIE model instigated a discussion within UKOPA regarding future recommendations on models to calculate pipeline failure frequency due to third party external interference. UKOPA ultimately decided that FFREQ would remain the recommended model for use in the industry. It was acknowledged however, that updates of the Incident-Rates and probability distributions used in FFREQ were required to take account of more recent operational data; and that these updates should be continuous and take place on a regular basis.

In 2010 UKOPA commissioned Penspen to update the probability distributions and Incident-Rates for FFREQ (Goodfellow, 2012). This section outlines the results of this study and presents the updated rates and distributions. A separate failure frequency model is not specifically considered in this section, however the importance of using Incident-Rates and probability distributions derived from the most up to date data (as of 2010) in an external interference failure frequency model warrants its inclusion.

Despite the fact that the motivation for the study was to provide an update to FFREQ, the particular probability distributions and Incident-Rate derived by Penspen are actually more suited to the simplified nature of the PIE model. This is likely to be because of the lack of definitive information relating to the FFREQ model combined with the recent publication of the PIE model.

Like the PIE model only one Incident-Rate was derived by Penspen and this is given in Table 2.16 (Goodfellow, 2012). The Incident-Rate makes no distinction

between gouges and gouged dents, instead representing an overall frequency for which a pipeline is subject to mechanical damage.

The Incident-Rate is based upon an analysis of the 2009 UKOPA Fault Database (the most up to date version of the database at the time of the study). The value derived relates to pipelines located in R-type areas only. In the 2009 database the corresponding operational exposure was 763,289 km.yr and the number of mechanical damage incidents included in the study was 689.

Rural Incident-Rate (per km.yr)
9.03×10^{-4}

Table 2.16: Penspen Updated Incident-Rate for R-Type Areas

It is noted that no additional factors to provide appropriate damage specific Incident-Rates, similar to those used in the PIE model, were derived as part of the Penspen study. Given that only one Incident-Rate was derived, such factors would be required in order to be consistent with the failure frequency models described in this review.

Like the PIE model the Penspen study derived only three random variables to calculate the probability of failure (Goodfellow, 2012) gouge length, gouge depth and dent depth. The variables do not take into account pipeline area type and make no distinction between gouge and gouged dent damage in terms of the gouge length and gouge depth.

As with the PIE model, Weibull distributions were chosen to represent the variables. The Weibull distributions were based upon an analysis of pipeline damage data for gouges and gouged dents contained in the 2009 UKOPA Fault Database. In line with the reduced number of variables, it is assumed that the distributions for gouge length and gouge depth were derived using data sets which incorporated both gouge and gouged dent data; and that all three distributions included data from both R-type and S-type areas. The Weibull distributions were fitted using both the maximum likelihood and least squares methods and a sensitivity study was performed by using both sets of

distributions with an unspecified failure frequency model to compare the outcomes. The variables used and the final parameters selected defining their Weibull distributions are summarised in Table 2.17 (Goodfellow, 2012).

Random Variable	Distribution Type	α	β (mm)
Gouge Length	Weibull	0.573	125.4
Gouge Depth	Weibull	0.674	0.916
Dent Depth	Weibull	1.018	9.382

Table 2.17: Penspen Updated Weibull Parameters

It is not known if the data sets used to derive the Weibull distributions given in Table 2.17 included data from punctures, punctures which were caused by drilling operation in-error or failures as a result of damage to branches and fittings. In the Hazard Analysis model (and by extension FFREQ), data from the latter two categories was acknowledged to be the result of a different failure mechanism and was only included in the historical data component of the model. This issue was not addressed by the PIE model, which included data from all categories in its distributions.

2.8 Failure Frequency Model Discussion

The previous sections have reviewed a number of models which have been used within the pipeline industry to calculate the failure frequency (or failure probability) due to third party external interference. The review has highlighted the similarities and differences between the models. It is noted that all of the models considered have the same basic structure which originated with the Hazard Analysis model. That is, they are rooted in probabilistic, structural reliability methods; use semi-empirical fracture mechanics failure models to define limit state functions; and probability distributions based on historical operational pipeline damage data. Variation between the models exists in the form of additional expressions or factors which have been included in an attempt to provide a more accurate description of the damage and failure mechanisms in effect. In addition some of the models have augmented their structural reliability procedure with additional historical operational data.

An important point to note is that the structural reliability methods used in Hazard Analysis and the other failure frequency models are not dependent on pipeline wall thickness or any other quantity related to the transport of dense phase CO_2 by pipeline. The methods themselves are non-specific and are used for a wide variety of applications throughout engineering. The applicability of a structural reliability method to any given situation depends entirely upon the applicability of the models and data contained within them. A structural reliability based model can be used to calculate the failure frequency for a dense phase CO_2 pipeline. However, in order to construct such a model using the basic structure of the Hazard Analysis model a further review must be undertaken to consider the applicability of available pipeline failure models and historical operational data to dense phase CO_2 pipelines. This review will be addressed in the next chapter. The remainder of this section will discuss the failure frequency models described above and consider which individual aspects could be included in the development of a failure frequency model for dense phase CO_2 pipelines.

The first point of consideration regards the differences between the Hazard Analysis and PIE models and the Cosham model in the calculation of the probability of failure of a gouge and a gouged dent. The implementation of an infinite upper limit in the integrals in the Cosham model would make the most sense mathematically rather than applying a cut off of 55 inches. In each of these models the gouge length distribution(s) have been derived from historical operational data and extend to infinity. The cut-off point suggests that no gouges longer than 55 inches will occur which directly contradicts the derived distributions, even if gouges longer than this would be extremely unlikely. The Cosham model is also more accurate than the Hazard Analysis and PIE models when considering failures where the gouge depth exceeds the critical depth. In the Hazard Analysis and PIE models this situation is not addressed for gouged dent damage, the integral considers gouged dents with a gouge depth up to the critical depth only. Documentation relating to the development of the Hazard Analysis model attempts to justify this by noting that failure would occur for a gouge with a depth greater than the critical depth without the presence of a dent and therefore the failures are counted by the integral for gouge failure. However, if a gouge occurs in the presence of a dent it should be treated as a

gouged dent regardless of whether or not failure would occur without the presence of the dent. It is also noted that the use of an infinitely long gouge to calculate the critical gouge depth in the gouged dent probability of failure in the Cosham model is more consistent with the use of the BGDGFM as a limit state function. It would therefore be preferable to use this with the BGDGFM in any future model.

The separation of Incident-Rate into different values for R-type and S-type areas appears to be justified given the differences observed between the two sets of Incident-Rates in the Hazard Analysis model. The PIPIN model also indicates that a factor of 4 difference exists between the Incident-Rates for the two area classes. To distinguish between pipelines located in R-type and S-type areas in the failure frequency model for dense phase CO_2 pipelines, the derivation of a similar factor would therefore be recommended. The Hazard Analysis work to separate the gouge and gouged dent random variables into R-type and S-type areas was well intentioned, however the documentation concedes that there was insufficient data to perform this in the desired way. Only gouges provided enough data for separate distributions to be derived and for this damage type, the distributions for gouge length were found to be almost identical. Subsequent models neglected to perform a similar analysis and as a result it has not been performed for this work.

The use of additional distributions in PIPIN giving the uncertainty in parameters such as the diameter, wall thickness and the limit state functions themselves could produce a more realistic representation of failure frequency. This method attempts to model the uncertainties which will be present in reality. The distributions used however must be realistic and therefore must be derived from relevant operational data. The source of the distributions giving uncertainty to the limit state functions used in the PIPIN model is not known and an attempt to derive such distributions for dense phase CO_2 pipelines would be impossible given the current lack of operational data. It is likely that the distributions used for the design parameters in PIPIN were derived for specific pipeline cases at the design stage, where exact operation parameters and manufacturing tolerances were well known. Contrastingly, this work is concerned with the development of a general failure frequency model for dense phase CO_2

pipelines, for which there is currently no operational experience and no design parameters available. Consequently the use of probability distributions in the same way as PIPIN would be speculative at best. It is also likely that distributions for design parameters manufactured to certain tolerance limits will show little variation and therefore have little effect on the failure frequency overall. If the additional distributions from PIPIN are not included in the failure frequency model for dense phase CO_2 pipelines then the use of numerical integration is preferred over Monte-Carlo techniques to perform the probability of failure calculations.

In the Hazard Analysis and FFREQ models, the historical data component is used to supplement the structural reliability component. It provides additional external interference failure frequencies for failures from branches and fittings; and drilling operations in-error, which are types of failure outside of the scope of those calculated using the limit state functions and probability distributions. It is important to include these types of failure in any failure frequency addressing third party external interference. In PIPIN, the historical data component does not consider external interference at all. The historical data component of the Hazard Analysis model has no direct analogue in PIPIN. It is unclear how data regarding punctures and failures from branches and fittings was treated when probability distributions were derived for PIPIN. It is reasonable to assume that conventional puncture data was included in the distributions; however a satisfactory conclusion regarding branches and fittings; and drill puncture data cannot be made. It is noted however that if PIPIN includes this data in the distributions, this would not give an accurate representation of the failure of either of these types of damage. A drill puncture is caused by a repeated boring action into the pipe wall, the probability of a drill puncture exceeding the pipe wall is therefore not the same as the probability of a conventional puncture occurring. Branches and fittings failures will not be described by the exact same limit state functions as the parent pipe, even if the causes of failure are of the same type. Branches and fittings may be of a different size to the parent pipe, including them in the standard gouge and gouged dent data will force failures of this type to be treated in the same way as standard gouge and gouged dent data, which is not correct. The PIE model and the Cosham model lack an historical data component. In these cases it is known that the failure data from

branches and fittings; and drilling operations in-error was included in the derivation of the probability distributions for the structural reliability calculations. Failures of those types are therefore not adequately addressed by the models. It is not known how the data was treated in the updated Penspen distributions, however given the distributions consider only three random variables, they are compatible with only the PIE and Cosham models and would therefore suffer the same shortcomings. It can be concluded that the only models considered as part of this review which address failures from damage to branches and fittings; and drilling operations in-error in an appropriate way are the Hazard Analysis and FFREQ models. The development of specific failure models for these damage types could be considered for future research work and used in the structural reliability component of a failure frequency model, as an alternative to the use of an historical data component. The use of such models would depend on there being sufficient relevant historical operational data available.

The reduced number of random variables in the PIE model; the Cosham model; and the updated Penspen distributions, requires investigation. From a statistical perspective it must be established whether the populations of gouge length and gouged dent gouge length are the same or different and whether the populations of gouge depth and gouged dent gouge depth are the same or different. In other words, does the presence of a dent affect the size of the gouge which would be produced by mechanical damage. The use of larger, non-separated data sets would provide more data points from which more accurate probability distributions could be derived. Conversely, incorrectly assuming the use of one random variable when in fact two distinct variables are required could lead to errors in the values of failure frequency calculated.

The additional elements included in the FFREQ, PIPIN and Cosham models concerning the behaviour of pipes subject to denting are considered to provide improvement to the methodology of the structural reliability component of the Hazard Analysis model. These elements should be considered for inclusion into a failure frequency model for dense phase CO_2 pipelines. Depth of cover is also an important consideration; an updated depth of cover factor curve was derived in 2012 by GL Noble Denton (GLND) on behalf of UKOPA (Mumby, 2012). This updated curve could also be included in the failure frequency model.

Chapter 3. Failure Models and Historical Operational Data

In section 2.8 it was noted that the applicability of the existing failure frequency models to a given situation depends entirely upon the applicability of the pipeline failure models and historical operational data contained within them. In order to construct a similar model for dense phase CO_2 pipelines based upon the same methodology, the constituent failure models and data should be applicable to thick wall pipelines.

This chapter presents a review of existing failure models and operational pipeline damage databases which could potentially be used in a failure frequency model for dense phase CO_2 pipelines. The failure models and databases are considered from the perspective of their applicability to thick wall pipelines.

3.1 Failure Models

In the failure frequency models described in Chapter 2, failure models are used to define the limit state functions. Separate limit state functions are required for:

- Leak / rupture
- Gouge failure
- Gouged dent failure

Therefore in order to develop a failure frequency model for dense phase CO_2 pipelines, suitable failure models must be included to describe each of these three mechanisms.

3.1.1 *Leak / Rupture and Gouge Models*

3.1.1.1 *The NG-18 Equations*

In the Hazard Analysis model, FFREQ, the PIE model and the Cosham model the limit state functions for leak / rupture and gouge failure, were derived from the through-wall and part-wall NG-18 equations respectively[12].

The NG-18 equations were developed by Battelle in the 1970s (Cosham, 2002). Because of the accuracy and simplicity of the NG-18 equations they have become accepted as the industry standard for defect assessment and have been included as part of defect assessment codes and used extensively since their introduction. The equations are semi-empirical and are based upon the Dugdale strip-yield model and series of full scale experimental burst tests of vessels with through-wall and part-wall defects (Cosham, 2002).

The through-wall NG-18 equation is used to determine, based upon the current operating conditions of the pipeline, whether an axially oriented through-wall defect in a pipeline will lead to a full-bore rupture or remain as a leak.

The part-wall NG-18 equation is used to determine, based upon the current operating conditions of the pipeline, whether an axially oriented part-wall defect (for the purposes of this work, a gouge) will progress into a through-wall defect.

Both the through-wall and the part-wall NG-18 equations exist in two forms: toughness dependent and flow stress dependent. The toughness dependent form of each NG-18 equation is recommended for use in assessing defects when the pipeline steel has a low toughness.

The failure of defects in pipelines occurs due to a combination of brittle fracture and plastic collapse. The fracture toughness, measured here using the Charpy

---

[12] It will be shown by the analysis in section 4.2.2 that the limit state functions in PIPIN also originate from the NG-18 equations.

v-notch impact energy, is a measure of a material's resistance to brittle fracture. If the pipe steel has a high fracture toughness then the failure of a defect in the pipeline is dominated by plastic collapse and the failure stress of the defect is independent of the value of the toughness. If however the pipe steel has low fracture toughness, the influence of brittle fracture is included in the failure and the failure stress of the defect will be sensitive to the value of the toughness.

The toughness dependent forms of the NG-18 equations are applicable over the full range of pipe steel toughness. If the toughness is greater than some minimum value (suggested to be a 2/3 Charpy v-notch impact energy of approximately 21 J (Cosham, 2002)), then the flow stress dependent forms of the equations can be used to give a conservative value for the defect failure stress. The flow stress dependent forms of the NG-18 equations do not include a fracture toughness term.

If the pipe steel toughness is sufficiently high, the failure is controlled entirely by plastic collapse. It has been suggested that a failure may become fully ductile if the Charpy v-notch impact energy for a full size specimen of pipe steel is between 81 J and 102 J (Cosham, 2002).

In the failure frequency models in Chapter 2 the flow stress dependent forms of the through-wall and part-wall NG-18 equations are used over the toughness dependent form due to the high toughness of modern pipe steels.

The toughness dependent and flow stress dependent forms of the **through-wall** NG-18 equation are as follows:

Toughness dependent

$$\frac{K_{IC}^2 \pi}{8c\overline{\sigma}^2} = \ln \sec\left(\frac{\pi M \sigma_H}{2\overline{\sigma}}\right) \qquad (3.1)$$

Flow Stress dependent

$$\sigma_H = M^{-1}\overline{\sigma} \qquad (3.2)$$

Where K_{IC} is the material's fracture toughness (in Nmm$^{-3/2}$); c is half of the axial defect length (in mm); σ_H is the circumferential hoop stress at failure (in Nmm^{-2}); $\overline{\sigma}$ is the flow stress (in Nmm^{-2}) (see below); and M is the Folias factor (see below).

The toughness dependent and flow stress dependent forms of the **part-wall** NG-18 equation are as follows:

Toughness dependent

$$\frac{K_{IC}^2 \pi}{8c\overline{\sigma}^2} = \ln \sec\left(\frac{\pi M_P \sigma_H}{2\overline{\sigma}}\right) \quad (3.3)$$

Flow stress dependent

$$\sigma_H = M_P^{-1}\overline{\sigma} \quad (3.4)$$

Where M_P is given by:

$$M_P = \left[\frac{1-\frac{d}{t}\left(\frac{1}{M}\right)}{1-\frac{d}{t}}\right] \quad (3.5)$$

Where d is the depth of the part-wall defect (in mm), t is the pipeline wall thickness (in mm) and M is the Folias factor.

In the toughness dependent forms of both the part-wall and through-wall NG-18 equations, the material fracture toughness is determined using a correlation with the Charpy v-notch energy. This correlation was empirically derived using the results of the series of full scale experimental burst tests of vessels with through-wall defects. The correlation used is as follows (in metric units):

$$K_{IC}^2 = C_v \frac{1000}{A} E \quad (3.6)$$

Where C_V is the 2/3 Charpy v-notch upper shelf impact energy (in J), A is the cross-sectional area (in mm^2) of the Charpy specimen, and E is the Young's

Modulus of steel (in Nmm^{-2}). The cross-sectional area of a 2/3 size Charpy specimen is 53.33 mm^2, Young's Modulus of steel is 210,000 Nmm^{-2}.

It is noted that in the NG-18 equations the circumferential hoop stress is calculated using Barlow's formula, equation (2.5):

$$\sigma_H = \frac{PD}{20t}$$

3.1.1.2 *The Folias Factor*

The Folias factor in the NG-18 equations described above is a quantity used to account for the additional stress concentration due to defect bulging. Bulging is caused by the action of the internal pressure of a pipeline on a part-wall or through-wall defect. The pipe material surrounding the defect is forced radially outwards by the internal pressure and causes the bulging deformation in the pipe wall. At the ends of the defect the bulging is resisted by the pipe material and this creates a stress concentration (Cosham, 2002).

In reality the Folias factor can only be completely described using an infinite series. The factor can be approximated however, using simple expressions. Folias' original approximation of the factor was a two term expression. This expression is given by equation (2.39):

$$M = \sqrt{1 + 0.40\left(\frac{2c}{\sqrt{Rt}}\right)^2}$$

The original two term expression is only applicable to small values of $2c/\sqrt{Rt}$; strictly, the expression should therefore only be applied to short defects. The original two term expression however, is not the only approximation for the Folias factor. An alternative two term expression was also derived by Folias and this is applicable to longer defects. The expression is given by equation (2.35):

$$M = \sqrt{1 + 0.26\left(\frac{2c}{\sqrt{Rt}}\right)^2}$$

The alternative two term expression has been shown to be accurate to within an error of 7% (Cosham, 2002).

When developing the NG-18 equations Battelle initially used the original two term expression. However they subsequently derived a three term expression to use in place of the original. This approximation was shown to be more accurate than the original two term expression. The three term expression is also limited by defect length and is only valid in the range $0 \leq 2c/\sqrt{Rt} \leq 8$. The three term expression is given by:

$$M = \sqrt{1 + 0.314\left(\frac{2c}{\sqrt{Rt}}\right)^2 - 0.00084\left(\frac{2c}{\sqrt{Rt}}\right)^4} \qquad (3.7)$$

Where the NG-18 equations have been employed in defect assessment codes and failure frequency models both the alternative two term and the three term expressions for the Folias factor have been used as alternatives to the original two term expression, for example:

- The original two term expression is used in the ASME B31G assessment method (Anon., 1991a). It is also used in defect assessment codes such as BS 7910 (Anon., 2007b), British Energy R6 (Anon., 2001a) and the failure frequency model PIPIN.
- The alternative two term expression of the Folias factor is used with the NG-18 equations in the FFREQ, PIE and Cosham failure frequency models.
- The modified B31G failure assessment method (Kiefner, 1989), uses a Folias factor based upon the Battelle three term expression.

As the approximations to the Folias factor are all slightly different, each will give slightly different predictions for the failure of part-wall and through wall defects when used with the NG-18 equations. PDAM notes that the most accurate predictions of part-wall defect failure are obtained using the alternative two term expression (along with a flow stress equal to the average of the yield and tensile strength) (Cosham, 2002). In terms of which approximation is closest to the infinite series, a comparison performed by Cosham (Cosham, 2002) has shown

the original two term expression to be the most conservative of the three; and that there is little difference between the alternative two term expression and the three term expression over the range of applicability of the three term expression, although the modified two term expression is slightly less conservative.

It is noted that the origin of the form of the Folias factor used in the Hazard Analysis model is unknown. The expression was replaced with the modified two term expression however, in the FFREQ model.

3.1.1.3 *The Flow Stress*

The flow stress is a measure of the stress at which unconstrained plastic flow occurs. The NG-18 equations described above are semi-empirical, however the definition of the flow stress used in the NG-18 equations is empirical. The flow stress in general is not precisely defined however, it has been estimated to have a value somewhere between the yield strength and the ultimate tensile strength of the material.

In the development of the NG-18 equations a value for the flow stress was empirically determined by considering a fit to the results of the series of full scale experimental burst tests of vessels with through-wall and part-wall defects. The flow stress defined by Battelle and used in the NG-18 equations is given by (Cosham, 2002):

$$\bar{\sigma} = \sigma_Y + 68.95 \text{ MPa} \qquad (3.8)$$

Since the introduction of the NG-18 equations further experimental tests have been performed and different definitions of the flow stress have been developed. A number of these different definitions are listed below (Cosham, 2002):

$$\bar{\sigma} = 1.1\sigma_Y \qquad (3.9)$$

$$\bar{\sigma} = 1.15\sigma_Y \quad (3.10)$$

$$\bar{\sigma} = \frac{\sigma_Y + \sigma_U}{2} \quad (3.11)$$

$$\bar{\sigma} = j^{n+1}(1/2)^n\sigma_U \quad (3.12)$$

$$\bar{\sigma} = 0.9\sigma_U \quad (3.13)$$

$$\bar{\sigma} = (\sigma_U)^{\nu}(\sigma_Y)^{1-\nu} \quad (3.14)$$

$$\bar{\sigma} = \sigma_U \quad (3.15)$$

Where in equation (3.12) j is a constant from the yield criterion and n is the hardening index. The value of the exponent ν in equation (3.14) depends upon the stress and strain properties of the material beyond yield. Where the flow stress has been employed in defect assessment codes, fracture models and failure frequency models, including the use of the NG-18 equations, some of the different expressions have been used as alternatives to equation (3.8), for example (Cosham, 2002):

- The flow stress defined by equation (3.8) is used in the modified B31G failure assessment method (Kiefner, 1989).
- The flow stress defined by equation (3.9) is used in the ASME B31G assessment method (Anon., 1991a).
- The flow stress defined by equation (3.10) is used in the BGDGFM (Cosham, 2001a). By extension it is also used in the Hazard Analysis, FFREQ, PIE and Cosham failure frequency models in both the NG-18 equations and the BGDGFM.
- The flow stress defined by equation (3.11) is used in defect assessment codes such as BS 7910 (Anon., 2007b) and British Energy R6 (Anon., 2001a); and the failure frequency model PIPIN.

As the definitions of the flow stress are all slightly different, each will give slightly different predictions for the failure of part-wall and through-wall defects

when used with the NG-18 equations. PDAM notes that many different recommendations have been made as to which definition to use, usually depending on which set of experimental tests are analysed. Overall the document recommends the use of the flow stress as defined using equation (3.11) (Cosham, 2002).

3.1.1.4 *Applicability of the NG-18 Equations*

The NG-18 equations are semi-empirical, they were calibrated using series of full scale experimental burst tests of vessels with through-wall and part-wall defects. The range of applicability of each equation with regards to wall thickness can be inferred from the range of vessel wall thicknesses used in the corresponding set of burst tests used to derive it.

The through-wall NG-18 equations were calibrated using the results of 92 burst tests on vessels with axially orientated, artificially machined, through-wall defects. The tests were carried out by Battelle between 1965 and 1974. The range of experimental parameters for the through-wall tests is shown in Table 3.1 (Cosham, 2002).

Parameter	Minimum Value	Maximum Value
Pipe Diameter (mm)	167.6	1219.2
Wall Thickness (mm)	4.9	21.9
Grade (API 5L)	A	X100
Yield Strength (Nmm^{-2})	220.6	735.0
Tensile Strength (Nmm^{-2})	337.9	908.1
2/3 Charpy V-Notch Impact Energy (J)	13.6	90.9
Defect Length ($2c$) (mm)	25.4	508.0
Burst Pressure (Nmm^{-2})	2.21	18.69
Burst Stress (Nmm^{-2})	97.9	486.8
Burst Stress (% Yield)	22.6	135.8

Table 3.1: Battelle Through-Wall Defect Burst Test Parameter Ranges

The part-wall NG-18 equations were calibrated using the results of 48 burst tests on vessels with axially orientated, artificially machined, part-wall defects (v-shaped notches). The tests were carried out by Battelle between 1965 and

1974. The range of experimental parameters for the part-wall tests is shown in Table 3.2 (Cosham, 2002).

Parameter	Minimum Value	Maximum Value
Pipe Diameter (mm)	406.4	1066.8
Wall Thickness (mm)	6.4	15.6
Grade (API 5L)	X52	X65
Yield Strength (Nmm^{-2})	379.2	509.5
Tensile Strength (Nmm^{-2})	483.3	633.7
2/3 Charpy V-Notch Impact Energy (J)	13.6	46.1
Defect Length ($2c$) (mm)	63.5	609.6
Defect Depth (d) (mm)	3.1	11.2
Burst Pressure (Nmm^{-2})	1.84	12.4
Burst Stress (Nmm^{-2})	61.4	506.1
Burst Stress (% Yield)	13.7	132.5

Table 3.2: Battelle Part-Wall Defect Burst Test Parameter Ranges

The parameter ranges in Table 3.1 and Table 3.2 suggest that the through-wall NG-18 equations are applicable to pipelines with a wall thickness between 4.9 mm and 21.9 mm and the part-wall NG-18 equations are applicable to pipelines with a wall thickness between 6.4 mm and 15.6 mm.

3.1.1.5 *The Ductile Flaw Growth Model*

Due to the widespread success of the NG-18 equations within the industry, the number of alternative pipeline specific models for describing leak / rupture or gouge failure is limited. The only notable example is the Ductile Flaw Growth Model (DFGM). The DFGM was developed in the 1980s when the Pipeline Research Council International (PRCI) commissioned work to update the through-wall and part-wall NG-18 equations; it had been acknowledged that the occurrence of stress corrosion cracking (SCC) in North American pipelines required the development of a less conservative, more accurate assessment method (Cosham, 2002).

The DFGM is based upon elastic-plastic fracture mechanics and is more complex than the simple through-wall and part-wall NG-18 equations; explicitly

considering the time dependent behaviour of crack growth. The DFGM is implemented in the form of a software package known as the Pipe Axial Failure Criterion (PAFFC). It has been reported that the DFGM is more accurate than the NG-18 equations (Cosham, 2002). However, due to its complexity, the DFGM is unsuitable for inclusion in a failure frequency model based upon structural reliability methods. It is therefore not considered any further in this work.

3.1.1.6 *BS 7910 and Generic Assessment Codes*

In the absence of further pipeline specific methods, an alternative way to describe leak / rupture and gouge failure is use the models contained in generic defect assessment codes. Assessment codes such as BS 7910 (Anon., 2007b), API 579 (Anon., 2007a) and British Energy R6 (Anon., 2001a) were developed to provide generic assessment methods for defects in metallic structures and can be applied to pipelines. In the PIPIN failure frequency model the limit state functions are based upon an assessment using British Energy R6 rev. 3 (Anon., 1986). This section describes an assessment using BS 7910; however, a very similar approach is used in the other codes.

In BS 7910 defects can be assessed to three levels of complexity (Anon., 2007b):

- A level 1 assessment is the most simple and provides a basic screening method for defects when information about the material properties is limited. It is the most conservative of the three assessment levels.
- A level 2 assessment is more in-depth and requires knowledge of the specific operating conditions, geometry and material properties of the structure. This method is termed the “normal assessment route” and presents an assessment method which uses data that would most commonly be available to the assessor. The level 2 assessment is less conservative than the level 1 assessment.
- A level 3 assessment is the most detailed assessment method and would be used when considering ductile materials for which a full tearing

resistance analysis could be performed. A large amount of data is required to complete a level 3 assessment which would very rarely be available to the assessor. The level 3 assessment is the most accurate and the least conservative of the three assessment methods.

The level 2 “normal assessment” method could be considered as analogous to that of the NG-18 equations when applied to the defect assessment of a pipeline in terms of the complexity and the information required. Therefore, for the purposes of this review, a level 2 assessment will be described. The assessment described, including any assumptions made, will address axially orientated through-wall (leak / rupture) and part-wall (gouge) defects in a pipeline. These defects are the most relevant to the failure frequency models. The defects are assumed to be located in the pipe body away from any areas of local stress concentration, structural discontinuities or misalignment.

In all three levels in BS 7910 the assessment of a defect is performed using a failure assessment diagram (FAD) approach. This method is derived from fracture mechanics theory and considers that failure of the structure can occur due to either brittle fracture or plastic collapse. Based on the geometry of the structure, its operating conditions and the dimensions of the defect two separate quantities are calculated, one representing brittle fracture and one representing plastic collapse (Anon., 2007b).

The quantity representing brittle fracture is known as the Fracture Ratio, K_r, and this is calculated as from equation (2.40):

$$K_r = \frac{K_I}{K_{IC}}$$

In equation (2.40) K_{IC} is the material fracture toughness (in Nmm$^{-3/2}$) and K_I is a quantity known as the stress intensity factor (in Nmm$^{-3/2}$)[13]. The form of the stress intensity factor is dependent on the type and the dimensions of the defect

[13] Note that the units used for the terms in the Fracture Ratio in BS 7910 differ slightly from those used in the PIPIN model.

and the geometry and operating conditions of the structure being assessed (Anon., 2007b).

The quantity representing plastic collapse is known as the Load Ratio, L_r, and this is calculated as follows:

$$L_r = \frac{\sigma_{ref}}{\sigma_Y} \quad (3.16)$$

Where σ_Y is the yield stress of the structure (in Nmm^{-2}) and σ_{ref} is a quantity known as the reference stress (in Nmm^{-2}) which is also dependent on the type and dimensions of the defect and the geometry and operating conditions of the structure being assessed (Anon., 2007b).

Once the specific K_r and L_r for the defect and structure have been calculated they can be plotted as a point on a FAD. A FAD is a plot with axes of K_r and L_r and shows a function relating acceptable values of the two quantities to each other, the failure assessment curve, to which the values of K_r and L_r must be compared. An example of a FAD for a level 2 assessment taken from BS 7910 is shown in Figure 3.1 below (Anon., 2007b):

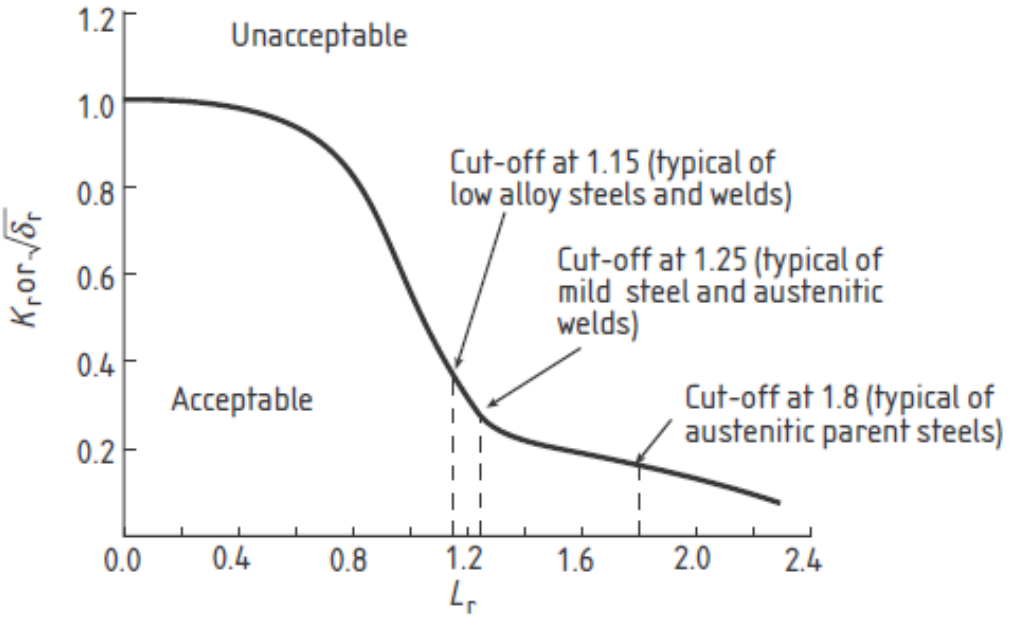

Figure 3.1: Example Failure Assessment Diagram for a Level 2 Assessment to BS 7910[14]

If the calculated values of K_r and L_r lie within the failure assessment curve then the defect is considered acceptable. Conversely, if they lie outside of the curve then the defect is considered unacceptable. The form of the failure assessment curve for a level 2 assessment is:

$$K_r = (1 - 0.14L_r^2)\{0.3 + 0.7\exp(-0.65L_r^6)\} \quad (3.17)$$

A cut-off point is also applicable once L_r is greater than some maximum value given by:

$$L_{rmax} = \frac{\sigma_Y + \sigma_U}{2\sigma_Y} \quad (3.18)$$

Beyond this point the value of K_r becomes zero (i.e. all values of fracture ratio are unacceptable) (Anon., 2007b).

For the BS 7910 level 2 assessment the circumferential hoop stress (in Nmm^{-2}) is calculated using Lamé's equations:

[14] δ_r is the Fracture Ratio defined using CTOD parameters.

$$\sigma_H = P\frac{{r_i}^2}{{r_0}^2-{r_i}^2}\left(1+\frac{{r_0}^2}{r^2}\right) \quad (3.19)$$

Where P is the internal pressure (in Nmm^{-2}), r_i is the internal shell radius (in mm), r_0 the external shell radius (in mm) and r the shell radius at the point of interest (in mm). The hoop stress is linearised into primary membrane, σ_m, and bending, σ_b, components using the following figure from section 6.4 of BS 7910:

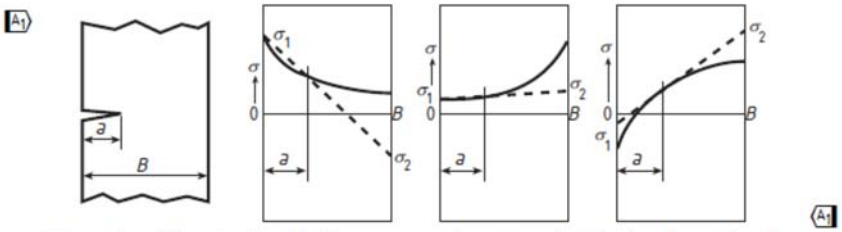

i) Examples of linearization of primary or secondary stress distributions for surface flaws

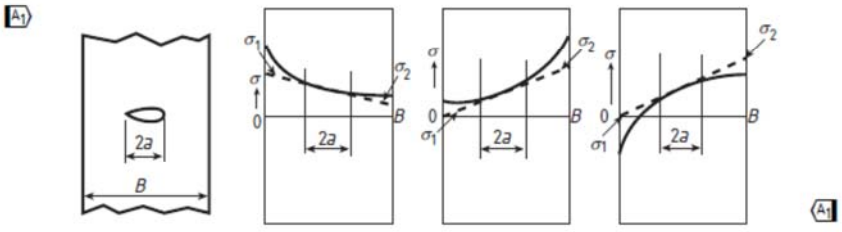

ii) Examples of linearization of primary or secondary stress distributions for embedded flaws

P_m, Q_m and P_b, Q_b can be determined from the distributions in i) and ii) using the following equations:

$$P_m, Q_m = \frac{\sigma_1+\sigma_2}{2} \qquad P_b, Q_b = \frac{\sigma_1-\sigma_2}{2}$$

NOTE Any linearized distribution of stress is acceptable provided that it is greater than or equal to the magnitude of the real distribution over the flaw surface.

Figure 3.2: Linearisation of Stress Distributions

The membrane and bending components (in Nmm^{-2}) are given by:

$$\sigma_m = \frac{\sigma_i+\sigma_0}{2} \quad (3.20)$$

$$\sigma_b = \frac{\sigma_i-\sigma_0}{2} \quad (3.21)$$

Where the subscripts i and o denote the stress on the internal and external wall of the pipe respectively.

The general form of the stress intensity factor, required for the fracture ratio (equation (2.40)) is:

$$K_I = (Y\sigma)\sqrt{\pi X} \quad (3.22)$$

Where, X, is a parameter used to represent the defect size. This is half the defect length, c (in mm), in the case of a through-wall defect, or the defect depth, d (in mm), in the case of a part-wall defect. Y is a function which depends the specific conditions of the assessment; and σ represents the stress state in the pipe wall (in Nmm^{-2}).

For a level 2 assessment the $(Y\sigma)$ term in equation (3.22) is split into components originating from primary and secondary stresses (in Nmm^{-2}) in the structure:

$$Y\sigma = (Y\sigma)_P + (Y\sigma)_S \quad (3.23)$$

Where the subscripts P and S refer to primary and secondary respectively. For the defects under consideration it is assumed that secondary stress contributions, $(Y\sigma)_S$, are zero. The primary stress component is given by:

$$(Y\sigma)_P = Mf_w[M_m\sigma_m + M_b\sigma_b] \quad (3.24)$$

Where M is the bulging correction factor for an axial through-wall or part-wall defect in a cylinder, f_w is the area correction term for a through-wall or part-wall defect in a curved shell, M_m is the membrane stress magnification factor for a through-wall or part-wall defect and M_b is the bending stress magnification factor for a through-wall or part-wall defect. In equation (3.24) factors due to regions of local stress concentration, structural discontinuities and misalignment (M_{km}, M_{kb}, k_t, k_{tm}, k_{tb}, k_m) do not appear as these are assumed to be equal to 1 in accordance with section 6.4.4 and Annex D of BS 7910. The finite width correction factor f_w is calculated using:

$$f_w = \{\sec(\pi A_1/2A_2)\}^{0.5} \quad (3.25)$$

Where A_2 (in mm^2) is given by:

$$A_2 = Wt \quad (3.26)$$

Where W is the length of a typical pipe spool (12 m or 6 m). For a through-wall defect A_1 (in mm^2) can be calculated by:

$$A_1 = 2ct \quad (3.27)$$

For a part-wall defect A_1 can be calculated using:

$$A_1 = 2cd \quad (3.28)$$

For the case of a through-wall defect, the bulging correction factor, M[15] is given by:

$$M = \{1 + 3.2(c^2/2r_m t)\}^{0.5} \quad (3.29)$$

Where r_m is the average pipe radius (between the internal and external pipe wall surfaces) (in mm). For the case of a part-wall defect M[16] is given by:

$$M = \frac{1-\{d/(M_T t)\}}{1-(d/t)} \quad (3.30)$$

Where M_T is given by:

$$M_T = \{1 + 3.2(c^2/2r_m t)\}^{0.5} \quad (3.31)$$

The membrane and bending load factors, M_m and M_b respectively, are equal to 1 for a through-wall defect. For a part-wall defect M_m is given by:

$$M_m = \{M_1 + M_2(d/t)^2 + M_3(d/t)^4\} g f_\theta / \emptyset \quad (3.32)$$

Where:

---

[15] The bulging correction factor in BS 7910 for a through-wall defect is analogous to the Folias factor used in the through-wall NG-18 equations, both denoted using the letter "M".

[16] The bulging correction factor in BS 7910 for a part-wall defect is analogous to the function M_P (equation (3.5)) used in the part-wall NG-18 equations.

$$M_1 = 1.13 - 0.09(d/c) \quad \text{for} \quad 0 \le d/2c \le 0.5 \quad (3.33)$$

$$M_1 = (c/d)^{0.5}\{1 + 0.04(c/d)\} \quad \text{for} \quad 0.5 < d/2c \le 1 \quad (3.34)$$

$$M_2 = [0.89/\{0.2 + (d/c)\}] - 0.54 \quad \text{for} \quad 0 \le d/2c \le 0.5 \quad (3.35)$$

$$M_2 = 0.2(c/d)^4 \quad \text{for} \quad 0.5 < d/2c \le 1 \quad (3.36)$$

$$M_3 = 0.5 - 1/\{0.65 + (d/c)\} + 14\{1 - (d/c)\}^{24} \quad \text{for} \quad d/2c \le 0.5 \quad (3.37)$$

$$M_3 = -0.11(c/d)^4 \quad \text{for} \quad 0.5 < d/2c \le 1 \quad (3.38)$$

$$g = 1 + \{0.1 + 0.35(d/t)^2\}(1 - \sin\theta)^2 \quad \text{for} \quad d/2c \le 0.5 \quad (3.39)$$

$$g = 1 + \{0.1 + 0.35(c/d)(d/t)^2\}(1 - \sin\theta)^2 \quad \text{for} \quad 0.5 < d/2c \le 1 \quad (3.40)$$

$$f_\theta = \{(d/c)^2 \cos^2\theta + \sin^2\theta\}^{0.25} \quad \text{for} \quad 0 \le d/2c \le 0.5 \quad (3.41)$$

$$f_\theta = \{(c/d)^2 \sin^2\theta + \cos^2\theta\}^{0.25} \quad \text{for} \quad 0.5 < d/2c \le 1 \quad (3.42)$$

$$\emptyset = \{1 + 1.464(d/c)^{1.65}\}^{0.5} \quad \text{for} \quad 0 \le d/2c \le 0.5 \quad (3.43)$$

$$\emptyset = \{1 + 1.464(c/d)^{1.65}\}^{0.5} \quad \text{for} \quad 0.5 < d/2c \le 1 \quad (3.44)$$

For equation (3.32) to apply the following conditions must be satisfied:

$$0 \le d/2c \le 1 \quad (3.45)$$

$$0 \le \theta \le \pi \quad (3.46)$$

$$d/t < 1.25(d/c + 0.6) \quad \text{for} \quad 0 \le d/2c \le 0.1 \quad (3.47)$$

$$d/t < 1.0 \quad \text{for} \quad 0.1 \le d/2c \le 1.0 \quad (3.48)$$

And if $d/2c > 1$ then the solutions for $d/2c = 1$ can be used. θ is an angle along the front of the defect (into the pipe wall thickness) measured from a plane tangential to the pipe surface at the point where the defect is located.

For a part-wall defect M_b is given by:

$$M_b = H_b M_m \quad (3.49)$$

Where M_m is calculated as in equation (3.32) and H_b is calculated using:

$$H_b = H_1 + (H_2 - H_1)\sin^q\theta \quad (3.50)$$

Where:

$$q = 0.2 + (d/c) + 0.6(d/t) \quad \text{for} \quad 0 \le d/2c \le 0.5 \quad (3.51)$$

$$q = 0.2 + (c/d) + 0.6(d/t) \quad \text{for} \quad 0.5 < d/2c \le 1 \quad (3.52)$$

$$H_1 = 1 - 0.34(d/t) - 0.11(d/c)(d/t) \quad \text{for} \quad 0 \le d/2c \le 0.5 \quad (3.53)$$

$$H_1 = 1 - \{0.04 + 0.41(c/d)\}(d/t) + \{0.55 - 1.93(c/d)^{0.75} + 1.38(c/d)^{1.5}\}(d/t)^2$$

$$\text{for} \quad 0.5 < d/2c \le 1 \quad (3.54)$$

$$H_2 = 1 + G_1(d/t) + G_2(d/t)^2 \quad (3.55)$$

Where:

$$G_1 = -1.22 - 0.12(d/c) \quad \text{for} \quad 0 \le d/2c \le 0.5 \quad (3.56)$$

$$G_1 = -2.11 + 0.77(c/d) \quad \text{for} \quad 0.5 < d/2c \le 1 \quad (3.57)$$

$$G_2 = 0.55 - 1.05(d/c)^{0.75} + 0.47(d/c)^{1.5} \quad \text{for} \quad 0 \le d/2c \le 0.5 \quad (3.58)$$

$$G_2 = 0.55 - 0.72(c/d)^{0.75} + 0.14(c/d)^{1.5} \quad \text{for} \quad 0.5 < d/2c \le 1 \quad (3.59)$$

For equation (3.50) to apply the conditions given by equations (3.45), (3.46), (3.47) and (3.48) must be satisfied and if $d/2c > 1$ then the solutions for $d/2c = 1$ can be used.

The reference stress term in the load ratio (equation (3.16)) for a through-wall defect is given by:

$$\sigma_{ref} = M_{Ti}\sigma_m + \frac{2\sigma_b}{3\left(1-\frac{2c}{W}\right)} \quad (3.60)$$

Where:

$$M_{Ti} = \{1 + 1.6(c^2/r_i t)\}^{0.5} \quad (3.61)$$

Where r_i is the internal radius of the pipe (in mm). For a part-wall defect the reference stress is given by:

$$\sigma_{ref} = M_{Si}\sigma_m + \frac{2\sigma_b}{3(1-\alpha'')^2} \quad (3.62)$$

Where:

$$M_{Si} = \frac{1-\{d/(M_{Ti}t)\}}{1-(d/t)} \quad (3.63)$$

$$\alpha'' = \left(\frac{d}{t}\right) / \left(1 + \frac{t}{c}\right) \quad \text{for} \quad W \geq 2(c+t) \quad (3.64)$$

$$\alpha'' = 2\left(\frac{d}{t}\right)\left(\frac{c}{\pi r_i}\right) \quad \text{for} \quad W \leq 2(c+t) \quad (3.65)$$

Where M_{Ti} is given by equation (3.61). In equations (3.60) and (3.62) a factor of 1.2 which occurs in the first term of both equations in BS 7910 has not been applied. This factor was originally introduced in order to increase the level of conservatism in the reference stress solutions for curved shells and therefore a more accurate comparison with the NG-18 equations can be achieved by ignoring it.

The material fracture toughness is calculated using a correlation with the Charpy v-notch energy for a full size specimen. The fracture toughness value used is the minimum of those calculated using the "lower shelf and transitional behaviour" correlation (equation (3.66)) and the "upper limit for fracture toughness" correlation (equation (3.67)):

$$K_{IC} = \left[\left(12\sqrt{C_{vfull}} - 20\right)(25/t)^{0.25}\right] + 20 \quad (3.66)[17]$$

Where C_{vfull} is the lower bound Charpy v-notch impact energy for a full size specimen at the operating temperature of the pipeline (in J) (Anon., 2007b).

$$K_{IC} = 0.54C_{vfull} + 55 \quad (3.67)$$

It is noted that in the PIPIN model the material fracture toughness is not defined by equation (3.66) or (3.67) but instead uses the fracture toughness correlation from the NG-18 equations (equation (3.6))[18].

---

[17] Note that equations (3.66) and (3.67) both calculate the fracture toughness in units of MPa√m. A conversion factor must therefore be applied before they can be used with the stress intensity factor to calculate the Fracture Ratio.

[18] Allowing for a change in the units of E from Nmm^{-2} to GPa.

3.1.1.7 *Applicability of BS 7910 Level 2 Assessment*

BS 7910 and similar defect assessment codes are generic, they are designed to be applicable to any and all metallic structures containing defects. Consequently, there is no limit to the wall thickness of pipelines to which the code can be applied. The range of applicability of BS 7910 with regards to wall thickness is unlimited. In this way the BS 7910 level 2 assessment should be suitable for inclusion in a failure frequency model for thick wall dense phase CO_2 pipelines to define limit state functions for leak / rupture and gouge failure.

3.1.2 *Gouged Dent Models*

Unlike gouge failure, the number of models describing gouged dent failure is large and a full review of each model is beyond the scope of this thesis. This review will provide an overall summary of the models and give descriptions of those which are most relevant to the current work, selected on the basis of their accuracy, level of acceptance within the industry and the amount of information known about them.

The most accepted model in the pipeline industry for describing gouged dent failure is the semi-empirical BGDGFM. The model is recommended by PDAM and the EPRG (Cosham, 2001a). This model is used in the majority of the failure frequency models described in Chapter 2 and is described separately in section 3.1.2.1.

Both empirical and semi-empirical alternatives to the BGDGFM exist. Empirical models are based solely upon a fit to experimental data. Empirical gouged dent models have been developed by (Cosham, 2001a):

- British Gas (Early 1980s)
- EPRG (1995, 2000)
- Battelle (1979, 1986)

The empirical gouged dent models were developed to determine simple criteria for the acceptance of gouged dent defects in pipelines. The models are significantly less accurate in determining the failure conditions of a gouged dent defect than the semi-empirical BGDGFM which was developed specifically for that purpose (Cosham, 2001a). The empirical models are therefore considered to be less suitable for inclusion in a failure frequency model based upon structural reliability methods than the BGDGFM. They have therefore not been considered any further in this work.

Semi-empirical models are based upon a combination of fracture mechanics theory and a fit to experimental data. Alternative semi-empirical models have been developed by (Cosham, 2001a; Jandu, 2008):

- Gasunie (1986)
- British Gas (1997)
- Bai and Song (1997)
- HSE/W.S. Atkins (Late 1990s)
- Advantica (2004)
- AFAA/KAI (2008)

The Gasunie, British Gas (1997) and Bai and Song semi-empirical models are slight variations on the original BGDGFM. Certain elements of the British Gas (1997) and Bai and Song models have not been published and therefore these models cannot be considered for inclusion in a failure frequency model based upon structural reliability methods (Cosham, 2001a). In addition PDAM (Cosham, 2001a) notes that the Gasunie model contains several errors, which would also make it an unsuitable candidate. These models have therefore not been considered any further in this work.

The HSE/W.S. Atkins model is included in the PIPIN failure frequency model. This model is also based on the BGDGFM and is discussed separately in section 3.1.2.3.

Advantica and AFAA/KAI are the most recently published gouged dent models. Many of the team responsible for the Advantica model were also involved in the

development of the AFAA/KAI model; and the AFAA/KAI model builds upon a number of principles considered in the Advantica model. The Advantica model is discussed in section 3.1.2.4. The AFAA/KAI model currently requires further development and validation against experimental data (Jandu, 2008). Consequently it has not been considered any further for this work.

3.1.2.1 *The British Gas Dent-Gouge Fracture Model*

In the Hazard Analysis model, FFREQ, the PIE model and the Cosham model, the limit state function for gouged dent failure is derived from the BGDGFM.

The BGDGFM was developed by British Gas in the early 1980s (Cosham, 2001a). The model was adopted as the standard model for the assessment of gouged dent defects in pipelines by the EPRG. The model is semi-empirical and is based upon a modified version of the Dugdale strip-yield model and series of experimental ring and vessel tests with artificial gouged dent defects created at zero pressure. The majority of the tests were ring tests (111 ring tests and 21 vessel tests). A ring test simulates an infinitely long gouge in an infinitely long dent (Cosham, 2001a).

The BGDGFM is used to determine, based upon the current operating conditions of the pipeline, whether a part-wall gouged dent defect will progress into a through-wall defect. In the model both the gouge and dent are assumed to be axially orientated and infinitely long (a consequence of the experimental data). The gouge is assumed to be located at the deepest point of the dent. The dent is assumed to be of constant width and the gouge is assumed to be of constant depth.

The BGDGFM was calibrated using experimental tests for which the gouged dent damage was created and measured in an unpressurised pipeline. The dent depth used in the model is therefore considered to be the dent depth at zero pressure. If an assessment of a gouged dent defect is required for which the dent depth was measured when the pipeline was pressurised, a re-rounding

correction must be applied to the dent depth before the BGDGFM can be applied.

In SI units, the BGDGFM is given by equation (2.10):

$$\frac{\sigma_H}{\tilde{\sigma}} = \frac{2}{\pi}\cos^{-1}\left[\exp -\left\{113\frac{1.5\pi E}{\tilde{\sigma}^2 Ad}\left[Y_1\left(1-\frac{1.8H}{2R}\right)+Y_2\left(10.2\frac{R}{t}\frac{H}{2R}\right)\right]^{-2}\exp\left[\frac{\ln(0.738C_v)-K_1}{K_2}\right]\right\}\right]$$

Where from equations (2.11), (2.12), (2.13), (2.14), (2.15):

$$\tilde{\sigma} = 1.15\sigma_Y\left(1-\frac{d}{t}\right)$$

$$Y_1 = 1.12 - 0.23\left(\frac{d}{t}\right) + 10.6\left(\frac{d}{t}\right)^2 - 21.7\left(\frac{d}{t}\right)^3 + 30.4\left(\frac{d}{t}\right)^4$$

$$Y_2 = 1.12 - 1.39\left(\frac{d}{t}\right) + 7.32\left(\frac{d}{t}\right)^2 - 13.1\left(\frac{d}{t}\right)^3 + 14.0\left(\frac{d}{t}\right)^4$$

$$K_1 = 1.9$$

$$K_2 = 0.57$$

Note that H in equation (2.10) is the depth of a dent in an unpressurised pipeline. In the Hazard Analysis model and the PIE model the BGDGFM is used (equation (8)) however the dent depth used in those models is (incorrectly) the depth in a pressurised pipeline (as derived from the ERS and UKOPA Fault Databases).

The function $\tilde{\sigma}$ is the plastic collapse stress (in Nmm^{-2}). If the fracture toughness of the pipe material is high (high value of Charpy v-notch impact energy), the failure is dominated by plastic collapse and this term dominates the failure stress predicted by the BGDGFM. Note that this function is the same as the flow stress dependent part-wall NG-18 equation if a gouge of infinite length is assumed and a flow stress defined using equation (3.10):

$$\bar{\sigma} = 1.15\sigma_Y$$

It is noted that because the BGDGFM assumes the gouge is of infinite length, the gouge length is not included in the model. The functions Y_1 and Y_2 are stress intensity magnification factors for membrane and bending stresses for a long surface defect in a flat plate. These functions are included in generic defect assessment codes such as BS 7910 (labelled as M_m and M_b) (Anon., 2007b).

K_1 and K_2 are empirical regression constants derived using the results of experimental ring and vessel tests with artificial gouged dent defects. In these tests, the fracture toughness was measured using 2/3 size Charpy specimens. Consequently, the value of C_V and A in equation (2.10) are for a 2/3 size Charpy specimen. As the BGDGFM was originally derived using imperial units K_1 and K_2 have units of ftlbf.

3.1.2.2 *Applicability of the British Gas Dent-Gouge Fracture Model*

The BGDGFM is semi-empirical, it was calibrated using the experimental results of 111 ring and 21 vessel tests with artificial gouged dent defects created at zero pressure. The tests were carried out by British Gas in 1982. The range of applicability of the BGDGFM with regards to wall thickness can be inferred from the range of wall thicknesses used in the experimental tests to derive it. The range of experimental parameters for the tests is shown in Table 3.3 (Cosham, 2001a):

Parameter	Minimum Value	Maximum Value
Pipe Diameter (mm)	323.9	1066.8
Wall Thickness (mm)	6.6	16.4
Grade (API 5L)	X42	X65
Yield Strength (Nmm^{-2})	348.2	522.6
Tensile Strength (Nmm^{-2})	494.0	577.8
2/3 Charpy V-Notch Impact Energy (J)	15.0	70.5
Dent Depth (H) (mm)	1.9	77.7
Gouge Depth (d) (mm)	0.2	7.9
Burst Stress (% Yield)	7.1	144.9

Table 3.3: British Gas Gouged Dent Ring and Burst Test Parameter Ranges

The parameter ranges in Table 3.3 suggest that the BGDGFM is applicable to pipelines with a wall thickness between 6.6 mm and 16.4 mm.

3.1.2.3 *The PIPIN Gouged Dent Limit State Function*

The method used to model gouged dent failure in the PIPIN failure frequency model is semi-empirical and is detailed in section 2.4.1.3.

Only a limited amount of information is available regarding the origin of the PIPIN gouged dent limit state function. The function appears to be a compilation of 3 different models; it is mainly based upon the BGDGFM but contains additional elements taken from a British Energy R6 rev. 3 assessment and a micro-crack analysis performed by Linkens (Linkens, 1997; Chaplin, 2012). On the basis of the equations described in section 2.4.1.3 it appears that all of the empirical constants used in the function originate with the various models from which it is comprised. In other words, it appears that no empirical calibration of the final 'composite' function to experimental data was performed. It is not known whether the function was validated against the results of experimental tests on pipelines with gouged dent defects. Consequently the accuracy and range of applicability of the function is unknown.

Given its composite nature, it is perhaps likely that the PIPIN gouged dent limit state function is less accurate than other bespoke semi-empirical models such as the BGDGFM. Confirmation of this however would require a detailed comparison with experimental data. The PIPIN limit state has not been considered any further as part of this work, the model is regarded as a slight variation on the BGDGFM and the additional elements it incorporates such as the FAD approach, the plasticity correction factor and micro-cracks are included in the more recent Advantica model, described in the next section.

3.1.2.4 *The Advantica "New Limit State Function"*

In 2004, UKOPA commissioned Advantica to develop a new model to describe gouged dent failure. An assessment of the various methods used for pipeline QRA had suggested that the BGDGFM, which was in use as part of FFREQ, UKOPA's adopted failure frequency model, was "behind the times". It was noted that sophisticated models for other aspects of the QRA process had recently been developed following extensive experimental and theoretical research work. Conversely, the BGDGFM was unchanged following its development in the early 1980s. It was acknowledged that developments had been made in fracture mechanics techniques and in understanding the behaviour of pipeline defects and that improvements to the model could be made. It was also acknowledged that the HSE had already included a more contemporary model using the FAD approach from British Energy R6 rev. 3 as part of their PIPIN failure frequency model (Francis, 2004).

The model developed by Advantica was known as the "New Limit State Function" for the failure of gouged dents. For the purposes of this review it will be referred to as the Advantica model. In developing the Advantica model, the aims were to (Francis, 2004):

- Provide alignment with the assessment techniques used in PIPIN
- Improve modelling of the dent via the inclusion of residual stresses
- Improve modelling of the gouge via the inclusion of micro-cracking

Like PIPIN the model is based upon generic defect assessment codes such as R6 rev. 3 or BS 7910. The assessment of a gouged dent is performed using a FAD approach and therefore closely follows the BS 7910 level 2 assessment methodology described in section 3.1.1.6. In the Advantica model the Fracture Ratio, K_r, is calculated using (Francis, 2004):

$$K_r = \frac{K_I}{K_{IC}} + \rho \qquad (3.68)$$

Where ρ is the plasticity correction factor (introduced with PIPIN in section 2.4.1.3). The Load Ratio, L_r, is calculated using same expression from BS 7910, equation (3.16):

$$L_r = \frac{\sigma_{ref}}{\sigma_Y}$$

The form of the failure assessment curve used in the Advantica model is modified from that used in British Energy R6 rev. 3 and BS 7910 to take into account the work hardening properties of the pipe steel:

$$K_r = \left(1 + 0.5{L_r}^2\right)^{-1/2}\left(0.3 + 0.7\exp\left(-0.6{L_r}^6\right)\right) \quad (3.69)$$

The cut-off point for the value of L_r is given by the ratio of the flow stress to the yield stress:

$$L_{rmax} = \frac{\bar{\sigma}}{\sigma_Y} \quad (3.70)$$

The Advantica model uses the same definition of flow stress as used in the BGDGFM, defined by equation (3.10):

$$\bar{\sigma} = 1.15\sigma_Y$$

In the Advantica model, the circumferential hoop stress is defined using Barlow's formula, equation (2.5):

$$\sigma_H = \frac{PD}{20t}$$

The primary membrane and primary bending stress components (in Nmm^{-2}) are derived from the hoop stress. These are modified from those used for gouge defects in the BS 7910 level 2 assessment, due to the presence of the dent and a micro-crack located at the base of the gouge:

$$\sigma_m^P = \sigma_H\left(1 - 1.8\frac{H}{2R}\right)K_t \quad (3.71)$$

$$\sigma_b^P = 0 \tag{3.72}$$

The gouged dent defect also produces secondary stress contributions (in Nmm^{-2}) given by:

$$\sigma_m^S = (1-\xi)\Phi\left(\frac{H}{2R}\right)\sigma_Y \tag{3.73}$$

$$\sigma_b^S = 10.2\sigma_H \frac{R}{t}\frac{H}{2R}K_t + \xi\Phi\left(\frac{H}{2R}\right)\sigma_Y \tag{3.74}$$

Where ξ is a constant between 0 and 1 and Φ is a function of $H/2R$ given by:

$$\Phi = \frac{H}{2R} \qquad \text{for} \qquad \frac{H}{2R} < \zeta \tag{3.75}$$

$$\Phi = 1 \qquad \text{for} \qquad \frac{H}{2R} \geq \zeta \tag{3.76}$$

Where ζ is a constant. In equations (3.71) and (3.74) the function K_t is a notch stress concentration factor, given by:

$$K_t = 1 + 2\sqrt{d/r_r} \tag{3.77}$$

Where r_r is the radius of the root of the gouge (in mm). The general form of the stress intensity factor (in $Nmm^{-3/2}$), required for the fracture ratio (equation (3.68)) is:

$$K_I = (Y\sigma)\sqrt{\pi a_m} \tag{3.78}$$

Where, a_m, is the depth of the micro-crack (in mm) located at the base of the gouge. In the Advantica model this parameter is preferred to gouge depth, d, as the gouge itself is assumed to be a blunt defect which provides no contribution to the stress intensity factor.

As with a BS 7910 level 2 assessment, the $(Y\sigma)$ term in equation (3.78) is split into components originating from primary and secondary stresses (in Nmm^{-2}) in the structure (equation (3.23)):

$$Y\sigma = (Y\sigma)_P + (Y\sigma)_S$$

The primary stress component is given by:

$$(Y\sigma)_P = \sigma_m^P Y_1\left(a_m/(t-d)\right) \tag{3.79}$$

And the secondary stress component is given by:

$$(Y\sigma)_S = \sigma_m^S Y_1\left(a_m/(t-d)\right) + \sigma_b^S Y_2\left(a_m/(t-d)\right) \tag{3.80}$$

Where:

$$Y_1 = 1.12 - 0.23\left(\frac{a_m}{(t-d)}\right) + 10.6\left(\frac{a_m}{(t-d)}\right)^2 - 21.7\left(\frac{a_m}{(t-d)}\right)^3 + 30.4\left(\frac{a_m}{(t-d)}\right)^4 \tag{3.81}$$

$$Y_2 = 1.12 - 1.39\left(\frac{a_m}{(t-d)}\right) + 7.32\left(\frac{a_m}{(t-d)}\right)^2 - 13.1\left(\frac{a_m}{(t-d)}\right)^3 + 14.0\left(\frac{a_m}{(t-d)}\right)^4 \tag{3.82}$$

Hence the overall stress intensity factor is given by:

$$K_I = \left[(\sigma_m^P + \sigma_m^S)Y_1\left(a_m/(t-d)\right) + \sigma_b^S Y_2\left(a_m/(t-d)\right)\right]\sqrt{\pi a_m} \tag{3.83}$$

The reference stress term in the load ratio (equation (3.16)) is given by:

$$\sigma_{ref} = \frac{\sigma_m^P[1-(d+a_m)/Mt]}{K_t[1-(d+a_m)/t]} \tag{3.84}$$

Where M is the Folias factor defined using the alternative two term expression equation (2.35):

$$M = \sqrt{1 + 0.26\left(\frac{2c}{\sqrt{Rt}}\right)^2}$$

The material fracture toughness (in MPa√m)[19] is calculated using a correlation with the Charpy v-notch energy for a 2/3 size specimen (in J). The correlation was empirically derived using the experimental results of 111 ring and 21 vessel tests with artificial gouged dent defects created at zero pressure performed by British Gas during the development of the BGDGFM:

$$K_{IC} = 3.2{C_v}^{1.1} \quad (3.85)$$

The plasticity correction factor is calculated from equations (2.57), (2.58), (2.59), (2.60) and (2.62), used in PIPIN (taken from BS 7910 and R6 rev. 3):

If $L_r \leq 0.8$ $\quad \rho = \rho_1$

If $0.8 < L_r < 1.05$ $\quad \rho = 4\rho_1(1.05 - L_r)$

If $L_r \geq 1.05$ $\quad \rho = 0$

Where ρ_1 is defined:

$$\rho_1(z) = 0.1z^{0.714} - 0.007z^2 + 0.00003z^5$$

And z is defined:

$$z = \frac{K_{Is}}{K_{Ip}/L_r}$$

Where (in Nmm$^{-3/2}$):

$$K_{Ip} = (Y\sigma)_P\sqrt{\pi a_m} \quad (3.86)$$

$$K_{Is} = (Y\sigma)_S\sqrt{\pi a_m} \quad (3.87)$$

[19] A conversion factor to Nmm$^{-3/2}$ must be applied before the fracture toughness can be used with the stress intensity factor to calculate the Fracture Ratio.

In addition to the fracture toughness correlation given by equation (3.85), fits to the British Gas experimental data were also used to determine the values of several constants which appear in the equations used for the Advantica model. From equations (3.73), (3.74), (3.75) and (3.76), the values of ξ and ζ were set as zero. The gouge radius, r_r, from equation (3.77) was given a value of 0.2 m. An expression for the depth of the micro-crack, a_m, was proposed by assuming a dependence on the amount of remaining wall thickness and plastic straining:

$$a_m = C\left(\frac{d}{t}\right)^{\gamma}\left(\frac{H}{2R}\right)^{\mu} \tag{3.88}$$

Where C (in mm), γ and μ are constants determined from the fit to experimental data. These were given values of:

$$C = 0.023 \tag{3.89}$$
$$\mu = 0.5 \tag{3.90}$$
$$\gamma = 1.5 \tag{3.91}$$

A mean value for the micro-crack depth was determined to be:

$$a_m = 0.4 \text{ mm} \tag{3.92}$$

With a standard deviation of 0.2 mm.

3.1.2.5 *Applicability of the Advantica "New Limit State Function"*

The Advantica model uses contemporary fracture mechanics techniques developed since the publication of the BGDGFM and makes an attempt to model the gouged dent defect more accurately. However the empirical constants used within the model were determined using fits to the same set of experimental data used to calibrate the BGDGFM. It can therefore be concluded that the range of applicability of the Advantica model is the same as that of the BGDGFM. The experimental data comprised of 111 ring and 21 vessel tests with artificial gouged dent defects created at zero pressure. The tests were carried out by British Gas in 1982. A table showing the range of experimental

parameters for the tests is given in section 3.1.2.2 (Table 3.3). The Advantica model is applicable to pipelines with a wall thickness between 6.6 mm and 16.4 mm.

3.2 Historical Operational Data

In the failure frequency models described in Chapter 2, historical operational data is used to derive Incident-Rate values; cumulative probability distributions for the random variables representing gouge and gouged dent damage and; failure frequencies for failures resulting from damage to branches and fittings and drilling operations in-error.

In order to develop a failure frequency model for dense phase CO_2 pipelines using the same methods an appropriate source of historical operational data must be found.

Pipeline failure data is collected by a large number of organisations worldwide. For example:

- In the United States, the Pipeline and Hazardous Material Safety Administration (PHMSA) publishes reports on pipeline failure incidents over the previous 20 years and has recorded failure data since 1970 for gas distribution, gas gathering, gas transmission, hazardous liquid and Liquefied Natural Gas (LNG) Pipelines (Anon., 2015b).
- In Canada, the National Energy Board (NEB) has recorded data on pipeline rupture events since 1972 (Anon., 2014).
- Gas pipeline failures in Europe are recorded by the European Gas Pipeline Incident Data Group (EGIG). The EGIG database contains data from 1970 onwards (Anon., 2011a).
- Oil pipeline failures in Europe are recorded by the COnservation of Clean Air and Water in Europe group (CONCAWE). CONCAWE's database contains data from 1971 onwards (Davis, 2013)

Unfortunately the data required for a failure frequency model is very specific. The number, length, depth and type of individual defects affecting operational pipelines and caused by third party external interference are required; including those which did not lead to a failure.

Considering the sources listed above, PHMSA provides data relating to incident cause only (Anon., 2015b). The NEB gives only the cause along with a brief description of the incident (Anon., 2014). The EGIG database records the size of the damage to the pipeline (hole size), however this is only given using very broad classifications (Anon., 2011a). CONCAWE's main concern lies with pollution and consequently details of the spillage volume and the area of contaminated land are recorded instead of pipeline damage data (Davis, 2013). Additionally only the NEB and CONCAWE provide details of each individual incident as part of their reporting process; PHMSA and EGIG present their data in the form of statistics only. It is also noted that all of the above sources record only details of pipeline failures. Incidents in which the pipe was damaged but did not fail are not considered. The use of failure data from regions other than the United Kingdom also presents issues. Topography and land-use can differ substantially between countries, which could lead to differences in the size and frequency of damage affecting pipelines.

The historical operational data used in the failure frequency models from Chapter 2 originates from either the UKOPA Fault Database or its predecessor the ERS Fault Database. Currently this is the only pipeline fault database which provides sufficient information from which cumulative probability distributions and Incident-Rates suitable for a failure frequency model based on structural reliability methods can be derived.

It is noted that the data contained in the UKOPA and ERS Fault Databases is appropriate for the failure frequency models described in Chapter 2 since its content is concerned specifically with the type of pipelines the failure frequency models are designed for.

In terms of developing a failure frequency model for dense phase CO_2 pipelines operating in the UK, the most appropriate historical operational data to use

would ideally originate only from dense phase CO_2 pipelines. More specifically, the data would concern dense phase CO_2 pipelines with wall thicknesses covering the full range over which the model could potentially be applied. However, since there are currently no dense phase CO_2 pipelines operating in the UK and therefore no historical operational data regarding them a compromise must be made if a failure frequency model is to be developed.

3.3 Failure Models and Historical Operational Data Discussion

Useable models to describe leak / rupture and gouge failure are the NG-18 equations and generic assessment codes such as BS 7910. The DFGM is a more accurate method to describe gouge failure however this model requires its own software and is too complex to include in a failure frequency model based on structural reliability methods.

The range of applicability of the NG-18 equations is between 4.9 mm and 21.9 mm for the through-wall NG-18 equations and between 6.4 mm and 15.6 mm for the part-wall NG-18 equations. The BS 7910 method is not limited by wall thickness. On the basis of the range of applicability of the equations it would appear that a generic assessment method such as BS 7910 would be more appropriate for leak / rupture and gouge failure than the NG-18 equations. The two assessment methods however are compared in more detail in the next chapter, which presents an analysis intended to validate the use of the NG-18 equations for thick wall pipelines outside the wall thickness range given above.

The NG-18 equations make use of the flow stress and the Folias factor. Numerous different expressions for these quantities have been published. The use of a different expression for the Folias factor or flow stress in the NG-18 equations will give slightly different predictions for leak / rupture and gouge failure. It appears that the most appropriate form of the Folias factor to use with the NG-18 equations is the alternative two term expression, which is more accurate than the original two term expression; and can be applied to longer defects, unlike both the original two term expression and the three term expression. In terms of the flow stress, equation (3.11), which is the average of

the yield and tensile stress, is used in BS 7910 and R6 rev. 3 and this is recommended by PDAM for use in the absence of detailed stress and strain data. If the NG-18 equations are to be used in conjunction with the BGDGFM for a failure frequency model however, equation (3.10) should be used to describe the flow stress in order to maintain consistency.

On the basis of accuracy and range of applicability the best models to describe gouged dent failure are the BGDGFM and the Advantica model. The AFAA/KAI model also has potential however this model is not yet completed.

Both the BGDGFM and the Advantica model have the same range of applicability between 6.6 mm and 16.4 mm. The wall thickness of a dense phase CO_2 pipeline could potentially be outside this range of applicability. Due to the complexity of the models and the lack of thick wall experimental data for gouged dents, validation of the BGDGFM or the Advantica model for thick wall pipelines is considered to be outside of the scope of this work. The BGDGFM and the Advantica model however, are currently the best published gouged dent models and in the absence of any alternative a failure frequency model for dense phase CO_2 pipelines must use one of them.

It is concluded and recommended that further research must be done in order to develop a gouged dent model for thick wall pipelines or to validate the current gouged dent models for thick wall pipelines using experiments on thick wall pipes with gouged dent defects.

The Advantica model was developed more recently than the BGDGFM. It includes new fracture mechanics techniques developed since the BGDGFM was published and takes into account additional parameters such as micro-cracking and the plasticity correction factor. The model however was calibrated using the same experimental data as the BGDGFM.

As the two models have the same range of applicability, the choice of which to use in a failure frequency model can be determined by their accuracy. A paper by Seevam et al. (Seevam, 2008) has compared the models using the set of British Gas experimental data which was used to calibrate both. The paper

concluded that the BGDGFM was more accurate than the Advantica model in predicting the failure pressure of a gouged dent defect. It was also noted that although the Advantica model includes a separate micro-cracking parameter, the parameter was empirically derived using the British Gas experimental data for which the presence of micro-cracking would have been extremely unlikely. This casts doubt on the validity of the explicit definition of the micro-crack used. It is noted in PDAM and the Seevam et al. paper that micro-cracking is implicitly described by the BGDGFM in that the gouge depth, d, is assumed to be the total depth comprising of the gouge and any associated micro-cracking.

Taking the above points into consideration it can be concluded that the most appropriate model to use for gouged dent failure at present is the BGDGFM.

The most recent UKOPA Fault Database (2010 at the time of the study) is the most appropriate source of historical operational data to use for a failure frequency model based upon structural reliability methods.

The limitations of the UKOPA Fault Database with regards to thick wall pipelines are acknowledged. However, if the Incident-Rates and probability distributions used within failure frequency models are regularly updated using the most recent version of the UKOPA Fault Database, then the data will eventually become more relevant to dense phase CO_2 pipelines as more of those pipelines are constructed and operated.

Chapter 4. Validation of the NG-18 Equations for Thick Wall Pipelines

In section 3.3 it was noted that the NG-18 equations and generic assessment codes such as BS 7910 are models which could potentially be used to describe leak / rupture and gouge failure in a failure frequency model for dense phase CO_2 pipelines. The applicability of codes such as BS 7910 is not limited by pipeline wall thickness; however the validity of the NG-18 equations in terms of wall thickness would appear to have an upper limit of 21.9 mm for through-wall defects and 15.6 mm for part-wall defects, on the basis of the experimental test data used in their derivation. The wall thickness of a dense phase CO_2 pipeline could potentially be outside this range of applicability. This chapter details a study intended to provide a validation of the applicability of the NG-18 equations to thick wall pipelines.

A definitive assessment as to the applicability of the NG-18 equations to thick wall dense phase CO_2 pipelines would require a detailed numerical analysis including finite element analysis and an experimental test programme. For the purposes of this work, a simpler approach has been proposed which considers a comparison between the components of the NG-18 equations and the components of BS 7910. This comparison can be used to determine whether an increase in pipeline wall thickness introduces effects which are not accounted for by the NG-18 equations. This simple approach can, in principle, be applied because modern linepipe steel has a high toughness. The lower limit of toughness for which this justification is applicable is not currently known and a recommendation has been made for further work.

In addition, the accuracy of the NG-18 equations and a BS 7910 level 2 assessment when compared to experimental data is considered, in order to determine the most appropriate model to use.

4.1 The Potential Importance of Pipeline Wall Thickness

The transportation of dense phase CO_2 by pipeline requires operational pressures in excess of the CO_2 triple point, potentially up to 200 barg when incorporating an appropriate margin to ensure single phase flow. Additionally, a high operating pressure will increase pipeline efficiency. The design pressure requirement necessitates the use of thick wall linepipe in pipeline construction; potentially with dimensions outside of the limits of current operational experience.

The NG-18 equations are semi-empirical and were originally developed using experimental failure data relating predominantly to standard pipeline wall thickness (Cosham, 2002). Consequently, their applicability to thick wall pipelines outside the limits of operational experience is uncertain.

In the context of fracture mechanics, an increase in pipeline wall thickness will result in an increase in both the constraint and the bending stress (illustrated below); and reduce the toughness. The accuracy of the NG-18 equations when applied to thick wall pipelines could therefore be affected. Providing validation for the use of the equations is therefore justified.

An operational pipeline experiences stresses in the axial, radial and hoop directions. The largest of the stresses is the hoop stress. For thin wall pipelines an accurate calculation of the hoop stress can be made using Barlow's formula (equation (2.5)):

$$\sigma_H = \frac{PD}{20t}$$

Where σ_H is the hoop stress (in Nmm^{-2}), P the internal pressure (in barg), D the external pipe diameter (in mm) and t the pipe wall thickness (in mm). The thin wall formula is slightly conservative and assumes that the hoop stress is constant radially through the pipe wall thickness. This is a reasonable approximation for thin wall pipelines.

Thick wall theory predicts that the hoop stress varies through the wall thickness, increasing from the outside to the inside surface. For thick wall pipelines the value of the hoop stress at any radial distance, r (in mm), within the pipe wall is calculated using Lamé's equations (equation (3.19)):

$$\sigma_H = P\frac{{r_i}^2}{{r_0}^2-{r_i}^2}\left(1+\frac{{r_0}^2}{r^2}\right)$$

Where P is the internal pressure (in Nmm^{-2}), r_i is the internal pipe radius (in mm), and r_0 is the external pipe radius (in mm).

The hoop stress through the pipe wall can be considered as a sum of a membrane component and a bending component. The membrane stress is the average stress through the pipe wall thickness and the bending stress is the difference in the total stress. The operational hoop stress through the pipe wall can be linearised into the membrane and bending components (in Nmm^{-2}) using the simple method from BS 7910 detailed in section 3.1.1.6 and given by equations (3.20) and (3.21) (Anon., 2007b):

$$\sigma_m = \frac{\sigma_i+\sigma_0}{2}$$

$$\sigma_b = \frac{\sigma_i-\sigma_0}{2}$$

Equations (3.19), (3.20) and (3.21) show that in standard thin wall pipelines, the bending stress component is small. A pipeline with an external diameter of 610 mm and a wall thickness of 9.5 mm, operating at a pressure of 40 barg would have a membrane stress of 124.45 Nmm^{-2} but a bending stress of only 2 Nmm^{-2}. As the pipeline wall thickness is increased however, the bending stress as a proportion of the total stress increases. Figure 4.1 shows how the bending stress proportion increases with an increase in wall thickness for a 610 mm external diameter pipeline operating at a design factor of 0.72. The total hoop stress in the pipeline remains constant with the influence of the membrane stress decreasing and the influence of the bending stress increasing.

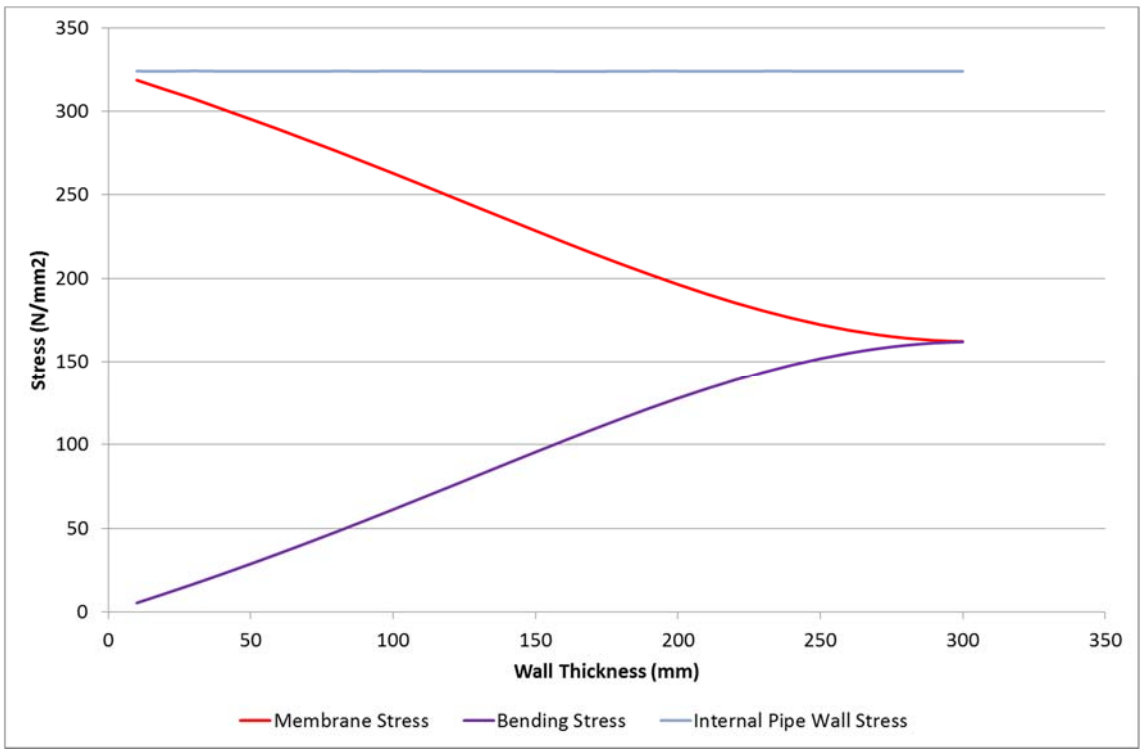

Figure 4.1: Membrane and Bending Stress as a Proportion of Total Hoop Stress Calculated Using Lamé's Formula with Wall Thickness for A 610 mm External Diameter Pipeline Operating at a Design Factor of 0.72

4.2 Failure Model Comparison

This study will provide verification of the applicability of the NG-18 equations to thick wall pipelines in the following way:

- An analysis and comparison of the component parts of the thick wall validated BS 7910 level 2 assessment method and the non-validated **toughness dependent** NG-18 equations will be made in order to show the similarities and differences between the two methods in terms of their basic structure.
- The component parts of each assessment method will then be illustrated graphically in order to show the effect of increased wall thickness.
- On the basis of this analysis, conclusions will be drawn regarding the use of the toughness dependent or flow stress dependent through-wall and part-wall NG-18 equations.

- A comparison will then be made between experimental failure data for thick wall pressure vessels and failure predictions made using the **flow stress dependent** NG-18 equations and BS 7910 in order to show the accuracy of the NG-18 equations when applied to thick wall pipelines.

The first three points outlined above are detailed in section 4.2, with the last point detailed in section 4.3.

It is noted that the justification made using the above approach will only apply if the linepipe steel under consideration is high toughness.

4.2.1 *Failure Model Parameters*

In this section the definitions of quantities such as the flow stress and Folias factor in the NG-18 equations and the particular geometry solutions for BS 7910 level 2 used in the study are stated.

4.2.1.1 *The NG-18 Equations*

For both the through-wall and part-wall NG-18 equations:

The material fracture toughness K_{IC} (in $Nmm^{-3/2}$) is defined as in equation (3.6) (Cosham, 2002):

$$K_{IC}^2 = C_v \frac{1000}{A} E$$

The cross-sectional area of a 2/3 size Charpy specimen is 53.33 mm^2, Young's Modulus of steel is taken to be 210,000 Nmm^{-2}.

As noted in sections 3.1.1.2 and 3.1.1.3 the flow stress and Folias factor can be defined using a number of different expressions. In this study two forms of each have been used.

For the purposes of the comparison between the **toughness dependent** NG-18 equations and the BS 7910 level 2 assessment method, the expressions used are in line with those used in BS 7910. In this instance, the flow stress (in Nmm^{-2}) has been defined using equation (3.11), the average of the yield strength and the tensile strength:

$$\bar{\sigma} = \frac{\sigma_Y + \sigma_U}{2}$$

The Folias factor has been defined as the original two-term expression (equation (2.39)):

$$M = \sqrt{1 + 0.40\left(\frac{2c}{\sqrt{Rt}}\right)^2}$$

For the purposes of the comparison between the **flow stress dependent** NG-18 equations and thick wall experimental data, the expressions used are those which are considered the most appropriate for use in a failure frequency model, as discussed in section 3.3. In this instance, the flow stress has been defined using equation (3.10) in order to be consistent with the BGDGFM:

$$\bar{\sigma} = 1.15\sigma_Y$$

The Folias factor has been defined as the alternative two-term expression applicable to longer defects (equation (2.35)):

$$M = \sqrt{1 + 0.26\left(\frac{2c}{\sqrt{Rt}}\right)^2}$$

For the NG-18 equations the pipe wall hoop stress (in Nmm^{-2}) is calculated using Barlow's formula (equation (2.5)):

$$\sigma_H = \frac{PD}{20t}$$

Where P is the operating pressure (in barg), D is the external diameter of the pipe (in mm) and t is the pipe wall thickness (in mm).

4.2.1.2 *BS 7910 Level 2*

For the BS 7910 level 2 assessment method, the equations used are those given in section 3.1.1.6 for through-wall and part-wall defects (Anon., 2007b).

4.2.2 *Component Analysis*

4.2.2.1 *Equation Analysis*

The NG-18 equations show the lower bound for unacceptable values of pipeline parameters such as pressure, diameter, wall thickness, grade and fracture toughness when a defect is present in a pipeline. This is very similar to the failure assessment line used in BS 7910 which bounds the acceptable values of the brittle fracture and plastic collapse parameters K_r and L_r.

The defect assessment code PD 6493:1991 (Anon., 1991b) is a precursor to BS 7910:2005 and includes a similar defect assessment method to that of BS 7910 level 2. If the equation for the failure assessment diagram in PD 6493 is considered:

$$K_r = S_r \left\{ \frac{8}{\pi^2} \ln \sec \left(\frac{\pi}{2} S_r \right) \right\}^{-0.5} \qquad (4.1)$$

It can be seen that the form of the equation is very similar to that of the toughness dependent NG-18 equations (equations (3.1) and (3.3)):

$$\frac{K_{IC}^2 \pi}{8c\overline{\sigma}^2} = \ln \sec \left(\frac{\pi M \sigma_H}{2\overline{\sigma}} \right)$$

$$\frac{K_{IC}^2 \pi}{8c\overline{\sigma}^2} = \ln \sec \left(\frac{\pi M_P \sigma_H}{2\overline{\sigma}} \right)$$

This is because the NG-18 equations and the FAD in PD 6493 are both based on the Dugdale strip yield model (Dugdale, 1960). Note that in equation (4.1)

which is taken directly from PD 6493, the quantity S_r has been used. This term represents plastic collapse and is similar to the Load Ratio, L_r defined in equation (3.16) but instead uses the flow stress in place of the yield stress. The FAD used in BS 7910 is similar to that of PD 6493 but has a slower decay with respect to L_r to allow different cut off points for different steel types, as seen in Figure 3.1. Figure 4.2 shows a comparison between the FADs in PD 6493 and BS 7910. It is noted that in Figure 4.2 S_r has been converted to L_r by assuming a material grade of L450 (SMYS of 450 Nmm^{-2} and SMUTS of 535 Nmm^{-2}) and the relation:

$$L_r \sigma_Y = S_r \bar{\sigma} \tag{4.2}$$

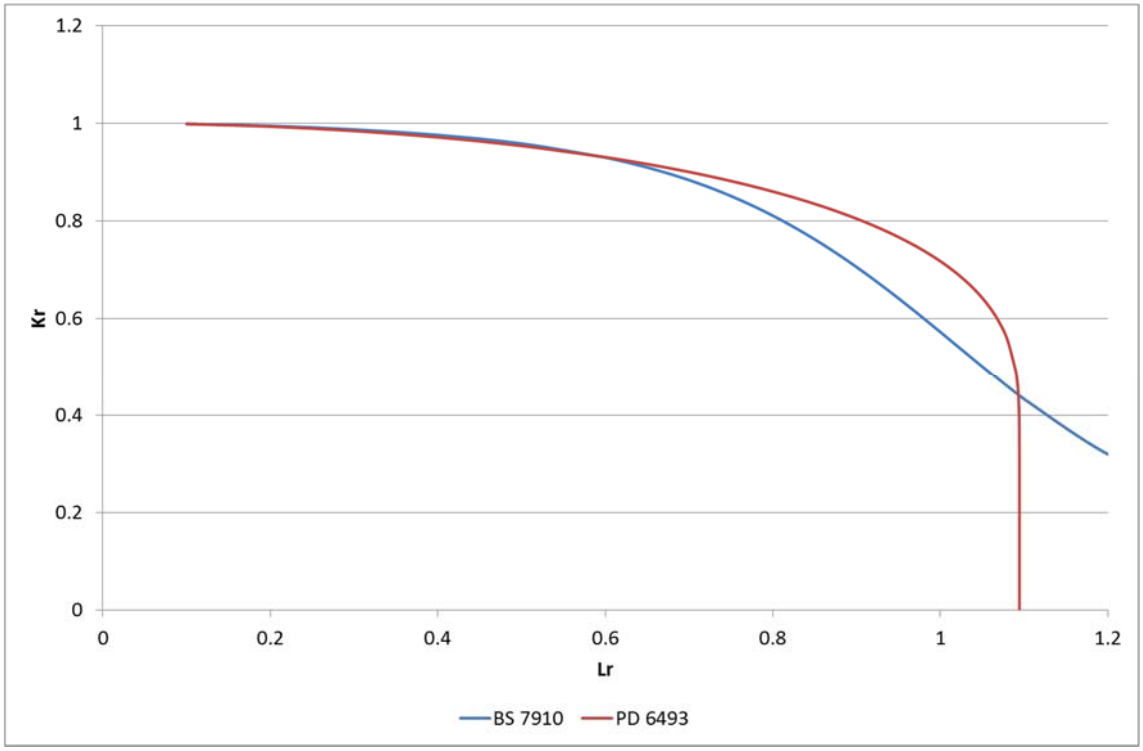

Figure 4.2: Comparison between FADs BS 7910 and PD 6493

Taking this into consideration, the toughness dependent NG-18 equations can be written in terms of a failure assessment line with their own brittle fracture and plastic collapse terms. If we consider the toughness dependent form of the through-wall NG-18 equation (equation (3.1)) this can be rearranged (Cosham, 2012):

$$K_{IC}^2 = c\overline{\sigma}^2 \frac{8}{\pi} \ln\left[\sec\left(\frac{\pi}{2}\left\{\frac{M\sigma_H}{\overline{\sigma}}\right\}\right)\right] \tag{4.3}$$

$$\frac{1}{K_{IC}^2} = \frac{1}{c\overline{\sigma}^2}\left\{\frac{8}{\pi}\ln\left[\sec\left(\frac{\pi}{2}\left\{\frac{M\sigma_H}{\overline{\sigma}}\right\}\right)\right]\right\}^{-1} \quad (4.4)$$

$$\frac{M^2\sigma_H^2\pi c}{K_{IC}^2} = \frac{M^2\sigma_H^2\pi c}{c\overline{\sigma}^2}\left\{\frac{8}{\pi}\ln\left[\sec\left(\frac{\pi}{2}\left\{\frac{M\sigma_H}{\overline{\sigma}}\right\}\right)\right]\right\}^{-1} \quad (4.5)$$

$$\frac{M^2\sigma_H^2\pi c}{K_{IC}^2} = \left\{\frac{M\sigma_H}{\overline{\sigma}}\right\}^2\left\{\frac{8}{\pi^2}\ln\left[\sec\left(\frac{\pi}{2}\left\{\frac{M\sigma_H}{\overline{\sigma}}\right\}\right)\right]\right\}^{-1} \quad (4.6)$$

$$\left\{\frac{M\sigma_H\sqrt{\pi c}}{K_{IC}}\right\}^2 = \left\{\frac{M\sigma_H}{\overline{\sigma}}\right\}^2\left\{\frac{8}{\pi^2}\ln\left[\sec\left(\frac{\pi}{2}\left\{\frac{M\sigma_H}{\overline{\sigma}}\right\}\right)\right]\right\}^{-1} \quad (4.7)$$

$$\left\{\frac{M\sigma_H\sqrt{\pi c}}{K_{IC}}\right\} = \left\{\frac{M\sigma_H}{\overline{\sigma}}\right\}\left\{\frac{8}{\pi^2}\ln\left[\sec\left(\frac{\pi}{2}\left\{\frac{M\sigma_H}{\overline{\sigma}}\right\}\right)\right]\right\}^{-0.5} \quad (4.8)$$

If the left hand side of equation (4.8) is defined as the brittle fracture term, K_r, and the expression $\left\{\frac{M\sigma_H}{\overline{\sigma}}\right\}$ on the right hand side is defined as the plastic collapse term, S_r, then the equation becomes:

$$K_r = S_r\left\{\frac{8}{\pi^2}\ln\sec\left(\frac{\pi}{2}S_r\right)\right\}^{-0.5}$$

The failure assessment line implied within the toughness dependent NG-18 equations is therefore identical to that of PD 6493 (equation (4.1)).

A comparison of the brittle fracture and plastic collapse terms in equation (4.8) with their equivalent definitions in BS 7910, equations (2.40), (3.16), (3.22) and (4.2), implies that:

- The Folias factor, M, in the NG-18 equation is analogous to the function Y in BS 7910
- The hoop stress, σ_H in the NG-18 equation is analogous to the stress state, σ in BS 7910
- The half defect length, c, is analogous to the defect parameter, X, in BS 7910

- The product of the Folias factor and hoop stress in the NG-18 equation, $M\sigma_H$, is analogous to the reference stress, σ_{ref}, in BS 7910

Table 4.1 shows the respective brittle fracture and plastic collapse components of each model:

BS 7910	NG-18
Fracture Ratio	
$K_r = \frac{K_I}{K_{IC}}$	$K_r = \frac{K_I}{K_{IC}}$ (implied by equation (4.8))
Stress Intensity Factor	
$K_I = (Y\sigma)\sqrt{\pi X}$ ($(Y\sigma)$ given by equations in section 3.1.1.6)	$K_I = (M\sigma_H)\sqrt{\pi c}$ (Implied by equation (4.8))
Fracture Toughness	
$K_{IC} = \left[\left(12\sqrt{C_{vfull}} - 20\right)(25/t)^{0.25}\right] + 20$ (Equation (3.66)) $K_{IC} = 0.54C_{vfull} + 55$ (Equation (3.67))	$K_{IC} = \sqrt{C_v \frac{1000}{A} E}$
Load Ratio	
$L_r = \frac{\sigma_{ref}}{\sigma_Y}$	$L_r = \frac{\sigma_{ref}}{\sigma_Y}$ (implied by equation (4.8) and $S_r - L_r$ relationship)
Reference Stress	
$\sigma_{ref} = M_{Ti}\sigma_m + \frac{2\sigma_b}{3\left(1 - \frac{2c}{W}\right)}$ (Equation (3.60))	$\sigma_{ref} = M\sigma_H$ (implied by equation (4.8) and $S_r - L_r$ relationship)

Table 4.1: Brittle Fracture and Plastic Collapse Components from BS 7910 and the Toughness Dependent Through-Wall NG-18 Equation

A similar analysis can be performed using the part-wall NG-18 equation. As the part-wall NG-18 equation simply involves the substitution of the Folias factor with the function M_P (equation (3.5)), this is fairly straightforward. The respective brittle fracture and plastic collapse components from BS 7910 and NG-18 for the part-wall case are shown in Table 4.2 (using the BS 7910 equations described in section 3.1.1.6):

BS 7910	NG-18
Fracture Ratio	
$K_r = \frac{K_I}{K_{IC}}$	$K_r = \frac{K_I}{K_{IC}}$ (implied by equation (3.3) and analysis from equations (4.3) to (4.8))
Stress Intensity Factor	
$K_I = (Y\sigma)\sqrt{\pi X}$ ($Y\sigma$) given by equations in section 3.1.1.6)	$K_I = (M_P\sigma_H)\sqrt{\pi d}$ (implied by equation (3.3) and analysis from equations (4.3) to (4.8))
Fracture Toughness	
$K_{IC} = \left[\left(12\sqrt{C_{vfull}} - 20\right)(25/t)^{0.25}\right] + 20$ (Equation (3.66)) $K_{IC} = 0.54C_{vfull} + 55$ (Equation (3.67))	$K_{IC} = \sqrt{C_v \frac{1000}{A} E}$
Load Ratio	
$L_r = \frac{\sigma_{ref}}{\sigma_Y}$	$L_r = \frac{\sigma_{ref}}{\sigma_Y}$ (implied by equation (3.3), analysis from equations (4.3) to (4.8) and S_r – L_r relationship)
Reference Stress	
$\sigma_{ref} = M_{Si}\sigma_m + \frac{2\sigma_b}{3(1-\alpha'')^2}$ (Equation (3.62))	$\sigma_{ref} = M_P\sigma_H$ (implied by equation (3.3), analysis from equations (4.3) to (4.8) and S_r – L_r relationship)

Table 4.2: Brittle Fracture and Plastic Collapse Components from BS 7910 and the Toughness Dependent Part-Wall NG-18 Equation

In Table 4.1 and Table 4.2 the quantities M_{Ti} and M_{Si} in BS 7910 are based on the Folias factor, using the original two term expression. As noted in section 4.2.1.1 for the purposes of comparison, the same definitions of the Folias factor and the flow stress used in BS 7910 have been used in the NG-18 equations.

It is clear from the analysis that the toughness dependent NG-18 equations and the BS 7910 level 2 assessment method are structurally very similar.

For the through-wall case, both models have similar expressions for the stress intensity factor, K_I, and the reference stress, σ_{ref}. The only difference between these components for BS 7910 and NG-18 is the presence of bending stress terms in the BS 7910 case. The comparisons made in section 4.2.2.2 will show that the effect of the bending terms is small and remains small as the pipeline

wall thickness is increased. It is clear from the analysis that the main source of difference between the two models is the correlation between the material fracture toughness, K_{IC}, and the Charpy v-notch impact energy. The difference in fracture toughness is illustrated in section 4.2.2.2.

For the part-wall case, the function M_P is used in the expressions for the stress intensity factor, K_I, and the reference stress, σ_{ref} for the NG-18 equations. For the reference stress, this function is identical to M_{Si} used in BS 7910. As a result, the reference stress solutions used in each model once again differ only due to the presence of bending stress terms in BS 7910. The comparisons made in section 4.2.2.2 will show that the effect of the bending terms is small and remains small as the pipeline wall thickness is increased. For the stress intensity factor, the presence of M_P is a source of difference between BS 7910 and NG-18. This difference is illustrated in the comparisons in section 4.2.2.2. The correlations between the material fracture toughness, K_{IC}, and the Charpy v-notch impact energy are identical to those in the through-wall case.

4.2.2.2 *Graphical Illustration with Wall Thickness*

In order to illustrate the similarities and differences between the BS 7910 and NG-18 approaches highlighted in section 4.2.2.1 and to show the effect of increased wall thickness, comparisons have been made between the stress intensity factor, K_I, reference stress, σ_{ref} and fracture toughness correlation, K_{IC}, for each model, considering both through-wall and part-wall defects. The comparisons show the variation in each component with increasing wall thickness for a range of defect dimensions.

For each of the comparisons made between the components of the through-wall and part-wall NG-18 equations and the BS 7910 level 2 assessment a single set of pipeline parameters was used. These parameters are shown in Table 4.3:

Input	Value
External Diameter	610 mm
Material Grade	L450
Yield Strength	450 Nmm^{-2}
Tensile Strength	535 Nmm^{-2}
Charpy V-Notch Impact Energy (2/3 Size)	100 (66.67) J

Table 4.3: Pipeline Parameters for NG-18 and BS 7910 Level 2 Comparison

To select a range of reasonable defect dimensions to be used in each comparison case, the UKOPA Fault Database (Anon., 2011c) was consulted. As noted in section 3.2 this database contains information on specific defect dimensions for third party external interference damage incidents affecting gas and liquid pipelines in the UK. The dimensions of three through-wall defects and three part-wall defects were chosen directly from the database with the intention that these would provide a sample of defects which could realistically be expected to occur. It is assumed that the defect dimensions (length and depth) are independent of the dimensions of the pipeline in which they are located. The dimensions of the through-wall and part-wall defects taken from the UKOPA Fault Database are shown in Table 4.4 and Table 4.5:

Defect No.	Length (mm)
1	203
2	89
3	5

Table 4.4: Through-Wall Defect Dimensions for NG-18 and BS 7910 Level 2 Comparison

Defect No.	Length (mm)	Depth (% wall thickness)
1	1350	14
2	480	54
3	20	63

Table 4.5: Part-Wall Defect Dimensions for NG-18 and BS 7910 Level 2 Comparison

Through-Wall Defects

For through-wall defects the comparison has been performed using the three defects listed in Table 4.4. with pipeline parameters from Table 4.3. In order to counteract the effect of a reduction in the hoop stress in the pipe wall with an increase in wall thickness, the pressure has also been varied such that the stress at the internal pipe wall (calculated using Lamé's equation for the hoop stress in a thick wall cylinder) always remains at a value of 0.72 of the yield strength of the pipeline, a value of 324 Nmm^{-2}. For BS 7910, the specific equations used for the stress intensity factor, fracture toughness correlation[20] and reference stress are the same as those listed for the through-wall case in section 3.1.1.6. The equations used for NG-18 are listed in Table 4.1. The results of the investigation are shown in Figure 4.3, Figure 4.4 and Figure 4.5 and are presented as the ratio of the value calculated using BS 7910 to the value calculated using the NG-18 equations. If the ratio is greater than one then the value calculated using BS 7910 is smaller, and if it is less than one then the value calculated using BS 7910 is larger.

[20] In line with the BS 7910 level 2 assessment method the units for the fracture toughness have been changed from $MPa\sqrt{m}$ to $Nmm^{-3/2}$ for the comparison.

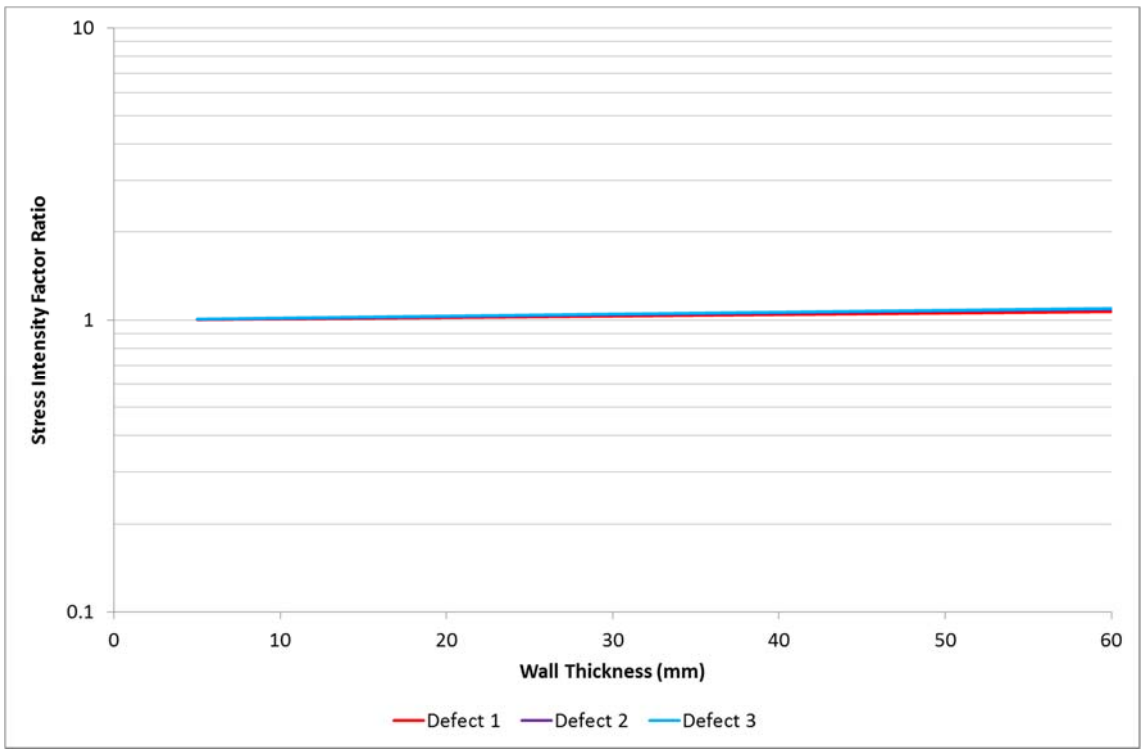

Figure 4.3: Stress Intensity Factor Ratio of NG-18 and BS 7910 Level 2 with Increasing Wall Thickness for Three Different Axial Through-Wall Defects

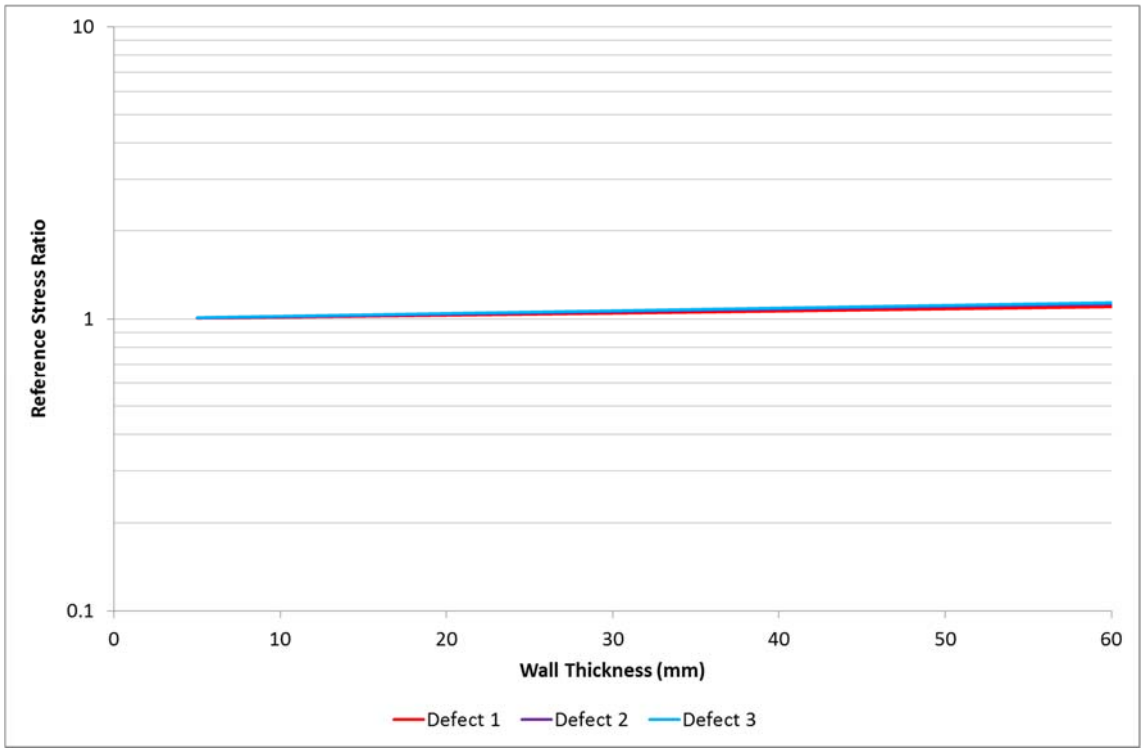

Figure 4.4: Reference Stress Ratio of NG-18 and BS 7910 Level 2 with Increasing Wall Thickness for Three Different Axial Through-Wall Defects

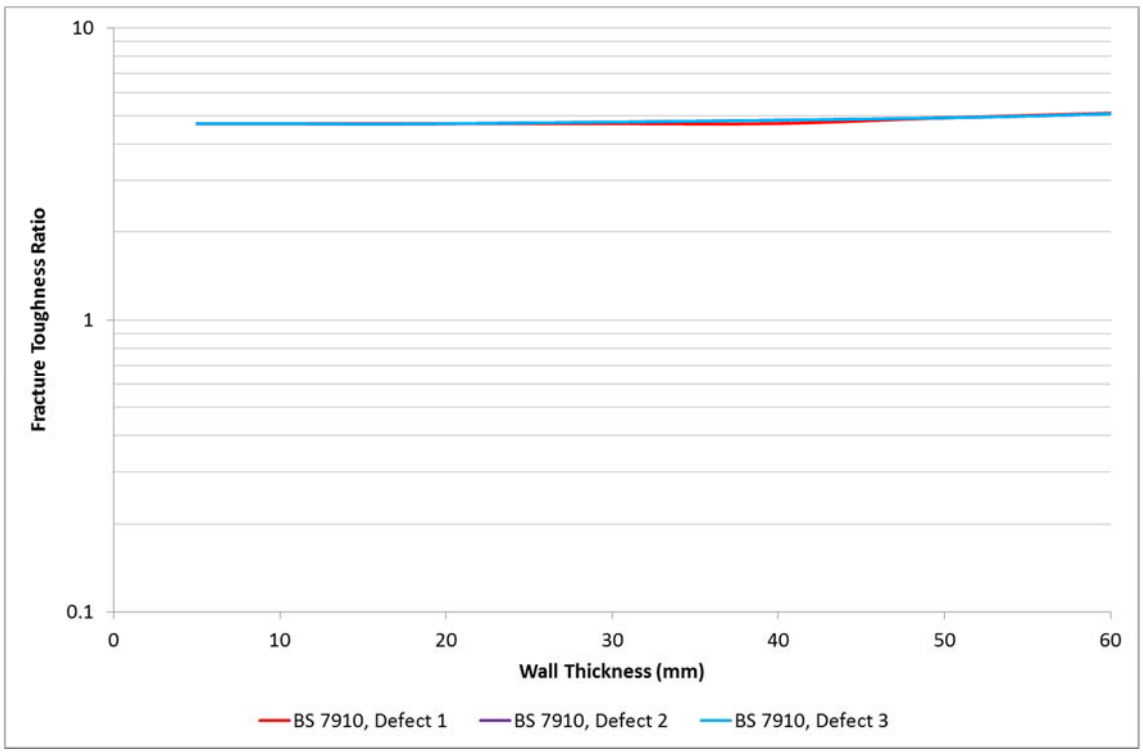

Figure 4.5: Fracture Toughness Ratio of NG-18 and BS 7910 Level 2 with Increasing Wall Thickness for Three Different Axial Through-Wall Defects

The proximity of the data to unity in Figure 4.3 and Figure 4.4 illustrates the similarity between the stress intensity factors and reference stress solutions used in the through-wall NG-18 equations and BS 7910 level 2. Almost exactly the same values are produced for each of the three defects investigated. It is noted that the presence of the bending terms in the BS 7910 assessment produces negligible difference at low wall thickness. As the wall thickness and bending stress increase the bending stress terms lead to a slightly increasing difference between the two models, however this difference remains very small as the wall thickness approaches 60 mm. The difference is shown by the data diverging from unity.

Figure 4.5 shows that the fracture toughness correlation used in the through-wall NG-18 equation gives substantially different values for fracture toughness than the correlation used for BS 7910 level 2. In this chart the results for each defect are overlaid as the toughness correlation is independent of defect dimensions. The toughness values calculated in the NG-18 equation are over four times as large as those from BS 7910. As was shown in section 4.2.2.1, this is the largest source of differences between BS 7910 and NG-18 in the through-wall case.

Figure 4.3, Figure 4.4 and Figure 4.5 together show that an increase in wall thickness produces only a very small difference between the two models. It is illustrated that the largest difference between the models is due to the difference in the fracture toughness correlation. It is noted that the fracture toughness correlation used in the toughness dependent NG-18 equation was derived empirically using the results of full scale tests on thin wall pipe sections and may not be applicable to thick wall pipelines. Verification of the application of the toughness dependent through-wall NG-18 equation would therefore require a detailed numerical analysis including finite element analysis and an experimental test programme. However, if the linepipe used in pipeline construction is very tough then defect failure is controlled by plastic collapse rather than brittle fracture. The flow stress dependent through-wall NG-18 equation would be the most appropriate form of NG-18 equation to apply for high toughness steel. In a plastic collapse failure, the fracture toughness, by definition, has no effect. Furthermore, the flow stress dependent form of the NG-18 equation does not include a fracture toughness correlation. Therefore for high toughness steel, the main source of contention regarding the application of the NG-18 equation to thick wall pipelines is negated. It is therefore concluded that in principle, the flow stress dependent through-wall NG-18 equation would be suitable for application to thick wall pipelines, provided the pipe material was of a high toughness.

The lower limit of toughness for which this justification is applicable is not currently known. It is therefore recommended that further work is carried out in order to determine the toughness at which it is acceptable to ignore the effect of fracture toughness and brittle fracture.

Part-Wall Defects

Similarly, for part-wall defects a comparison has been performed using the three defects listed in Table 4.5 with pipeline parameters from Table 4.3. In order to counteract the effect of a reduction in the hoop stress in the pipe wall with an increase in wall thickness the pressure has also been varied such that the stress at the internal pipe wall (calculated using Lamé's equation for the hoop stress in a thick wall cylinder) always remains at a value of 0.72 of the

yield strength of the pipeline, a value of 324 Nmm^{-2}. For BS 7910, the specific equations used for the stress intensity factor, fracture toughness correlation[21] and reference stress are the same as those listed for the part-wall case in section 3.1.1.6. The equations used for NG-18 are listed in Table 4.2. The results are shown in Figure 4.6 and Figure 4.7 and are presented as the ratio of the value calculated using BS 7910 to the value calculated using the NG-18 equations. If the ratio is greater than one then the value calculated using BS 7910 is smaller, and if it is less than one then the value calculated using BS 7910 is larger. The comparison for fracture toughness correlation has not been shown as this is identical to that of Figure 4.5.

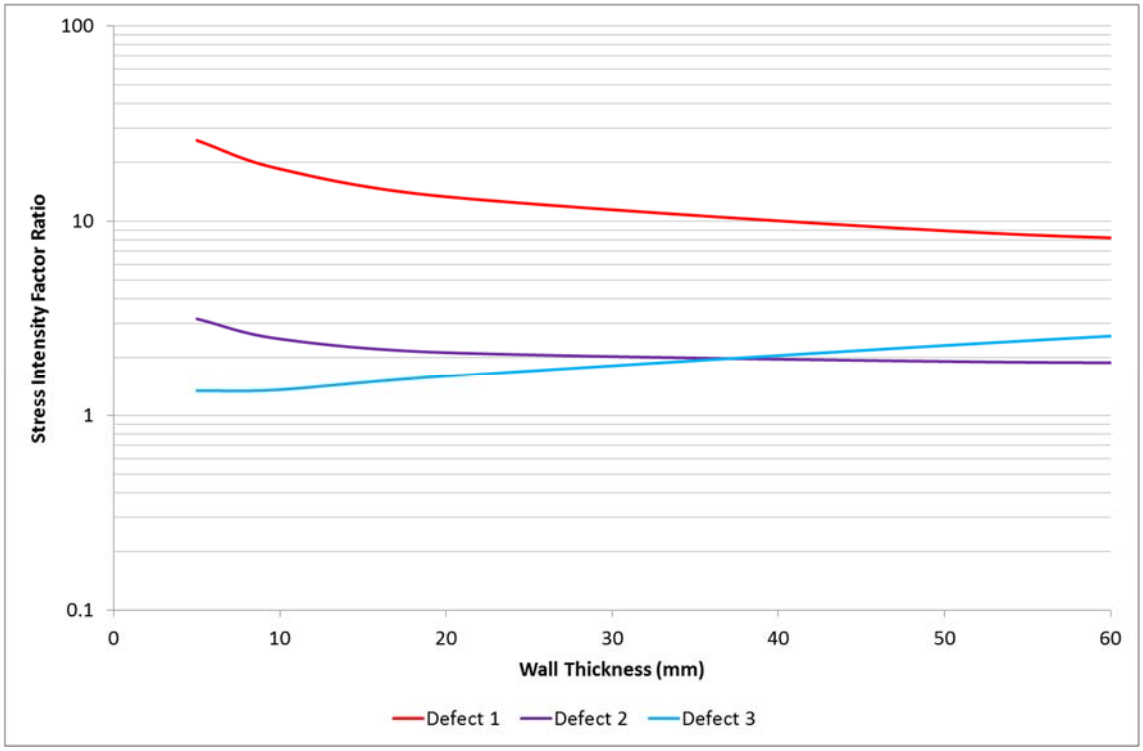

Figure 4.6: Stress Intensity Factor Ratio of NG-18 and BS 7910 Level 2 with Increasing Wall Thickness for Three Different Axial Part-Wall Defects

[21] In line with the BS 7910 level 2 assessment method the units for the fracture toughness have been changed from MPa√m to $Nmm^{-3/2}$ for the comparison.

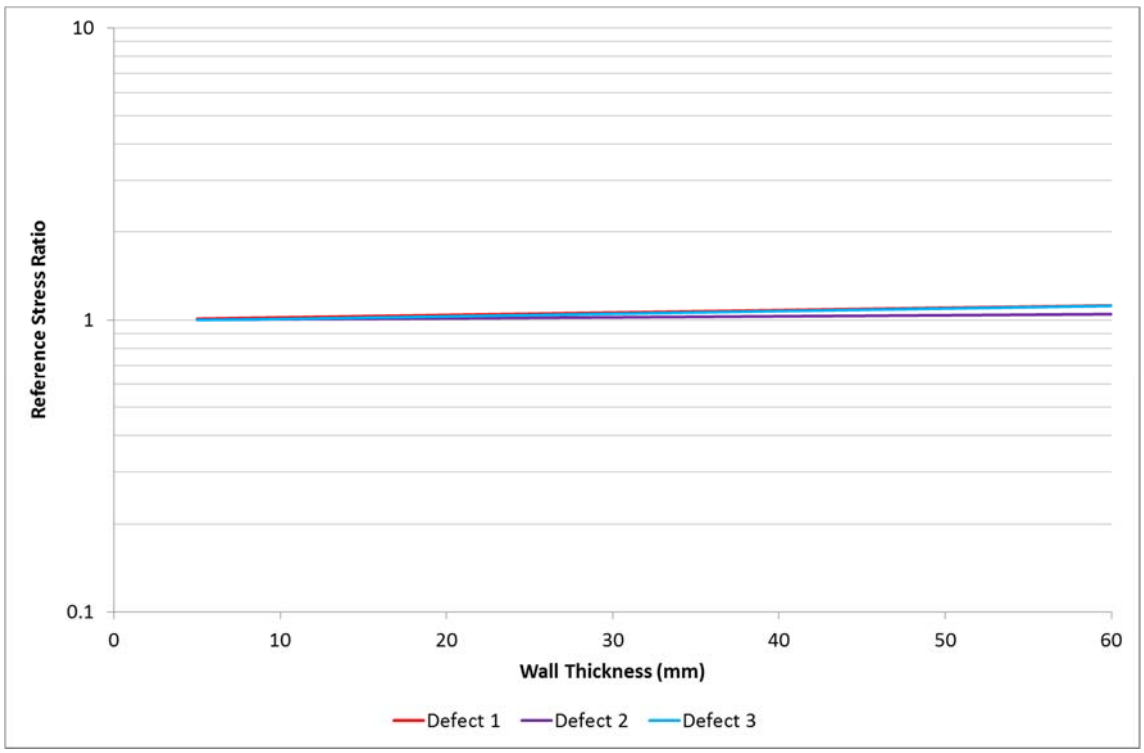

Figure 4.7: Reference Stress Ratio of NG-18 and BS 7910 Level 2 with Increasing Wall Thickness for Three Different Axial Part-Wall Defects

As can be seen from Figure 4.6, the presence of the function M_P in the part-wall NG-18 equation produces a large difference between the BS 7910 and NG-18 stress intensity factors. Defect 1, which is long and shallow, shows the greatest difference between the two models, the NG-18 stress intensity factor is over seven times as large as BS 7910's equivalent value for all wall thickness values considered. As the defect length is reduced and the defect depth increased the difference between the NG-18 and BS 7910 values is reduced. From the defects considered it is not possible to identify the cause because both the length and the depth are changing when moving from defect 1 through to defect 3. The shortest and deepest defect shows the closest agreement in stress intensity factor between the two models however the difference here is still considerable. Defect 3 also displays an opposite trend to that of the other two defects with increasing wall thickness. In this case the stress intensity factors become more different as pipeline wall thickness is increased.

The proximity of the data to unity in Figure 4.7 illustrates the similarity between the reference stress solutions used in the through-wall NG-18 equations and BS 7910 level 2. Almost exactly the same values are produced for each of the three defects investigated. It is noted that the presence of the bending terms in the

BS 7910 assessment produces negligible difference at low wall thickness. As the wall thickness and bending stress increase the bending stress terms lead to a slightly increasing difference between the two models, however this difference remains very small as the wall thickness approaches 60 mm. The difference is shown by the data diverging from unity.

In the part-wall case, the differences between the two models lie in the fracture toughness correlation (as in Figure 4.5) and the stress intensity factors. As both of these factors contribute to the approach to brittle failure then it is demonstrated that it is the fracture toughness dependence and not the approach to plastic collapse that is responsible for the differences. As noted for the through-wall case, if the linepipe used in pipeline construction is very tough then defect failure is controlled by plastic collapse rather than brittle fracture. Therefore, the **flow stress dependent** part-wall NG-18 equation would then be the most appropriate form of the NG-18 equation to apply for high toughness steel. This form of the NG-18 equation does not include a brittle fracture, toughness dependent component. Therefore for high toughness steel, the main source of contention regarding the application of the NG-18 equation to thick wall pipelines is negated. It is therefore concluded that in principle, the flow stress dependent part-wall NG-18 equation would be suitable for application to thick wall pipelines, provided the pipe material was of a high toughness.

The lower limit of toughness for which this justification is applicable is not currently known. It is therefore recommended that further work is carried out in order to determine the toughness at which it is acceptable to ignore the effect of fracture toughness and brittle fracture.

4.3 Comparison with Real Failure Data

In section 4.2 it was shown that the largest source of the difference between the NG-18 equations (which are validated for thin wall pipelines) and the BS 7910 level 2 assessment (which is validated for thin and thick wall pressure vessels) are the different expressions for brittle fracture behaviour. It was also noted that by imposing a high toughness requirement on linepipe steel, the effect of

fracture toughness on defect failure would be negated. It was therefore concluded that the flow stress dependent NG-18 equations would, in principle, be a suitable method to apply to thick wall pipelines, provided that the pipe material was of a high toughness.

However, in order to satisfactorily determine the accuracy of the flow stress dependent NG-18 equations when applied to thick wall pipelines, a comparison between predicted values of failure pressure and experimental test data is required.

In this section the accuracy of the predictions from both models will be compared with through-wall and part-wall defect burst tests on thick wall pipe sections and pressure vessels taken from a search of available literature.

It is noted that for this section the comparison is between each model and experimental data not between the models themselves. Taking this into consideration, the expressions used in the NG-18 equations for the flow stress and Folias factor are those which are considered the most appropriate for use in a failure frequency model, as discussed in section 3.3. The NG-18 equations in this form represent how they would be used in practice. This requires replacing the Folias factor with the alternative two term approximation applicable to larger defects (equation (2.35)):

$$M = \sqrt{1 + 0.26\left(\frac{2c}{\sqrt{Rt}}\right)^2}$$

And the flow stress with the form used in the BGDGFM (equation (3.10)):

$$\bar{\sigma} = 1.15\sigma_Y$$

The BS 7910 level 2 assessment method remains as outlined in section 3.1.1.6.

4.3.1 *Through-Wall Defects*

4.3.1.1 *Through-Wall Failure Data*

The experimental failure data available for burst tests of through-wall defects on thick wall vessels originates from Sturm and Stoppler in 1985 (Sturm, 1990; Cosham, 2002; Staat, 2004).

Three tests were performed on vessels constructed from 20 MnMoNi 55 grade manganese-molybdenum-nickel alloy steel and one test was performed on a vessel constructed from 22 NiMoCr 37 mod nickel-molybdenum-chromium alloy steel. Details of the vessels and tests are summarised in Table 4.6.

Input	Value
External Diameter (mm)	798
Wall Thickness (mm)	47.2
Material Grade	20 MnMoNi 55, 22 NiMoCr 37 mod
Yield Strength (Nmm^{-2})	428, 417
Tensile Strength (Nmm^{-2})	605, 622
Charpy V-Notch Impact Energy (J) Full-Size	150, 50
Defect Length Range ($2c$) (mm)	650 – 1105

Table 4.6: Thick Wall, Through-Wall Burst Test Vessel Details, Sturm and Stoppler, 1985

Data from burst tests of through-wall defects on thin wall vessels have also been included in order to provide a comparison. This data originates from Battelle in 1973 (Kiefner, 1973; Cosham, 2002). Data from 90 burst tests of through-wall defects on thin wall pressure vessels has been included. These tests were performed for a range of different vessels and parameters. Details are summarised in Table 4.7:

Input	Value
External Diameter Range (mm)	168 – 1219
Wall Thickness Range (mm)	4.9 – 21.9
Yield Strength Range (Nmm^{-2})	220 – 735
Tensile Strength Range (Nmm^{-2})	338 – 908
Charpy V-Notch Impact Energy (J) Full-Size	20 – 136
Defect Length Range ($2c$) (mm)	25 – 508

Table 4.7: Thin Wall, Through-Wall Burst Test Vessel Details, Kiefner et al., 1973

4.3.1.2 *Failure Data Comparison*

A comparison has been made between the actual failure pressures for the set of axial through-wall defects in thick wall pressure vessels, reported by Sturm and Stoppler in 1985 and summarised in Table 4.6; and those predicted for the same set of defects by the through-wall NG-18 equation and a BS 7910 level 2 assessment. The results are shown in Figure 4.8 with the failure stress as a percentage of the yield stress. For BS 7910 the failure stress is assumed to be the stress on the internal pipe wall at the failure pressure and has been calculated using Lamé's equation for the hoop stress in a thick wall pressure vessel. For the NG-18 equation the failure stress is assumed to be the hoop stress at the failure pressure as calculated using Barlow's formula.

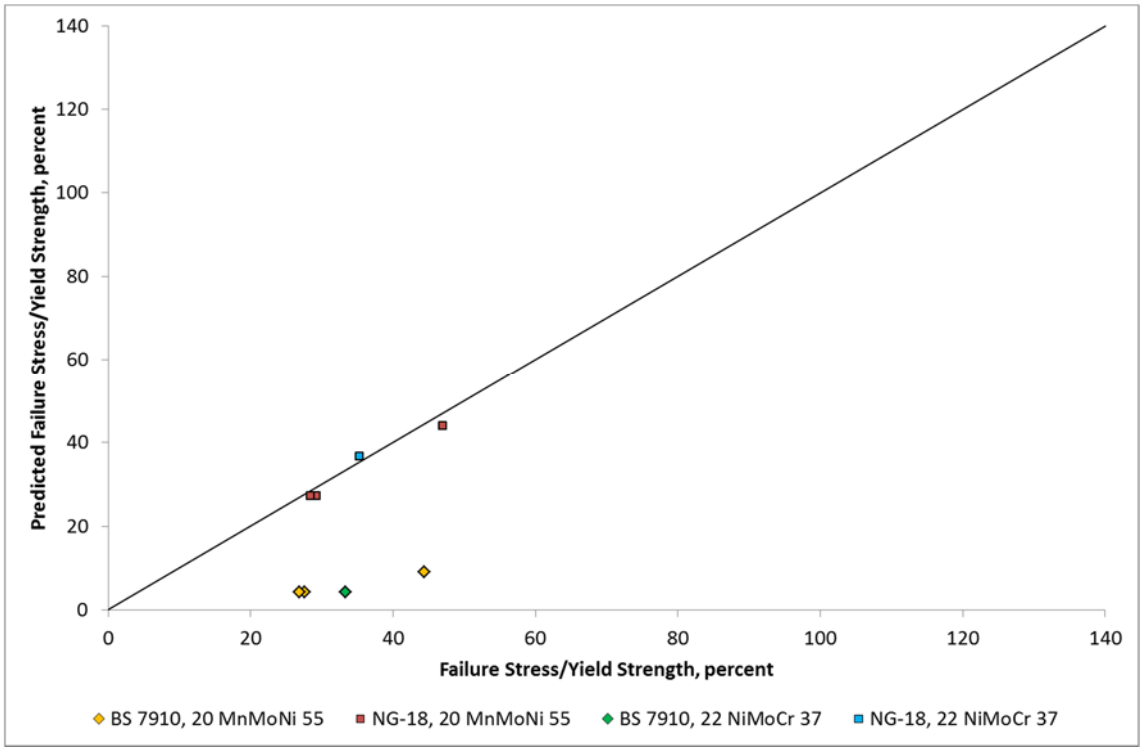

Figure 4.8: Predicted versus Actual Failure Stress for Axial Through-Wall Defects in Thick Wall Pipe Sections According to NG-18 and BS 7910 Level 2, Sturm and Stoppler

Figure 4.9 shows the same data from Figure 4.8 and also includes the results of the burst tests on axial through-wall defects in thin wall pressure vessels from Battelle in 1973, summarised in Table 4.7.

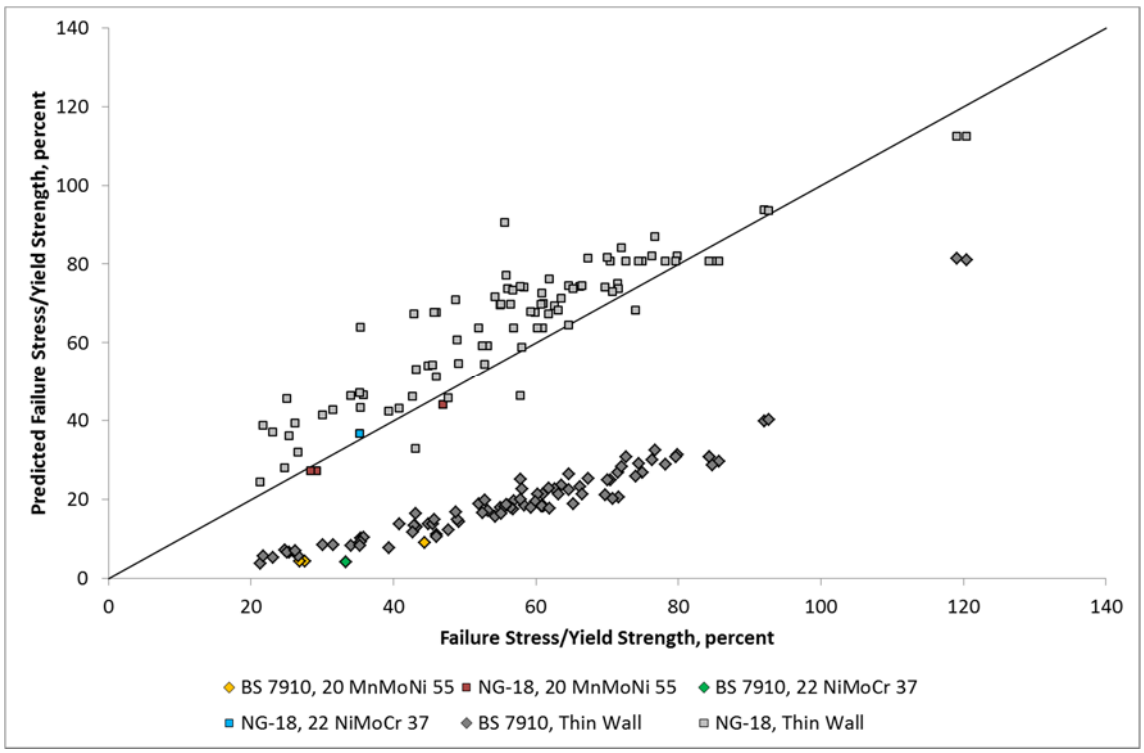

Figure 4.9: Predicted versus Actual Failure Stress for Axial Through-Wall Defects in Thick and Thin Wall Pipe Sections According to NG-18 and BS 7910 Level 2, Sturm and Stoppler, Kiefner et al.

In Figure 4.8 and Figure 4.9 data points which lie below the line of unity are conservative, with the model predicting a failure stress below that of the experimental failure stress. Conversely, data points which lie above the line of unity are non-conservative. The closer data points are to the line of unity, the more accurate the prediction of failure stress.

Figure 4.8 implies that the predictions of BS 7910 are more conservative than those of NG-18. The failure stresses calculated by NG-18 are approximately four to eight times as large as those calculated by BS 7910 for the experimental cases considered. Figure 4.8 shows that the flow stress dependent NG-18 equation is the most accurate of the two models in calculating predictions of pipeline failure stress for through-wall defects in thick wall pipelines.

Figure 4.9 includes the thin wall failure data from which the NG-18 equations were originally calibrated. It is clear that for NG-18, the thick wall data is contained within the scatter of the data points of the thin wall data.

Figure 4.8 and Figure 4.9 suggest that the flow stress dependent NG-18 equation is a valid model for through-wall defects in pipelines up to at least 47.2 mm wall thickness, provided that the toughness is high.

On the basis of the accuracy of the two models it can be concluded that the flow stress dependent through-wall NG-18 equation is the most appropriate model to use to describe leak / rupture in a failure frequency model for dense phase CO_2 pipelines.

4.3.2 *Part-Wall Defects*

4.3.2.1 *Part-Wall Failure Data*

The experimental failure data available for burst tests of part-wall defects on thick wall vessels originates from Eibner in 1971 (Staat, 2004), Wellinger and Sturm in 1971 (Wellinger, 1971; Staat, 2004), Sturm and Stoppler in 1985 (Sturm, 1990; Cosham, 2002; Staat, 2004), Keller in 1990 (Keller, 1987; Cosham, 2002; Staat, 2004) and Demofonti et al. in 2001 (Demofonti, 2000; Cosham, 2002; Staat, 2004).

As reported by Eibner, four tests were performed on vessels constructed from A 106 B grade steel, two tests were performed on vessels constructed from Type 316 steel and one test was performed on a vessel constructed from A 316 steel. Details of the vessels and tests are summarised in Table 4.8. It should be noted that for the Eibner data there was no information available on the internal/external classification of the part-wall defects. Due to the practicalities of machining part-wall defects in a vessel, the defects have been assumed to be external. It should also be noted that the Charpy v-notch impact energy values were not given for two of the tests. Values of 81 J and 200 J were assumed for these tests, which are in line with values from the rest of the data.

Input	Value
External Diameter (mm)	609.6
Wall Thickness Range (mm)	38.1 – 43.7
Material Grade	A 106 B, Type 316, A 316
Yield Strength (Nmm^{-2})	155, 241
Tensile Strength (Nmm^{-2})	426, 570
Charpy V-Notch Impact Energy (J) Full-Size Range	81 – 200
Defect Length Range ($2c$) (mm)	76 – 361
Defect Depth Range (d) (% wall thickness)	47 – 88

Table 4.8: Thick Wall, Part-Wall Burst Test Vessel Details, Eibner 1971

As reported by Wellinger and Sturm, 23 tests were performed on vessels constructed from St 35 grade steel and two tests were performed on vessels constructed from FB 70 grade steel. Details of the vessels and tests are summarised in Table 4.9. It should be noted that for the Wellinger and Sturm data the Charpy v-notch impact energy values were not given for 24 of the tests. Values of 56 J were assumed for 22 of the tests and 71 J for the remaining two, in line with values from the rest of the data.

Input	Value
External Diameter (mm)	88.9
Wall Thickness (mm)	22.2
Material Grade	St 35, FB 70
Yield Strength Range (Nmm^{-2})	199 – 473
Tensile Strength Range (Nmm^{-2})	438 – 614
Charpy V-Notch Impact Energy (J) Full-Size Range	56 – 71
Defect Length Range ($2c$) (mm)	40.5 – 123
Defect Depth Range (d) (% wall thickness)	18.9 – 88.7

Table 4.9: Thick Wall, Part-Wall Burst Test Vessel Details, Wellinger and Sturm 1971

As reported by Sturm and Stoppler, four tests were performed on vessels constructed from 20 MnMoNi 55 grade steel and three tests were performed on vessels constructed from 22 NiMoCr 37 grade steel. Details of the vessels and tests are summarised in Table 4.10.

Input	Value
External Diameter (mm)	797.9, 793.9
Wall Thickness (mm)	47.2
Material Grade	20 MnMoNi 55, 22 NiMoCr 37
Yield Strength (Nmm^{-2})	428, 417
Tensile Strength (Nmm^{-2})	622, 605
Charpy V-Notch Impact Energy (J) Full-Size	150, 50
Defect Length Range ($2c$) (mm)	709 – 1500
Defect Depth Range (d) (% wall thickness)	74 – 81

Table 4.10: Thick Wall, Part-Wall Burst Test Vessel Details, Sturm and Stoppler 1985

As reported by Keller, two tests were performed on vessels constructed from 34 CrMo 4 grade steel. Details of the vessels and tests are summarised in Table 4.11.

Input	Value
External Diameter (mm)	564.8, 565.4
Wall Thickness (mm)	20.4, 21.7
Material Grade	34 CrMo 4
Yield Strength (Nmm^{-2})	878, 866
Tensile Strength (Nmm^{-2})	990, 979
Charpy V-Notch Impact Energy (J) Full-Size	64, 65
Defect Length ($2c$) (mm)	48, 32.5
Defect Depth (d) (% wall thickness)	78.9, 66.8

Table 4.11: Thick Wall, Part-Wall Burst Test Vessel Details, Keller 1990

As reported by Demofonti et al., two tests were performed on vessels constructed from API 5L X100 grade steel. Details of the vessels and tests are summarised in Table 4.12. It should be noted that for the Demofonti data there was no information available on the internal/external classification of the part-wall defects. Due to the practicalities of machining part-wall defects in a vessel, the defects have been assumed to be external.

Input	Value
External Diameter (mm)	1422.4
Wall Thickness (mm)	19.25, 20.1
Material Grade	API 5L X100
Yield Strength (Nmm^{-2})	740, 795
Tensile Strength (Nmm^{-2})	774, 840
Charpy V-Notch Impact Energy (J) 2/3-Size	261, 171
Defect Length ($2c$) (mm)	180, 385
Defect Depth (d) (% wall thickness)	54, 18.9

Table 4.12: Thick Wall, Part-Wall Burst Test Vessel Details, Demofonti et al. 2001

Data from burst tests of part-wall defects on thin wall vessels has also been included in order to provide a comparison. This data originates from Battelle in 1973 (Kiefner, 1973; Cosham, 2002). Data from 33 burst tests of part-wall defects on thin wall pressure vessels has been included. These tests were performed for a range of different vessels and parameters. Details are summarised in Table 4.13.

Input	Value
External Diameter Range (mm)	762 – 1067
Wall Thickness Range (mm)	9.1 – 15.6
Yield Strength Range (Nmm^{-2})	379 – 510
Tensile Strength Range (Nmm^{-2})	531 – 634
Charpy V-Notch Impact Energy (J) Full-Size	24 – 69
Defect Length Range ($2c$) (mm)	64 – 610
Defect Depth Range (d) (% wall thickness)	25 – 92

Table 4.13: Thin Wall, Part-Wall Burst Test Vessel Details, Kiefner et al., 1973

4.3.2.2 *Failure Data Comparison*

A comparison has been made between the actual failure pressures for the set of axial part-wall defects in thick wall pressure vessels, reported by Eibner in 1971, Wellinger and Sturm in 1971, Sturm and Stoppler in 1985, Keller in 1990 and Demofonti et al. in 2001, summarised in Table 4.8 to Table 4.12; and those predicted for the same set of defects by the part-wall NG-18 equation and a BS 7910 level 2 assessment. The results are shown in Figure 4.10 and Figure 4.11

with the failure stress as a percentage of the yield stress. For BS 7910 the failure stress is assumed to be the stress on the internal pipe wall at the failure pressure and has been calculated using Lamé's equation for the hoop stress in a thick wall pressure vessel. For the NG-18 equation the failure stress is assumed to be the hoop stress at the failure pressure as calculated using Barlow's formula.

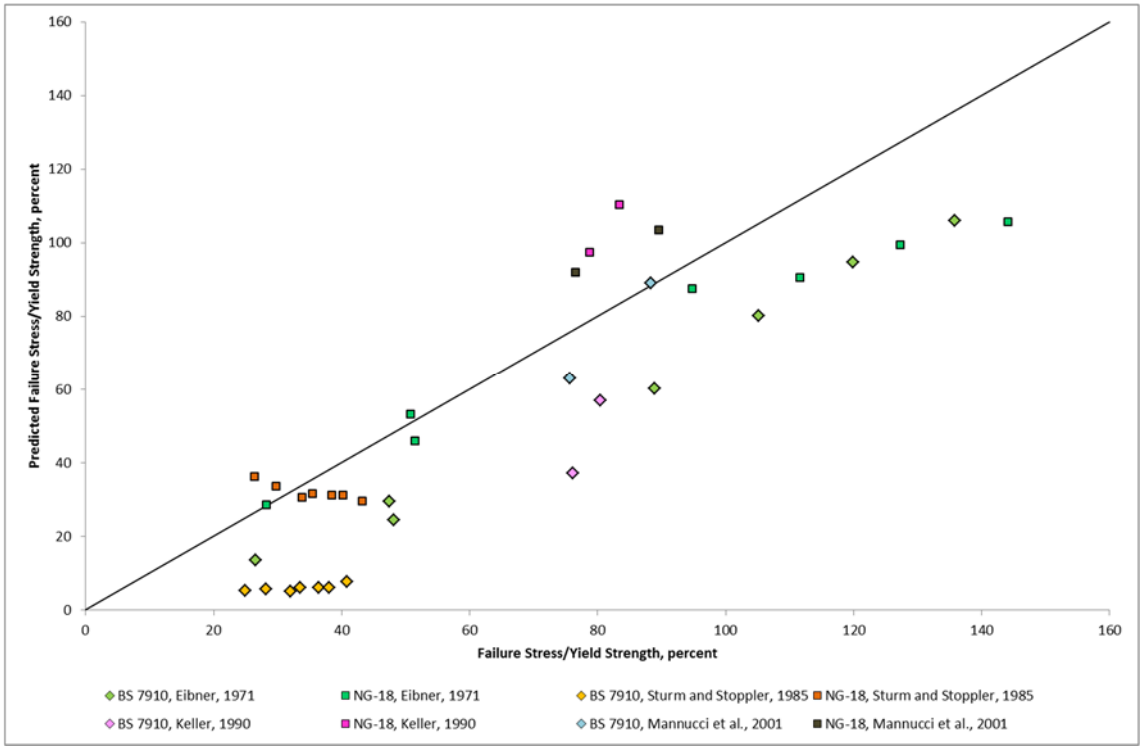

Figure 4.10: Predicted versus Actual Failure Stress for Axial Part-Wall Defects in Thick Wall Pipe Sections According to NG-18 and BS 7910 Level 2, Eibner, Sturm and Stoppler, Keller and Demofonti et al.

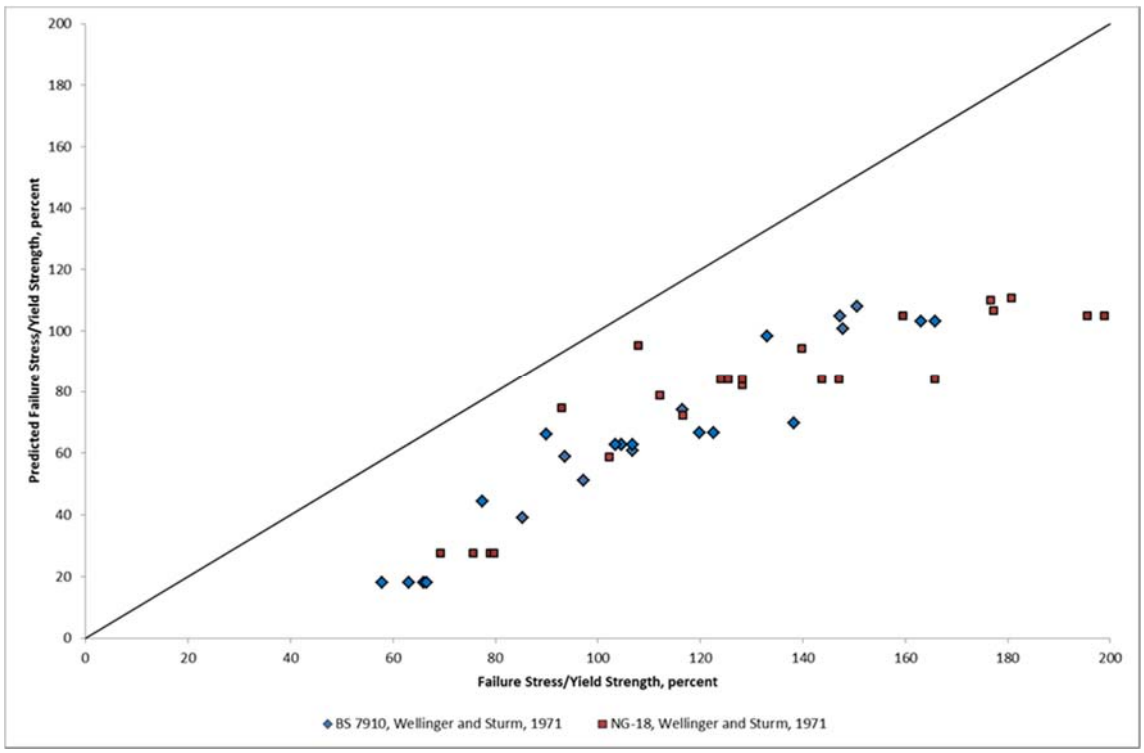

Figure 4.11: Predicted versus Actual Failure Stress for Axial Part-Wall Defects in Thick Wall Pipe Sections According to NG-18 and BS 7910 Level 2, Wellinger and Sturm

Figure 4.12 and Figure 4.13 show the same data from Figure 4.10 and Figure 4.11 and also include the results of the burst tests on axial part-wall defects in thin wall pressure vessels from Battelle in 1973, summarised in Table 4.13.

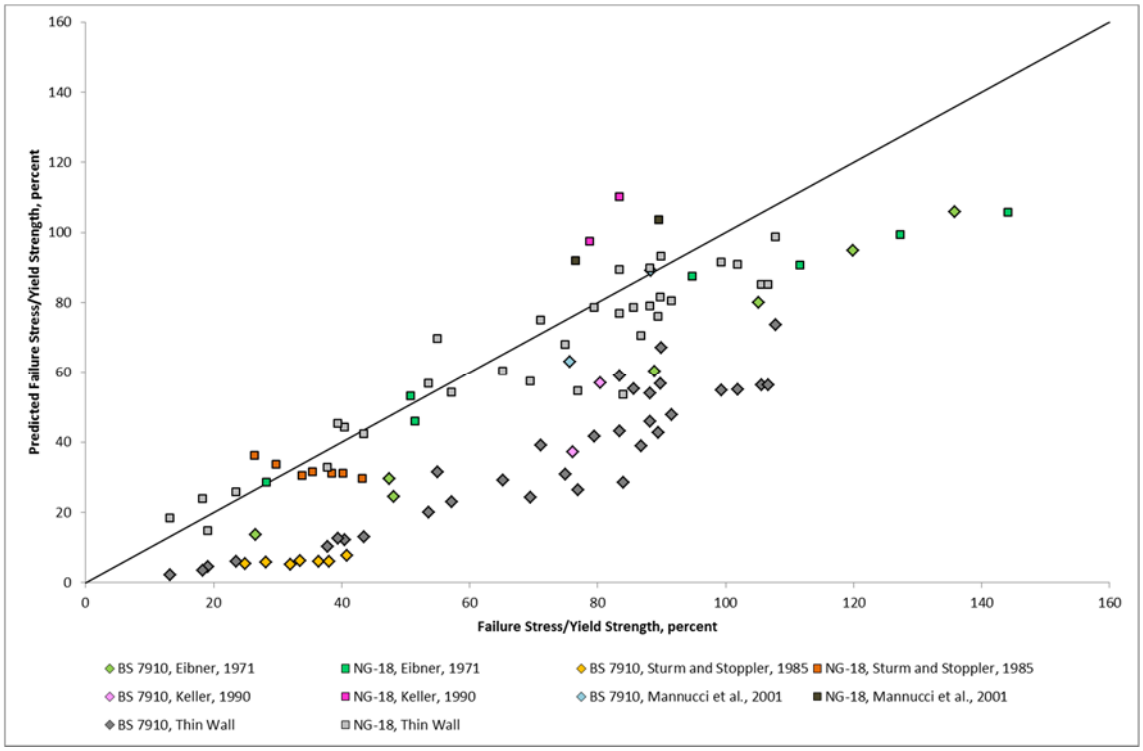

Figure 4.12: Predicted versus Actual Failure Stress for Axial Part-Wall Defects in Thick and Thin Wall Pipe Sections According to NG-18 and BS 7910 Level 2, Eibner, Sturm and Stoppler, Keller, Demofonti et al. and Kiefner et al.

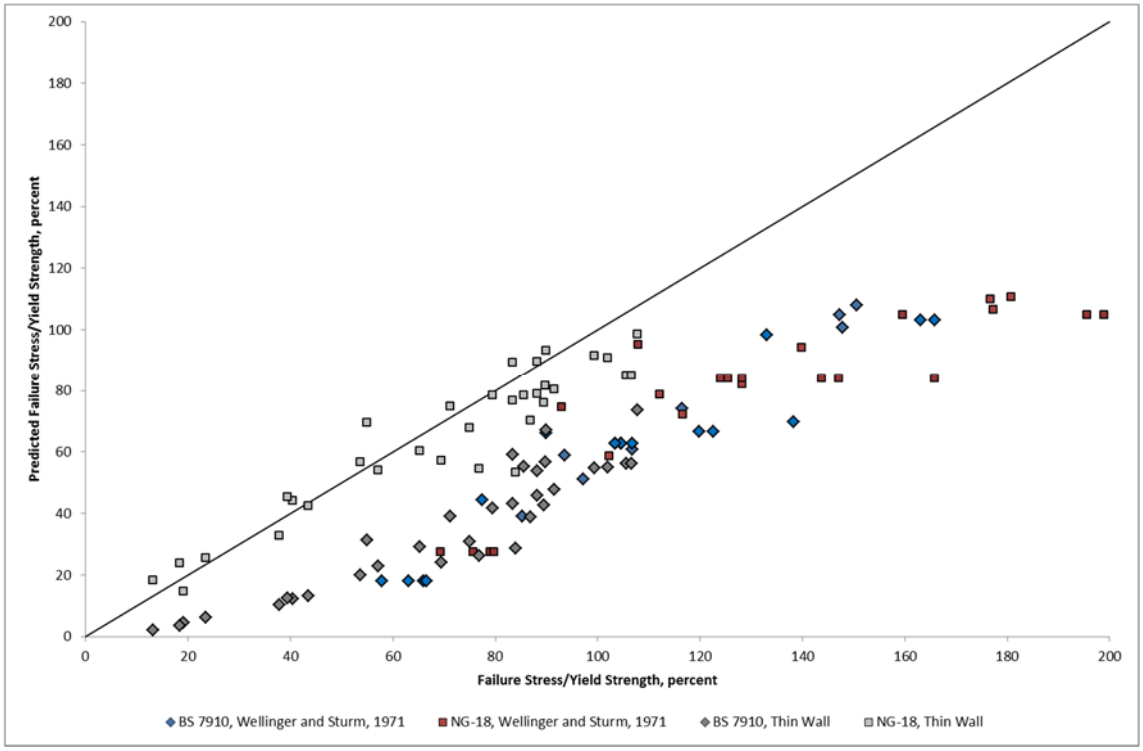

Figure 4.13: Predicted versus Actual Failure Stress for Axial Part-Wall Defects in Thick and Thin Wall Pipe Sections According to NG-18 and BS 7910 Level 2, Wellinger and Sturm, Kiefner et al.

In Figure 4.10, Figure 4.11, Figure 4.12 and Figure 4.13 data points which lie below the line of unity are conservative, with the assessment method predicting

a failure stress below that of the experimental failure stress. Conversely, data points which lie above the line of unity are non-conservative. The closer data points are to the line of unity, the more accurate the prediction of failure stress.

For the experimental data considered in Figure 4.10 the predictions of BS 7910 are generally conservative in comparison to those of NG-18. The failure stresses calculated by NG-18 range from being approximately equal to 6.8 times larger than those calculated by BS 7910 for the experimental cases considered. For the experimental data considered in Figure 4.11, the predictions of BS 7910 are slightly more conservative than those of NG-18. The failure stresses calculated by NG-18 range from being approximately equal to 1.7 times larger than those calculated by BS 7910 for the experimental cases considered. The conservatism of the failure stresses calculated by BS 7910 over NG-18 in the part-wall case reflects that of the through-wall case, however in this case the conservatism is less evident.

The experimental data considered in Figure 4.10 suggests that the accuracy of NG-18 in calculating pipeline failure stress for part-wall defects in thick wall pipelines may be slightly higher than that of BS 7910. The experimental data considered in Figure 4.11 suggests that the accuracy of NG-18 and BS 7910 are approximately equal.

Figure 4.12 and Figure 4.13 include the thin wall failure data from which the NG-18 equations were originally calibrated. In Figure 4.12 the thick wall data for NG-18 is contained within the scatter of the data points of the thin wall data. In Figure 4.13 the thick wall data for NG-18 does not lie within the scatter of the data points of the thin wall data. The reason for this is the atypically large, pipe radius to wall thickness ratio of the vessels used in these tests. The large size of the ratio emphasises the conservative nature of Barlow’s equation for thin wall pipelines when applied to thick wall pipelines, as was noted in section 4.1. Regardless of this conservatism, the accuracy of the NG-18 equation can be considered as approximately equal to BS 7910 when considering these particular tests.

Figure 4.12 and Figure 4.13 suggest that the flow stress dependent NG-18 is a valid model for part-wall defects in pipelines up to at least 47.2 mm wall thickness, provided that the toughness is high.

On the basis of the accuracy of the two models both the flow stress dependent part-wall NG-18 equation and the BS 7910 level 2 assessment are appropriate to use to describe gouge failure in a failure frequency model. However, the flow stress dependent NG-18 equation would be preferred over BS 7910 due to its simplicity.

4.4 Validation of the NG-18 Equations for Thick Wall Pipelines Conclusions

This chapter has presented a study to validate the application of the NG-18 equations to thick wall pipelines. The NG-18 equations were derived using tests on thin wall pressure vessels. In the context of fracture mechanics, an increase in pipeline wall thickness will result in an increase in both the constraint and the bending stress; and reduce the toughness. The accuracy of the NG-18 equations when applied to thick wall pipelines could therefore potentially be affected.

The approach taken has considered a comparison between the component parts of the NG-18 equations and the component parts of the defect assessment code BS 7910, which is valid for application to both thin and thick walled pressure vessels. The aim was to determine whether an increase in pipeline wall thickness introduces effects which are not accounted for by the NG-18 equations. In addition, the accuracy of the NG-18 equations and a BS 7910 level 2 assessment when compared to thick wall experimental failure data was considered, in order to determine the most appropriate model to use in a failure frequency model for dense phase CO_2 pipelines.

It was found that the through-wall and part-wall toughness dependent NG-18 equations can be written in the form of a failure assessment diagram which is

analogous to the BS 7910 level 2 assessment method and mathematically identical to the failure assessment diagram used in PD 6493.

Comparisons between the BS 7910 level 2 assessment method; and the through-wall and part-wall toughness dependent NG-18 equations written in the same form; indicated that the two models are structurally very similar. Wall thickness effects were shown to be minimal and the main source of difference between the two models is the calculation of the fracture ratio, particularly for part-wall defects. These differences arise from the correlation used for material fracture toughness and the calculation of the stress intensity factor.

For modern, high toughness linepipe steel, defect failure will occur as a result of plastic collapse rather than brittle fracture. The flow stress dependent NG-18 equations are therefore the most appropriate form of the NG-18 equations to apply for high toughness steel.

In a plastic collapse failure the fracture toughness, by definition, has no effect. Furthermore, the flow stress dependent form of the NG-18 equations do not include a brittle fracture, toughness dependent component. Therefore for high toughness steel, the main source of the difference between BS 7910 and NG-18 is negated. In principle, the flow stress dependent NG-18 equations would be suitable for application to thick wall pipelines, provided the pipe material was of a high toughness.

On the basis of the above points and the comparison made with thick wall experimental failure data, it is concluded that the flow stress dependent through-wall NG-18 equation is a valid model for through-wall axial defects in pipelines up to at least 47.2 mm wall thickness, provided that the linepipe steel has a high toughness.

On the basis of the comparison made with thick wall experimental failure data, it is concluded that the flow stress dependent through-wall NG-18 equation is a more appropriate model to use than the BS 7910 level 2 assessment to describe leak / rupture in a failure frequency model for dense phase CO_2 pipelines.

On the basis of the above points and the comparison made with thick wall experimental failure data, it is concluded that the flow stress dependent part-wall NG-18 equation is a valid model for part-wall axial defects in pipelines up to at least 47.2 mm wall thickness, provided that the linepipe steel has a high toughness.

On the basis of the comparison made with thick wall experimental failure data, it is concluded that both the flow stress dependent part-wall NG-18 equation and the BS 7910 level 2 assessment are appropriate to use to describe gouge failure in a failure frequency model. However, the flow stress dependent NG-18 equation would be preferred over BS 7910 due to its simplicity.

It is noted that verification for the application of the toughness dependent NG-18 equation would require a detailed numerical analysis including finite element analysis and an experimental test programme.

It is recommended that further work is carried out in order to determine the toughness limit at which it is acceptable to ignore the effect of fracture toughness and brittle fracture.

Chapter 5. Development of the AFFECT Failure Frequency Model for Dense Phase CO_2 Pipelines (Part 1)

Chapter 2 to Chapter 4 have considered the suitability of available models and data, for the purposes of developing a model to calculate the failure frequency of a dense phase CO_2 pipeline due to third party external interference. Chapter 5 to Chapter 7 detail the development of the model, to be known as AFFECT: A Failure Frequency Estimation model for dense phase CO_2 Transport.

As previously noted, pipeline failure frequency models are typically based upon probabilistic structural reliability methods which use limit state functions defined by pipeline failure models; and probability distributions derived from historical operational data. In terms of using structural reliability techniques to develop the AFFECT model, it was concluded in Chapter 3 and Chapter 4 that:

- The NG-18 equations are the most appropriate models to describe leak / rupture and gouge failure.
- The BGDGFM is the most appropriate model to describe gouged dent failure

The most basic failure frequency model considered in Chapter 2 incorporating these aspects is the PIE model. The PIE model has therefore been used as a template from which to develop the AFFECT model.

All of the pipeline failure frequency models which use structural reliability methods are based upon a methodology originally developed by British Gas. It was shown in Chapter 2 however, that many of the models incorporate modifications to this methodology on the basis of further research into damage modelling; improved operational data; or different interpretations of the problem. These modifications are discussed in section 2.8. AFFECT has been developed in a stepwise manner by considering the effect of including some of these modifications in the model.

From the starting point of the PIE model Chapter 5 to Chapter 7 will detail the step by step construction of the AFFECT model. The first four stages are covered in Chapter 5, an analysis of the most recent UKOPA Fault Database is presented in Chapter 6 and the final two stages are detailed in Chapter 7. Each modification made to the PIE model is outlined and estimates of pipeline failure frequency calculated at each stage are presented. In this way the effect of each modification on the estimated value of failure frequency can be observed.

The modifications considered in Chapter 5 include:

- Changes to the probability of failure calculation;
- The re-rounding effect of the pipeline internal operating pressure on a dent;
- The force which causes a dent;
- Distributions derived from recent historical operational damage data.

It is noted that the PIE model, as discussed in section 2.8, does not adequately address failures caused by damage to branches and fittings; and drilling operations in-error. In order that the AFFECT model address failures of these types, the development of an historical data component or additional damage specific failure models would be required. The development of these elements however, has not been performed as part of this work. It is therefore recommended that such a task is considered as part of further work.

5.1 The Modified PIE Model

The basis for the AFFECT model is the PIE model. The model is described in section 2.5, however it was noted in the discussion in section 2.8 that in comparing the PIE and Cosham failure frequency models, the expressions used for calculation of the probability of failure in the Cosham model are more accurate than those used in the PIE model. Therefore, for the purposes of this study, changes have been made to the probability of failure calculation in the PIE model to bring it more in line with the Cosham model. The model used as

the basis for the AFFECT model is therefore referred to as the “Modified PIE model”. The changes made to the PIE model are outlined below.

The total probability of failure for gouges in the PIE model, given by equation (2.73), is replaced in the Modified PIE model with the equivalent equation from the Cosham model (equation (2.84)):

$$P_{gougetotal} = \int_0^{\infty} f_{2c}(2c) R_d(d_{crit}) d2c$$

The probability of a gouge leak, $P_{gougeleak}$, and probability of a gouge rupture, $P_{gougerupture}$, are therefore given by equations (2.74) and (2.85):

$$P_{gougeleak} = \int_0^{L_{crit}} f_{2c}(2c) R_d(d_{crit}) d2c$$

$$P_{gougerupture} = \int_{L_{crit}}^{\infty} f_{2c}(2c) R_d(d_{crit}) d2c$$

The total probability of failure for gouged dents in the PIE model, given by equation (2.76), is replaced in the Modified PIE model by:

$$P_{gougeddenttotal} = \int_0^{\infty} f_{2c}(2c) d2c \,.\left[\int_0^{d_{critBGDGFM}} f_d(d) R_H(H_{crit}) dd + R_d(d_{critBGDGFM})\right] \qquad (5.1)$$

Where $d_{critBGDGFM}$ is given by equation (2.87). Note that although equation (5.1) uses the same form as the probability of failure for gouged dents in the Cosham model (equation (2.86)), the dent depth random variable, H, from the PIE model is retained. The value of H_{crit} is calculated using equation (2.16).

It follows from equation (5.1) that the probability of a gouged dent failing as a leak and a gouged dent failing as a rupture are given by:

$$P_{gougeddentleak} = \int_0^{L_{crit}} f_{2c}(2c) d2c \,.\left[\int_0^{d_{critBGDGFM}} f_d(d) R_H(H_{crit}) dd + R_d(d_{critBGDGFM})\right] \qquad (5.2)$$

$$P_{gougeddentrupture} = \int_{L_{crit}}^{\infty} f_{2c}(2c) d2c \,.\left[\int_0^{d_{critBGDGFM}} f_d(d) R_H(H_{crit}) dd + R_d(d_{critBGDGFM})\right] \qquad (5.3)$$

The critical length of the gouged dent gouge in equation (5.2) and (5.3) is the same as that used in the both the PIE and Cosham models, equation (2.72).

It should be noted that all other aspects of the Modified PIE model remain the same as the original PIE model. The Incident-Rate is given in Table 2.10, the probabilities that mechanical damage will be a gouge or a gouged dent in Table 2.11, the random variables in Table 2.12 and the Weibull probability distribution parameters in Table 2.13.

5.2 Modified PIE Model Results

Estimated pipeline failure frequency values have been calculated using the Modified PIE model for six example pipeline cases. In each case the leak, rupture and total failure frequency has been calculated. The example cases represent typical design parameters for 610 mm and 762 mm external diameter pipelines operating between 0.3 and 0.72 design factor, with a range of steel toughness.

The study has been performed for set values of external diameter, internal operating pressure, material and fracture toughness (as measured by the 2/3 Charpy v-notch impact energy). Variation in the failure frequency is presented as a function of the pipeline wall thickness. The only difference between examples 1, 2 and 3 is an increase in the material fracture toughness of the pipeline; likewise for examples 4, 5 and 6.

Details of the example pipeline cases are shown in Table 5.1.

Example No.	External Diameter (mm)	Wall Thickness (mm) (min/max)	Operating Pressure (barg)	Material Grade	Specified Minimum Yield Strength (Nmm^{-2})	Ultimate Tensile Strength (Nmm^{-2})	2/3 Charpy V-Notch Impact Energy (J)
1	610	12.7 / 25.4	135	L450	450	535	27
2	610	12.7 / 25.4	135	L450	450	535	43
3	610	12.7 / 25.4	135	L450	450	535	167
4	762	9.5 / 19.1	34	L450	450	535	27
5	762	9.5 / 19.1	34	L450	450	535	43
6	762	9.5 / 19.1	34	L450	450	535	167

Table 5.1: Example Pipeline Cases

The variation in leak, rupture and total failure frequency with wall thickness for example no.1 in Table 5.1, is shown in Figure 5.1. The variation in leak, rupture and total failure frequency with wall thickness for example no.4, is shown in Figure 5.2. Equivalent charts for the remaining examples are included in Appendix A .

A comparison between total failure frequency values calculated for examples 1, 2, and 3 is shown in Figure 5.3 indicating the effect of an increase in material fracture toughness. A similar comparison between total failure frequency values calculated for examples 4, 5 and 6 is shown in Figure 5.4.

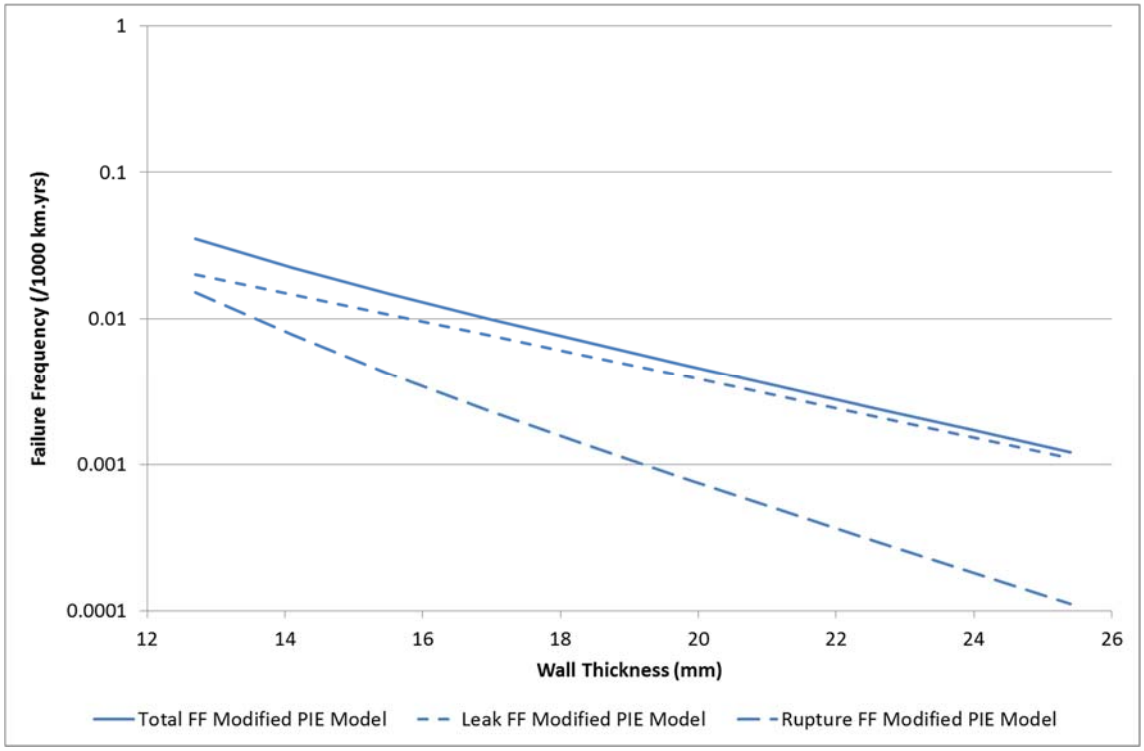

Figure 5.1: Leak Rupture and Total Failure Frequency as Calculated by the Modified PIE Model, for Example 1

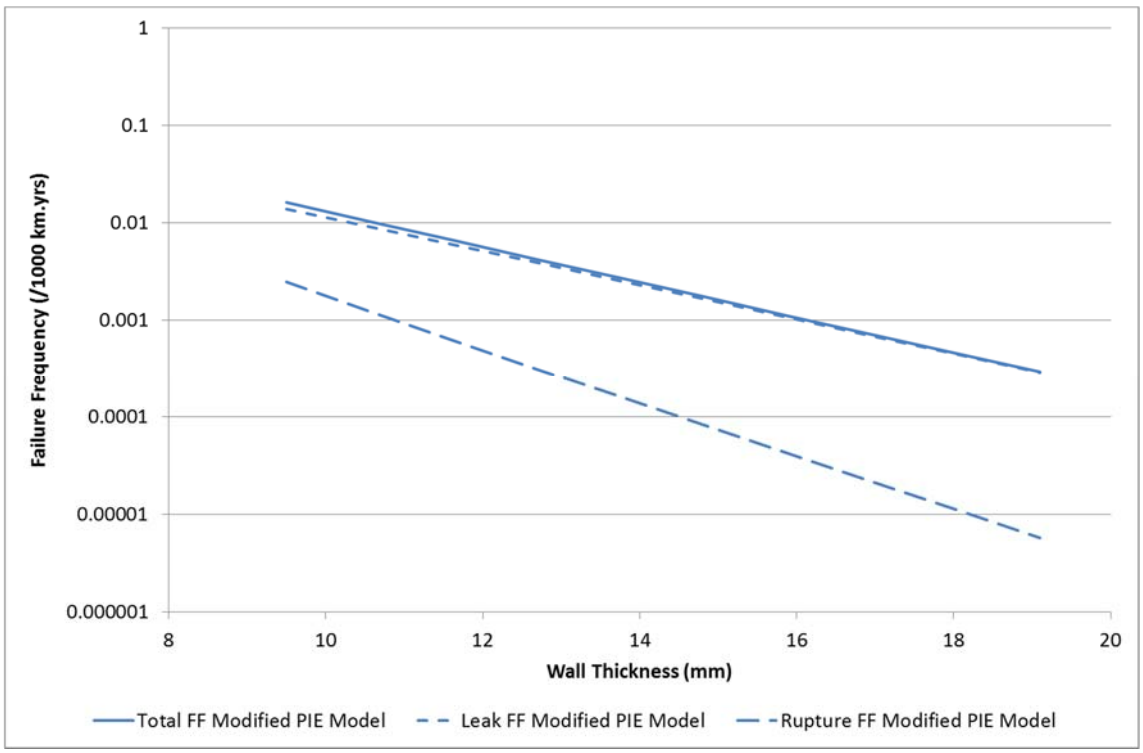

Figure 5.2: Leak Rupture and Total Failure Frequency as Calculated by the Modified PIE Model, for Example 4

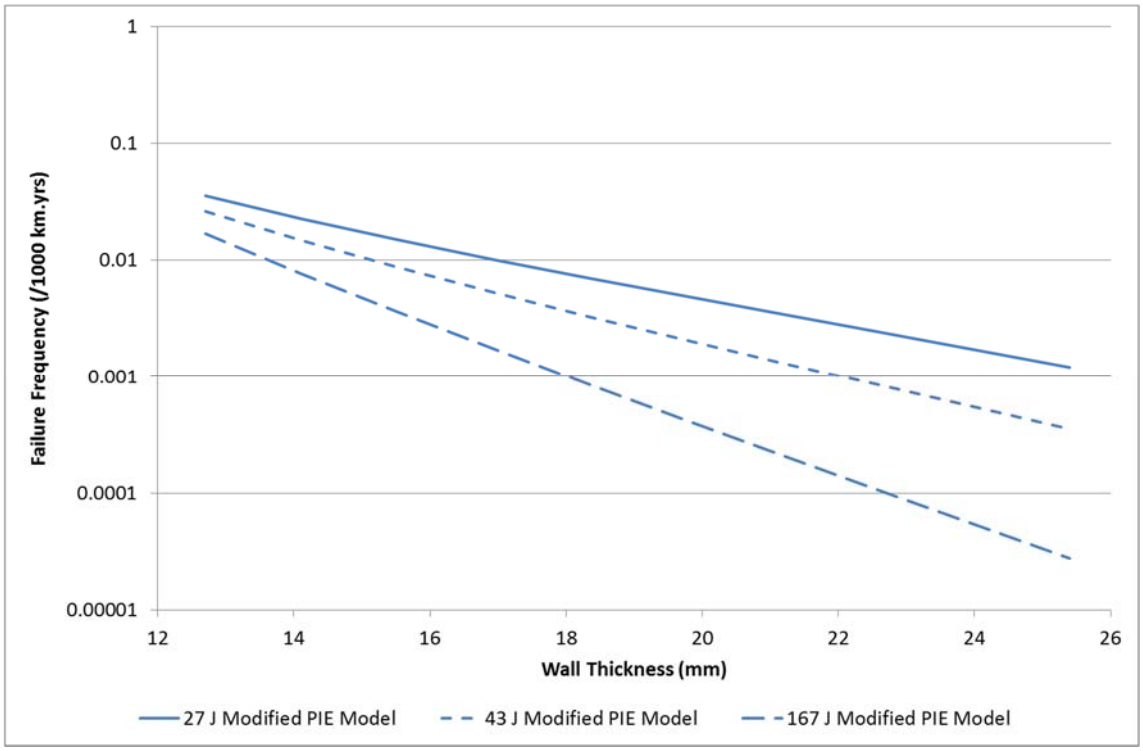

Figure 5.3: Total Failure Frequency as Calculated by the Modified PIE Model for Examples 1, 2 and 3

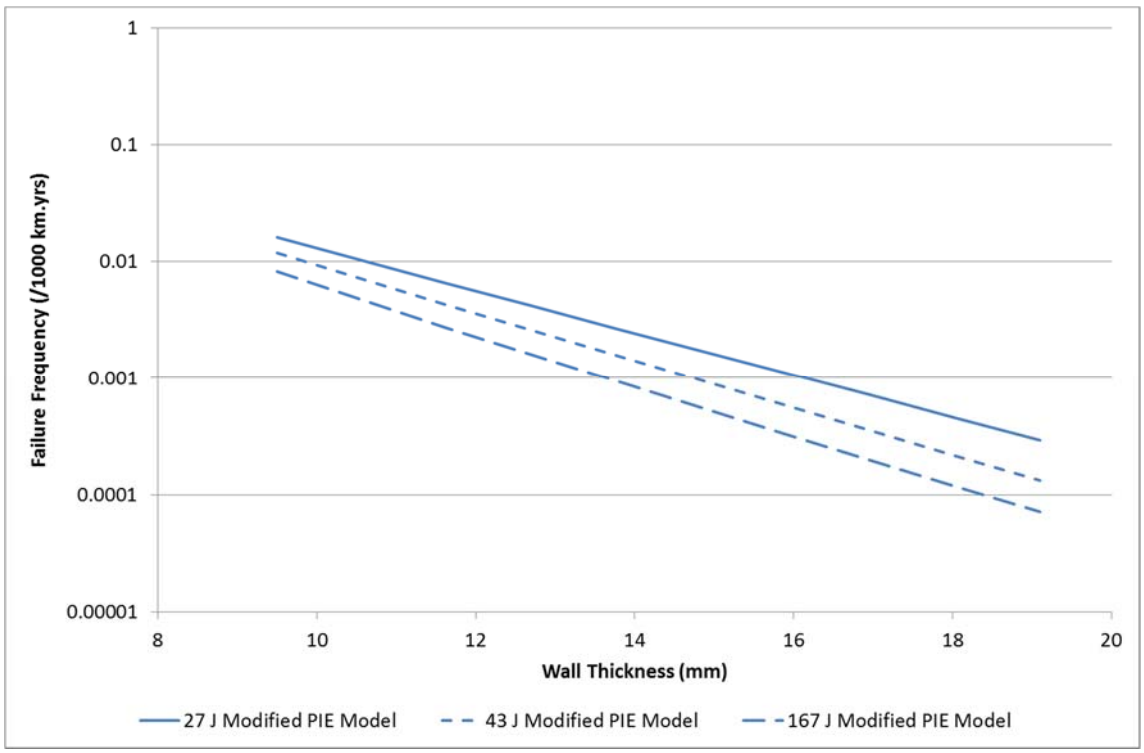

Figure 5.4: Total Failure Frequency as Calculated by the Modified PIE Model for Examples 4, 5 and 6

Based on the results, the following observations can be made regarding estimations of pipeline failure frequency made by the Modified PIE model.

The value of failure frequency decreases with increasing wall thickness. This result is expected; a thicker pipeline would require deeper and longer gouges to cause failure and deeper and longer gouges are less likely to occur (as indicated by the Weibull probability distributions which are shown in Figure 2.7 and Figure 2.8).

Taking into consideration all of the examples calculated, the leak failure frequency is, for the most part, in excess of the rupture failure frequency. This is also to be expected given that the rupture failure condition is based upon the defect length exceeding a minimum critical value; and that longer defects are less likely to occur. The pipeline examples with a higher operating pressure (numbers 1, 2 and 3) indicate that the rupture failure frequency becomes more dominant at the minimum value of wall thickness considered. In these cases an increased pipe wall hoop stress results in a critical length that is sufficiently small such that the majority of failures would occur as ruptures. The same effect is not observed when the operating pressure is lower in the considered

examples 4, 5 and 6, although the overall trend suggests this would happen if the wall thickness was sufficiently low.

The value of failure frequency decreases with increasing material toughness (Charpy 2/3 v-notch impact energy). This effect is to be expected; toughness is a measure of the resistance of a material to fracture and therefore an increase in this quantity would suggest a decrease in the number of failures. This decrease would be expected to tail off as the toughness increases and vulnerability to brittle fracture is minimised. The effect is due to the decreasing influence of the gouged dent failure probability as the toughness is increased (calculated by equations (5.1), (5.2) and (5.3)). From the gouged dent limit state function, equation (2.16), an increase in toughness increases the value of dent depth required to cause a gouged dent failure. From the dent depth Weibull distribution (Figure 2.9), deeper dents are less likely to occur; therefore the gouged dent failure probability is decreased. Note that the leak / rupture boundary and gouge failure probability are unaffected by an increase in toughness, the flow stress dependent NG-18 equations (equations (3.2) and (3.4)) have no toughness dependency.

5.3 The Re-Rounding Model

In the Modified PIE model, the BGDGFM is used to produce a limit state function for the failure of a gouged dent.

As explained in section 3.1.2.1, the BGDGFM is a semi-empirical model formulated using fracture mechanics theory and the results of experimental burst tests of gouged dent defects. In the burst tests used to calibrate the model, the dent damage was introduced and measured with the pipeline at zero pressure. The dent depth used in the BGDGFM is therefore defined as the dent depth in an unpressurised pipeline.

The dent depth recorded in the UKOPA Fault Database however, is (in most cases) the dent depth measured at pressure. Therefore, given that it was

derived using the UKOPA Fault data, the dent depth Weibull probability distribution used in the Modified PIE model will refer to dent depth at pressure.

This leads to the conclusion that the use of the BGDGFM in the Modified PIE model may produce non-conservative predictions of the behaviour of damage recorded during operation.

It was noted in section 3.1.2.1 that if an assessment of a gouged dent defect is required for which the dent depth was measured when the pipeline was pressurised, a re-rounding correction must be applied to the dent depth before the BGDGFM can be applied. The Cosham failure frequency model described in Chapter 2 acknowledges the potential for non-conservative predictions with the BGDGFM and applies a re-rounding correction factor developed by the EPRG and given by equation (2.82):

$$H = 1.43H_P$$

Where H is the dent depth in the unpressurised pipeline (in mm) and H_P is the dent depth in the pressurised pipeline (in mm).

The above relationship is considered to improve the accuracy of calculations made using the BGDGFM for damage recorded during operation. The relationship has therefore been added to the Modified PIE model as the second stage in the construction of AFFECT. This version of the model will be referred to as the “Re-Rounding model”.

In the Modified PIE model the dent depth required to cause a gouged dent to fail is calculated using equation (2.16). This value is then used in the calculation of the probability of failure. In the Re-Rounding model, the dent depth calculated by equation (2.16) is first transformed to an equivalent, pressurised dent depth using equation (2.82) before being used to calculate the probability of failure.

5.4 Re-Rounding Model Results

Estimated pipeline failure frequency values have been calculated using the Re-Rounding model for the six example pipeline cases listed in Table 5.1. As for the Modified PIE model, the leak, rupture and total failure frequency has been calculated.

The variation in leak, rupture and total failure frequency with wall thickness for example no.1 in Table 5.1, is shown in Figure 5.5. The variation in leak, rupture and total failure frequency with wall thickness for example no.4, is shown in Figure 5.6. Equivalent charts for the remaining examples are included in Appendix A .

A comparison between total failure frequency values for examples 1, 2, and 3 as calculated by the Re-Rounding model and the Modified PIE model, is shown in Figure 5.7. A similar comparison between total failure frequency values calculated for examples 4, 5 and 6 is shown in Figure 5.8.

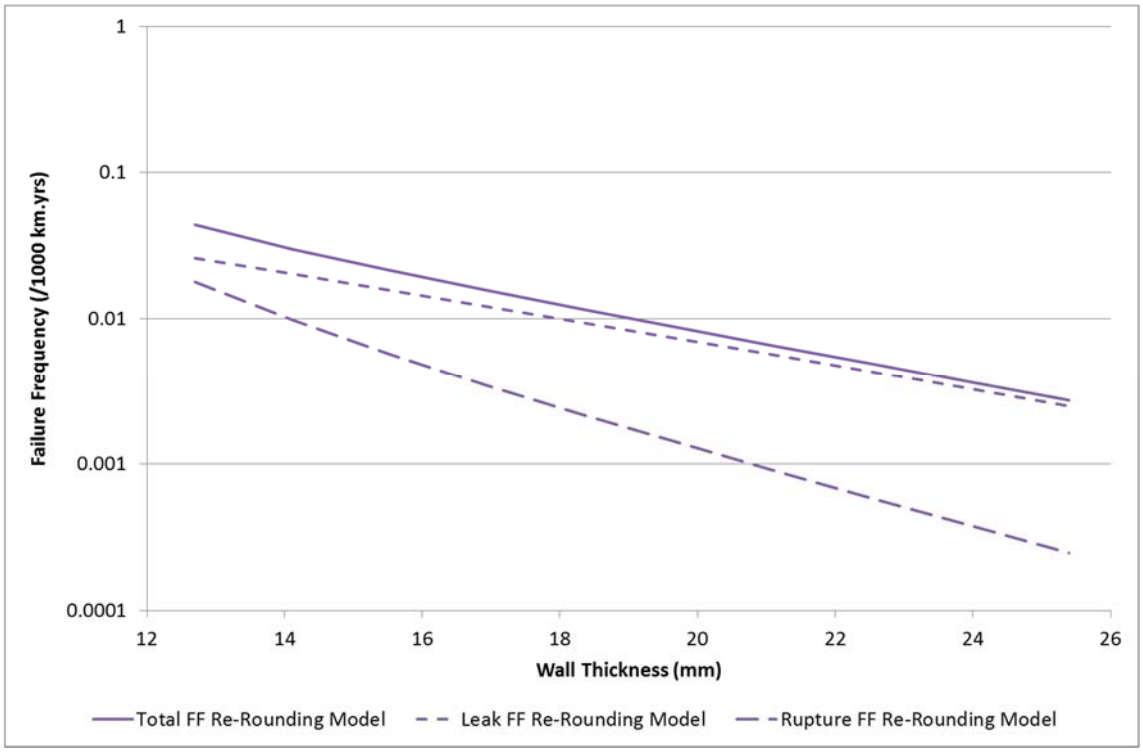

Figure 5.5: Leak, Rupture and Total Failure Frequency as Calculated by the Re-Rounding Model, for Example 1

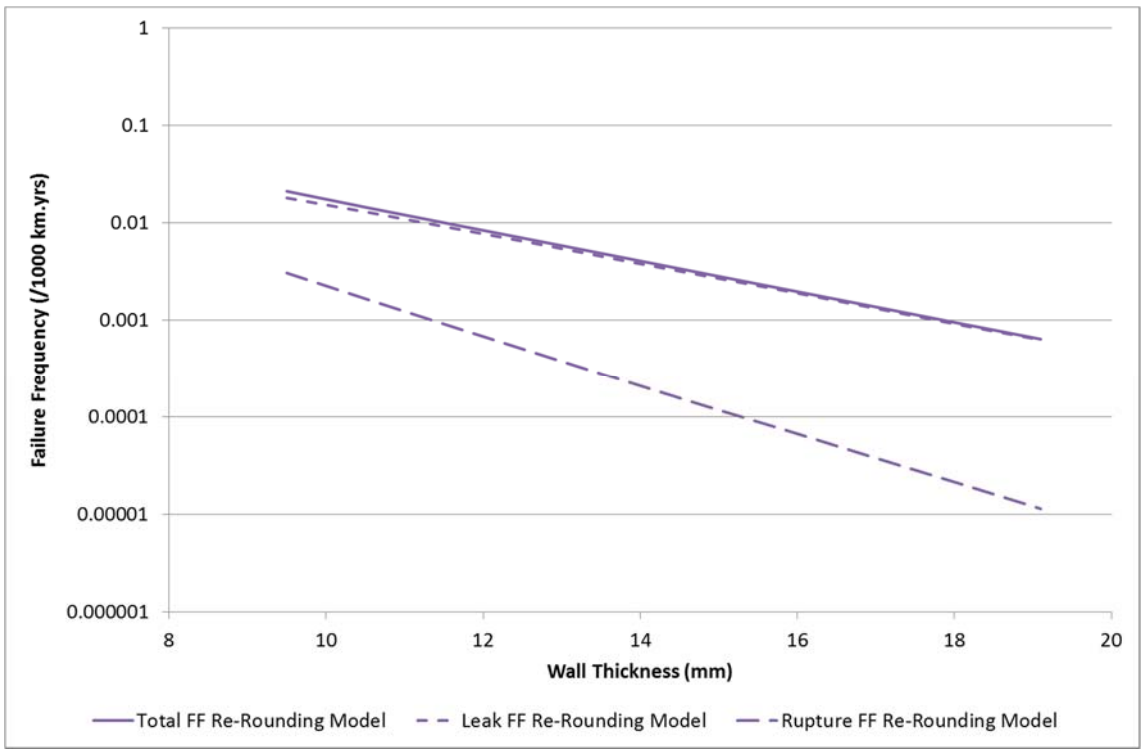

Figure 5.6: Leak, Rupture and Total Failure Frequency as Calculated by the Re-Rounding Model, for Example 4

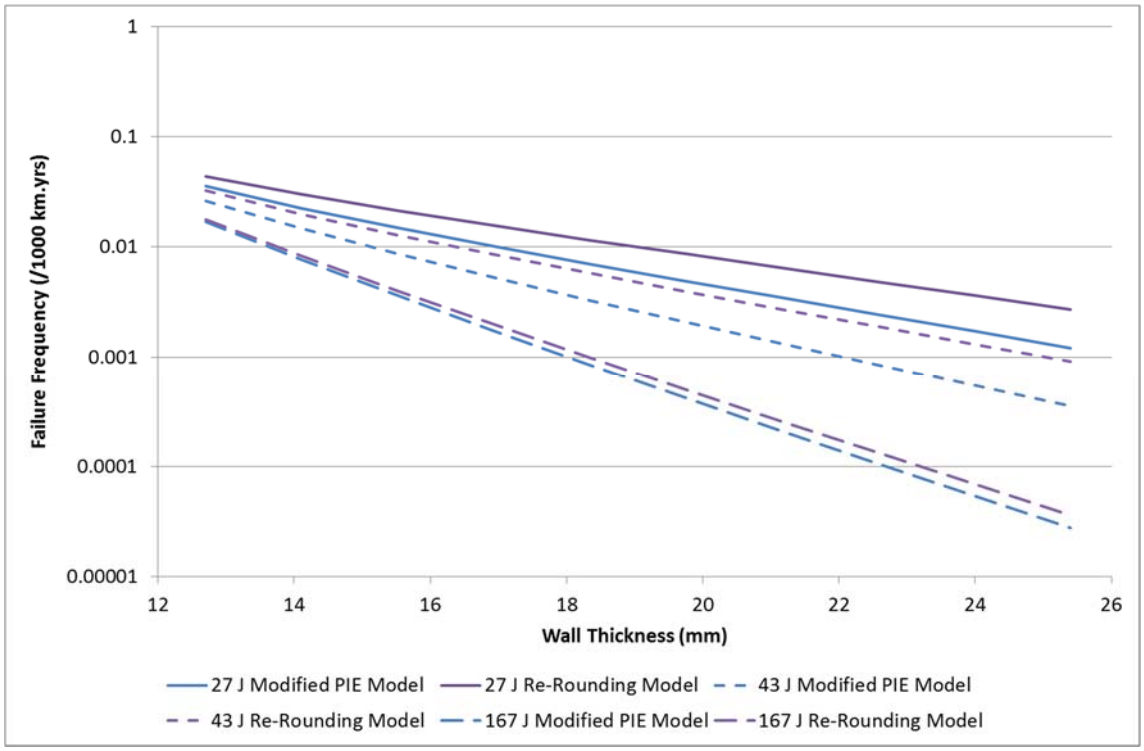

Figure 5.7: Total Failure Frequency as Calculated by the Re-Rounding Model and the Modified PIE Model for Examples 1, 2 and 3

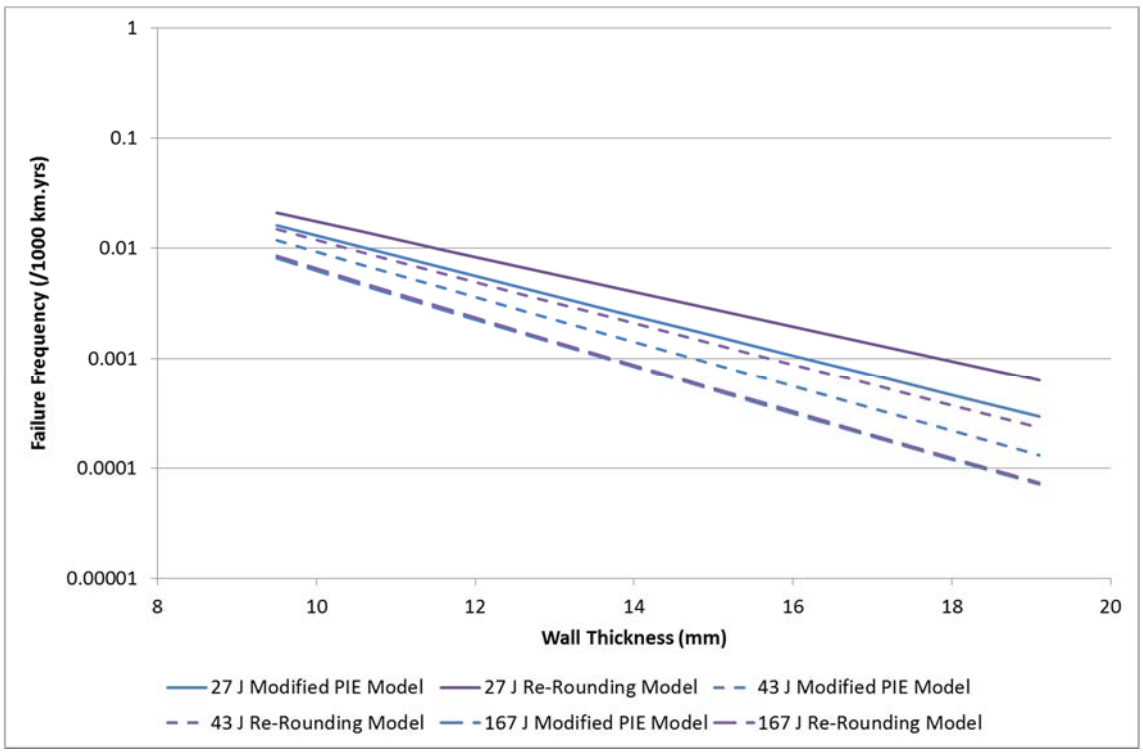

Figure 5.8: Total Failure Frequency as Calculated by the Re-Rounding Model and the PIE Model for Examples 4, 5 and 6

Based on the results, the following observations can be made regarding estimations of pipeline failure frequency made by the Re-Rounding model.

A direct comparison between the results calculated for each example using the Modified PIE model and the Re-Rounding model indicates that the Re-Rounding model estimates higher values of failure frequency. The use of the re-rounding relationship given by equation (2.82) lowers the value of the dent depth required to cause a gouged dent failure. From the dent depth Weibull distribution (Figure 2.9), shallower dents are more likely to occur; therefore the overall probability of failure is increased.

The leak and rupture failure frequencies for each example follow an identical trend to that shown by the Modified PIE model. From the leak / rupture limit state function (equation (2.72)), the leak / rupture boundary is determined by the gouge length. Gouge length is not affected by the introduction of equation (2.82) to the model; therefore a change in the relative significance of leak and rupture failure frequencies would not be expected.

The effect on the estimated failure frequency of introducing equation (2.82) to the model decreases with increasing material toughness (Charpy 2/3 v-notch impact energy). A deeper dent is required as the toughness increases, therefore the effect of dent depth (and therefore equation (2.82)) on the failure frequency decreases as the toughness increases.

5.5 The Dent Force Model

In the Modified PIE and Re-Rounding models the dent depth probability distribution is based upon an analysis of all dent depth data in the 2005 UKOPA Fault Database.

A dent is a deformation in the shape of the pipe; therefore its dimensions will be influenced by the pipe geometry in a way that gouge defects are not.

A probability distribution derived from a dent damage database will not only be influenced by the size of the dents but also by the geometry of the pipelines in the database.

A more desirable situation would be to remove the influence of pipe geometry from the dent depth distribution, allowing more accurate values of probability to be calculated in the case of a specific pipeline.

This issue is addressed by the FFREQ, PIPIN, and Cosham failure frequency models described in Chapter 2, which take into account the resistance of a pipe to denting. The probability of failure of a gouged dent in these models is determined from the force required to cause the dent, rather than the dent depth.

In the PIPIN and Cosham models[22] the dent force is incorporated into the gouged dent limit state function, through the use of a semi-empirical relationship

[22] In FFREQ the exact implementation is unknown (section 2.3.5).

developed by the EPRG (Corder, 1995b) which relates it to dent depth (equation (2.83)):

$$F_{dent} = 0.49\sqrt{Res}H_P^{0.42}$$

Where F_{dent} is the dent force (in kN) and Res (in $N^{1/2}mm$) is defined using:

$$Res = \sqrt{L\sigma_Y t}\left(t + \frac{0.7PD}{10\sigma_U}\right) \quad (5.4)$$

Where L is the length of the excavator tooth (in mm), assumed by both models to be 80 mm. Documentation relating to the development of the Cosham model indicates that this assumption is consistent with a paper by Linkens (Linkens, 1998; Cosham, 2007). The use of a relationship such as that given by equations (2.83) and (5.4), allows dent force to be introduced as a random variable in place of the dent depth.

The use of a dent force variable would remove the influence of pipe geometry and provide a more realistic calculation of the gouged dent failure probability. A dent force variable has therefore been substituted for the dent depth variable in the Re-Rounding model as the third stage in the construction of AFFECT. This version of the model will be referred to as the “Dent Force model”.

In the Re-Rounding model, pressurised dent depth is calculated using equations (2.16) and (2.82) before the dent depth Weibull probability distribution (Figure 2.9) is used to calculate dent depth probability. In the Dent Force model, the EPRG relationship given by equations (2.83) and (5.4) is used to transform the pressurised dent depth calculated by equations (2.16) and (2.82) into a dent force. A dent force Weibull distribution is then used to calculate dent force probability. In order to be consistent with the Cosham and PIPIN models the tooth length assumption of 80 mm from those models has been retained.

In principle, the dent force distribution can be derived from the dent depth distribution. For a specific pipeline the quantities, P, D, t, σ_Y and σ_U are constant, therefore from equations (2.83) and (5.4) and the definitions of Weibull

probability distributions given in section 2.2.1.3 (equations (2.17), (2.18), (2.19), (2.20) and (2.21)):

$$f_H(H)dH = f_{F_{dent}}(F_{dent})dF_{dent} \quad (5.5)$$

$$\int_0^H f_H(H)dH = \int_0^{F_{dent}(H)} f_{F_{dent}}(F_{dent})dF_{dent} \quad (5.6)$$

$$F(H) = F(F_{dent}(H)) \quad (5.7)$$

$$R_x(H) = R_x(F_{dent}(H)) \quad (5.8)$$

For the Dent Force model however, the dent force distribution from the PIPIN and Cosham models has been used. The parameters for this distribution are taken from the independent review of the QRA for the onshore pipeline of the Corrib Field Development Project conducted by Advantica (Acton, 2006; Cosham, 2007).

In the Dent Force model the dent depth random variable has been replaced with a dent force variable, however all other random variables remain unchanged from the Modified PIE and Re-Rounding models. The parameters defining the cumulative probability distributions in the Dent Force model are therefore identical to those used in the Cosham Model and are given in Table 2.15. The total probability of failure for gouged dents is expressed using equation (2.86) from the Cosham model, rather than equation (5.1):

$$p_{gougeddenttotal} = \int_0^\infty f_{2c}(2c)d2c \,.\left[\int_0^{d_{critBGDGFM}} f_d(d)R_F(F_{crit})dd + R_d(d_{critBGDGFM})\right]$$

Where $d_{critBGDGFM}$ is given by equation (2.87); the subscript F denotes the use of the dent force distribution; and the value of F_{crit} is dependent on d and calculated using equations (2.16), (2.82), (2.83) and (5.4).

Similarly, the probability of a gouged dent failing as a leak and a gouged dent failing as a rupture are given by equations (2.88) and (2.89), rather than equations (5.2) and (5.3):

$$p_{gougeddentleak} = \int_0^{L_{crit}} f_{2c}(2c)d2c \,.\left[\int_0^{d_{critBGDGFM}} f_d(d)R_F(F_{crit})dd + R_d(d_{critBGDGFM})\right]$$

$$p_{gougeddentrupture} = \int_{L_{crit}}^{\infty} f_{2c}(2c)d2c \,.\left[\int_0^{d_{critBGDGFM}} f_d(d)R_F(F_{crit})dd + R_d(d_{critBGDGFM})\right]$$

The critical length of the gouged dent gouge in equations (2.88) and (2.89) is the same as that used in the both the PIE and Cosham models, equation (2.72).

5.6 Dent Force Model Results

Estimated pipeline failure frequency values have been calculated using the Dent Force model for the 6 example pipeline cases listed in Table 5.1. As before, leak, rupture and total failure frequency has been calculated.

A comparison between total failure frequency values for example 1 as calculated by the Dent Force model, Re-Rounding model and the Modified PIE model, is shown in Figure 5.9. A similar comparison between total failure frequency values for example 4 is shown in Figure 5.10. Equivalent charts for the remaining examples are included in Appendix A .

A comparison between total failure frequency values for examples 1, 2, and 3 as calculated by the Dent Force model and the Re-Rounding model, is shown in Figure 5.11. A similar comparison between total failure frequency values calculated for examples 4, 5 and 6 is shown in Figure 5.12.

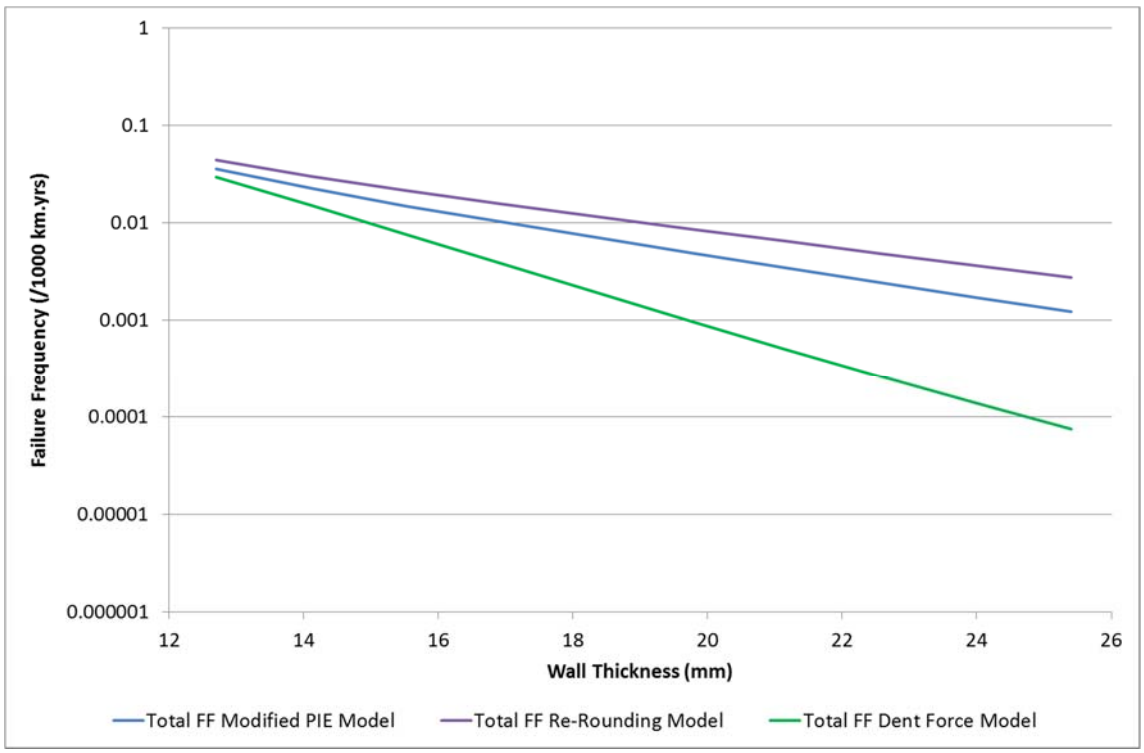

Figure 5.9: Total Failure Frequency as Calculated by the Dent Force Model, Re-Rounding Model and the Modified PIE Model for Example 1

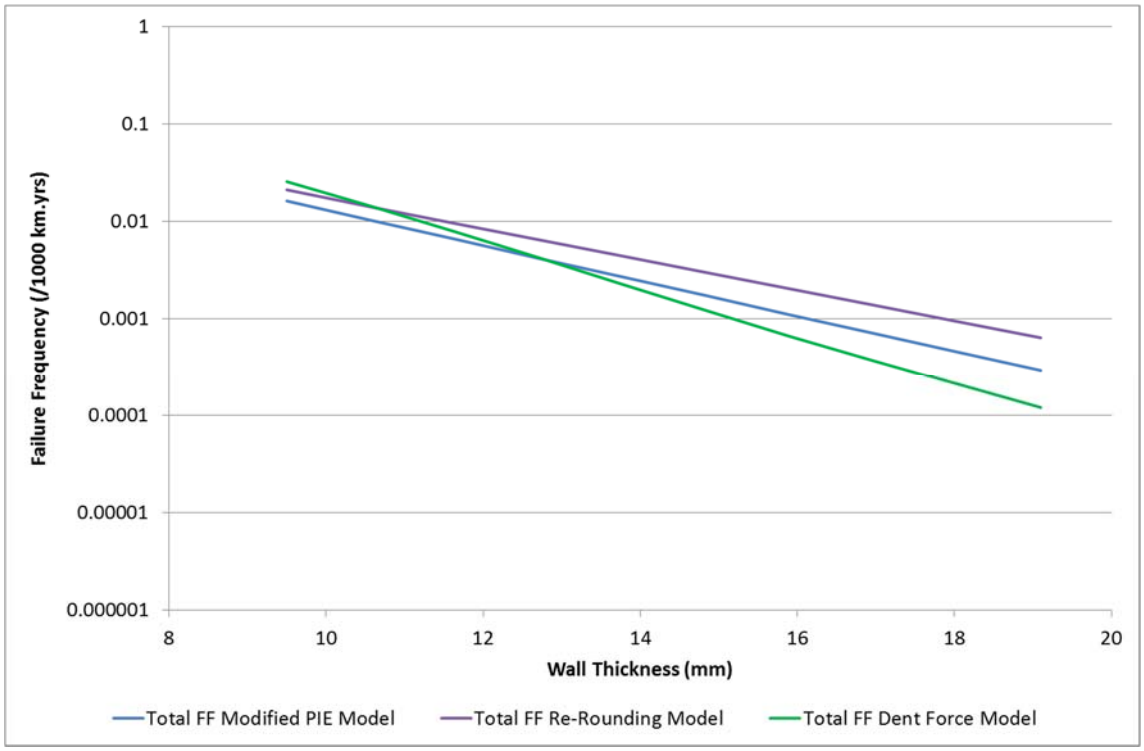

Figure 5.10: Total Failure Frequency as Calculated by the Dent Force Model, Re-Rounding Model and the Modified PIE Model for Example 4

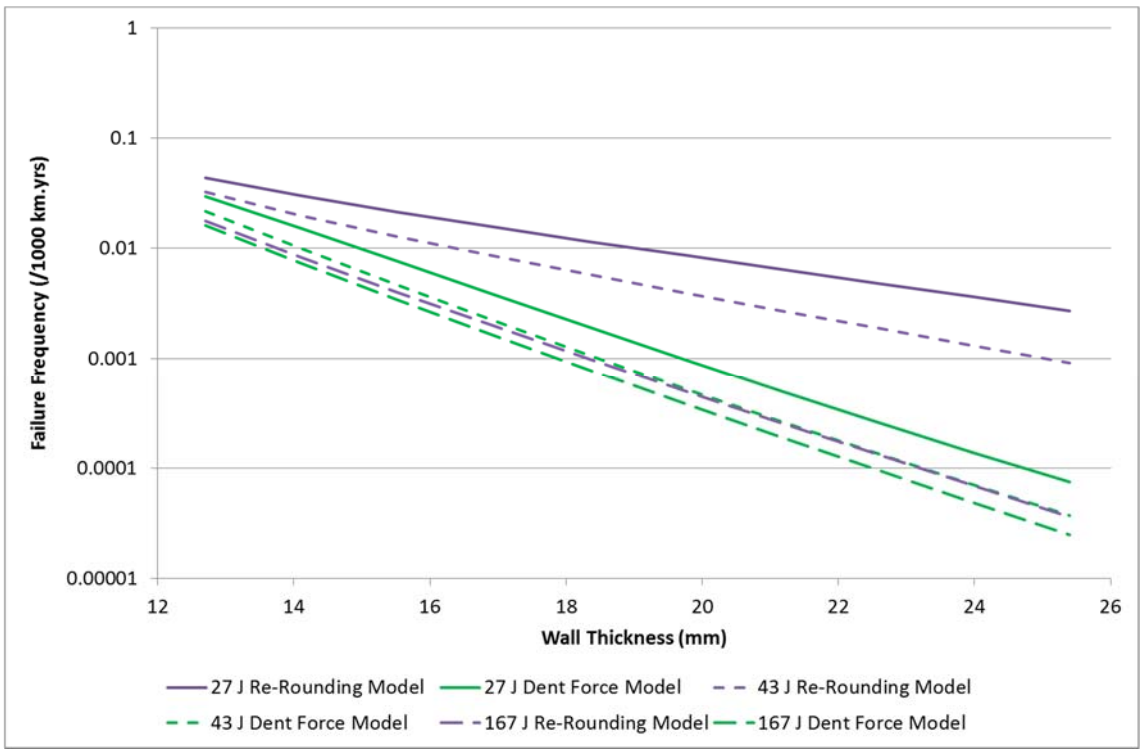

Figure 5.11: Total Failure Frequency as Calculated by the Dent Force Model and the Re-Rounding Model for Examples 1, 2 and 3

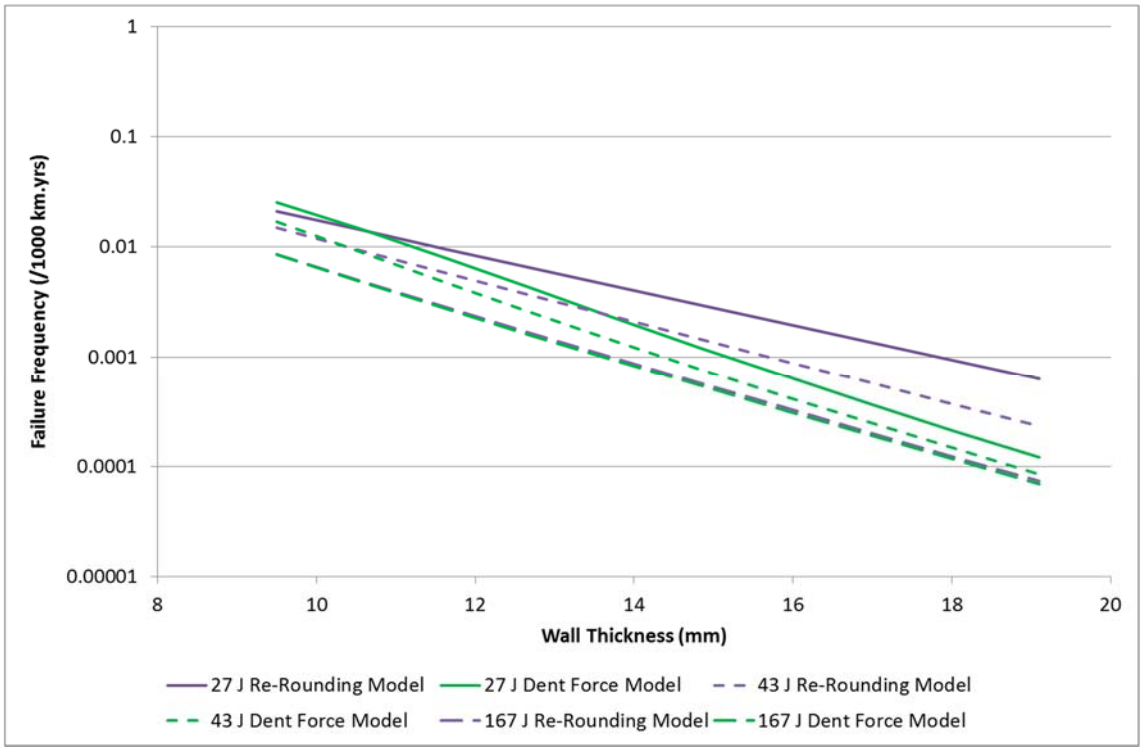

Figure 5.12: Total Failure Frequency as Calculated by the Dent Force Model and the Re-Rounding Model for Examples 4, 5 and 6

Based on the results, the following observations can be made regarding estimations of pipeline failure frequency made by the Dent Force model.

A direct comparison between the results calculated for each example using the Modified PIE model, Re-Rounding model and the Dent Force model indicates that the Dent Force model estimates lower values of failure frequency for high wall thicknesses and higher values of failure frequency for lower wall thicknesses. The use of the dent force distribution in the model allows the effect of the specific pipeline geometry being considered to have more influence on the probability of failure. The dent depth in thick pipe is smaller than in thin pipe resulting in a lower failure frequency.

The effect on estimated failure frequency of introducing the dent force distribution to the model decreases with increasing material toughness (Charpy 2/3 v-notch impact energy). The effect is due to the decreasing influence of the gouged dent failure probability as the toughness is increased (calculated by equations (2.86), (2.88) and (2.89)), as noted in the last paragraph of section 5.2. As with the Re-Rounding model the introduction of the dent force distribution to the model affects only the gouged dent failure probability. The influence of the changes which this model makes to the failure frequency are reduced as the influence of the gouged dent failure probability is reduced.

5.7 The New Distributions Model

Alongside the conclusions stated at the beginning of this chapter, a conclusion was also made in Chapter 3 regarding the use of historical operational data in the development of AFFECT. It was concluded that the most recent UKOPA Fault Database is the most appropriate source of historical operational data to use for the model.

In 2010 UKOPA commissioned Penspen to update the probability distributions and Incident-Rates for the FFREQ failure frequency model, as detailed in section 2.7 (Goodfellow, 2012). An assessment of the 2009 UKOPA Fault Database was performed by Penspen for this purpose. It was noted in section 2.7 that despite the fact that the motivation was to provide an update to FFREQ, the particular probability distributions and Incident-Rate derived by Penspen are actually more suited to the PIE model (and by extension the AFFECT model).

In comparison to the values used by the Modified PIE model, the Re-Rounding model and the Dent Force model, the updated Penspen parameters take into account four additional years of historical operational data related to pipeline mechanical damage[23]. On the basis of the conclusion from Chapter 3, they are therefore considered to be a more accurate representation of the occurrence and size of mechanical damage. Taking this into consideration the updated parameters have been substituted for the Incident-Rate and probability distributions used in the Re-Rounding model as the fourth stage in the construction of AFFECT. This version of the model will be referred to as the New Distributions model. It should be noted that the changes have been made to the Re-Rounding model (the second stage in the construction of AFFECT) rather than the Dent Force model (the third stage) as the 2010 Penspen analysis fitted only a dent depth distribution from the UKOPA Fault Database and dent force was not considered. A corresponding update to the dent force distribution is considered in Chapter 7. It is also noted that the updated Penspen Incident-Rate refers to pipelines located in R-type areas only. The original PIE Model Incident-Rate used in the Modified PIE, Re-Rounding and Dent Force models made no distinction between S-type and R-type areas. The New Distributions model and subsequent models using this Incident-Rate are therefore applicable only to rural pipelines. In order apply the model to pipelines located in S-type areas a factor must be applied to the Incident-Rate, as explained in the discussion in section 2.8. Further details are given in section 7.7.

The updated Incident-Rate used in the New Distributions model is given in Table 2.16. The parameters defining the probability distributions are given in Table 2.17. The distributions are shown in comparison with those from the Modified PIE / Re-Rounding models in Figure 5.13, Figure 5.14 and Figure 5.15. In considering the probabilities that mechanical damage will be a gouge or a gouged dent, no analysis regarding this aspect was performed by Penspen. The values therefore remain unchanged from the Modified PIE / Re-Rounding models.

[23] The PIE model uses the 2005 UKOPA Fault Database as a source of historical operational data.

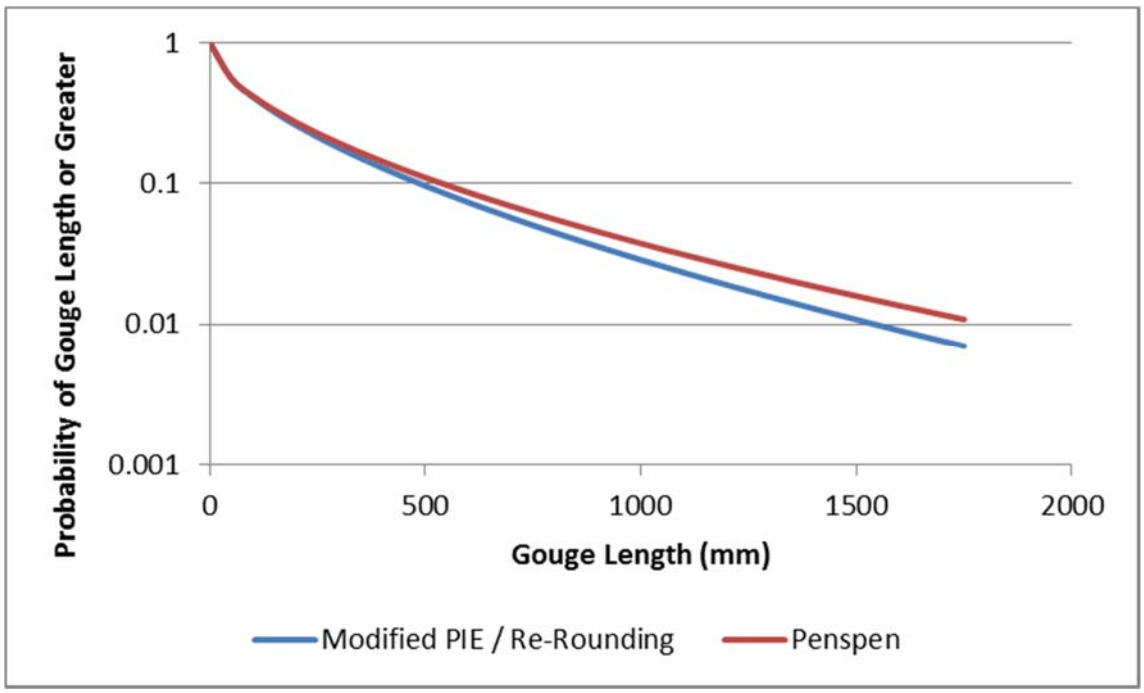

Figure 5.13: Gouge Length Distribution, Modified PIE / Re-Rounding and Penspen Comparison

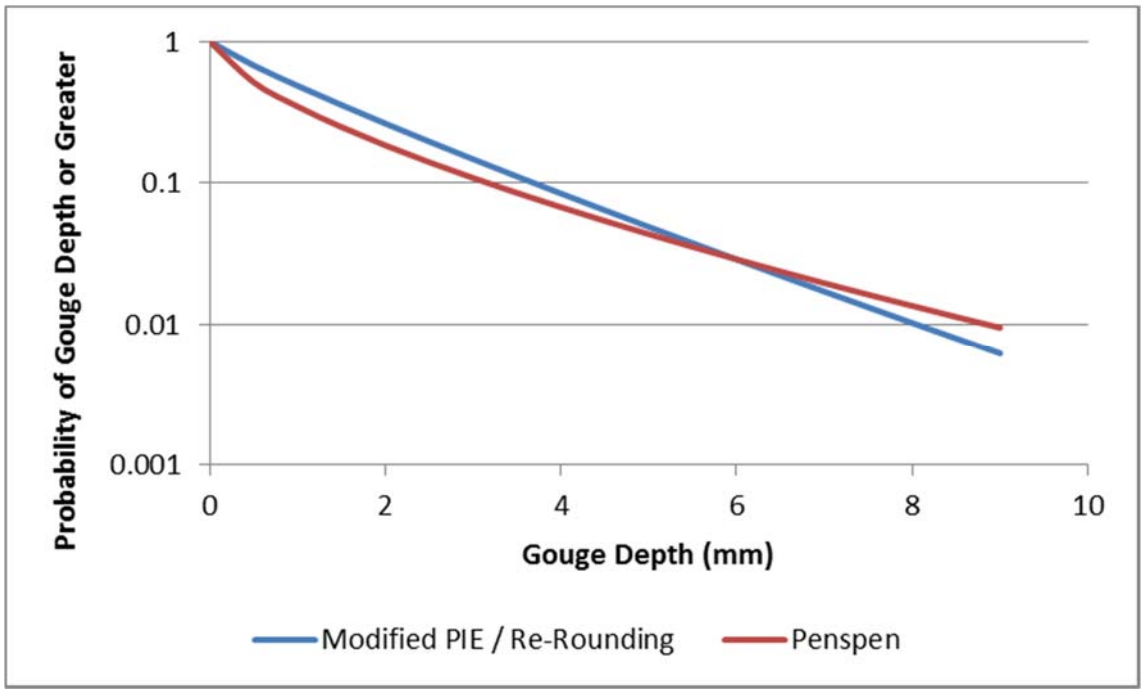

Figure 5.14: Gouge Depth Distribution, Modified PIE / Re-Rounding and Penspen Comparison

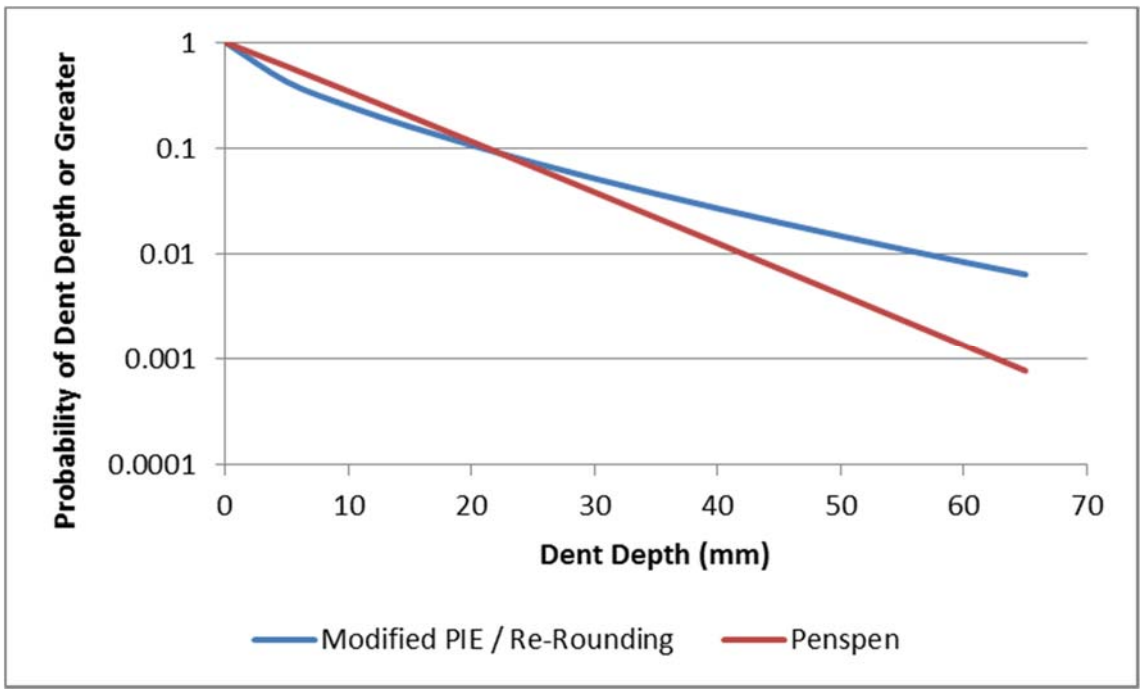

Figure 5.15: Dent Depth Distribution, Modified PIE / Re-Rounding and Penspen Comparison

5.8 New Distributions Model Results

Estimated pipeline failure frequency values have been calculated using the New Distributions model for the six example pipeline cases listed in Table 5.1. As before, leak, rupture and total failure frequency has been calculated.

A comparison between total failure frequency values for example 1 as calculated by the New Distributions model, Dent Force model, Re-Rounding model and the Modified PIE model, is shown in Figure 5.16. A similar comparison between total failure frequency values for example 4 is shown in Figure 5.17. Equivalent charts for the remaining examples are included in Appendix A .

A comparison between total failure frequency values for examples 1, 2, and 3 as calculated by the New Distributions model and the analogous Re-Rounding model, is shown in Figure 5.18. A similar comparison between total failure frequency values calculated for examples 4, 5 and 6 is shown in Figure 5.19.

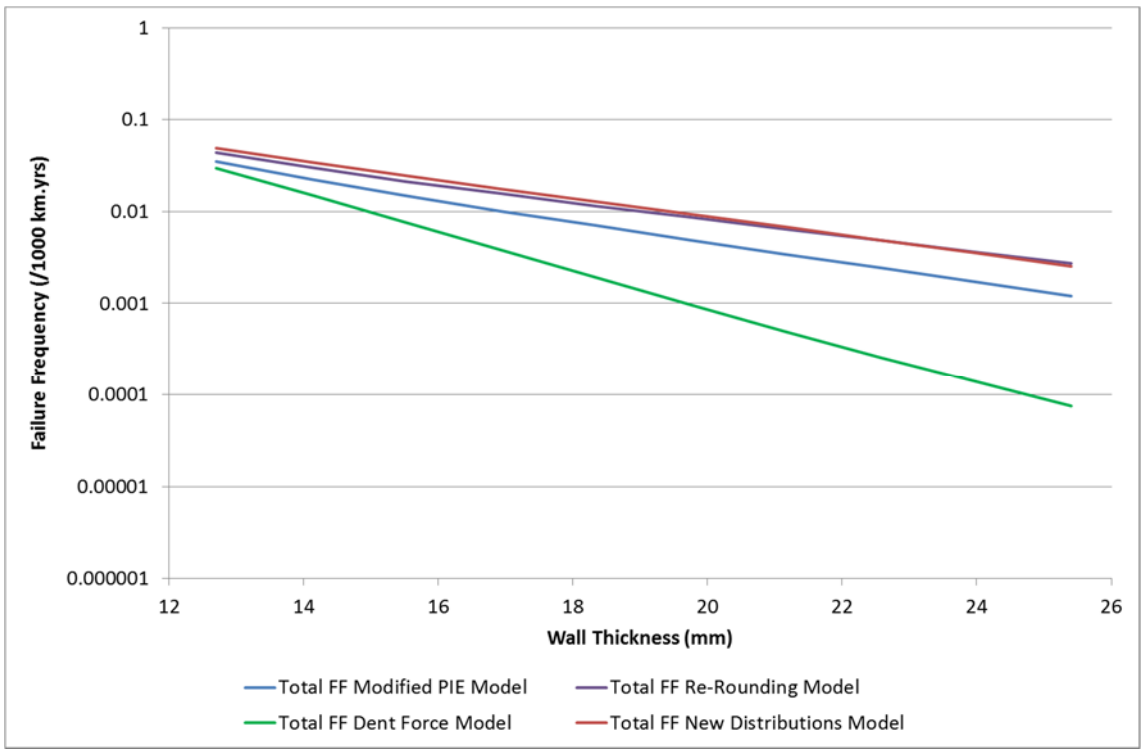

Figure 5.16: Total Failure Frequency as Calculated by the New Distributions Model, Dent Force Model, Re-Rounding Model and the Modified PIE Model for Example 1

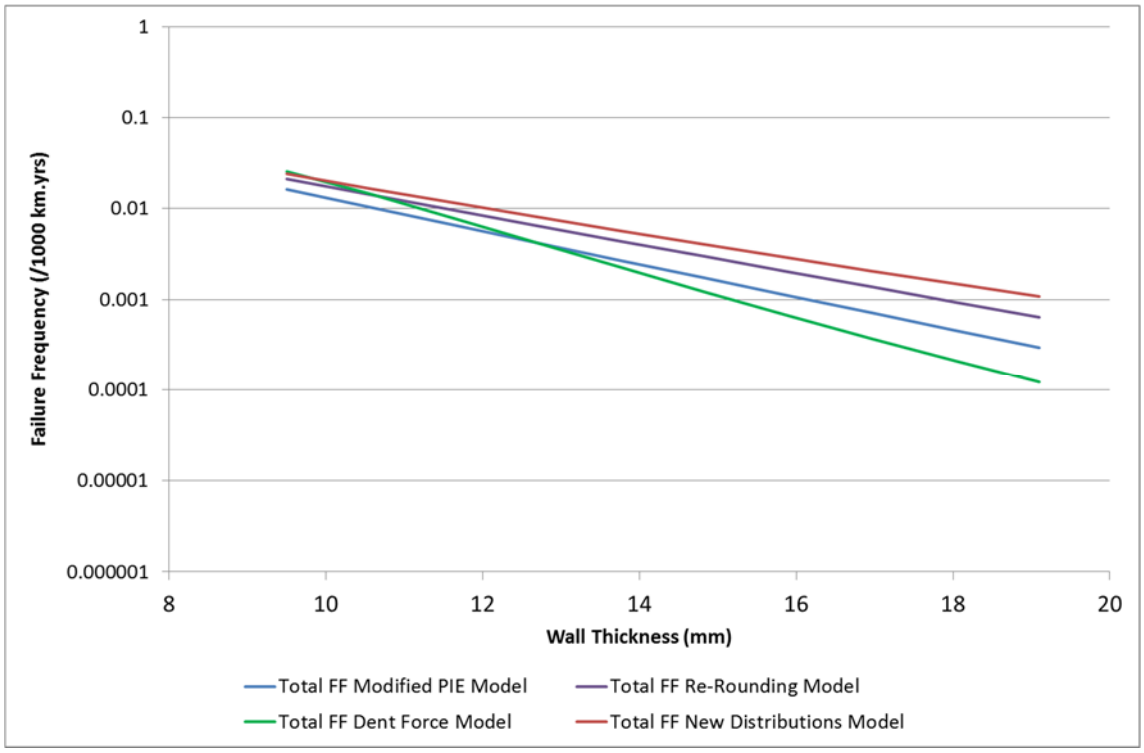

Figure 5.17: Total Failure Frequency as Calculated by the New Distributions Model, Dent Force Model, Re-Rounding Model and the Modified PIE Model for Example 4

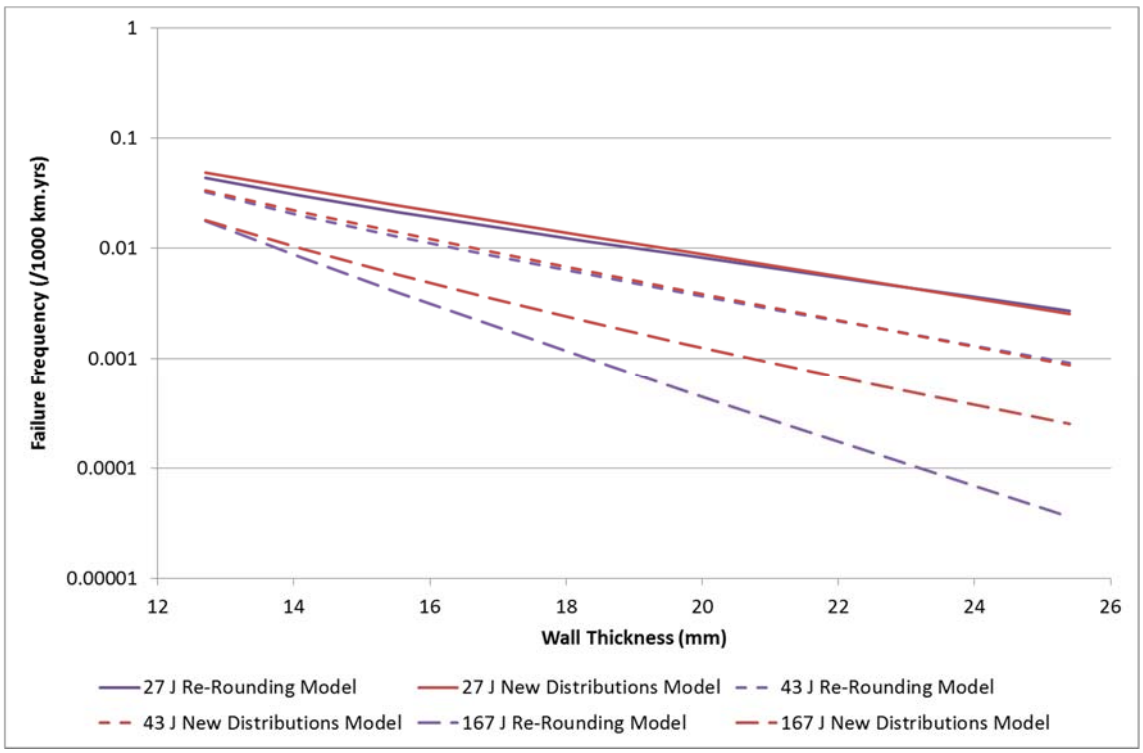

Figure 5.18: Total Failure Frequency as Calculated by the New Distributions Model and the Re-Rounding Model for Examples 1, 2 and 3

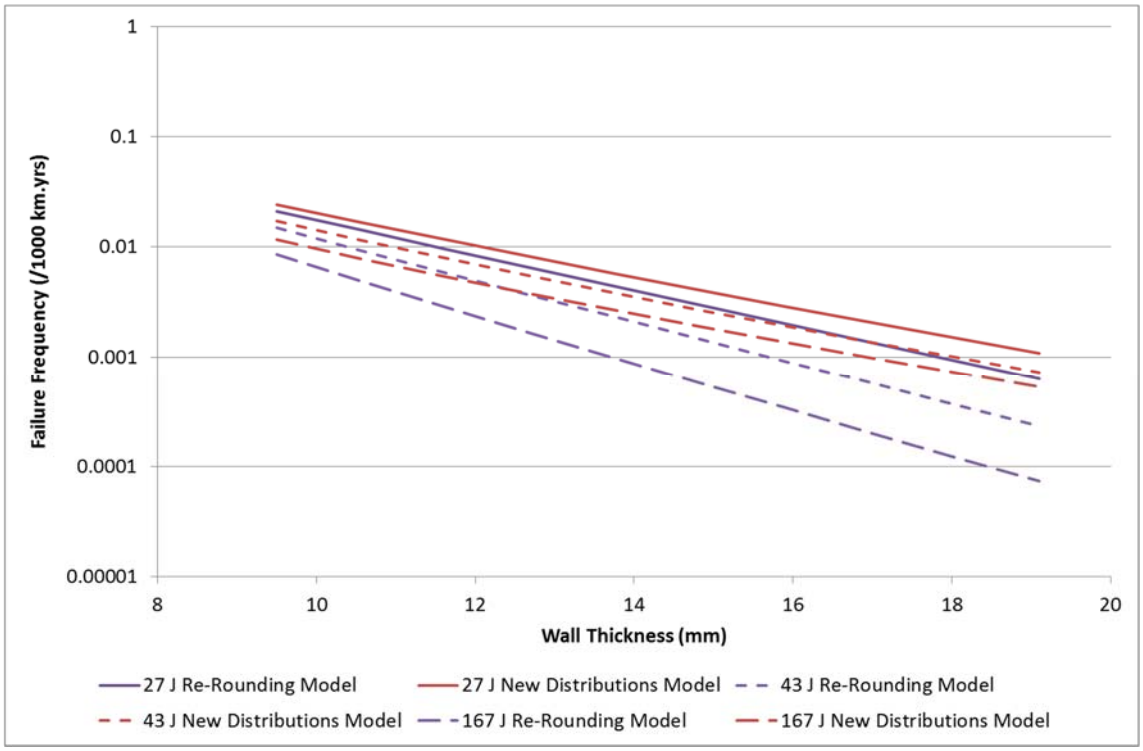

Figure 5.19: Total Failure Frequency as Calculated by the New Distributions Model and the Re-Rounding Model for Examples 4, 5 and 6

Based on the results, the following observations can be made regarding estimations of pipeline failure frequency made by the New Distributions model.

A direct comparison between the results calculated for each example using the Modified PIE Model, the Re-Rounding model, the Dent Force model and the New Distributions model indicates that the New Distributions model generally estimates higher values of failure frequency than the other models. Values are observed to drop slightly below the Re-Rounding model for higher wall thicknesses in the high pressure examples (1, 2 and 3) for the two lowest material toughnesses. The Dent Force model is also seen to estimate slightly higher values than the New Distributions model for the lowest wall thicknesses in the low pressure example with the lowest material toughness (example 4).

The effect on estimated failure frequency of introducing the new parameters to the model shows an increase with increasing material toughness (Charpy 2/3 v-notch impact energy). This effect is due to the differences between the Modified PIE / Re-Rounding and Penspen distributions observed in Figure 5.13, Figure 5.14 and Figure 5.15 and the decreasing influence of the gouged dent failure probability as the toughness is increased (as noted in the last paragraph of section 5.2). For the examples considered, the majority of the gouge failures integrated within equation (2.84) have depths above approximately 6 mm. These gouges reside in the region of Figure 5.14 where the Penspen distribution probability exceeds the Modified PIE / Re-Rounding distribution probability meaning that the overall gouge failure probability is higher for the New Distributions model than the Re-Rounding model. Using similar arguments it can be shown that the overall gouged dent probability is higher for the Re-Rounding model than the New Distributions model. At lower toughnesses, where the gouged dent probability has more influence, the differences cancel for the most part. This can be seen in the very similar estimations of failure frequency in the high pressure examples with the two lowest material toughnesses. In the low pressure examples, the difference in gouge depth failure probability between the Penspen and Modified PIE / Re-Rounding distributions is larger, which is seen as an increase in the New Distributions model estimations over the Re-Rounding model. As toughness is increased the gouged dent failure probability reduces but the gouge failure probability is unaffected. The Re-Rounding model, with its higher gouged dent failure probabilities, therefore shows a large drop off with toughness whilst the New Distributions model is affected to a much lesser extent.

5.9 Development of AFFECT (Part 1) Conclusions

This chapter has charted the first four stages in the construction of AFFECT, a failure frequency model for dense phase carbon dioxide pipelines based upon probabilistic structural reliability methods. The AFFECT model has been developed by making modifications to the PIE model, a basic failure frequency model which uses appropriate failure models identified in Chapter 3 and Chapter 4. The modifications made in this chapter consider damage modelling; operational data and calculation methods. Table 5.2 summarises the basis and benefits of each discrete stage in the model development; a flow chart showing the progression of the model is shown in Figure 5.20.

Each of the modifications addressed is considered to provide improvement to the PIE model. The Modified PIE model improves the probability of failure calculations. The Re-Rounding model and the Dent Force model provide improvement in defining failure limit states by modelling pipeline mechanical damage in a more accurate way, allowing for damage in thicker walled pipelines, in particular, to be modelled more appropriately. The New Distributions model provides improvement to the probability distributions describing the nature of pipeline mechanical damage.

Model	Basis / Development	Benefits
Modified PIE	Structural reliability model based upon a simplified version of the British Gas methodology. Updated with calculations from the Cosham model.	Use of most appropriate models for leak / rupture, gouge failure and gouged dent failure. Probability of failure calculated accurately
Re-Rounding	As Modified PIE model but with EPRG dent re-rounding equation	Dent depth is modelled more accurately
Dent Force	As Re-Rounding model but with EPRG dent force equation used to derive dent force distribution in place of dent depth	Denting modelled more accurately, dependence on geometry is removed
New Distributions	As Re-Rounding model but with updated distributions	Distributions up to date as of 2009

Table 5.2: Summary of the Basis and Benefits of the First Four Stages in the Construction of AFFECT

Following the modifications made for the New Distributions model, the next logical stage in the construction of AFFECT is an update to the dent force distribution using recent operational data. In this way the improvements introduced in The Dent Force model can be combined with those from the New

Distributions model. In the absence of any existing studies providing a new dent force distribution an analysis of the most recent UKOPA Fault Database must be performed in order to derive the updated distribution.

An analysis of the UKOPA Fault Database also allows the number of random variables used in the AFFECT model to be investigated. In Chapter 2 it was highlighted that the original Hazard Analysis model, FFREQ and PIPIN all assumed the gouge length and gouge depth variables to be separate to those for gouged dent gouge length and gouged dent gouge depth. In the PIE and Cosham models and the updated Penspen distributions the variables were consolidated. The importance in determining the correct approach was noted in the discussion in section 2.8 and will provide scope for an additional stage in the construction for the AFFECT model.

At the time of writing the most recent UKOPA Fault Database is 2010. The analysis of the 2010 UKOPA Fault Database is detailed in Chapter 6.

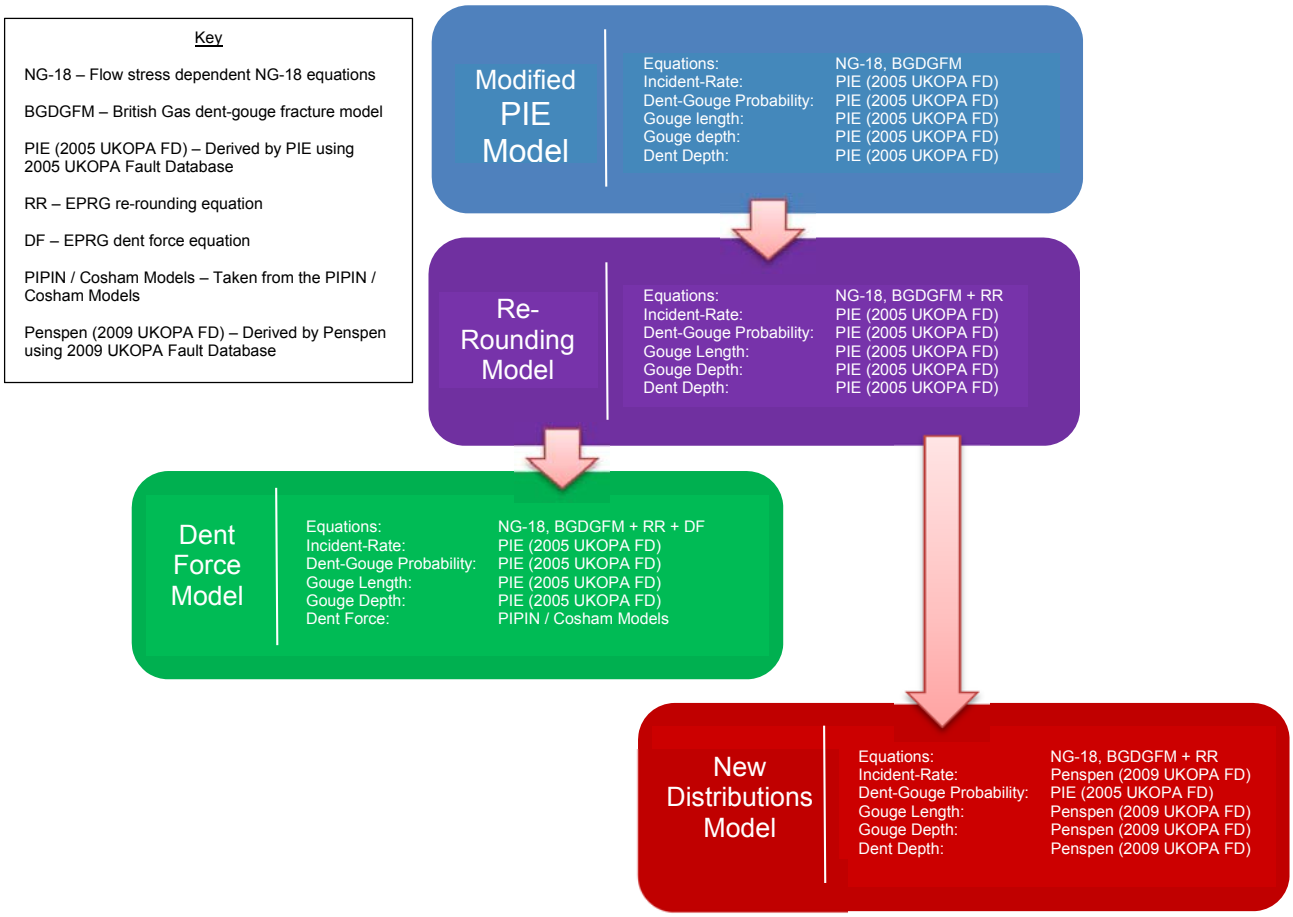

Figure 5.20: The First Four Stages in the Construction of AFFECT

Chapter 6. An Assessment of the 2010 UKOPA Fault Database

Details of historical operational damage and failures caused by external interference are recorded in the UKOPA Pipeline Fault Database (Anon., 2011c). This chapter presents a detailed filtering and assessment process of the 2010 UKOPA Fault Database. The data has been provided by UKOPA for use in the development of the AFFECT model.

The aims of this chapter are: firstly, to derive from the UKOPA Fault Database suitable pipeline damage data sets to which probability distributions for dent force, gouge depth and gouge length can be fitted and used in the AFFECT model; and secondly to provide a comprehensive statistical analysis of the database in order to identify trends and assist in the refinement of the model.

6.1 Description of the UKOPA Fault Database

The UKOPA Pipeline Fault Database contains details of pipeline faults and failures which have been subject to an excavation and on-site assessment dating back to 1962. The database covers approximately 23,000 km of gas and liquid pipelines (both operating and decommissioned) in the UK. It includes information about the affected pipeline including its external diameter, wall thickness, steel grade, operating pressure and the specific component affected. For the fault, its type, date of discovery, orientation and the extent of the damage are recorded. In line with other recognised pipeline databases, the cause of the fault is stated, including comments providing additional information. The UKOPA Fault Database is unique in that it also contains detailed information on the size of pipeline defects, both for cases of part-wall damage and through-wall failures, which have resulted in a of loss of containment.

6.1.1 *Data Requirements for the AFFECT Model*

The causes of pipeline faults recorded within the UKOPA Fault Database include construction damage, external interference, corrosion, material and

welding defects (Anon., 2011c; McConnell, 2011). Given that AFFECT is a model for calculating the failure frequency due to third party external interference, only the faults resulting from external interference damage are of concern.

The data required from the UKOPA Fault Database for the development of the AFFECT model includes:

- The total number of external interference damage incidents;
- The operating parameters for the pipelines affected in each damage incident;
- The type of the damage caused in each incident;
- The size of the damage caused in each incident;

In addition to the total operational exposure of pipelines covered by UKOPA, this data allows derivation of: the Incident-Rate[24], the probability that external interference damage will be a gouge or a gouged dent; and probability distributions for each of the random variables in the model.

Regarding the “type of the damage”, in line with its basis in the PIE and Cosham models, AFFECT considers the probability of failure due to part-wall and through-wall damage from gouges and gouged dents only. As noted in Chapter 2, external interference damage to branch pipes or fittings; or due to drilling operations in-error, can in some cases result in a pipeline failure. These types of pipeline failure are not considered to be the same as failure of part-wall and through-wall gouges and gouged dents. Data from the UKOPA Fault Database relating to these types of failure must not be included in any derivations relating to gouge and gouged dent damage. It is therefore important to determine the mode of failure from the UKOPA Fault Database in order to ensure that AFFECT is constructed correctly.

[24] Note however that in this analysis a new value for Incident-Rate has not been derived. The value derived in the Penspen analysis is considered to be perfectly adequate.

In order to incorporate failures from branches and fittings and drilling operations in-error into a failure frequency model either separate branch / fitting failure and drill puncture models must be developed; or an additional historical data component (see section 2.2.2) is required. The development of such components for AFFECT has not been considered as part of this work.

The “size of the damage” relates to the measured damage dimensions which are random variables in the model. The important dimensions for gouge damage are the gouge length and gouge depth. The important dimensions for gouged dent damage are the dent depth, gouge length and gouge depth. Dent force can be derived from the dent depth using equations (2.83) and (5.4). Information taken from the UKOPA Fault Database allows probability distributions to be derived for each damage dimension of importance.

6.1.2 *Overview of External Interference Damage Data*

A detailed review of the damage and failure data recorded within the UKOPA Fault Database as being due to external interference has been carried out. A summary of the “type of damage” category as described in section 6.1.1 following this review is given in Table 6.1. A complete description of the review process is included in Appendix B .

It is noted that due to non-standardised methods of data reporting and a wide variety of contributing sources, much of the information recorded within the UKOPA Fault Database is uncertain or non-specific, particularly regarding the type of damage. The row headings listed in Table 6.1 are not taken directly taken from the database, but rather the data has been categorised using judgement based upon the available information.

Table 6.1 indicates which damage records within the database can be used in the development of the AFFECT model. Where the term “Damage” is used, this refers to either gouge, dent or gouged dent damage. This subdivision is explored further in section 6.2. Note that damage to pipeline components other than the pipe body or bends are not included (damage to branches and fittings).

As previously noted the AFFECT model is not applicable to these components. Damage to the pipeline within operator compounds is also not included. These areas are not accessible to the general public and the damage does not qualify as third party external interference. Damage classed as “coating damage” is considered to be superficial and cannot be considered as dent, gouge or gouged dent damage. Unknown damage has not been included due to a lack of information associated with those records. Table 6.1 also includes a category for “not external interference”. Damage within this category was recorded as “external interference” in the database but a review of the available information subsequently highlighted this to not be the case. This data has not been used in the development of the AFFECT model.

Table 6.1 also includes a column indicating that 307 of the total 1292 recorded external interference damage records contained no information on the dimensions of the damage. With regards to the AFFECT model, only damage data with recorded dimensions is included in the derivation of the probability distributions. It is noted however, that where impact damage is recorded without damage dimensions, the data can still be taken into account in determining the probability that external interference damage will be a gouge or a gouged dent. Furthermore, if an impact is recorded but specific dent or gouge damage to the pipe wall does not occur, the data remains adequate for inclusion into the Incident-Rate.

Description of damage	No. Of Defects	No. w/out dimensions	Comments
Not external interference	64	13	Not included in derivations from dent and gouge data
Coating damage to pipe/bend	104	23	May be used to adjust Incident-Rate
Damage to pipe/bend	932	222	Only data with recorded dimensions can be used for probability distributions. Otherwise, gouge/gouged dent probability only
Damage to pipe/bend with corrosion	29	4	As above
Damage to weld on pipe/bend	7	2	As above
“Leak” of pipe/bend	24	7	As above. 10 separate incidents.
“Fracture” of pipe/bend	13	2	As above. 7 separate incidents.
Drill damage to pipe/bend	21	1	As above
Drill “leak” of pipe/bend	7	1	Not included in derivations from dent and gouge data and require a separate treatment
Damage to above ground or within complex pipe/bend	33	9	Not included in derivations from dent and gouge data
Damage to tee, weldolet, sleeve, valve, branch, dome end etc.	35	10	Not included in derivations from dent and gouge data. Failures require a separate treatment.
Unknown damage incidents to pipe/bend/weld	17	10	Not included in derivations from dent and gouge data
Unknown “leak”/”fracture” on pipe/bend	1	1	Not included in derivations from dent and gouge data and require a separate treatment.
Damage to unknown components	5	2	Not included in derivations from dent and gouge data
Total	1292	307	

Table 6.1: Overview of External Interference Damage and Failure Data

6.2 Damage Data

As noted in section 6.1.1, the damage data of primary interest in the development of the AFFECT model is that concerning gouges and gouged dents. Probability distributions must be derived relating to the damage dimensions. Damage dimensions are recorded for each record within the UKOPA Fault Database, giving the length, width and depth of a particular incident. Dents and gouges within the database have separate records, each with their own set of dimensions. Each record also has a “defect number” and a “fault number”. The “defect number” is simply an individual identifier for each damage record contained within the database. The “fault number” is a group identifier assigned to one or more defects located on the same pipeline, in close proximity to each other, and discovered during the same excavation. A dent record may be associated with a gouge record by the “fault number”. Due to the uncertain nature of the information within the UKOPA Fault Database it has conservatively been assumed that a dent and gouge sharing the same “fault number” can be classed as gouged dent damage. Gouge records which do not

share a “fault number” with a dent record have been classed as gouge damage and dent records which do not share a “fault number” with a gouge record have been classed as dent damage.

An assessment of the dent depth, gouge depth and gouge length data is made in this chapter in order to determine which of the records contained within the database are appropriate for the derivation of damage dimension probability distributions. Discussion is also made regarding trends within the data. The dimensions are considered directly as recorded from the UKOPA Fault Database, however considering the level of uncertainty within the database, it is likely some error exists.

The database classifies pipeline failures simply as “dents” or “gouges”. As noted in section 6.1.1 pipeline failures from branches and fittings and drilling operations in-error must not be included in any derivations relating to gouge and gouged dent damage. Damage to branches and fittings is easily identified by an “affected component” field included in the database. This data is not included in the following assessments. A specific identifier relating to drilling however does not exist; and failures caused by drilling are grouped together with other pipeline damage and classified as “dent” or “gouge”. Judgement must therefore be made as to whether drilling was the cause of the failure. In the following assessments, all damage data relating to the pipe or bend, either in the pipe body or on a weld is included. For this reason pipe or bend failures caused by drilling are included in the assessment, despite the fact that they must be excluded from any subsequent derivations. The classification of drilling failures is addressed in section 6.3.

6.2.1 *Dents*

As described in section 2.1.1, a dent is a plastic deformation of the pipe profile, which causes a concentration of stress and therefore reduces the pressure at which the pipe may fail. There are 107 external interference dents to pipe or a bend recorded within the UKOPA Fault Database. Two of the dents were

recorded as being associated with the coating only, as a result these have been removed from the assessment.

Of the remaining 105 dents, 85 are recorded with associated gouges, five are recorded with associated gouges and corrosion[25], and five are recorded with associated gouges and lead to a pipeline failure ("leak" or "fracture"); ten of the dents are considered to be plain dents (with no associated gouge).

Of the 105 dents, only 66 have a recorded dent depth. Figure 6.1 shows the depths of these dents, plotted against the wall thickness of the pipeline in which they occurred, in terms of their measured depth. Figure 6.2 shows the depths in terms of the percentage of the pipeline's external diameter (%OD).

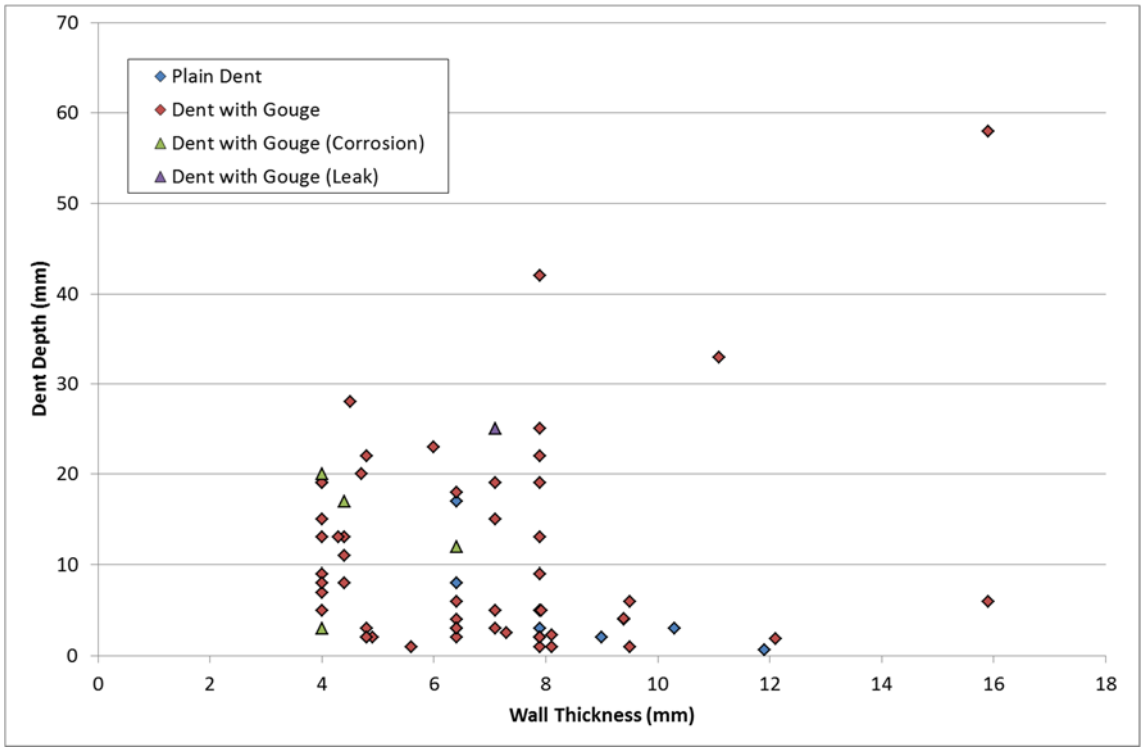

Figure 6.1: Dent Depth (mm) vs. Wall Thickness

[25] Corrosion develops as a result of damage to the pipeline coating when the dent occurs. It can add to the damage severity by increasing the size of any associated gouging.

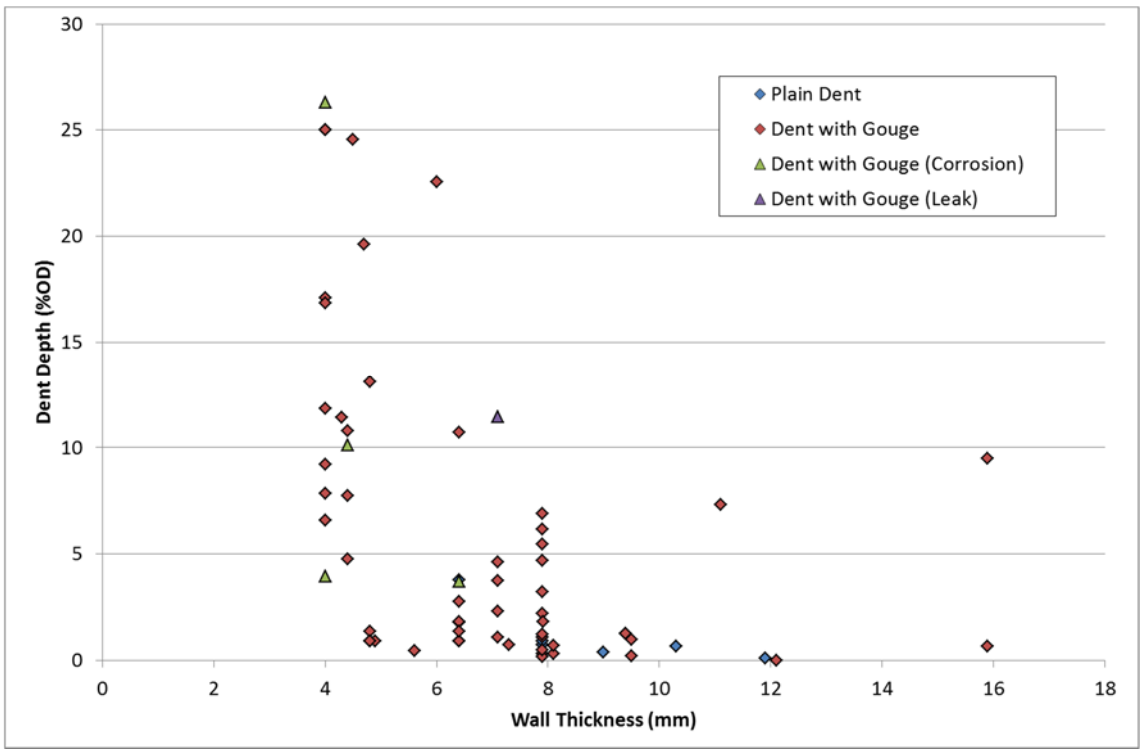

Figure 6.2: Dent Depth (%OD) vs. Wall Thickness

The deepest dent in the database is a dent associated with a gouge. This dent was located in a pipeline of wall thickness 15.9 mm and external diameter 610 mm. The dent was recorded to be 58 mm deep or 9.5 %OD, with an associated gouge of 1.5 mm deep. The deepest dent, relative to pipeline external diameter, in the database is a dent associated with a gouge and corrosion. This dent was located in a pipeline of wall thickness 4 mm and external diameter 76 mm. The dent was recorded to be 20 mm deep or 26.3 %OD. The associated gouge/corrosion does not have a recorded depth.

The deepest recorded plain dent was located in a pipeline of wall thickness 6.4 mm and external diameter 450 mm. The dent was recorded to be 17 mm deep or 3.8 %OD.

The dent associated with a pipeline failure (“leak”) was located in a pipeline of wall thickness 7.1 mm and external diameter 218 mm. The dent was recorded to be 25 mm deep or 11.5 %OD, with an associated gouge of 7.1 mm. The failure was caused by an excavator.

Table 6.2 summarises six significant dents in the database.

Description	Operating Pressure (barg)	Pipe Diameter (mm)	Wall Thickness (mm)	Dent Length (mm)	Dent Width (mm)	Dent Depth (mm)	Dent Depth (%OD)	Fault Comment
Plain Dent	7	450	6.4	210	120	17	3.8	TWO DENTS: #2 ENTERED AS GOUGE
Dent with gouge	17	610	15.9	1400	320	58	9.5	DENT&SPALLING. FALLING MASONRY
Dent with gouge	6.5	610	7.9	700	250	42	6.9	DMGE BY IMPACT CORE DRILL
Dent with gouge	50	450	11.1	160	110	33	7.3	INTERF/BOREHOLE SURVEY/W.MAIN
Dent with gouge (corrosion)	14	76	4	50	50	20	26.3	DENT & EXT. CORROSION OLI4
Dent with gouge (leak)	6.9	218	7.1	133	133	25	11.5	Damaged by FE20 excavator during landscaping

Note: The dents highlighted in yellow were caused by drilling machines

Table 6.2: Summary of Significant Dents

Note that in Table 6.2 the plain dent record refers to “Two dents: #2 entered as a gouge”, in this case the comment has been used to reclassify the type of damage from gouge to dent and this has been included in the above totals.

Figure 6.2 shows that the maximum depth of dents, relative to the pipeline external diameter, decreases with increasing wall thickness. This is an expected trend as pipeline external diameter typically increases with wall thickness whereas the machinery (in terms of impact force delivered) involved in creating pipeline denting will be the same regardless of the pipeline they are hitting. From Figure 6.1 it is clear that the majority of dents are below 30 mm deep suggesting that the typical machinery working in the vicinity of pipelines is capable of delivering a force large enough to cause a maximum dent depth of 30 mm. Furthermore, as can be seen from Table 6.2, of the three dents with depths greater than 30 mm, two were caused by powerful drilling machines capable of delivering a sustained force to the pipeline, rather than an instantaneous impact; and one was caused by falling masonry, which is an atypical damage mechanism. Both Figure 6.1 and Figure 6.2 appear to show that the depth of dents decreases significantly for pipelines subject to external interference with a wall thickness in excess of 8 mm. This suggests that thicker walled pipelines are more difficult to dent. It should be noted however that substantially fewer dents occurred in pipelines with wall thicknesses greater than 8 mm.

On the basis of the above assessment it is concluded that the 66 dents with a recorded depth dimension are suitable for the derivation of a probability distribution to be used in the AFFECT model.

6.2.2 *Gouges*

As described in section 2.1.1, a gouge is a loss of material which results in a reduction of wall thickness, which may include crack like defects.

There are 1027 external interference gouges to a pipe or bend recorded within the UKOPA Fault Database. 99 of the gouges were recorded as being associated with the coating only, as a result these have been removed from the following assessment.

Of the remaining 928 gouges, 194 are recorded as being associated with dents[26]. Of these 194, 15 are recorded with associated corrosion[27], 15 lead to a pipeline failure ("leak" or "fracture") and six have been classified as being caused by drilling.

734 of the gouges are recorded with no associated dent. Of these, nine are recorded with associated corrosion, 20 were caused by drilling and 24 lead to a pipeline failure (seven of the 24 failures were caused by drilling).

In terms of dimensions, the severity of a part-wall gouge is a function of its depth as a proportion of wall thickness, and length as a multiple of external pipeline radius.

6.2.2.1 *Gouge Depth*

Of the 928 gouges, only 596 have a recorded gouge depth which is sensible[28]. Of these, 110 are recorded as being associated with dents and 486 are recorded with no associated dent.

---

[26] Some dents are associated with multiple gouges.
[27] Corrosion develops as a result of damage to the pipeline coating when the gouge occurs. It can add to the damage severity by increasing the size of the gouge over time.
[28] 16 gouges have a recorded gouge depth which exceeds the pipeline wall thickness, nine as a result of the wall thickness being omitted from the database and one with a potentially erroneous depth of 99 mm. The remainder are gouges associated with dents, possibly suggesting that gouge depths have been recorded as a combination of dent depth and gouge depth.

Figure 6.3 shows the depths of these gouges, plotted against the wall thickness of the pipeline in which they occurred in terms of their measured depth. Gouge depth frequency is shown in Figure 6.4.

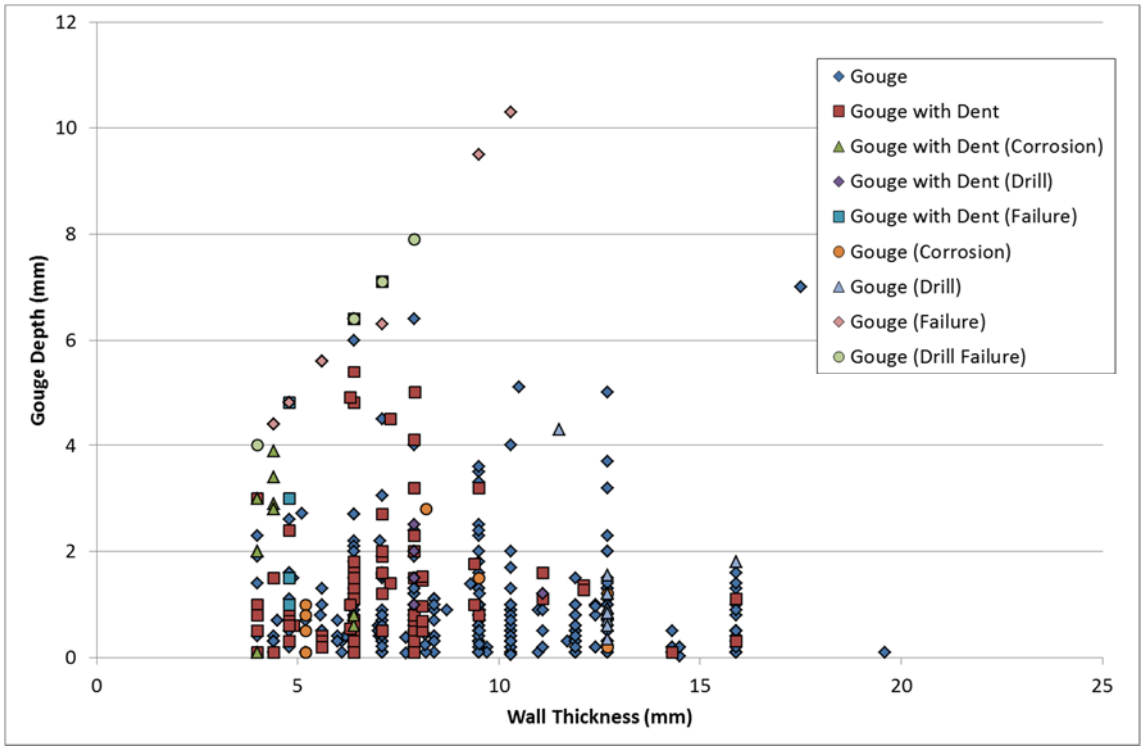

Figure 6.3: Gouge Depth vs. Wall Thickness

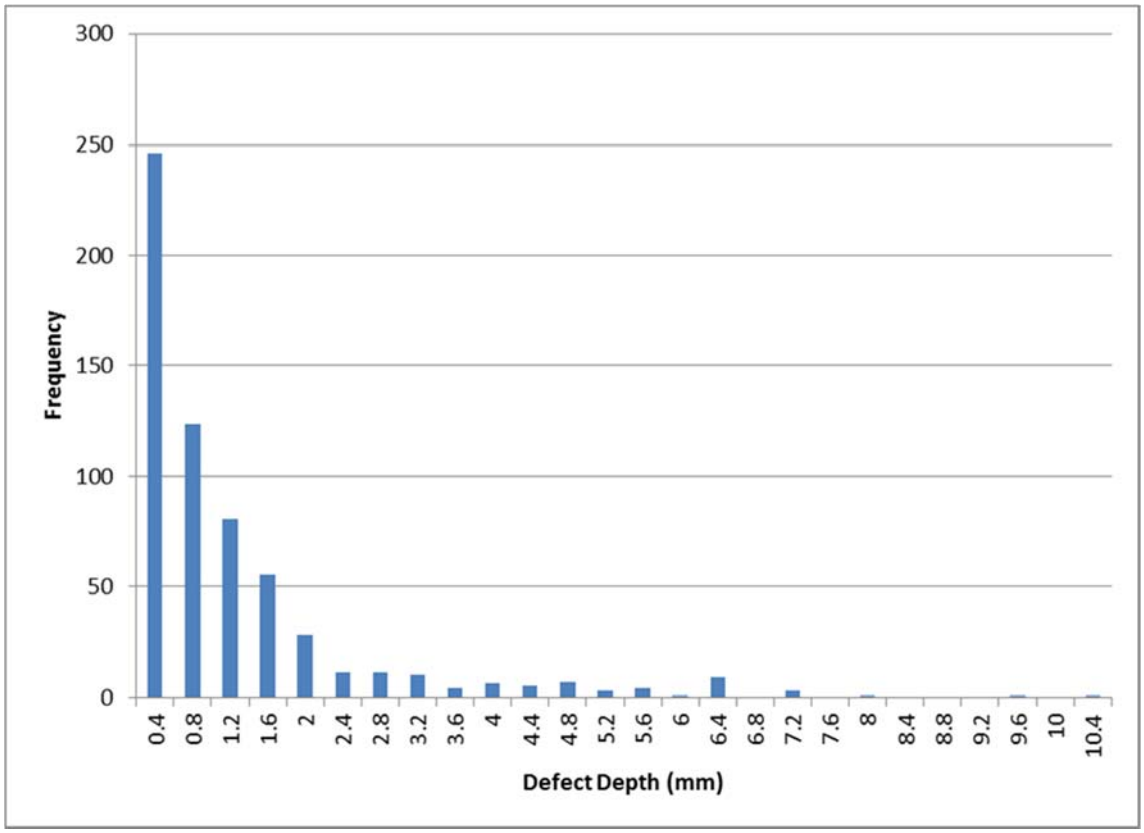

Figure 6.4: Gouge Depth Frequency

Pipeline failures caused by drilling have been explicitly shown in Figure 6.3. As noted in section 6.1.1 these defects are not considered to be the same as failure of severe part-wall or through-wall gouges in the context of the AFFECT model. A drill will deliver a sustained boring action to the pipe wall, whereas typical gouges are metal loss defects caused by an instantaneous transmission of energy when machinery accidentally strikes a pipeline. Consequently, the chances of a failure resulting from a drill puncture are not reduced in thicker wall pipelines in the same way as typical gouges. Failures as a result of this damage mechanism are considered to be wall thickness independent.

The deepest recorded gouge in the database was a through-wall failure located in a pipeline of wall thickness 10.3 mm and external diameter 457 mm. This gouge was not associated with a dent. The failure either occurred during a welded sleeve repair or was repaired by a welded sleeve (details are uncertain).

The deepest gouge which did not result in a failure was located in a pipeline of wall thickness 17.5 mm and external diameter 914 mm. The gouge was recorded to be 7 mm deep and was not associated with a dent. Table 6.3 summarises the 15 deepest gouges in the database in order of depth.

Description	Operating Pressure (barg)	Pipe Diameter (mm)	Wall Thickness (mm)	Defect Length (mm)	Defect Width (mm)	Defect Depth (mm)	Fault Comment
Gouge (Failure)	14.1	457	10.3	0	0	10.3	WELDED SLV REPAIR
Gouge (Failure)	21.4	457	9.5	0	0	9.5	SHEETPILERSLICEDTHRUSIDEOFPIPE
Gouge (Drill Failure)	10.3	325	7.9	23	23	7.9	// LINES-WRONG 1 DRILLED-25MMH
Gouge (Drill Failure)	15.9	274	7.1	11	11	7.1	GAS LINE MISTAKEN FOR WATER PI
Gouge with Dent (Failure)	6.9	218	7.1	5	5	7.1	Damaged by FE20 excavator during landscaping
Gouge	0	914	17.5	25	10	7	JACK HAMMER CHISEL GOUGE
Gouge (Drill Failure)	12.3	325	6.4	50	50	6.4	DRILLED IN ERROR BY DISTN.
Gouge with Dent (Failure)	14.5	324	6.4	89	89	6.4	HOLE , INDENTATION
Gouge	6.9	406	7.9	0	0	6.4	GOUGES
Gouge (Drill Failure)	10.3	168	6.4	0	0	6.4	[MS]SERVICE LAYER DRILLED WRONG MN
Gouge (Failure)	6.9	218	6.4	8	8	6.4	LINE HOLED BY PNEUMATIC DRILL
Gouge with Dent (Failure)	6.2	324	6.4	25	3	6.4	4 HITS , 1 PENETRATION
Gouge (Failure)	16.5	325	6.4	64	13	6.4	TRENCH CUTTER HOLED PIPE
Gouge (Failure)	13.8	168	6.4	0	0	6.4	JCB HIT DIVERTED PIPE-ROADWRKS
Gouge (Failure)	30.1	218	7.1	8	3	6.3	PIPE CUT BY GRINDER IN ERROR

Table 6.3: Summary of Deepest Gouges

In Figure 6.3 a diagonal line of data with positive gradient, where gouge depth is equal to wall thickness, bounds the remaining data points. This line represents the pipeline failures classified in the database as gouges. Below this it is clear that the majority of gouges are below 6 mm deep; Figure 6.4 shows that 87% of gouges are 2 mm deep or less, with only 2.6% at 6 mm or greater. This suggests that the typical machinery working in the vicinity of pipelines is capable of delivering a force large enough to cause a maximum gouge depth of 6 mm. The majority of these gouges are not significant and did not result in failure. Furthermore, as can be seen from Table 6.3, of the 15 gouges with depths greater than 6 mm; four were caused by drill damage; three were caused by machines similar to drills (jack hammer chisel, pneumatic drill, grinder); and two were caused by powerful slicing machines (sheet-piler and trench cutter). Of the remaining six gouges, four of the records do not provide enough information to draw satisfactory conclusions as to their origin; leaving only two gouges with a depth greater than 6 mm definitively indicated as typical gouge damage. These gouges are highlighted in Table 6.3.

It can also be seen from Figure 6.3 that the maximum depth of gouges associated with dents decreases with increasing wall thickness, whilst the maximum depth of gouges not associated with dents remains approximately constant. Considering this trend in conjunction with the trends shown in section 6.2.1 suggests that because additional force is required to dent a pipeline of higher wall thickness, less force will be available to create an associated gouge on impact, thus reducing the depth of these gouges as pipeline wall thickness increases.

In a similar way to pipeline denting in section 6.2.1, Figure 6.3 also appears to show that the depth of gouges decreases for pipelines subject to external interference with a wall thickness in excess of 12.7 mm (outlier at 17.5 mm wall thickness noted). However, contrary to the case of dents, which are deformations in the shape of the pipe wall, which the wall thickness would work directly against; a gouge is a metal loss defect and would therefore not be affected by the pipeline wall thickness. Intuitively, there is no reason why such a relationship would occur. It should be noted that substantially fewer gouges

occurred in pipelines with wall thicknesses greater than 12.7 mm which could possibly explain the trend.

On the basis of the above assessment it is concluded that the 570 gouges with a sensible gouge depth dimension are suitable for use in the development of the AFFECT model. 26 gouges associated with pipeline failure are addressed further in section 6.3.

6.2.2.2 *Gouge Length*

Of 928 gouges, only 636 have a recorded gouge length. Of these 118 are recorded as being associated with dents and 518 are recorded with no associated dent. Figure 6.5 shows the lengths of these gouges, plotted against the wall thickness of the pipeline in which they occurred in terms of their measured length[29]. Gouge length frequency is shown in Figure 6.6.

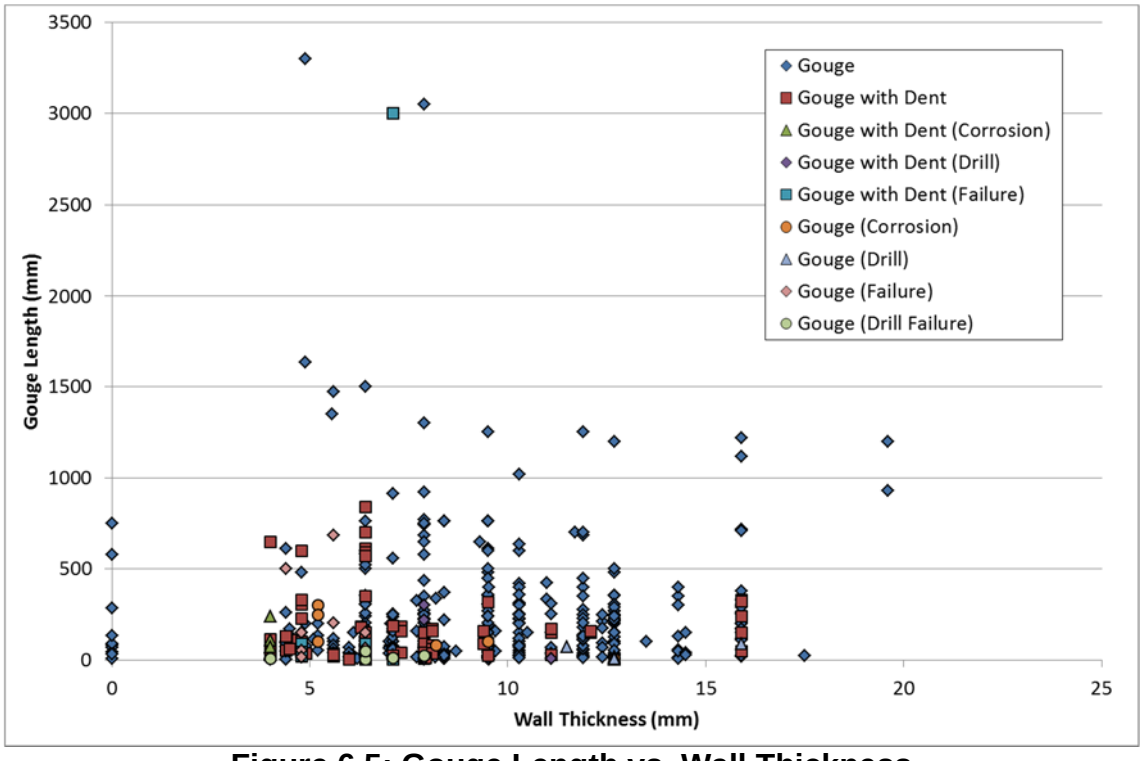

Figure 6.5: Gouge Length vs. Wall Thickness

[29]Note that ten gouges lie on the y-axis due to the wall thickness of the pipeline in which they were located being omitted from the database.

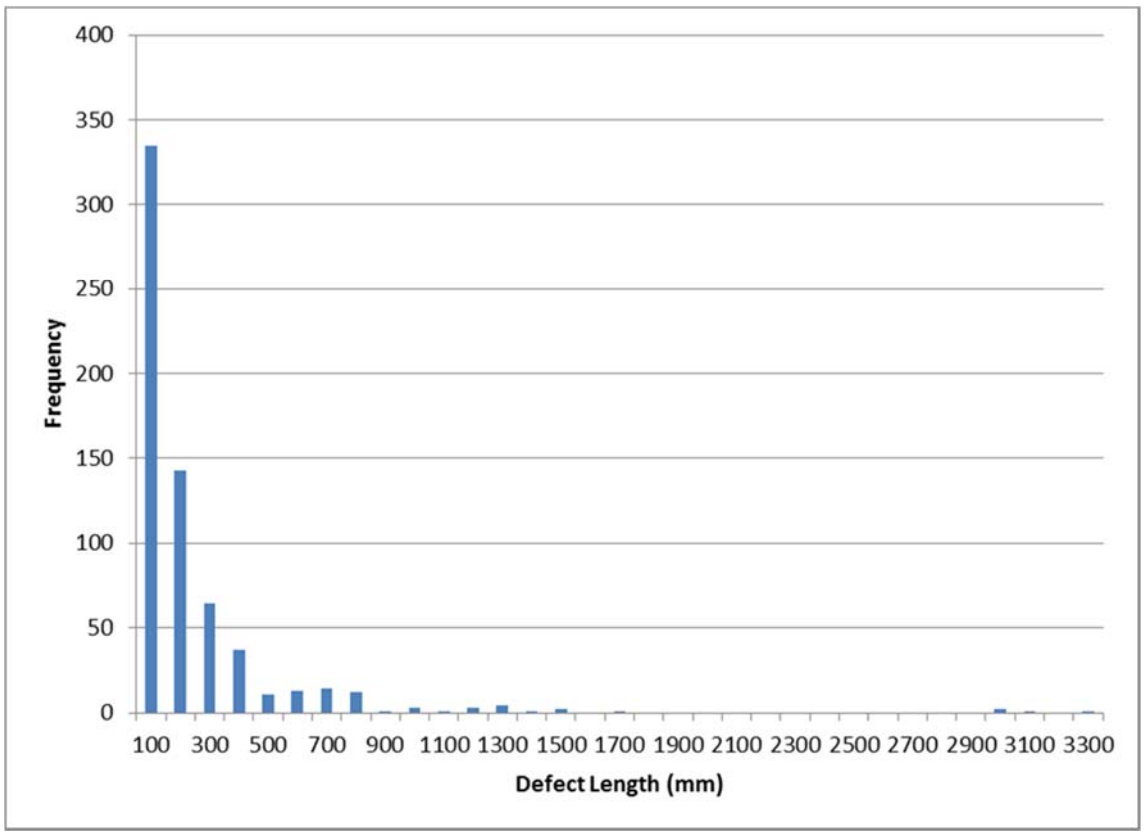

Figure 6.6: Gouge Length Frequency

The longest recorded gouge in the database was located in a pipeline of wall thickness 4.88 mm and external diameter 219 mm. The gouge was recorded to be 3300 mm long and was not associated with a dent.

The longest gouges associated with a failure were located in a pipeline of wall thickness 7.1 mm and external diameter 218 mm. The gouges were both recorded to be 3000 mm long and were associated with a dent. Both gouges occurred as a result of the same incident. It should be noted that neither of these gouges were the cause of the failure itself, they share a “fault number” with a much shorter 5 mm long gouge which failed. The dent defect and other gouge defects associated with this failure appear both in the tables of important dents and deepest gouges in sections 6.2.1 and 6.2.2.1 respectively. The failure was caused by an excavator during landscaping.

Table 6.4 summarises the 15 longest gouges in the database in order of length.

Description	Operating Pressure (barg)	Pipe Diameter (mm)	Wall Thickness (mm)	Defect Length (mm)	Defect Width (mm)	Defect Depth (mm)	Fault Comment
Gouge	19.8	219	4.88	3300	0	1.5	186k cable laying - pipe was pegged-out
Gouge	24.1	325	7.9	3048	0	0	2 LARGE GOUGES IN DITCH
Gouge with Dent (Failure)	6.9	218	7.1	3000	0	0	Damaged by FE20 excavator during landscaping
Gouge with Dent (Failure)	6.9	218	7.1	3000	0	0	Damaged by FE20 excavator during landscaping
Gouge	19.8	219	4.88	1640	0	1.5	186k cable laying - pipe was pegged-out
Gouge	7	325	6.4	1500	0	0	MINOR(ABRASNS&WRAP).DRAINLAYER
Gouge	22.1	218	5.6	1473	0	0	BUCKET SCRATCHED PIPE
Gouge	98	273	5.56	1350	350	0.8	ROSEN IP SURVEY
Gouge	37.2	274	7.9	1300	75	0.3	PIPE IN DYKE - DURING CLEARING
Gouge	36	610	11.9	1252	20	1.5	3 SMALL GOUGES
Gouge	12.1	457	9.5	1250	0	0	2(SCORE/WRAP DAMAGE) HYMAC
Gouge	15	450	15.9	1220	5	0.9	18 INCH COLESHILL/TIPTON PIPELINE
Gouge	44.8	610	12.7	1198	2	1	DUE TO COLD CUTTING MACHINE
Gouge	0	762	19.6	1197	0	0.1	LINE AIR PURGED FOR STN. MODS.
Gouge	8.3	610	15.9	1118	0	0.4	7SCRATCHES-22.5DEG BEND SECTN.
Gouge	40.3	457	10.3	1020	5	0.3	3GOUGES,3CRACKS&1SCC-FORESTRYC

Table 6.4: Summary of Longest Gouges

Figure 6.5 shows that the majority of the longest gouges are not associated with dents. Of the 15 longest gouges, only one was associated with a dent. Furthermore, this gouge was located in a grouping with at least four other gouges, one of which was considerably shorter and deeper (as highlighted in Table 6.3) and which resulted in a pipeline failure. It can be seen from the gouge depths in Table 6.4 that the longest gouges in the UKOPA Fault Database are also very shallow, with the deepest recorded as 1.5 mm. This point is discussed further in section 6.2.2.3. If the four outlying data points are excluded, a relatively constant maximum gouge length of between 1100 and 1600 mm exists across all wall thicknesses. Figure 6.6 shows that 74% of gouges are 200 mm or less and only 10.8% are 500 mm or greater. This suggests that the typical machinery working in the vicinity of pipelines is unlikely to produce gouges with lengths in excess of this. Gouges associated with dents are generally shorter than those not associated with dents, the majority of which are below 350 mm long. Figure 6.5 also shows that the majority of gouges associated with failures are short, this suggests that most failures occur as leaks rather than ruptures. Gouges and failures caused by drills are shown to

be very short. This is expected as the gouge defects associated with drills are generally limited to the diameter of the impinging drill bit.

Figure 6.5 indicates that there is no obvious relationship between gouge length and wall thickness. The lack of such a trend would be expected as gouge length and wall thickness represent measurements in two orthogonal dimensions.

On the basis of the above assessment it is concluded that 611 gouges with a recorded gouge length dimension are suitable for use in the development of the AFFECT model. 25[30] gouges associated with pipeline failure are addressed further in section 6.3.

6.2.2.3 *Gouge Severity*

As mentioned in section 6.2.2 the severity of a part-wall gouge depends on both the gouge length and gouge depth. Of the 928 gouges, only 516 have both a recorded gouge length and gouge depth which is sensible. Figure 6.7 shows the depth of gouges caused by external interference, plotted against their corresponding length. Gouge depth and gouge length frequency are shown in Figure 6.8.

[30] This value differs from the gouge depth value because in some cases a depth but no length is recorded, the opposite is also true.

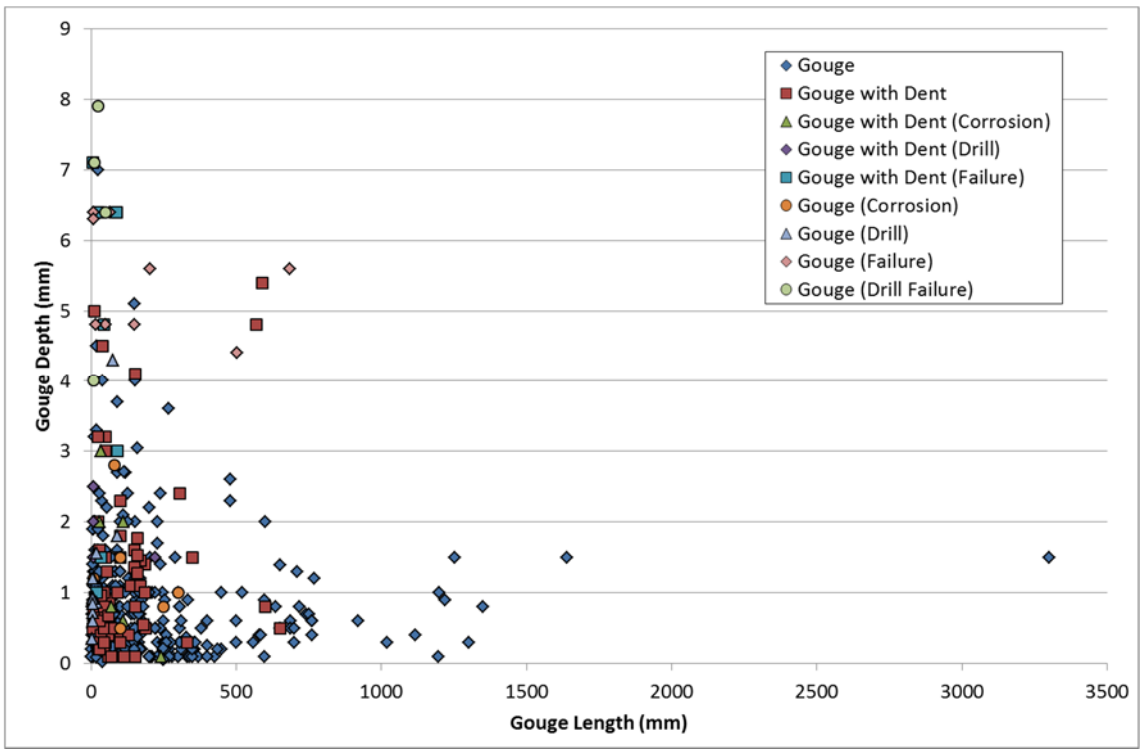

Figure 6.7: Gouge Depth vs. Gouge Length

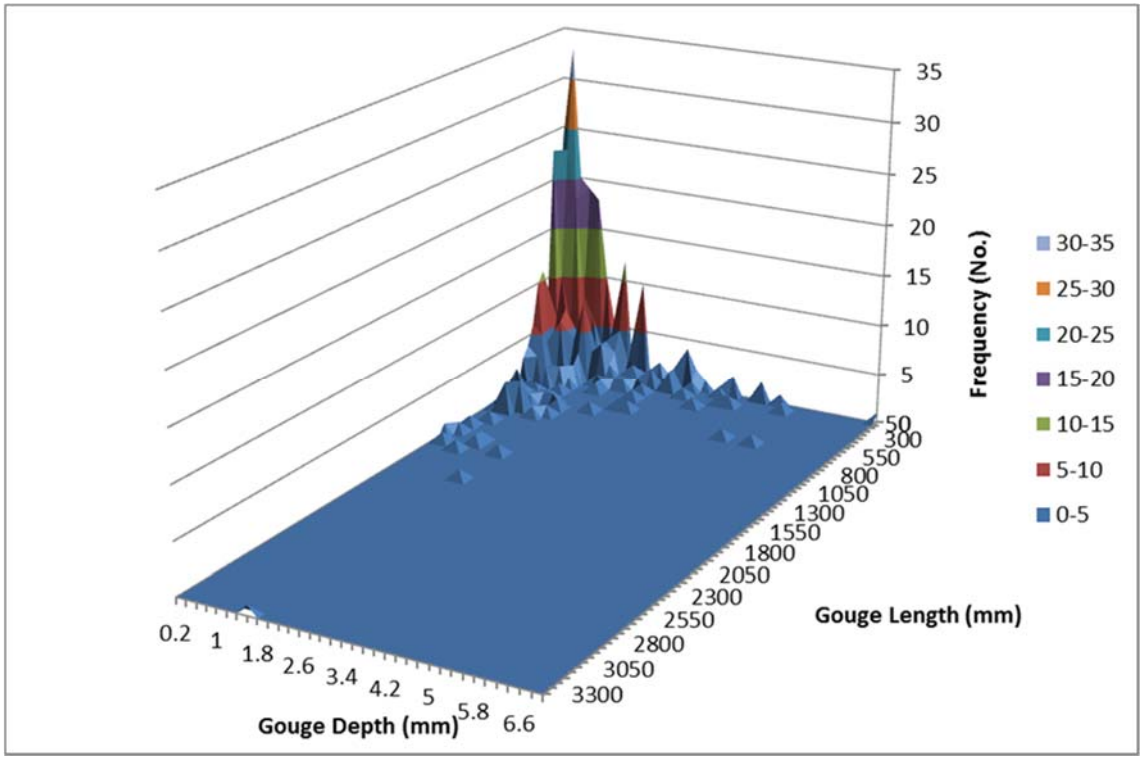

Figure 6.8: Gouge Depth vs. Gouge Length Frequency

In Figure 6.7 the gouge data is distributed close to the chart axes with the greatest concentration of data points occurring around the origin. The pattern suggests that long gouges are more likely to be shallow and deep gouges are more likely to be short; and confirms trends illustrated in Table 6.3 and Table

6.4. It can be seen that the majority of gouges which have failed lie towards the extremes of the recorded data, as would be expected. Gouges associated with failures with dimensions not at the extremes of the data tend to be those associated with dents, highlighting the onerous nature of this form of damage. The majority of gouges associated with a failure are short and deep suggesting that gouge depth is a more important factor than gouge length in terms of gouge severity. Figure 6.7 also shows that gouges associated with dents have a similar range of values to gouges not associated with dents when considering gouge depth. However, the range for gouge length is shorter.

Analysis of the data presented in Figure 6.8 shows that 235 out of 487 combined gouge depth/length records (48%) are of depths 2 mm or less and length 100 mm or less, and 335 combined gouge depth/length records (69%) are of depths 2 mm or less and lengths 200 mm or less. 336 combined gouge depth/length records (75%) are of depth 7mm or less and length 200 mm or less, and 39 records (8%) are of depth 7 mm or less and length greater than 500 mm.

In terms of the AFFECT model, the severity of a part-wall gouge is determined using the flow stress dependent part-wall NG-18 equation (equations (3.4) and (3.5)). Figure 6.9 shows the severity of external interference gouges, represented in terms of the failure stress calculated using the flow stress dependent part-wall NG-18 equation; plotted against the wall thickness of the pipeline in which they occurred[31]. In producing this chart the quantities of pipeline operating pressure, external diameter, wall thickness and grade associated with damage are taken directly as recorded from the UKOPA Fault Database. Gouges which are associated with failures have not been included in the chart. Pipeline failures are addressed in section 6.3.

[31] Note that of the 516 gouges displayed in Figure 6.7, 12 are not included in Figure 6.9 due to the grade of the pipeline in which they occurred being omitted from the database and two are not included in Figure 6.9 due to the external diameter of the pipeline in which they occurred being omitted from the database.

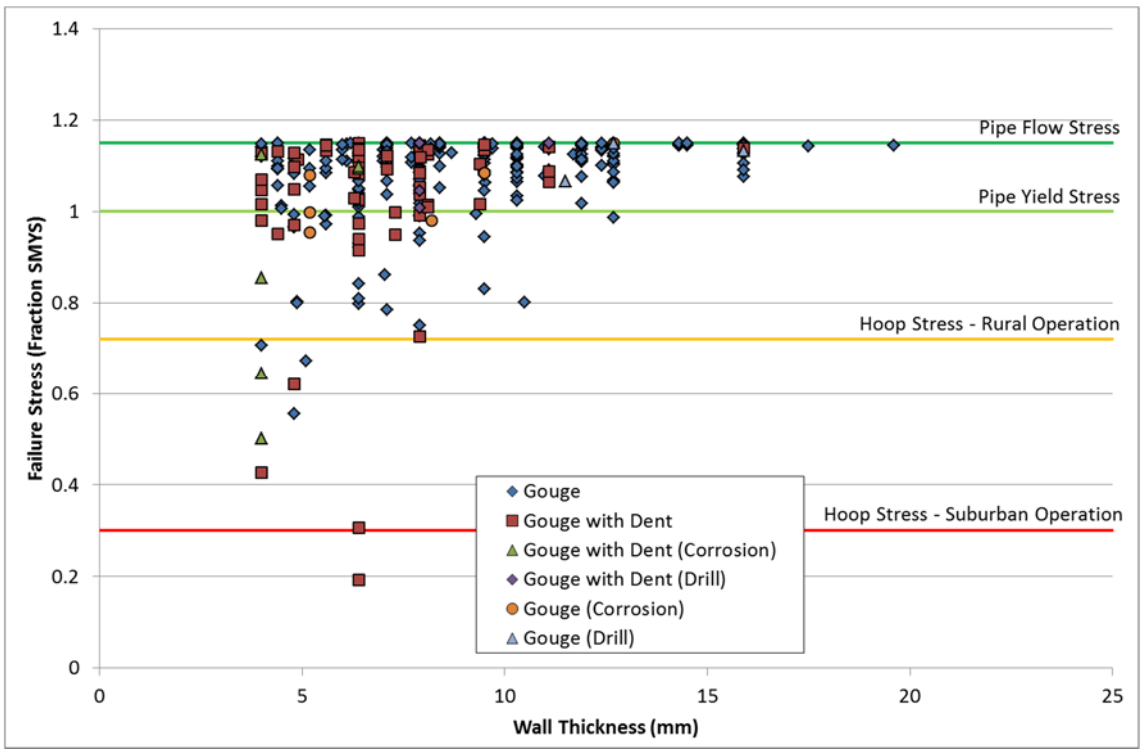

Figure 6.9: Gouge Severity vs. Wall Thickness

The most severe gouge in the database which did not fail is a gouge associated with a dent. This gouge was located in a pipeline of wall thickness 6.4 mm and external diameter 168 mm. The gouge was recorded to be 5.4 mm deep, with a length of 590 mm. The associated dent does not have a recorded depth and the gouge occurred during ditch clearing.

The most severe gouge not associated with a dent was located in a pipeline of wall thickness 4.8 mm and external diameter 218 mm. The gouge was recorded to be 2.6 mm deep, with a length of 480 mm and was caused by a JCB during a fencing procedure.

Table 6.5 summarises the gouges with a failure stress less than 0.72 of the pipeline SMYS in descending order of severity.

Description	Operating Pressure (barg)	Pipe Diameter (mm)	Wall Thickness (mm)	Defect Length (mm)	Defect Width (mm)	Defect Depth (mm)	Failure Stress (Fraction SMYS)	Fault Comment
Gouge with Dent	19	168	6.4	590	40	5.4	0.19	Discovered by tenant, ditch clearing, 3 dents
Gouge with Dent	19	168	6.4	570	35	4.8	0.31	Discovered by tenant, ditch clearing, 3 dents
Gouge with Dent	14	76	4	50	6	3	0.43	(DENT<12%DIA&GOUGE<76%WT) OLI4
Gouge with Dent (Corrosion)	14	76	4	35	20	3	0.50	DT/G/AB+DENT+GOUGE+EXT.CR. OLI4
Gouge	16.6	218	4.8	480	186	2.6	0.56	JCB WHILE FENCING DAMAGE<55%WT
Gouge with Dent	13.8	218	4.8	305	102	2.4	0.62	DENT,GOUGES&SCRATCHES-GRASSCUT
Gouge with Dent (Corrosion)	14	76	4	110	5	2	0.64	DT/G/AB+DENT+GOUGE+EXT.CR. OLI4
Gouge	19	219	5.1	114.7	10	2.713	0.67	Ditch Crossing, Damage caused by Plough.
Gouge	14	76	4	38	0	2.3	0.71	GOUGE OLI4

Table 6.5: Summary of the Most Severe Gouges

Figure 6.9 clearly shows that the severity (according to the part-wall NG-18 equation) of the external interference gouges decreases with increasing wall thickness. Based on the trends seen in Figure 6.3 and Figure 6.5 relating to the maximum length and depth of gouges caused by machinery typically working in the vicinity of a pipeline, this relationship would be expected. The force capable of being exerted on a pipeline to cause damage is limited and therefore as the pipeline wall thickness increases the severity of the gouges produced will decrease. The majority of the most severe gouges for each wall thickness in Figure 6.9 follow a curve. There are two outlying points at 6.4 mm which do not follow the general trend. These gouges are highlighted in Table 6.5. It should be noted that these gouges also make up two of the outlying points in Figure 6.7. In the database, these two gouges are grouped with a further gouge and a dent. The gouge defects have recorded dimensions whereas the dent defect does not. The fault comments in the UKOPA Fault Database note the presence of three dents, however gouging is not mentioned. The damage is also quoted as being “Slight” rather than “Severe” which contradicts the evidence shown in Figure 6.9. On this basis it could be speculated that the three “gouges” in this fault grouping actually refer to dent defects and that the “dent” defect without dimensions is more a placeholder or notification and refers to the other three defects rather than being an actual defect itself.

It should be noted that the failure stress assigned to gouges associated with dents in Figure 6.9 will be non-conservative due to the presence of the dent.

Figure 6.9 shows gouge severity according to the part-wall NG-18 equation only. Gouged dents are assessed using the BGDGFM.

6.2.3 *Probability of a Gouge and a Gouged Dent*

Using the data from sections 6.2.1 and 6.2.2, an analysis has been performed in order to determine the probability that external interference damage will manifest as either a gouge or a gouged dent. The updated probabilities for gouges and gouged dents are given in Table 6.6. The probabilities are unchanged from those determined from the 2005 UKOPA Fault Database and used in the PIE and Cosham models.

Damage Type	Symbol	Probability
Gouge	$P_{gougedamage}$	0.82
Gouged Dent	$P_{gougeddentdamage}$	0.18

Table 6.6: Probabilities that External Interference Damage will be a Gouge or a Gouged Dent

6.2.4 *Statistical Difference between Gouge and Gouged Dent*

For the AFFECT model the required damage dimensions are gouge length, gouge depth and dent depth. Values for gouge length and gouge depth exist in the database for damage classed as both gouge and gouged dent. Probability distributions can therefore be derived for gouge length and gouge depth considering either the gouge and gouged dent data as a whole (2 distributions):

- Gouge length;
- Gouge depth.

or separately (four distributions):

- Gouge length;
- Gouged dent gouge length;

- Gouge depth;
- Gouged dent gouge depth.

A statistical analysis of the filtered UKOPA Fault Database has been carried out by the Newcastle University Industrial Statistics Research Department (ISRU) (Coleman, 2013).The statistical report by ISRU has suggested that the dimensions of gouge damage should be treated separately to those of gouged dent damage. In order to investigate this conclusion further, two additional statistical tests have been performed on the data. These are:

- 2 Sample Kolmogorov-Smirnov Test.
- Mann-Whitney U Test.

The Kolmogorov-Smirnov and Mann-Whitney tests are non-parametric tests which test whether the underlying probability distributions for two data samples are different (Anon., 2010).

The tests have been performed using Minitab (Anon., 2010), all tests were performed using a p-value of 0.05, i.e. the confidence limit was set at 95%. The tests have been performed separately on the gouge length dimensions and the gouge depth dimensions. The two samples in each case are gouges and gouges associated with dents. Two sets of data were used in each case. The first was the data concluded as suitable in sections 6.2.2.1 and 6.2.2.2. In an attempt to remove information from the data which could possibly skew the outcome of the tests, the tests were also performed on a second set of data. This data set was a subset of the first data set ignoring all incidents of pipeline failure and gouges associated with corrosion. Details of the sample size of each data set are presented in Table 6.7.

	Sample Size (Large Data Set)	Sample Size (Small Data Set)
Gouge Length	518	484
Gouged Dent Gouge Length	118	92
Gouge Depth	486	445
Gouged Dent Gouge Depth	110	86

Table 6.7: Sample Sizes for Non-Parametric Tests of Gouge Length and Gouge Depth

Details of the Kolmogorov-Smirnov test statistics are presented in Table 6.8.

	Sample Size (Large Data Set)		Sample Size (Small Data Set)	
	Test Statistic	Critical Value	Test Statistic	Critical Value
Gouge Length Data	0.135	0.138	0.174	0.154
Gouge Depth Data	0.262	0.143	0.216	0.160

Table 6.8: 2 Sample Kolmogorov – Smirnov Test Statistics

Details of the Mann-Whitney calculated p-values are presented in Table 6.9.

	Sample Size (Large Data Set)		Sample Size (Small Data Set)	
	P Value	Critical Value	P Value	Critical Value
Gouge Length Data	0.099	0.050	0.092	0.050
Gouge Depth Data	0.000	0.050	0.000	0.050

Table 6.9: Mann – Whitney U Test P Values

The results of the test outcomes are summarised in Table 6.10.

	Sample Size (Large Data Set)		Sample Size (Small Data Set)	
	Kolmogorov – Smirnov	Mann – Whitney U	Kolmogorov – Smirnov	Mann – Whitney U
Gouge Length Data	Insufficient evidence to conclude	Insufficient evidence to conclude	Distributions concluded as different	Insufficient evidence to conclude
Gouge Depth Data	Distributions concluded as different	Distributions concluded as different	Distributions concluded as different	Distributions concluded as different

Table 6.10: Summary of Test Outcomes

From Table 6.10 it can be seen that for the gouge depth data sets every test led to the conclusion that the underlying distributions were different. For the gouge length data sets the outcome was less certain, a conclusion that the underlying distributions were different was only possible in one of the four tests made, with there being insufficient evidence to accept a conclusion of different distributions in the other three cases.

On the basis of five of the eight total tests showing gouge and gouged dent damage to be statistically different to each other it is concluded that for the purposes of the AFFECT model, gouge dimension data and gouged dent dimension data should be treated separately and used to derive separate probability distributions.

On the basis of the above assessment it is concluded that the 570 gouges with a sensible gouge depth dimension suitable for use in the development of the AFFECT model (section 6.2.2.1) are split into 467 gouges and 103 gouges associated with dents for the purposes of derivation of damage dimension probability distributions.

On the basis of the above assessment it is concluded that the 611 gouges with a recorded gouge length dimension suitable for use in the development of the AFFECT model (section 6.2.2.2) are split into 503 gouges and 108 gouges associated with dents for the purposes of derivation of damage dimension probability distributions.

6.3 Failure Data

The dent and gouge data discussed in section 6.2 includes damage which resulted in through-wall pipeline failure.

There are 44 external interference defects to a pipe or bend associated with pipeline failures within the UKOPA Fault Database. Considering the “fault number” grouping within the database, these defects comprise 24 separate incidents of pipeline failure[32]. Of the 44 defects, five are dents with associated gouges; 15 are the gouges associated with these dents; 24 are gouges not associated with dents, of which seven are gouges caused by drilling. Of the five dents associated with failures, only one has a recorded dent depth. Of the 39 gouges, 26 have a recorded gouge depth and 25 have a recorded gouge length, with only 20 having both a length and depth measurement.

From a risk assessment point of view, the most important factor in pipeline failure is whether the failure will occur as a leak or as a rupture. Whether a failure will occur as a leak or a rupture is determined by the critical defect length, which is based on the pipeline geometry and operating conditions. Defects with a length in excess of the critical length, are expected to fail as ruptures. A rupture is significantly worse than a leak in consequence terms. The UKOPA Fault Database records classify all pipeline failure incidents as either a “leak” or a “fracture”. These classifications can be assumed to refer to leak and rupture failures respectively.

Table 6.11 collates all of the defects associated with pipeline failures. These are grouped by each particular pipeline failure.

[32] Some failures consist of multiple defects.

Description	Operating Pressure (barg)	Pipe Diameter (mm)	Wall Thickness (mm)	Defect Length (mm)	Defect Width (mm)	Defect Depth (mm)	Extent of Damage	Fault Comment
Gouge (drill failure)	10.3	168	6.4	0	0	6.4	Leak	[MS]SERVICE LAYER DRILLED WRONG MN
Gouge (drill failure)	19	218	4.8	0	0	0	Leak	NO CUSTOMER LOSS WRONG P.DRILLED
Gouge (failure)	6.9	218	6.4	8	8	6.4	Leak	LINE HOLED BY PNEUMATIC DRILL
Gouge (failure)	5.5	102	4.8	51	6	4.8	Leak	2 HOLES
Gouge (failure)	5.5	102	4.8	16	5	4.8	Leak	2 HOLES
Gouge (drill failure)	11.7	457	6.4	2	2	0	Leak	HOLE DRILLED TO FIND PIPE
Dent with Gouge (failure)	6.2	324	6.4	0	0	0	Leak	4 HITS , 1 PENETRATION
Gouge with Dent (failure)	6.2	324	6.4	25	3	6.4	Leak	4 HITS , 1 PENETRATION
Gouge with Dent (failure)	6.2	324	6.4	0	0	0	Leak	4 HITS , 1 PENETRATION
Gouge with Dent (failure)	6.2	324	6.4	0	0	0	Leak	4 HITS , 1 PENETRATION
Gouge with Dent (failure)	6.2	324	6.4	0	0	0	Leak	4 HITS , 1 PENETRATION
Dent with Gouge (failure)	6.9	218	7.1	133	133	25	Leak	Damaged by FE20 excavator during landscaping
Gouge with Dent (failure)	6.9	218	7.1	5	5	7.1	Leak	Damaged by FE20 excavator during landscaping
Gouge with Dent (failure)	6.9	218	7.1	3000	0	0	Leak	Damaged by FE20 excavator during landscaping
Gouge with Dent (failure)	6.9	218	7.1	3000	0	0	Leak	Damaged by FE20 excavator during landscaping
Gouge with Dent (failure)	6.9	218	7.1	0	0	0	Leak	Damaged by FE20 excavator during landscaping
Gouge with Dent (failure)	6.9	218	7.1	0	0	0	Leak	Damaged by FE20 excavator during landscaping
Gouge (drill failure)	10.3	325	7.9	23	23	7.9	Leak	// LINES-WRONG 1 DRILLED-25MMH
Gouge (failure)	0	218	5.6	685	0	5.6	Fracture	No Loss, severed pre commission
Gouge (failure)	0	218	5.6	0	0	5.6	Fracture	No Loss, severed pre commission
Gouge (failure)	0	218	5.6	0	0	0	Fracture	No Loss, severed pre commission
Dent with Gouge (failure)	14.5	324	6.4	127	127	0	Leak	HOLE , INDENTATION
Gouge with Dent (failure)	14.5	324	6.4	89	89	6.4	Leak	HOLE , INDENTATION
Gouge (failure)	16.5	325	6.4	64	13	6.4	Leak	TRENCH CUTTER HOLED PIPE
Gouge (failure)	16.5	325	6.4	152	102	0	Leak	TRENCH CUTTER HOLED PIPE
Gouge (drill failure)	12.3	325	6.4	50	50	6.4	Leak	DRILLED IN ERROR BY DISTN.
Gouge (failure)	30.1	218	7.1	8	3	6.3	Leak	PIPE CUT BY GRINDER IN ERROR
Gouge (drill failure)	15.9	274	7.1	11	11	7.1	Leak	GAS LINE MISTAKEN FOR WATER PI
Gouge (failure)	21.4	457	9.5	0	0	9.5	Fracture	SHEETPILERSLICEDTHRUSIDEOFPIPE
Gouge (failure)	7.6	168	4.4	502	0	4.4	Fracture	LINE SHEARED BY MOLE PLOUGH
Gouge (drill failure)	17.2	76	4	10	10	4	Leak	DRILLED IN ERROR-TO BE CUT OUT
Dent with Gouge (failure)	17.2	168	4.8	0	0	0	Fracture	36 cust. Line holed by trencher during excavation for water main
Gouge with Dent (failure)	17.2	168	4.8	90	21	3	Fracture	36 cust. Line holed by trencher during excavation for water main
Gouge with Dent (failure)	17.2	168	4.8	19	4	1	Fracture	36 cust. Line holed by trencher during excavation for water main
Gouge with Dent (failure)	17.2	168	4.8	34	15	1.5	Fracture	36 cust. Line holed by trencher during excavation for water main
Gouge with Dent (failure)	17.2	168	4.8	23	18	0	Fracture	36 cust. Line holed by trencher during excavation for water main
Gouge (failure)	13.8	168	6.4	0	0	6.4	Leak	JCB HIT DIVERTED PIPE-ROADWRKS
Gouge (failure)	13.8	168	6.4	0	0	0	Leak	JCB HIT DIVERTED PIPE-ROADWRKS
Dent with Gouge (failure)	22.8	168	4.8	45	45	0	Leak	Mole plough holed pipe
Gouge with Dent (failure)	22.8	168	4.8	45	45	4.8	Leak	Mole plough holed pipe

Description	Operating Pressure (barg)	Pipe Diameter (mm)	Wall Thickness (mm)	Defect Length (mm)	Defect Width (mm)	Defect Depth (mm)	Extent of Damage	Fault Comment
Gouge (failure)	15.8	102	4.4	0	0	4.4	Fracture	EXCV.FRACTUREDPIPE-LANDDRAINAG
Gouge (failure)	15.8	168	4.8	149	149	4.8	Fracture	30 cust. Line sliced longitudinally by D6 Bogmaster during roadworks
Gouge (failure)	21	168	5.6	203	152	5.6	Fracture	203x152mm hole punched by CAT 977 Traxcavator during drainage work
Gouge (failure)	14.1	457	10.3	0	0	10.3	Leak	WELDED SLV REPAIR

Table 6.11: External Interference Failure Data

In Table 6.11, lines between rows are used to show the end of one incident of pipeline failure and the start of another based upon the “fault number”. Considering the information regarding the damage in groupings of multiple defects it can be seen that in the majority of cases, each group has a standout “gouge” defect with a depth equal to that of the pipeline wall thickness. For these cases it can reasonably be assumed that this individual defect is the source of the failure and that the other associated defects are less severe non-failing damage. Two exceptions to this are noted:

- The failure incident highlighted in yellow includes two defects for which the comment in the database clearly reads “2 holes”. In this case each defect in the grouping has been assumed to represent a separate failure.
- The failure incident highlighted in green includes a dent and four gouge defects. None of the defects have a recorded gouge depth equal to the pipeline wall thickness. In this case the available information does not allow which of the gouges failed to be determined.

Seven failures can be concluded as having being caused by drills from the information included in the database, these are highlighted in blue. Drill punctures must be separated from the data used in the derivation of probability distributions for part-wall and through-wall gouge and gouged dent damage. Drill punctures are unlike conventional through-wall punctures in that they are assumed to be wall thickness independent. A separate historical data component or drill-puncture model would therefore need to be developed in order to incorporate them into the AFFECT model. It should be noted that classification of the drill failure data is made solely on the basis of the

comments associated with the defects in each case and interpretation of this information is largely subjective. Only the non-drill failure data from the UKOPA Fault Database has been in used in the derivation of the damage dimension probability distributions for use in AFFECT. The development of either a drill puncture model or an historical data component for AFFECT is recommended.

Table 6.11 shows that the majority of pipeline failures occurred on small external diameter, low wall thickness pipelines. Furthermore, six out of seven pipeline ruptures occurred on pipelines with external diameters below 220 mm. Rupture type failures generally occurred as a result of gouge defects which were not associated with dents. This is potentially due to the shorter gouge length which is found in gouges associated with dents, as illustrated in section 6.2, which means the majority of gouges associated with dents remain below the critical length. It is clear that the thickest pipelines to suffer a failure generally did so as a result of drill or drill-type defects (grinder, welding torch), which failed as stable leaks. The most concerning failure is the rupture of a pipeline with wall thickness 9.5 mm and external diameter 457 mm, caused by a sheet-piler machine.

It is concluded that 14 gouges associated with a failure with a sensible gouge depth dimension and no failures caused by drilling should be included with the 467 gouges for the purposes of derivation of damage dimensions probability distributions. It is concluded that seven gouges associated with dents and associated with failures, with a sensible gouge depth dimension and no failures caused by drilling should be included with the 103 gouges associated with dents for the purposes of derivation of damage dimensions probability distributions.

It is concluded that ten gouges associated with a failure with a recorded gouge length dimension and no failures caused by drilling should be included with the 503 gouges for the purposes of derivation of damage dimensions probability distributions. It is concluded that ten gouges associated with dents and associated with failures with recorded length dimensions and no failures caused by drilling should be included with the 108 gouges associated with dents for the purposes of derivation of damage dimensions probability distributions.

6.4 Assessment of the 2010 UKOPA Fault Database Conclusions

This chapter has presented a detailed filtering and assessment of the 2010 UKOPA Fault Database. As a result of the assessment process appropriate data sets were derived to which probability distributions can be fitted and used in the AFFECT failure frequency model. A comprehensive statistical analysis performed on the database indicated that gouge dimension data and gouged dent dimension data should be treated separately and used to derive separate probability distributions. The data sets derived for use in the AFFECT model therefore relate to gouge depth, gouged dent gouge depth, gouge length, gouged dent gouge length and dent depth / dent force. A summary of the size of the data sets and the number of incidents of pipeline failure included in each data set is shown in Table 6.12.

The assessment of the database also showed the probabilities of external interference damage manifesting as either a gouge or a gouged dent are unchanged from the values determined from the 2005 UKOPA Fault Database and used in the PIE and Cosham models.

	Total Number	Split Category	Number	Number of Failures
Gouge Depth	570	Gouge Depth	467	14
		Gouged Dent Gouge Depth	103	7
Gouge Length	611	Gouge Length	503	10
		Gouged Dent Gouge Length	108	10
Dent Depth / Dent Force	66			1

Table 6.12: UKOPA Fault Database Data Set Summary

Chapter 7. Development of the AFFECT Failure Frequency Model for Dense Phase CO_2 Pipelines (Part 2)

Chapter 5 to Chapter 7 of this thesis detail the step by step construction of the AFFECT model to calculate the failure frequency of a dense phase CO_2 pipeline due to third party external interference. The first four stages of development have been covered in Chapter 5 and an analysis of the 2010 UKOPA Fault Database has been described in Chapter 6. In Chapter 7 the final two stages are considered. As with Chapter 5, each modification made to the model is outlined and estimates of pipeline failure frequency calculated at each stage are presented. In this way the effect of each modification on the estimated value of failure frequency can be observed.

The modifications considered in Chapter 7 include:

- A dent force distribution derived from the 2010 UKOPA Fault Database;
- Separate depth and length distributions for gouges and gouged dents.

7.1 The Lognormal Force Model

In the New Distributions model described in section 5.7, updated distributions and Incident-Rates derived by Penspen in 2010 were included. It was noted that that a dent force distribution was not fitted by Penspen and therefore the New Distributions model uses dent depth instead of dent force.

As outlined in section 5.5, including a dent force distribution over dent depth is beneficial in terms of improving the accuracy of the probability of failure calculation. Taking this into account, a dent force distribution has been derived using data from the 2010 UKOPA Fault Database. The distribution has been used to provide an update for dent force which is analogous to the update provided for dent depth by the Penspen distributions.

In order to derive a dent force distribution, the depth data for the 66 dents concluded as suitable in section 6.2.1 (along with corresponding geometry,

operating and material parameters) was transformed using equations (2.83) and (5.4). A distribution was then fitted to the resulting force data.

The probability distributions used to describe the random variables in the Hazard Analysis, FFREQ, PIE and Cosham models, as well as for the 2010 Penspen updates, are Weibull distributions. In the PIPIN model, the majority of the distributions are Weibull; however normal and lognormal distributions are used to describe some of the random variables. As part of the derivation of a dent force distribution, an assessment of the data was performed using the statistical software package Minitab (Anon., 2010) in order to determine if Weibull was the most appropriate distribution to use in order to describe the data. Figure 7.1 shows a comparison between a Weibull fit and the dent force data; and a lognormal fit and the dent force data. This chart compares the data to the regression line in each case; a graphical comparison between the two distributions is shown in Figure 7.2.

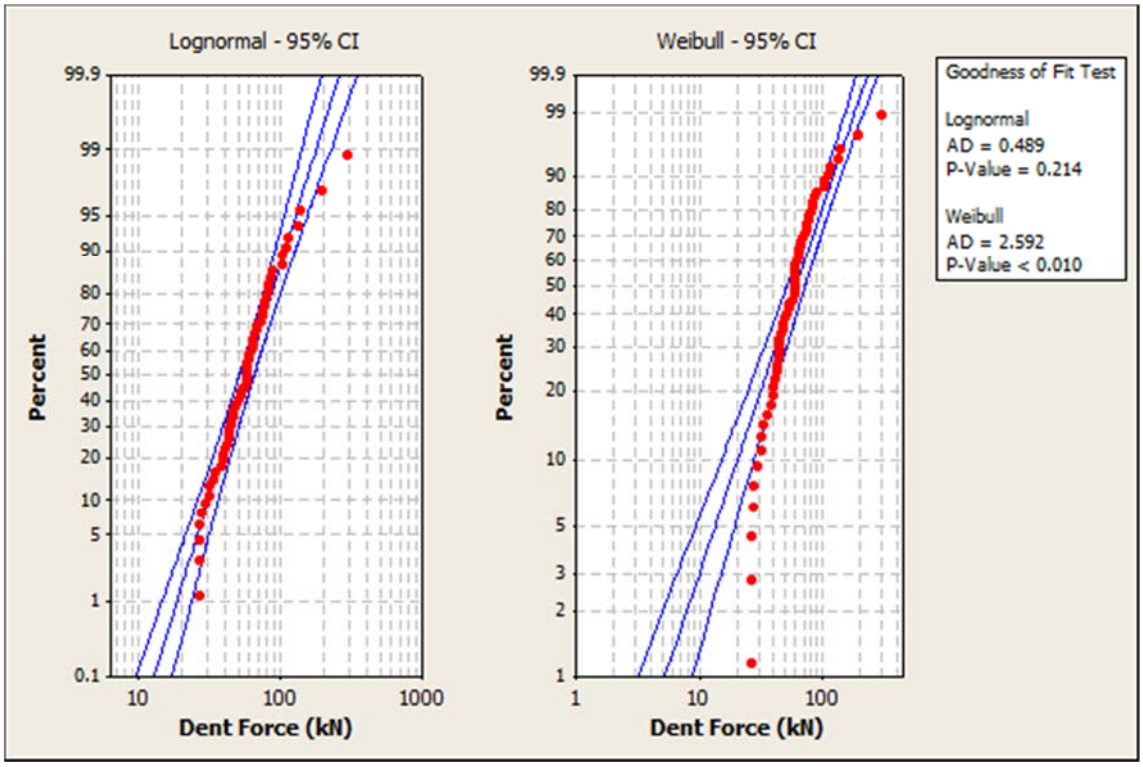

Figure 7.1: Dent Force Lognormal and Weibull Comparison

The lognormal probability density function describing a random variable x has the form:

$$f(x) = \frac{1}{x\sigma_d\sqrt{2\pi}} \exp\left[-\frac{(\ln x - \mu_d)^2}{2{\sigma_d}^2}\right] \quad (7.1)$$

Where σ_d and μ_d are distribution parameters. The cumulative probability density function is given by:

$$F(x) = \frac{1}{2} + \frac{1}{2}\,\mathrm{erf}\left[\frac{\ln x - \mu_d}{\sigma_d\sqrt{2}}\right] \quad (7.2)$$

Where erf is the error function.

A distribution is considered to be a good fit for the data if its statistical p-value exceeds 0.05. In Figure 7.1, the low p-value of <0.010 for the Weibull distribution indicates that a Weibull is not a good fit to the dent force data. Conversely, the lognormal distribution has a p-value of 0.214. The Minitab analysis suggests that a more accurate representation of the dent force random variable would be obtained if a lognormal distribution is fitted to the data.

A comparison between the dent force probability distributions for Weibull and lognormal when fitted to the data from the 2010 UKOPA Fault Database is shown in Figure 7.2 alongside the original data points. Figure 7.2 gives visual confirmation that the lognormal distribution is a better fit to the data than the Weibull.

In Figure 7.2 the dent force distribution from the Corrib QRA, used in the Dent Force model in section 5.5 is included for reference. This curve is significantly different to the lognormal and Weibull fits. The curve was derived using an alternative method, detailed in Espiner (Espiner, 1996a). A comparison showing the specific effect on the values of failure frequency of selecting either this curve or the lognormal dent force distribution is detailed in section 7.3.

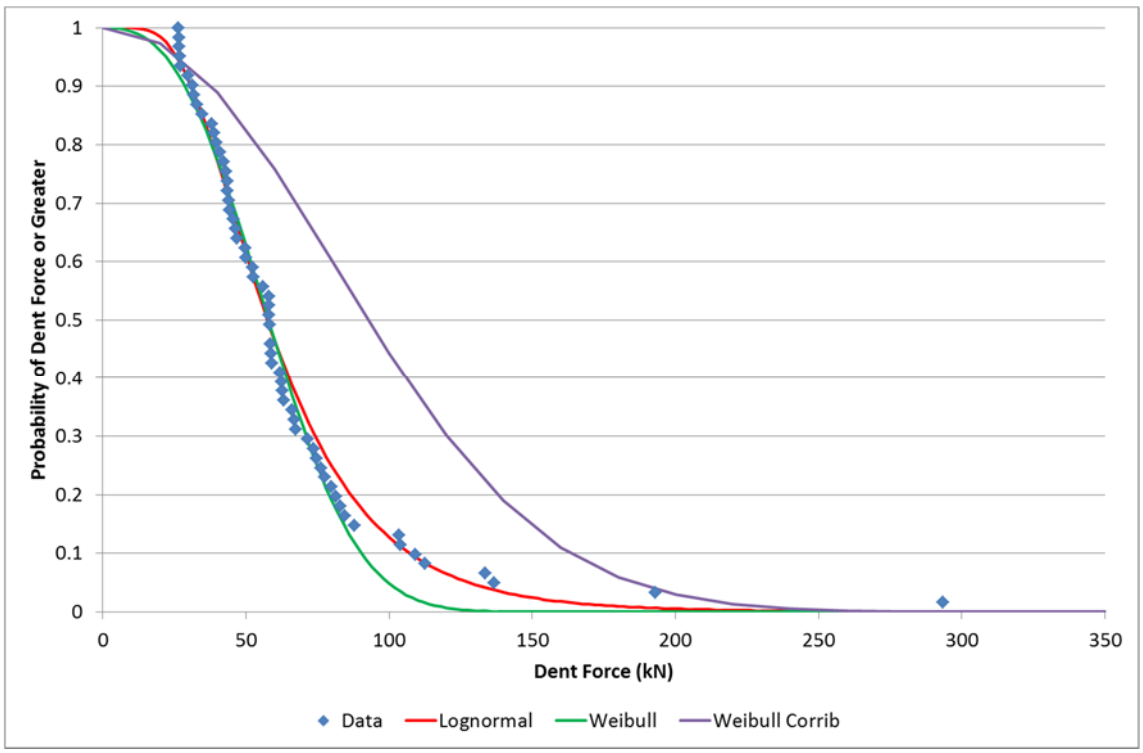

Figure 7.2: Dent Force Distribution Lognormal and Weibull Comparison

A lognormal distribution for dent force has been derived based on the 2010 UKOPA Fault Database. This has been used in conjunction with the updated Incident-Rate, gouge length and gouge depth distributions, derived by Penspen and used in the New Distributions model[33], as the fifth stage in the construction of AFFECT. This version of the model will be referred to as the Lognormal Force model. The parameters defining the cumulative probability distributions used in the Lognormal Force model are summarised in Table 7.1.

Variable	Distribution	α (Weibull) μ_d (Lognormal)	β (Weibull) σ_d (Lognormal)
Gouge Length	Weibull	0.573	125.4
Gouge Depth	Weibull	0.674	0.916
Dent Force	Lognormal	4.052	0.486

Table 7.1: Lognormal Force Model Distribution Parameters

[33] Note that at this stage, following the analysis of the 2010 UKOPA Fault Database, the probabilities that mechanical damage will be a gouge or a gouged dent taken from the original PIE model and given in Table 2.11 should also be updated in line with Table 6.6. In this case however, the values are identical.

7.2 Lognormal Force Model Results

Estimated pipeline failure frequency values have been calculated using the Lognormal Force model for the six example pipeline cases listed in Table 5.1. As before, leak, rupture and total failure frequency has been calculated.

A comparison between the total failure frequency values for example 1 as calculated by the Lognormal Force model, New Distributions model, Dent Force model, Re-Rounding model and the Modified PIE model, is shown in Figure 7.3. A similar comparison between total failure frequency values for example 4 is shown in Figure 7.4. Equivalent charts for the remaining examples are included in Appendix A .

A comparison between the total failure frequency values for examples 1, 2, and 3 as calculated by the Lognormal Force model and the analogous Dent Force model, is shown in Figure 7.5. A similar comparison between the total failure frequency values calculated for examples 4, 5 and 6 is shown in Figure 7.6.

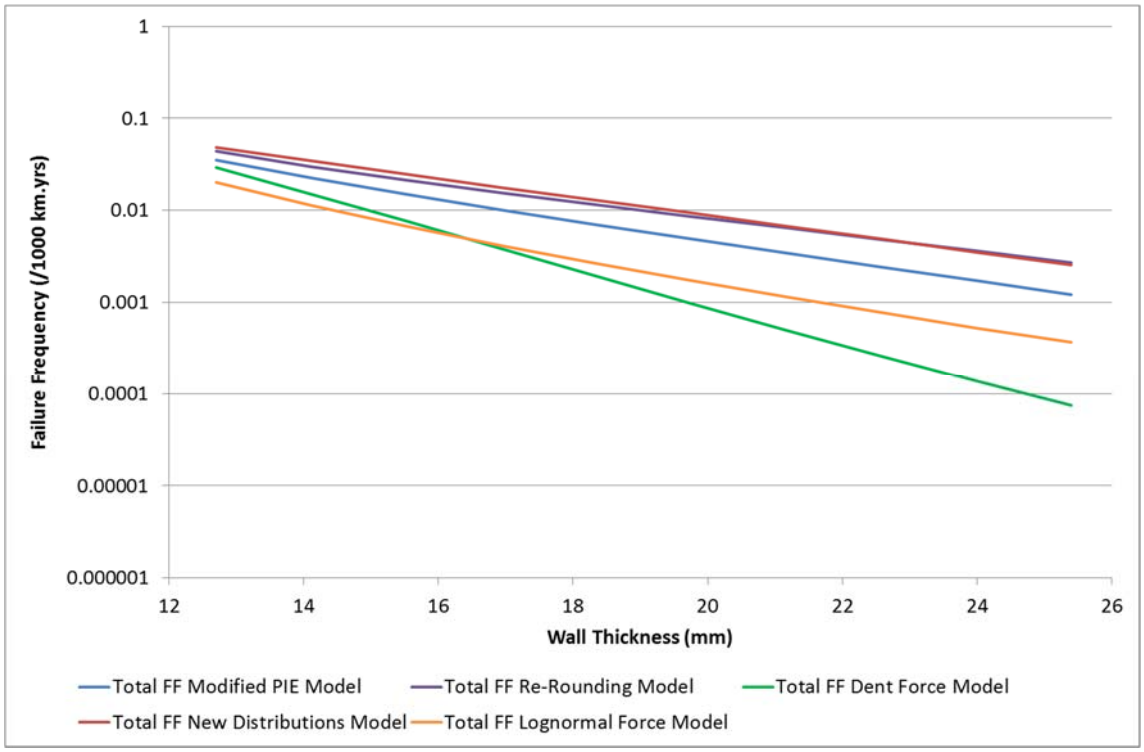

Figure 7.3: Total Failure Frequency as Calculated by the Lognormal Force Model, New Distributions Model, Dent Force Model, Re-Rounding Model and the Modified PIE Model for Example 1

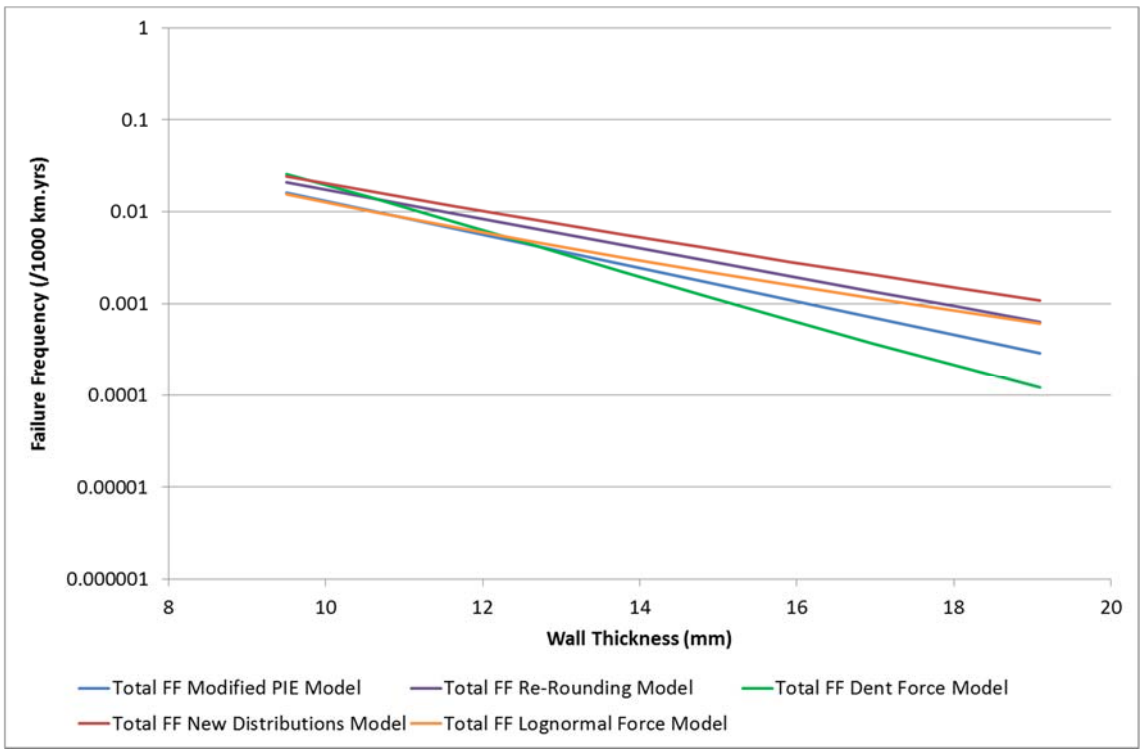

Figure 7.4: Total Failure Frequency as Calculated by the Lognormal Force Model, New Distributions Model, Dent Force Model, Re-Rounding Model and the Modified PIE Model for Example 4

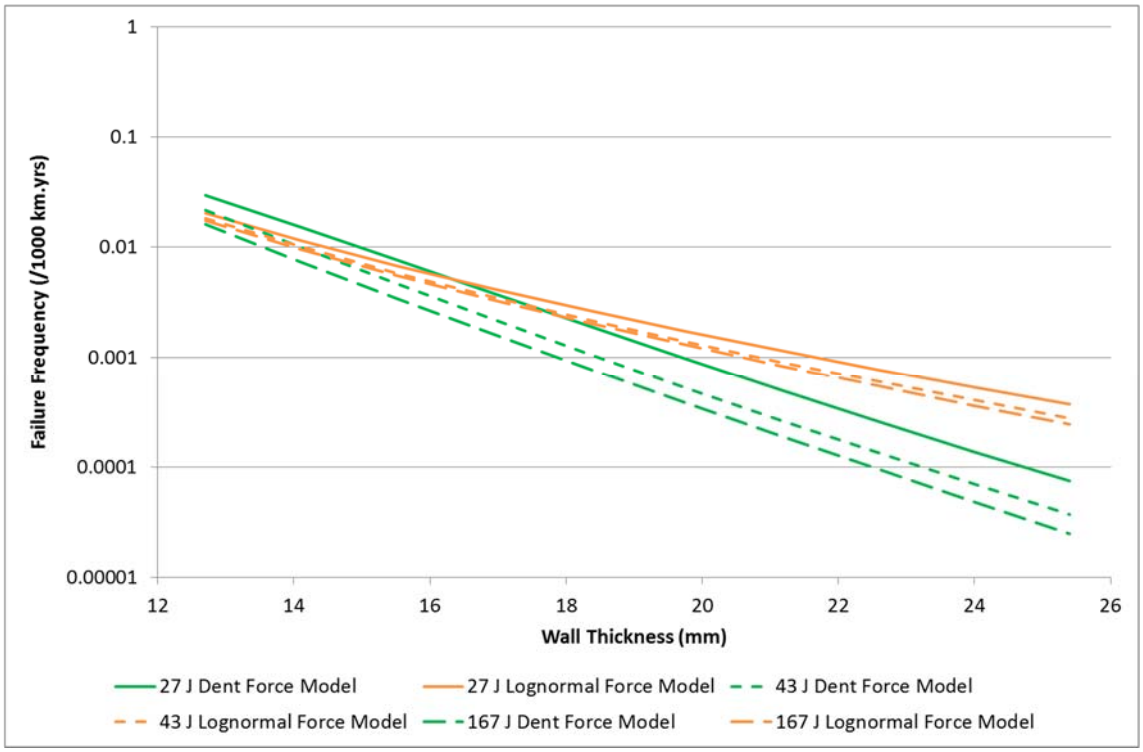

Figure 7.5: Total Failure Frequency as Calculated by the Lognormal Force Model and the Dent Force Model for Examples 1, 2 and 3

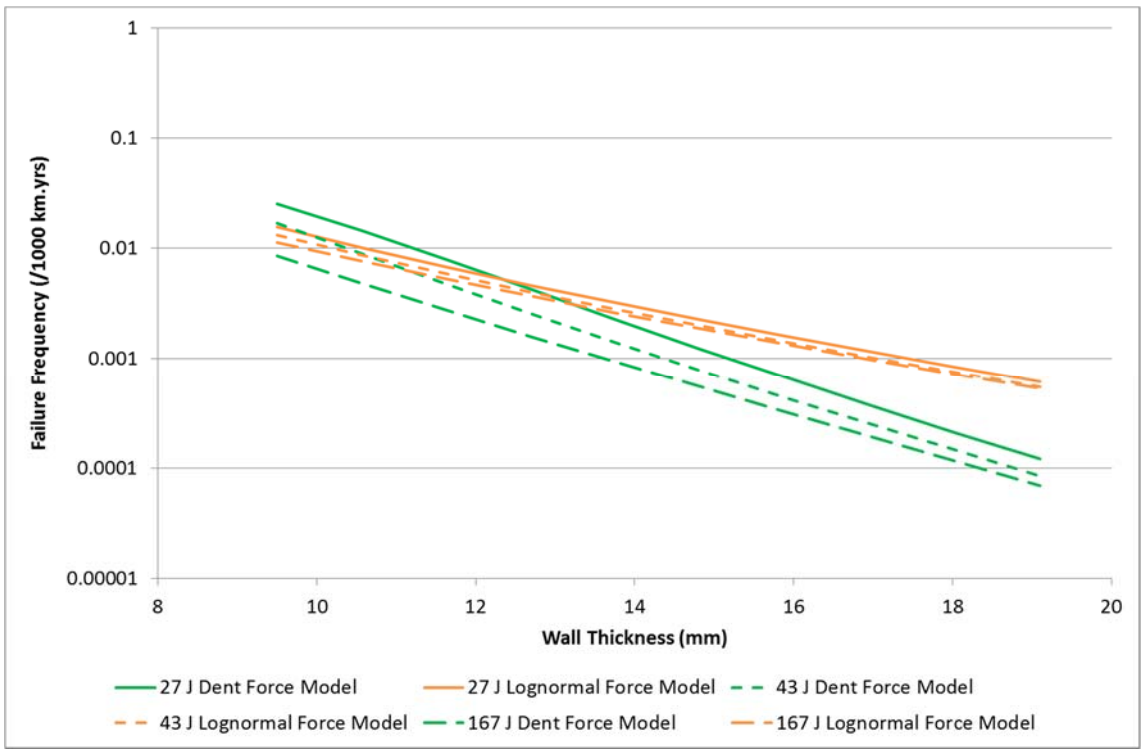

Figure 7.6: Total Failure Frequency as Calculated by the Lognormal Force Model and the Dent Force Model for Examples 4, 5 and 6

Based on the results, the following observations can be made regarding estimations of pipeline failure frequency made by the Lognormal Force model.

A direct comparison between the results calculated for each example indicates that the Lognormal Force model generally mirrors the behaviour of the New Distributions model from section 5.7 but estimates lower values of failure frequency. The model does not display the level of drop off in its results that is observed in models based upon the 2005 UKOPA Fault Database. This is highlighted in the comparison with the analogous Dent Force model. The difference between the two models is due to the differences between the distributions. Not only do the updated gouge length and gouge depth parameters have an effect (as explained in section 5.8) but the dent force distribution is significantly different, as highlighted by Figure 7.2.

7.3 The Effect of Dent Force Distribution on Failure Frequency

In section 7.1, Figure 7.2 compares the lognormal dent force distribution used in the Lognormal Force model with the Corrib QRA dent force distribution used in

the Dent Force model. Figure 7.2 shows that the two distributions are significantly different to each other.

In order to investigate the effect that the difference in the two distributions has on calculated values of failure frequency a further analysis has been performed. For this analysis the failure frequencies calculated by two separate models, Model A and Model B, have been compared. Model A is the Lognormal Force model described in section 7.1. Model B is identical to Model A but with the lognormal dent force distribution replaced by the Corrib QRA dent force distribution (in Figure 7.5 and Figure 7.6, the gouge length and gouge depth distributions are different).

Estimated pipeline failure frequency values have been calculated using Model A and Model B for the six example pipeline cases listed in Table 5.1. A comparison between total failure frequency values for example 1 is shown in Figure 7.7. Equivalent charts for the remaining examples are included in Appendix A .

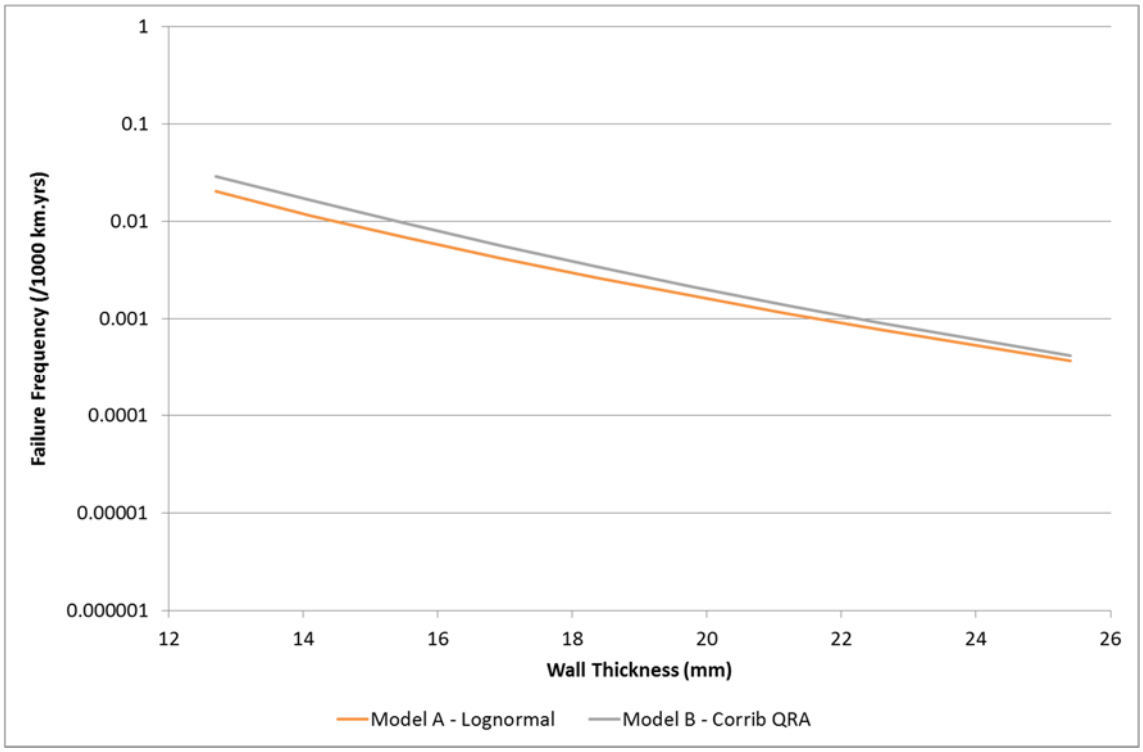

Figure 7.7: Total Failure Frequency as Calculated by Model A and Model B for Example 1

A direct comparison between the results calculated for each example indicates that Model A generally estimates lower values of failure frequency than Model B. It can be concluded that the use of the Corrib QRA dent force distribution within a failure frequency model produces higher values of failure frequency than the use of the lognormal dent force distribution, when all other components are equal. The reason for this is evident from the behaviour of the dent force distributions shown in Figure 7.2. For the majority of dent force values shown in Figure 7.2 (above approximately 27 kN), the probability given by the Corrib QRA distribution exceeds that given by the lognormal force distribution by up to a maximum of approximately 0.35. In regions of Figure 7.2 in which the lognormal dent force distribution gives higher probabilities than the Corrib QRA distribution, the difference between the two curves is small. The combined effect of this is that the overall gouged dent failure probability will be higher when using the Corrib QRA distribution if all other aspects of the model are equal.

The difference between the lognormal and Corrib QRA distributions decreases beyond approximately 75 kN. As pipeline wall thickness is increased, larger dent force values will be required in order to cause a gouged dent failure. This will cause the difference in failure frequencies calculated by models using the lognormal and Corrib QRA distributions to decrease, an effect which can be seen in Figure 7.7.

The difference in failure frequencies calculated by the models due to the dent force distributions is also reduced by increasing the pipeline material toughness. This is because the gouged dent contribution to the failure frequency reduces with increasing toughness.

Overall, Figure 7.7 shows that differences between the results are small, and that it is the changes to the other distributions that are the cause of the larger differences between the ‘Dent Force model’ and the ‘Lognormal Force model’.

7.4 The Split Distributions Model

In Chapter 2 it was highlighted that the original Hazard Analysis model, FFREQ and PIPIN assumed the gouge length and gouge depth random variables to be separate to those for gouged dent gouge length and gouged dent gouge depth. In the PIE and Cosham models and the updated Penspen distributions however, the variables were consolidated. In order to determine the correct approach, a statistical analysis of the gouge and gouged dent data from the 2010 UKOPA Fault Database was performed and is detailed in section 6.2.4. From the analysis it was concluded that gouges and gouges existing as part of a gouged dent come from different populations and therefore should be treated separately.

Based on these findings, a further stage in the construction of AFFECT has been investigated through the use of separate probability distributions for gouge length and gouge depth based on whether a defect is a gouge or a gouged dent. Taking the findings of the statistical analysis into consideration, the gouge length and depth data from the 2010 UKOPA Fault Database concluded as suitable in sections 6.2.2.1 and 6.2.2.2 has been split into:

- Gouge length;
- Gouged dent gouge length;
- Gouge depth;
- Gouged dent gouge depth.

Probability distributions can be fitted to the split data sets in order to describe the behaviour of the now four random variables. These can then be incorporated into the failure frequency model in place of the gouge length and gouge depth distributions used in the Lognormal Force model. In accordance with the conclusions made in section 6.3, data from gouges and gouged dents which resulted in through-wall pipeline failure should be included in the derivation of the probability distributions, with the exception of failures caused by drilling. As previously explained, drill puncture data must be implemented into a failure frequency model through the use of a separate historical data component or a drill puncture model.

7.4.1 *Probability Distributions*

Following removal of the drill puncture data, probability distributions have been fitted to the gouge length, gouge depth, gouged dent gouge length and gouged dent gouge depth data sets. In a similar way to the dent force distribution in section 7.1, a Minitab analysis considering common probability distributions was performed (Anon., 2010) in order to determine the most appropriate distribution to use in order to describe the data. The analysis suggested the most accurate representation of the variables as follows:

- Gouge length – Weibull distribution.
- Gouge depth – Lognormal distribution.
- Gouged dent gouge length – Lognormal distribution.
- Gouged dent gouge depth – Weibull distribution.

Figure 7.8, Figure 7.9, Figure 7.10 and Figure 7.11 show the selected fits to the data. The fits were selected by choosing the lowest Anderson-Darling coefficient in each case apart from that of the gouge depth. For this variable, the distribution which best fitted the data with the highest depth values was chosen. According to the use of the gouge limit state function (equations (3.4) and (3.5)) in the model, only depth probabilities of the critical depth and above are considered within the model. The fit of the distribution is therefore more important at higher depths than lower ones. This condition does not follow for the other variables where a failure state can occur at any value. For gouge depth a reliability/survival analysis was also performed on the data to censor the probability fits to lower depth values in an attempt to achieve a closer fit to higher depth values. The analysis was performed using no censorship, censoring values below 0.5 mm depth, and censoring values below 1 mm depth. The best fit to high depth data was chosen by observation. It should be noted that the probability distributions considered in the Minitab analysis do not represent an exhaustive collection of all possible distributions for each variable. Furthermore the choice of distribution for a variable can have a significant effect on the values of failure frequency calculated by the model. A further study investigating this effect has been performed in section 7.6.

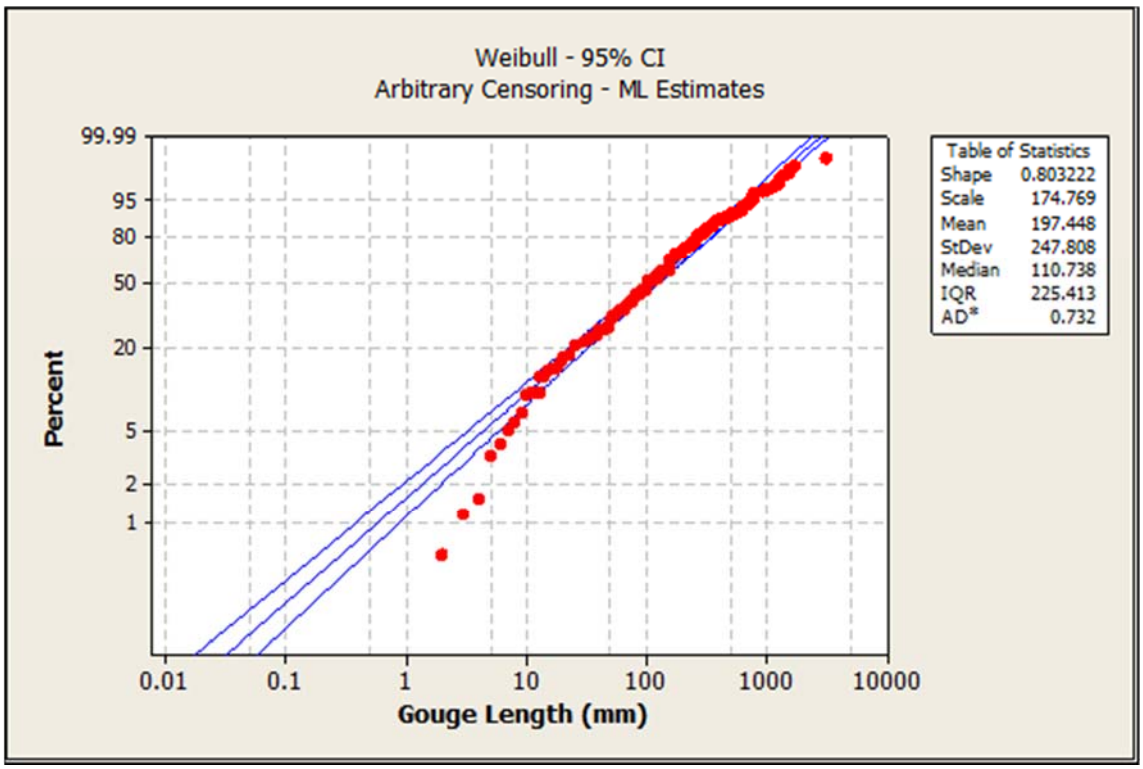

Figure 7.8: Gouge Length Weibull Distribution

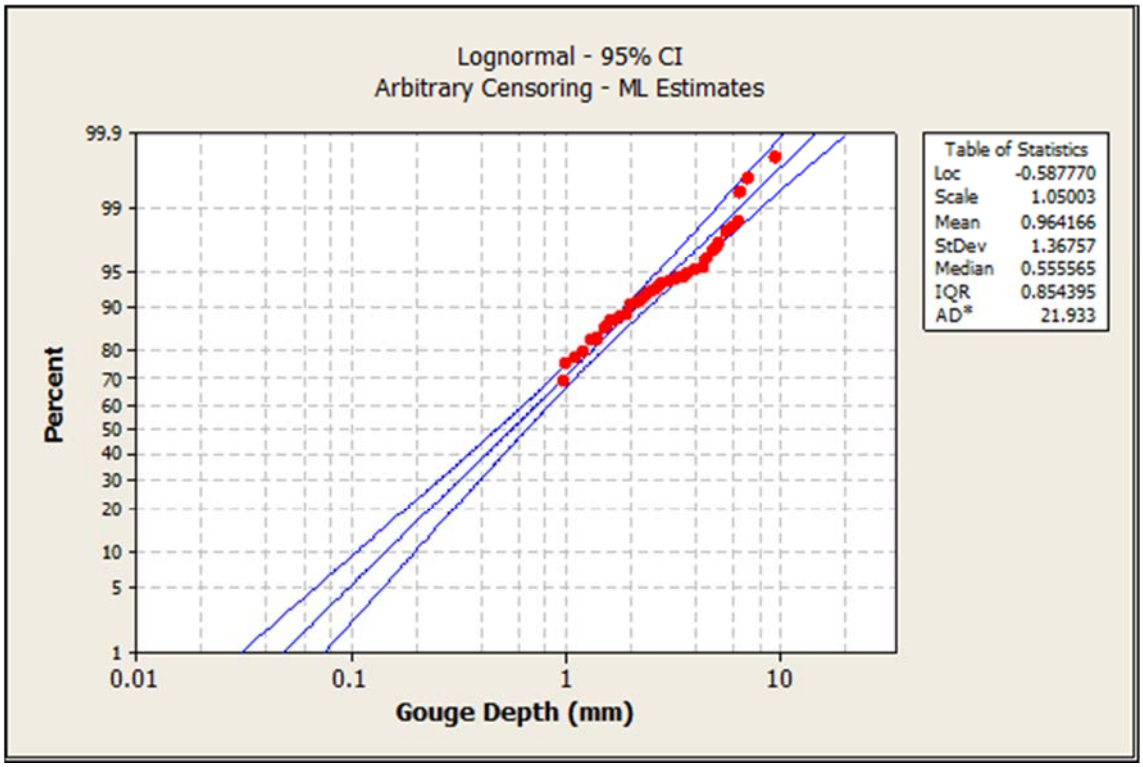

Figure 7.9: Gouge Depth Lognormal Distribution

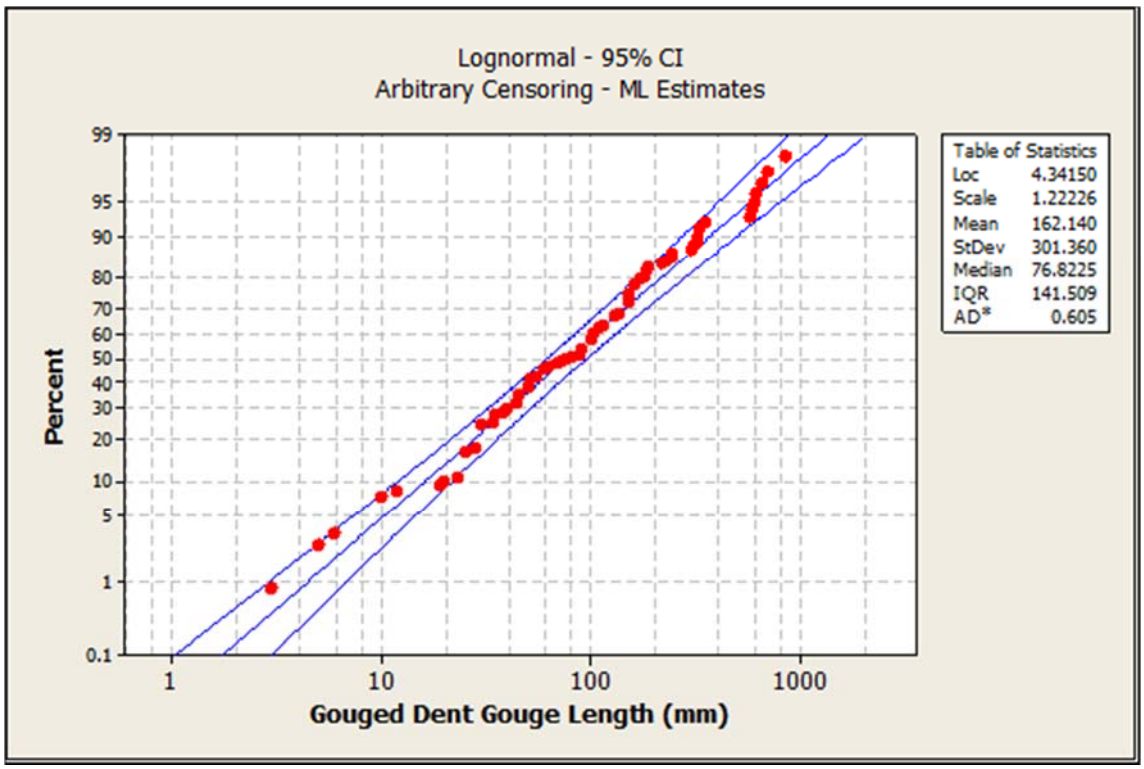

Figure 7.10: Gouged Dent Gouge Length Lognormal Distribution

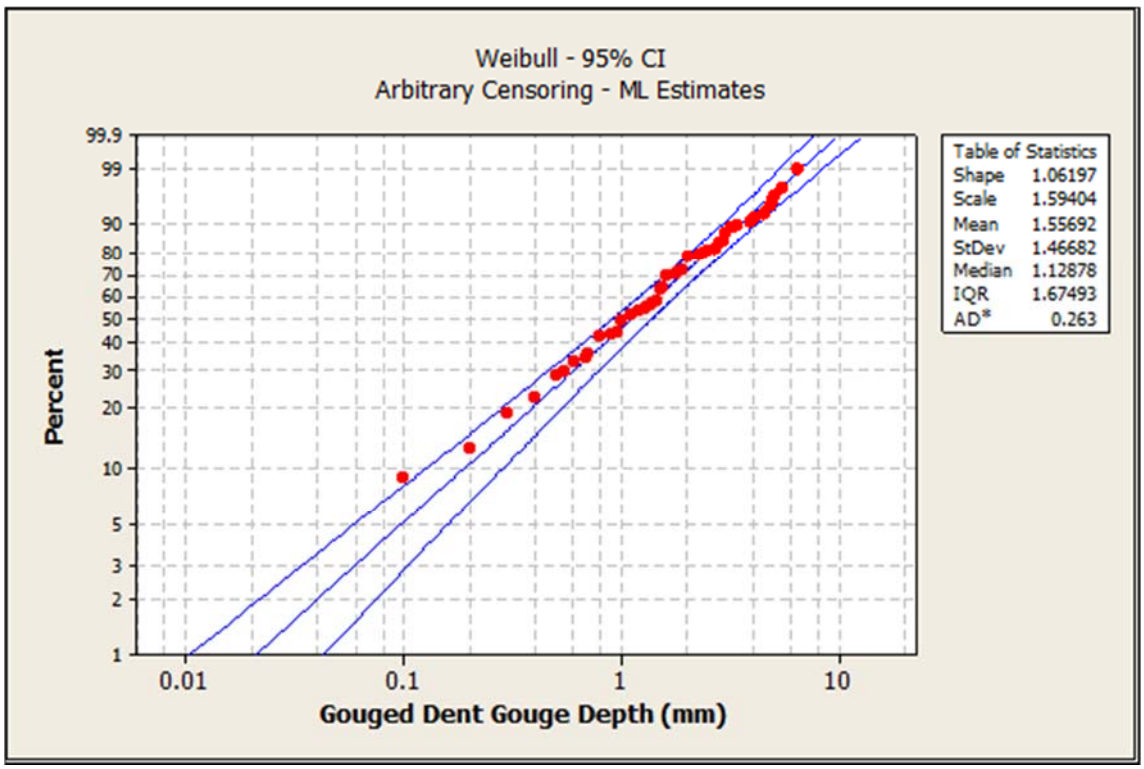

Figure 7.11: Gouged Dent Gouge Depth Weibull Distribution

The distributions for gouge length, gouge depth, gouged dent gouge length and gouged dent gouge depth based on the 2010 UKOPA Fault Database have been incorporated into the failure frequency model in place of the gouge length and gouge depth distributions used in the Lognormal Force model, as the sixth

stage in the construction of AFFECT. This version of the model will be referred to as the Split Distributions model. The parameters defining the cumulative probability distributions used in the Split Distributions model are summarised in Table 7.2. Comparisons between the gouge and gouged dent, gouge depth and gouge length probability distributions used in the Split Distributions model and those used in the Lognormal Force model are shown in Figure 7.12 and Figure 7.13.

Variable	Distribution	α (Weibull) μ_d (Lognormal)	β (Weibull) σ_d (Lognormal)
Gouge Length	Weibull	0.803	174.769
Gouge Depth	Lognormal	-0.587	1.050
Gouged Dent Gouge Length	Lognormal	4.342	1.222
Gouged Dent Gouge Depth	Weibull	1.062	1.594
Dent Force	Lognormal	4.052	0.486

Table 7.2: Split Distributions Model Distribution Parameters

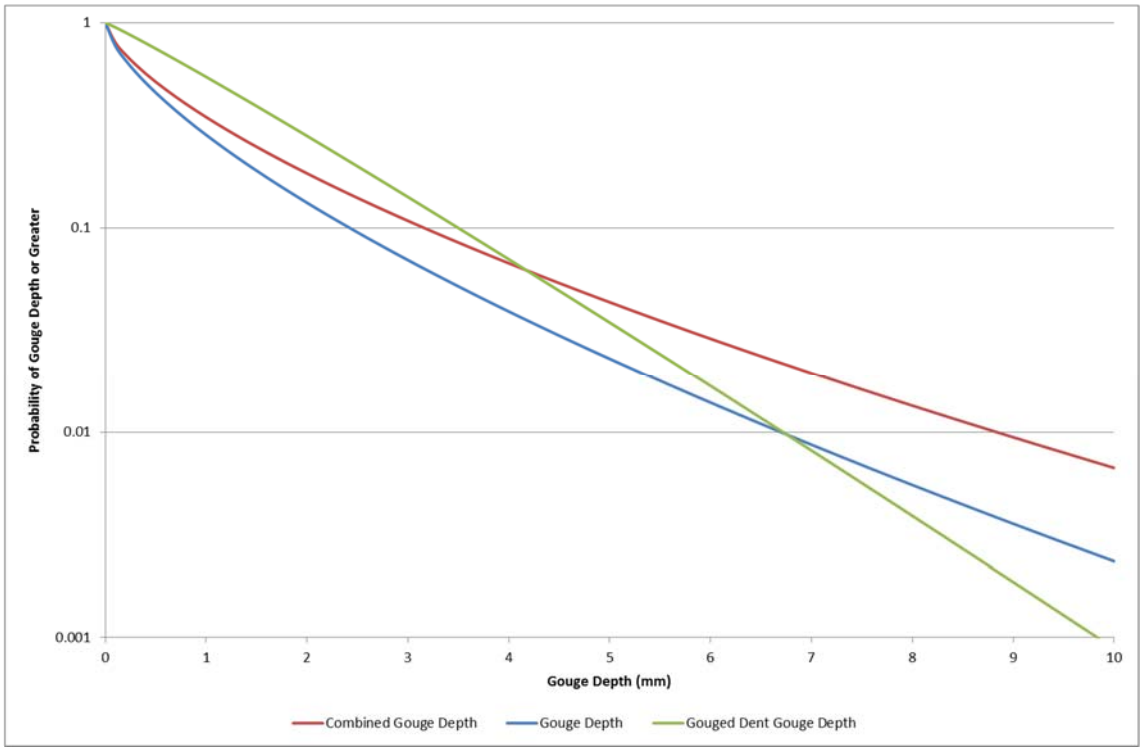

Figure 7.12: Gouge Depth Distribution Comparison, Split Distributions Model and Lognormal Force Model

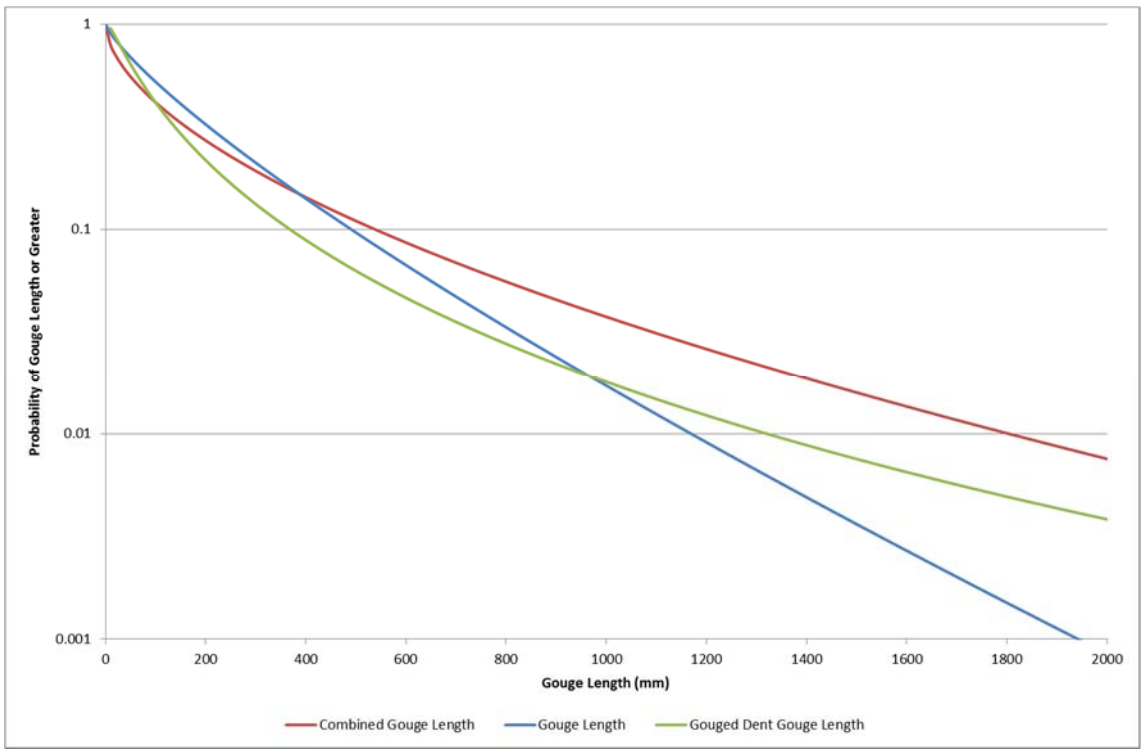

Figure 7.13: Gouge Length Distribution Comparison, Split Distributions Model and Lognormal Force Model

The additional probability distributions are implemented by modifying the expressions for gouge and gouged dent failure probability. The probability of failure for gouges (equation (2.84)) becomes:

$$P_{gougetotal} = \int_0^{\infty} f_{g2c}(2c) R_{gd}(d_{crit}) d2c \qquad (7.3)$$

Where the subscripts $g2c$ and gd denote the use of the gouge length and gouge depth distribution parameters respectively.

Similarly the probability of failure of gouged dents (equation (2.86)) becomes:

$$P_{gougeddenttotal} = \int_0^{\infty} f_{gd2c}(2c) d2c \,.\left[\int_0^{d_{critBGDGFM}} f_{gdd}(d) R_F(F_{crit}) dd + R_{gdd}(d_{critBGDGFM})\right] \qquad (7.4)$$

Where the subscript F denotes the use of the dent force distribution and F_{crit} being the critical force required to cause a failure in combination with a gouge of depth d. The integrals for leak and rupture (equations (2.88), (2.89)) become:

$$P_{gougeddentleak} = \int_0^{L_{crit}} f_{gd2c}(2c) d2c \,.\left[\int_0^{d_{critBGDGFM}} f_{gdd}(d) R_F(F_{crit}) dd + R_{gdd}(d_{critBGDGFM})\right] \qquad (7.5)$$

$$P_{gougeddentrupture} = \int_{L_{crit}}^{\infty} f_{gd2c}(2c)d2c \,.\left[\int_{0}^{d_{critBGDGFM}} f_{gdd}(d)R_F(F_{crit})dd + R_{gdd}(d_{critBGDGFM})\right] \quad (7.6)$$

Where the subscripts *gdd* and *gd2c* denote the use of the gouged dent gouge depth and gouged dent gouge length distribution parameters respectively.

7.5 Split Distributions Model Results

Estimated pipeline failure frequency values have been calculated using the Split Distributions model for the six example pipeline cases listed in Table 5.1. As before, leak, rupture and total failure frequency have been calculated.

A comparison between total failure frequency values for example 1 as calculated by the Split Distributions model, Lognormal Force model, New Distributions model, Dent Force model, Re-Rounding model and the Modified PIE model, is shown in Figure 7.14. A similar comparison between total failure frequency values for example 4 is shown in Figure 7.15. These charts show the progression of the models. Equivalent charts for the remaining examples are included in Appendix A .

A comparison between total failure frequency values for examples 1, 2, and 3 as calculated by the Split Distributions model and the Lognormal Force model, is shown in Figure 7.16. A similar comparison between total failure frequency values calculated for examples 4, 5 and 6 is shown in Figure 7.17.

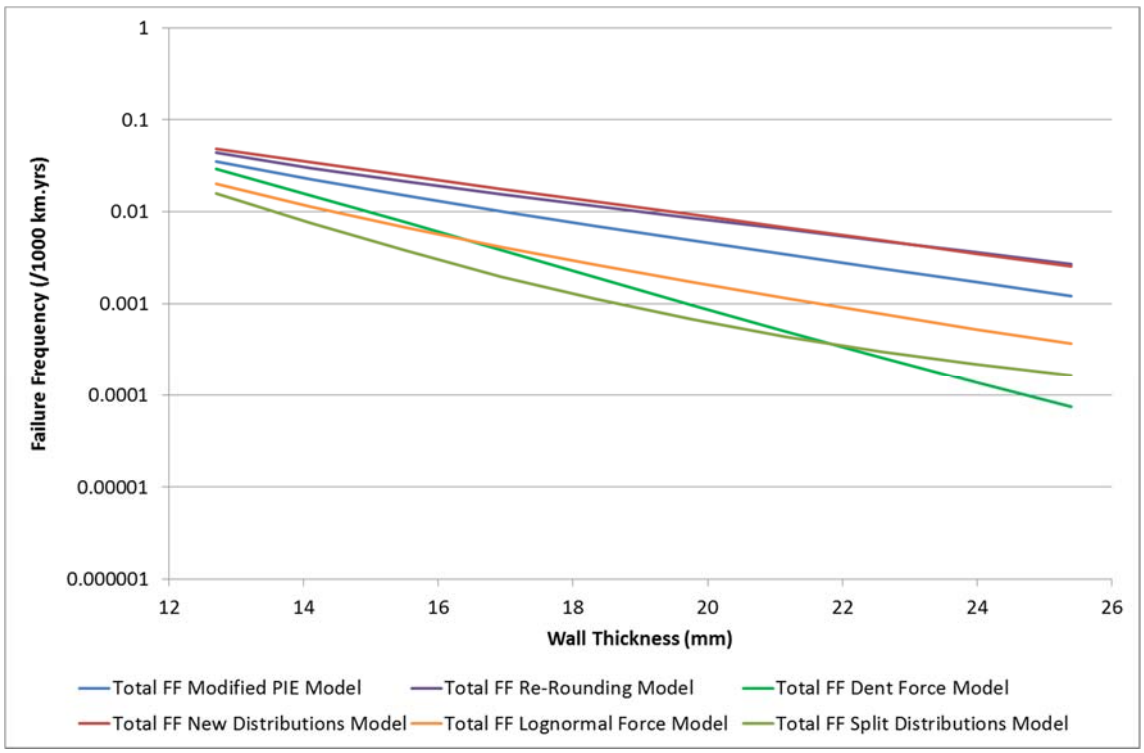

Figure 7.14: Total Failure Frequency as Calculated by the Split Distributions Model, Lognormal Force Model, New Distributions Model, Dent Force Model, Re-Rounding Model and the Modified PIE Model for Example 1

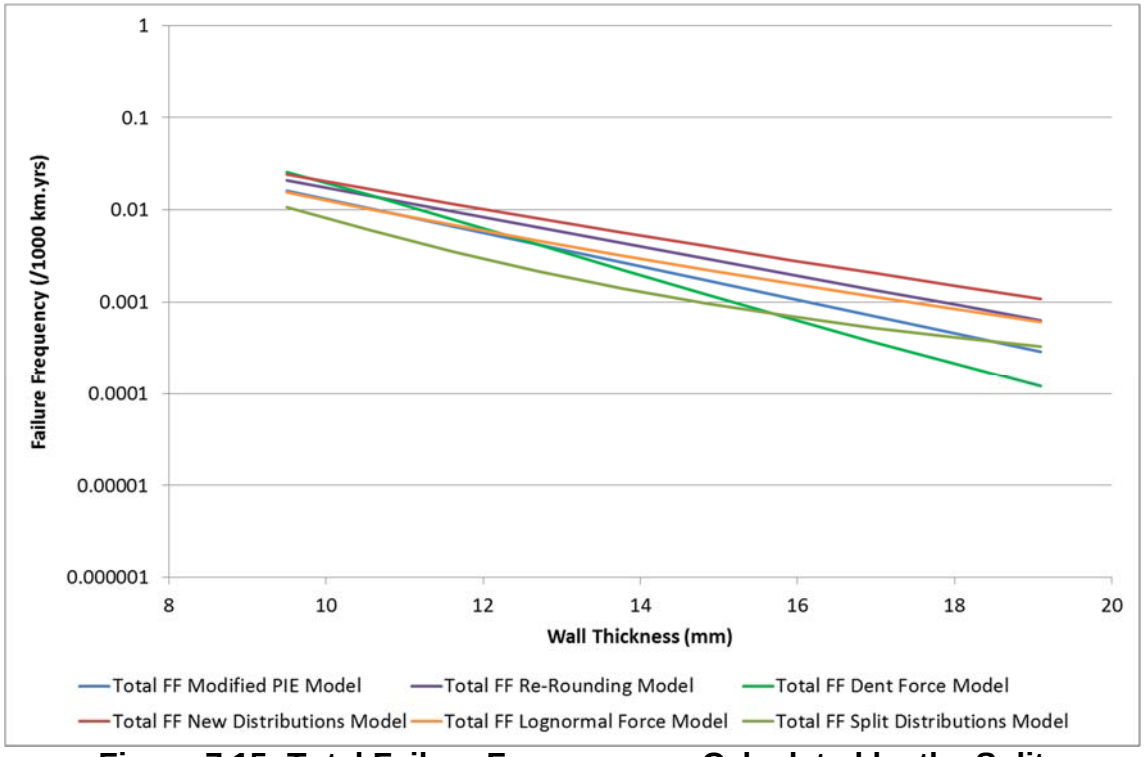

Figure 7.15: Total Failure Frequency as Calculated by the Split Distributions Model, Lognormal Force Model, New Distributions Model, Dent Force Model, Re-Rounding Model and the Modified PIE Model for Example 4

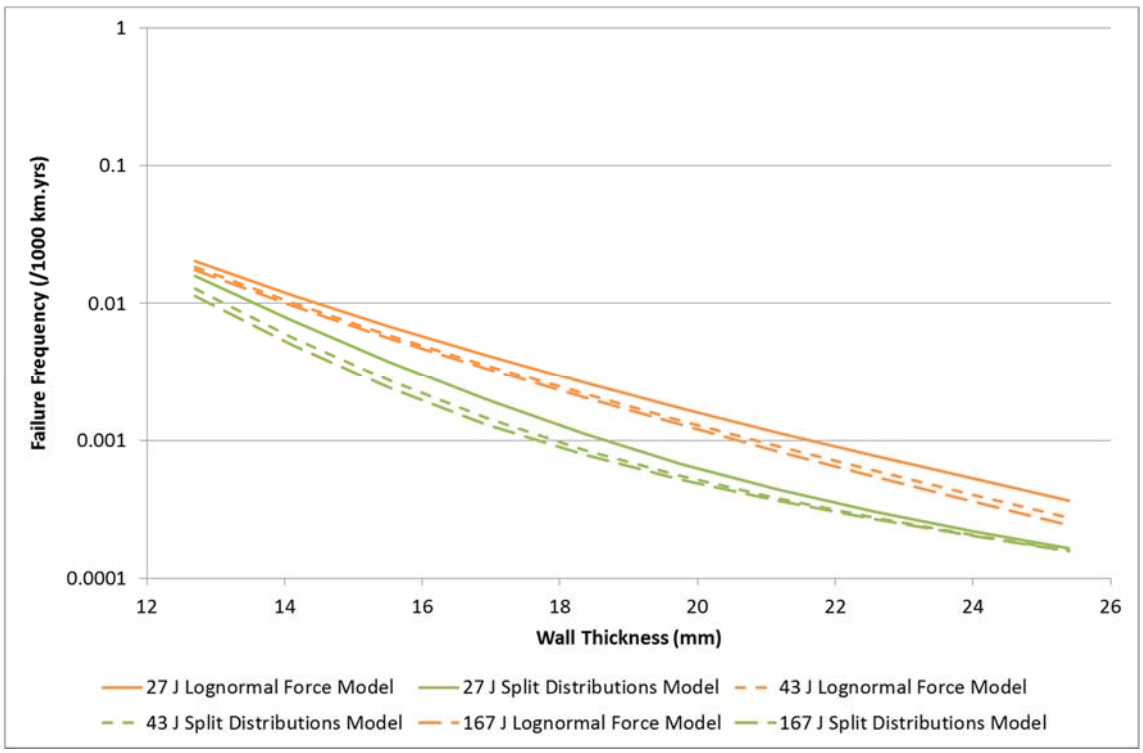

Figure 7.16: Total Failure Frequency as Calculated by the Split Distributions Model and the Lognormal Force Model for Examples 1, 2 and 3

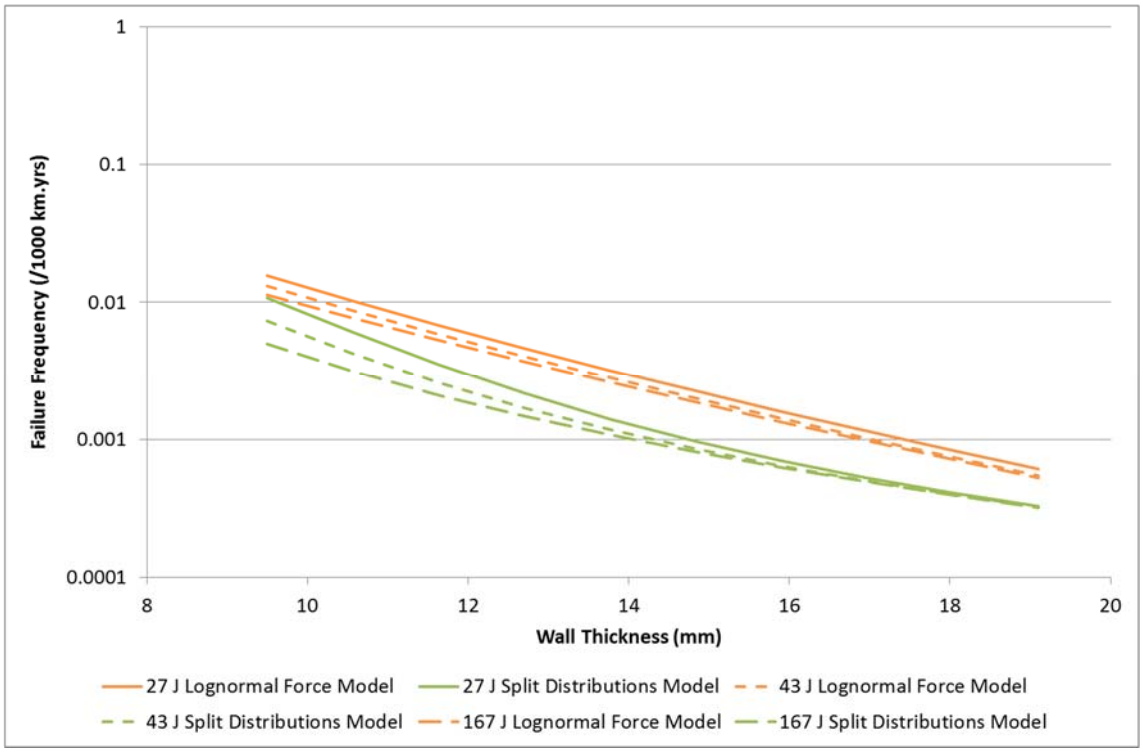

Figure 7.17: Total Failure Frequency as Calculated by the Split Distributions Model and the Lognormal Force Model for Examples 4, 5 and 6

Based on the results, the following observations can be made regarding estimations of pipeline failure frequency made by the Split Distributions model.

A direct comparison between the results calculated for each example indicates that at low wall thickness, the Split Distributions model estimates the lowest values of failure frequency of all the models considered so far. The model however, displays a reduced rate of decay in values of failure frequency with increasing wall thickness in comparison to the other models. The effect of this is that at higher wall thicknesses, depending on the conditions, the Split Distributions model can produce failure frequencies in excess of the other models.

The depth and length distributions used in the Split Distributions model from Figure 7.12 and Figure 7.13 give an insight into the behaviour of the model. A similar trend in the gouge depth and gouged dent gouge length probability distributions with increasing depth and length can be seen in these charts as is observed for the Split Distributions failure frequencies with increasing wall thickness. From Table 7.2, these curves are lognormal fits. It is clear that the presence of the lognormal fits within the model is strongly influencing the estimated failure frequencies.

7.6 The Effect of Distribution Choice on Failure Frequency

In section 7.4.1, an analysis to determine the most appropriate probability distributions for the random variables introduced in the Split Distributions model was performed. The analysis was performed using the statistical software package Minitab. In this analysis a range of distributions were fitted for each of the four variables using different distribution types and fitting methods. For each random variable two different distributions types and two different curve fitting methods were used. The distribution types used were chosen on the basis of their historical use in failure frequency models such as Hazard Analysis and PIPIN. The distributions fitted for each variable are given in Table 7.3:

Distribution Type	Curve Fitting Method
Weibull	Maximum Likelihood
Weibull	Least Squares
Lognormal	Maximum Likelihood
Lognormal	Least Squares

Table 7.3: Distribution Range for Each Variable for Minitab Analysis

In addition, a further range of distributions were fitted for the gouge depth variable using a reliability/survival analysis. The aim of the reliability/survival analysis was to censor the curve fitting method to lower depth values in an attempt to achieve distributions closer fit to higher depth values. As explained in section 7.4.1, the fit of the gouge depth distribution is more important at higher depths than lower ones as this is where the failure states occur. This condition does not follow for the other variables where a failure state can occur at any value. The additional distributions fitted for gouge depth are given in Table 7.4:

Distribution Type	Curve Fitting Method	Censoring Depth (mm)
Weibull	Maximum Likelihood	1
Weibull	Least Squares	1
Lognormal	Maximum Likelihood	1
Lognormal	Least Squares	1
Weibull	Maximum Likelihood	0.5
Weibull	Least Squares	0.5
Lognormal	Maximum Likelihood	0.5
Lognormal	Least Squares	0.5

Table 7.4: Additional Distributions for Gouge Depth for Minitab Analysis

From the distributions given in Table 7.3 and Table 7.4 the best fit was selected for each different variable on the basis of either the lowest calculated Anderson-Darling coefficient; or, in the case of gouge depth, the observed best fit to the data points at the highest depth values.

Using the above method a best fit distribution was selected for each variable from a range of at least four different fits. It should be noted however that the different fits considered by the method do not represent an exhaustive collection of all possible distributions for each variable. Other distribution types such as

exponential, gamma, logistic and loglogistic could be used to produce fits to the data. In addition, further options are also available to influence the procedure of curve fitting. It is possible that through some combination of these a better fit to the data sets for each variable could be achieved. Performing such an exercise would prove to be inconsequential however, due to the nature of the data source itself. Because of the level of uncertainty of the UKOPA Fault Database, the data sets derived for each variable depend upon a subjective interpretation of the data made by the assessor during their derivation. A separate analysis performed by a different assessor would yield different data sets regardless of the fact that the data source is the same. The data sets would be similar, however even small differences would affect the outcome of curve fitting leading to different “best fit” probability distributions. In conclusion, there is no definitive method of analysis of the UKOPA Fault Database to derive the true data sets for each of the random variables and therefore no way to determine the absolute best fit probability distributions. It must be accepted that the probability distributions derived from any analysis of the UKOPA Fault Database will have an associated error.

In order to investigate the effect that differences in the probability distribution fits can have on the values of failure frequency calculated by the model a further analysis has been performed. For this analysis the failure frequencies calculated by three separate models, Model C, Model D and Model E have been compared. Model D is the Split Distributions model described in section 7.4. Model C and Model E are identical to Model D, but use different gouge length probability distributions, selected from the distributions fitted as part of the Minitab analysis described above. The gouge length probability distributions derived as part of the Minitab analysis are shown in Figure 7.18 alongside the raw data points.

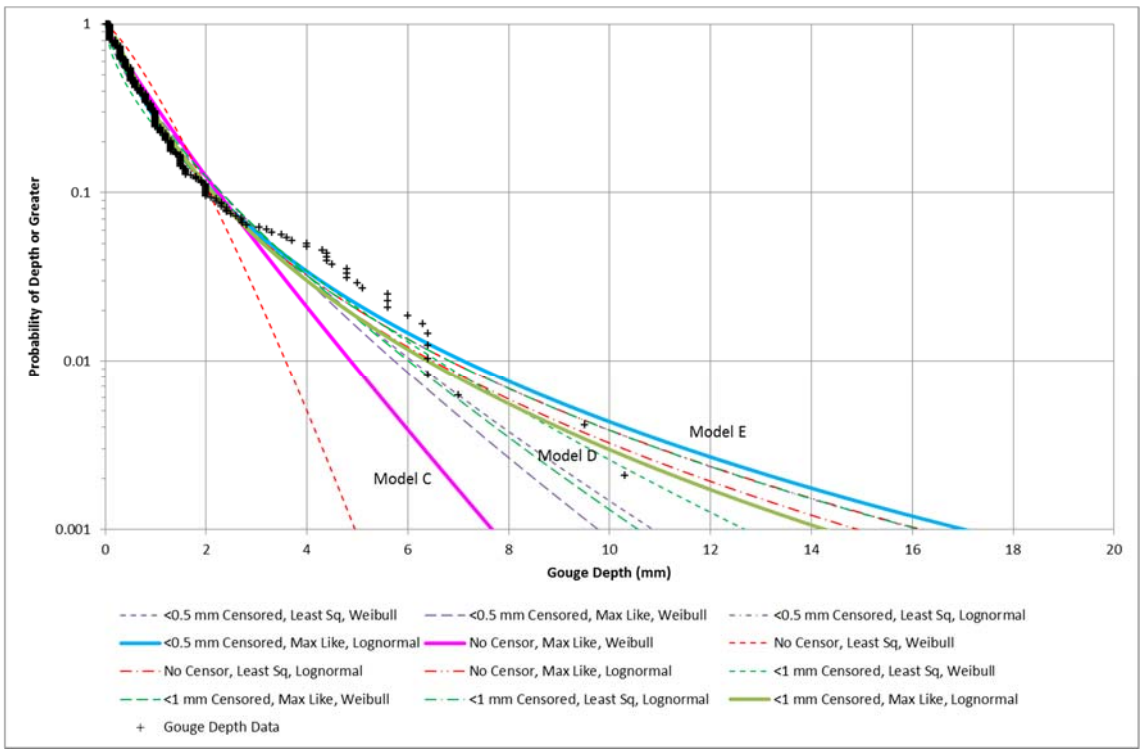

Figure 7.18: Gouge Depth Distributions Fitted for Minitab Analysis

In Figure 7.18 the distributions selected for this analysis have been highlighted as thicker coloured lines. Note that in this case the distributions have been chosen because they represent the range of the different fits produced in the Minitab analysis in relation to the gouge depth data points, rather than the accuracy of their fit as determined by their goodness-of-fit parameters. A summary of the gouge depth distributions selected for models C, D and E is given in Table 7.5. The distributions for the other variables are identical and equivalent to those used in the Split Distributions model.

Model	Distribution Type	Curve Fitting Method	Censoring Depth (mm)
C	Weibull	Maximum Likelihood	N/A
D	Lognormal	Maximum Likelihood	0.5
E	Lognormal	Maximum Likelihood	1

Table 7.5: Gouge Depth Distributions for Models in the "Effect of Distribution Choice on Failure Frequency" Comparison

Estimated pipeline failure frequency values have been calculated using Model C, Model D and Model E for the six example pipeline cases listed in Table 5.1. A comparison between total failure frequency values for example 1 is shown in

Figure 7.19. Equivalent charts for the remaining examples are included in Appendix A .

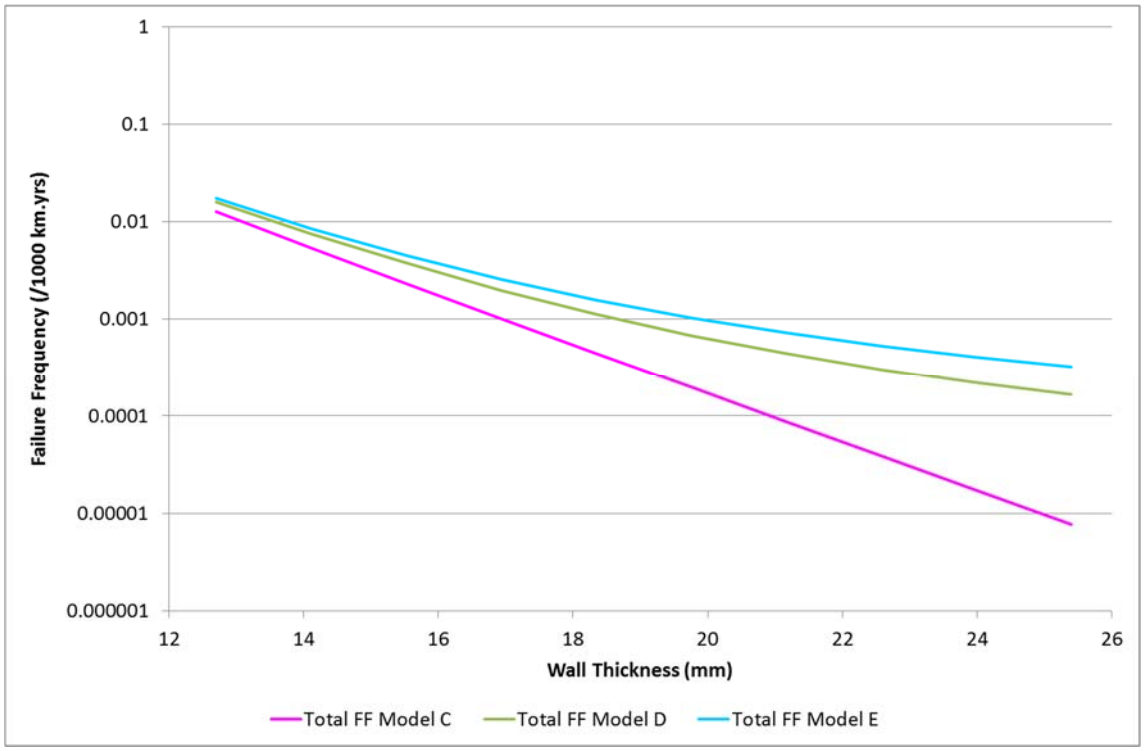

Figure 7.19: Total Failure Frequency as Calculated by Model C, Model D and Model E for Example 1

The results show that the model using the gouge depth distribution which gives the lowest gouge depth probabilities of those selected in Figure 7.18, Model C, produces the lowest values of calculated failure frequency. Similarly the model which gives the highest gouge depth probabilities in Figure 7.18 produces the highest calculated values of failure frequency, Model E.

From the results it can be concluded that failure frequency is strongly influenced by the distributions used in its calculation. In terms of the models used in this analysis, if a comparison is made between the differences produced by introducing the modifications to the model explained in Chapter 5 and Chapter 7 (shown in Figure 7.14 for example 1); and the differences produced by changing the gouge depth distribution only, distribution choice is shown to be a significant factor, especially at high wall thickness. At approximately 20 mm wall thickness Model C produces values of failure frequency which are almost an order of magnitude lower than those produced by Model E. The difference becomes increasingly divergent as wall thickness is increased further. In

comparison the differences produced over the whole range of model modifications shown in Figure 7.14 is of approximately the same order. Furthermore, the differences shown account for changes in the distributions of only one of the five random variables. Further differences, either additive or subtractive depending on the chosen distributions, would occur if the distributions for the other random variables were also changed between models. It is also noted that the values of failure frequency calculated using Model C are the lowest of all the models considered so far. A particular choice of distribution could therefore potentially lead to non-conservative results.

It is recommended that further work is performed towards investigating the potential error in failure frequencies as a result of interpretation of the UKOPA Fault Database and selecting a distribution fit.

7.7 Additional Model Considerations for AFFECT

The Split Distributions model described in section 7.4 represents the final stage in the construction of the AFFECT model. However, following on from the discussion in section 2.8 there are two additional considerations to be addressed.

Firstly, as noted in section 5.7, the updated value for the Penspen Incident-Rate used in the AFFECT model refers to pipelines located in R-type areas only. The basic AFFECT model is therefore applicable only to rural pipelines. In the discussion from section 2.8 it was suggested that an appropriate factor applied to the R-type Incident-Rate could be used to account for pipelines located in S-type areas. The PIPIN failure frequency model employs such a system, using a factor of 4. An analysis has been performed using the 2010 UKOPA Fault Database in order to derive a similar factor for the AFFECT model. This factor is given in Table 7.6. The factor is derived by calculating the ratio of the total number of external interference incidents affecting pipelines in R-type areas to the total number of external incidents affecting pipelines in S-type areas.

Incident-Rate Factor
3.6

Table 7.6: R-Type/S-Type Area Incident-Rate Factor for AFFECT

Secondly, as noted in the discussion in section 2.8, pipeline depth of cover is an important consideration when applying a failure frequency model to a specific pipeline. For the basic AFFECT model a pipeline is assumed to have the average depth of cover for all of the pipelines considered in the UKOPA Fault Database. This follows from the probability distributions and Incident-Rate used in the model, which are derived from an amalgamation of the data from each damaged pipeline. Both the FFREQ and PIPIN models included a facility to take into account the pipeline depth of cover by applying modifying factors to the Incident-Rate. These factors were derived from separate analyses performed when the models were originally developed. An updated analysis was performed in 2012 by GLND on behalf of UKOPA, which can be used to provide similar factors for the AFFECT model. The modifying factors were derived from historical operational data contained in the 2010 UKOPA Fault Database by relating the number of pipeline damage incidents to the depth of cover (Mumby, 2012). The modifying factors for depth of cover derived by GLND are shown graphically in Figure 7.20. For comparison the equivalent factors from FFREQ and PIPIN are also shown.

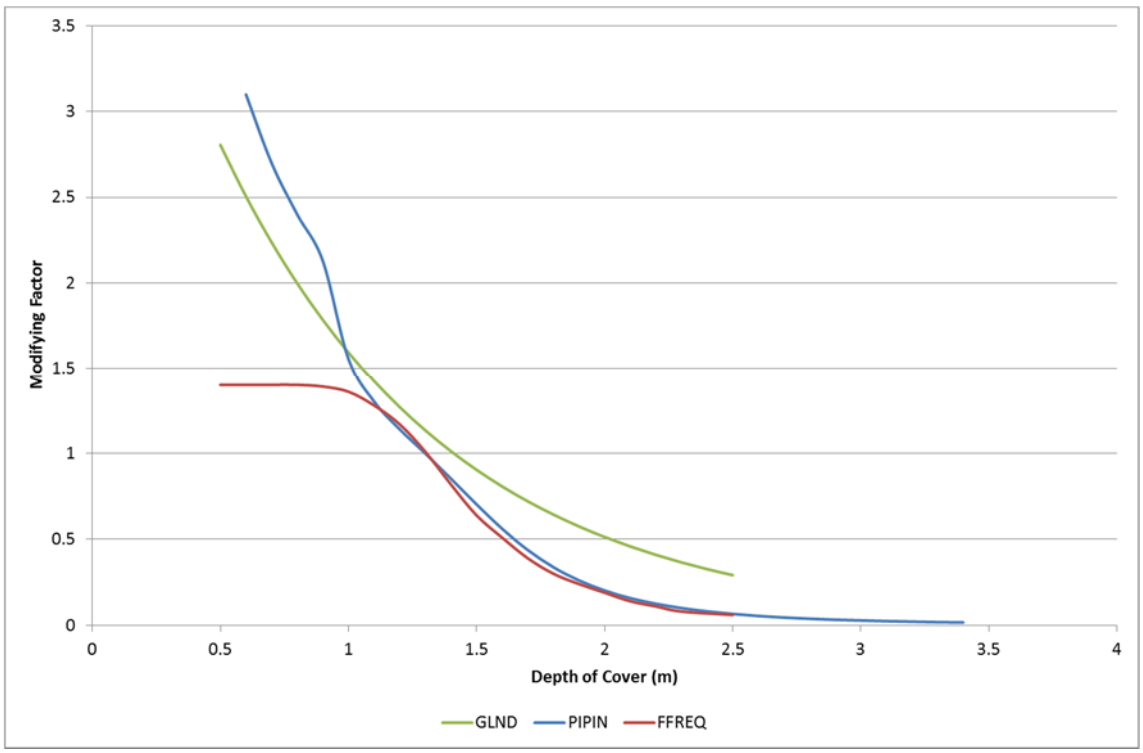

Figure 7.20: Depth of Cover Factors from GLND with PIPIN and FFREQ

Figure 7.20 shows that for the GLND analysis the modifying factor has a value of 1 when the depth of cover is 1.6 m. It follows logically that if the depth of cover factor is omitted, the assumption is that the particular pipeline under consideration is buried with a depth of 1.6 m. This value is higher the value derived for FFREQ but approximately equal to that from PIPIN. Above 1 m depth of cover the modifying factors are higher than those used in both FFREQ and PIPIN.

7.8 Development of AFFECT (Part 2) Conclusions

This chapter has charted the final two stages in the construction of AFFECT, a failure frequency model for dense phase carbon dioxide pipelines based upon probabilistic structural reliability methods. Additional factors have also been proposed to enable the AFFECT model to take account of pipelines located in S-type areas and pipeline depth of cover. The AFFECT model has been developed by making modifications to the PIE model, a basic failure frequency model which uses appropriate failure models identified in Chapter 3 and Chapter 4. The modifications made in this chapter consider the results of a statistical analysis of the 2010 UKOPA Fault Database. Table 7.7 summarises

the basis and benefits of each discrete stage in the model development; a flow chart showing the progression of the entire AFFECT model is shown in Figure 7.21.

Each of the modifications addressed is considered to provide improvement to the PIE model. In addition to the stages detailed in Chapter 5, the Lognormal Force model and the Split Distributions model provide further improvement to the probability distributions describing the nature of pipeline mechanical damage.

It is noted that the AFFECT model does not adequately address failures caused by damage to branches and fittings; and drilling operations in-error. In order that the model address failures of these types, the development of an historical data component or additional damage specific failure models would be required. The development of these elements however, has not been performed as part of this work. It is therefore recommended that such a task is considered as part of further work.

It is concluded that differences in the probability distribution fits used to describe the random variables in a failure frequency model can have a significant effect on the values of failure frequency calculated by that model. It is recommended that further work is performed towards investigating the potential error in failure frequencies as a result of interpretation of the UKOPA Fault Database and selecting a distribution fit.

Further comparison studies have been performed using AFFECT. These include an analysis of the trends observed when the model is applied to different pipeline scenarios and also comparison calculations with the observed failure rate of the UK pipeline system. This work provides validation of the model. Details are included in Chapter 8. It is recommended that the additional factors detailed in section 7.7 are used depending on the depth of cover of the pipeline and if the AFFECT model is to be applied to pipelines located in S-type areas.

Model	Basis / Development	Benefits
Modified PIE	Structural reliability model based upon a simplified version of the British Gas methodology. Updated with calculations from the Cosham model.	Use of most appropriate models for leak / rupture, gouge failure and gouged dent failure. Probability of failure calculated accurately
Re-Rounding	As Modified PIE model but with EPRG dent re-rounding equation	Dent depth is modelled more accurately
Dent Force	As Re-Rounding model but with EPRG dent force equation used to derive dent force distribution in place of dent depth	Denting modelled more accurately, dependence on geometry is removed
New Distributions	As Re-Rounding model but with updated distributions	Distributions up to date as of 2009
Lognormal Force	New Distributions and Dent Force models effectively combined	Distributions up to date as of 2010 including dent force distribution
Split Distributions	Gouge and gouged dent parameters treated separately, new distributions for each derived	Acknowledges the difference between the two forms of damage

Table 7.7: Summary of the Basis and Benefits of All Stages in the Construction of AFFECT

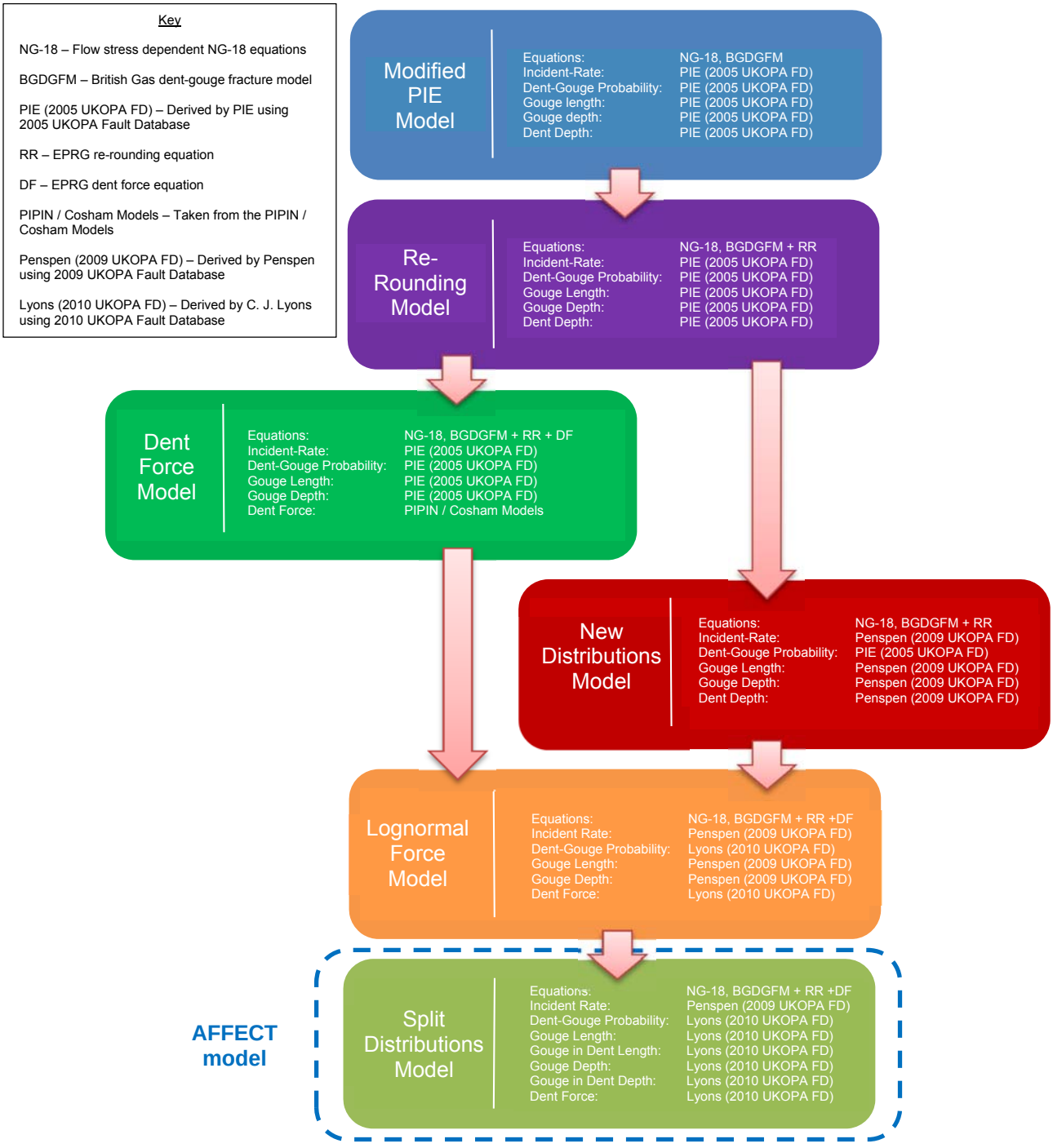

Figure 7.21: All Stages in the Construction of AFFECT

Chapter 8. Trends of the AFFECT Failure Frequency Model for Dense Phase CO_2 Pipelines

Chapter 5 to Chapter 7 have detailed the development of the AFFECT model to calculate the failure frequency due to third party external interference of a dense phase CO_2 pipeline. This chapter details an analysis of the trends observed when the AFFECT model is applied to different pipeline scenarios. Validation of the model is also provided through a comparison between model predictions, historical operational data and the current industry standard failure frequency model FFREQ.

The studies included in this chapter are:

- A comparison between the number of failures recorded historically for pipelines in the UKOPA Pipeline Database; and the number which would be expected as calculated using both the AFFECT and FFREQ models.
- A sensitivity study of pipeline failure frequency calculated using the AFFECT model, to wall thickness.
- A sensitivity study of pipeline failure frequency calculated using the AFFECT model, to design factor.
- An example comparison between the operating stress of a 610 mm external diameter dense phase CO_2 pipeline operating at 135 barg; and its proximity to the leak/rupture boundary for a long defect, calculated using the AFFECT model.

8.1 Comparison with Historical Operational Failure Data

Although AFFECT has been developed for the purpose of application to thick wall dense phase CO_2 pipelines, the model is based upon the methodology originally developed by British Gas for the Hazard Analysis model and can be used to estimate failure frequencies for both thin and thick wall pipelines. Taking this into consideration a validation study has been performed by comparing the number of failures of pipelines listed in the UKOPA Pipeline Database (McConnell, 2012) which would be expected when calculated by AFFECT, with

the true value from historical operational failure data (McConnell, 2011). A comparison with the industry standard failure frequency software FFREQ has also been included.

8.1.1 *AFFECT Calculation*

The UKOPA Pipeline Database contains details of 2,300 pipelines located in the UK, including both those currently operating and those decommissioned. Like the UKOPA Fault Database the UKOPA Pipeline Database includes information about the pipelines including their external diameter, wall thickness, steel grade and operating pressure. It also includes information on the length of each pipeline, their commissioning and decommissioning dates (where relevant), and whether they are routed through R-type, S-type or town (T-type) areas.

A value for the expected number of failures on pipelines listed in the UKOPA Pipeline Database can be calculated by the AFFECT model based on the operational exposure of pipelines in the database.

In the AFFECT model, the Incident-Rate is the number of times per unit of operational exposure that a pipeline is subject to damage due to third party external interference. By multiplying the Incident-Rate by the pipeline operational exposure, a value for the total predicted number of third party external interference damage incidents a pipeline has experienced in its lifetime can be derived:

Number of Third Party External Interference Damage Incidents = Incident-Rate x Operational Exposure

This value can then be multiplied by the probability of failure for the pipeline, calculated by AFFECT, in order to determine a value for the total number of failures a pipeline has suffered in its lifetime.

In order to calculate the total expected number of failures on pipelines listed in the UKOPA Pipeline Database, the above method has been applied to each pipeline in the database individually and the results summed.
The AFFECT model as described in Chapter 5 and Chapter 7 calculates failure frequencies for pipelines routed through R-type areas. In order to take account of pipelines in the UKOPA Pipeline Database routed through S-type and T-type areas in this study, the Incident-Rate factor of 3.6 described in section 7.7 has been applied. An increased Incident-Rate acknowledges the increased level of third party activity in these areas.

Note that specific depth of cover information for each pipeline in the UKOPA Pipeline Database was not provided. The depth of cover factors described in section 7.7 were therefore not applied as part of the calculation. In excluding these factors, the assumption is that each pipeline in the database has a depth of cover equal to the average depth of cover for the entire database. This was considered to be a reasonable assumption given that the calculation considers a sum over every pipeline within the database.

For each pipeline in the UKOPA Pipeline Database the external diameter and operational exposure for each area class have been taken as stated in the database. The pipe yield strength and tensile strength in each case have been assumed as the SMYS and the SMUTS of the reported pipe grade. The pipeline operating pressure and wall thickness have been taken from the fields “Maximum Operating Pressure” and “Main Nominal Wall Thickness” in the database, respectively. The 2/3 Charpy v-notch energy for each pipeline is not recorded in the UKOPA Pipeline Database. Conservatively a value of 27 J has been assumed for each case.

Note that in the UKOPA Pipeline Database seven pipelines do not have a reported pipe grade, 11 do not have a reported maximum operating pressure, 29 do not have a reported wall thickness and one pipeline does not have a reported external diameter, wall thickness or pipe grade. In the absence of this information these 48 pipelines have not been included in the calculation of the expected number of pipeline failures. The calculation therefore considers a total of 2,252 pipelines.

8.1.2 *Historical Operational Failure Data*

The historical operational failure data used in the comparison with the AFFECT calculation is taken from the 2010 UKOPA Fault Database described in Chapter 6.

By construction, the AFFECT model is used to calculate the pipeline failure frequency, due to third party external interference, which has resulted in part-wall or through-wall damage (either a gouge or a gouged dent), to a pipe body, or pipe bend. The UKOPA Fault Database includes the details of failures caused by third party external interference, which occurred to components such as weldolets, valves, tees, stand pipes etc. Failure incidents such as these are not appropriate for a comparison with calculations made by AFFECT and are therefore not included. In addition, punctures to the pipeline resulting from drilling operations in-error are not included in the comparison; pipeline failure resulting from this form of damage is not the same as a conventional through-wall failure. From a total of 39 historical incidents of pipeline failure caused by external interference recorded in the UKOPA Fault Database, there are conservatively 18 which are considered appropriate for comparison with calculations made using AFFECT. Further details on the UKOPA Fault Database and the suitability of data with respect to the AFFECT model are contained in Chapter 6.

Details of the 18 pipeline failure incidents used in the comparison are given in Table 8.1[34]:

[34] Note that in comparison with Table 6.11 in Chapter 6, only the individual defects considered to have been the source of the failure are shown in Table 8.1. Additional defects which share the same fault number as those in Table 8.1 but did not fail are not shown.

Description	Date Discovered	Pipeline Diameter (mm)	Wall Thickness (mm)	Extent of Damage	Fault Comment from the UKOPA Fault Database
Gouge (failure)	20 May 1980	218	6.4	Leak	LINE HOLED BY PNEUMATIC DRILL
Gouge (failure)	28 April 1978	102	4.8	Leak	2 HOLES
Gouge (failure)	28 April 1978	102	4.8	Leak	2 HOLES
Dent with Gouge (failure)	08 June 1972	324	6.4	Leak	4 HITS , 1 PENETRATION
Dent with Gouge (failure)	31 May 1988	218	7.1	Leak	Damaged by FE20 excavator during landscaping
Gouge (failure)	09 June 1970	218	5.6	Fracture	No Loss, severed pre commission
Dent with Gouge (failure)	30 September 1971	324	6.4	Leak	HOLE , INDENTATION
Gouge (failure)	28 September 1983	325	6.4	Leak	TRENCH CUTTER HOLED PIPE
Gouge (failure)	04 February 1992	218	7.1	Leak	PIPE CUT BY GRINDER IN ERROR
Gouge (failure)	03 May 1978	457	9.5	Fracture	SHEETPILERSLICEDTHRUSIDEOFPIPE
Gouge (failure)	27 April 1971	168	4.4	Fracture	LINE SHEARED BY MOLE PLOUGH
Dent with Gouge (failure)	02 April 1990	168	4.8	Fracture	36 cust. Line holed by trencher during excavation for water main
Gouge (failure)	01 December 1971	168	6.4	Leak	JCB HIT DIVERTED PIPE-ROADWRKS
Dent with Gouge (failure)	26 September 1984	168	4.8	Leak	Mole plough holed pipe
Gouge (failure)	17 November 1973	102	4.4	Fracture	EXCV.FRACTUREDPIPE-LANDDRAINAG
Gouge (failure)	03 April 1983	168	4.8	Fracture	30 cust. Line sliced longitudinally by D6 Bogmaster during roadworks
Gouge (failure)	21 October 1983	168	5.6	Fracture	203x152mm hole punched by CAT 977 Traxcavator during drainage work
Gouge (failure)	17 June 1969	457	10.3	Leak	WELDED SLV REPAIR

Table 8.1: Historical Operational Failure Data Used in Comparison with AFFECT

8.1.3 *FFREQ Calculation*

In addition to the calculation of the total expected number of failures on pipelines listed in the UKOPA Pipeline Database by AFFECT, a calculation has also been made using the FFREQ model. FFREQ is considered as the current industry standard for the calculation of pipeline failure frequency and has been used in pipeline QRA since the early 1990s (Corder, 1992; Corder, 1995a). Calculations made using FFREQ are included as a further comparison for the AFFECT model.

8.1.4 *Comparison Results*

The AFFECT failure frequency model has been used to calculate the total expected number of failures on pipelines listed in the UKOPA Pipeline Database based on their operational exposure and the results have been compared with a similar calculation made using FFREQ and the true value from historical operational failure data. In order to present the comparison the failure values have been split into groupings by pipeline diameter and by failure mode, i.e. whether they represent a leak or a rupture. In Table 8.1 the classification "Leak" in the "Extent of Damage" column is assumed to refer to a leak failure whereas the classification "Fracture" is assumed to refer to a rupture[35]. Table 8.2 shows the number of pipelines in each diameter group.

Diameter (mm)	No. of Pipelines	Operational Exposure (km.yr)
0 - 114	219	39239
127 - 273	618	161610
304 - 406	513	131519
457 - 559	363	115165
609 - 711	274	127103
762 - 863	78	37942
914 - 1219	187	172806
All	2252	785350

Table 8.2: Number of Pipelines and Operational Exposure per Diameter Group

Figure 8.1 shows a comparison between the number of leak failures calculated by AFFECT, FFREQ and the true value from historical operational data. The data from Figure 8.1 is presented in Table 8.3.

[35]In the AFFECT model, defects with an axial length longer than the critical length, for the specified operating conditions, are predicted to fail as a rupture. Defects with an axial length shorter or equal to the critical length are predicted to fail as a leak.

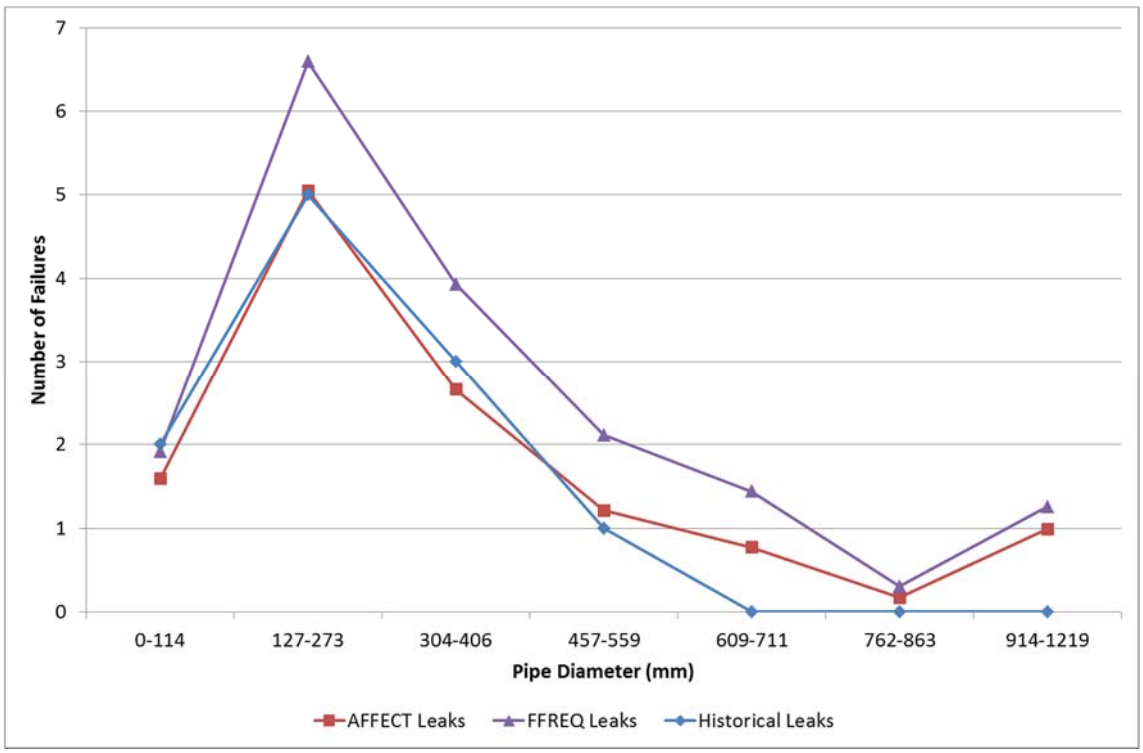

Figure 8.1: Comparison between AFFECT, FFREQ and Historical Operational Data for Leaks

Diameter (mm)	AFFECT Leaks	FFREQ Leaks	Historical Leaks
0 - 114	1.59	1.91	2
127 - 273	5.05	6.59	5
304 - 406	2.66	3.93	3
457 - 559	1.21	2.11	1
609 - 711	0.77	1.44	0
762 - 863	0.17	0.30	0
914 - 1219	0.99	1.26	0
All	12.44	17.55	11

Table 8.3: Number of Leaks from AFFECT, FFREQ and Historical Operational Data

From Figure 8.1, the historical operational data shows that all leak failures occurred on pipelines with diameters less than 609 mm (24”). The most failures occurred in the diameter group 127 to 273 mm (5 to 10”), in which there were five leaks. The overall trend of the historical operational data is a decrease in the number of failures per diameter group with an increase in diameter. This trend is due to the increased wall thickness as pipeline diameter increases, giving better resistance to damage. The smallest diameter group, 0 to 114 mm (0 to 4”) does not follow the trend shown by the other groups and contains only two leak failures. Pipelines in this group are the most susceptible to failure in the event of damage and therefore this group would be expected to show the

largest number of failures. The low number of leak failures in this case is due to the relatively low number of pipelines and operational exposure contained within this group compared with the other smaller diameter groups.

In terms of the calculated data, both failure frequency models are shown to closely follow the general trend of the historical operational data. For leaks the AFFECT model gives more accurate values than FFREQ. If the data is rounded to the nearest failure, which is considered reasonable given that fractional failures cannot occur, then AFFECT predicts the same values as observed in the historical operational data for five of the seven diameter groups. In the remaining two groups AFFECT gives calculated values which are conservative by one failure. Conversely, FFREQ is more conservative than the historical operational data. The values calculated by FFREQ are greater than observed in the historical operational data in five of the seven diameter groups.

It is concluded that, when applied to the UKOPA Pipeline Database, both AFFECT and FFREQ give a good approximation of the number of leak failures in comparison to historical operational data. Both models are conservative, however the AFFECT model produced the most accurate results.

Figure 8.2 shows a comparison between the number of rupture failures calculated by AFFECT, FFREQ and the true value from historical operational data. The data from Figure 8.2 is presented in Table 8.4.

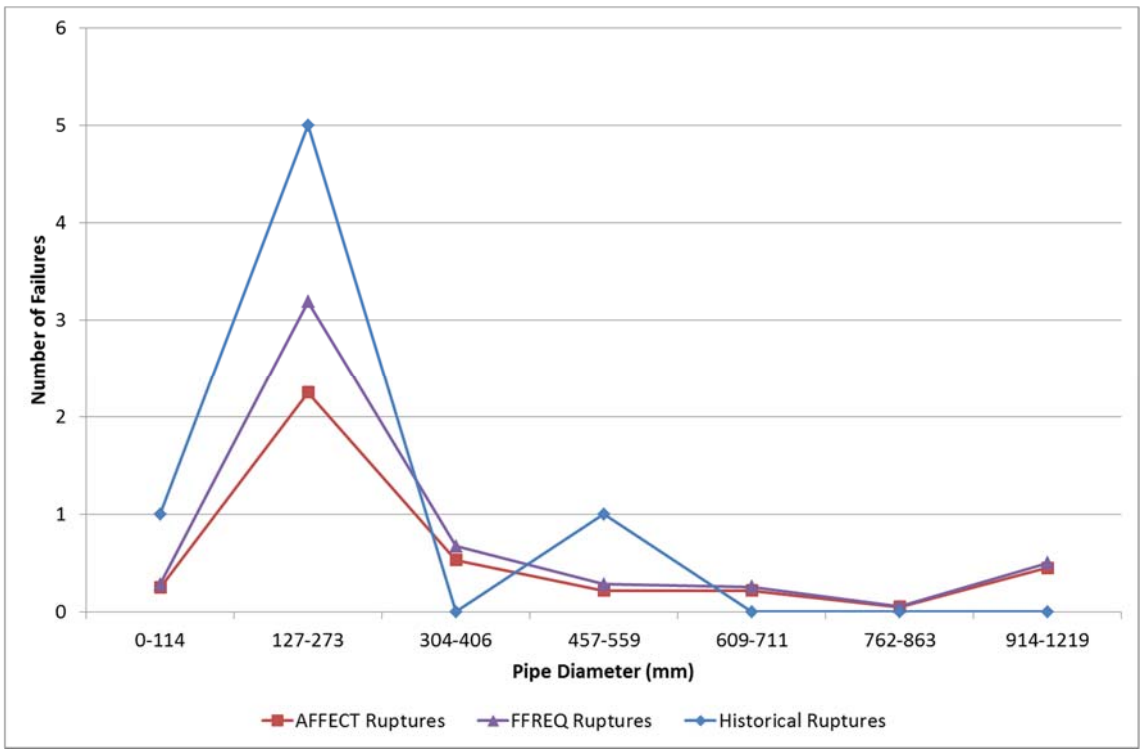

Figure 8.2: Comparison between AFFECT, FFREQ and Historical Operational Data for Ruptures

Diameter (mm)	AFFECT Ruptures	FFREQ Ruptures	Historical Ruptures
0 - 114	0.25	0.28	1
127 - 273	2.25	3.19	5
304 - 406	0.53	0.67	0
457 - 559	0.22	0.28	1
609 - 711	0.22	0.26	0
762 - 863	0.05	0.05	0
914 - 1219	0.45	0.50	0
All	3.97	5.23	7

Table 8.4: Number of Ruptures from AFFECT, FFREQ and Historical Operational Data

From a risk assessment point of view, ruptures are the most important of the two failure modes. A rupture is significantly worse than a leak in terms of the consequences. In a similar way to leaks Figure 8.2 shows a decrease in the number of failures with increasing diameter; all rupture failures occurred on pipelines with diameters less than 609 mm (24”). However, the majority of the data is contained within one diameter group, 127 to 273 mm (5 to 10”), and the drop off with increasing diameter is more abrupt than in the leak case. This can be explained by noting that an increase in diameter and wall thickness not only increases a pipeline’s resistance to failure, but also increases the margin

between defects which fail as a leak and those which fail as a rupture[36]. i.e. there is an additional factor of protection against ruptures in comparison with leaks. The low number of failures in the 0 to 114 mm (0 to 4") diameter group can again be explained by the relatively low number of pipelines and low operational exposure within this group.

In terms of the calculated data, both failure frequency models match the overall trend in the historical operational data, however neither model displays the same level of accuracy in predicted values as was observed for the leak case. For diameter groups in which ruptures were recorded, both AFFECT and FFREQ give non-conservative values.

It should be noted however that determining which historical operational rupture data would be suitable for a comparison to failure frequency model calculations is difficult. Both failure frequency models define rupture in terms of the failure of severe part-wall damage or punctures to the pipeline. The models do not address severed or broken pipe type failures, which are also defined as a form of pipeline rupture. The failure data contained within Table 8.1 is conservatively considered to be appropriate for comparison to the failure frequency models. However, it is noted that five of the total seven pipeline ruptures in the table include words in the "Comment" field such as "severed", "sliced", "sheared" and "fractured" which could suggest that a severed or broken pipe was the source of the rupture in these cases. If this data was removed from the comparison then the number of pipeline ruptures would be reduced to two residing in the 127 to 273 mm diameter group. In this case the calculations of the failure frequency models would be more in line with the historical operational data.

It should also be noted however, that this argument should only serve to highlight the difficulty of making a comparison between historical operational rupture data and failure frequency model calculations, rather than to imply the accuracy of AFFECT. If the data was removed from the comparison then the

[36] Considering the effect of increased diameter and wall thickness on the critical length, which determines the leak / rupture behaviour of severe part-wall defects or punctures. Intuitively, a similar pattern would be expected between leaks and severed / broken pipe type ruptures.

probability distributions used in the AFFECT model would need to be refitted and AFFECT would produce different calculated values. All of the rupture data has been included in the development of the model and therefore also included in the comparison.

The decision to include all of the rupture data in the development of AFFECT was made because of the uncertain nature of the UKOPA Fault Database. Despite the presence of the terms noted above for five of the seven pipeline ruptures, the limited information available for each damage record in the database makes it difficult to ascertain the exact nature of each failure. Unlike failures caused by drilling operations in-error, which are more readily identified by the “Comment” field and thus can justifiably be removed, the descriptors used for rupture are more open to subjective interpretation. The data was retained for the purposes of the model development as the evidence for its removal was considered to be insufficient.

The fact that the results from this study do not match up to the historical operational rupture data suggests that this interpretation may be incorrect and that the data should be removed and used in the development of a separate failure model or historical data component to address severed or broken pipes. An additional component to the model such as this may be necessary in order to provide a complete description of failure frequency due to third party external interference.

It is concluded that, when applied to the UKOPA Pipeline Database, both AFFECT and FFREQ agree with the overall trend of historical operational rupture data. Both models are non-conservative, however an accurate comparison with rupture failures is difficult, due to the uncertain nature of the historical operational data.

8.2 Wall Thickness Sensitivity Study

A sensitivity study has been performed in order to determine the variation in pipeline failure frequency calculated using the AFFECT model, with pipeline wall thickness.

For the sensitivity study, the pipeline diameter, material grade (yield strength) and 2/3 Charpy v-notch impact energy have been set to fixed values, whilst the wall thickness is varied. Details of the fixed pipeline parameters are provided in Table 8.5.

Parameter	Value
External Diameter (mm)	610
Material Grade	L450
SMYS (Nmm^{-2})	450
SMUTS (Nmm^{-2})	535
2/3 Charpy V–Notch Impact Energy (J)	167[37]

Table 8.5: Fixed Pipeline Parameters for Sensitivity Studies

The study has been performed for three different design factors, 0.72, 0.5 and 0.3, representing the defined operational limits for the area classes in the Institution of Gas Engineers and Managers (IGEM) standard for steel natural gas pipelines, IGEM/TD/1 (Anon., 2009). Pipeline design factor is related to the other operational parameters using Barlow's formula:

$$\sigma_H = \sigma_Y . df = \frac{PD}{20t} \qquad (8.1)$$

Where σ_H is the hoop stress in the pipe wall (in Nmm^{-2}), σ_Y is the yield stress (in Nmm^{-2}), df is the design factor, P is the internal operating pressure (in barg), D is the external diameter of the pipeline (in mm) and t is the wall thickness (in mm). In the study, in order to counteract the effect of wall thickness variation on the design factor, the pipeline operating pressure has been varied in accordance with equation (8.1).

[37] The equivalent full size Charpy v-notch impact energy is 250 J.

For the wall thickness sensitivity study the depth of cover and S-type area factors have not been applied to AFFECT. The results therefore apply to pipelines located in R-type areas with the average depth of cover for a UK pipeline.

Figure 8.3 shows the variation in failure frequency, as calculated by AFFECT, with wall thickness, for a pipeline with the fixed parameters from Table 8.5, operating at a design factor of 0.72. The results are presented for both the rupture and total failure frequency.

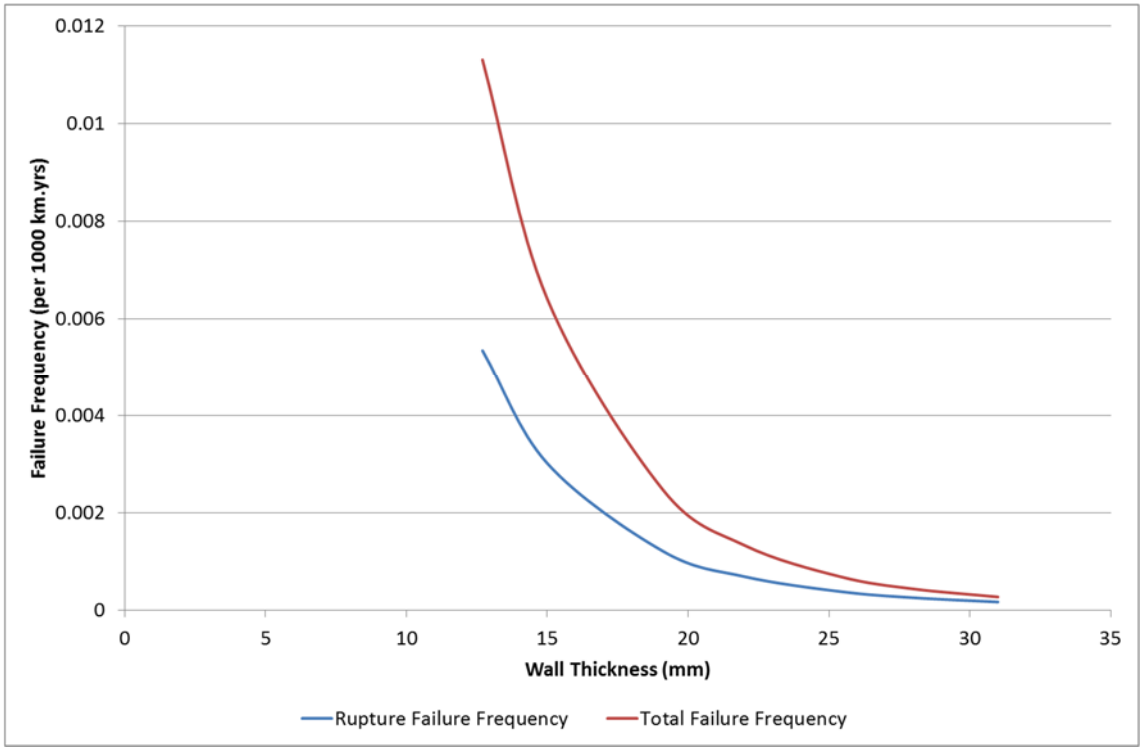

Figure 8.3: Variation in Failure Frequency with Wall Thickness for 0.72 Design Factor

Figure 8.4 shows the variation in failure frequency, as calculated by AFFECT, with wall thickness, for a pipeline with the fixed parameters from Table 8.5, operating at a design factor of 0.5. The results are presented for both the rupture and total failure frequency.

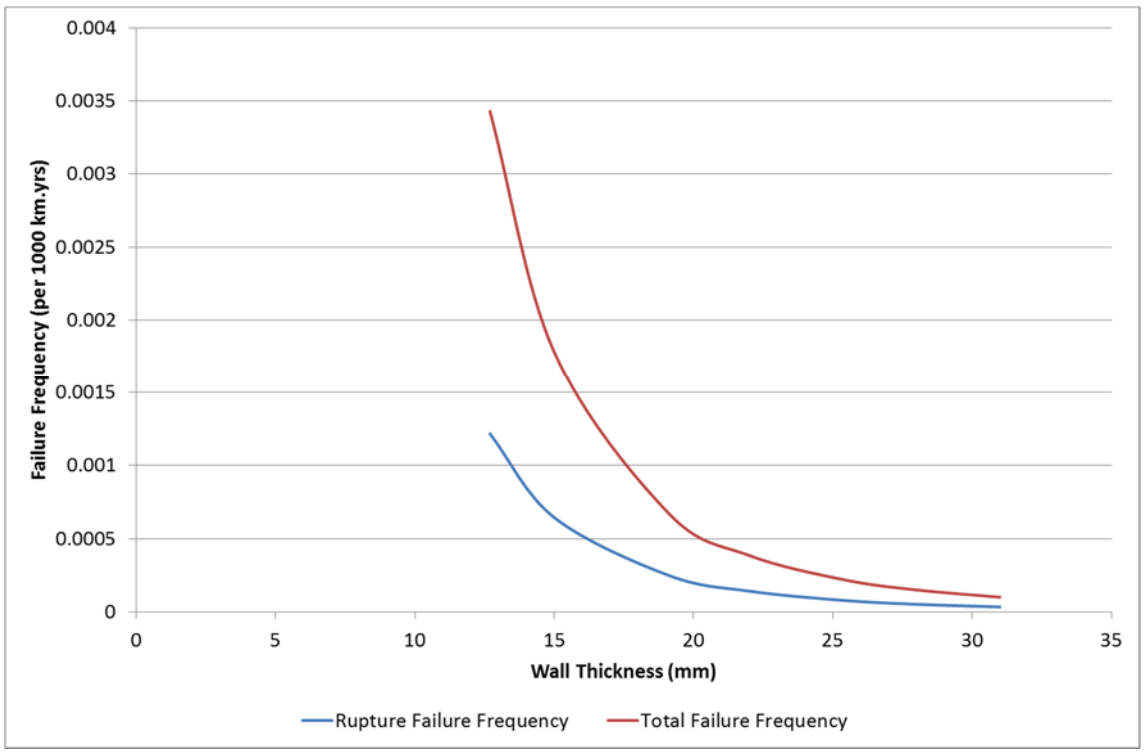

Figure 8.4: Variation in Failure Frequency with Wall Thickness for 0.5 Design Factor

Figure 8.5 shows the variation in failure frequency, as calculated by AFFECT, with wall thickness, for a pipeline with the fixed parameters from Table 8.5, operating at a design factor of 0.3. The results are presented for both the rupture and total failure frequency.

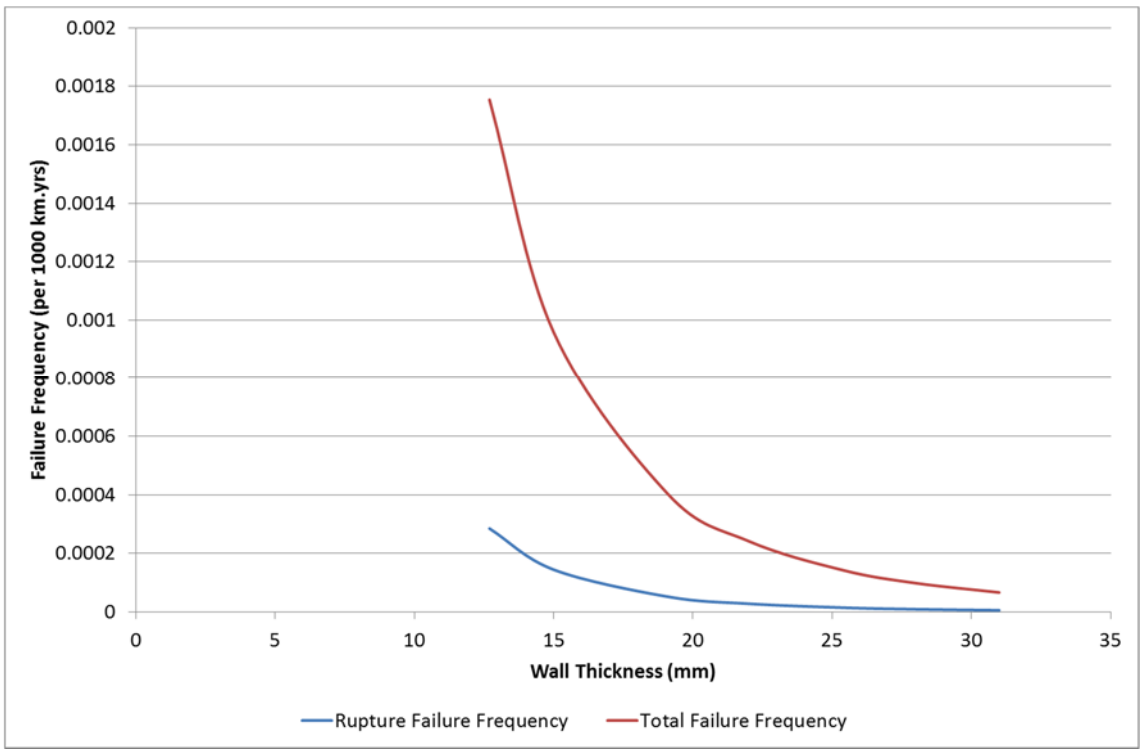

Figure 8.5: Variation in Failure Frequency with Wall Thickness for 0.3 Design Factor

Figure 8.3, Figure 8.4 and Figure 8.5 show that pipeline failure frequency is strongly dependent on wall thickness. An increase in wall thickness results in a decrease in failure frequency. The same trend is seen for both rupture and total failure frequencies and at each design factor considered. The reason for this trend is that severe part-wall defects and through-wall punctures are less likely to occur in thick pipelines than thin ones, assuming the machinery and tools used by third parties in the vicinity of pipelines remain constant. The critical defect depth for part-wall failure increases with wall thickness and deeper defects are less common. For each design factor considered, both the rupture and the total failure frequency fall by approximately 1.5 orders of magnitude when the wall thickness is increased from 12.7 mm to 31 mm. The decrease in failure frequency with wall thickness is non-linear, meaning the relative benefit on failure frequency value decreases as the wall thickness increases, in addition to the absolute value.

8.3 Design Factor Sensitivity Study

A sensitivity study has been performed in order to determine the variation in pipeline failure frequency calculated using the AFFECT model, with pipeline design factor.

For the sensitivity study, the pipeline diameter, material grade (yield strength) and 2/3 Charpy v-notch impact energy have been set to fixed values, whilst the design factor is varied. Details of the fixed pipeline parameters are provided in Table 8.5.

The study has been performed for two different wall thicknesses, 12.7 mm and 19.1 mm. In the study, in order to allow a constant wall thickness to be used while design factor is varied, the pipeline operating pressure has been varied in accordance with equation (8.1).

For the design factor sensitivity study the depth of cover and S-type area factors have not been applied to AFFECT. The results therefore apply to pipelines located in R-type areas with the average depth of cover for a UK pipeline.

Figure 8.6 shows the variation in failure frequency, as calculated by AFFECT, with design factor, for a pipeline with the fixed parameters from Table 8.5, and a wall thickness of 19.1 mm. The results are presented for both the rupture and total failure frequency.

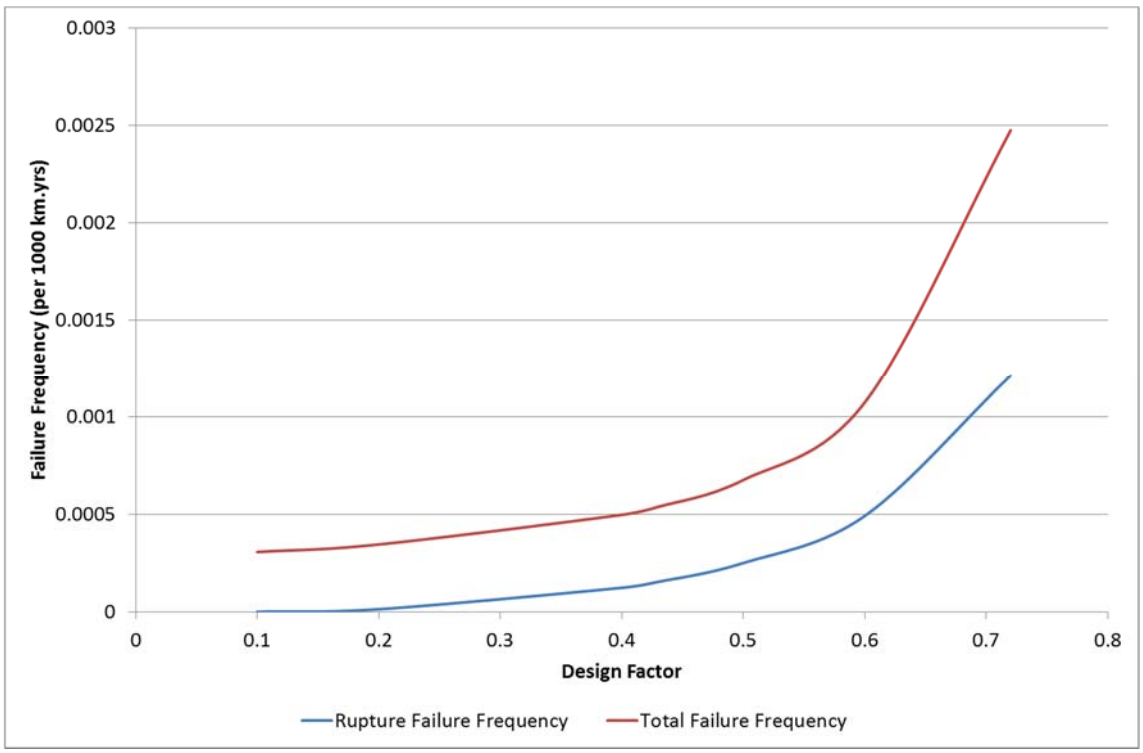

Figure 8.6: Variation in Failure Frequency with Design Factor for 19.1 mm Wall Thickness

Figure 8.7 shows the variation in failure frequency, as calculated by AFFECT, with design factor, for a pipeline with the fixed parameters from Table 8.5, and a wall thickness of 12.7 mm. The results are presented for both the rupture and total failure frequency.

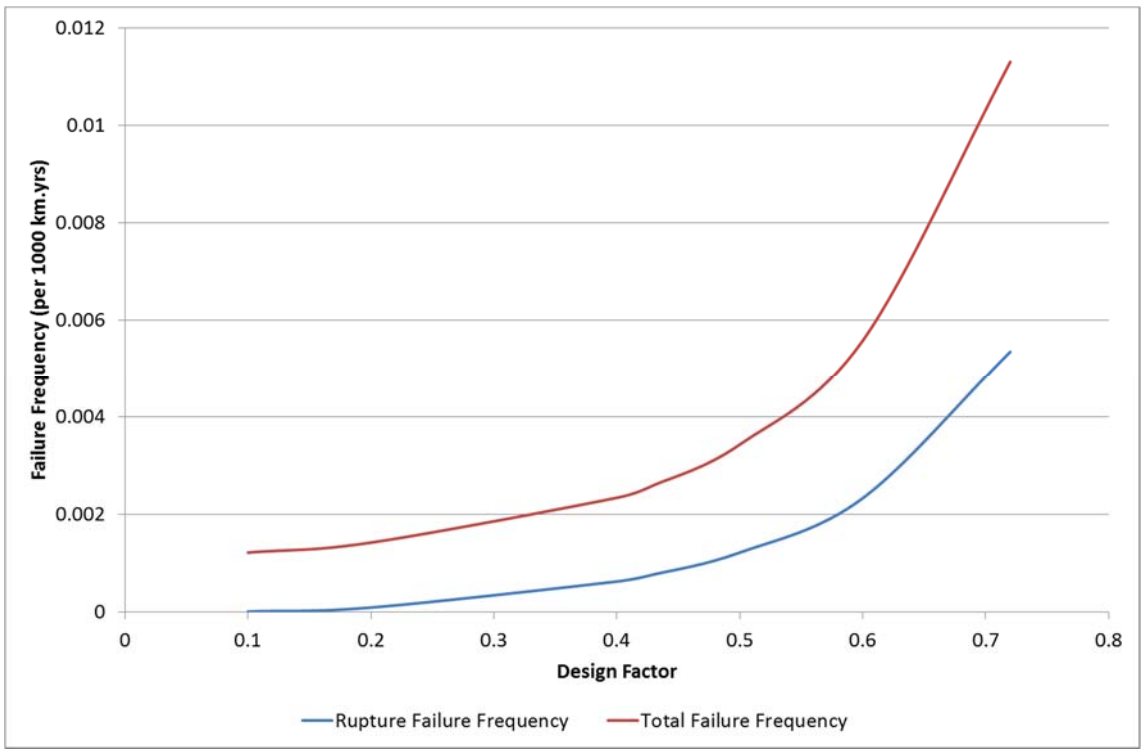

Figure 8.7: Variation in Failure Frequency with Design Factor for 12.7 mm Wall Thickness

Figure 8.6 and Figure 8.7 show that pipeline failure frequency is strongly dependent on design factor. An increase in design factor results in an increase in failure frequency. The same trend is seen for both rupture and total failure frequencies and at each wall thickness considered. The reason for this trend is that a pipeline operating at a higher design factor is under higher stress than a pipeline at lower design factor. Severe part-wall defects are more likely to occur in high stress pipelines than low stress ones, assuming the machinery and tools used by third parties in the vicinity of pipelines remain constant. The critical defect depth for part-wall failure decreases with increasing stress and smaller defects are more common. For each wall thickness considered, the rupture failure frequency increases by approximately three orders of magnitude as the design factor is increased from 0.1 to 0.72; and the total failure frequency increases by approximately one order of magnitude. The increase in failure frequency with design factor is non-linear, meaning the relative detriment to the failure frequency value increases as the design factor is increased, in addition to the absolute value.

8.4 Leak / Rupture Example Calculation

In this section an example calculation has been performed in order to demonstrate how pipeline failure mode can vary with wall thickness. The example considers a 610 mm external diameter dense phase CO_2 pipeline, constructed from L450 grade steel and operating at a pressure of 135 barg. A comparison has been made between the operating stress of the pipeline at different wall thicknesses; and its proximity to the leak / rupture boundary for a hypothetical 508 mm (20”) long defect, calculated using the AFFECT model.

For this example, the pipeline diameter, material grade (yield strength) and operating pressure have been set to fixed values, whilst the wall thickness is varied. In accordance with equation (8.1) this will result in a variation of the pipeline operating stress. Details of the fixed pipeline parameters are provided in Table 8.6.

Parameter	Value
External Diameter (mm)	610
Material Grade	L450
SMYS (Nmm^{-2})	450
SMUTS (Nmm^{-2})	535
Operating Pressure (barg)	135

Table 8.6: Fixed Pipeline Parameters for Leak/Rupture Example

The leak / rupture boundary for a 508 mm (20”) long defect in the pipeline has been calculated using the AFFECT model at each wall thickness considered. A 508 mm defect has been chosen as an example of a long defect which could be introduced by third party external interference. In the UKOPA Fault Database approximately 90% of third party external interference defects are shorter than 508 mm (Chapter 6).

In the AFFECT model the leak / rupture boundary is defined by the flow stress dependent through-wall NG-18 equation (equation (3.2)):

$$\sigma_H = M^{-1}\overline{\sigma}$$

Where the flow stress, $\overline{\sigma}$, is defined using equation (3.10):

$$\overline{\sigma} = 1.15\sigma_Y$$

And the Folias factor, M, is given by equation (2.35):

$$M = \sqrt{1 + 0.26\left(\frac{2c}{\sqrt{Rt}}\right)^2}$$

A hoop stress greater than the right hand side of equation (3.2) will cause the defect to fail as a rupture; if the hoop stress is less than the right hand side of equation (3.2) then the defect will fail as a leak.

Figure 8.8 shows the comparison between the operating stress of the pipeline and its proximity to the leak / rupture boundary at different wall thicknesses. The operating stress and leak / rupture boundary are presented in terms of the pipeline design factor. The leak / rupture boundary can be written in terms of the design factor using equation (8.1):

$$df = \frac{M^{-1}\overline{\sigma}}{\sigma_Y} \qquad (8.2)$$

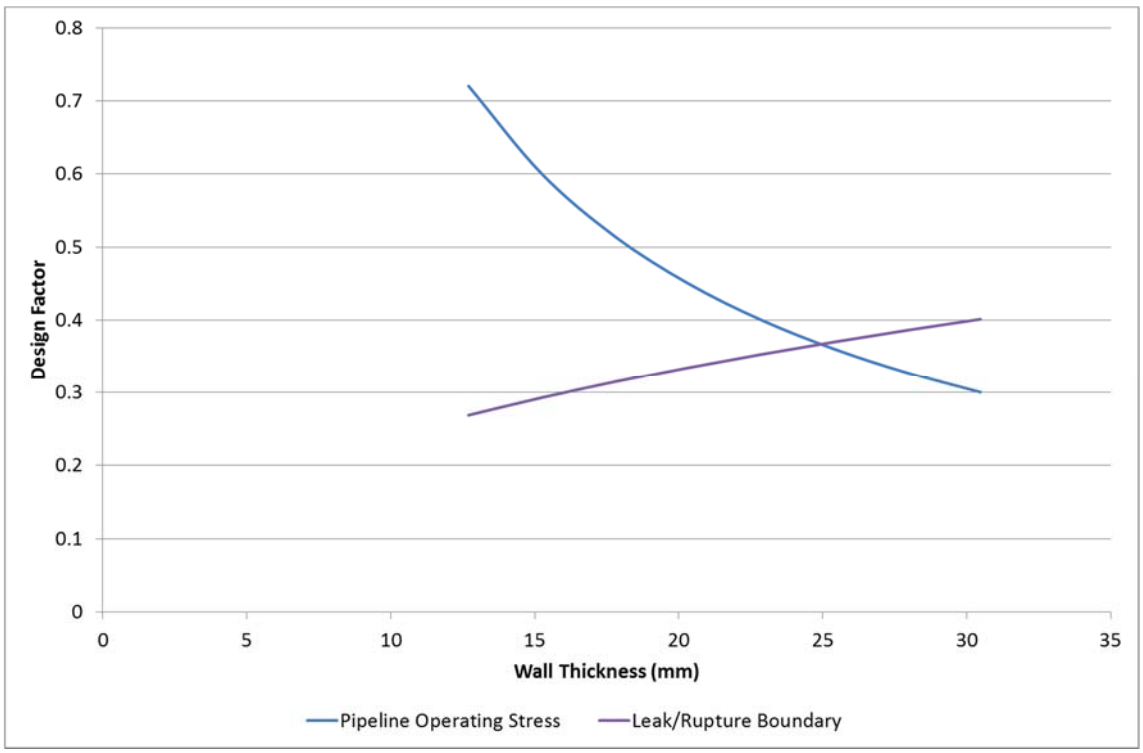

Figure 8.8: Operating Stress and Leak / Rupture Boundary Comparison for 610 mm External Diameter, L450 Grade, 135 barg Pipeline with a 508 mm Long Defect

Figure 8.8 shows that the operating stress (design factor) of the pipeline decreases as wall thickness is increased. The purple line represents the leak / rupture boundary of the 508 mm long defect. If the defect was to fail with the pipeline operating in the region above the boundary, the failure would occur as a rupture; if the defect was to fail with the pipeline operating in the region below the boundary, the failure would occur as a leak. The operating stress of the pipeline crosses the leak / rupture boundary at a wall thickness of approximately 25 mm. As noted in section 8.1.4, a rupture is significantly worse than a leak in terms of the consequences. A leak failure is preferable to a rupture. In this example a wall thickness of at least 25 mm would ensure that all severe third party external interference defects and punctures up to a length of 508 mm would fail only as leaks. This would correspond to the pipeline operating at a maximum design factor of 0.37. It should be noted that as the wall thickness of the pipeline is increased, the chances of a through-wall puncture are reduced; and a severe part-wall defect would be less likely to occur as the critical defect depth for failure would increase and deeper defects are less common.

8.5 Trends of the AFFECT Failure Frequency Model Conclusions

This chapter has considered an analysis of the trends observed when the AFFECT model is applied to different pipeline scenarios. Validation of the model has also been provided through a comparison between model predictions, historical operational data and the current industry standard failure frequency model FFREQ.

When applied to the UKOPA Pipeline Database, it is concluded that both AFFECT and FFREQ give a good approximation of the number of leak failures in comparison to historical operational data. Both models are conservative, however the AFFECT model produced the most accurate results of the two. In terms of ruptures, both AFFECT and FFREQ agree with the overall trend of historical operational data. Both models are non-conservative, however an accurate comparison with rupture failures is difficult, due to the uncertain nature of the historical operational data.

An analysis of failure frequency trends with wall thickness indicated that both rupture and total failure frequency calculated by AFFECT are strongly dependent on wall thickness. An increase in wall thickness results in a decrease in failure frequency.

Similarly an analysis of failure frequency trends with design factor indicated that both rupture and total failure frequency calculated by AFFECT are strongly dependent on design factor. An increase in design factor results in an increase in failure frequency.

It is recommended that further work is performed regarding the inclusion of historical operational rupture data in the development of AFFECT. The development of a separate failure model or historical data component to address severed and broken pipes may be necessary in order to provide a complete description of failure frequency due to third party external interference.

Chapter 9. A Shelter Model for Consequence Predictions Following A CO_2 Pipeline Release

The background and development of the AFFECT model detailed in Chapter 2 to Chapter 8 is concerned with the likelihood of failure side of a QRA for a dense phase CO_2 pipeline; the aim being to reduce the probability of occurrence of a catastrophic pipeline failure. The other side of the QRA procedure is the assessment of the potential consequences to any surrounding population in the event of such a failure. In Chapter 9 and Chapter 10 elements of the consequences of failure side are considered through an investigation into shelter and escape in the event of a rupture of a dense phase CO_2 pipeline.

A rupture to a pipeline carrying dense phase CO_2 could have dramatic consequences for people located in the vicinity of the release. CO_2 is both toxic and acts as an asphyxiant in high concentrations. Due to the high density of CO_2 in comparison to air, a CO_2 cloud emitted during a pipeline rupture could remain at ground level, therefore increasing the probability that people could be affected by such concentrations.

It is assumed that in the event of a pipeline rupture, people outdoors in the vicinity will attempt to run from the CO_2 cloud to safety. It is also reasonable to assume that nearby buildings could offer some form of shelter against the harmful effects of CO_2. As the CO_2 enters the building through open windows, doors or via the adventitious openings characteristic of all buildings, the concentration of CO_2 within a building engulfed in a CO_2 cloud is a matter of importance. For example, if the release was constant and continuous, eventually the concentration inside could increase to match that of the external atmosphere. However it is considered that the time required for this process to occur could provide those taking shelter in the building with additional time before a harmful concentration is reached, increasing the chance of help arriving. In the case of a decaying release, it may be that the maximum concentration experienced indoors would be limited due to the effects of the decaying nature of the release and the closing of valves.

To investigate the level of shelter that buildings can provide; and the potential for escape on foot, in the event of a rupture of a dense phase CO_2 pipeline, two models have been developed:

- An indoor “shelter” model considering the ingress of CO_2 into a building surrounded by an environment with a high CO_2 concentration.
- An outdoor “escape” model considering escape on foot from a moving cloud of CO_2.

The effect of CO_2 exposure on humans is quantified in the form of a time-accumulated dose which is calculated within both models. The development of the shelter model is described in Chapter 9 and the escape model is described in Chapter 10. In each chapter results are presented which have been produced using the models for a number of simulated releases of dense phase CO_2 from a pipeline.

A number of factors are considered between the two models. These include atmospheric conditions; the distance to the source of the CO_2 release; the size of the air flow pathways into/out of the building; and the conditions of the pipeline failure. In terms of the escape model, starting position and direction of travel are also considered.

Input data for the models has been provided by DNV-GL. The data was generated by simulating pipeline failure events using DNV-GL’s own custom built flat terrain computer model (Cleaver, 2014e). Input data produced using the Phast model (Anon., 2011b) has also been provided by HSL. In addition, the shelter model has been verified using experimental data from the Spadeadam test site. All of the input data has been produced from release and dispersion studies performed as part of the wider COOLTRANS research programme.

9.1 Shelter Model Background and Development

The shelter model considers the ingress of CO_2 into a single building and the subsequent effect this has on the building occupants. The model is based on the principles of natural building ventilation which are explained by Etheridge and Sandberg (Etheridge, 1996) and form the basis for the simple ventilation equations in British Standard BS 5925 (Anon., 1995).

In the model it is assumed that initially the concentration of CO_2 in the building is the low background level in the atmosphere. It is assumed that the pipeline release occurs and that, as a result, the building is subject to a cloud of CO_2 that drifts past the building. The concentration of CO_2 in the external atmosphere is transient and will change with time as the CO_2 cloud released from the pipeline disperses. Similarly, the concentration of CO_2 within the building will change as CO_2 is drawn in from the concentrations outside through the process of natural ventilation. The change in the internal concentration of CO_2 is modelled over the course of the rupture event.

For the purposes of the model a building is represented as a three dimensional rectangular structure of specified length, width and height (l_b, w_b, h_b), located at a fixed distance from a pipeline rupture. Openings in the building envelope between the indoor and the outdoor environment are used to represent the doors, windows and adventitious openings found in real buildings. The building is assumed to have no internal partitions, an assumption which is considered to be conservative and the concentration within the interior is assumed to be uniform.

Air flow between the internal and external atmospheres in the building occurs due to a pressure difference across the openings in the building envelope. Air will flow from a region of higher pressure to a region of lower pressure. The pressure difference can arise as result of wind effects externally and/or buoyancy effects internally. An example of ventilation air flow incorporating both of these effects is shown in Figure 9.1.

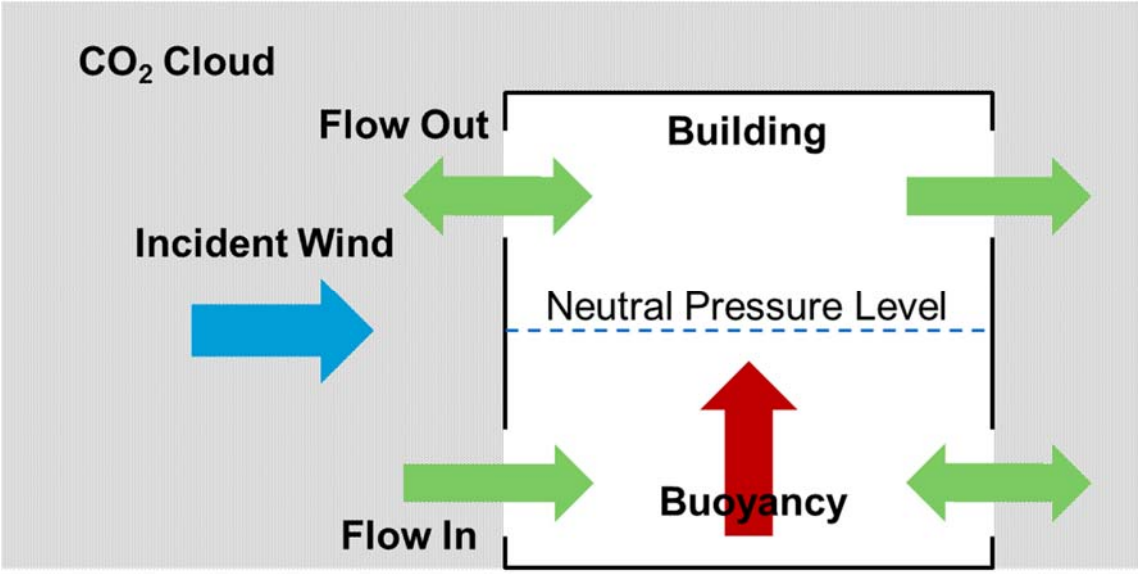

Figure 9.1: Air Flow through Openings due to Pressure Difference (Side View)

9.1.1 *Wind Pressure*

The dynamic pressure (in Pa) due to the (free stream) wind flow is given by (Etheridge, 1984; Etheridge, 1996):

$$P_{wind} = \frac{1}{2}\rho_{air}U_{wind}^2 \qquad (9.1)$$

Where ρ_{air} is the density of the outside air (in kgm^{-3}) and U_{wind} is the wind speed (in ms^{-1}).

Wind blowing against the surfaces of a building will cause an increase in the air pressure at those surfaces and any openings on those surfaces. Conversely, the surfaces and openings of the building sheltered from the wind will experience a decrease in air pressure. In order to determine the change in air pressure due to the effect of the wind on a particular building surface, equation (9.1) is multiplied by a surface pressure coefficient, C_p. The value of C_p depends upon the angle at which the wind impacts the surface in question.

9.1.2 *Buoyancy Pressure*

Pressure differences due to buoyancy arise as a result of a difference in temperature between the internal and external environments. Due to the principle of hydrostatics, atmospheric air pressure decreases with increasing altitude (Etheridge, 1984; Etheridge, 1996). The pressure change (in Pa) from the bottom to the top of a building can be represented using the following equation:

$$P_{atmos} = P_{reference} + \rho_{reference} g_a z_h \quad (9.2)$$

Where $P_{reference}$ is the atmospheric pressure at the top of the building (in Pa), $\rho_{reference}$ is the density of the air at the top of the building[38] (in kgm^{-3}), g_a is the acceleration due to gravity (9.81 ms^{-2}) and z_h is the height above ground level at any point subtracted from the height of the building (in m).

The density of the air in equation (9.2) can be approximated using the ideal gas equation:

$$\rho_{reference} = \frac{P_{reference}}{R_I T} \quad (9.3)$$

Where R_I the ideal gas constant (8.31 Jmol^{-1}K^{-1}) and T the air temperature (in K).

If the building is not air-tight and the internal atmosphere is at the same temperature as the external atmosphere then the internal and external pressure will be the same (assuming there is no wind) and will display an identical variation with height.

An increased internal air temperature however, results in a reduction in the internal air density, from equation (9.3). Because of the principle of hydrostatics,

[38] Note that equation (9.2) assumes that the change in air density with height is negligible. This is a reasonable approximation when considering values of height of the order of the height of a building.

the less dense air within the building will rise resulting in an increased number of air molecules at the top of the building and a decreased number at the bottom. The internal air pressure is therefore increased from its initial value at the top of the building and decreased from its initial value at the bottom of the building. The resultant outcome is one of a steeper pressure gradient within the building than that outside, given by equation (9.2). At some point within the building above ground level there will exist a plane in which the internal pressure equals the external pressure, this is the neutral pressure level shown in Figure 9.1 and its position depends on the magnitude of the temperature difference between the internal and external atmospheres. Air will flow from high pressure to low pressure, therefore any openings in the envelope of the building below the neutral pressure level will draw air in from the outside and any openings above the neutral pressure level will push air outside. This sets up a flow of air within the building from the floor to the ceiling.

9.1.3 *Pressure Differences and Building Air Flow*

Within the shelter model, pressure differences across the openings in the envelope of the building are calculated by combining the effects of wind and buoyancy.

Taking into account wind and hydrostatic effects, an expression for the external air pressure (in Pa) on a particular building face, at some value of z_h, can be written as:

$$P_{external}(z_h) = P_{reference} + \frac{1}{2}\rho_{external}U_{wind}^2 C_p + \rho_{external} g_a z_h \qquad (9.4)$$

Similarly, the corresponding expression for the internal air pressure (in Pa) on the same face at the same value of z_h can be written as:

$$P_{internal}(z_h) = P_{reference} + P' + \rho_{internal} g_a z_h \qquad (9.5)$$

For some value of P' (in Pa), as yet undefined, that is determined by the location of the neutral pressure level and volume conservation. From equations

(9.4) and (9.5), the difference in pressure (in Pa) across an opening in the envelope of the building at z_h is given by:

$$\Delta P(z_h) = \frac{1}{2}\rho_{external} U_{wind}^2 C_p - P' + g_a z_h(\rho_{external} - \rho_{internal}) \quad (9.6)$$

As explained in section 9.1, a pressure difference between the internal and external environments causes air flow through openings in the building envelope. The magnitude of the air flow (in m^2s^{-1}) across an opening at z_h can be calculated using (Etheridge, 1984; Etheridge, 1996):

$$Q(z_h) = C_d W_o(z_h)\sqrt{\frac{2|\Delta P|}{\rho_{air}}} \quad (9.7)$$

Where C_d is the coefficient of discharge for the particular type of opening under consideration, $W_o(z_h)$ is the width of the opening (in m) at z_h and ρ_{air} is the internal or external air density (in kgm^{-3}).

By imposing a boundary condition for the conservation of volume, i.e. all air flow into the building must equal all air flow out of the building; the unknown pressure P' in equations (9.5) and (9.6) can be calculated and the air flow (in m^3s^{-1}) for the building solved:

$$\int_{h_b}^{z_0} Q_{in}\, dz_h = \int_{z_0}^{0} Q_{out} dz_h \quad (9.8)$$

Where h_b is the height of the building (in m) and z_0 (in m) is the value of z_h corresponding to the neutral pressure level from Figure 9.1 at which it is known that:

$$P_{internal}(z_0) = P_{external}(z_0) \quad (9.9)$$

9.1.4 *Shelter Model Example Flow Rates*

For illustrative purposes, Figure 9.2 shows an example of how the ventilation flow rate for a building changes with an increasing wind speed, as calculated by the shelter model.

In this particular example the flow rate is shown for constant temperature differences between the internal and external environment of 10, 20 and 30 degrees Celsius[39] as the wind speed changes from 0 ms^{-1} to 7 ms^{-1}. For the purposes of this example the external and internal CO_2 concentrations are equal to zero. Figure 9.2 presents the ventilation rate in terms of the number of air changes in the building per hour (AC/hr). This is a standard unit used in building ventilation studies (Anon., 1995) and is calculated by dividing the volume flow rate per hour by the total building volume.

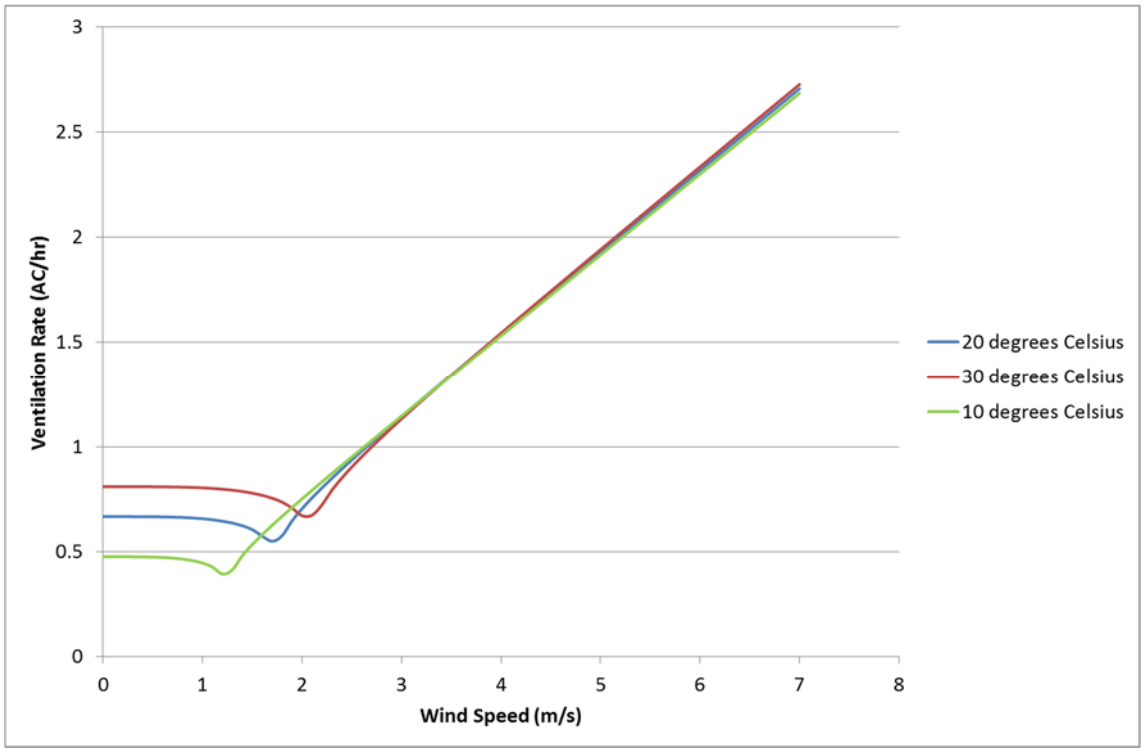

Figure 9.2: Example of Ventilation Rate with Increasing Wind Speed

[39] The choice of temperature differences for Figure 9.2 is arbitrary as the purpose is simply to illustrate the transition between buoyancy driven and wind driven ventilation as the wind speed increases. The values chosen however are within the range of typical values expected for a building located in the UK.

Figure 9.2 shows the relative strengths of wind driven and buoyancy driven ventilation and how these can change depending on the conditions. At low wind speeds (<1 ms^{-1}) the chart shows that the ventilation rate is independent of the wind speed. In this region pressure differences arising due to the wind are negligible and the flow rate is driven by buoyancy arising from the temperature differences between the internal and external environments; a larger temperature difference produces a higher ventilation rate. As the wind speed is gradually increased the wind pressure gains more influence. In the region between 1 ms^{-1} and 2 ms^{-1} wind driven and buoyancy driven effects are of a similar magnitude and compete against each other in terms of the total air flow rate into and out of the building. This is shown by the slight dip in ventilation rate for each example. As the wind speed increases further the wind pressure becomes the dominant cause of pressure difference. The lines on the chart converge with each other beyond approximately 3 ms^{-1} showing that at wind speeds beyond this, the flow rate is driven by wind pressure only and buoyancy effects have become negligible.

9.1.5 *CO_2 Concentration*

In equations (9.4) to (9.8) the flow rate of air into and out of a building is dependent on both the external and internal density of air. In the shelter model, the building is surrounded by a cloud of CO_2 from a ruptured dense phase CO_2 pipeline resulting in a high external concentration of CO_2 in the air. The external concentration of CO_2 will change over time as the rupture event evolves. Furthermore the internal concentration of CO_2 will change with time as more CO_2 is drawn in from outside. An increased presence of CO_2 compared to normal air will affect the air density. The internal and external air densities (in kgm^{-3}) at any one time can be calculated by assuming an air/CO_2 mixture which behaves as an ideal gas:

$$\rho_{external} = \frac{P_{external}}{R_I}\left[\frac{c_{external}m_{CO_2}}{T_{external}} + \frac{(1-c_{external})m_{air}}{T_{external}}\right] \quad (9.10)$$

$$\rho_{internal} = \frac{P_{internal}}{R_I}\left[\frac{c_{internal}m_{CO_2}}{T_{internal}} + \frac{(1-c_{internal})m_{air}}{T_{internal}}\right] \quad (9.11)$$

Where $P_{external}$ and $P_{internal}$ are the external and internal pressures (in Pa) respectively; R_I is the ideal gas constant (in $Jmol^{-1}K^{-1}$); $T_{external}$ and $T_{internal}$ are the external and internal temperatures (in K); $c_{external}$ and $c_{internal}$ are the internal and external volume concentrations of CO_2; and m_{CO2} and m_{air} are the molar masses of CO_2 and air (in $kgmol^{-1}$). For the purposes of the model the internal and external pressures in equations (9.10) and (9.11) are assumed to be the same and equal to $P_{reference}$ in equations (9.4) and (9.5). For cases of interest, associated with relatively higher external concentrations of CO_2, this makes only a small difference to the calculated value of the density compared to the changes resulting from concentration variations and so is ignored.

In the shelter model equation (9.8) is solved in order to determine the rate of air flow by ventilation into and out of the building at any instant in time. The air/CO_2 mixture from the outside drawn into the building is assumed to mix perfectly with the internal air/CO_2 causing the internal concentration of CO_2 to change. The internal concentration of CO_2 is calculated using the following method (Harris, 1989):

The volume of CO_2 flowing in to the building (in m^3) in a time period dt (in s) is:

$$\Delta V_{CO_2\,in} = Q_{in} c_{external} dt \tag{9.12}$$

And the volume of CO_2 flowing out of the building (in m^3) over dt is:

$$\Delta V_{CO_2\,out} = Q_{out} c_{internal} dt \tag{9.13}$$

Therefore the total change in internal CO_2 concentration over dt is:

$$dc_{internal}(dt) = \frac{\left(\Delta V_{CO_2\,in} - \Delta V_{CO_2\,out}\right)}{V_{building}} \tag{9.14}$$

Where $V_{building}$ is the total volume of the building (in m^3). The total internal concentration at a time $t + dt$ will therefore be:

$$c_{internal}(t + dt) = c_{internal}(t) + dc_{internal}(dt) \tag{9.15}$$

9.1.6 *Temperature Change*

Section 9.1.2 outlined the importance of internal and external temperature difference in establishing a ventilation flow rate due to buoyancy. CO_2 vapour from a dense phase pipeline rupture can be released into the atmosphere at temperatures of approximately -80 degrees Celsius due to the Joule-Thomson effect. A low vapour temperature such as this can change the temperature of the external environment surrounding the building and therefore affect its density and the ventilation flow rate. Furthermore, as external air is drawn into the building as the event progresses the temperature of the internal environment will also be affected. These considerations are taken into account in the model by considering energy conservation. The energy equation is approximated to equation (9.16), which is derived assuming that heat changes from inside to outside are not significant and that any inflow caused by temperature changes in the interior can be neglected.

$$M_{internal}\frac{dT_{internal}}{dt} = \frac{dm_{in}}{dt}(T_{external} - T_{internal}) \qquad (9.16)$$

Where $M_{internal}$ and m_{in} are the masses of air/CO_2 mixture (in kg) within the building and entering the building in time dt respectively; and $T_{internal}$ and $T_{external}$ are the internal and external temperatures. Using equation (9.16) the change in internal temperature over dt can be calculated.

9.2 CO_2 Toxic Dose and Probit

In the shelter model the effect that an increased atmospheric concentration of CO_2 has on people is quantified in terms of a toxic dose. The toxic dose is cumulative over time meaning that duration of increased CO_2 exposure is equally as important as the value of the concentration.

A generalised equation for the toxic dose of exposure to some contaminant (in (ppm^nmin) is:

$$D_o = \int c_o(t)^{n_o} dt \quad (9.17)$$

Where $c_o(t)$ is the concentration of the contaminant a person is exposed to in parts per million (ppm), and t is the time of the exposure in minutes. n_o is the toxic index which can take different values depending on the nature of the contaminant. For CO_2 the HSE specify that the value n_o = 8 is used (Halford, 2011; HSE, 2015).

9.2.1 *Dangerous Toxic Loads*

Dangerous toxic loads (DTL) are values of dose specified by the HSE[40] which represent harmful levels of exposure to a contaminant (Halford, 2011):

- The Specified Level of Toxicity (SLOT). For an average population exposed to the SLOT dose, 3% of people would be expected to die. The SLOT dose for CO_2 is 1.5 x 10^{40} ppm^8.min.
- The Significant Likelihood of Death (SLOD). For an average population exposed to the SLOD dose, 50% of people would be expected to die. The SLOD dose for CO_2 is 1.5 x 10^{41} ppm^8.min.

9.2.2 *Probit*

The DTL values for CO_2 can be used as part of a Probit analysis. In general, it is assumed that the percentage of fatalities (lethality) due to contaminant exposure in an average population follows a cumulative lognormal distribution with increasing toxic dose (Lees, 1996).

$$F = \frac{1}{2}\left[1 + \mathrm{erf}\left(\frac{\ln x - \mu_d}{\sigma_d\sqrt{2}}\right)\right] \quad (9.18)$$

Where $erf(x)$ is the error function.

---

[40] The HSE define fatalities from a SLOT dose as being between 1% and 5%. A value of 3% has been assumed in line with assumptions made by DNV-GL.

However, in a probit analysis the lethality response to increasing toxic dose is represented as a straight line, with the percentage lethality measured using a new unit, “probits”. By transforming known dose-lethality coordinates onto the probit scale, a straight line probit relationship for a particular contaminant can be derived. This relationship can provide a simple way to determine the percentage lethality in an average population at a specific dose.

For the purposes of determining CO_2 lethality in the shelter model, a straight line probit relationship has been derived using the SLOT and SLOD values given in section 9.2.1. The probit equation is:

$$probit = 0.82 \ln(dose) - 72.41 \quad (9.19)$$

In this way, the chances of death for a building occupant can be plotted with exposure time for the model.

9.3 Shelter Model Validation

The shelter model has been validated for use using experimental data from the COOLTRANS test programme at Spadeadam (Allason, 2012). This section provides details of the test case used for the validation and shows a comparison between the results of the test case and predictions made using input data from the test case in the shelter model with the same conditions. In this way, the validity of the shelter model for predicting the change in the internal concentration of CO_2 in a building following the rupture of a nearby dense phase CO_2 pipeline is confirmed.

9.3.1 *Validation Test Case*

The validation test case was that of a scaled pipeline rupture experiment, with measurements taken of gas accumulation within a specific building, placed in the path of the drifting cloud produced by the rupture (Cleaver, 2013a; Cleaver, 2013b).

In the rupture experiment, a simulated building was situated downwind of the source of release. The structure used for this purpose was a welding hut normally used to provide protection during pipe welding operations on the test site. The hut was a metal framed building with sheet metal sides and a roof. The majority of the openings that are normally present on the building were deliberately sealed for the experiments. However, two openings on opposing side walls were left open to provide a path for CO_2 ingress and egress from the building. Figure 9.3 shows a sketch of the building and provides a record of the instrumentation that was used to record the CO_2 concentration and temperatures at the inlet, within and at the outlet of the building.

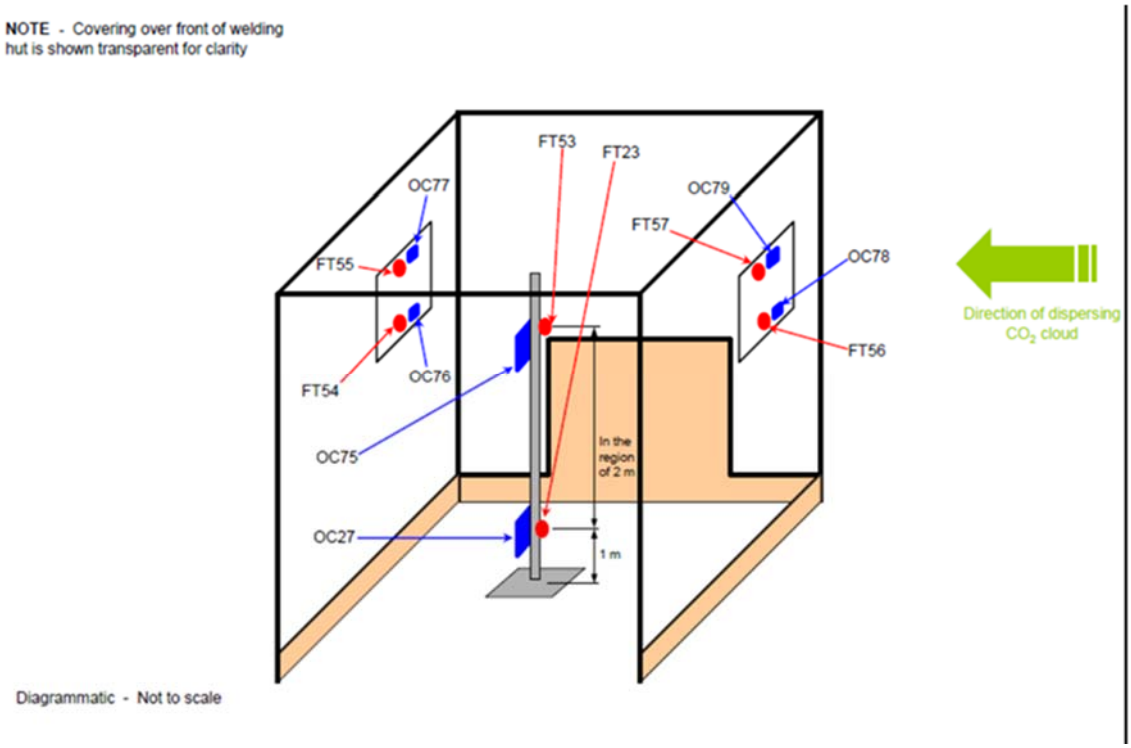

Figure 9.3: Schematic Drawing of the Welding Hut and Instrumentation

The welding hut was installed downwind of the source of the release, on a line that is 15 degrees to the north of the measurement array centreline. The hut dimensions remain proprietary information to National Grid, but the actual dimensions to the nearest cm were used as input in the calculations that follow.

A plot of the variation of concentration (as measured by sensors OC78 and OC79) and temperature (as measured by sensors FT56 and FT57) at the inlet against time is given in Figure 9.4 and Figure 9.5. These show that the measurements made at the upper and lower levels of the inlet follow the same

trends and have a similar magnitude. This suggests that the average of the upper and lower values provides a reasonable estimate of the concentration and temperature of the air/CO_2 mixture that entered the welding hut.

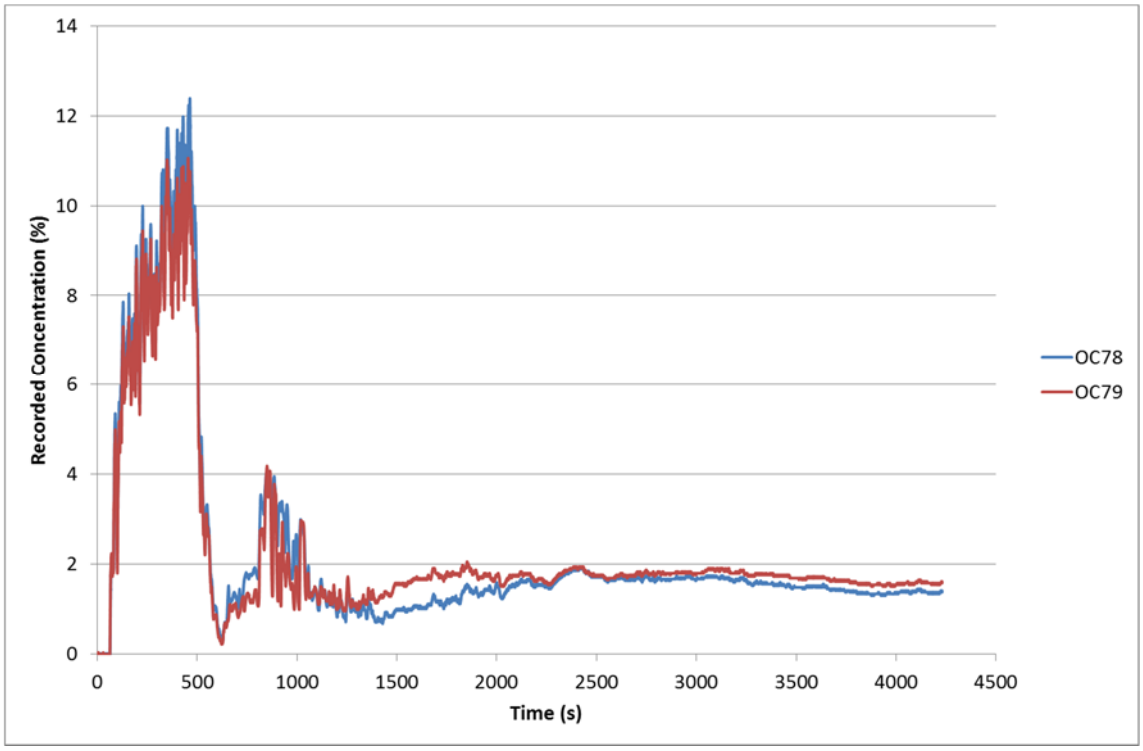

Figure 9.4: Plot of the Concentration Values Recorded at the Inlet on the Front Face of the Welding Hut

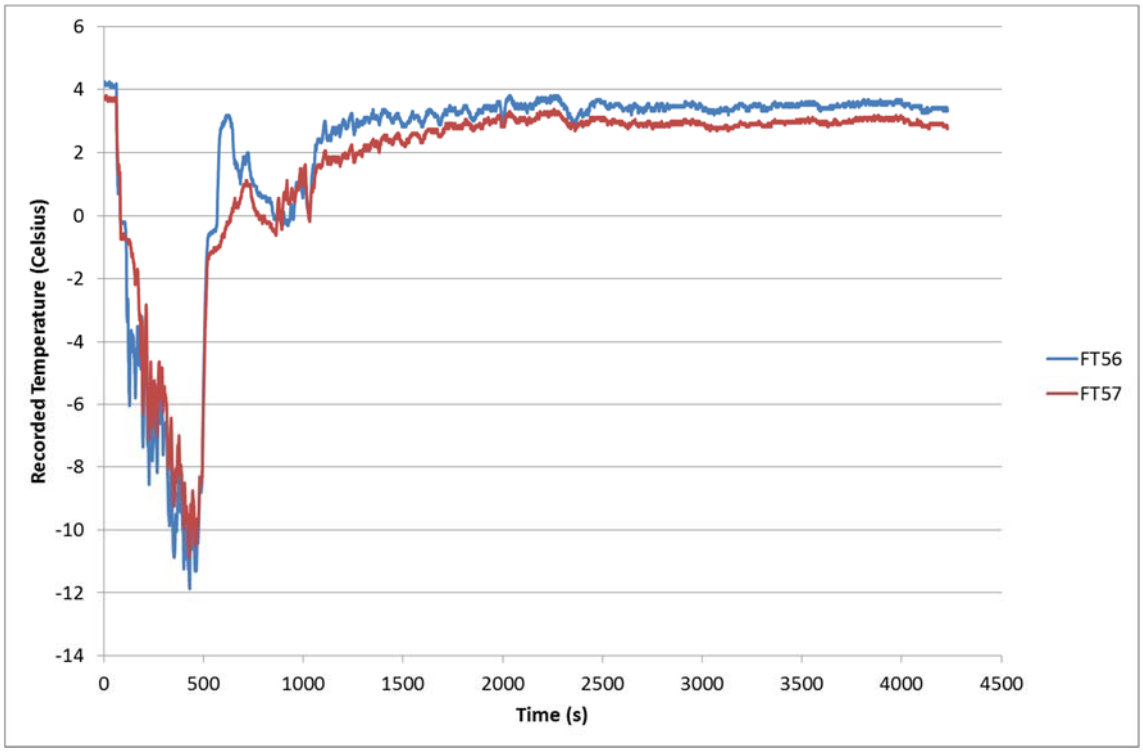

Figure 9.5: Plot of the Temperature Values Recorded at the Inlet on the Front Face of the Welding Hut

The average wind speed measured during the release was 1.15 ms^{-1} in a direction of 235° relative to the instrumentation centreline, the values are plotted in Figure 9.6 and Figure 9.**7**. The wind is incident on the front face of the hut at an angle of approximately 20° from the normal.

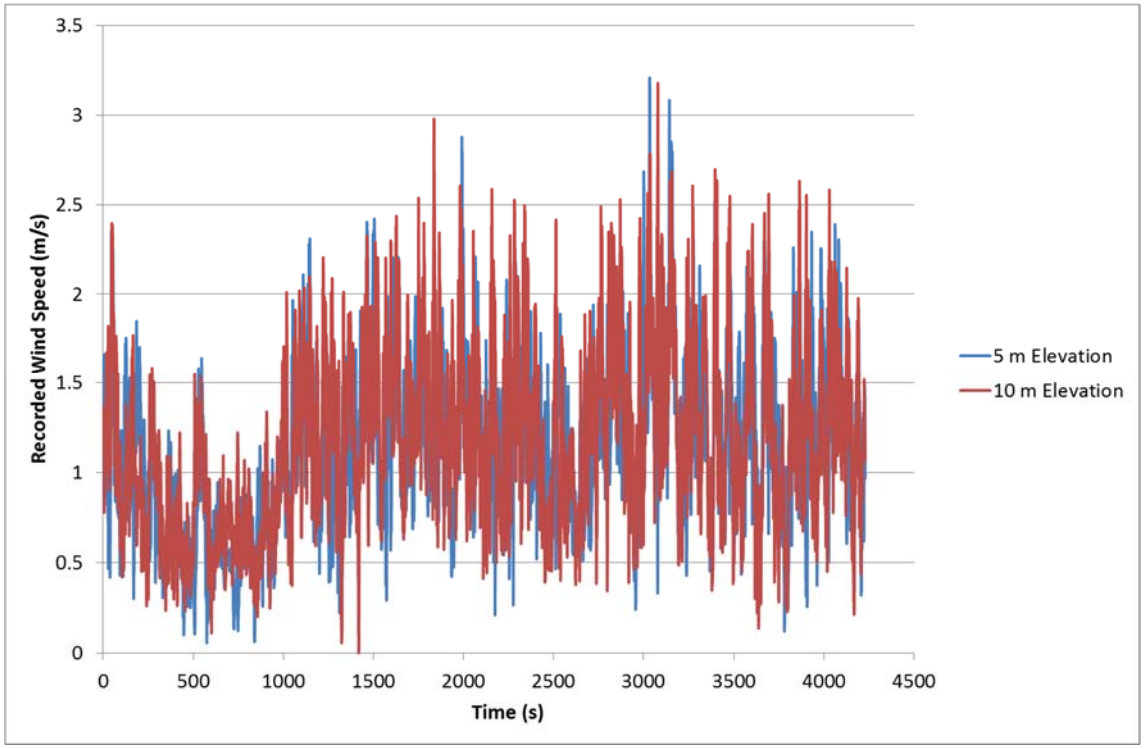

Figure 9.6: Recorded Wind Speed Upstream of Release

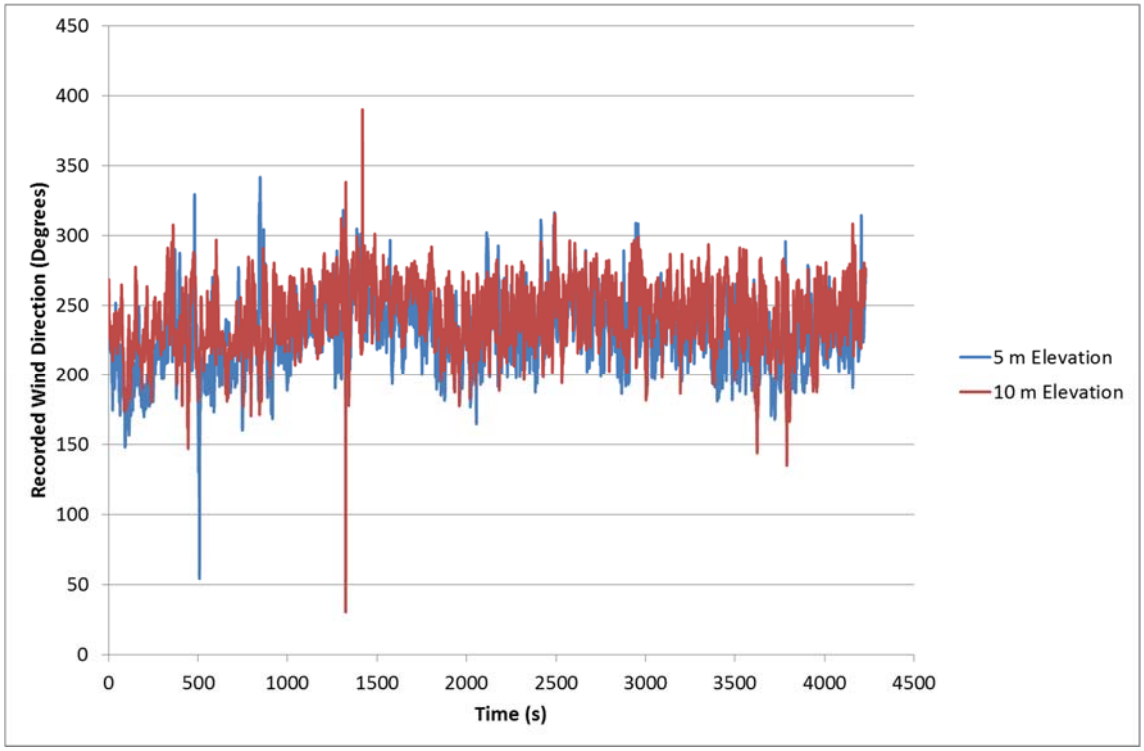

Figure 9.7: Recorded Wind Direction Upstream of the Release

9.3.2 *Shelter Model Test Case Predictions*

The shelter model was run using the same conditions and the external CO_2 concentration and temperature data from the experimental test case outlined in section 9.3.1 in order to calculate predictions of the internal CO_2 concentration and temperature. These predictions were compared with the internal CO_2 concentration and temperature recorded in the test in order to provide validation for the shelter model.

The experimental test case was not designed exclusively for the purposes of validating the shelter model. Consequently, certain minor differences exist between the allowable input for the model and the design of the test case. In order to allow for these differences a number of assumptions were made regarding the input to the model. The assumptions are listed below:

- All experimental input data from non-integer times (2.1s, 2.2s, 2.3s etc.) was removed in order to reduce processing time.
- The single rectangular windows front and back in the test case were replaced with two closely spaced square windows front and back in the shelter model. The windows were spaced with a vertical gap of 0.04 m between them.
- The windows both front and back in the shelter model are identically sized, unlike those in the experimental test case. The individual window area in the shelter model has been selected as the area of the rectangular window on the upwind face divided by 2 (i.e the total window area on the upwind face is identical to that of the experiment).
- The experimental data included a number of negative values for external concentration. This was a side-effect of the particular instrumentation used for recording. For the external concentration input to the shelter model, these negative values were replaced with the lowest positive value in the data set.
- External CO_2 concentration and temperature input data was averaged over both sensors as suggested in section 9.3.1.
- It was assumed that the wind was directly incident onto the face of the building with no angle to the normal.

- The front and back face pressure coefficients C_{pf} and C_{pb} were assumed to be 0.7 and -0.25 respectively and were taken from BS 5925 (Anon., 1995) for a directly incident wind onto a building with the same dimensions as those in the experimental test case.
- The window discharge coefficient C_d was assumed to be 0.61 and was taken from BS 5925 (Anon., 1995).
- The wind speed used was an average of the entire set of wind speed measurements and had a value of 1.168 ms^{-1}.
- The initial internal temperature in the welding hut was assumed to be the same as the initial external temperature.

Figure 9.8 shows the comparison between values of internal CO_2 concentration predicted using the shelter model and those recorded during the experimental test case. For the experimental data in Figure 9.8 an average taken between values recorded at sensors OC75 and OC27 from Figure 9.3 represents the concentration inside the welding hut. An average between values recorded at sensors OC75, OC27, OC77 and OC76 is also shown, which incorporates additional measurements from the outlet to the hut.

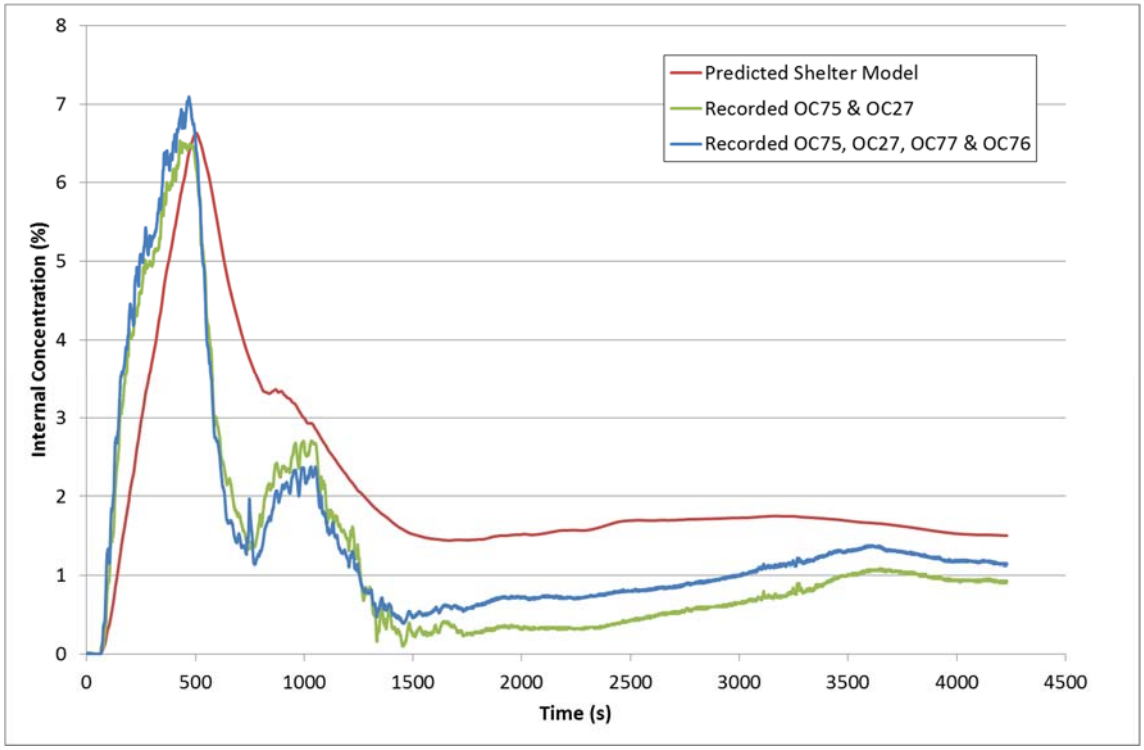

Figure 9.8: Comparison between Recorded and Predicted Values of Internal CO_2 Concentration for the Validation Test Case

Figure 9.8 shows that the initial build-up of CO_2 in the welding hut occurs faster in the experiment than predicted by the model, however the difference between model and experiment is reduced as the maximum concentration is approached. The predicted maximum CO_2 concentration is reached within approximately 50 seconds of the experimental maximum. The maximum CO_2 concentration predicted by the model is only approximately 0.05% of CO_2 higher than experiment when considering the two internal sensors alone, and approximately 0.6% of CO_2 lower than experiment when incorporating the outlet data. After the peak value is reached, the shelter model shows conservative behaviour, as the decay in CO_2 concentration is slower than that recorded by the experiment. The general trend of the model follows the experimental data.

Similarly, Figure 9.9 shows the comparison between the predicted and recorded values of internal temperature. For the experimental data in Figure 9.9 an average taken between values recorded at sensors FT23 and FT53 from Figure 9.3 represents the concentration inside the welding hut. An average between values recorded at sensors FT23, FT53, FT54 and FT55 is also shown, which incorporates additional measurements from the outlet to the hut.

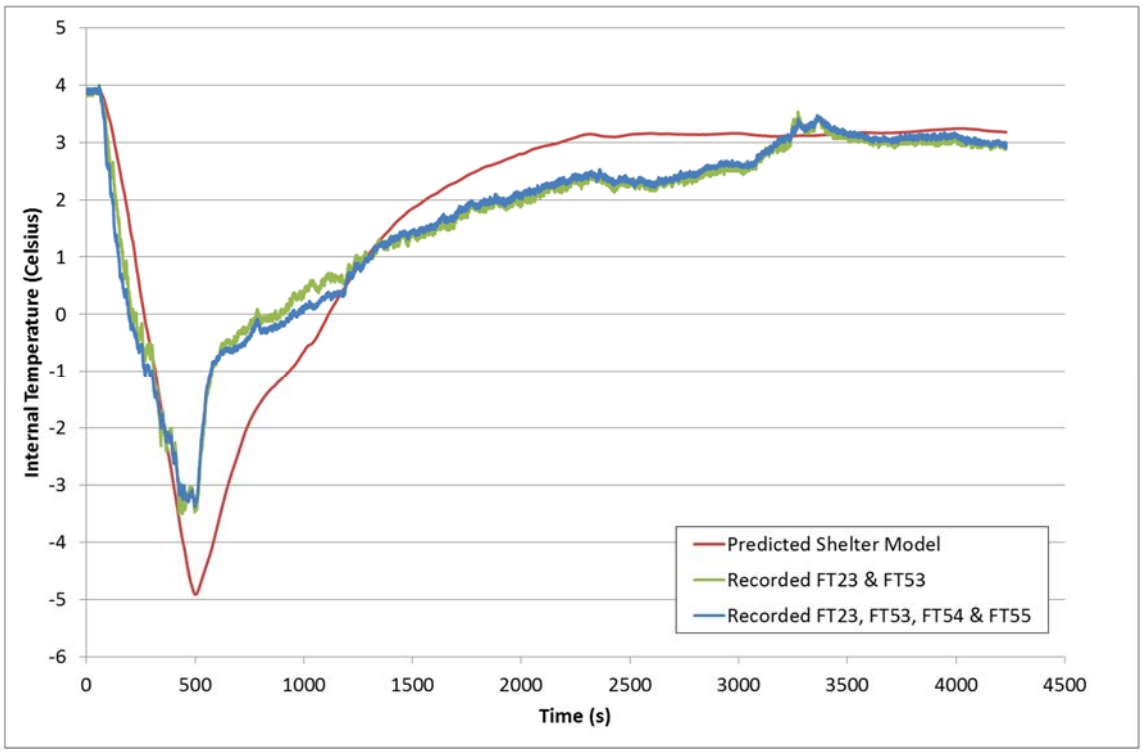

Figure 9.9: Comparison between Recorded and Predicted Values of Internal Temperature for the Validation Test Case

Figure 9.9 shows that the initial drop in welding hut temperature occurs faster in the experiment than predicted by the model, however the difference between model and experiment is reduced as the minimum temperature is approached. The predicted minimum temperature is reached within 60 seconds of the experimental minimum. The minimum temperature predicted by the model is approximately 1.5 degrees lower than that of the experiment. After the minimum value is reached, the shelter model initially shows the temperature increase to be slower than that recorded by the experiment. After approximately 750 seconds however, this trend is reversed and model temperatures exceed those of the experiment after approximately 1200 seconds. From this point onwards the model and experimental curves slowly converge.

From the comparisons shown in Figure 9.8 and Figure 9.9 it can be concluded that the shelter model gives a good approximation to experimental data for both internal CO_2 concentration and internal temperature. The shelter model is considered suitable for the purpose of predicting the change in the internal concentration of CO_2 in a building following the rupture of a nearby dense phase CO_2 pipeline.

9.4 Model Simulations

9.4.1 *DNV-GL Cases*

For the purposes of the COOLTRANS research programme, DNV-GL have performed simulations of a dense phase CO_2 pipeline rupture using their in-house, custom built, flat terrain dispersion model developed from the results of COOLTRANS experiments (Cleaver, 2014e). The DNV-GL model simulates the dispersion of the released CO_2 cloud and provides values for atmospheric CO_2 concentration and vapour temperature variation with time and distance from the release.

The data from these simulations has been used as input to the shelter model in order to investigate the level of shelter a nearby building can provide in the

event of a real dense phase CO_2 pipeline rupture (Cleaver, 2014e; Cleaver, 2014b; Cleaver, 2014c; Cleaver, 2014d; Cleaver, 2014a).

In order to explore shelter under different conditions, the results of four different simulation cases have been provided. Each simulation is based upon a double ended guillotine break type rupture at the mid-point of a 96 km long dense phase CO_2 pipeline. Details of the input conditions which remain constant between each simulation are provided in Table 9.1.

Input	Value
Pipeline Length	96 km
Pipeline Outside Diameter	610 mm
Pipeline Wall Thickness	19.4 mm
Pipeline Internal Pressure	150 barg
Material	Carbon Dioxide

Table 9.1: DNV-GL Dispersion Model Input Conditions

The input conditions which vary between each simulation are the atmospheric conditions, the temperature of the CO_2 in the pipeline and whether or not shut-off valves are operated in the event of a rupture. The four cases considered are:

1. CO_2 at 30°C in the pipeline, atmospheric conditions 5D (day with 5 m/s wind speed), valve closure after 15 minutes.

2. CO_2 at 10°C in the pipeline, atmospheric conditions 5D (day with 5 m/s wind speed), valve closure after 15 minutes.

3. CO_2 at 30°C in the pipeline, atmospheric conditions 5D (day with 5 m/s wind speed), no valve closure.

4. CO_2 at 30°C in the pipeline, atmospheric conditions 2F (night with 2 m/s wind speed), valve closure after 15 minutes.

Case 1 is regarded as the default case, with the remaining three cases each providing sensitivity in one of the variable input conditions, whilst keeping the

others constant. In the simulations, atmospheric conditions of 5D are used to represent a rupture during daylight hours whereas conditions of 2F represent a rupture at night. The implications these conditions have for the shelter model are the presence of different wind speeds in each case.

The shelter model has been applied to the results of the above four simulations from DNV-GL. The main variable considered in the investigation was the distance of the building from the release. For the purposes of the investigation all other variables were kept constant. The distances used in the investigation were exclusively along the centreline axis in the simulated release and the wind was assumed to be blowing directly onto the face of the building closest to the rupture source (angle of 0° to the normal). In each of the four cases DNV-GL has modelled the CO_2 cloud dispersion for two hours following the rupture or until the external CO_2 concentration returned to the pre-release level.

The data from the DNV-GL simulations includes two values for atmospheric CO_2 concentration and one value for external temperature. The concentration values are termed “C-mean” and “C-equiv”. “C-mean” is a value for the mean atmospheric CO_2 concentration and “C-equiv” is an “equivalent” higher value adjusted so that concentration fluctuations are included. For the cases considered, the values for “C-mean” have been used in conjunction with the temperature values in order to calculate the air flow rates between the internal and external atmospheres in the shelter model. The values of “C-equiv” have been used in conjunction with the calculated air flow rates to determine the toxic dose and lethality within the building. It is assumed in the analysis that the CO_2 cloud completely envelopes the building over all dimensions.

Table 9.2 provides the assumptions and input conditions for the shelter model used in the investigation.

Input	Value
Starting Internal Temperature	293 K (20° C)
Initial Internal CO_2 Concentration	0.039%
Wind Direction	0° to the normal
Initial External CO_2 Concentration	0.039%
Building Height	5 m
Building Length	10 m
Building Width	10 m
C_p Front Face	0.7
C_p Back Face	-0.2
Window Discharge Coefficient, C_d	0.61
Number of Windows on Front/Back Face	2 on each
Height of Bottom of Lowest Window	0.25 m
Vertical Separation of Windows	2 m
Window Area	0.02125 m^2

Table 9.2: Shelter Model Input Conditions and Assumptions

The window discharge coefficient and pressure coefficients for the specified wind direction were taken from BS 5925 (Anon., 1995).

The building used in the analysis was a single cuboid structure with dimensions given in Table 9.2, the interior of the building did not contain different rooms or partitions. The dimensions of the building are taken from the DNV-GL report 9500 (Halford, 2011) which presented a similar study based on a simple wind driven ventilation model. The windows in the building were square shaped and identically sized. For the investigation the window area has been chosen as 0.02125 m^2. A starting internal temperature of 20° C was chosen as an example of a typical room temperature.

The choice of input conditions and assumptions produces a ventilation flow rate of approximately 0.65 AC/hr when the building is subject to a direct wind of 5 m/s with a 10° C temperature difference between the internal and external environment. As explained in section 9.1 the ventilation flow rate will vary depending on the wind speed; internal and external CO_2 concentration; and internal and external temperature difference. The ventilation flow rate is therefore subject to continuous variation throughout the course of each simulation. Typical ventilation rates for a real dwelling with internal partitions range between 0.5 and 3 AC/hr (Harris, 1989). If internal partitions were

included in the model it is anticipated that the flow rate would vary between different rooms, and that the predicted CO_2 concentration would be higher in rooms on the side facing the wind than those on the opposite side; and higher on the ground floor than on the upper floor.

9.4.2 *Investigation Results*

The change in internal CO_2 concentration and temperature with time has been modelled for a building, located at eight distances along the centreline axis, using the shelter model with the DNV-GL simulations. In each case, following the rupture there is a period of time before the cloud reaches the building in which the internal and external conditions remain constant at their initial levels. The duration of this time period is determined by the wind speed, which controls the speed of the released CO_2 cloud; and the distance of the building from the rupture. The distances considered and respective times that the CO_2 cloud takes to reach the building, for each of the wind speeds investigated are shown in Table 9.3.

It is noted that the building is located downwind on the centreline axis in each case. The results produced may be different for a similar distance crosswind or upwind. The downwind case is assumed to be the worst case direction. In a full QRA, other locations throughout the cloud would be also need to be considered.

Distance (m)	Time at Wind Speed of 2 m/s (s)	Time at Wind Speed of 5 m/s (s)
100	50	20
150	75	30
200	100	40
300	150	60
400	200	80
500	250	100
700	350	140
1000	500	200

Table 9.3: Time Taken for the Arrival of CO_2 Cloud with Distance from Rupture

Mean Concentration

Figure 9.10 shows the change in the mean internal concentration of CO_2 (C-mean) calculated using the shelter model for the eight distances given in Table 9.3 for case 1: CO_2 at 30°C in the pipeline, atmospheric conditions 5D (day with 5 m/s wind speed), valve closure after 15 minutes. The mean external concentration with time is also shown. Charts for the remaining cases are included in Appendix C .

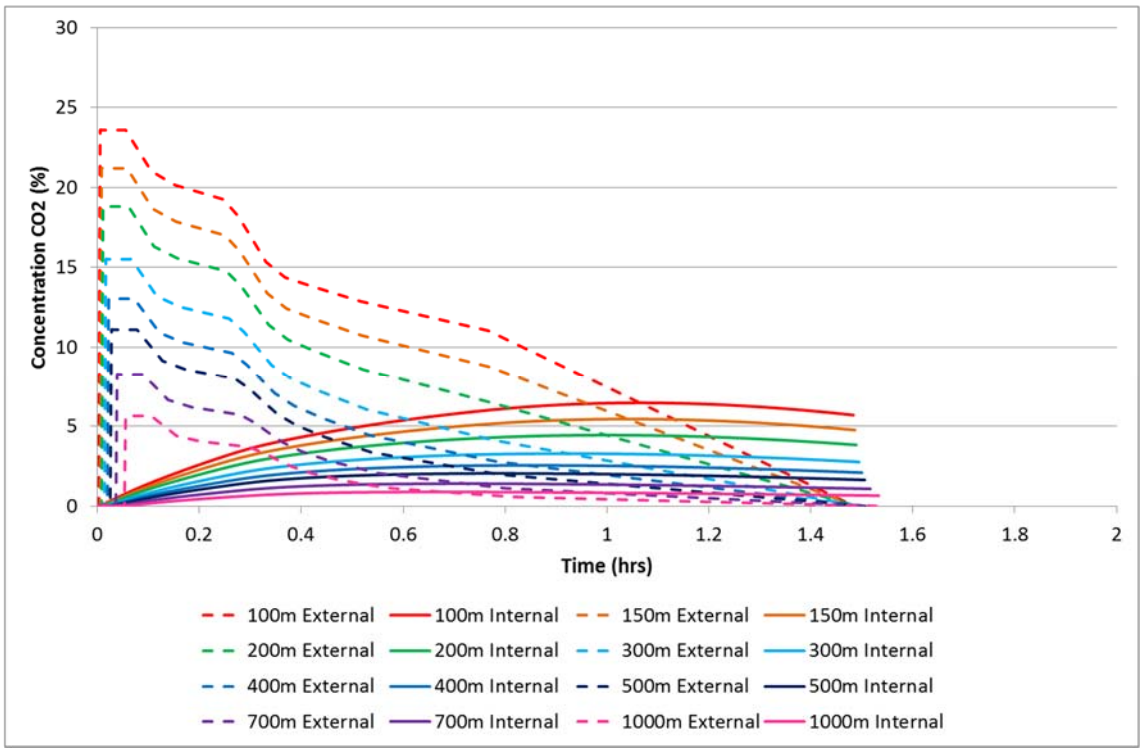

Figure 9.10: Change in Mean Internal CO_2 Concentration with Time and Distance for Case 1

For each case considered, the calculated internal concentration follows a trend of diminishing increase. The reason for this is that the internal concentration always acts to match the time-decaying external concentration. As a result, the maximum mean internal concentration of CO_2 is reached when it equals the external concentration, after this point it begins to fall.

For the purposes of this investigation, the mean internal and external CO_2 concentrations contribute to the value of air flow rate between the internal and external atmospheres.

Temperature

Figure 9.11 shows the change in the internal temperature calculated using the shelter model for the eight distances given in Table 9.3 for case 1: CO_2 at 30°C in the pipeline, atmospheric conditions 5D (day with 5 m/s wind speed), valve closure after 15 minutes. The external temperature with time is also shown. Charts for the remaining cases are included in Appendix C .

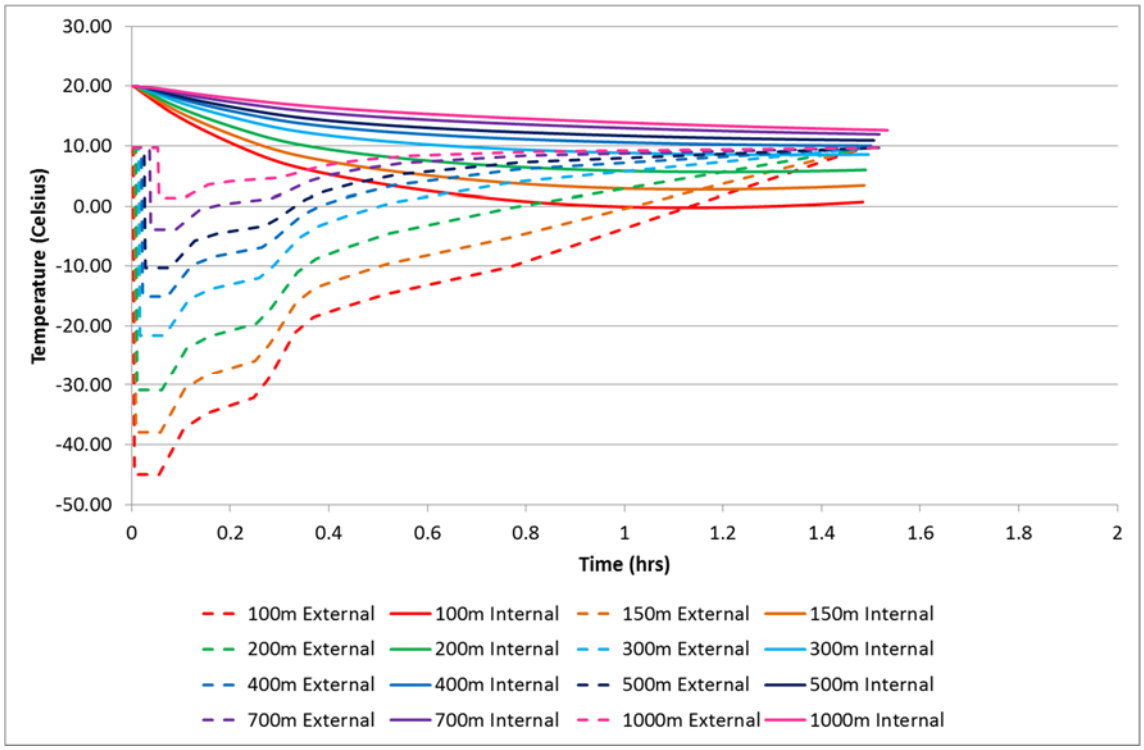

Figure 9.11: Change in Internal Temperature with Time and Distance for Case 1

For each case considered, the calculated internal temperature follows a trend of diminishing decrease. The reason for this is that the internal temperature always acts to match the time-increasing external temperature. As a result, the minimum internal temperature is reached when it equals the external temperature, after this point it begins to rise.

In the shelter model, the internal and external temperatures contribute to the value of air flow rate between the internal and external atmospheres.

Equivalent Concentration

Figure 9.12 shows the change in the equivalent internal concentration of CO_2 (C-equiv) calculated using the shelter model for the eight distances given in Table 9.3 for case 1: CO_2 at 30°C in the pipeline, atmospheric conditions 5D (day with 5 m/s wind speed), valve closure after 15 minutes. The equivalent external concentration with time is also shown. Charts for the remaining cases are included in Appendix C .

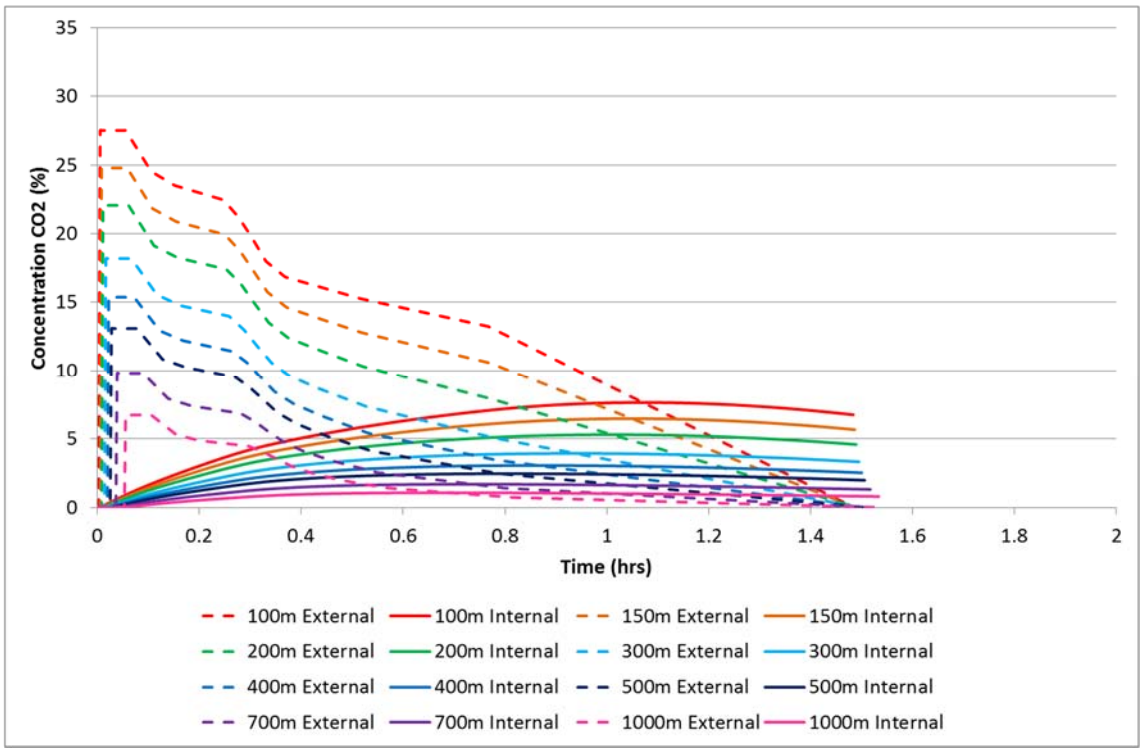

Figure 9.12: Change in Equivalent Internal CO_2 Concentration with Time and Distance for Case 1

For each case considered, the calculated internal concentration follows a trend of diminishing increase. The reason for this is that the internal concentration always acts to match the time-decaying external concentration. As a result, the maximum equivalent internal concentration of CO_2 is reached when it equals the external concentration, after this point it begins to fall.

For the purposes of this investigation, the equivalent internal CO_2 concentration is used to calculate the toxic dose for occupants of the building.

Toxic Dose

Figure 9.13 shows the CO_2 dose that a building occupant would receive, as calculated using the equivalent internal concentration from the shelter model for the eight distances given in Table 9.3 for case 1: CO_2 at 30°C in the pipeline, atmospheric conditions 5D (day with 5 m/s wind speed), valve closure after 15 minutes. Lines for the SLOT and SLOD DTLs are also shown. Charts for the remaining cases are included in Appendix C .

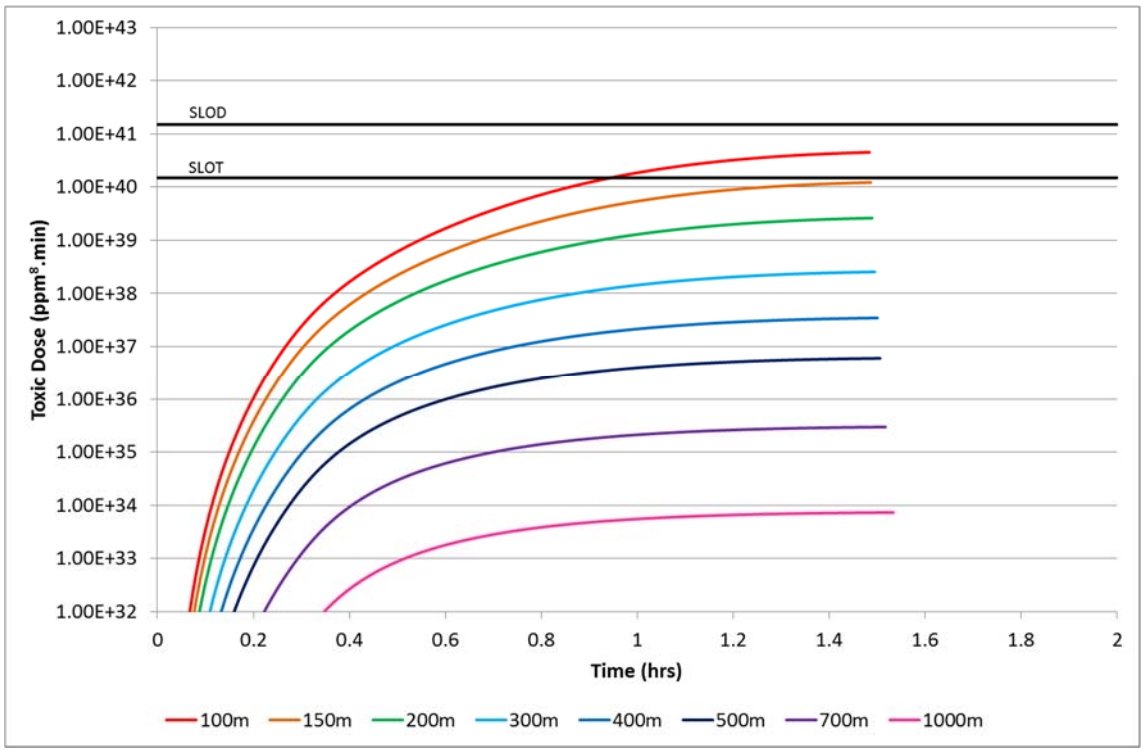

Figure 9.13: Dose Received by a Building Occupant with Time and Distance for Case 1

The toxic dose is a cumulative quantity; this is reflected in the charts, which show a continuous increase in dose for each case. In the cases with valve closure, the magnitude of the increase diminishes as the simulation progresses because the internal equivalent CO_2 concentration reaches its maximum value and begins to fall (Figure 9.12). As the external concentration of CO_2 returns to atmospheric levels the toxic dose value for each case will become constant.

The toxic dose is used to calculate the lethality for occupants of the building.

Lethality

Figure 9.14 shows the chances of lethality for a building occupant, as calculated using the toxic dose for the eight distances given in Table 9.3 for case 1: CO_2 at 30°C in the pipeline, atmospheric conditions 5D (day with 5 m/s wind speed), valve closure after 15 minutes. Lines for the SLOT and SLOD percentages are also shown. Charts for the remaining cases are included in Appendix C .

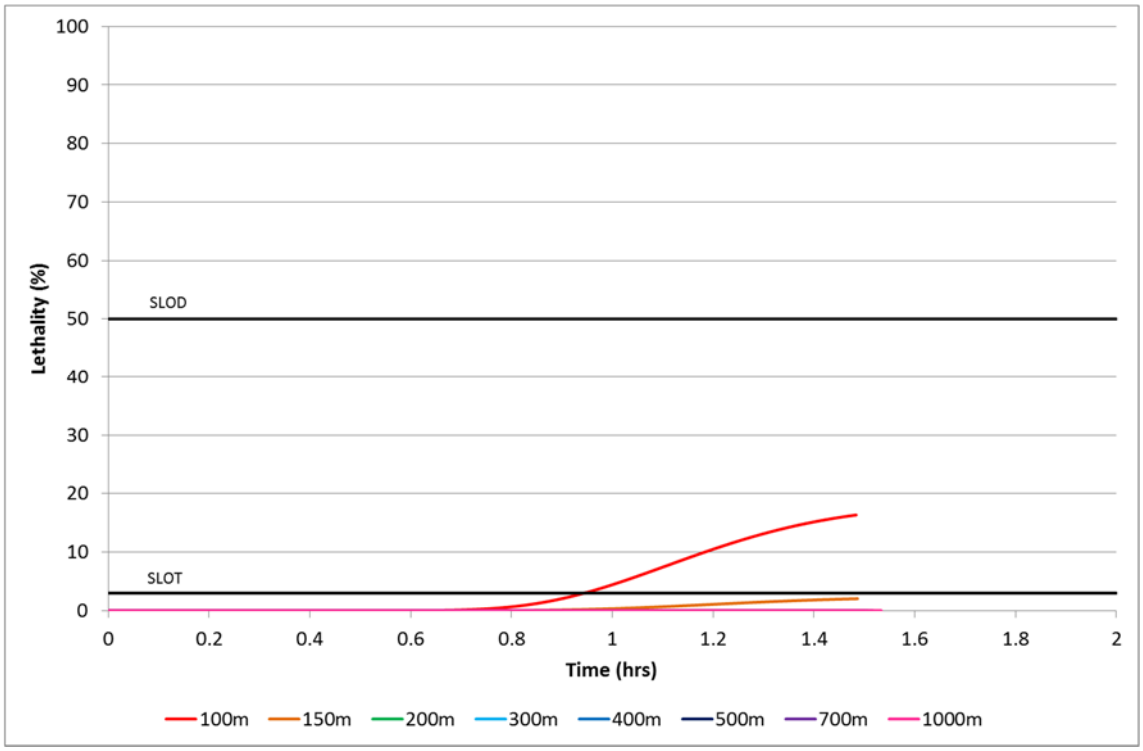

Figure 9.14: Percentage Lethality for a Building Occupant with Time and Distance for Case 1

Lethality is represented as a cumulative percentage and is derived from the toxic dose. Its value therefore increases as the toxic dose increases (Figure 9.13). A summary of the times taken for the lethality to exceed the SLOT and SLOD percentages of 3% and 50% for each case considered is given in Table 9.4. Note that in Table 9.4 an entry of "-" indicates that the specific DTL was not exceeded during the course of the simulation.

Dangerous Toxic Load/ Percentage Lethality	Distance (m)	Time (hours)			
		Case 1	Case 2	Case 3	Case 4
SLOT	100	0.95	0.91	0.75	-
	150	-	1.2	0.89	-
	200	-	-	1.11	-
	300	-	-	1.69	-
	400	-	-	-	-
	500	-	-	-	-
	700	-	-	-	-
	1000	-	-	-	-
SLOD	100	-	-	1.13	-
	150	-	-	1.39	-
	200	-	-	1.84	-
	300	-	-	-	-
	400	-	-	-	-
	500	-	-	-	-
	700	-	-	-	-
	1000	-	-	-	-

Table 9.4: Times until The SLOT and SLOD Dangerous Toxic Loads are Exceeded for Building Occupants with Distance

From Table 9.4 and the lethality charts, it can be concluded that the time period before a specific percentage lethality is reached within the building in question, increases with distance from the source of the release for all of the cases considered. Additionally, the maximum lethality reached over the duration of the simulation decreases with distance from the source of the release. These trends are inherent from the concentration and temperature input data which shows a reduction in the mean and equivalent external concentration of CO_2 with distance and external temperatures which are closer the pre-release ambient temperature. The trend is carried through the shelter model as shown in the mean and equivalent concentration, temperature and toxic dose charts.

A decrease in the initial temperature of the CO_2 in the pipeline between 30 degrees and 10 degrees (i.e. the difference between case 1 and case 2) results in a decrease in the time period before a specific percentage lethality is reached within the building, at each distance. Additionally, the maximum lethality reached over the duration of the simulation increases for each distance. Assuming the DNV-GL model produces a realistic representation of CO_2

dispersion following a rupture, the analysis suggests that a decrease in the temperature of CO_2 in the pipeline may lead to worse consequences for nearby building occupants in the event of a rupture. However, in order to fully investigate this possibility, a more comprehensive sensitivity study into CO_2 temperature would need to be carried out.

If shut-off valves are not operated 15 minutes after the release then the result is a decrease in the time period before a specific lethality is reached within the building, at each distance. Additionally, the maximum lethality reached over the duration of the simulation increases for each distance. This effect is much larger than that observed between case 1 and case 2. The effect is a clear reflection of the input data which shows that in case 3, the external CO_2 concentration remains significantly higher than the standard atmospheric value two hours after the release at each distance. In case 1, the presence of the shut-off valves limits the volume of CO_2 which can escape to the atmosphere and ensures that the external CO_2 concentration and external temperature are disturbed for a much shorter period. Assuming the DNV-GL model produces a realistic representation of CO_2 dispersion following a rupture, it can be concluded from this analysis that shut-off valves can be used to reduce the consequences for nearby building occupants in the event of a rupture.

A change in the atmospheric conditions from 5D to 2F (i.e. the difference between case 1 and case 4) results in an increase in the time period before a specific percentage lethality is reached within the building, at each distance. Additionally, the maximum lethality reached over the duration of the simulation decreases for each distance. In case 4 the different atmospheric conditions lead to a lower external concentration of CO_2 and an external temperature which is closer to that of the pre-release ambient temperature. These conditions in turn lead to a lower air flow rate into the building and a lower lethality percentage. Assuming the DNV-GL model produces a realistic representation of CO_2 dispersion following a rupture, it can be concluded from this analysis that a rupture in atmospheric conditions of 2F would have fewer consequences for nearby building occupants than an identical rupture in 5D conditions.

For a case 1 release, the minimum distance for which the internal concentration of CO_2 in the building considered will remain below the level required for a SLOT DTL is between 100 m and 150 m. The minimum distance for which the internal concentration in the building will remain below the level required for a SLOD DTL is less than 100 m.

For a case 2 release, the minimum distance for which the internal concentration of CO_2 in the building considered will remain below the level required for a SLOT DTL is between 150 m and 200 m. The minimum distance for which the internal concentration in the building will remain below the level required for a SLOD DTL is less than 100 m.

For a case 3 release, the minimum distance for which the internal concentration of CO_2 in the building considered will remain below the level required for a SLOT DTL is between 300 m and 400 m. The minimum distance for which the internal concentration in the building will remain below the level required for a SLOD DTL is between 200 m and 300 m. For all of the simulations considered, the highest maximum percentage lethality and the shortest time to a specific percentage lethality within the building at each particular distance occur in the case without valve closure.

For a case 4 release, the minimum distance for which the internal concentration of CO_2 in the building considered will remain below the level required for both SLOT and SLOD DTLs is less than 100 m. For all of the simulations considered, the lowest maximum percentage lethality and the longest time to a specific percentage lethality within the building at each particular distance are seen in the case with F2 atmospheric conditions.

It is noted however, that the above results are for a building located downwind on the centreline axis which is considered to be the worst case. The results produced may be different for a building located crosswind or upwind, which should be considered as part of future work.

It is also noted that the CO_2 cloud in the analysis was assumed to completely envelope the building, a recommendation for future work would be to consider

clouds which only cover a fraction of the building's height. In addition, the building considered in the analysis was a single cuboid structure and therefore a simplified representation of the majority of buildings which could be occupied. A recommendation for future work would therefore be to introduce partitions within the building to simulate different rooms, thereby refining the analysis.

9.4.3 *Ventilation Rate Study*

The input conditions and assumptions given in Table 9.2 and used for the investigation detailed in sections 9.4.1 and 9.4.2 produce a ventilation flow rate of approximately 0.65 AC/hr when the building in question is subject to a direct wind of 5 m/s with a 10° C temperature difference between the internal and external environment. However, it was also noted in section 9.4.1 that that typical ventilation rates for a real dwelling can range from between 0.5 to 3 AC/hr. Taking this into consideration, a study has been performed in order to investigate the effect of ventilation flow rate on the level of shelter a nearby building can provide in the event of a dense phase CO_2 pipeline rupture.

For this study the shelter model has been applied to the results of the case 1 simulation from DNV-GL only. The main variable considered in the study was the building window area, which was used to dictate the size of the ventilation flow rates. Three different window areas were selected as input for the model in order to produce small, medium and large ventilation flow rates. For the purposes of the study all other variables were kept constant. Other than the window area, the assumptions and input conditions for the shelter model used in the study are identical to those given in Table 9.2.

The distance of the building from the source of the rupture was set at 100 m along the centreline axis in the simulated release. As with the investigation in sections 9.4.1 and 9.4.2 the wind was assumed to be blowing directly onto the face of the building closest to the rupture source.

Table 9.5 provides the values of window area used in the study in addition to the value of ventilation flow rate which would be produced if the building were

subject to a direct wind of 5 m/s with a 10° C temperature difference between the internal and external environment.

Window Area (m^2)	Ventilation Flow Rate (AC/hr)
0.02125	0.65
0.0425	1.3
0.085	2.6

Table 9.5: Window Areas for Ventilation Rate Study

Note that the flow rates given in Table 9.5 are for constant atmospheric conditions and in the absence of a nearby pipeline rupture. Ventilation flow rate is dependent on wind speed; internal and external CO_2 concentration; and internal and external temperature difference. The conditions experienced by the building over the course of the case 1 simulation therefore lead to continuous variation in the ventilation flow rate. In the study, the different window area values in Table 9.5 produce ventilation rates which vary over the course of the simulation but remain small, medium and large relative to each other. The ventilation flow rates with time for the study are shown in Figure 9.15.

9.4.4 *Ventilation Study Results*

The change in internal CO_2 concentration and temperature with time has been modelled for a building, located at a distance of 100 m along the centreline axis from the source of the release, using the shelter model with the case 1 DNV-GL simulation. Modelling has been performed three times using different window area values in order to investigate the effect of ventilation flow rate.

Ventilation Flow Rate

Figure 9.15 shows the change in the ventilation flow rate calculated using the shelter model for the three window area values given in Table 9.5 for case 1: CO_2 at 30°C in the pipeline, atmospheric conditions 5D (day with 5 m/s wind speed), valve closure after 15 minutes.

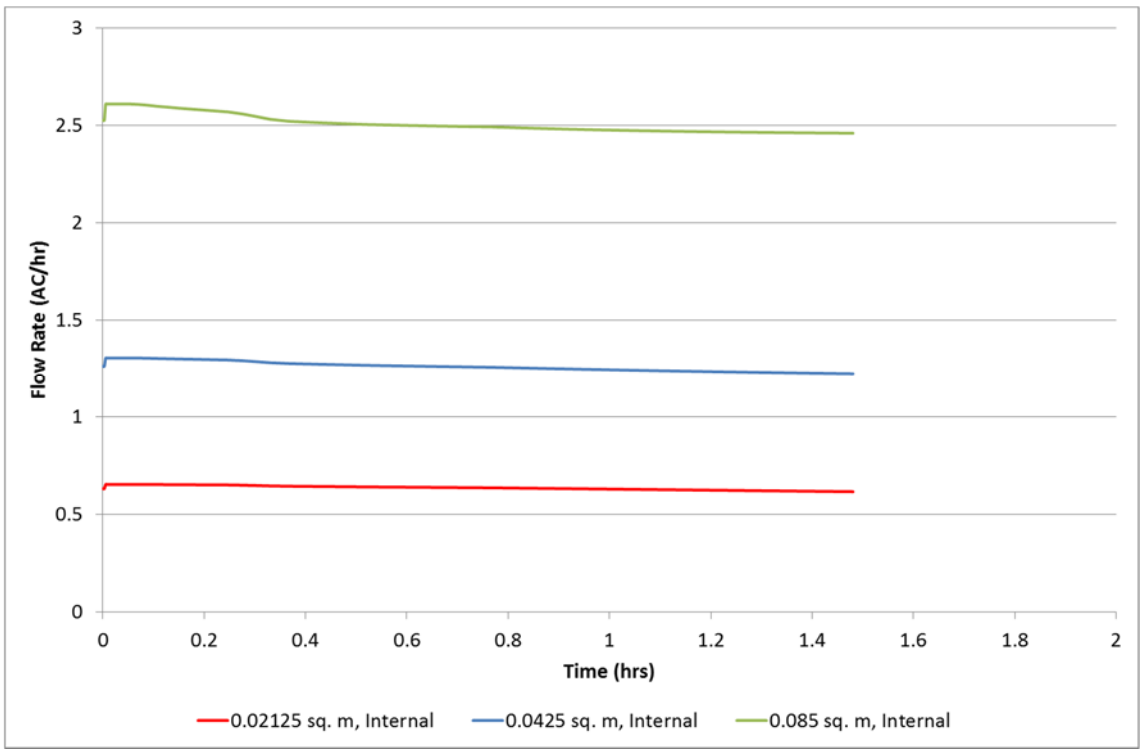

Figure 9.15: Change in Ventilation Flow Rate with Time and Window Area for Case 1

For each different window area, the ventilation flow rate is initially similar to its respective value in Table 9.5. This represents the period of time before the cloud reaches the building in which the internal and external conditions remain constant at their initial levels. An increase in the window area by a factor of two produces an increase in the ventilation flow rate by a factor of two for constant internal and external conditions.

Once the building is surrounded by the CO_2 cloud the ventilation flow rates change in line with the variation in internal and external conditions. The flow rates vary continuously throughout the course of the simulation with the extent of the variation increasing with increasing window area. The reason for this is the larger the window area, the higher the overall flow rate and the quicker the internal conditions will change to match the external conditions.

Mean Concentration

Figure 9.16 shows the change in the mean internal concentration of CO_2 (C-mean) calculated using the shelter model for the three window area values given in Table 9.5 for case 1: CO_2 at 30°C in the pipeline, atmospheric conditions 5D (day with 5 m/s wind speed), valve closure after 15 minutes. The mean external concentration with time is also shown.

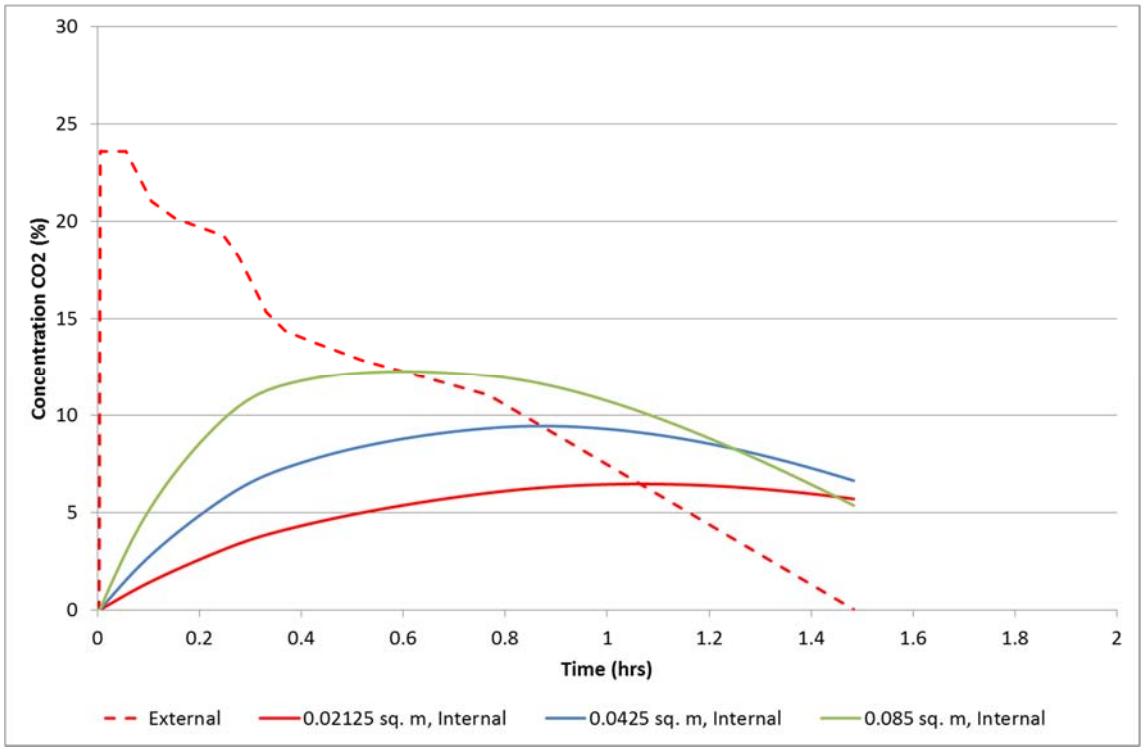

Figure 9.16: Change in Mean Internal CO_2 Concentration with Time and Window Area for Case 1

Temperature

Figure 9.17 shows the change in the internal temperature calculated using the shelter model for the three window area values given in Table 9.5 for case 1: CO_2 at 30°C in the pipeline, atmospheric conditions 5D (day with 5 m/s wind speed), valve closure after 15 minutes. The external temperature with time is also shown.

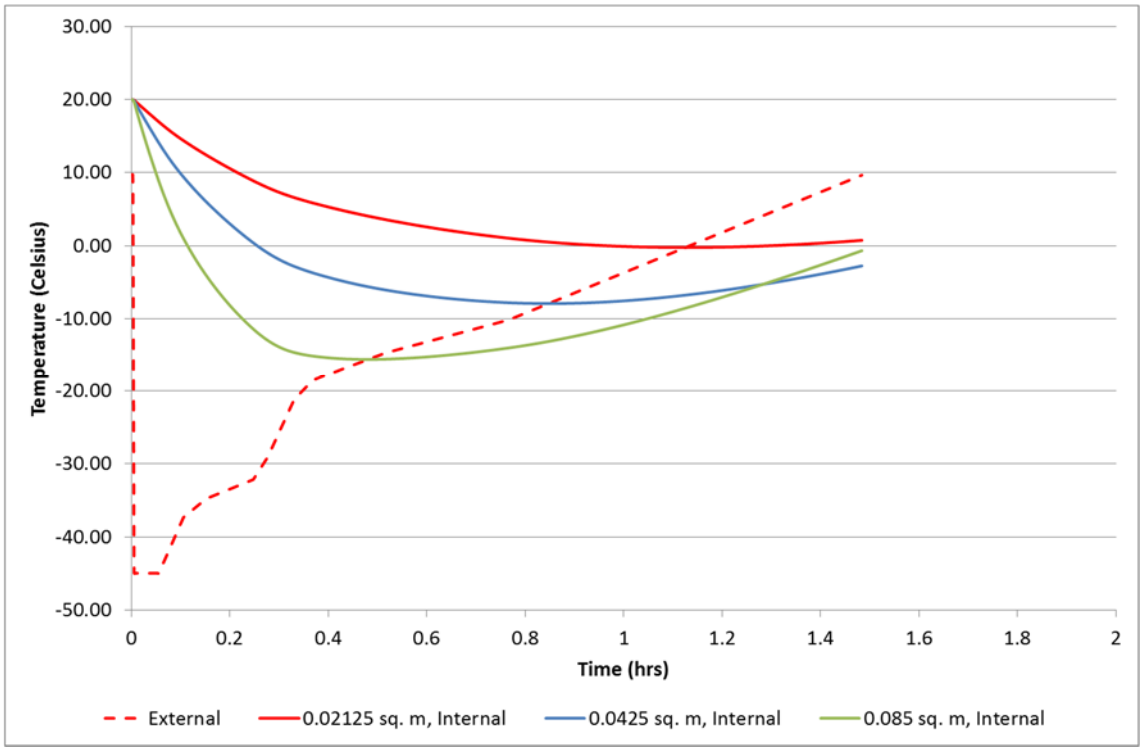

Figure 9.17: Change in Internal Temperature with Time and Window Area for Case 1

Equivalent Concentration

Figure 9.18 shows the change in the equivalent internal concentration of CO_2 (C-equiv) calculated using the shelter model for the three window area values given in Table 9.5 for case 1: CO_2 at 30°C in the pipeline, atmospheric conditions 5D (day with 5 m/s wind speed), valve closure after 15 minutes. The equivalent external concentration with time is also shown.

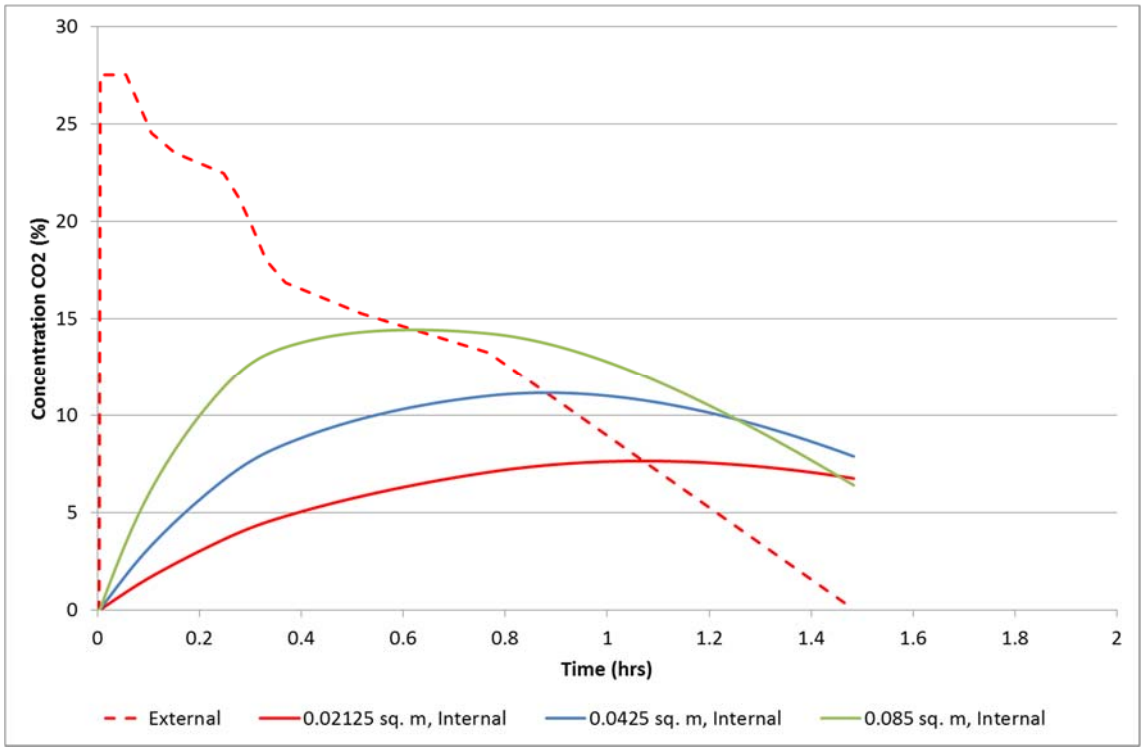

Figure 9.18: Change in Equivalent Internal CO_2 Concentration with Time and Window Area for Case 1

Toxic Dose

Figure 9.19 shows the CO_2 dose that a building occupant would receive, as calculated using the equivalent internal concentration from the shelter model for the three window area values given in Table 9.5 for case 1: CO_2 at 30°C in the pipeline, atmospheric conditions 5D (day with 5 m/s wind speed), valve closure after 15 minutes. Lines for the SLOT and SLOD DTLs are also shown.

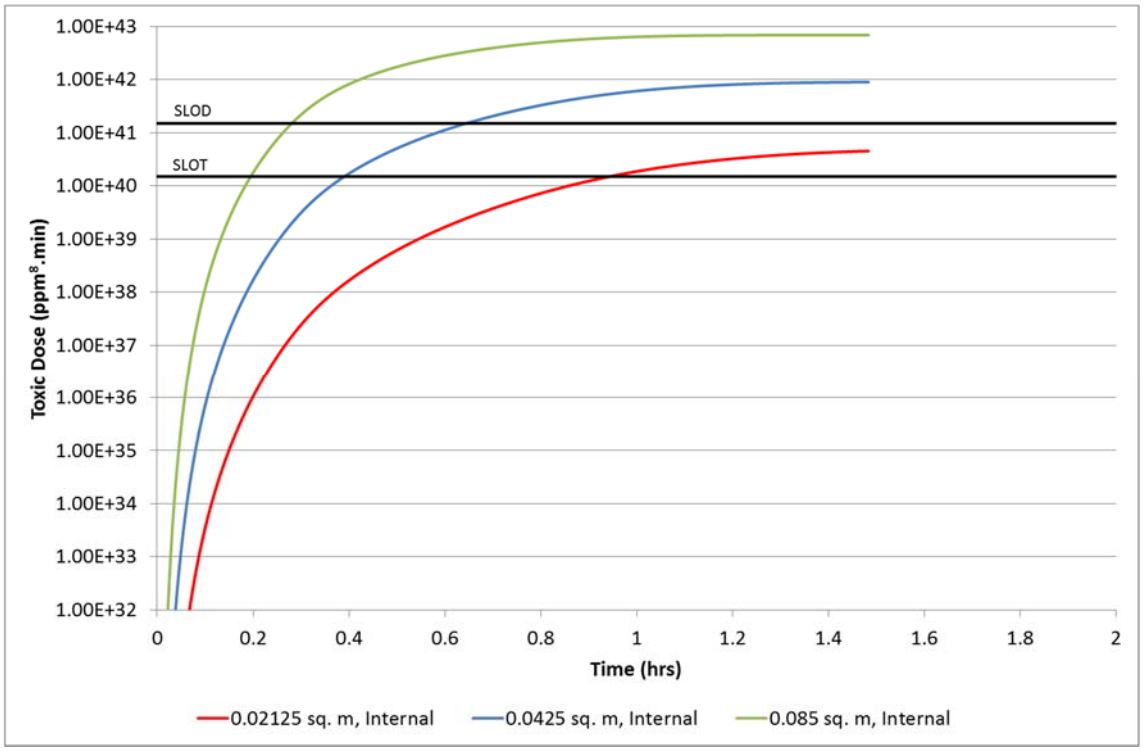

Figure 9.19: Dose Received by a Building Occupant with Time and Window Area for Case 1

Lethality

Figure 9.20 shows the chances of lethality for a building occupant, as calculated using the toxic dose for the three window area values given in Table 9.5 for case 1: CO_2 at 30°C in the pipeline, atmospheric conditions 5D (day with 5 m/s wind speed), valve closure after 15 minutes. Lines for the SLOT and SLOD percentages are also shown.

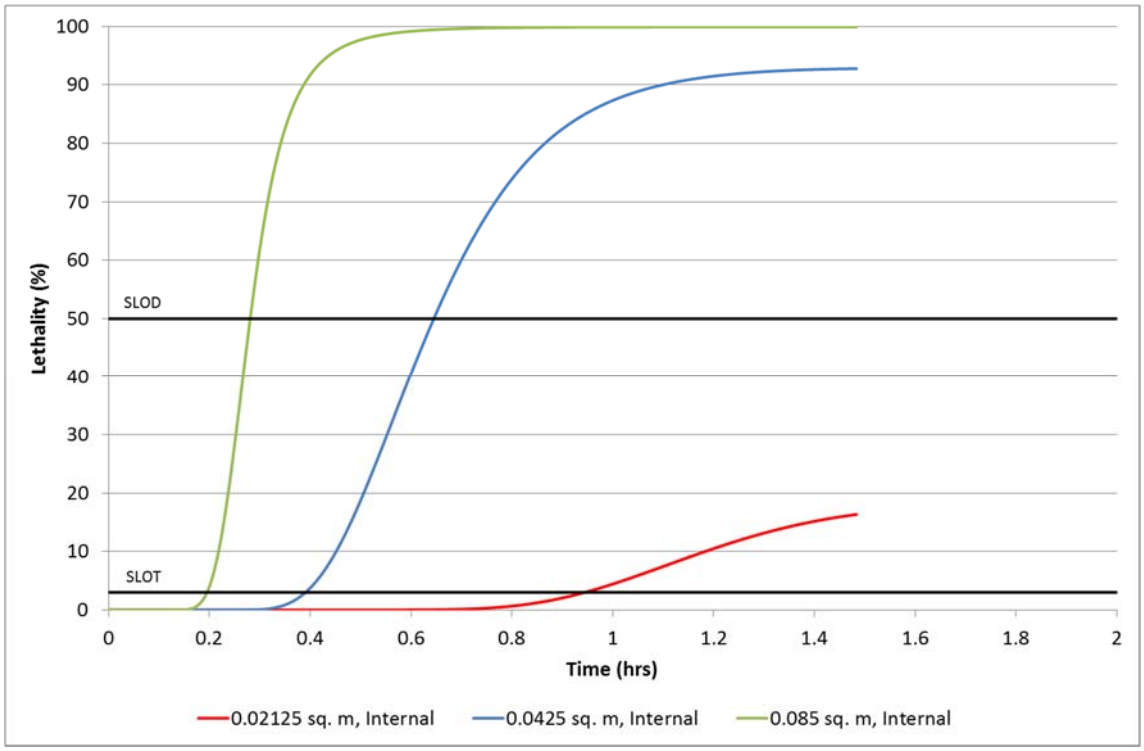

Figure 9.20: Percentage Lethality for a Building Occupant with Time and Window Area for Case 1

A summary of the times taken for the lethality to exceed the SLOT and SLOD percentages of 3% and 50% respectively for each window area considered is given in Table 9.6. Note that in Table 9.6 an entry of "-" indicates that the specific DTL was not exceeded during the course of the simulation.

Dangerous Toxic Load/ Percentage Lethality	Window Area (m^2)	Time (hours)
SLOT	0.02125	0.95
	0.0425	0.39
	0.085	0.20
SLOD	0.02125	-
	0.0425	0.65
	0.085	0.28

Table 9.6: Times until The SLOT and SLOD Dangerous Toxic Loads are Exceeded for Building Occupants with Window Area

From Table 9.6 and the lethality charts, it can be concluded that the time period before a specific percentage lethality is reached within the building in question, decreases with increasing ventilation flow rate (window area). Additionally, the maximum lethality reached over the duration of the simulation increases with increasing ventilation flow rate. The trend is carried through the shelter model as shown in the mean and equivalent concentration and toxic dose charts.

9.4.5 *Phast Examples*

The shelter model can also be used with output data from the industry hazard analysis software tool Phast (Anon., 2011b). In a similar way to the DNV-GL model, the Phast tool can be used to model the dispersion of a cloud of released CO_2 providing values for atmospheric CO_2 concentration and vapour temperature with distance away from the release. An example analysis using Phast data in the shelter model has been performed in order to demonstrate this functionality. Phast simulations of a dense phase CO_2 pipeline rupture have been performed for the study by HSL (Gant, 2014). The Phast tool models time-varying releases from pipelines in a different way to the DNV-GL model used in sections 9.4.1 and 9.4.2. There are two possible simulation methods:

1. The release is modelled using a single discharge rate calculated from the average over the first 20 seconds of the release. In this method, for any particular distance from the release, the external concentration of CO_2 is constant with time for the duration of the simulation.

2. The release is modelled using a time-varying discharge rate. The duration of the simulation is split into ten segments, each using a different release rate which diminishes over time.

For the example study, a single rupture event has been simulated twice, using each of the possible methods. Results were provided for a distance of 100 m from the source of the release along the centreline axis. The simulation case modelled by Phast for this investigation was that of a downward generic dispersion in 2F atmospheric conditions (night with 2 m/s wind speed). Table 9.7 provides the input details of the simulation:

Input	Value
Pipeline Length	96 km
Pipeline Outside Diameter	610 mm
Pipeline Wall Thickness	19.4 mm
Atmospheric Conditions	2F
Wind Speed	2 ms^{-1}
Material	Carbon Dioxide
Concentration Calculated at Height	1 m

Table 9.7: Phast Input Conditions

The shelter model has been applied to the results from the Phast tool. For comparison, the CO_2 cloud dispersion has been modelled until the external CO_2 concentration would have returned to pre-release levels in both cases. In contrast to the DNV-GL model, Phast provides only one value for atmospheric CO_2 concentration in addition to the external temperature. Consequently, the same value of external CO_2 concentration has been used for the calculation of air flow rates between the internal and external atmospheres as was used to calculate the toxic dose and lethality in the shelter model. The remaining input conditions and assumptions used for the shelter model are the same as those used for the DNV-GL cases and are detailed in section 9.4.1 and Table 9.2.

9.4.6 *Phast Results*

The change in internal CO_2 concentration and temperature with time has been modelled for a building, located at a distance of 100 m along the centreline axis from the source of the release, using the shelter model with Phast simulations.

Concentration

Figure 9.21 shows the change in internal concentration of CO_2 calculated using the shelter model at a distance of 100 m from the release, for the example Phast simulations. The external concentration with time is also shown.

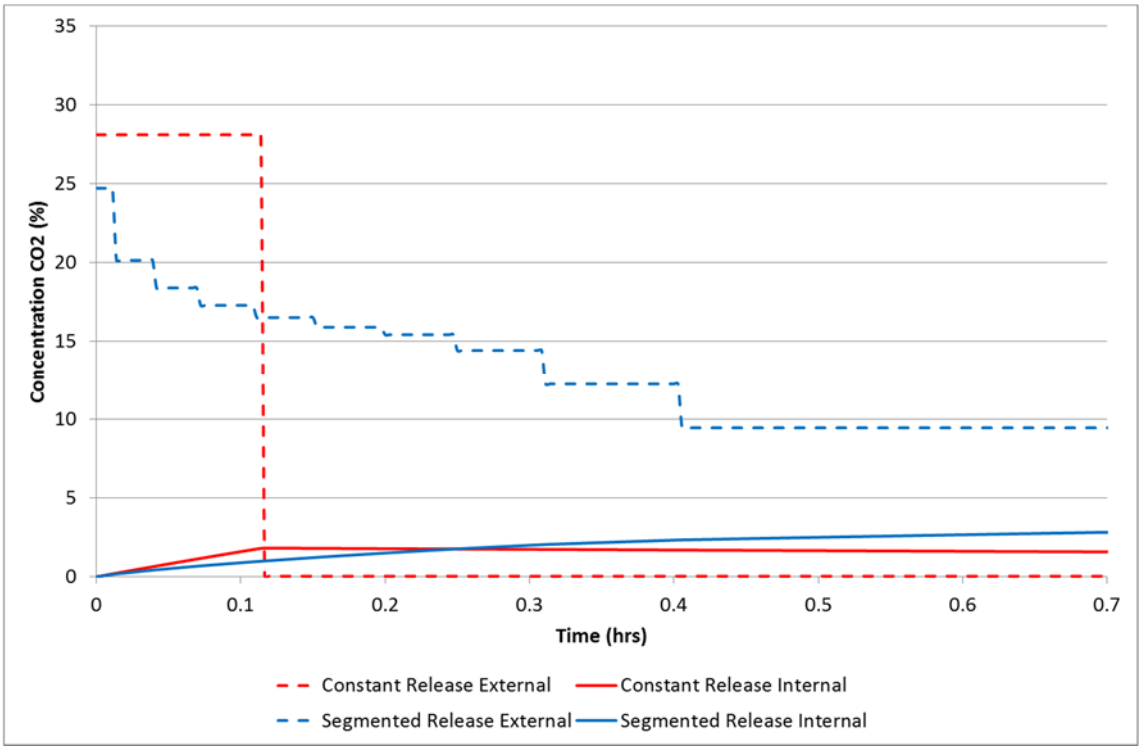

Figure 9.21: Change in Internal CO_2 Concentration with Time for Example Phast Cases

Temperature

Figure 9.22 shows the change in internal temperature calculated using the shelter model at a distance of 100 m from the release, for the example Phast simulations. The external temperature with time is also shown.

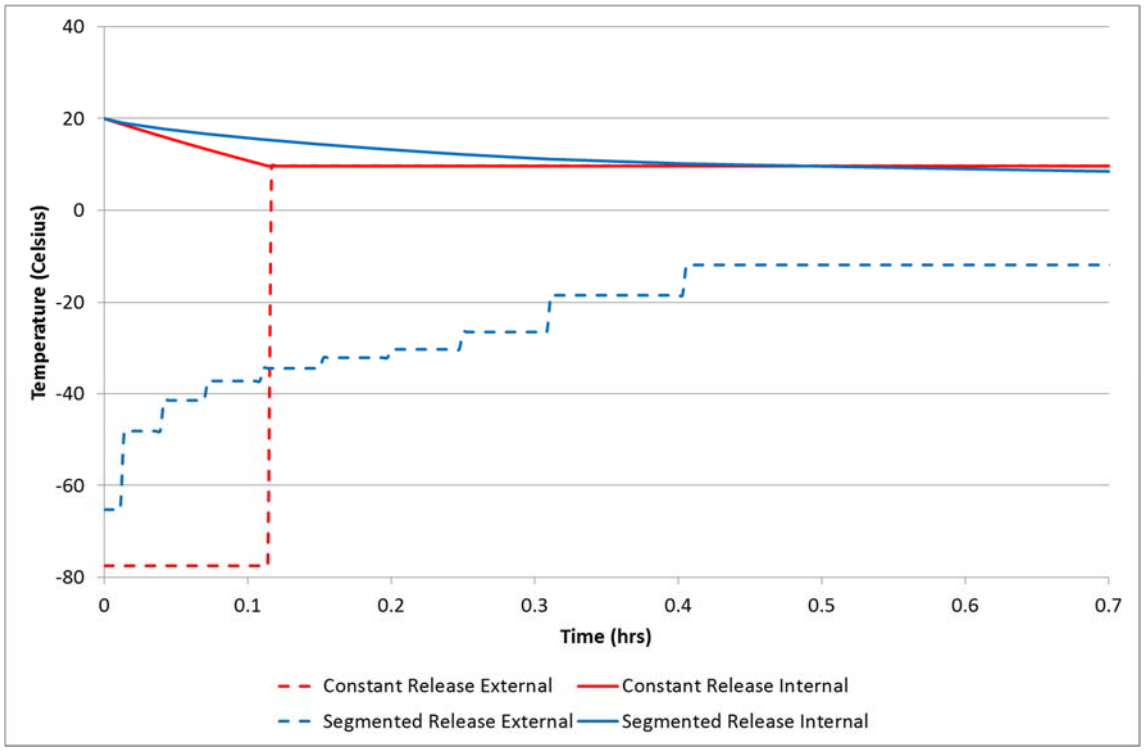

Figure 9.22: Change in Internal Temperature with Time for Example Phast Cases

Toxic Dose

Figure 9.23 shows the CO_2 dose that a building occupant would receive, as calculated using the internal concentration from the shelter model at a distance of 100 m from the release, for the example Phast simulations. Lines for the SLOT and SLOD DTLs are also shown.

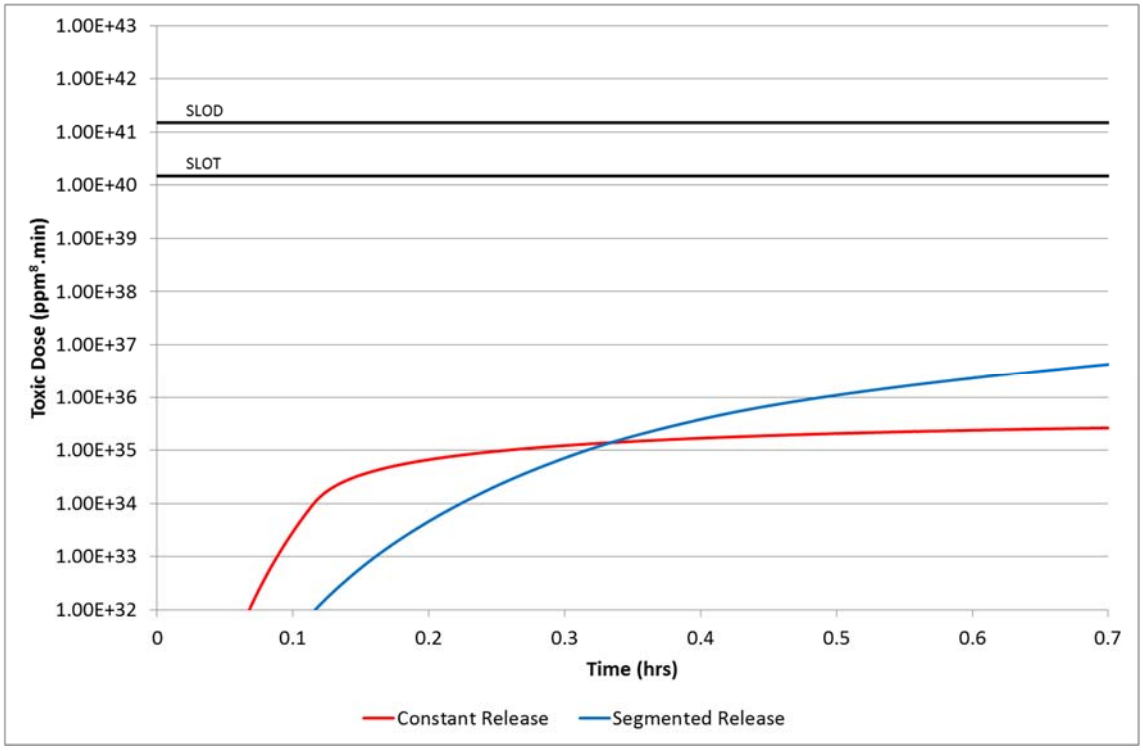

Figure 9.23: Dose Received by a Building Occupant with Time for Example Phast Cases

Lethality

Figure 9.24 shows the chances of lethality for a building occupant, as calculated using the toxic dose at a distance of 100 m from the release, for the example Phast simulations. Lines for the SLOT and SLOD DTLs are also shown.

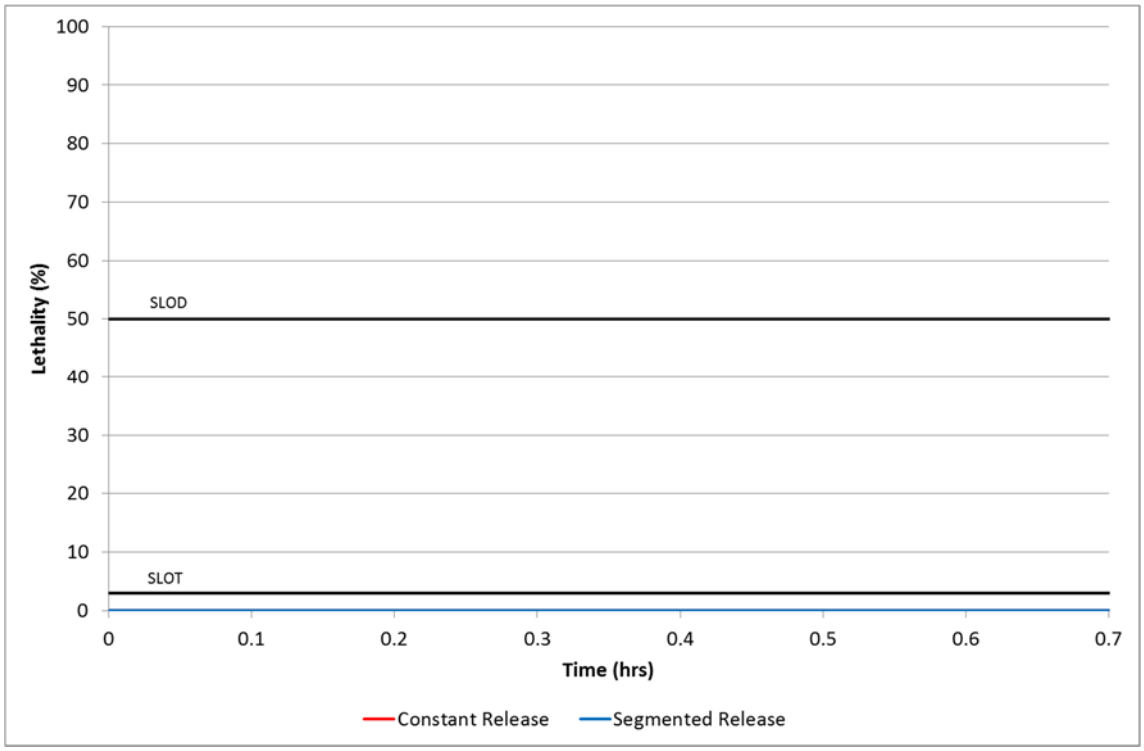

Figure 9.24: Percentage Lethality for a Building Occupant with Time for Example Phast Cases

From Figure 9.23 it is clear that the CO_2 dose received by building occupants increases quickest for the constant release case, in which the external concentration of CO_2 remains at its initial, highest value for the duration of the release (Figure 9.21). However, because the release rate is so high in this case, the volume of CO_2 in the pipeline is discharged very quickly and the external concentration returns to pre-release levels after only 0.12 hours. After this point the internal concentration begins to fall and this is reflected in Figure 9.23 as the increase in CO_2 dose is considerably less. For the segmented release case, the initial build-up of CO_2 in the building is slower (Figure 9.21), but the extended duration of an elevated external CO_2 concentration (Figure 9.23) means that the maximum CO_2 dose building occupants receive, exceeds that of the constant release case. Neither of the cases reach either the SLOT or SLOD DTLs and therefore the lethality remains low for both cases. The segmented release case

is a more realistic representation of a true rupture incident than the constant release case.

9.5 Shelter Model Conclusions

In this chapter the development of a shelter model for the prediction of the casualty probability for persons indoors subjected to a dispersing cloud of CO_2 vapour has been considered. The shelter model has demonstrated the ability to calculate a distance within the hazard range at which a building can provide safe shelter. The shelter model has been compared with experimental data. The model has demonstrated a clear illustration of the difference between the DNV-GL COOLTRANS model and the industry standard commercial package Phast.

In terms of the model results when applied to the DNV-GL dispersion predictions, the calculated mean and equivalent internal concentrations were found to follow a trend of diminishing increase for all of the simulated rupture cases analysed using the model. Conversely, the calculated internal temperature was found to follow a trend of diminishing decrease for all of the simulated rupture cases analysed.

The analysis suggests that a decrease in the temperature of CO_2 in the pipeline may lead to worse consequences for nearby building occupants in the event of a rupture. However, it can be concluded that shut-off valves can be used to reduce the consequences. A rupture in atmospheric conditions of 2F (night with 2 m/s wind speed) would also have fewer consequences for nearby building occupants than an identical rupture in 5D conditions (day with 5 m/s wind speed).

It can be concluded that the time period before a specific percentage lethality is reached within the building in question, increases with distance from the source of the release; and the maximum lethality reached over the duration of the simulation decreases with distance from the source of the release. Additionally, the time period before a specific percentage lethality is reached decreases with increasing ventilation flow rate (window area); and the maximum lethality

reached over the duration of the simulation increases with increasing ventilation flow rate.

It is noted that for each case performed as part of the analysis the building was located downwind on the centreline axis. This is considered to be the worst case direction and the results produced may be different for a building located crosswind or upwind. It is recommended that buildings located in different directions be considered as part of future work.

In order to fully investigate the possibility that a decrease in the temperature of CO_2 in the pipeline may lead to worse consequences for nearby building occupants in the event of a rupture, it is recommended that a more comprehensive sensitivity study into CO_2 temperature is carried out.

It is noted that the CO_2 cloud in the analysis was assumed to completely envelope the building, a recommendation for future work would be to consider clouds which only cover a fraction of the building's height. Furthermore, it is noted that the building considered in the analysis was a single cuboid structure and therefore a simplified representation of the majority of buildings which could be occupied. A recommendation for future work would therefore be to introduce partitions within the building to simulate different rooms, thereby refining the analysis.

Chapter 10. An Escape Model for Consequence Predictions Following A CO_2 Pipeline Release

In Chapter 9 the level of shelter that buildings can provide in the event of a rupture of a dense phase CO_2 pipeline was considered through the shelter model. The potential for escape on foot in these circumstances is considered in Chapter 10, through the development of an escape model.

10.1 Escape Model Background and Development

The escape model considers the potential for escape on foot, of a person located in close vicinity to the rupture of a dense phase CO_2 pipeline. The escaping person will be affected by the increased concentration of CO_2 in the local atmosphere resulting from a cloud of CO_2 released by the pipeline failure. As with the shelter model the concentration of CO_2 in the local atmosphere is transient and will change with time as the CO_2 cloud disperses.

In the escape model a person attempting escape is exposed to the atmospheric concentration of CO_2 at their location. Unlike the shelter model, the escaping person is not located at a fixed distance from the CO_2 release and therefore the concentration of CO_2 he/she is exposed to is determined not only by the dispersion of the CO_2 cloud but also by their position relative to it.

In the escape model a person is assumed to be located at ground level and is given initial location coordinates relative to the location of the pipeline rupture. A constant speed and angle of escape are chosen and the dose of CO_2 the escaping person accumulates over time is calculated based upon their changing location and the changing external concentration of CO_2.

Distances within the model are calculated using trigonometry and the simple equation of motion:

$$s(dt) = v_p.dt \qquad (10.1)$$

Where s is the distance travelled by the escaping person (in m) in the time period dt, v_p is their constant velocity (in ms^{-1}) and dt is the time period under consideration (in s). Hence the model requires that external CO_2 concentration data is provided for both the downwind and crosswind spatial dimensions at close to ground level and also how these data change with time.

If after a set time period the escaping person's location does not coincide with the location of a CO_2 concentration measurement then the concentration at their location is inferred using linear interpolation between the four closest surrounding (in space) concentration values.

For the escape model the method to calculate the toxic dose from exposure to CO_2 and the probit relationship giving the chances of death for an escaping person are identical to those used for the shelter model and detailed in section 9.2.

10.2 Model Simulations

The data from the DNV-GL simulations detailed in section 9.4.1 has also been used as input to the escape model in order to investigate the potential for escape on foot in the event of a real dense phase CO_2 pipeline rupture. The escape model considers an escaping individual moving away from a rupture event and therefore requires the input of atmospheric CO_2 concentration data, as a function of time and distance from the release in two dimensions in the plane of the Earth's surface.

The escape model has been applied to the results of the four simulations produced by DNV-GL using their flat terrain dispersion model developed from the results of COOLTRANS experiments. The input conditions and assumptions made for the simulations are identical to those described in section 9.4.1.

The escape model has been used to demonstrate the differences in the potential for escape which may occur when considering two different variables, these are:

- The initial location of the escaping individual at the time of the release; and
- The direction in which the escaping individual chooses to move

It has been assumed that the initial location of the escaping individual lies exclusively along the centreline axis in the simulated release and is analogous to the way in which building location was used for the shelter model. As with the shelter model, the wind was assumed to be blowing parallel to the centreline axis. For the direction of escape, the investigation has considered two possibilities; downwind escape, in which the individual travels from their initial location in a direction parallel to the centreline axis and directly away from the source of the release; and crosswind escape in which the individual travels from their initial location in a direction which is 90 degrees to the centreline axis. For each case, the direction of escape was set at the start and did not change throughout the course of the simulation. The individual has been assumed to start moving at the exact moment of release and their movement has been modelled until they leave the area covered by the simulation data. In all cases the speed of the escaping individual has been assumed to be 2.5 ms^{-1}. It should be noted that any potential physiological effects of an increasing CO_2 dose are ignored.

As for the shelter model, the data from the DNV-GL simulations includes values for the mean and equivalent atmospheric CO_2 concentrations; and for the external temperature. For the escape model there is no ventilation air flow and therefore the mean CO_2 concentration and external temperature values are redundant. For the cases considered the toxic dose and lethality experienced by the escaping individual are calculated using the equivalent CO_2 concentration.

10.2.1 *Investigation Results*

The effect of atmospheric CO_2 concentration with time on a person escaping either downwind or crosswind from a dense phase CO_2 pipeline rupture, has been modelled for eight starting distances along the centreline axis, using the escape model with the DNV-GL simulations. In each case, following the rupture

there is a period of time before the cloud reaches the escaping individual in which the external CO_2 concentration remains at its initial level. The duration of this time period is determined by; the wind speed, which controls the speed of the released CO_2 cloud; the starting distance of the individual from the rupture; and the direction of escape. The starting distances and escape directions considered and respective times that the CO_2 cloud takes to reach the individual, for each of the wind speeds investigated are shown in Table 10.1. Note that in Table 10.1 an entry of "-" indicates that the individual was able to elude the CO_2 cloud for the entire course of the simulation.

Direction of Escape	Starting Distance (m)	Time at Wind Speed of 2 m/s (s)	Time at Wind Speed of 5 m/s (s)
Downwind	100	-	40
	150	-	60
	200	-	80
	300	-	120
	400	-	160
	500	-	200
	700	-	280
	1000	-	400
Crosswind	100	50	20
	150	75	30
	200	100	40
	300	150	60
	400	200	80
	500	250	100
	700	350	140
	1000	-	200

Table 10.1: Time Taken for CO_2 Cloud to Reach Escaping Individual

Note that while the results of this investigation show that escape is possible downwind from a closer distance to the rupture than is possible crosswind, this is based upon simulations from the DNV-GL flat terrain dispersion model. In real cases, local topography could potentially cause differences in the atmospheric concentration of CO_2 with time and distance, which could in turn result in crosswind escape being safer than downwind.

Toxic Dose – Downwind

Figure 10.1 shows the CO_2 dose that an escaping individual would receive when travelling in the downwind direction, calculated using the escape model for the eight starting distances given in Table 10.1 for case 1: CO_2 at 30°C in the pipeline, atmospheric conditions 5D (day with 5 m/s wind speed), valve closure after 15 minutes. Lines for the SLOT and SLOD DTLs are also shown. Charts for the remaining cases are included in Appendix D .

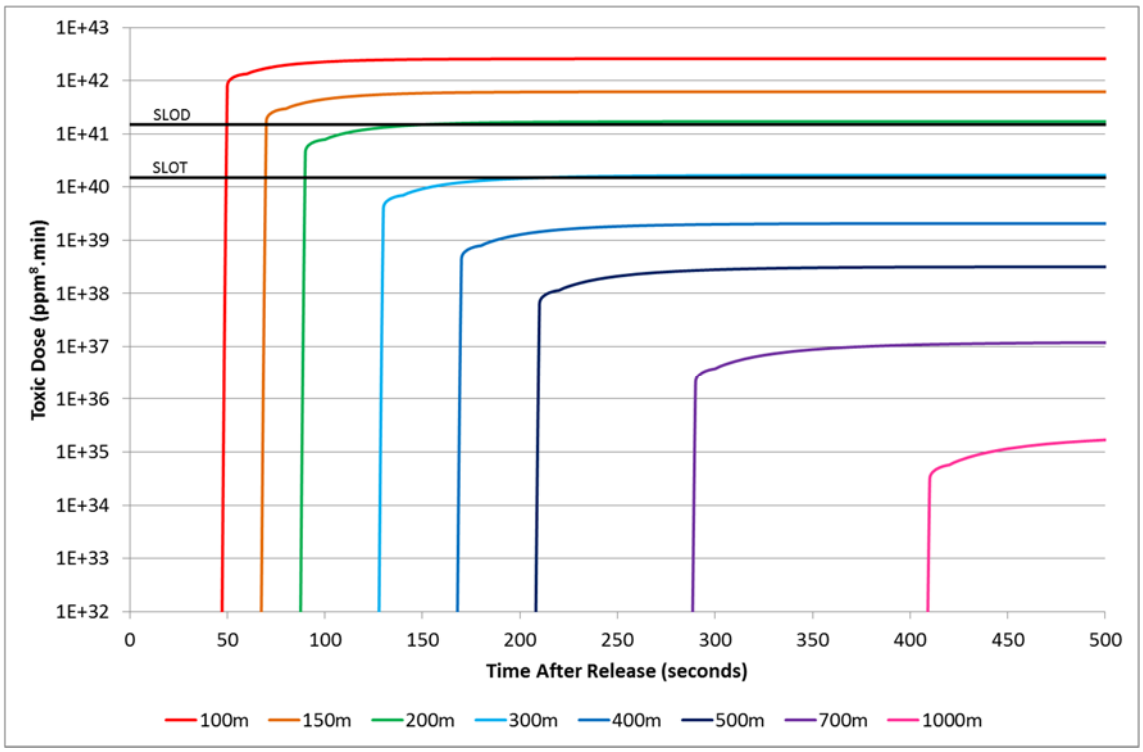

Figure 10.1: Dose Received by an Escaping Individual Travelling Downwind with Time and Distance for Case 1

For the escape model, the escaping individual receives the largest dose of CO_2 immediately after the cloud reaches their position. Following this, the individual (if they were to survive the initial dose) continues their path away from the source of the release. The atmospheric CO_2 concentration to which they are exposed to is reduced and the dose received per unit time decreases. This is reflected in the charts which show that the toxic dose received rapidly approaches a constant once the individual encounters the cloud.

Toxic Dose – Crosswind

Figure 10.2 shows the CO_2 dose that an escaping individual would receive when travelling in the crosswind direction, calculated using the escape model for the eight starting distances given in Table 10.1 for case 1: CO_2 at 30°C in the pipeline, atmospheric conditions 5D (day with 5 m/s wind speed), valve closure after 15 minutes. Lines for the SLOT and SLOD DTLs are also shown. Charts for the remaining cases are included in Appendix D .

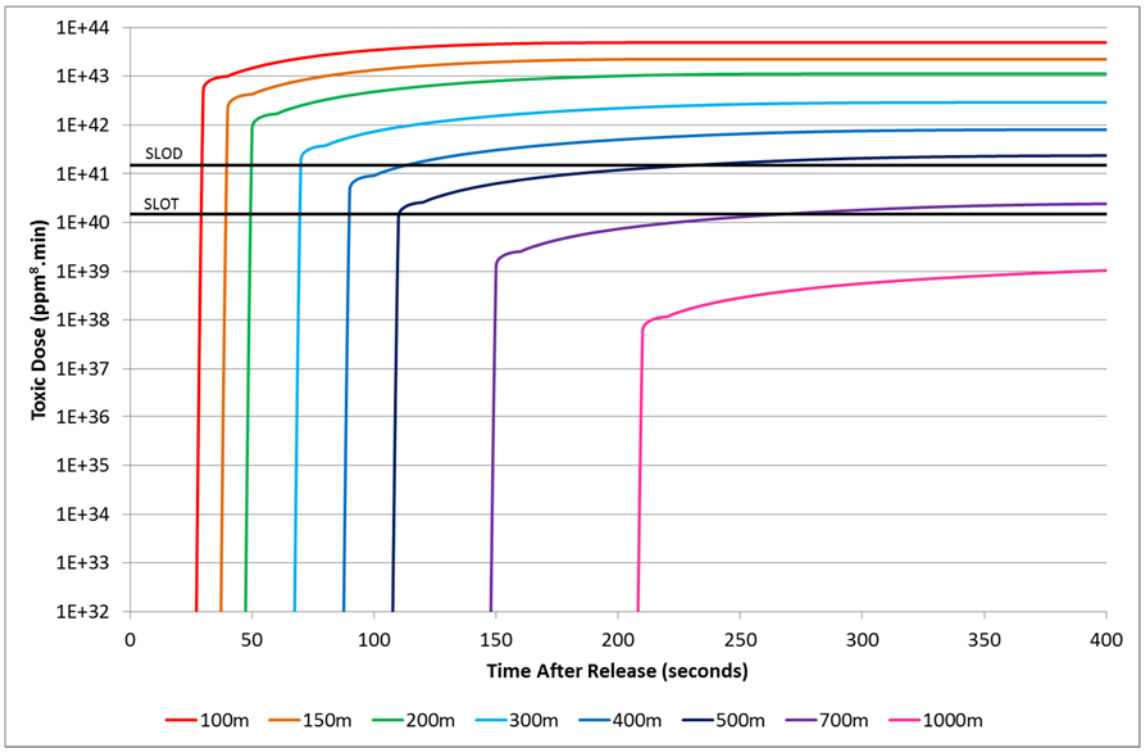

Figure 10.2: Dose Received by an Escaping Individual Travelling Crosswind with Time and Distance for Case 1

In the crosswind direction, the largest dose of CO_2 again occurs immediately after the cloud has reached the escaping individual. In this direction however, the atmospheric CO_2 concentration within the cloud does not decrease as quickly with distance from the starting position as in the downwind direction. As the individual continues their path, they are exposed to high concentrations of CO_2 for longer. This is reflected in the charts which show that the toxic dose received takes longer to approach a constant value than in the downwind analysis.

Lethality – Downwind

Figure 10.3 shows the chances of lethality for an escaping individual when travelling in the downwind direction, as calculated using the toxic dose for the eight distances given in Table 10.1 for case 1: CO_2 at 30°C in the pipeline, atmospheric conditions 5D (day with 5 m/s wind speed), valve closure after 15 minutes. Lines for the SLOT and SLOD percentages are also shown. Charts for the remaining cases are included in Appendix D .

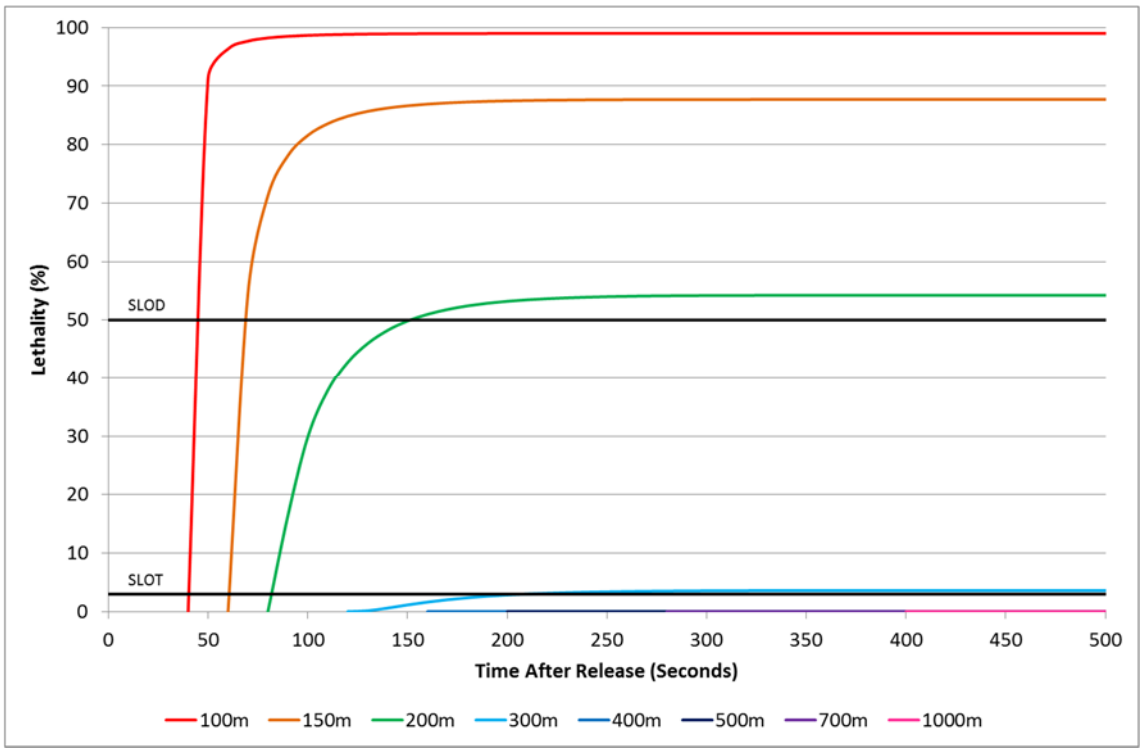

Figure 10.3: Percentage Lethality for an Escaping Individual Travelling Downwind with Time and Distance for Case 1

A summary of the times taken for the lethality to exceed the SLOT and SLOD percentages of 3% and 50% for each case considered is given in Table 10.2. Note that in Table 10.2 an entry of "-" indicates that the specific DTL was not exceeded during the course of the simulation.

Dangerous Toxic Load/ Percentage Lethality	Distance (m)	Time (seconds) Case 1	Case 2	Case 3	Case 4
SLOT	100	50	60	50	-
	150	70	80	70	-
	200	90	100	90	-
	300	210	-	210	-
	400	-	-	-	-
	500	-	-	-	-
	700	-	-	-	-
	1000	-	-	-	-
SLOD	100	50	60	50	-
	150	70	80	70	-
	200	160	-	160	-
	300	-	-	-	-
	400	-	-	-	-
	500	-	-	-	-
	700	-	-	-	-
	1000	-	-	-	-

Table 10.2: Times until The SLOT and SLOD Dangerous Toxic Loads are Exceeded for Downwind Escape

From Table 10.2 and the lethality charts, it can be concluded that the further away from the source the individual begins their escape, the more chance they have of survival for ruptures similar to those of cases 1, 2 and 3. For a case 4 rupture in which the atmospheric conditions are 2F (night with 2 m/s wind speed), the individual travels at a faster speed than the CO_2 cloud and always escapes regardless of their starting position. In cases 1, 2 and 3 it can be seen that for starting distances of less than 200 m from the release, both the SLOT and SLOD DTLs are exceeded at the same time. This highlights the magnitude of the initial CO_2 dose which the escaping individual receives the instant they encounter the cloud. Approximately 50% of the total dose the individual receives throughout the simulation occurs within 20 seconds of the cloud arriving at their position. The maximum lethality reached over the duration of the simulation decreases with starting distance from the source of the release. These trends are due to a reduction in the concentration of CO_2 within the cloud with distance. This behaviour can also be used to explain why the times at

which SLOT and SLOD DTLs are exceeded begin to differ with increasing starting distance.

A decrease in the initial temperature of the CO_2 in the pipeline between 30 degrees and 10 degrees (i.e. the difference between case 1 and case 2) results in little difference for the chances of survival for an individual escaping downwind. A slight increase in the time period before a specific percentage lethality is reached, at each distance; and a reduction in the maximum lethality reached over the duration of the simulation is observed. With reference to the differences observed between the same cases for the shelter model, it is likely that for the escape model, the timescales under consideration are too short for the temperature to have a notable effect.

If shut-off valves are not operated 15 minutes after the release (i.e. the difference between case 1 and case 3) then there is no difference to the chances of survival for an individual escaping downwind. This result is evident from the timescales under consideration. For the escape model the escaping individual, assuming they are able to survive, takes a maximum time of 880 seconds to escape the area covered by the simulation data. This value is less than the 900 seconds (15 minutes) required before valve closure in case 1 and therefore shut-off valve operation cannot influence the chances of escape of the individual.

A change in the atmospheric conditions from 5D to 2F (i.e. the difference between case 1 and case 4) has a large effect on the chances of survival for an individual escaping downwind. Assuming an escape speed of 2.5 ms^{-1}, the individual is easily able to outrun the approaching CO_2 cloud in 2F conditions where the wind speed is only 2 ms^{-1}. In this case, the starting distance of the individual is irrelevant. For 5D conditions, the cloud always reaches the individual eventually and the chances of survival are dependent on the starting position. It can be concluded from this analysis that a rupture in atmospheric conditions of 2F would have fewer consequences for escaping individuals than an identical rupture in 5D conditions.

For a case 1 release, the minimum starting distance for which the toxic dose an individual escaping downwind receives will remain below a SLOT DTL is between 300 m and 400 m. The minimum starting distance for which the dose will remain below a SLOD DTL is between 200 m and 300 m.

For a case 2 release, the minimum starting distance for which the toxic dose an individual escaping downwind receives will remain below a SLOT DTL is between 200 m and 300 m. The minimum starting distance for which the dose will remain below a SLOD DTL is between 150 m and 200 m.

For a case 3 release, the minimum starting distance for which the toxic dose an individual escaping downwind receives will remain below a SLOT DTL is between 300 m and 400 m. The minimum starting distance for which the dose will remain below a SLOD DTL is between 200 m and 300 m.

For a case 4 release, there is no minimum starting distance for which the toxic dose an individual escaping downwind receives will remain below both the SLOT and SLOD DTLs. In the cases with F2 atmospheric conditions an individual escaping downwind always outruns the approaching CO_2 cloud.

Lethality – Crosswind

Figure 10.4 shows the chances of lethality for an escaping individual when travelling in the crosswind direction, as calculated using the toxic dose for the eight distances given in Table 10.1 for case 1: CO_2 at 30°C in the pipeline, atmospheric conditions 5D (day with 5 m/s wind speed), valve closure after 15 minutes. Lines for the SLOT and SLOD percentages are also shown. Charts for the remaining cases are included in Appendix D .

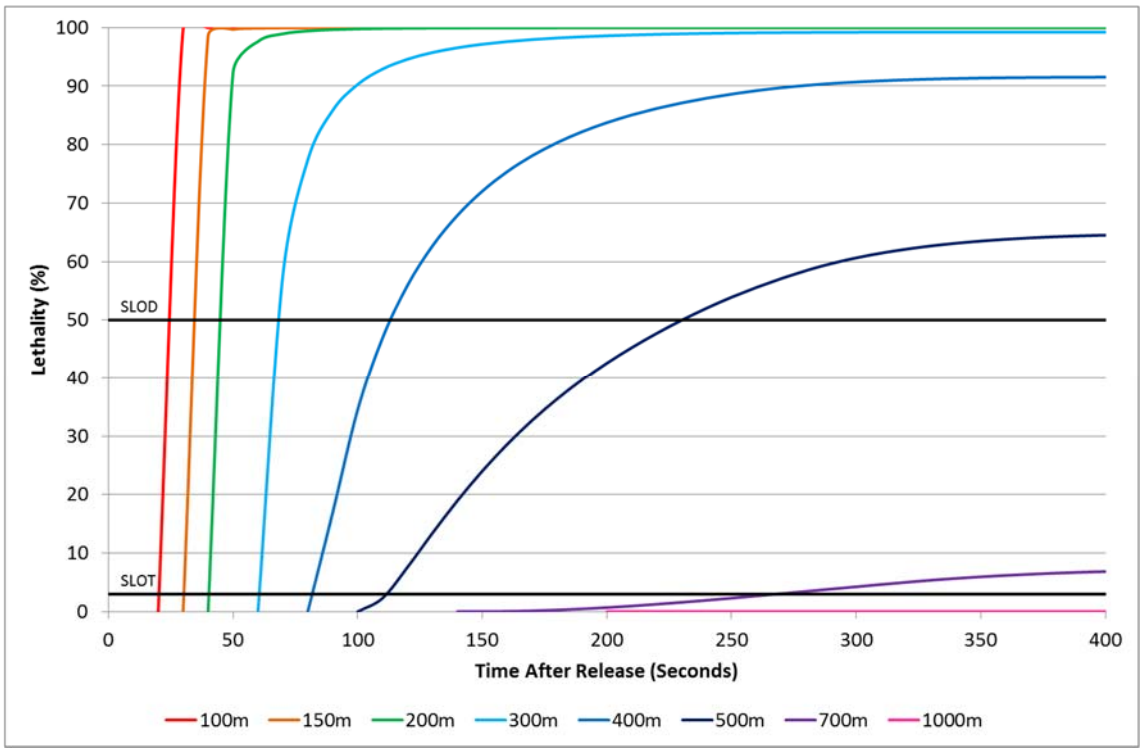

Figure 10.4: Percentage Lethality for an Escaping Individual Travelling Crosswind with Time and Distance for Case 1

A summary of the times taken for the lethality to exceed the SLOT and SLOD percentages of 3% and 50% for each case considered is given in Table 10.3. Note that in Table 10.3 an entry of "-" indicates that the specific DTL was not exceeded during the course of the simulation.

Dangerous Toxic Load/ Percentage Lethality	Distance (m)	Time (seconds) Case 1	Case 2	Case 3	Case 4
SLOT	100	30	40	30	60
	150	40	50	40	85
	200	50	60	50	110
	300	70	80	70	170
	400	90	100	90	250
	500	120	120	120	-
	700	270	-	270	-
	1000	-	-	-	-
SLOD	100	30	40	30	60
	150	40	50	40	85
	200	50	60	50	130
	300	70	80	70	290
	400	120	140	120	-
	500	240	316	240	-
	700	-	-	-	-
	1000	-	-	-	-

Table 10.3: Times until The SLOT and SLOD Dangerous Toxic Loads are Exceeded for Crosswind Escape

Similarly to downwind escape, it can be concluded from Table 10.3 and the lethality charts, that the further away from the source the individual begins their escape crosswind, the more chance they have of survival, for all of the cases considered. For the crosswind analysis, the individual is travelling in an orthogonal direction to the approaching cloud and therefore the cloud is not evaded for a case 4 rupture. It can be seen that for starting distances of less than 400 m from the release in cases 1, 2 and 3 and 200 m from the release for case 4, both the SLOT and SLOD DTLs are exceeded at the same time. This highlights the magnitude of the initial CO_2 dose which the escaping individual receives the instant they encounter the cloud. As with downwind escape, the maximum lethality reached over the duration of the simulation decreases with starting distance from the source of the release because of a reduction in the concentration of CO_2 within the cloud. It was previously noted that the CO_2 concentration within the cloud in the crosswind direction does not decrease as quickly as for the downwind direction. The result of this phenomenon is that the

maximum toxic dose experienced by an escaping individual is far greater in the crosswind direction than in the downwind direction. This is reflected in a comparison between Table 10.3 and Table 10.2 which shows that the number of escape analyses in which DTLs are exceeded is higher for crosswind. It should be noted that this outcome is contrary to normal industry safety procedure which recommends that the best escape route from a release plume is crosswind not downwind. The reason for this is the high value of n_0 specified for CO_2 in the toxic dose equation (9.17).

A decrease in the initial temperature of the CO_2 in the pipeline between 30 degrees and 10 degrees (i.e. the difference between case 1 and case 2) results in little difference for the chances of survival for an individual escaping crosswind. A slight increase in the time period before a specific percentage lethality is reached, at each distance; and a reduction in the maximum lethality reached over the duration of the simulation is observed. The differences between the results are not sufficient to conclude that the initial CO_2 temperature has an effect on crosswind escape. With reference to the differences observed between the same cases for the shelter model, it is likely that for the escape model, the timescales under consideration are too short for the temperature to have a notable effect.

As with downwind escape, if shut-off valves are not operated 15 minutes after the release (i.e. the difference between case 1 and case 3) then there is no difference to the chances of survival for an individual escaping crosswind. This result is due to each analysis being completed before the valves are due to close.

A change in the atmospheric conditions from 5D to 2F (i.e. the difference between case 1 and case 4) has a large effect on the chances of survival for an individual escaping crosswind. The reduced wind speed of 2 ms^{-1} in 2F conditions gives the individual additional time to travel further from their starting position than for the 5D conditions. In this way, when the individual eventually encounters the cloud they will be further from the highest concentrations of CO_2, found on the centreline axis of the release, and therefore more likely to survive the CO_2 dose they receive. Additionally, the maximum concentration of

CO_2 associated with a 2F conditions is less than that associated with 5D. This is reflected in Table 10.3 which shows longer times to each DTL and fewer instances in which a DTL was exceeded for case 4 compared to case 1. It can be concluded from this analysis that a rupture in atmospheric conditions of 2F would have fewer consequences for escaping individuals than an identical rupture in 5D conditions.

For a case 1 release, the minimum starting distance for which the toxic dose an individual escaping crosswind receives will remain below a SLOT DTL is between 700 m and 1000 m. The minimum starting distance for which the dose will remain below a SLOD DTL is between 500 m and 700 m.

For a case 2 release, the minimum starting distance for which the toxic dose an individual escaping crosswind receives will remain below a SLOT DTL is between 500 m and 700 m. The minimum starting distance for which the dose will remain below a SLOD DTL is between 500 m and 700 m.

For a case 3 release, the minimum starting distance for which the toxic dose an individual escaping crosswind receives will remain below a SLOT DTL is between 700 m and 1000 m. The minimum starting distance for which the dose will remain below a SLOD DTL is between 500 m and 700 m.

For a case 4 release, the minimum starting distance for which the toxic dose an individual escaping crosswind receives will remain below a SLOT DTL is between 400 m and 500 m. The minimum starting distance for which the dose will remain below a SLOD DTL is between 300 m and 400 m.

10.3 Escape Decision Tree

When considering the individual consequences to a person in the event of a rupture of a dense phase CO_2 pipeline, the models detailed in Chapter 9 and Chapter 10 can be combined to provide a complete overview of the chances of survival. Figure 10.5 and Figure 10.6 together show an example of the potential choices facing an individual located in the vicinity of a dense phase CO_2

pipeline rupture. These figures show how the shelter and escape models could be linked in order to provide the chances of survival of a person based upon the decisions he/she makes.

Figure 10.5 shows the decision process which can take place at any one instant in time following the rupture. The person may or may not find themselves with an opportunity to enter a nearby building (shelter). A decision is made as to whether the building is entered (if possible). A decision to enter a building would result in the shelter model being employed in order to calculate the dose the person would receive within the building as time passes. A decision to not enter the building (or if there is no building available) would result in another choice for the person, between running and standing still. In this branch of the diagram a person's dose is calculated by the escape model. A decision to stand still would result in an escape speed of 0 ms^{-1} in the escape model, they would be subject to the external concentration of CO_2 in that position until at some later time they decided to run or enter an available nearby building. Conversely, if the person decides to run they must then choose which direction they run in, effectively selecting their angle and escape speed within the model. Running in a particular direction may result in the discovery of a building with the potential for entry.

Figure 10.6 shows an overview of the process with the evolution of time, any one of the grey segments within the diagram represents an instant in time and one cycle of the decision tree in Figure 10.5. The outcome at the end of each time instant will depend on the decisions made within that time instant; and will affect what happens in the next time instant. After any one time instant, the person could be inside and therefore subject to the shelter model; outside and subject to the escape model; or making a switch between the shelter and escape models.

It is recommended that an analysis based upon Figure 10.5 and Figure 10.6 is performed as part of future work in order to further investigate the chances of survival for an individual in the event of a rupture of a dense phase CO_2 pipeline.

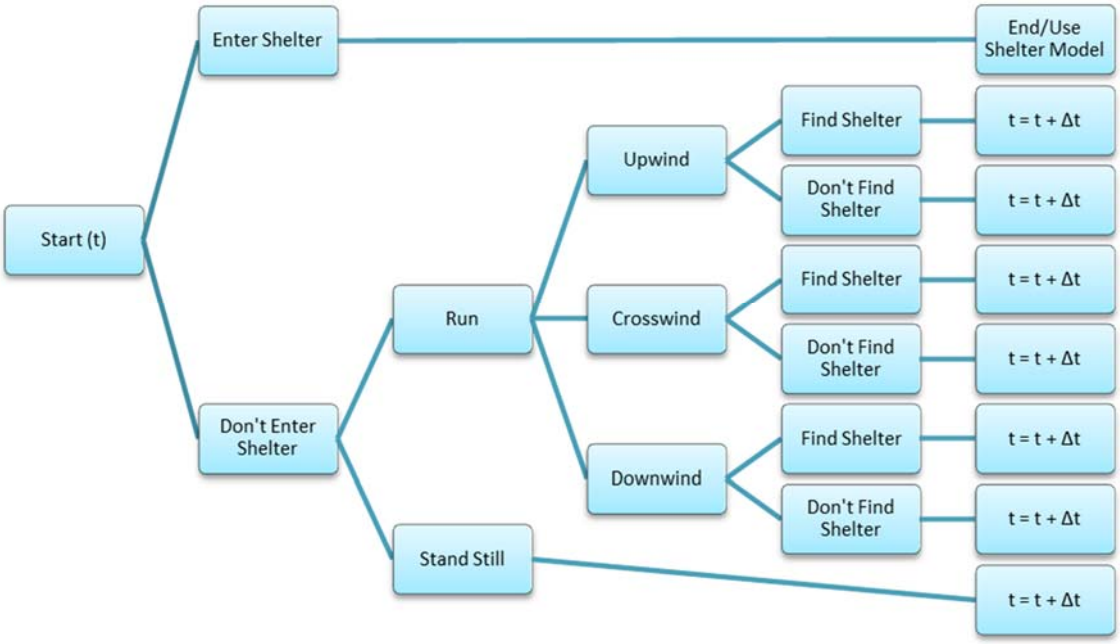

Figure 10.5: Escape Decision Tree – Part A

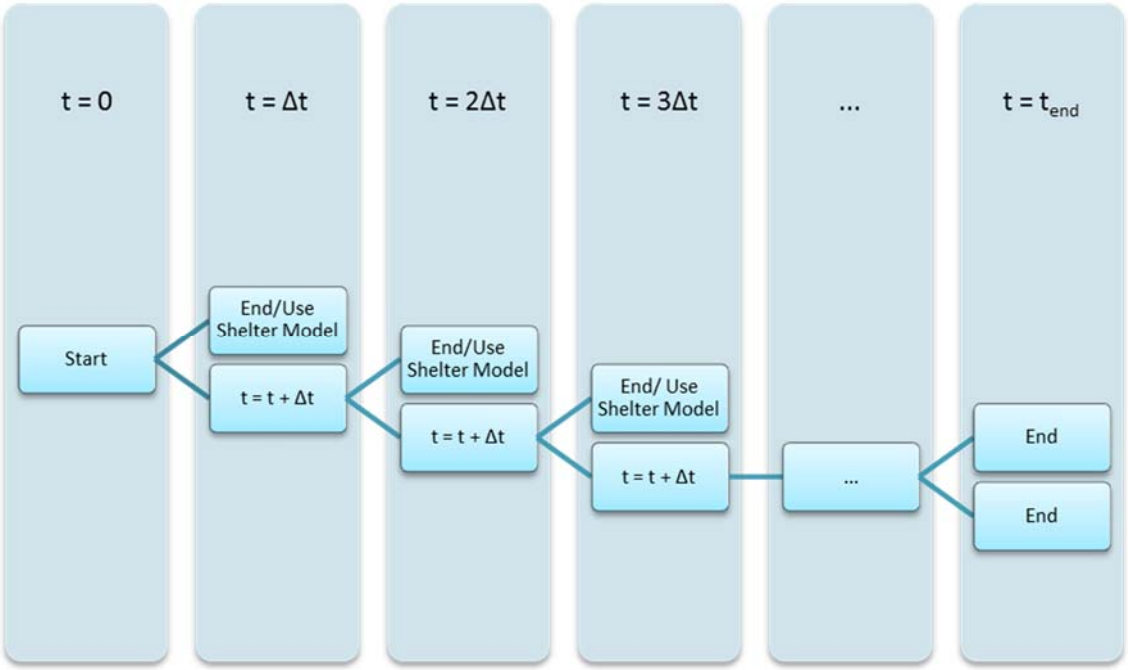

Figure 10.6: Escape Decision Tree – Part B

10.4 Escape Model Conclusions

In this chapter the development of an escape model for the prediction of the casualty probability for persons outdoors subjected to a dispersing cloud of CO_2 vapour has been considered. The escape model has demonstrated the ability to calculate a distance within the hazard range at which it is possible to escape to a safe distance.

In terms of the model results when applied to the DNV-GL dispersion predictions, it is concluded that for all of the simulated rupture cases analysed, an individual escaping receives the largest dose of CO_2 per unit time, immediately after the cloud reaches their position.

When considering downwind escape, the further away from the source the individual begins their escape, the more chance they have of survival for ruptures similar to those of cases 1, 2 and 3. For a case 4 rupture in which the atmospheric conditions are 2F, the individual travels at a faster speed than the CO_2 cloud and always escapes regardless of their starting position. A decrease in the initial temperature of the CO_2 in the pipeline between 30 degrees and 10 degrees results in negligible difference for the chances of survival for an escaping individual. Similarly, the chances of survival are unaffected by the use of shut-off valves within 15 minutes after the release. It can be concluded however, that a rupture in atmospheric conditions of 2F would have fewer consequences for escaping individuals than an identical rupture in 5D conditions.

When considering crosswind escape, the further away from the source the individual begins their escape, the more chance they have of survival for all of the simulated rupture cases considered. The CO_2 concentration within a cloud released in a rupture event does not decrease as quickly with distance in the crosswind direction as in the downwind direction. The result of this phenomenon is that the maximum toxic dose experienced by an escaping individual is far greater in the crosswind direction than in the downwind direction. It should be noted that this outcome is contrary to normal industry safety procedure which recommends that the best escape route from a release plume is crosswind not

downwind. The reason for this is the high value of n_0 specified for CO_2 in the toxic dose equation (9.17). As with the downwind case, a decrease in the initial temperature of the CO_2 in the pipeline between 30 degrees and 10 degrees results in negligible difference for the chances of survival for an escaping individual crosswind. Similarly, the chances of survival are unaffected by the use of shut-off valves within 15 minutes after the release; and a rupture in atmospheric conditions of 2F would have fewer consequences for escaping individuals than an identical rupture in 5D conditions.

It is recommended that future work consider the effects of local topography on the atmospheric concentration of CO_2 with time and distance; and the physiological effects of an increasing CO_2 dose, with respect to the potential for escape. An analysis linking the shelter and escape models together should also be performed in order to provide a more comprehensive description of an individual's behaviour in the event of a the rupture of a dense phase CO_2 pipeline and to calculate more accurate values for the chances of survival.

Chapter 11. Conclusions and Recommendations for Further Work

11.1 Conclusions

This thesis has presented the development of failure frequency, shelter and escape models to be used as part of the QRA methodology for dense phase CO_2 pipelines.

11.1.1 *Failure Frequency Model*

The failure frequency model has been named AFFECT. The model is used to calculate the failure frequency of a dense phase CO_2 pipeline due to third party external interference. The need to develop a failure frequency model arose from the design requirements for dense phase CO_2 pipelines. For oil and natural gas pipelines, the frequency of pipeline failure due to third party external interference is calculated using models based upon structural reliability methods. These models combine semi-empirical pipeline failure models with probability distributions derived from historical operational damage data. Dense phase CO_2 pipelines require the use of thick wall linepipe in pipeline construction, potentially with wall thickness dimensions outside the limits of operational experience for oil and natural gas. The reliance of the current failure frequency models on empirical data and semi-empirical relations suggested their application to dense phase CO_2 pipelines may be inappropriate.

There was a desire however to extend the use of structural reliability methods to calculate failure frequency for dense phase CO_2 pipelines. These methods have been employed for over 25 years, and as a result are tried, tested and well understood. A review of the available failure frequency models was therefore performed in order to assess their applicability to dense phase CO_2 pipelines. This review concluded that the applicability of structural reliability methods to thick wall pipelines depends entirely upon the applicability of the pipeline failure models and operational damage data contained within them.

A review of the available failure models and operational data was performed. The review considered the suitability of the models and data for inclusion into a failure frequency model and their applicability to thick wall pipelines. It was concluded that the NG-18 equations and generic assessment codes such as BS 7910 were suitable models to be used to describe the failure of gouges and leak / rupture behaviour in a failure frequency model based on structural reliability methods. It was also concluded that the British Gas Dent-Gouge Fracture Model (BGDGFM) was the most suitable model to be used to describe the failure of a gouged dent and that the UKOPA Fault Database was the most suitable source of historical operational damage data for the probability distributions.

It was found that the largest wall thickness in the experimental tests used to derive the NG-18 equations was 21.9 mm for the through-wall equations and 15.6 mm for the part-wall equations. The BS 7910 assessment method is not limited by wall thickness. A study was performed in order to provide a validation of the applicability of the flow stress dependent NG-18 equations to thick wall pipelines; and to compare the accuracy of the flow stress dependent NG-18 equations and the BS 7910 assessment method when applied to thick wall pipe. In this study predicted burst pressures for thick wall pipe were calculated using both the flow stress dependent NG-18 equations and BS 7910 and compared with values from experimental test data. Based upon the comparison with experimental test data, the flow stress dependent NG-18 equations were found to be the most accurate of the two models. From the range of the experimental test data used in the study, the flow stress dependent NG-18 equations are considered to be applicable to pipelines with a wall thickness of up to 47.2 mm, provided the linepipe steel has a high toughness.

It was found that the largest wall thickness in the experimental tests used to derive the BGDGFM was 16.4 mm. The wall thickness of a dense phase CO_2 pipeline could potentially be outside this range of applicability. However, due to complexity of the model and the lack of thick wall experimental data for gouged dents, validation of the BGDGFM for thick wall pipelines was considered to be outside of the scope of this work.

The wall thicknesses contained in the UKOPA Fault Database are limited by operational pipelines. Since there are no dense phase CO_2 pipelines currently in operation the database does not contain data covering the required wall thickness range. At present there is no solution to this problem, however the future construction and operation of dense phase CO_2 pipelines will ensure this data source becomes more relevant with time.

The AFFECT model has been developed using structural reliability methods. The flow stress dependent NG-18 equations have been used to describe the failure of gouges and leak / rupture behaviour in the model and the BGDGFM has been used to describe the failure of a gouged dent. The UKOPA Fault Database has been used as the source of historical operational damage data to derive the required probability distributions. The failure frequency models currently in use within the pipeline industry have been used as a basis for the AFFECT model. The model has been developed by making modifications to the PIE model, a basic failure frequency model which uses the appropriate failure models and historical operational data. The modifications made considered improvements in damage modelling and calculation methods. A statistical analysis of the most recent version of the UKOPA Fault Database was also performed as part of the development process. Each of the modifications is considered to provide improvement to the structure of the AFFECT model.

It is noted that the review of failure frequency models highlighted that in order to describe failures from branches and fittings; and from drilling operations in-error, in a failure frequency model, either separate branch / fitting failure and drill puncture models must be developed; or an additional historical data component is required. The development of such components for AFFECT has not been considered in this thesis.

It was concluded through the development of the AFFECT model and the statistical analysis that differences in the fit of the probability distributions used in a failure frequency model can have a significant effect on the values of failure frequency calculated by that model.

The AFFECT model has been validated through a comparison between model predictions, historical operational data and the current industry standard failure frequency model, FFREQ. When applied to the historical operational data from the UKOPA Pipeline Database, it is concluded that both AFFECT and FFREQ give a good approximation of the number of leak failures. Both models are conservative, however the AFFECT model produced the most accurate results of the two. In terms of ruptures, both AFFECT and FFREQ agree with the overall trend of historical data. Both models are non-conservative, however an accurate comparison with rupture failures is difficult, due to the uncertain nature of the historical operational data. It was noted that development of a separate failure model or historical data component to address severed and broken pipes may be necessary in order to provide a complete description of failure frequency due to third party external interference.

11.1.2 *Shelter Model*

Models have been developed to describe the impact of CO_2 on people sheltering inside buildings and those attempting to escape on foot during a pipeline release event. The need to develop shelter and escape models arose from the hazards and behaviour of dense phase CO_2 in the event of a pipeline rupture, which are significantly different to those of oil or natural gas and therefore not addressed by current models.

The indoor “shelter” model considers the ingress of CO_2 into a building surrounded by an environment with a high CO_2 concentration. The model is based on the principles of natural building ventilation for which air flow is driven by wind effects externally and buoyancy effects internally. The shelter model enables the prediction of the casualty probability for persons indoors subjected to a dispersing cloud of CO_2 vapour. The shelter model has been validated using experimental data and has demonstrated the ability to calculate a distance within the hazard range at which a building can provide safe shelter.

The shelter model has been applied to dispersion predictions made for a number of simulated releases of dense phase CO_2 from a pipeline. When

applied to the dispersion predictions, the internal concentration of CO_2 calculated by the model was found to follow a trend of diminishing increase for all of the simulated rupture cases analysed. Conversely, the calculated internal temperature was found to follow a trend of diminishing decrease for all of the simulated rupture cases analysed.

The analysis suggested that a decrease in the temperature of CO_2 in the pipeline may lead to worse consequences for nearby building occupants in the event of a rupture. However a more comprehensive sensitivity study into CO_2 temperature would be required in order to fully investigate this effect. It has been concluded that shut-off valves can be used to reduce the consequences. A rupture in atmospheric conditions of 2F (night with 2 m/s wind speed) would also have fewer consequences for nearby building occupants than an identical rupture in 5D conditions (day with 5 m/s wind speed).

It was also concluded that the time period before a specific percentage lethality is reached within the building in question, increases with distance from the source of the release; and the maximum lethality reached over the duration of the simulation decreases with distance from the source of the release. Additionally, the time period before a specific percentage lethality is reached decreases with increasing ventilation flow rate (window area); and the maximum lethality reached over the duration of the simulation increases with increasing ventilation flow rate.

It is noted that for each simulated rupture case performed as part of the analysis the building was located downwind on the centreline axis. This is considered to be the worst case direction and the results produced may be different for a building located crosswind or upwind.

It is also noted that the following simplifying assumptions were made as part of the analysis for each simulated rupture case: the CO_2 cloud was assumed to completely envelope the building; and the building considered was a single cuboid structure with no internal partitions.

11.1.3 *Escape Model*

The outdoor “escape” model considers the escape on foot from a moving cloud of CO_2. The model is based upon a simple equation of motion and distances are calculated using trigonometry. The escape model enables the prediction of the casualty probability for persons outdoors subjected to a dispersing cloud of CO_2 vapour. The escape model has demonstrated the ability to calculate a distance within the hazard range at which it is possible to escape to a safe distance.

The escape model has been applied to dispersion predictions made for a number of simulated releases of dense phase CO_2 from a pipeline. When applied to the dispersion predictions it was found that for all of the simulated rupture cases analysed, an individual escaping receives the largest dose of CO_2 per unit time, immediately after the CO_2 cloud reaches their position.

When considering downwind escape, it can be concluded that the further away from the source the individual begins their escape, the more chance they have of survival. A decrease in the initial temperature of the CO_2 in the pipeline between 30 degrees and 10 degrees results in negligible difference for the chances of survival for an escaping individual. Similarly, the chances of survival are unaffected by the use of shut-off valves within 15 minutes after the release. It can be concluded however, that a rupture in atmospheric conditions of 2F would have fewer consequences for escaping individuals than an identical rupture in 5D conditions.

When considering crosswind escape, it can also be concluded that the further away from the source the individual begins their escape, the more chance they have of survival. The CO_2 concentration within a cloud released in a rupture event does not decrease as quickly with distance in the crosswind direction as in the downwind direction. The result of this phenomenon is that the maximum toxic dose experienced by an escaping individual is far greater in the crosswind direction than in the downwind direction. It should be noted that this outcome is contrary to normal industry safety procedure which recommends that the best escape route from a release plume is crosswind not downwind. The reason for

this is the high value of n_0 specified for CO_2 in the toxic dose equation. As with the downwind case, a decrease in the initial temperature of the CO_2 in the pipeline between 30 degrees and 10 degrees results in negligible difference for the chances of survival for an escaping individual crosswind. Similarly, the chances of survival are unaffected by the use of shut-off valves within 15 minutes after the release; and a rupture in atmospheric conditions of 2F would have fewer consequences for escaping individuals than an identical rupture in 5D conditions.

It is noted that the following simplifying assumptions were made as part of the analysis for each simulated rupture case: the local topography was assumed to be perfectly flat; and the physiological effects of an increasing CO_2 dose were ignored.

11.2 Contributions of the Work

In terms of the contributions of this work to the wider body of knowledge of CCS; the failure frequency, shelter and escape models produced in this thesis have been included in the QRA methodology for dense phase CO_2 pipelines developed as part of the COOLTRANS research programme and to be used in planning the construction of dense phase CO_2 pipelines in the UK. Furthermore, the models have been used to inform the QRA studies for the design of the planned National Grid Carbon CO_2 network in the Humber and Yorkshire area of the UK (Barnett, 2014; Cooper, 2014).

In addition, the work has provided further contributions to pipeline defect assessment and failure frequency modelling. It has been shown that the flow stress dependent NG-18 equations are suitable to be applied to pipelines with a wall thickness of up to 47.2 mm, provided the linepipe steel has a high toughness. The review of existing failure frequency models has clearly outlined the structure and the similarities and differences between the various failure frequency models currently in use in the pipeline industry. Furthermore the process of analysing of the UKOPA Fault Database to derive probability distributions for the AFFECT model has been documented in detail for future

reference. The development of the AFFECT model has highlighted potential issues with the current use of failure frequency models, in terms of their treatment of failures resulting from damage to branches and fittings, drilling operations in-error and broken or severed pipelines. It has also been shown that the specific probability distribution fits made to the historical operational damage data in the models can significantly affect the values of failure frequency calculated by those models.

11.3 Recommendations

The recommendations for further work made in this thesis are as follows:

- Further research should be carried out in order to either develop a model to describe gouged dent failure which is applicable to thick wall pipelines; or to validate the current gouged dent models for thick wall pipelines through experimental tests on thick wall pipes with gouged dent defects.
- The Incident-Rates and probability distributions used within the AFFECT model should be regularly updated using the most recent version of the UKOPA database. This will ensure that the data becomes more relevant to dense phase CO_2 pipelines over time as more of those pipelines are constructed and operated.
- With reference to the applicability of the flow stress dependent NG-18 equations to thick wall pipe, further research should be carried out in order to determine the lower limit of material fracture toughness at which it is acceptable to ignore the effect of fracture toughness and brittle fracture.
- Further work should be performed towards investigating the potential error in failure frequencies as a result of interpretation of the UKOPA Fault Database and selecting a distribution fit.
- Either a separate drill puncture model or a separate historical data component should be developed and added to the AFFECT model in order to accurately describe pipeline failures due to drilling operations in-error.

- Either a separate branch or fitting puncture model or a separate historical data component should be developed and added to the AFFECT model in order to accurately describe third party external interference pipeline failures from branches and fittings.
- Either a separate severed or broken pipe failure model or a separate historical data component should be developed and added to the AFFECT model in order to accurately describe pipeline failures resulting in a severed or broken pipeline.
- For the analysis performed using the shelter model it is noted that for each simulated rupture case the building was located downwind on the centreline axis. This is considered to be the worst case direction and the results produced may be different for a building located crosswind or upwind. Buildings located in different directions should therefore be considered as part of further work.
- In order to fully investigate the possibility that a decrease in the temperature of CO_2 in the pipeline may lead to worse consequences for nearby building occupants in the event of a rupture, a more comprehensive sensitivity study into CO_2 temperature should be carried out as part of further work.
- Further work into shelter should consider clouds of CO_2 which cover only a fraction of the height of the buildings used for shelter, rather than completely envelope them.
- Further work into shelter should consider buildings with internal partitions in order to simulate different rooms.
- For the analysis performed using the escape model further work should consider the effects of local topography on the atmospheric concentration of CO_2 with time and distance; and the physiological effects of an increasing CO_2 dose, with respect to the potential for escape.
- Further work should consider an analysis linking the shelter and escape models together in order to provide a more comprehensive description of an individual's behaviour in the event of the rupture of a dense phase CO_2 pipeline and to calculate more accurate values for the chances of survival.

Chapter 12. References

Acton, M. (2011) *Damage Distributions and Hit Rates in FFREQ*. Germanischer Lloyd Industrial Services UK Ltd.

Acton, M., Andrews, R. (2006) *Independent Safety Review of the Onshore Section of the Proposed Corrib Gas Pipeline* (R 8391).

Allason, D., Armstrong, K., Cleaver, P., Halford, A., Barnett, J. (2012) 'Experimental Studies of the
Behaviour of Pressurised Release of Carbon Dioxide', *IChemE Symposium Series*, (No. 158), pp. 142-152.

Anon. (1986) 'R6 rev. 3' *Assessment of the Integrity of Structures Containing Defects*. 1986. British Energy Generation Ltd/BEG(UK)L.

Anon. (1991a) 'ASME B31G-1991' *Manual for Determining the Remaining Strength of Corroded Pipelines, A Supplement to ASME B31 Code for Pressure Piping*. 1991. The American Society of Mechanical Engineers, New York, USA.

Anon. (1991b) 'PD 6493:1991' *Guidance on Methods for Assessing the Acceptability of Flaws in Fusion Welded Structures*. 30 August 1991. British Standards Institution.

Anon. (1992) 'The Tolerability of Risk from Nuclear Power Stations'. 1992. HMSO, London.

Anon. (1993) 'Guidelines on Risk Issues'. 1993. The Engineering Council, London.

Anon. (1995) 'BS 5925:1991' *Code of Practice for Ventilation Principles and Designing for Natural Ventilation*. December 1995. British Standards Institution.

Anon. (1996) *The Pipelines Safety Regulations (SI 1996/825)*.

Anon. (2001a) 'R6 rev. 4' *Assessment of the Integrity of Structures Containing Defects*. 2001. British
Energy Generation Ltd/BEG(UK)L.

Anon. (2001b) 'Reducing Risks, Protecting People. HSE's Decision Making Process'. 2001. HMSO, London.

Anon. (2005) *Onshore Pipeline Quantified Risk Assessment* (368821/D835-01).

Anon. (2007a) 'API 579-1/ASME FFS-1' *Fitness-For-Service*. 5 June 2007. American Petroleum Institute.

Anon. (2007b) 'BS 7910:2005' *Guide to Methods for Assessing the Acceptability of Flaws in Metallic Structures*. 28 September 2007. British Standards Institution.

Anon. (2007c) 'Specification for Line Pipe, ANSI/SPI Specification 5L' Forty-Fourth. October 1 2007. API Publishing Services, 1220 L Street, N. W. Washington D. C. 20005.

Anon. (2009) *Steel Pipelines and Associated Installations for High Pressure Gas Transmission, Recommendations on Transmission and Distribution Practice, IGEM TD/1 Edition 5, Communication 1735*. The Institute of Gas Engineers and Managers.

Anon. (2010) *Minitab 16* (Version 16.1.0) [Computer program]. Minitab Inc.

Anon. (2011a) *8th Report of the European Gas Pipeline Incident Data Group* (EGIG 11.R.0402).

Anon. (2011b) *Phast* (Version 6.7) [Computer program]. DNV Software.

Anon. (2011c) 'UKOPA Pipeline Fault Database (1962 - 2010)'. September 2011. UKOPA.

Anon. (2013) 'PD 8010-3:2009' *Pipeline Systems - Part 3: Steel Pipelines on Land - Guide to the Application of Pipeline Risk Assessment to Proposed Developments in the Vicinity of Major Accident Hazard Pipelines Containing Flammables*. 31 July 2013. British Standards Institution.

Anon. (2014) *Pipeline Ruptures*. Available at: www.neb.gc.ca/sftnvrnmnt/sft/pplnrptr/index-eng.html.

Anon. (2015a) 'PD 8010-1:2015' *Code of Practice for Pipelines - Part 1: Steel Pipelines on Land*. March 2015. British Standards Institution.

Anon. (2015b) *Pipeline Incident 20 Year Trends*. Available at: www.phmsa.dot.gov/pipeline/library/datastatistics/pipelineincidenttrends.

Barnett, J., Cooper, R. (2014) 'IPC2014-33370: The COOLTRANS Research Programme - Learning for the Design of CO2 Pipelines', *10th International Pipeline Conference*. Calgary, Alberta, Canada, September 29 - October 3, 2014.

Butterfield, J.M., Baum, M.R. (1979) 'Studies of the Depressurisation of Gas Pressurised Pipes During Rupture', *Journal of Mechanical Engineering Science*, 21(4), pp. 253-261.

CCSA (2015) *Tackling Climate Change*. Available at: http://www.ccsassociation.org/why-ccs/tackling-climate-change/.

Chaplin, Z. (2012) *Rewriting The PIPIN Code to use a Monte Carlo Solution Approach* (MSU/2012/40).

Chaplin, Z. (2013) *Data Updates to HSE's PIPeline INtegrity Model (PIPIN)* (MSU/2011/34/1).

Cleaver, P. (2013a) 'Input Specification for Test Case 4: Scaled Rupture Experiment, Input Specification for University of Newcastle'. November 2013.

Cleaver, P. (2013b) Input To Allow Predictions To Be Made For Gas Accumulation In The Welding Hut, 29/11/2013.

Cleaver, P. (2014a) 'Data Only-Case study 5-2F-2014 methodology.xlsx'. March 2014. DNV-GL.

Cleaver, P. (2014b) 'Data Only-Case study 5-10deg-2014 methodology.xlsx'. March 2014. DNV-GL.

Cleaver, P. (2014c) 'Data Only-Case study 5-2014 methodology.xlsx'. March 2014. DNV-GL.

Cleaver, P. (2014d) 'Data Only-Case study 5-NoValves-2014 methodology.xlsx'. March 2014. DNV-GL.

Cleaver, P. (2014e) Updated Spreadsheets, 25/03/2014.

Coleman, S.Y. (2013) *Pipeline External Interference Data, Report for Julia Race and Christopher Lyons*.

Cooper, R., Barnett, J. (2014) 'Pipelines for Transporting CO2 in the UK', *12th International Conference on Greenhouse Gas Control Technologies, GHGT-12*. 2013. pp. 2412 - 2431.

Corder, I. (1985a) *Hazard Analysis of The Transmission System - External Interference (Dent and Gouge)* (ERS R.3244).

Corder, I. (1985b) *Hazard Analysis of The Transmission System - External Interference (Gouging)* (ERS R.3015).

Corder, I. (1986) *Hazard Analysis of Transmission System - External Interference* (ERS R.3245).

Corder, I. (1993) *A Users Guide to The Pipeline Failure Frequency Program FFREQ* (ERS R.5004).

Corder, I. (1995a) *The Application of Risk Techniques to The Design and Operation of Pipelines* (C502/016/95).

Corder, I., Chatain, P. (1995b) *EPRG/PRC 10th Biennial Joint Technical Meeting on Line Pipe Research*. Cambridge, UK, April 1995.

Corder, I., Fearnehough, G. D., Knott, R. N. (1992) 'Pipeline Design Using Risk Based Criteria', *Institute of Gas Engineers 129th Annual General Meeting and Spring Conference*. Eastbourne, UK.

Cosham, A. (2001a) *Assessment Methods for Dents and Gouges in Pipelines* (NR99015/4238.1.75/R3).

Cosham, A. (2001b) *Assessment Methods for Dents in Pipelines* (NR99014/4238.1.74/R3).

Cosham, A. (2002) *Assessment Methods for Gouges in Piplines* (NR99013/4238.1.73/R3).

Cosham, A. (2007) *Reduction Factors for Damage due to External Interference* (UKOPA/01-N/BR07084/1).

Cosham, A., Hopkins, P., Leis, B. (2012) 'IPC2012-90459: Crack-Like Defects in Pipelines: The Relevance of Pipeline-Specific Methods and Standards', *9th International Pipeline Conference*.
Calgary, Alberta, Canada, September 24 - 28, 2012.

Davis, P.M., Diaz, J-M., Gambardella, F., Sanchez-Garcia, E., Uhlig, F., den Haan, K., Larive, J-F. (2013) *Statistical Summary of Reported Spillages in 2012 and Since 1971* (12/13).

Demofonti, G., Mannucci, G., Barsanti, L., Spinelli, C.M., Hillenbrand, H.G. (2000) 'Fracture Behaviour and Defect Evaluation of Large Diameter, HSLA Steels, Very High Pressure Pipelines', *3rd International Pipeline Conference*. Calgary, Alberta, Canada, October 1 - 5, 2000.

Downie, M.J., Race, J.M., Seevam, P.N. (2007) 'SPE 109060: Transport of CO2 for Carbon Capture and Storage in the UK', *Offshore Europe 2007*. Aberdeen, Scotland, UK, 4-7 September 2007. SPE International.

Dugdale, D.S. (1960) 'Yielding of Steel Sheets Containing Slits', *Journal of the Mechanics and Physics of Solids*, 8, pp. 100 – 104.

Edwards, A.M., Espiner, R.J., Francis, A., Owen, R. (1998) *A Probabilistic Integrity Assessment in Support of Uprating 10, 11 and 12 Feeders* (R1571).

Espiner, R.J. (1996a) *Calculation of a Dent Depth Distribution for a Pipeline From the Distribution for the Whole System* (R1376).

Espiner, R.J., Francis, A. (1996b) *A Probabilistic Assessment of External Interference on 10, 11 & 12 Feeders* (GRC R1569).

Etheridge, D., Sandberg. M. (1984) 'A Simple Parametric Study of Ventilation', *Building & Environment*, 19(2), pp. 163 - 173.

Etheridge, D., Sandberg. M. (1996) *Building Ventilation: Theory and Measurement*. John Wiley & Sons Ltd.

Francis, A., Miles, T., Chauhan, V. (2004) *A New Limit State Function for the Instantaneous Failure of a Dent Containing a Gouge in a Pressurised Pipeline* (R 7423).

Gant, S. (2014) COOLTRANS Time-Varying Gas Concentrations At 100m For Case Study 5 From Phast, 19/03/2014.

Goodfellow, G., Haswell, J., (2006) 'IPC2006-10507: A Comparison of Inherent Risk Levels in ASME B31.8 and UK Gas Pipeline Design Codes', *6th International Pipeline Conference*. Calgary, Alberta, Canada, September 25-29, 2006.

Goodfellow, G., Turner, S., Haswell, J., Espiner, R. (2012) 'IPC2012-90247: An Update to the UKOPA Pipeline Damage Distributions', *9th International Pipeline Conference*. Calgary, Alberta, Canada, Septermber 24-28 2012.

Halford, A., Mumby, C. (2011) *Investigation of the Shelter Provided by a Building to a Drifting Carbon Dioxide Cloud* (Report Number 9500).

Harris, R.J. (1989) *The Investigation and Control of Gas Explosions in Buildings and Heating Plant*. British Gas Corporation.

Haswell, J.V., Lyons, C. (2008) *Failure Frequency Predictions due to 3rd Party Interference for Corrib Pipeline* (PIE/07/R0176).

Hay, R.J. (1998) *An Independent Detailed Statistical Analysis of Wall Thickness and Material Property Data in Support of The 85 Bar Uprating Programme* (GRTC R2168).

HSE (2003) *Planning Case Assessment Support (PCAS) Chapter 6O: PIPIN Pipeline Failure Frequency Software*.

HSE (2015) *Assessment of the Dangerous Toxic Load (DTL) for Specified Level of Toxicity (SLOT) and Significant Likelihood of Death (SLOD)*. Available at: http://www.hse.gov.uk/chemicals/haztox.htm.

IPCC (2014) *Climate Change 2014: Impacts, Adaptation and Vulnerability. Part A: Global and Sectoral Aspects*. Cambridge University Press, Cambridge, United Kingdom and New York, NY, USA.

Jandu, C., Francini, B., Taylor, M., Francis, A. (2008) 'IPC2008-64304: Towards a New Limit State Function for Determining the Failure Pressure of a Pipeline Containing Mechanical Damage', *7th International Pipeline Conference*. Calgary, Alberta, Canada, September 29 - October 03, 2008.

Keller, H.P., Junker, G., Merker, W. (1987) 'Fracture Analysis of Surface Cracks in Cylindrical Pressure Vessels Applying the Two Parameter Fracture Criterion (TPFC)', *International Journal of Pressure Vessels and Piping*, 29.

Kiefner, J.F., Maxey, W.A., Eiber, R.J., Duffy, A.R. (1973) *The Failure Stress Levels of Flaws in Pressurised Cylinders* (ASTM STP 536).

Kiefner, J.F., Vieth, P.H. (1989) *A Modified Criterion for Evaluating the Strength of Corroded Pipe*.

Lees, F.P. (1996) *Loss Prevention in the Process Industries: Hazard Identification, Assessment and Control*. Second edn. Butterworth - Heinemann.

Linkens, D. (1997) *Gas Pipeline Failure Frequency Predictions - Probabilistic Fracture Models* (Report No. AM5076/RSU8000/R1).

Linkens, D., Shetty, N.K., Bilo, M. (1998) 'A Probabilistic Approach to the Fracture Assessment of Onshore Gas Transmission Pipelines', *Pipes & Pipelines International*, pp. 5-16.

Lyons, C. (2006) *Failure Frequency Prediction for Pipelines Due to 3rd Party Interference* (PIE/2006/R121).

Lyons, C., Haswell, J.V., Hopkins, P., Ellis, R., Jackson, N. (2008) 'IPC2008-64375: A Methodology for The Prediction of Pipeline Faliure Frequency Due to External Interference', *7th International Pipeline Conference*. Calgary, Alberta, Canada, Septermber 30th - October 3rd 2008.

Matthews, Z., Cairns, A. (1984) *Statistical Treatment of Damage Information for The ERS Hazard Analysis Program* (ERS R.3012).

McConnell, R.A. (2012) 'UKOPA Pipeline Exposure for Newcastle University 16 May 2012.xls'. 16 May 2012.

McConnell, R.A., Haswell, J.V. (2011) *UKOPA Pipeline Product Loss Incidents (1962 - 2010)* (UKOPA/11/0076).
Mumby, C. (2012) *Influence of Pipeline Depth of Cover of failure Frequencies due to External Interference* (10074).

Owen, R. (1996) *A Compilation of Data Used in Support of Probabilistic Studies on 10, 11 and 12 Feeders* (GRC R1570).

Race, J.M., Seevam, P.N., Downie, M.J. (2007) 'OMAE2007-29720: Challenges for Offshore Transport of Anthropogenic Carbon Dioxide', *Proceedings of OMAE2007, 26th International Conference on Offshore Mechanics and Arctic Engineering*. San Diego, California USA, June 10-15, 2007.

Seevam, P., Lyons, C., Toft, M., Hopkins, P. (2008) 'IPC2008-64061: Modelling of Dent and Gouges and The Effect on The Failure Probability of Pipelines', *7th International Pipeline Conference*. Calgary, Alberta, Canada, September 29 - October 03, 2008.

Staat, M. (2004) 'Plastic Collapse Analysis of Longitudinally Flawed Pipes and Vessels', *Nuclear Engineering and Design*, 234.

Stern, N. (2006) *STERN REVIEW: The Economics of Climate Change*. HM Treasury Department.

Sturm, D., Stoppler, W. (1990) 'Strength Behaviour of Flawed Pipes under Internal Pressure and External Bending Moment: Comparison between Experiment and Calculation', *International Journal of Pressure Vessels and Piping*, 43.

Wellinger, K., Sturm, D. (1971) 'Festigkeitsverhalten von zylindrischen Hohlkörpern', *Fortschr-Ber VDI-Z*, 5(13).

Wild, F.D. (1994) *Programmers Guide to The Pipeline Failure Frequency Computer Program FFREQ* (ERS R.5043).

Wild, F.D., Corder, I. (1993) *FFREQ* (Version 2.5) [Computer program].

Appendix A Development of the AFFECT Failure Frequency Model for Dense Phase CO_2 Pipelines (Charts)

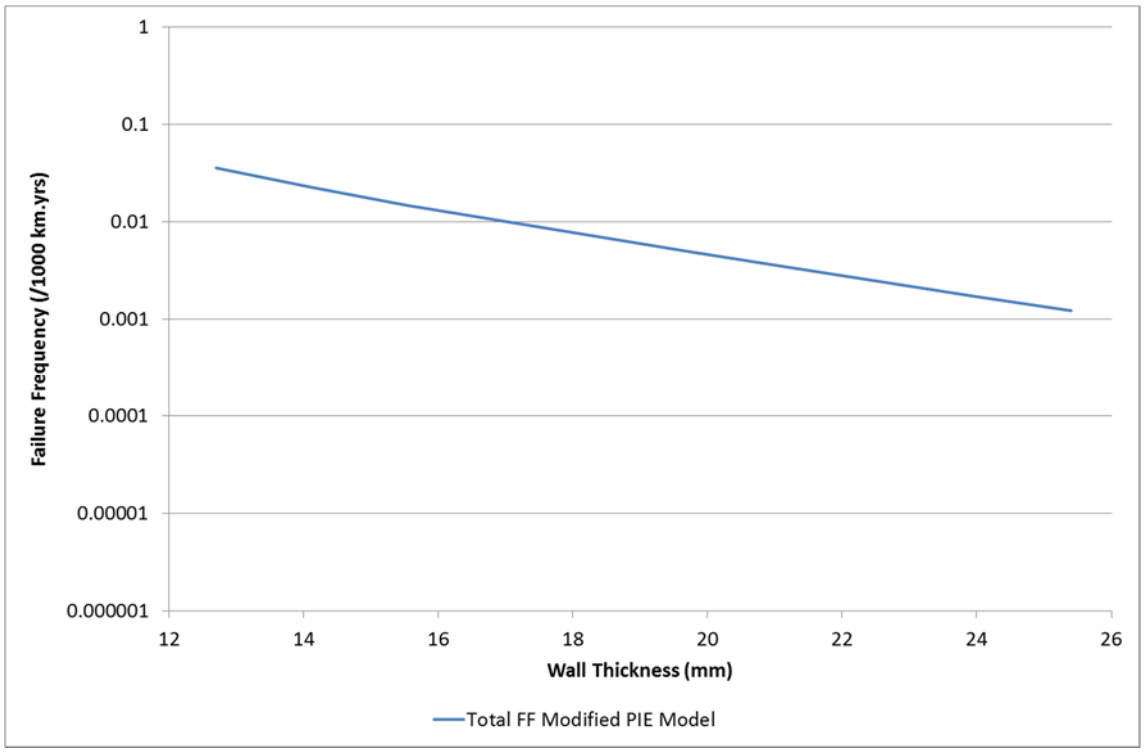

Figure A.1: Total Failure Frequency as Calculated by the Modified PIE Model for Example 1

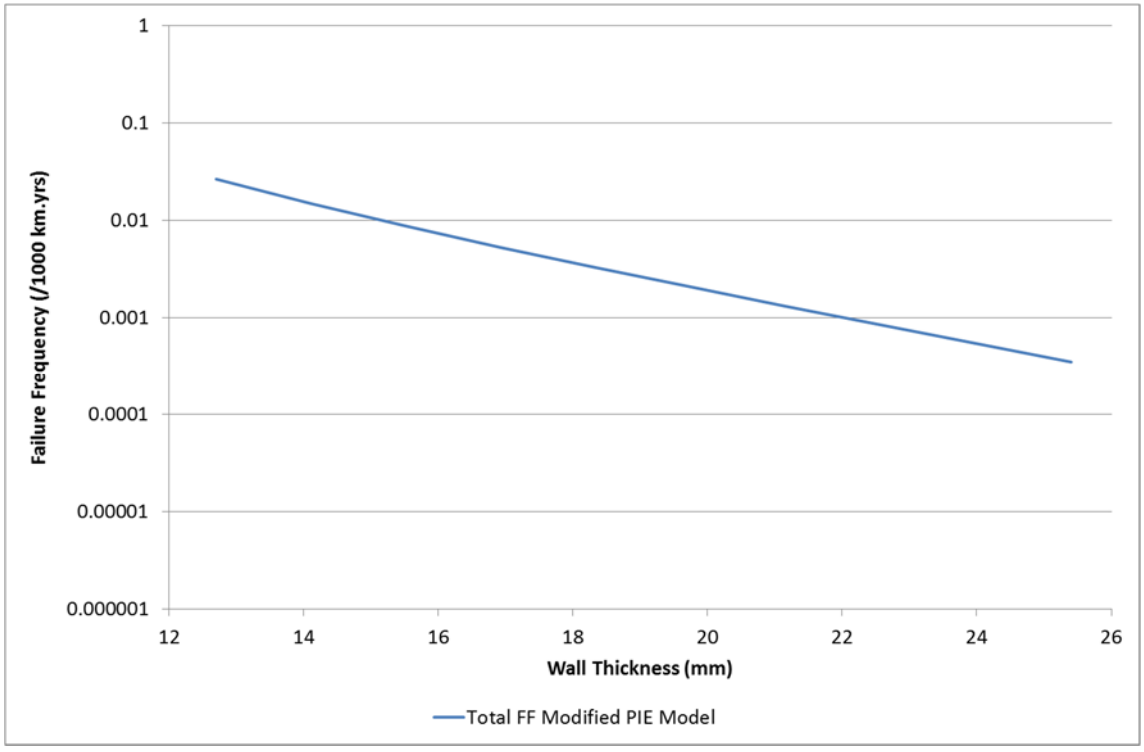

Figure A.2: Total Failure Frequency as Calculated by the Modified PIE Model for Example 2

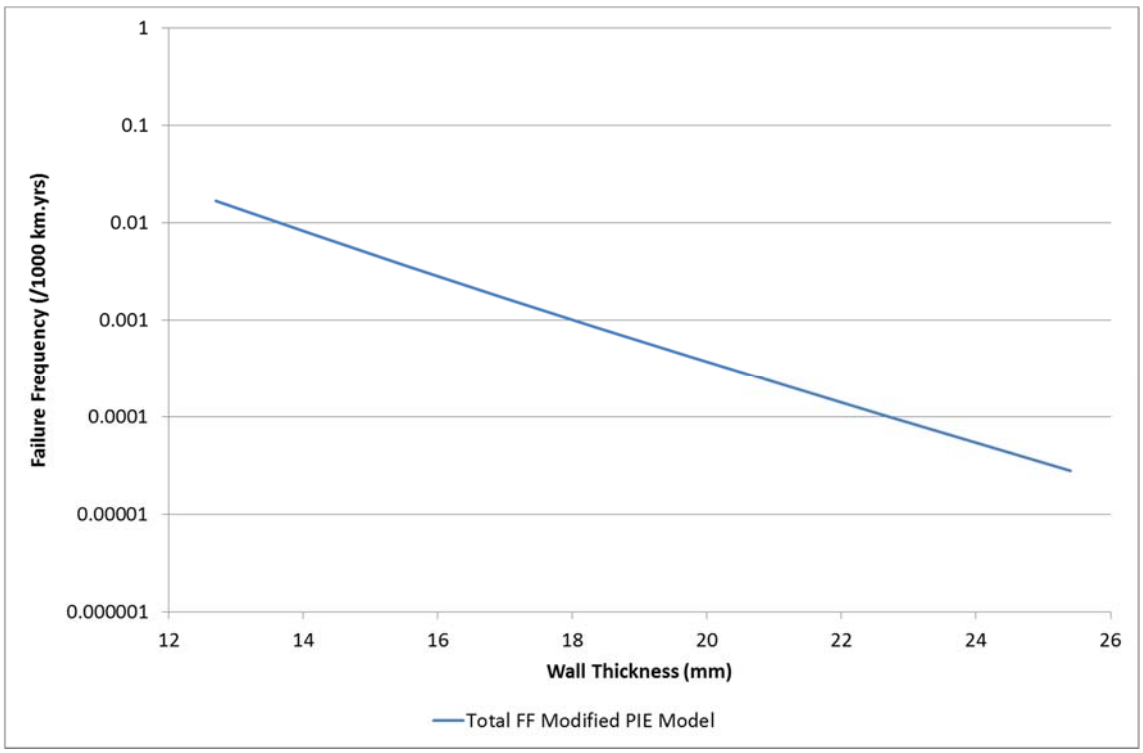

Figure A.3: Total Failure Frequency as Calculated by the Modified PIE Model for Example 3

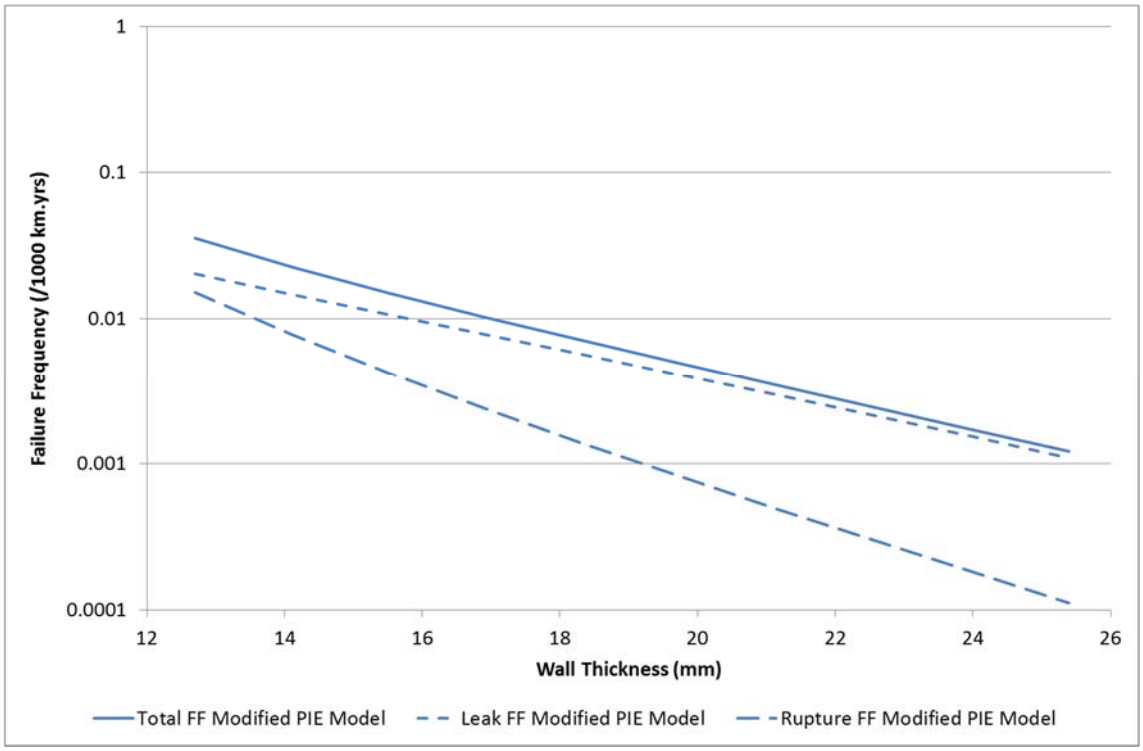

Figure A.4: Leak Rupture and Total Failure Frequency as Calculated by the Modified PIE Model, for Example 1

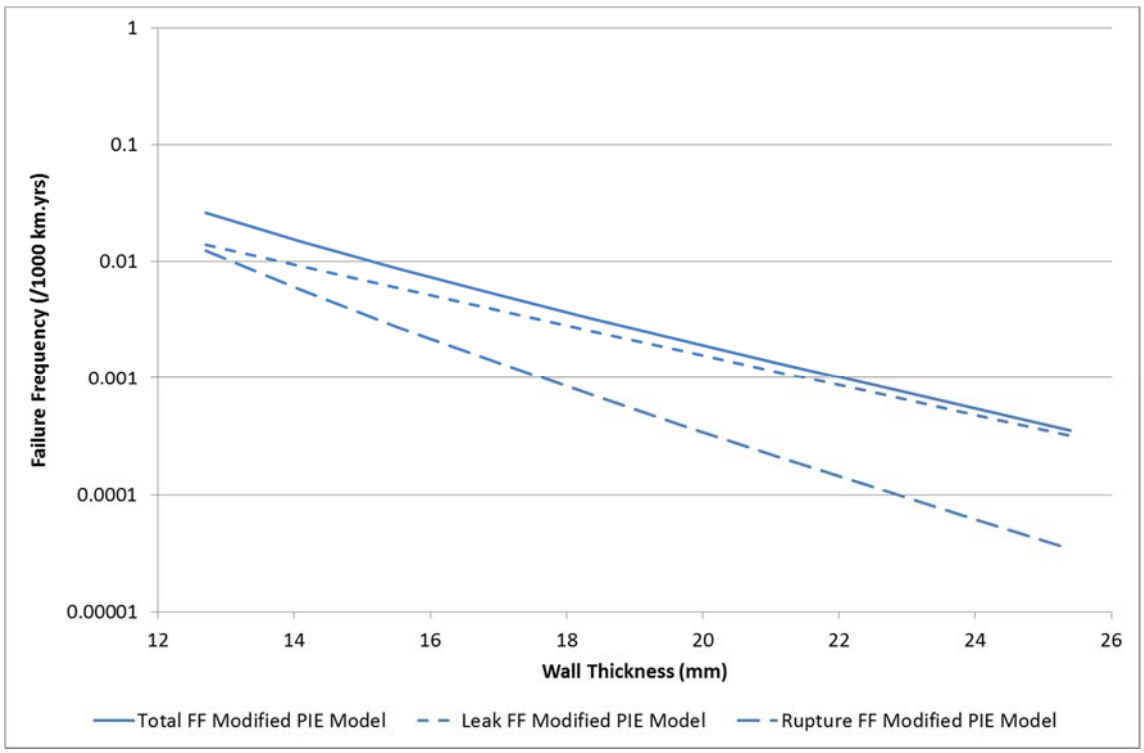

Figure A.5: Leak Rupture and Total Failure Frequency as Calculated by the Modified PIE Model, for Example 2

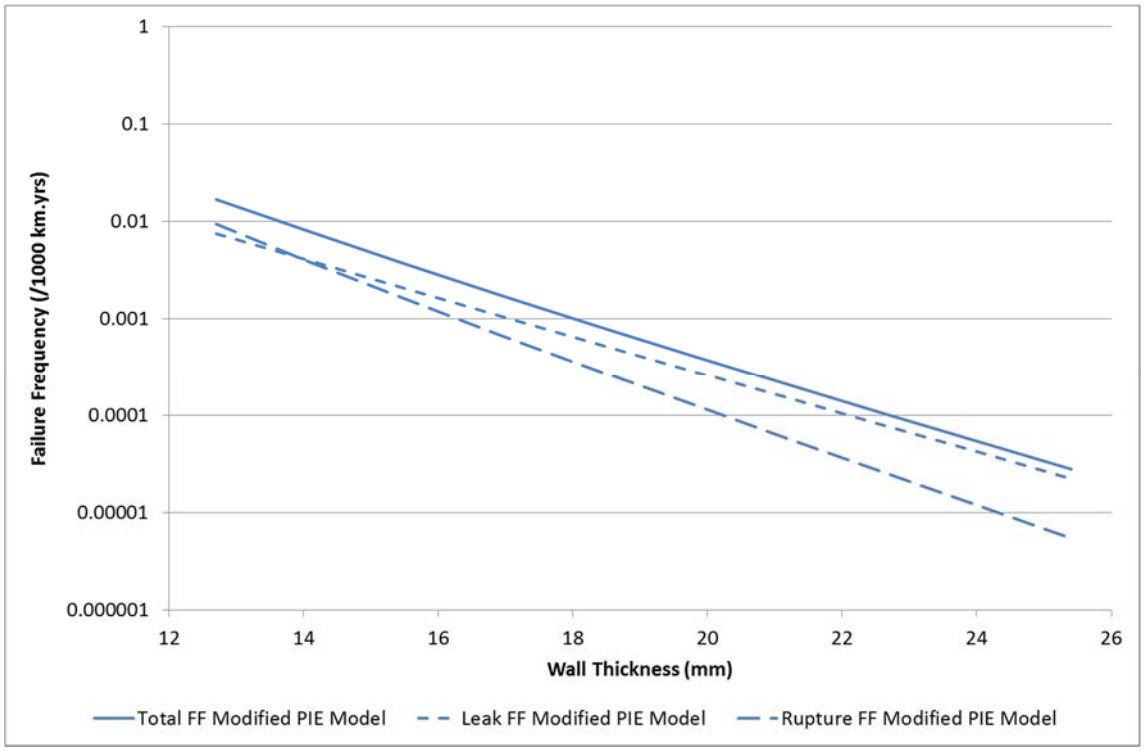

Figure A.6: Leak Rupture and Total Failure Frequency as Calculated by the Modified PIE Model, for Example 3

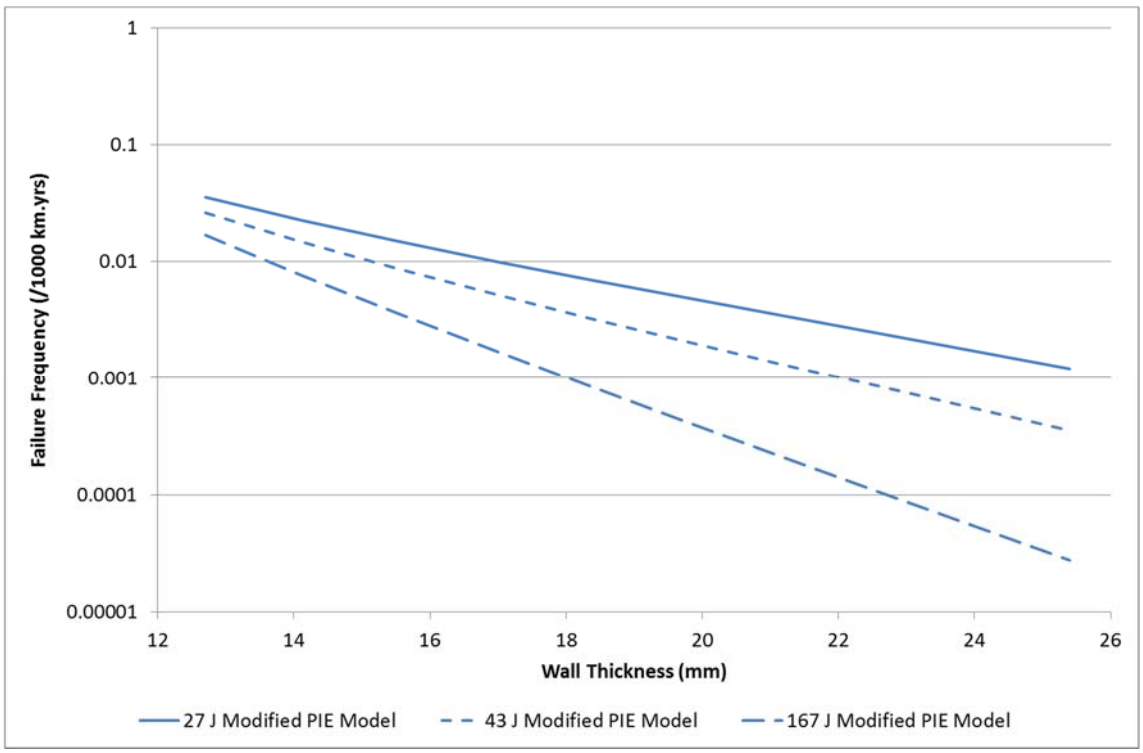

Figure A.7: Total Failure Frequency as Calculated by the Modified PIE Model for Examples 1, 2 and 3

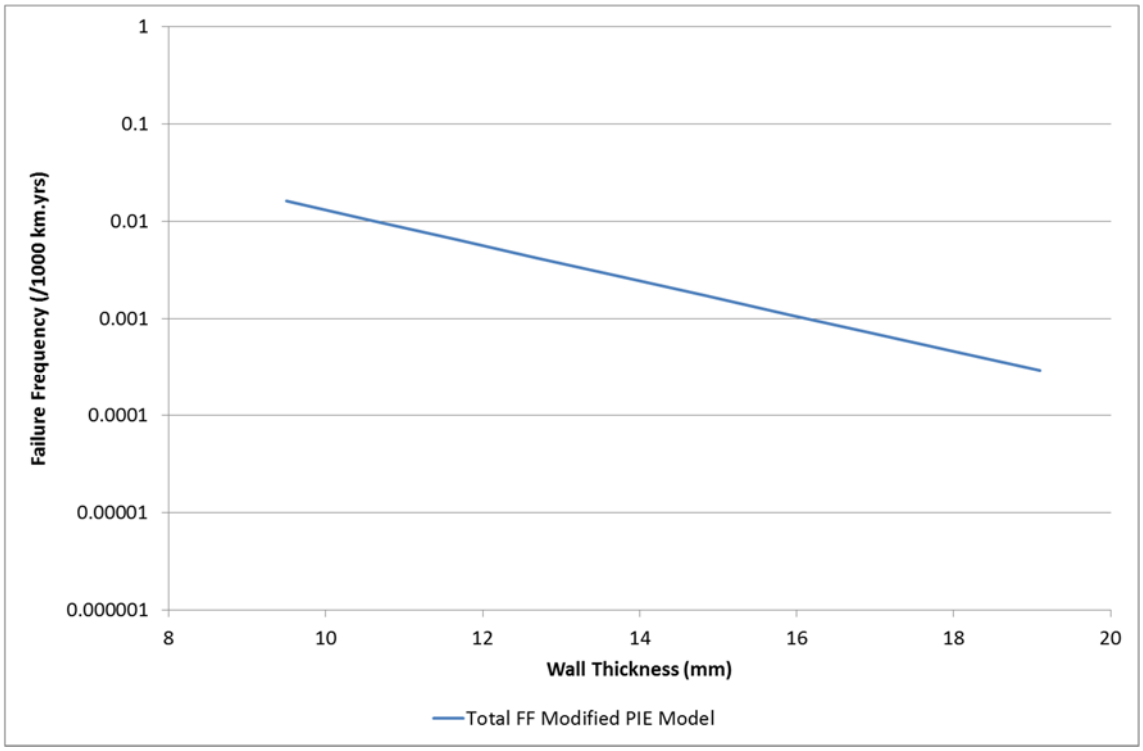

Figure A.8: Total Failure Frequency as Calculated by the Modified PIE Model for Example 4

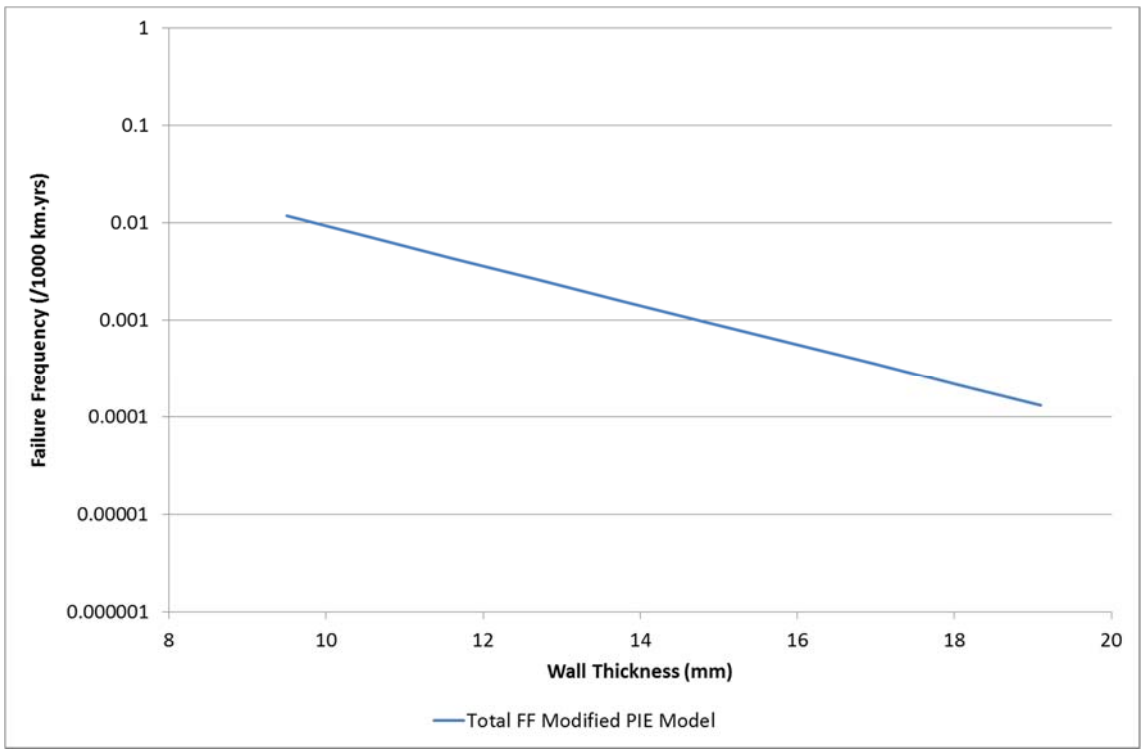

Figure A.9: Total Failure Frequency as Calculated by the Modified PIE Model for Example 5

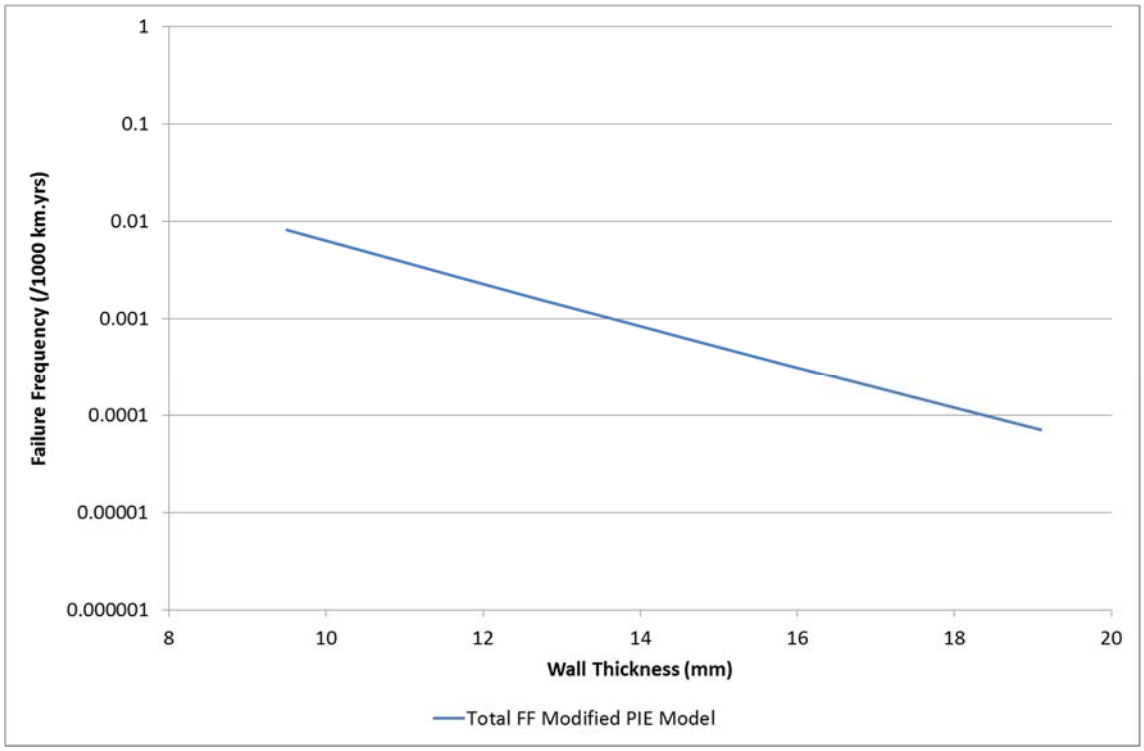

Figure A.10: Total Failure Frequency as Calculated by the Modified PIE Model for Example 6

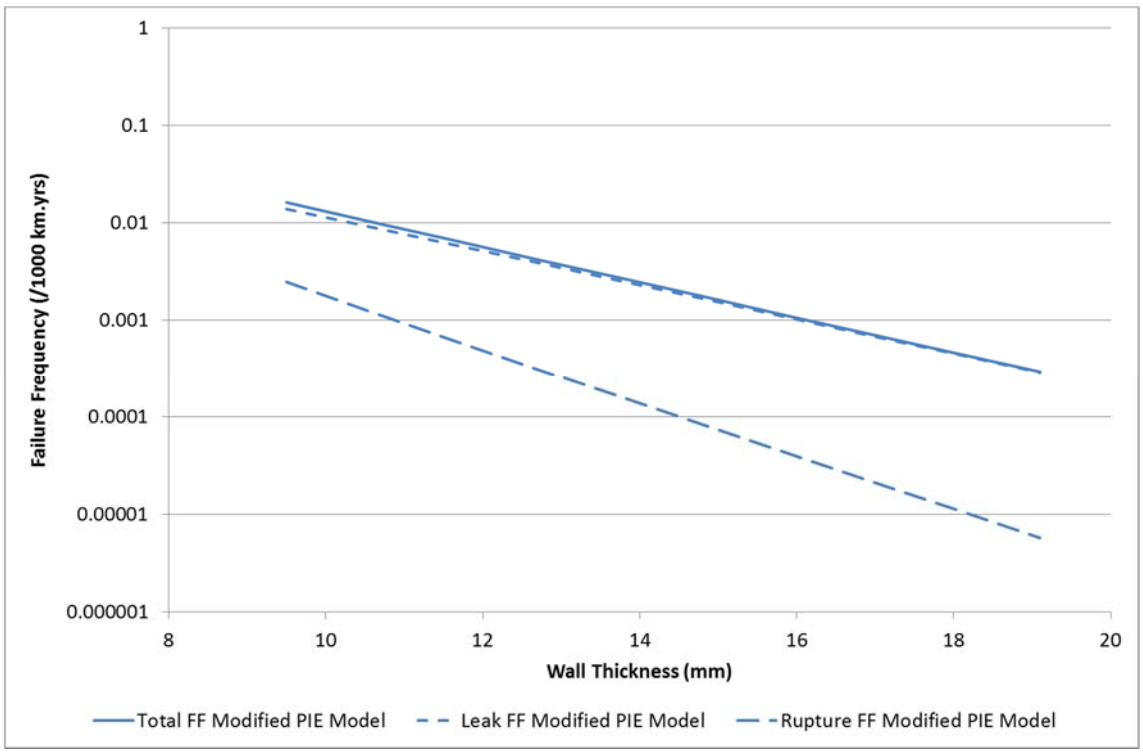

Figure A.11: Leak Rupture and Total Failure Frequency as Calculated by the Modified PIE Model, for Example 4

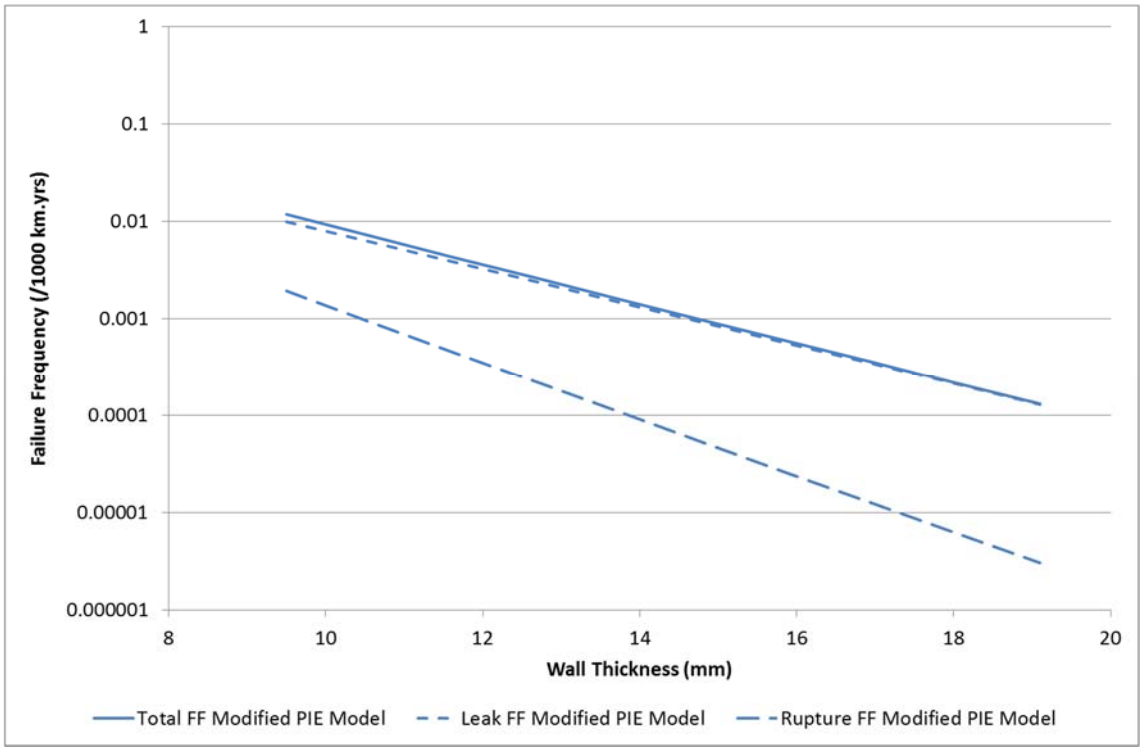

Figure A.12: Leak Rupture and Total Failure Frequency as Calculated by the Modified PIE Model, for Example 5

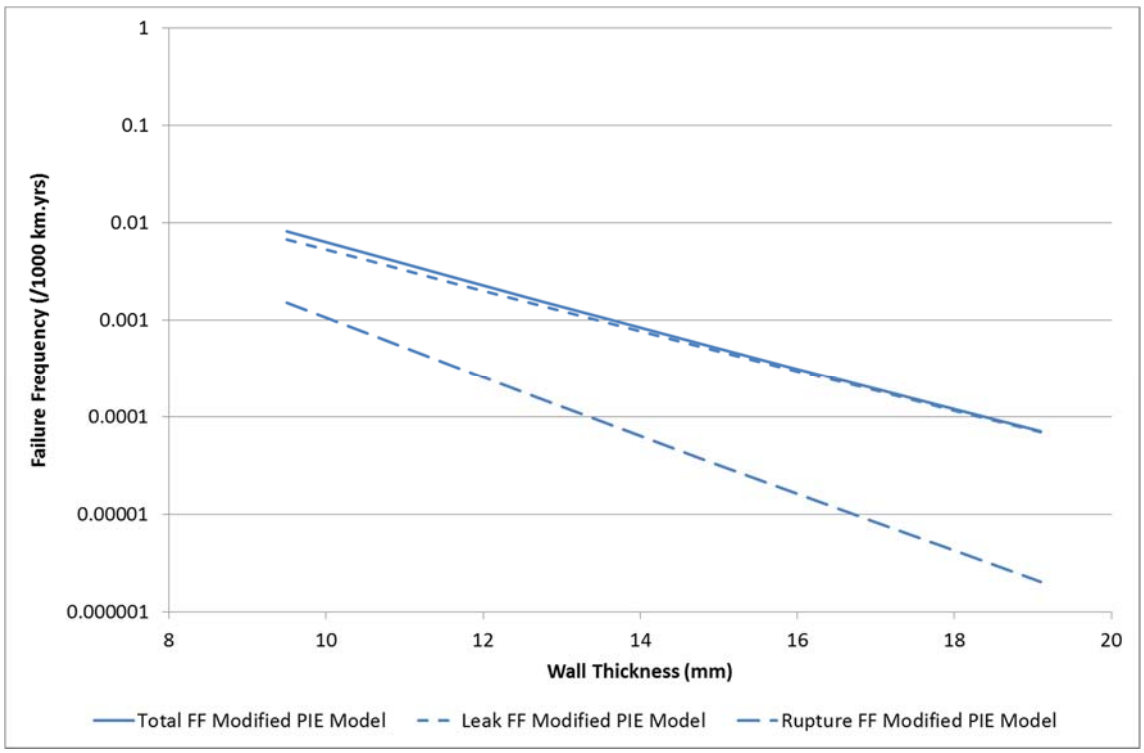

Figure A.13: Leak Rupture and Total Failure Frequency as Calculated by the Modified PIE Model, for Example 6

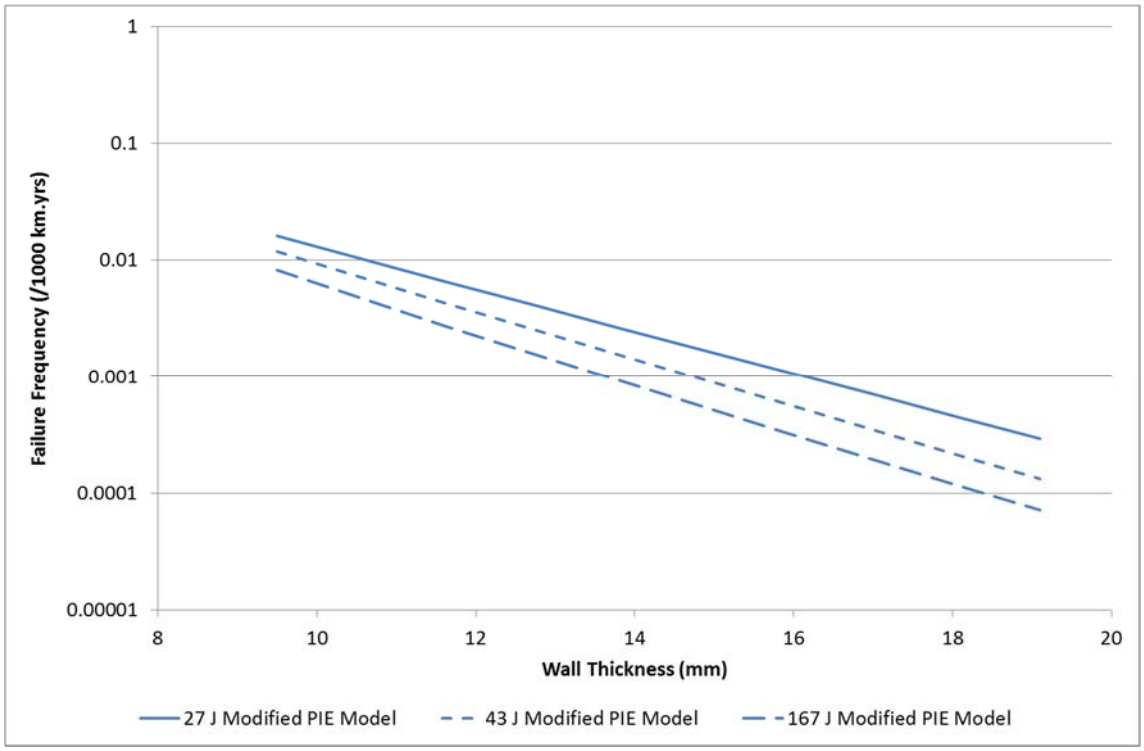

Figure A.14: Total Failure Frequency as Calculated by the Modified PIE Model for Examples 4, 5 and 6

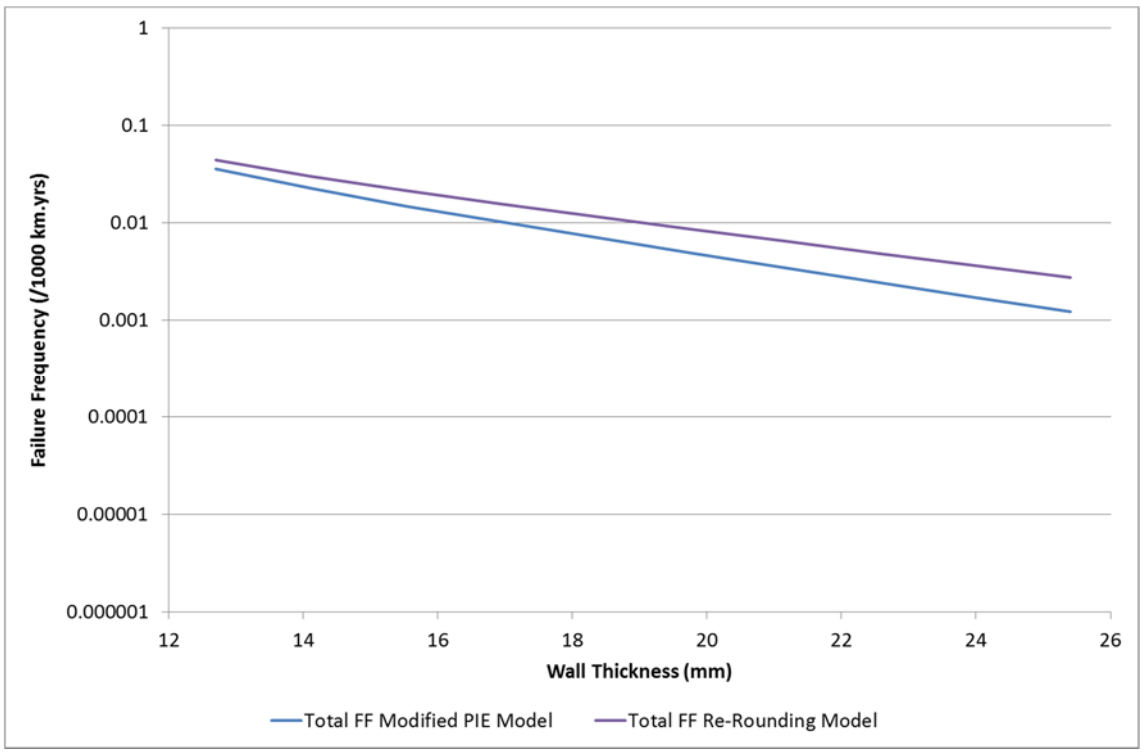

Figure A.15: Total Failure Frequency as Calculated by the Re-Rounding Model and the Modified PIE Model for Example 1

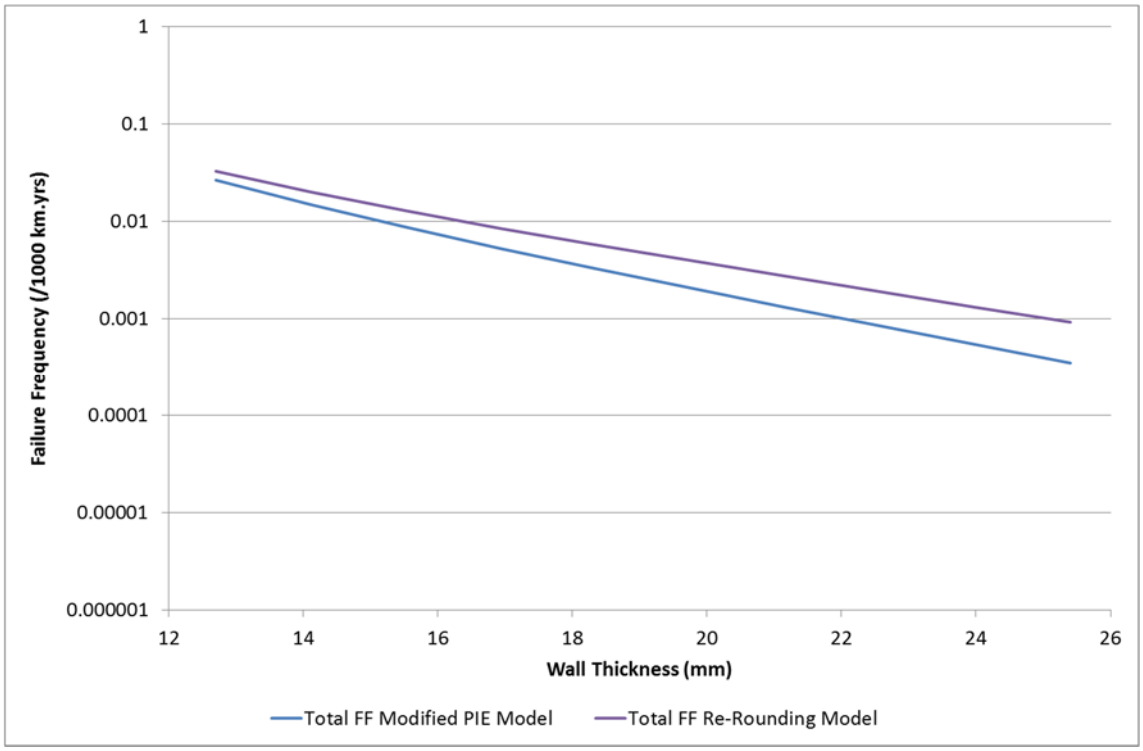

Figure A.16: Total Failure Frequency as Calculated by the Re-Rounding Model and the Modified PIE Model for Example 2

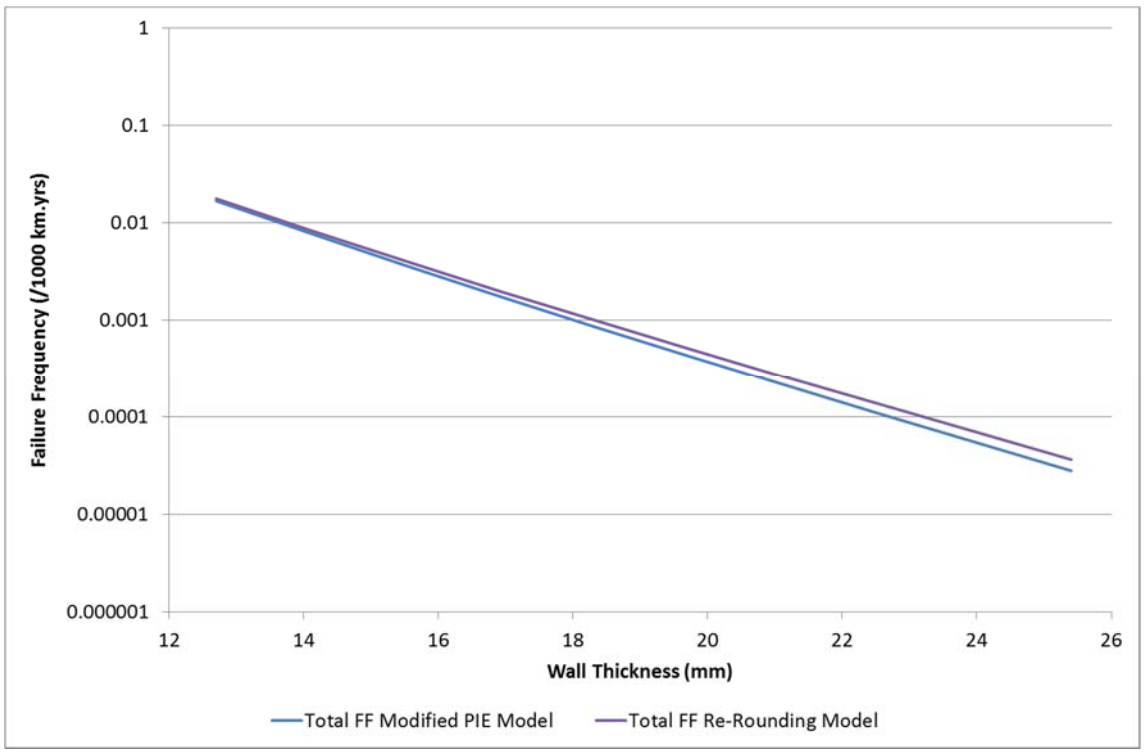

Figure A.17: Total Failure Frequency as Calculated by the Re-Rounding Model and the Modified PIE Model for Example 3

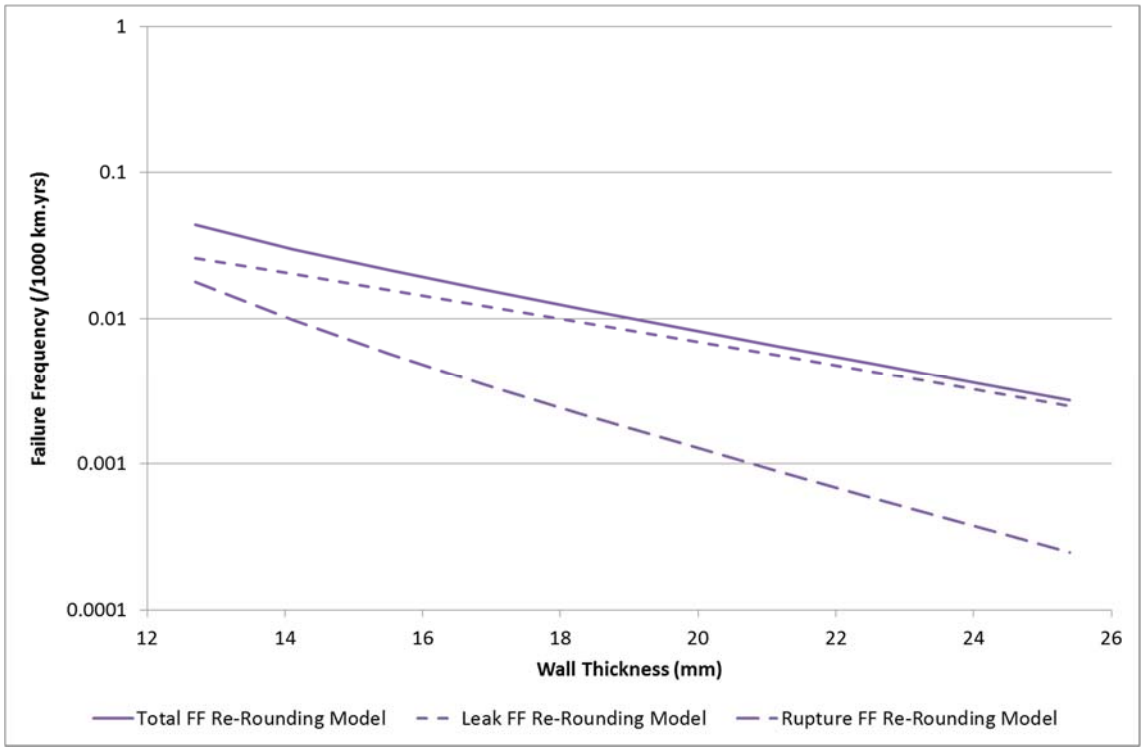

Figure A.18: Leak Rupture and Total Failure Frequency as Calculated by the Re-Rounding Model, for Example 1

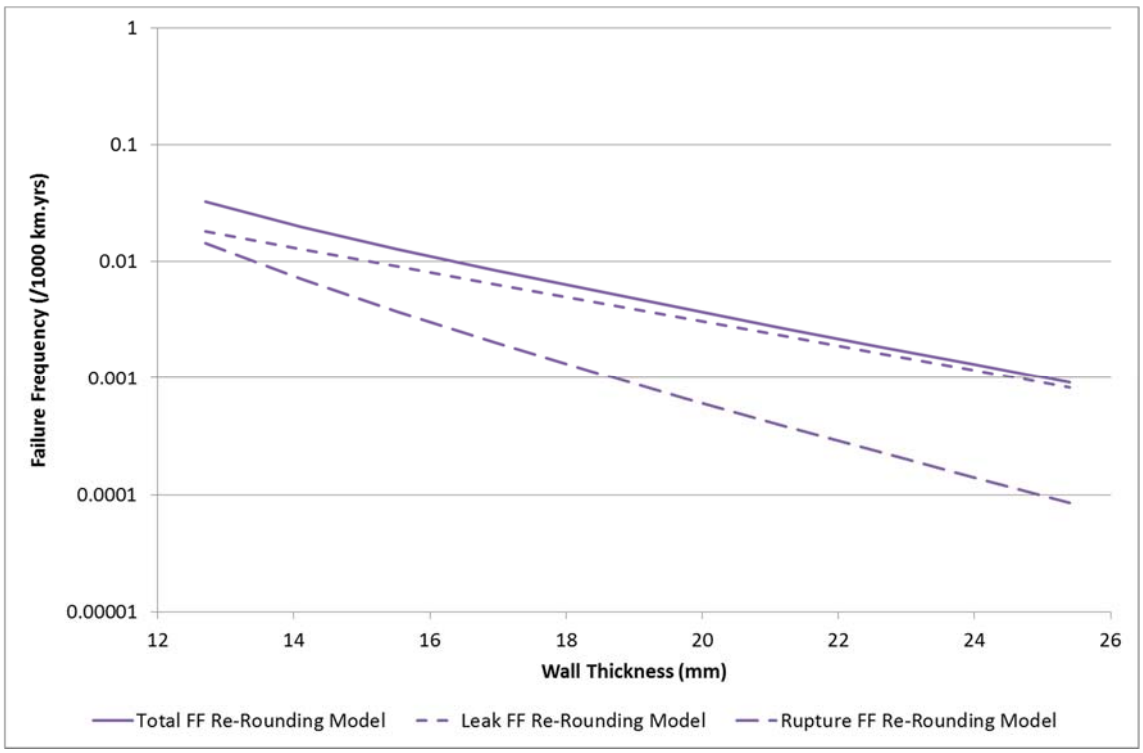

Figure A.19: Leak Rupture and Total Failure Frequency as Calculated by the Re-Rounding Model, for Example 2

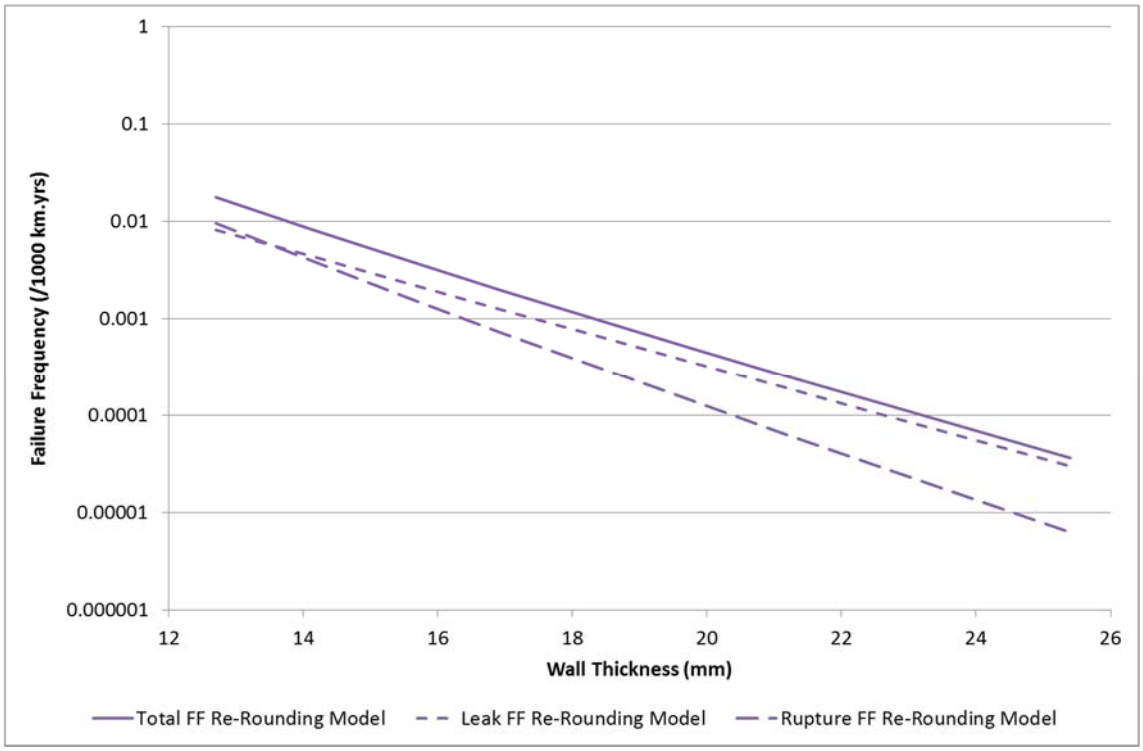

Figure A.20: Leak Rupture and Total Failure Frequency as Calculated by the Re-Rounding Model, for Example 3

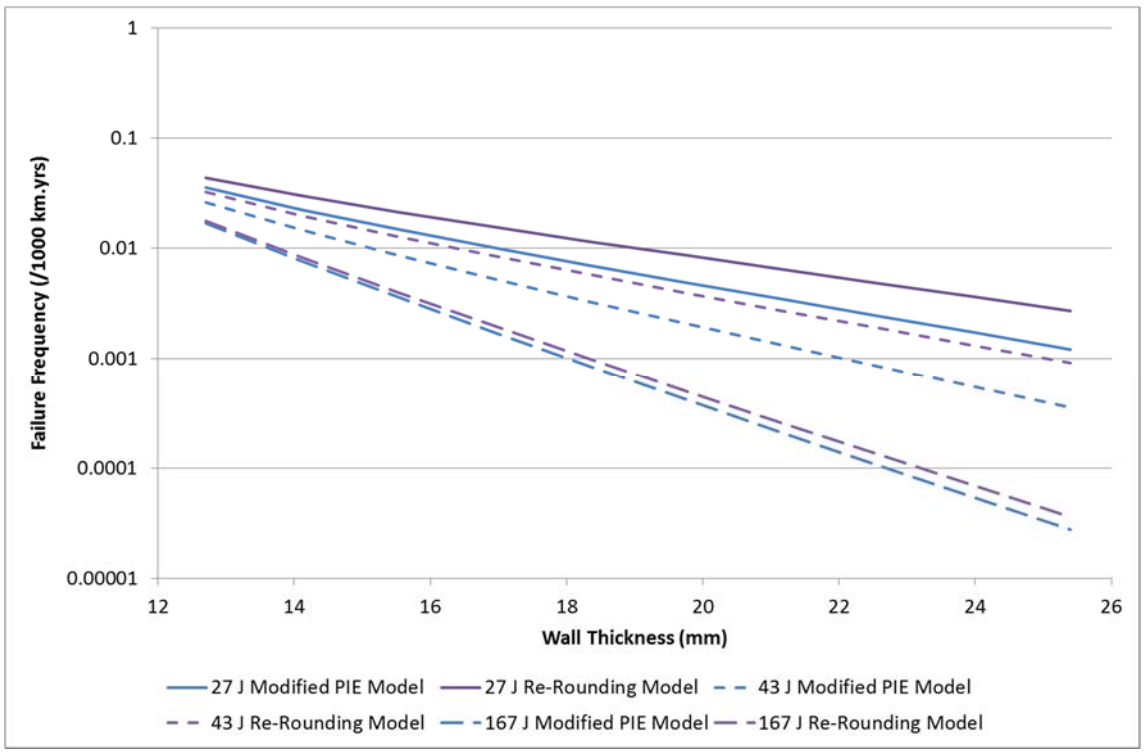

Figure A.21: Total Failure Frequency as Calculated by the Re-Rounding Model and the Modified PIE Model for Examples 1, 2 and 3

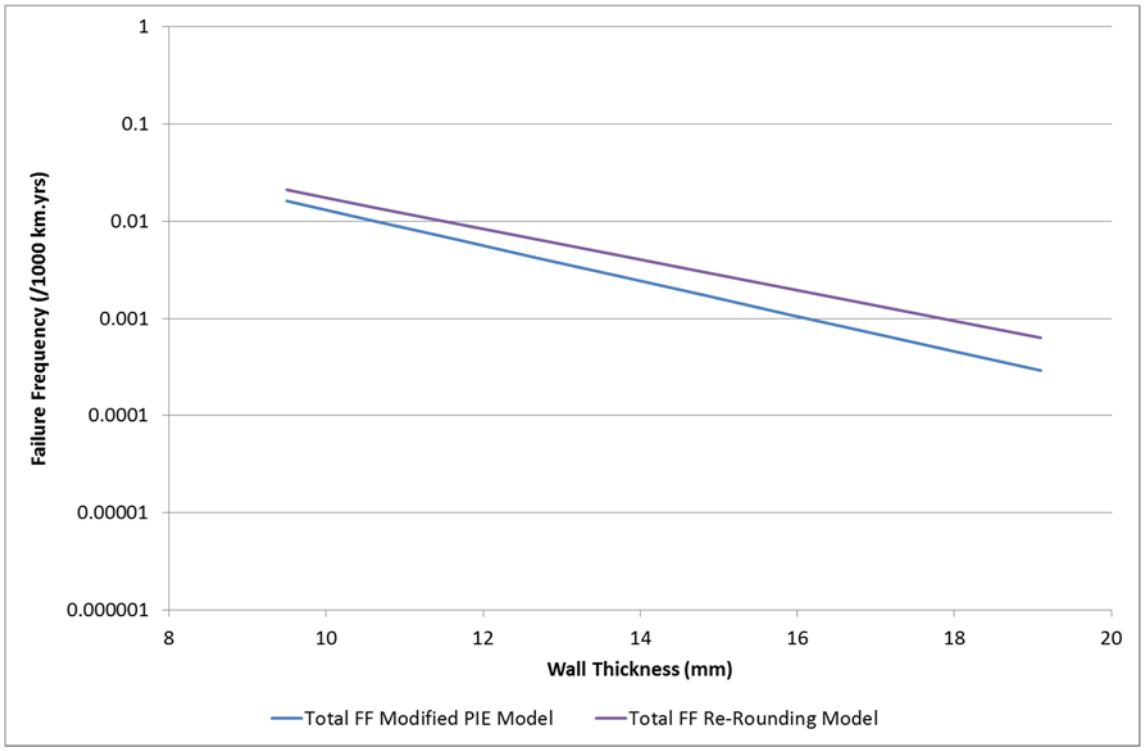

Figure A.22: Total Failure Frequency as Calculated by the Re-Rounding Model and the Modified PIE Model for Example 4

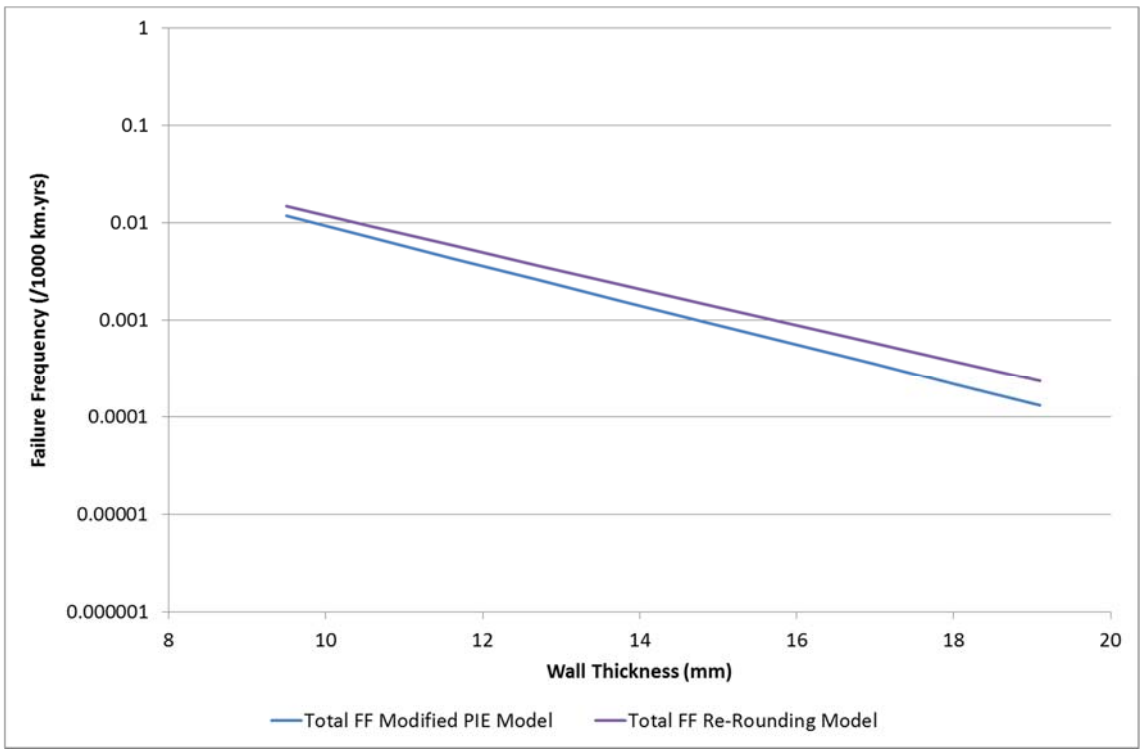

Figure A.23: Total Failure Frequency as Calculated by the Re-Rounding Model and the Modified PIE Model for Example 5

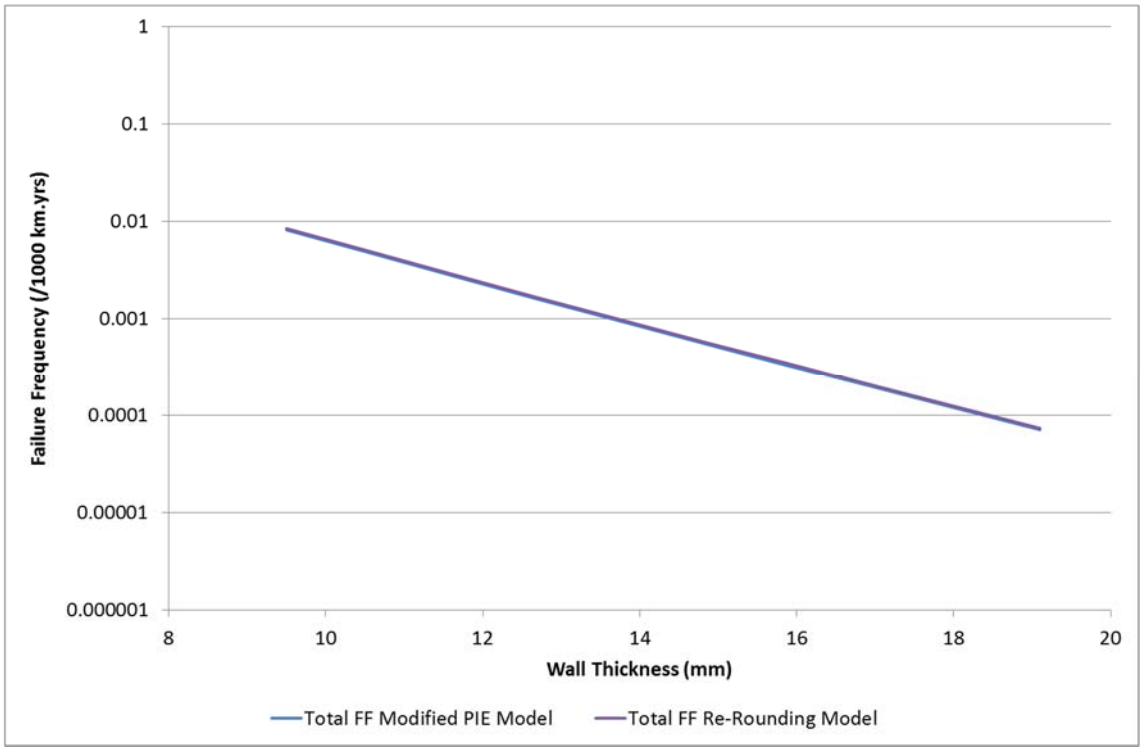

Figure A.24: Total Failure Frequency as Calculated by the Re-Rounding Model and the Modified PIE Model for Example 6

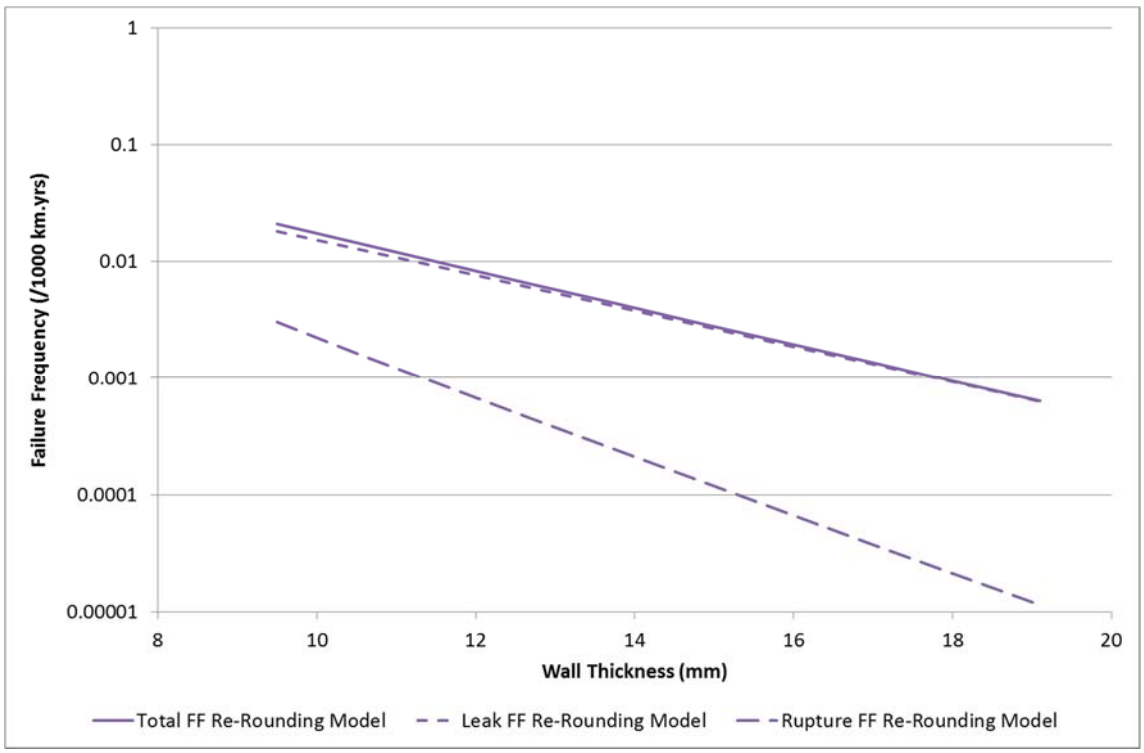

Figure A.25: Leak, Rupture and Total Failure Frequency as Calculated by the Re-Rounding Model, for Example 4

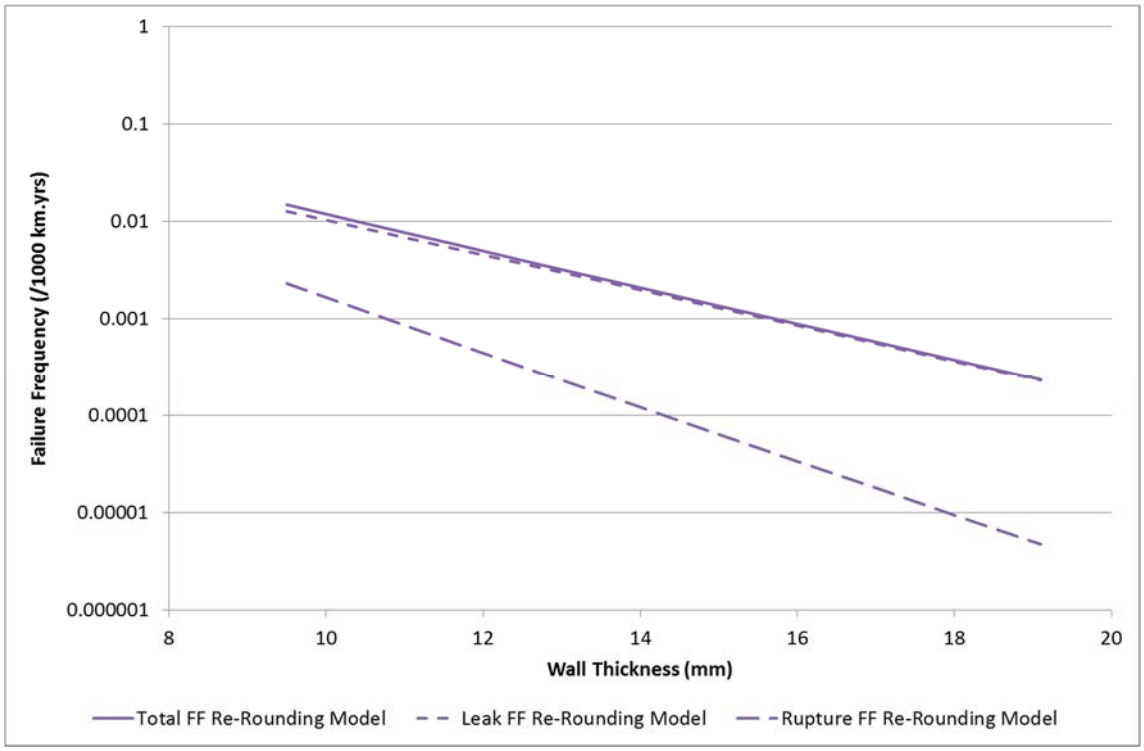

Figure A.26: Leak, Rupture and Total Failure Frequency as Calculated by the Re-Rounding Model, for Example 5

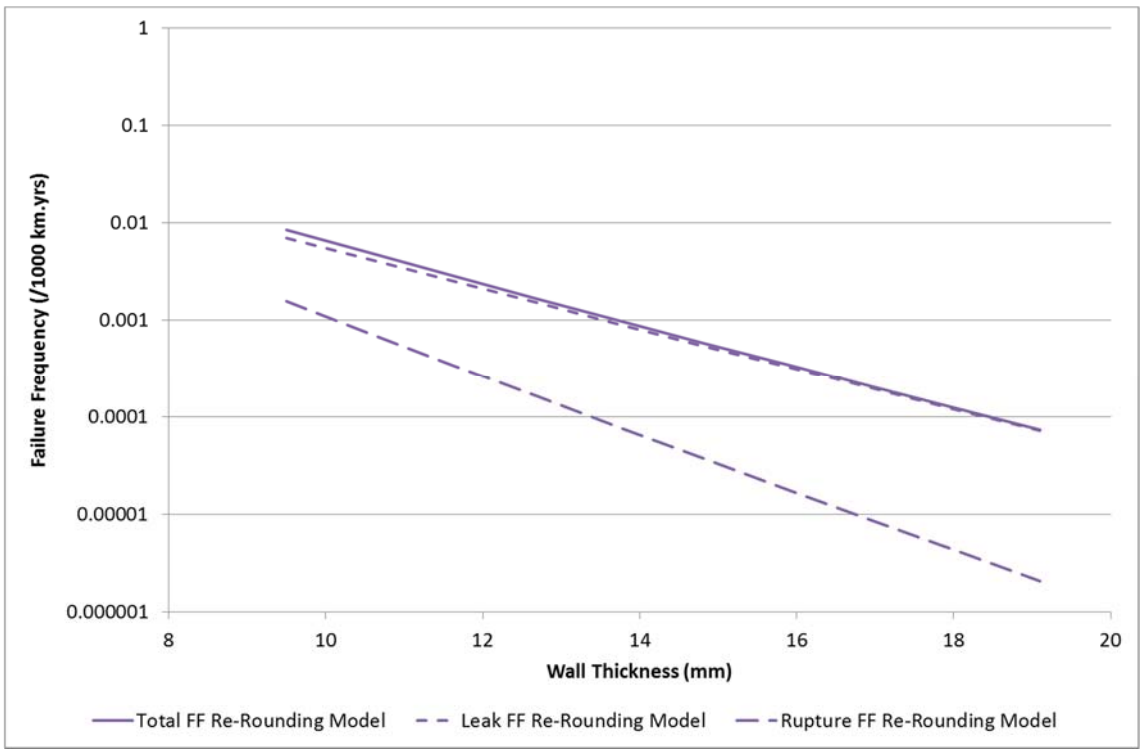

Figure A.27: Leak, Rupture and Total Failure Frequency as Calculated by the Re-Rounding Model, for Example 6

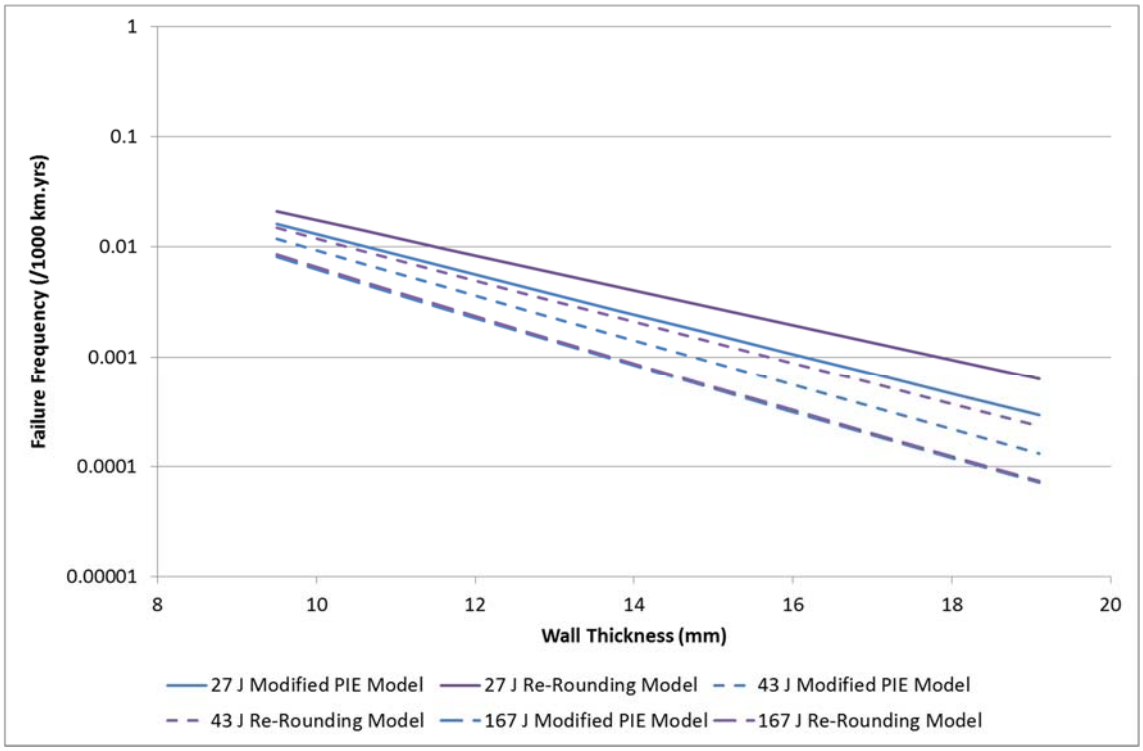

Figure A.28: Total Failure Frequency as Calculated by the Re-Rounding Model and the PIE Model for Examples 4, 5 and 6

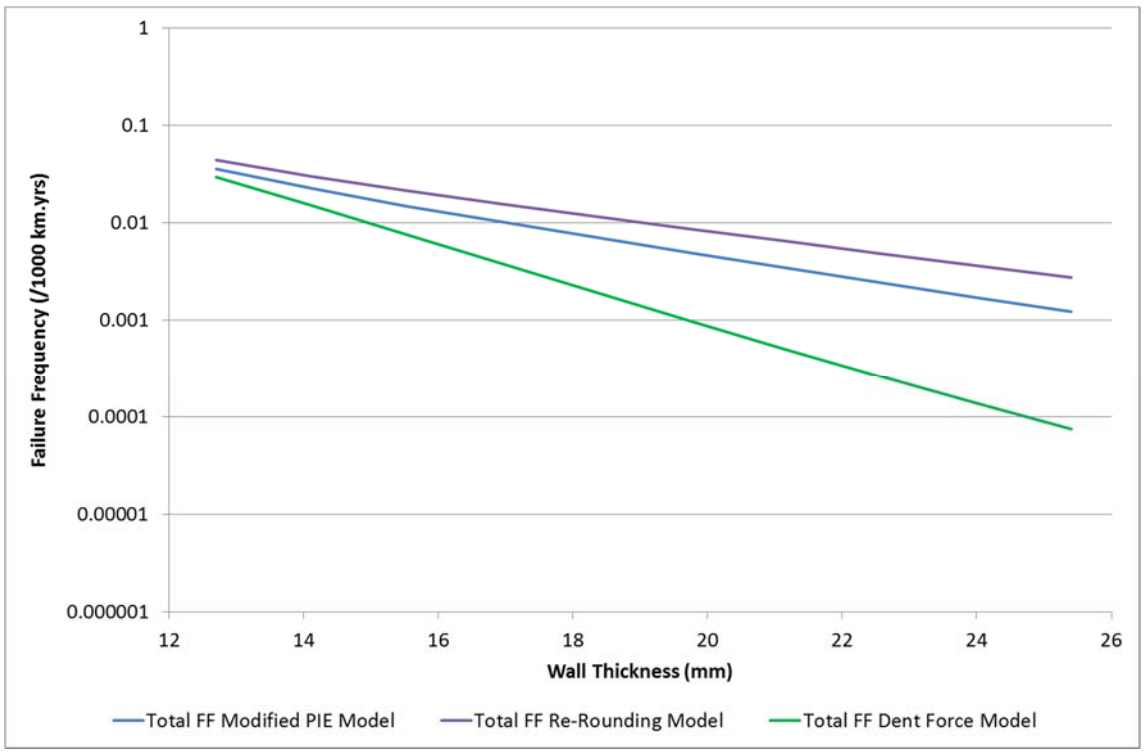

Figure A.29: Total Failure Frequency as Calculated by the Dent Force Model, Re-Rounding Model and the Modified PIE Model for Example 1

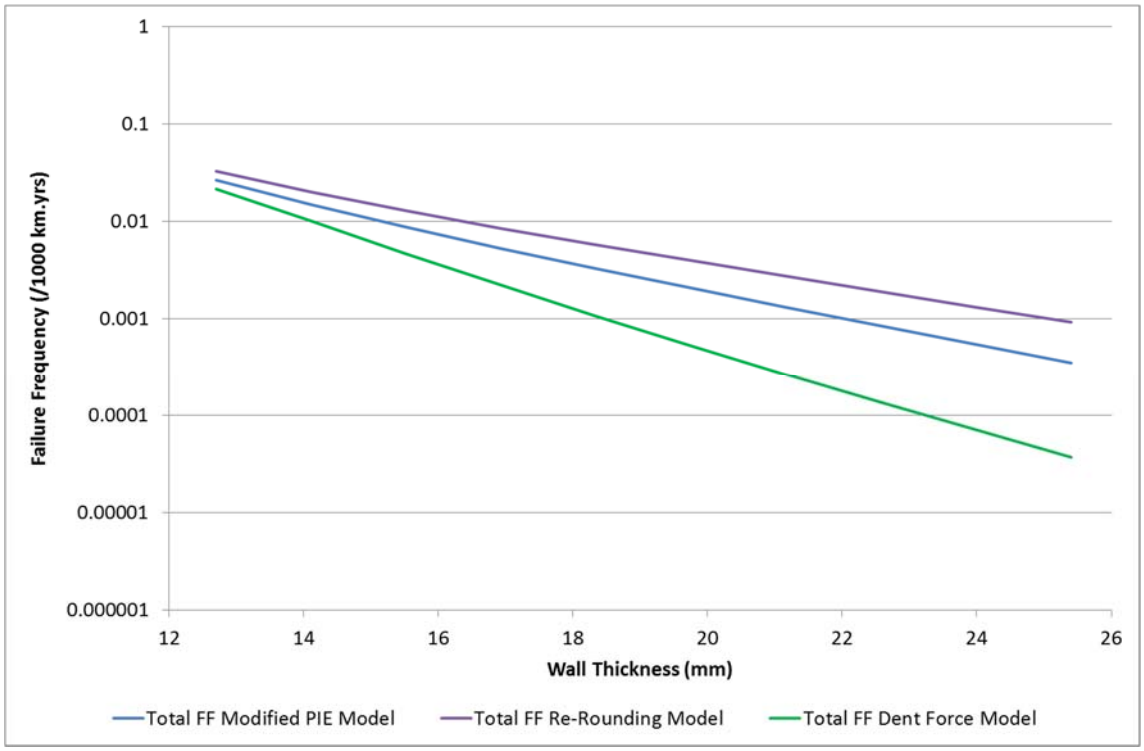

Figure A.30: Total Failure Frequency as Calculated by the Dent Force Model, Re-Rounding Model and the Modified PIE Model for Example 2

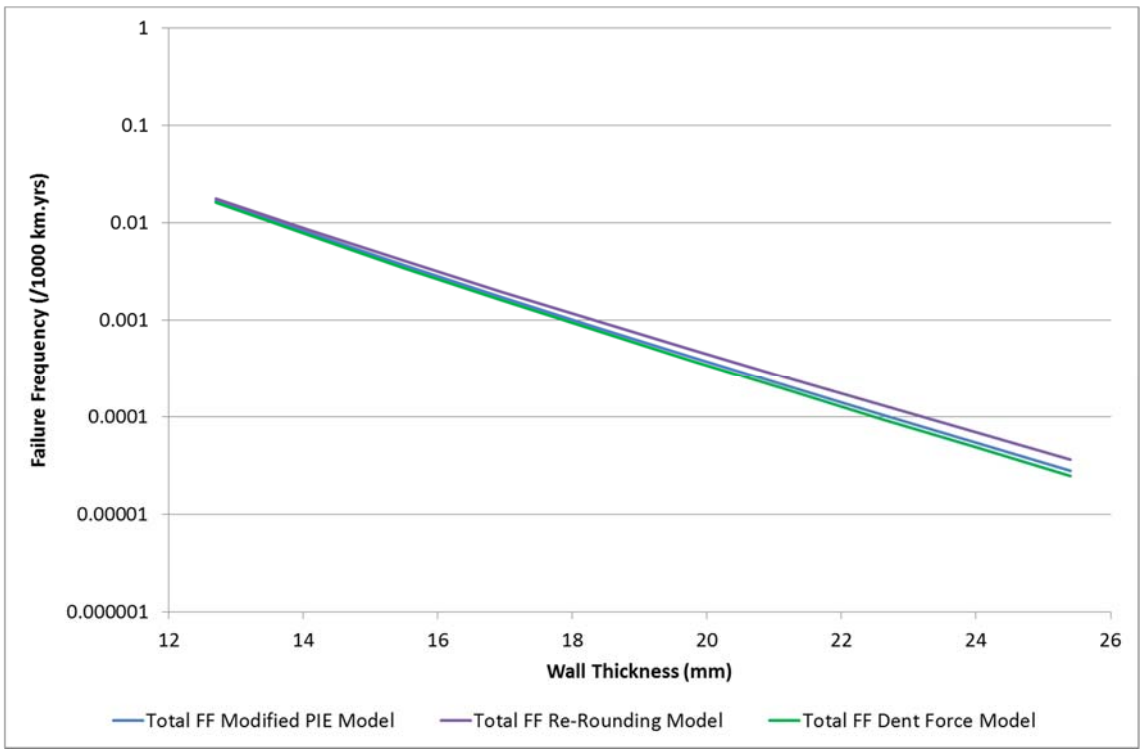

Figure A.31: Total Failure Frequency as Calculated by the Dent Force Model, Re-Rounding Model and the Modified PIE Model for Example 3

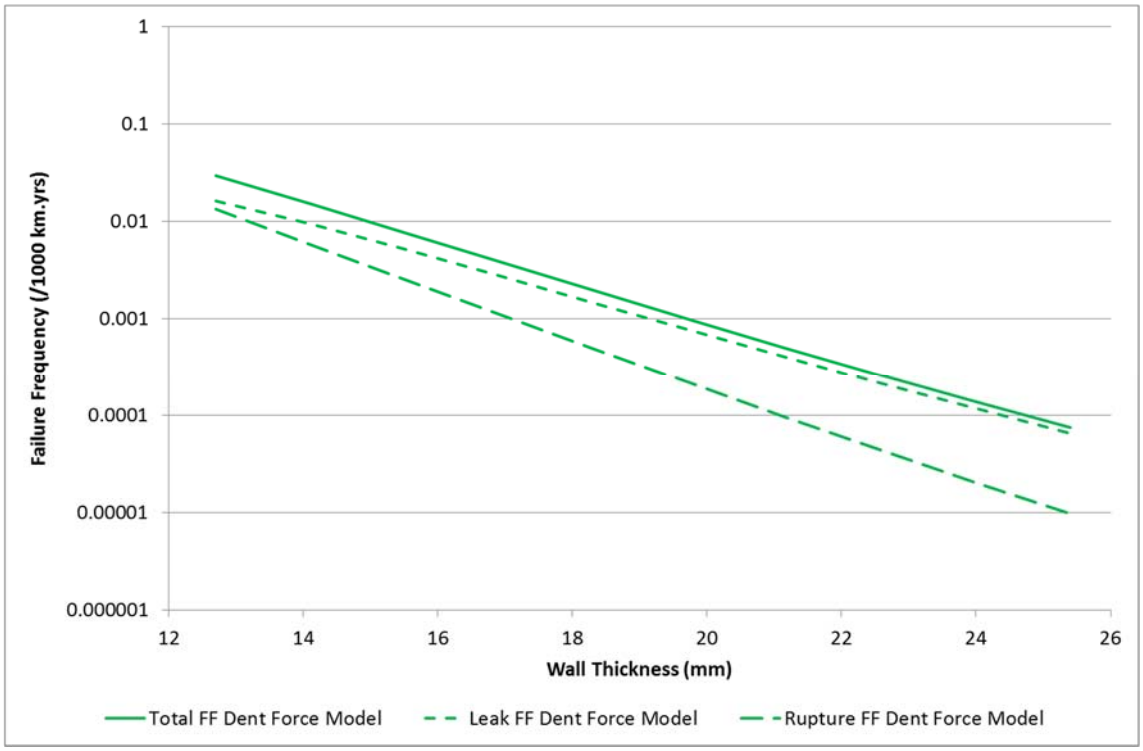

Figure A.32: Leak, Rupture and Total Failure Frequency as Calculated by the Dent Force Model, for Example 1

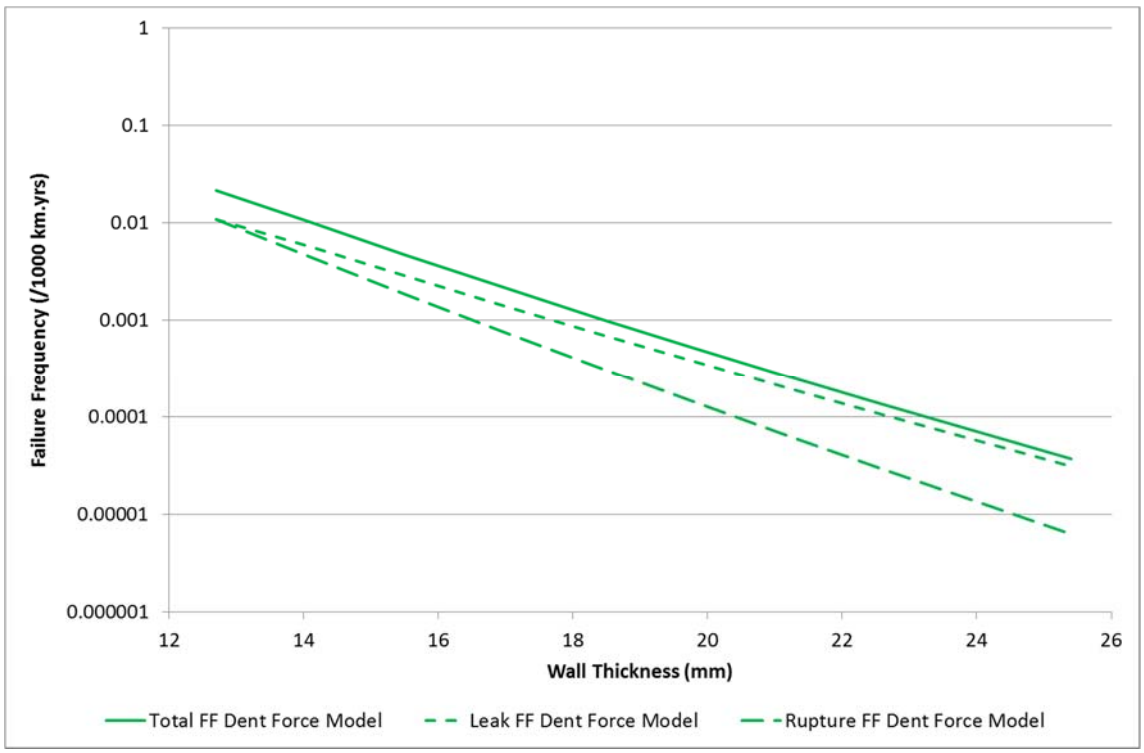

Figure A.33: Leak, Rupture and Total Failure Frequency as Calculated by the Dent Force Model, for Example 2

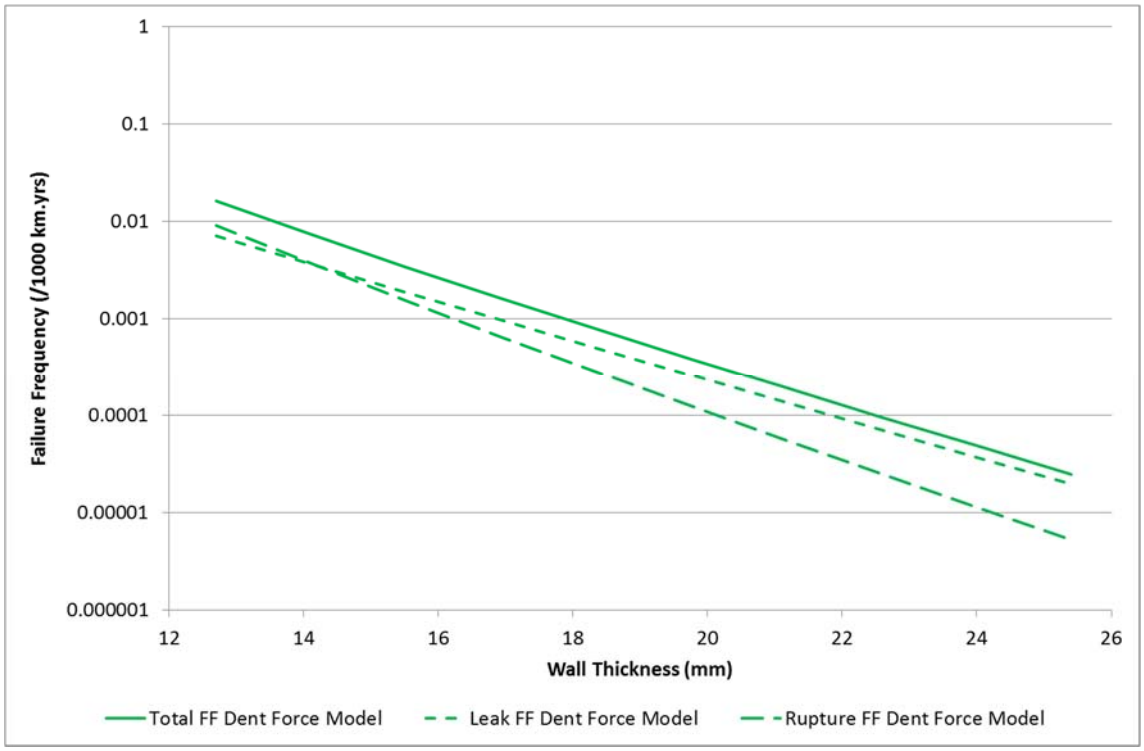

Figure A.34: Leak, Rupture and Total Failure Frequency as Calculated by the Dent Force Model, for Example 3

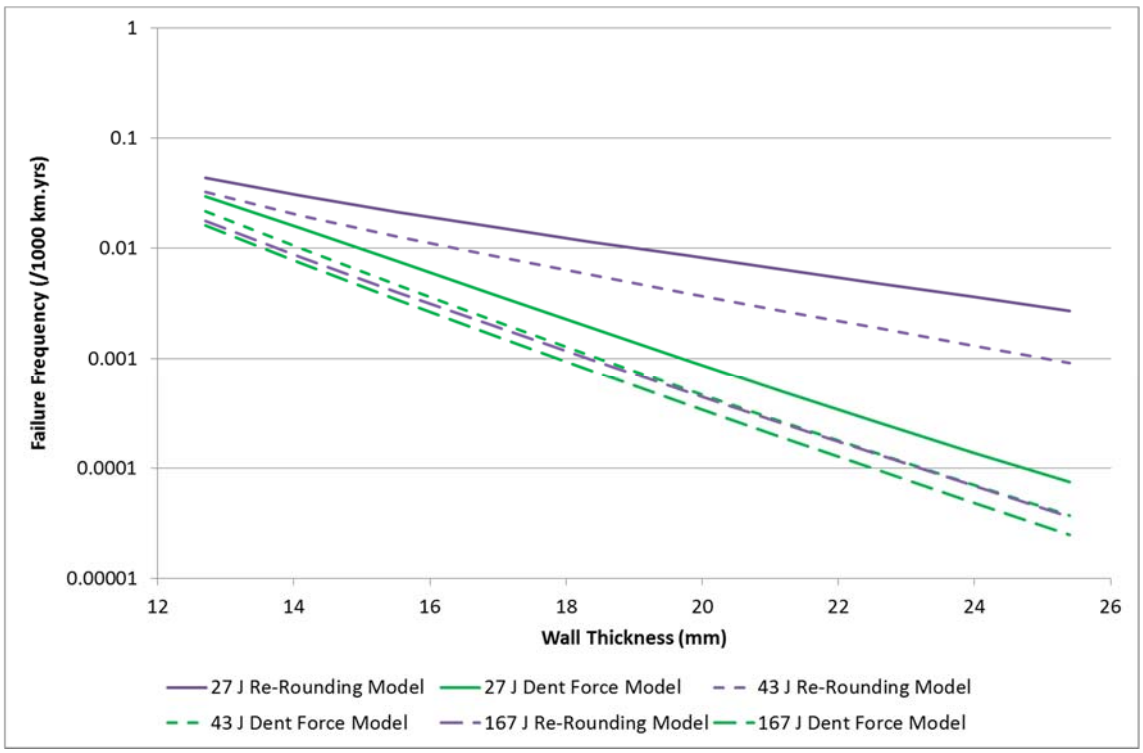

Figure A.35: Total Failure Frequency as Calculated by the Dent Force Model and the Re-Rounding Model for Examples 1, 2 and 3

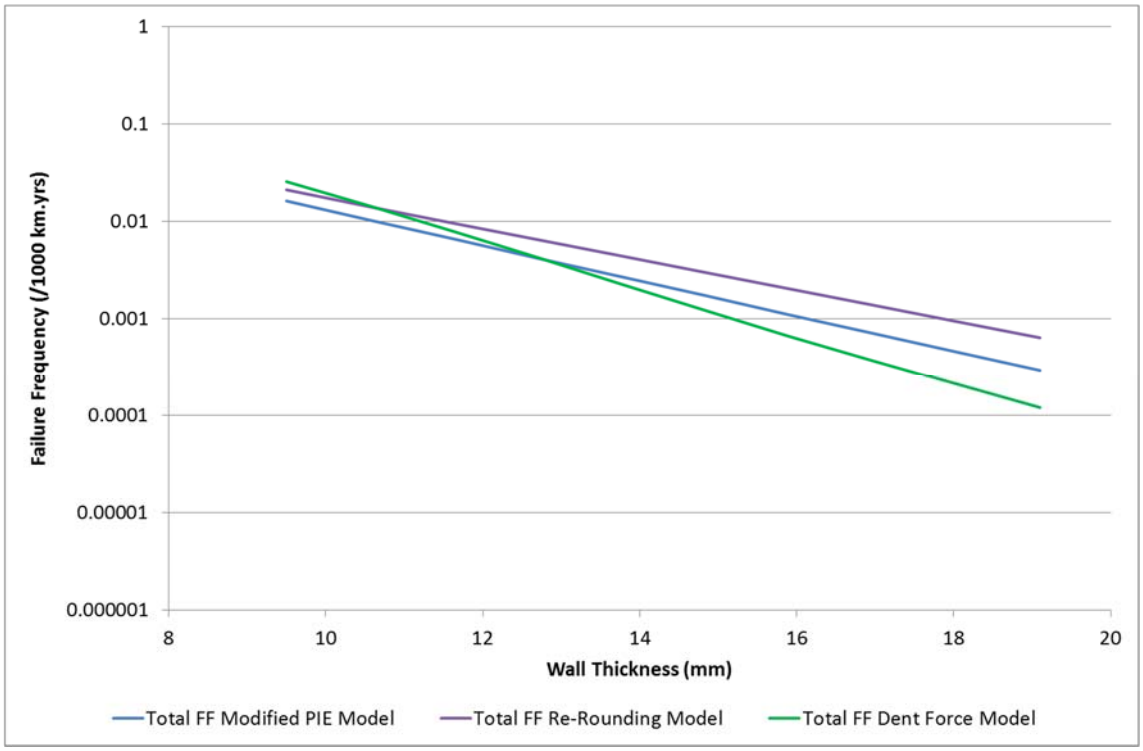

Figure A.36: Total Failure Frequency as Calculated by the Dent Force Model, Re-Rounding Model and the Modified PIE Model for Example 4

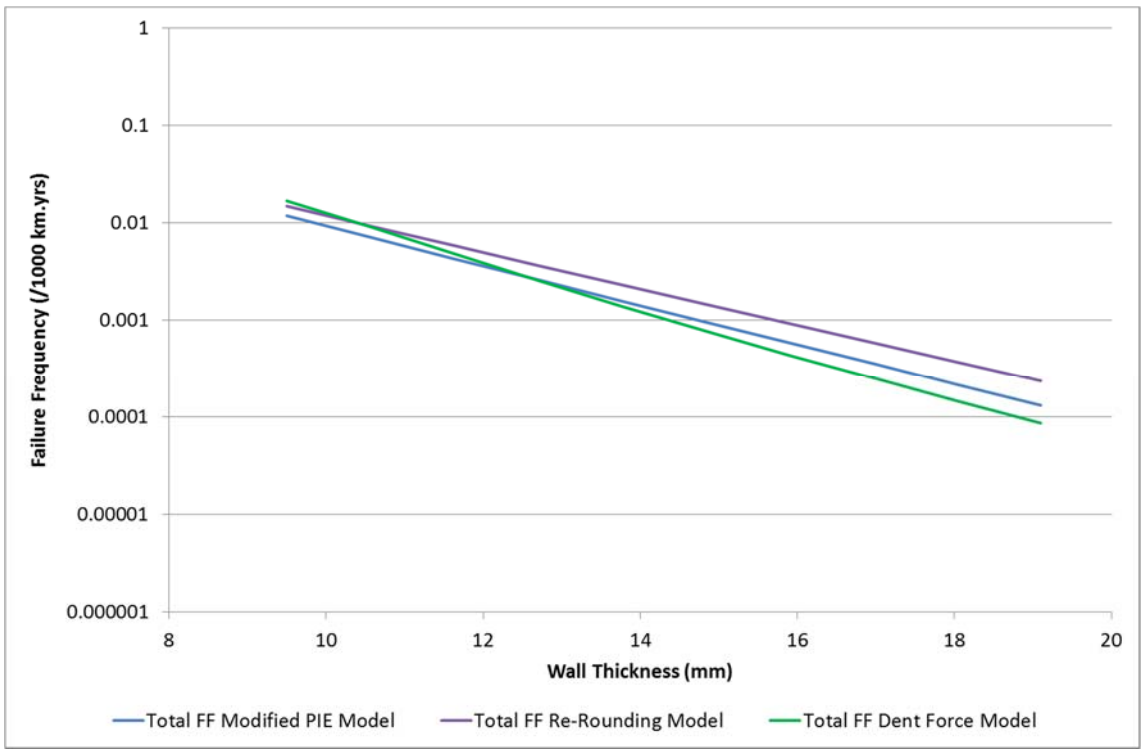

Figure A.37: Total Failure Frequency as Calculated by the Dent Force Model, Re-Rounding Model and the Modified PIE Model for Example 5

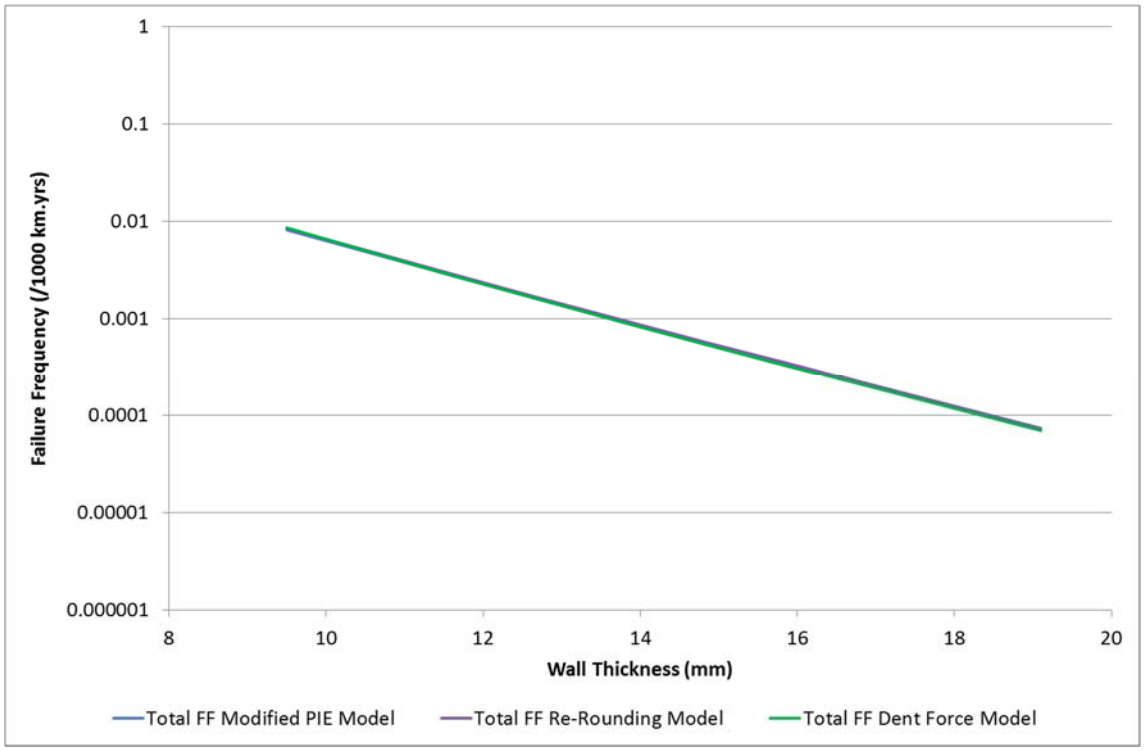

Figure A.38: Total Failure Frequency as Calculated by the Dent Force Model, Re-Rounding Model and the Modified PIE Model for Example 6

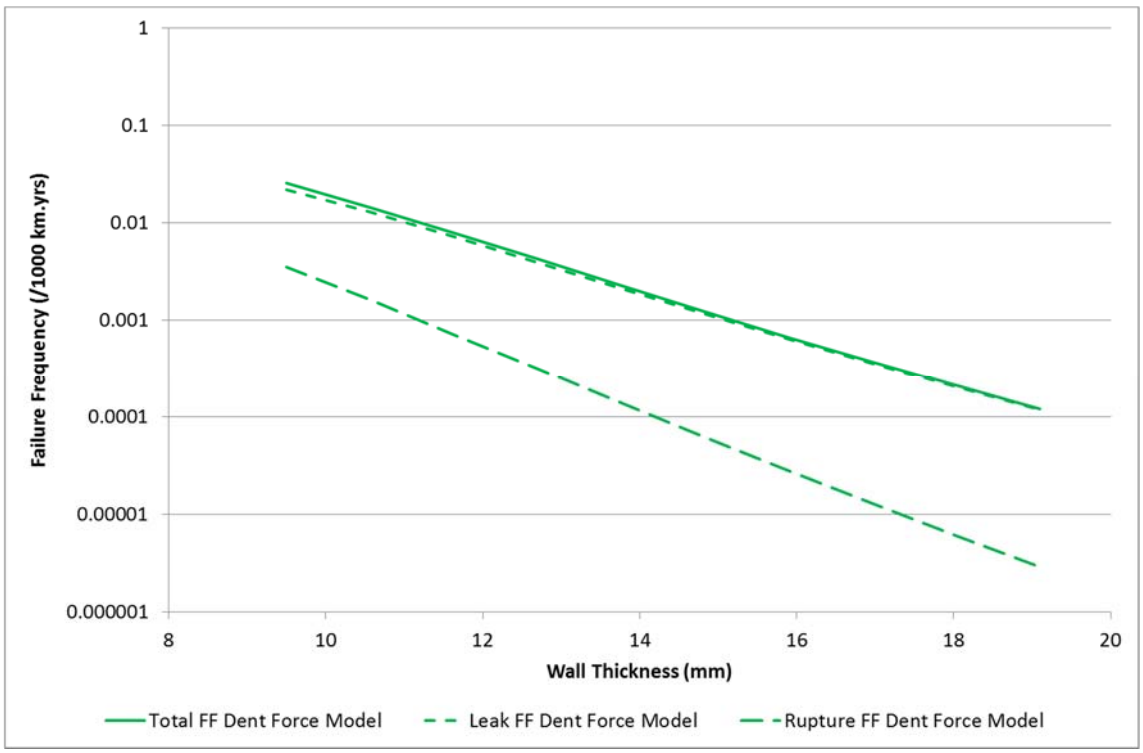

Figure A.39: Leak, Rupture and Total Failure Frequency as Calculated by the Dent Force Model, for Example 4

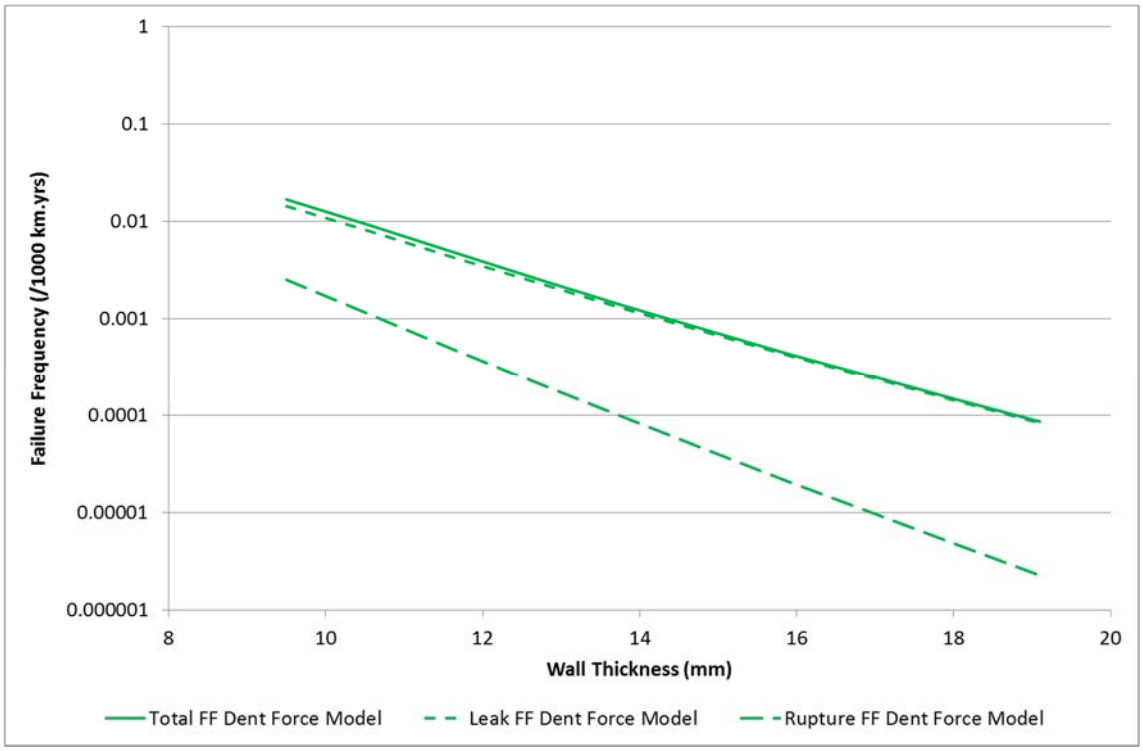

Figure A.40: Leak, Rupture and Total Failure Frequency as Calculated by the Dent Force Model, for Example 5

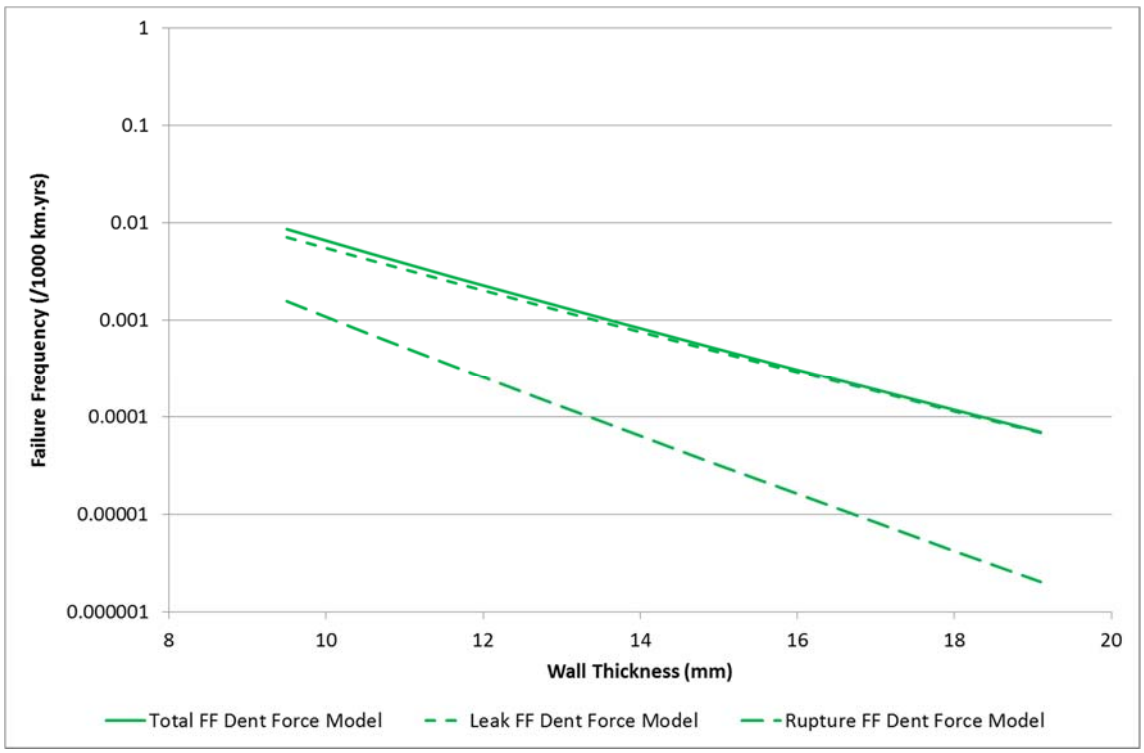

Figure A.41: Leak, Rupture and Total Failure Frequency as Calculated by the Dent Force Model, for Example 6

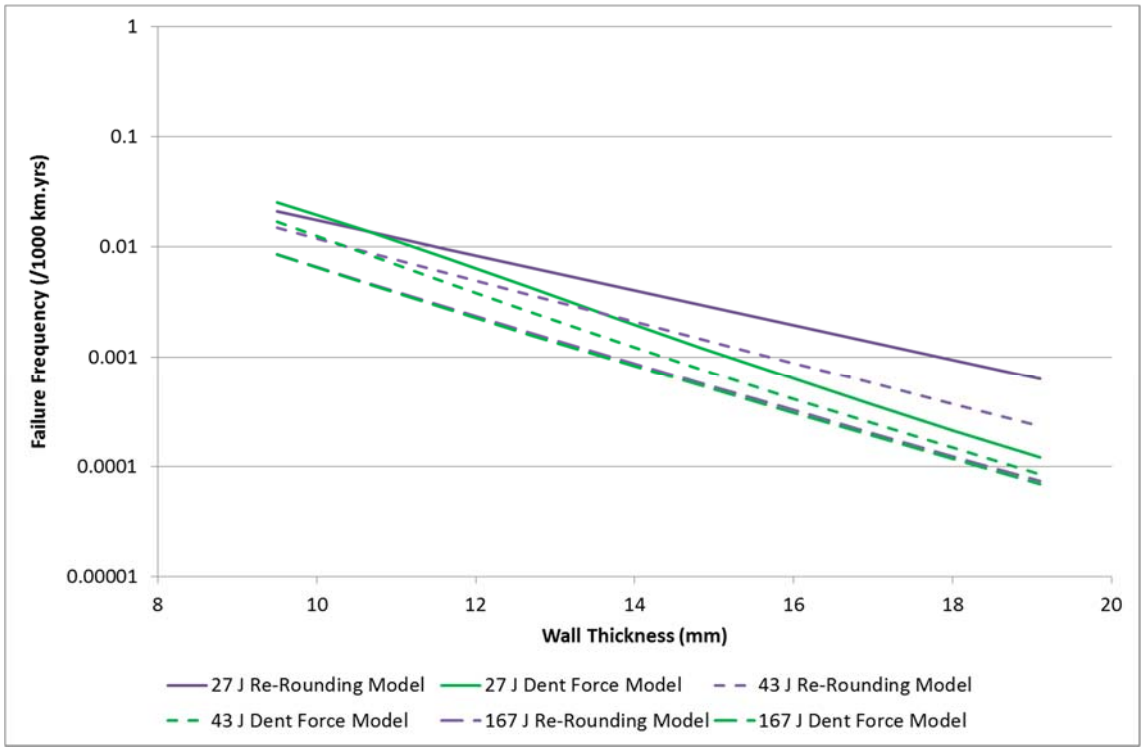

Figure A.42: Total Failure Frequency as Calculated by the Dent Force Model and the Re-Rounding Model for Examples 4, 5 and 6

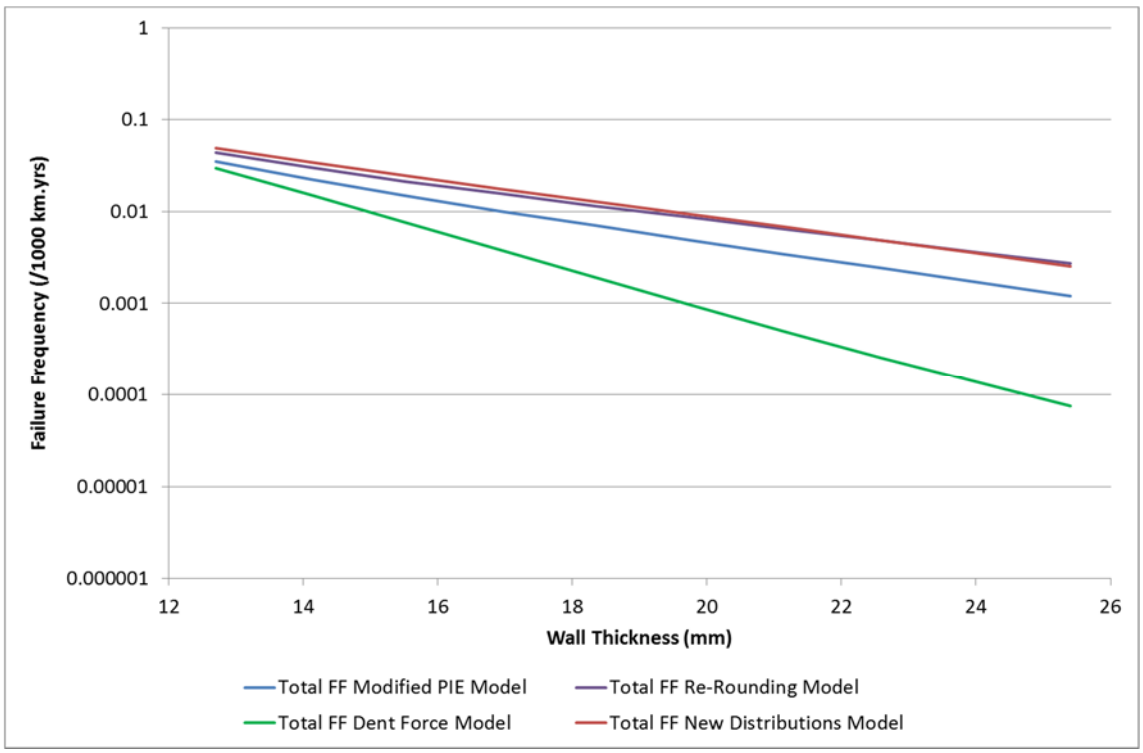

Figure A.43: Total Failure Frequency as Calculated by the New Distributions Model, Dent Force Model, Re-Rounding Model and the Modified PIE Model for Example 1

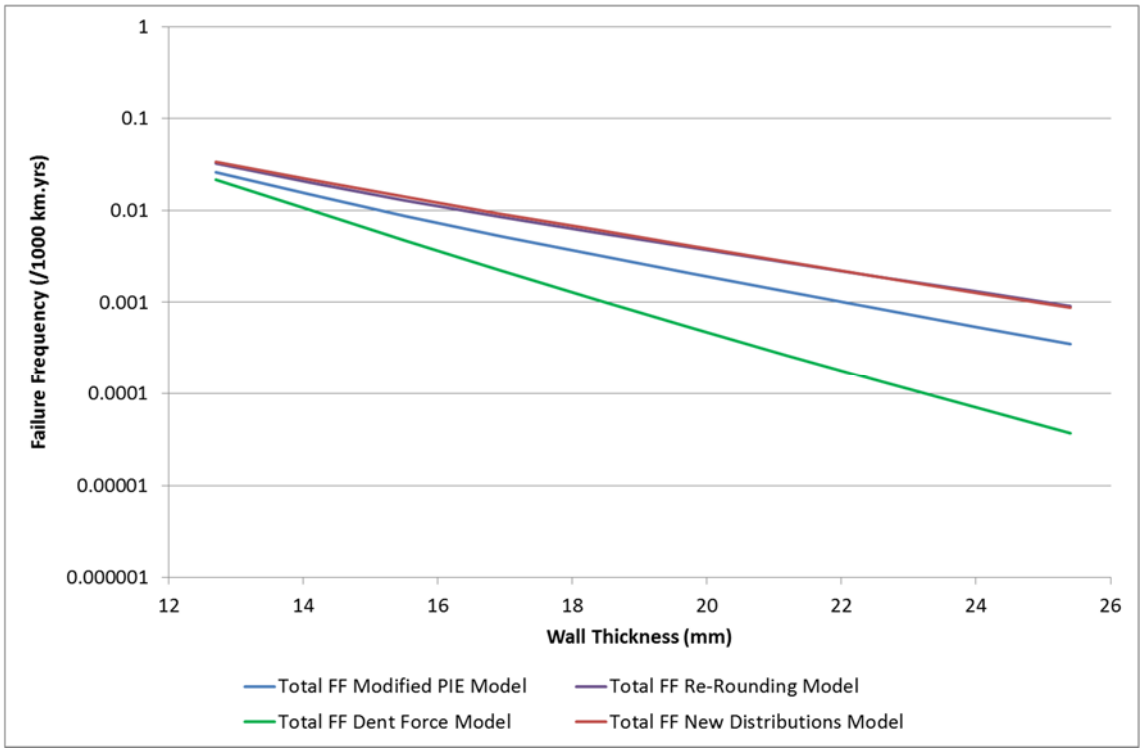

Figure A.44: Total Failure Frequency as Calculated by the New Distributions Model, Dent Force Model, Re-Rounding Model and the Modified PIE Model for Example 2

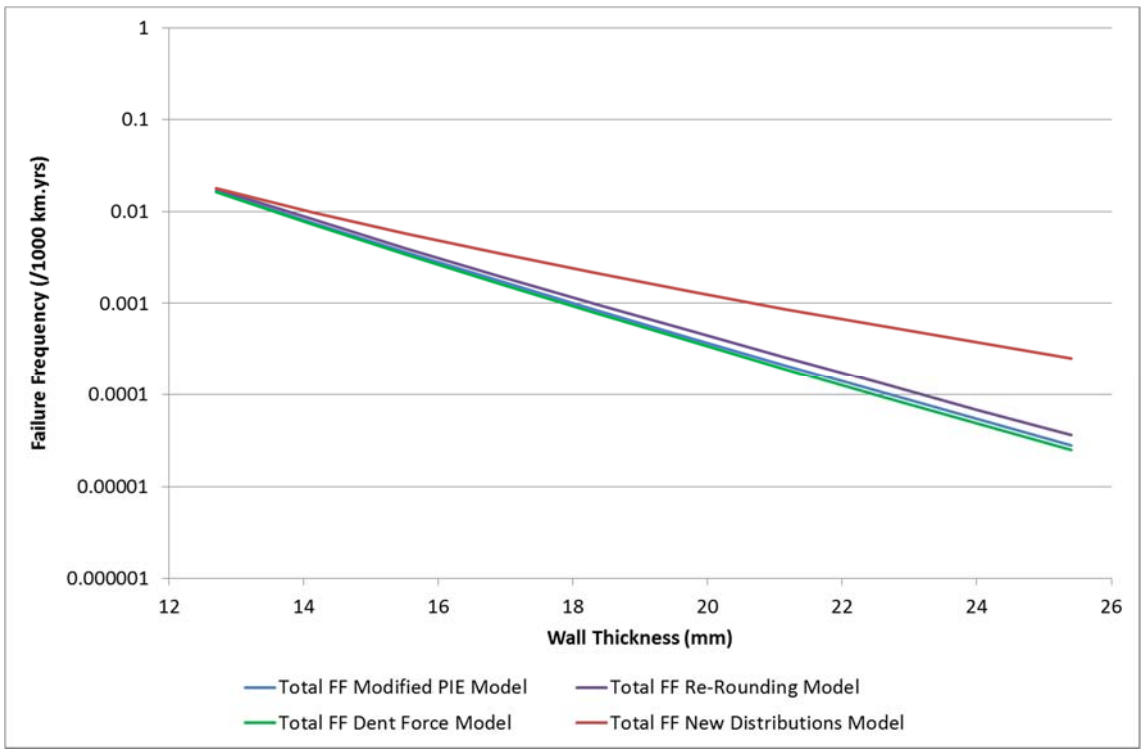

Figure A.45: Total Failure Frequency as Calculated by the New Distributions Model, Dent Force Model, Re-Rounding Model and the Modified PIE Model for Example 3

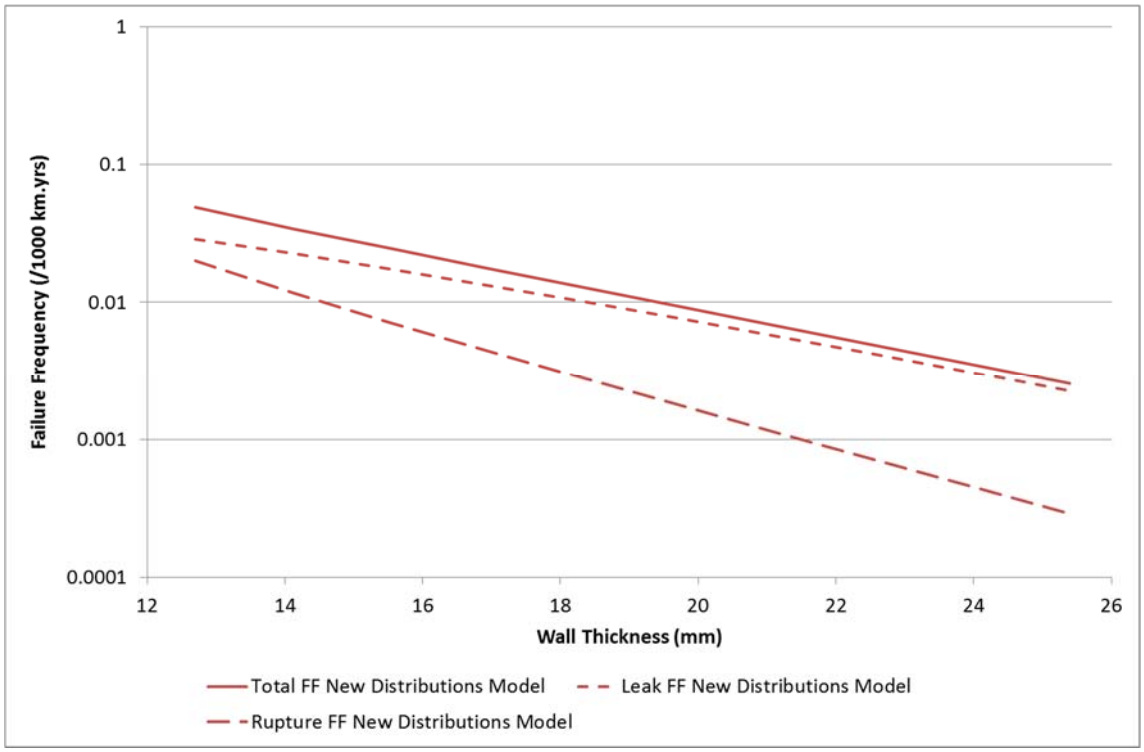

Figure A.46: Leak, Rupture and Total Failure Frequency as Calculated by the New Distributions Model, for Example 1

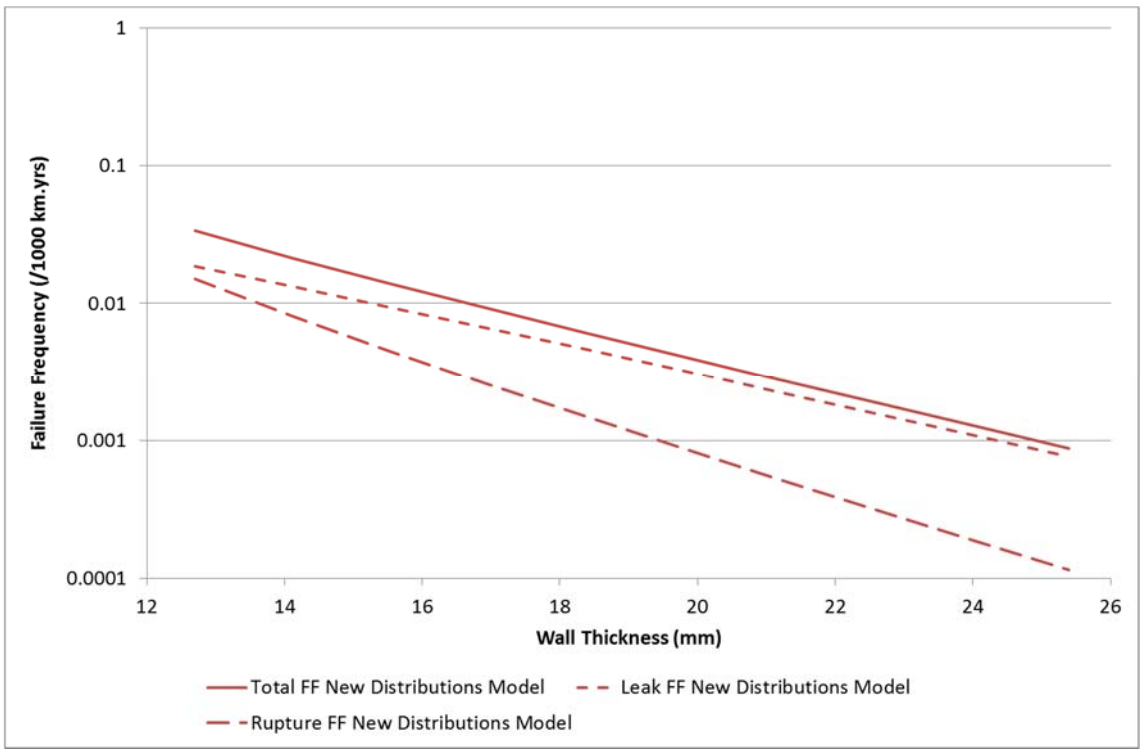

Figure A.47: Leak, Rupture and Total Failure Frequency as Calculated by the New Distributions Model, for Example 2

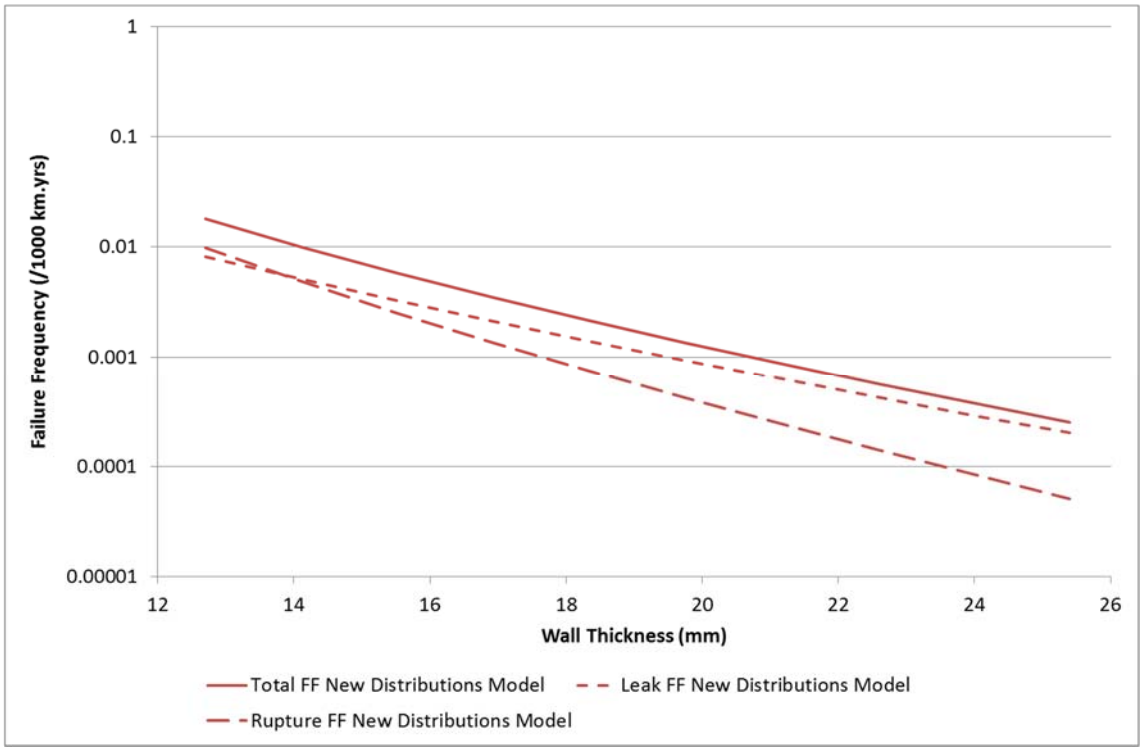

Figure A.48: Leak, Rupture and Total Failure Frequency as Calculated by the New Distributions Model, for Example 3

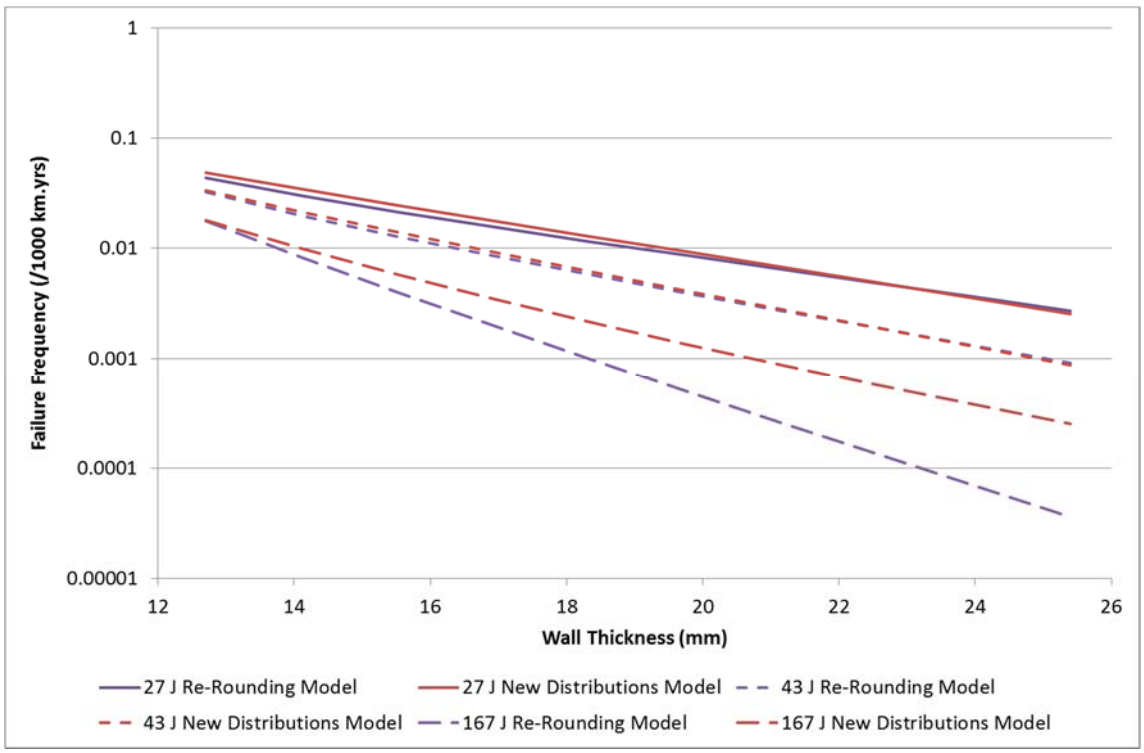

Figure A.49: Total Failure Frequency as Calculated by the New Distributions Model and the Re-Rounding Model for Examples 1, 2 and 3

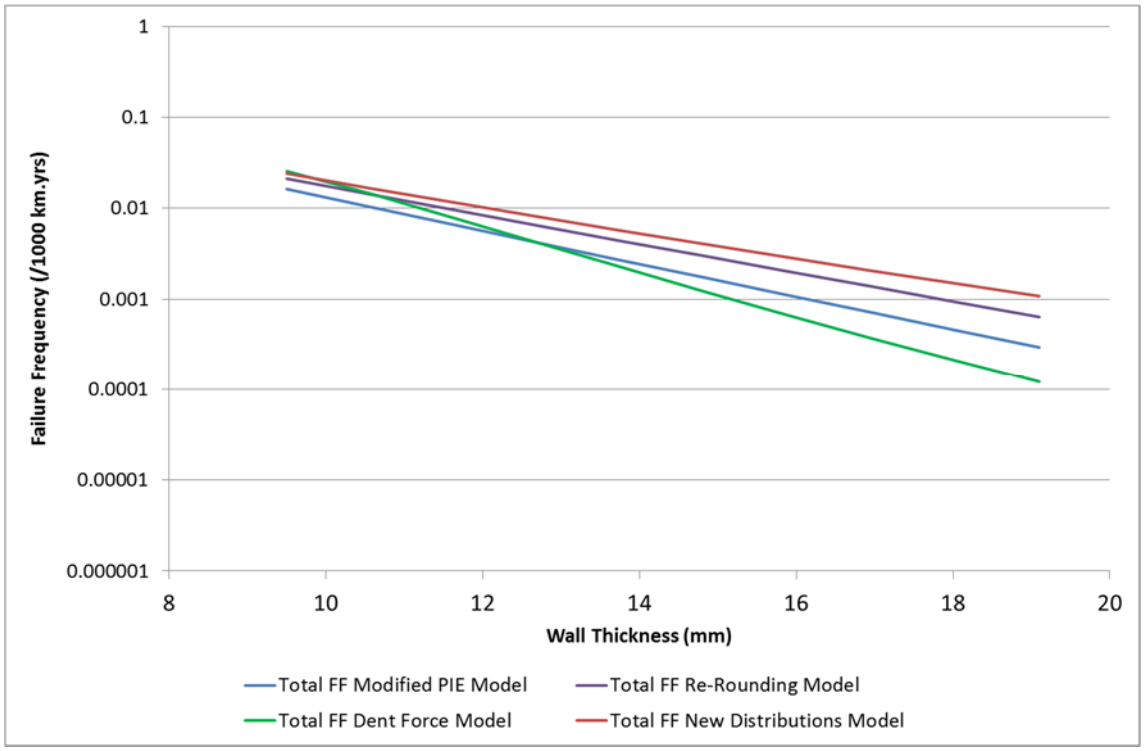

Figure A.50: Total Failure Frequency as Calculated by the New Distributions Model, Dent Force Model, Re-Rounding Model and the Modified PIE Model for Example 4

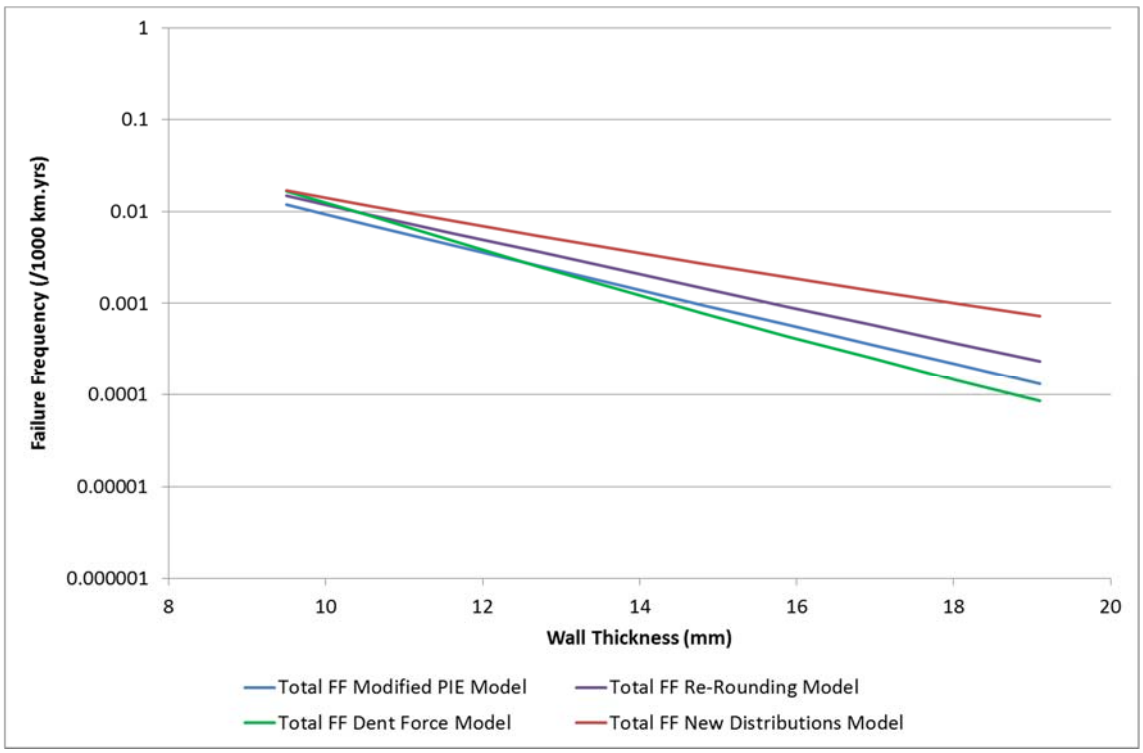

Figure A.51: Total Failure Frequency as Calculated by the New Distributions Model, Dent Force Model, Re-Rounding Model and the Modified PIE Model for Example 5

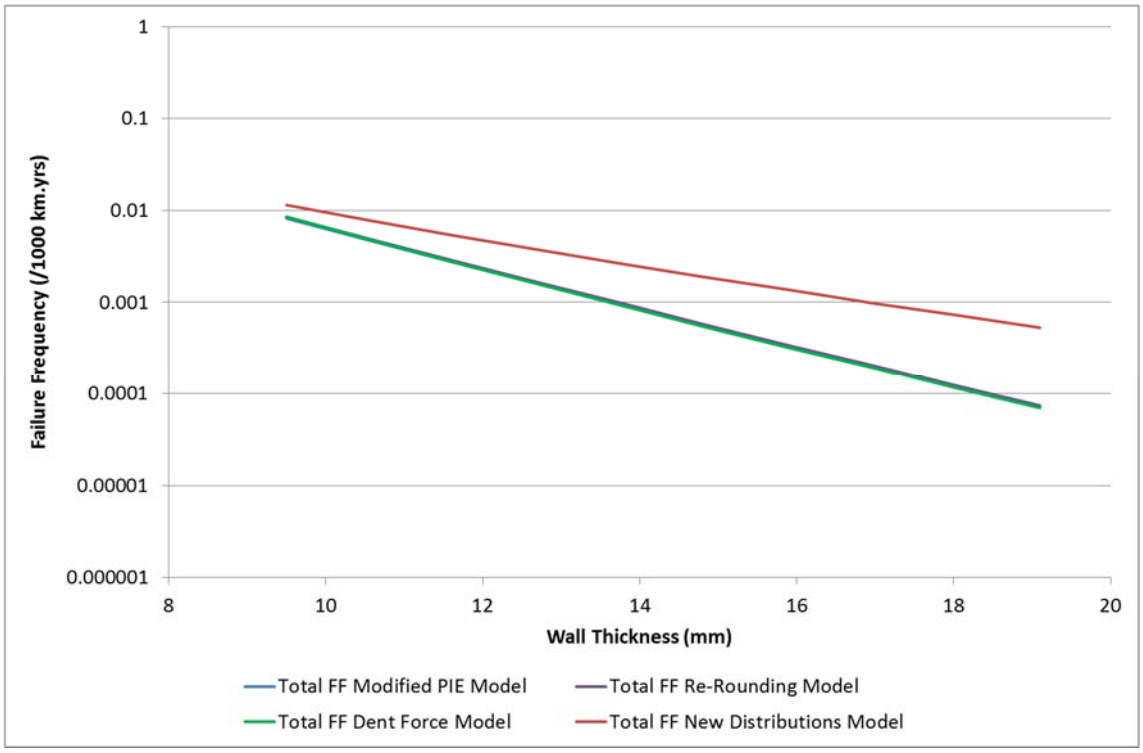

Figure A.52: Total Failure Frequency as Calculated by the New Distributions Model, Dent Force Model, Re-Rounding Model and the Modified PIE Model for Example 6

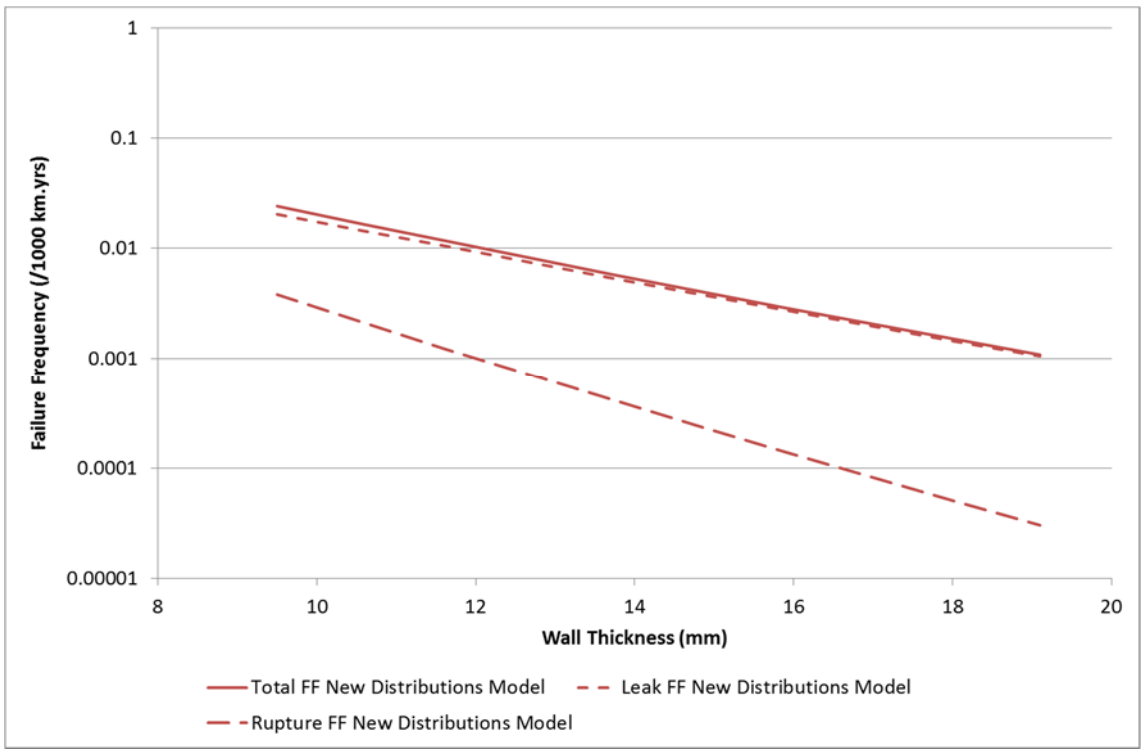

Figure A.53: Leak, Rupture and Total Failure Frequency as Calculated by the New Distributions Model, for Example 4

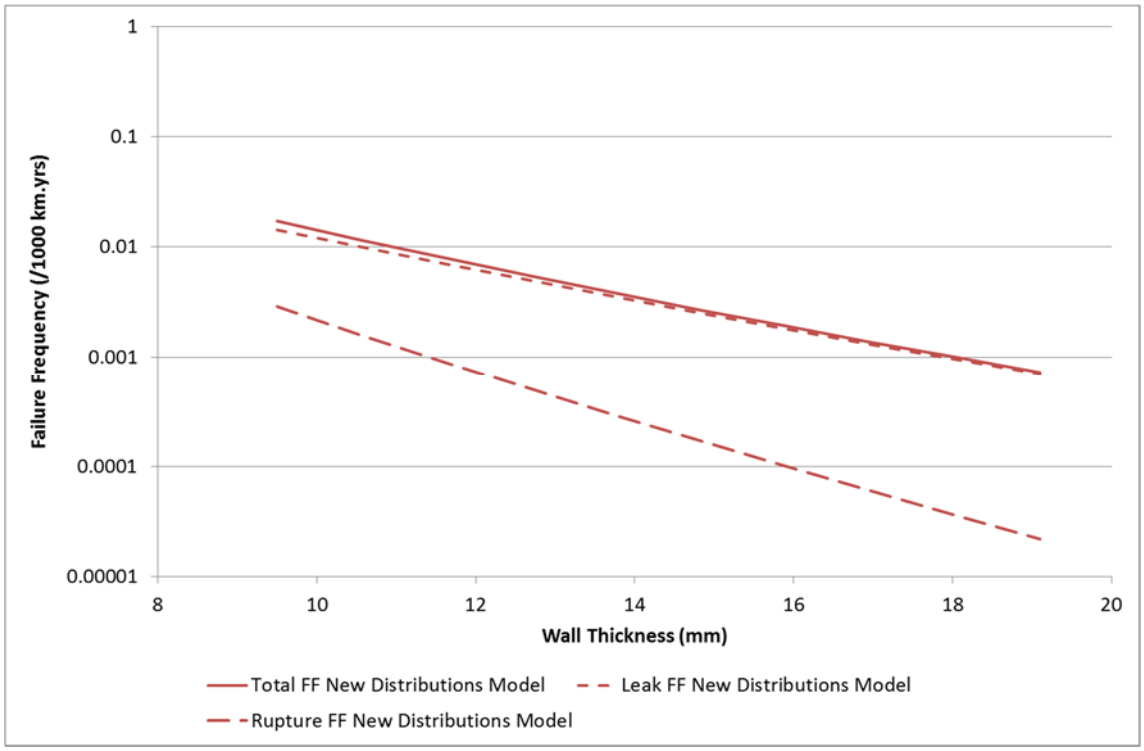

Figure A.54: Leak, Rupture and Total Failure Frequency as Calculated by the New Distributions Model, for Example 5

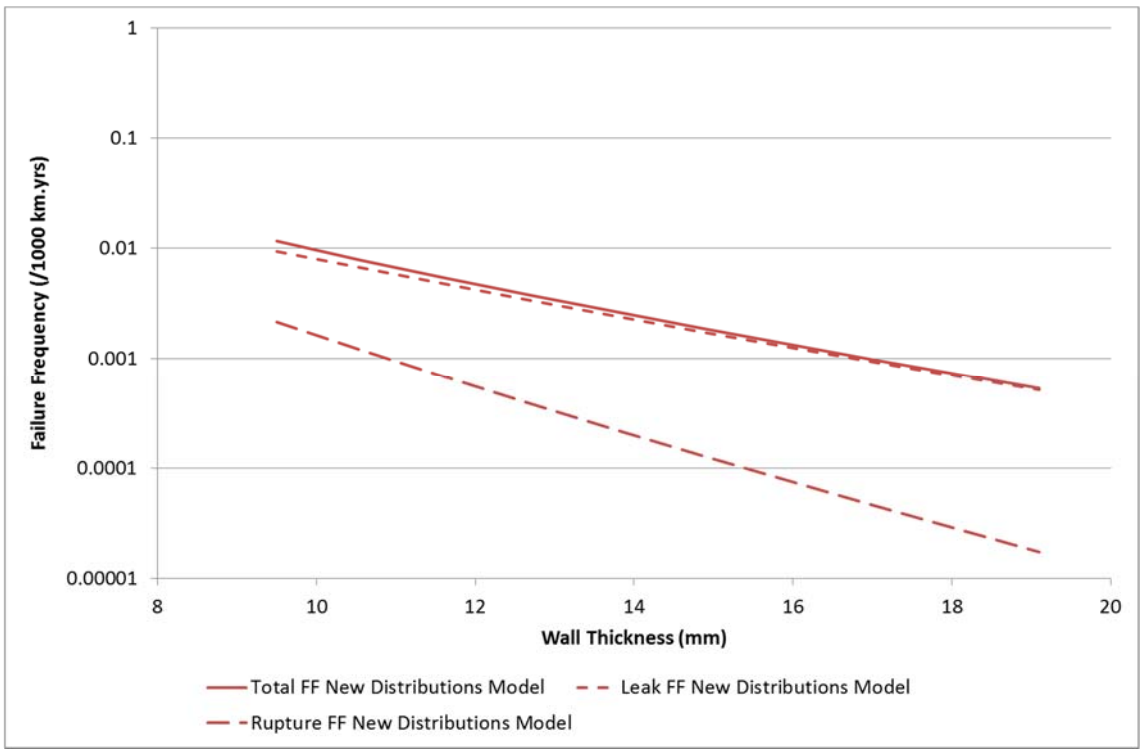

Figure A.55: Leak, Rupture and Total Failure Frequency as Calculated by the New Distributions Model, for Example 6

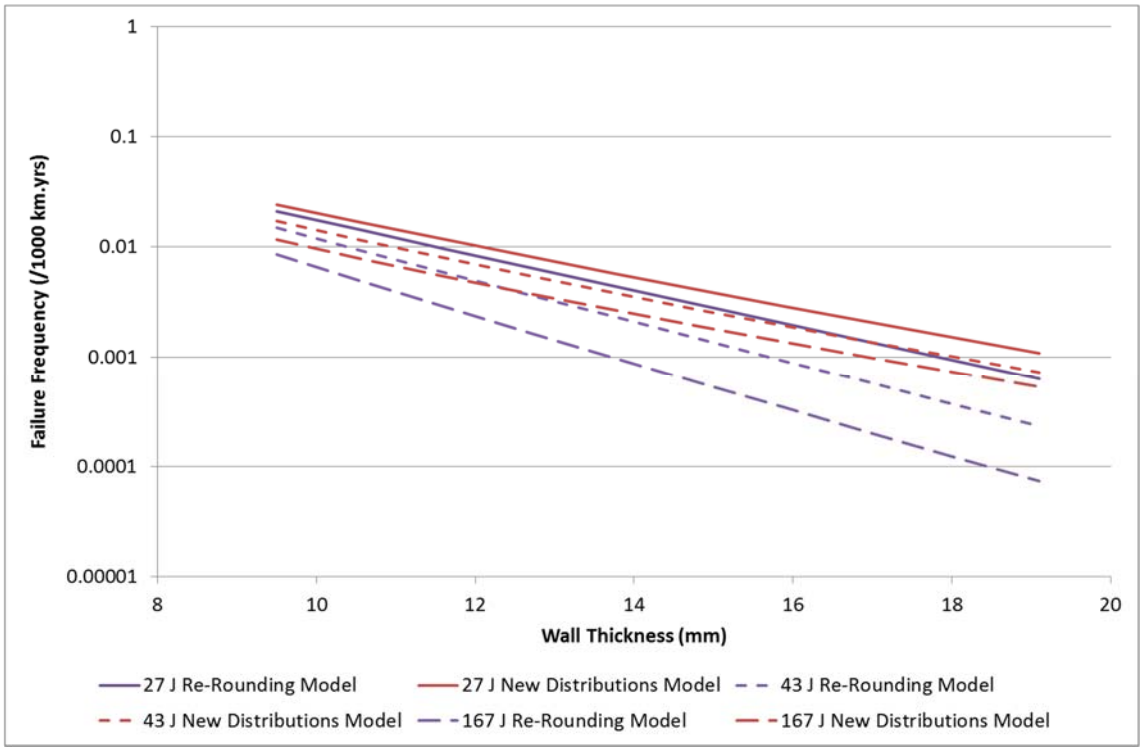

Figure A.56: Total Failure Frequency as Calculated by the New Distributions Model and the Re-Rounding Model for Examples 4, 5 and 6

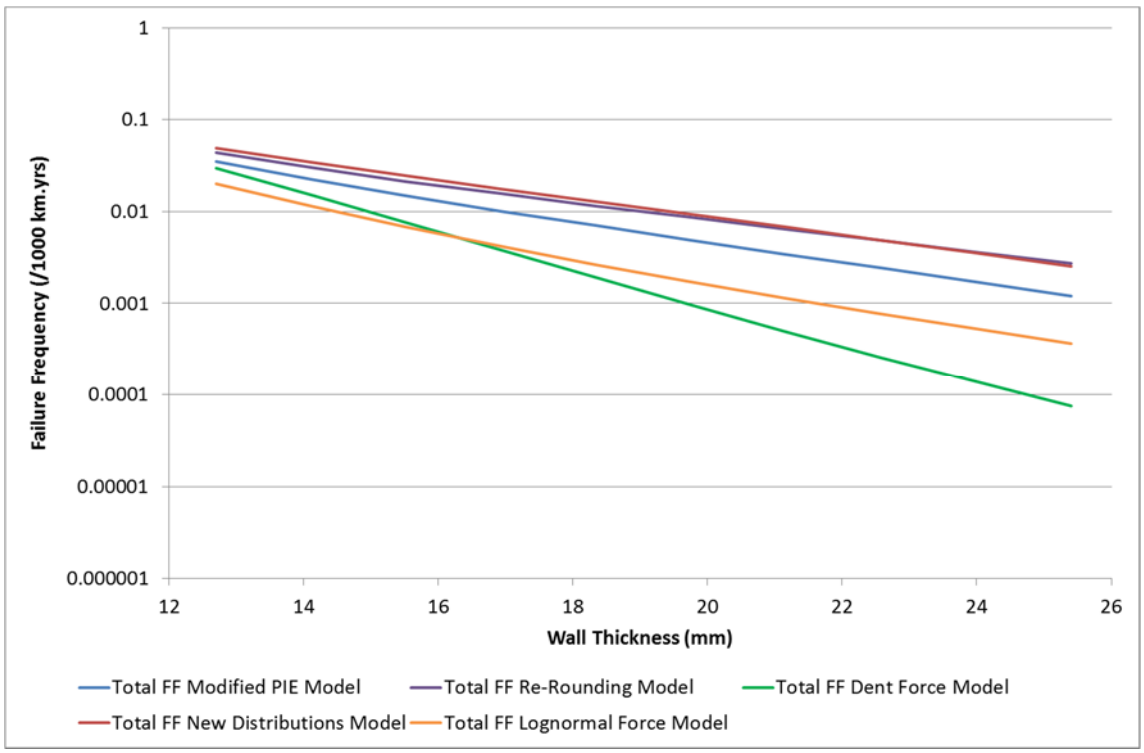

Figure A.57: Total Failure Frequency as Calculated by the Lognormal Force Model, New Distributions Model, Dent Force Model, Re-Rounding Model and the Modified PIE Model for Example 1

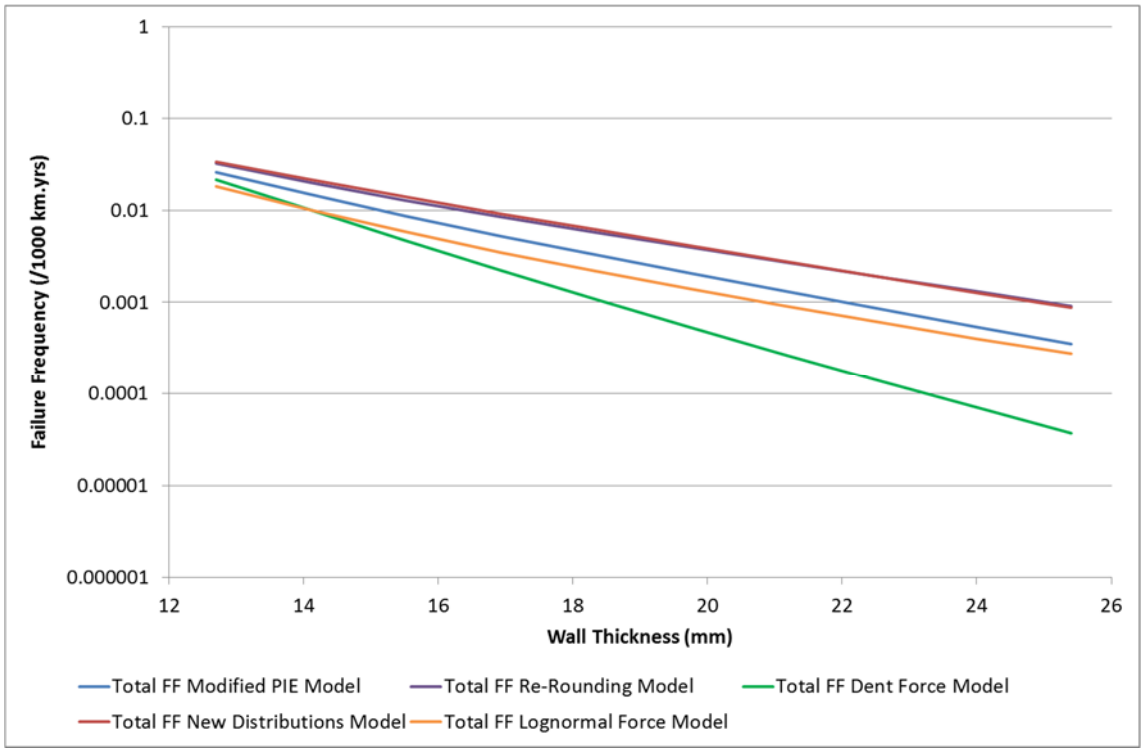

Figure A.58: Total Failure Frequency as Calculated by the Lognormal Force Model, New Distributions Model, Dent Force Model, Re-Rounding Model and the Modified PIE Model for Example 2

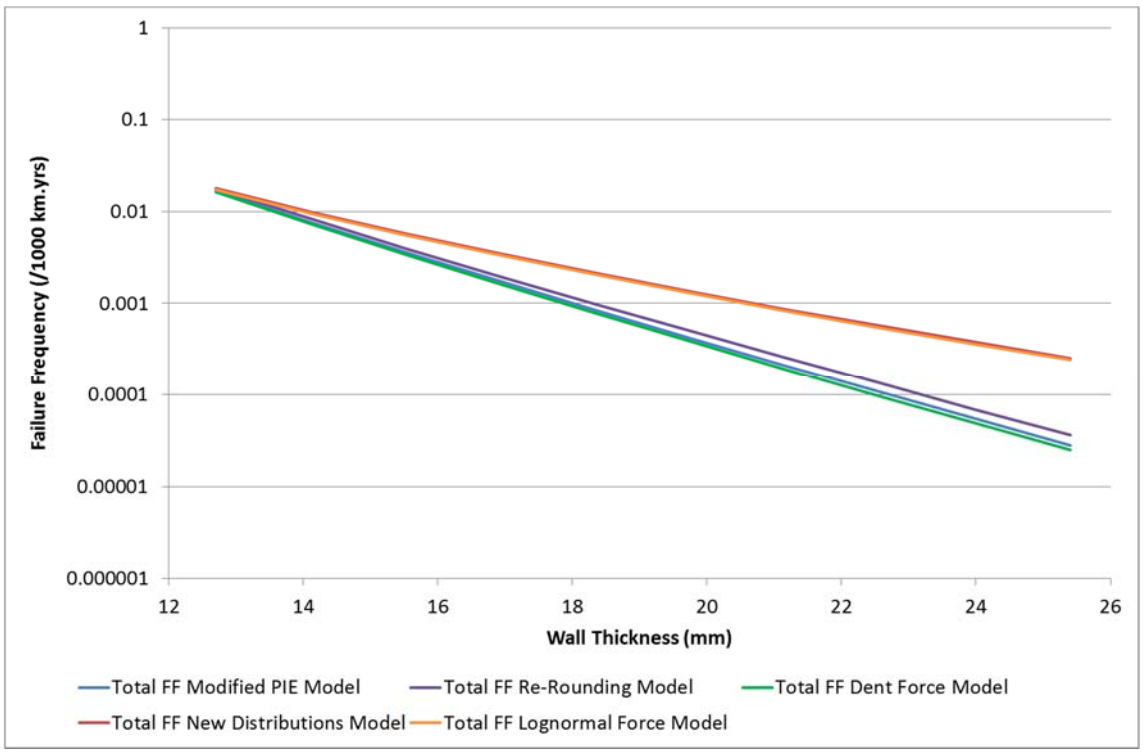

Figure A.59: Total Failure Frequency as Calculated by the Lognormal Force Model, New Distributions Model, Dent Force Model, Re-Rounding Model and the Modified PIE Model for Example 3

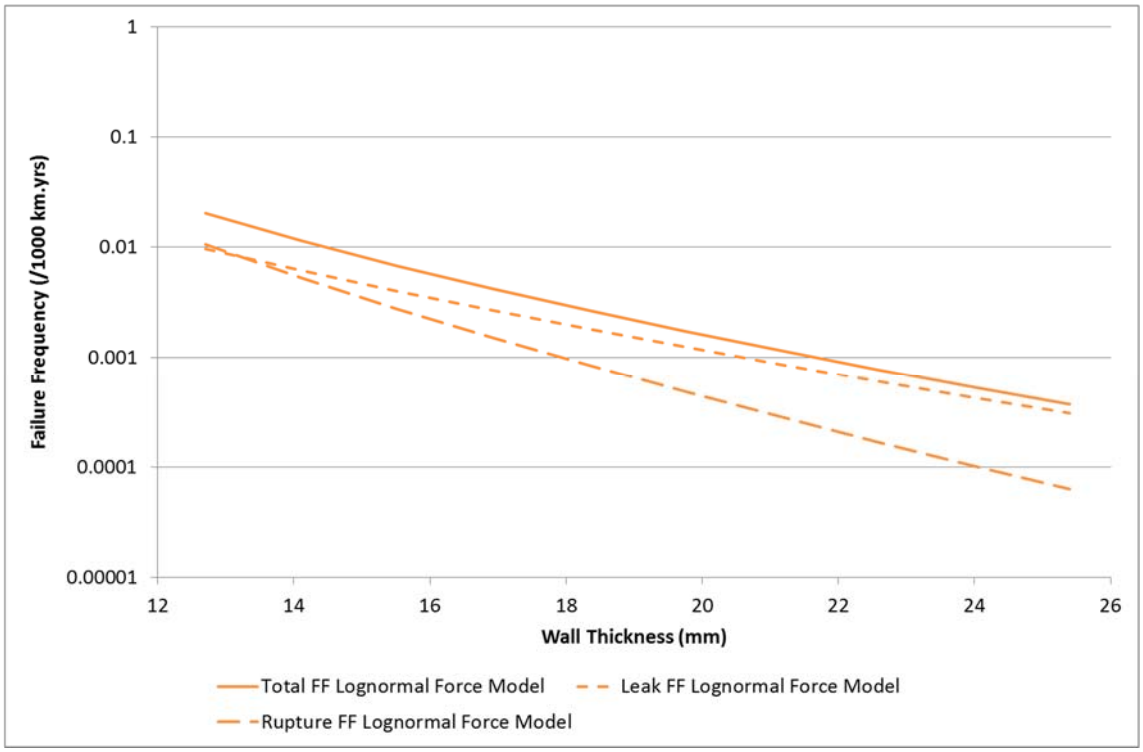

Figure A.60: Leak, Rupture and Total Failure Frequency as Calculated by the Lognormal Force Model, for Example 1

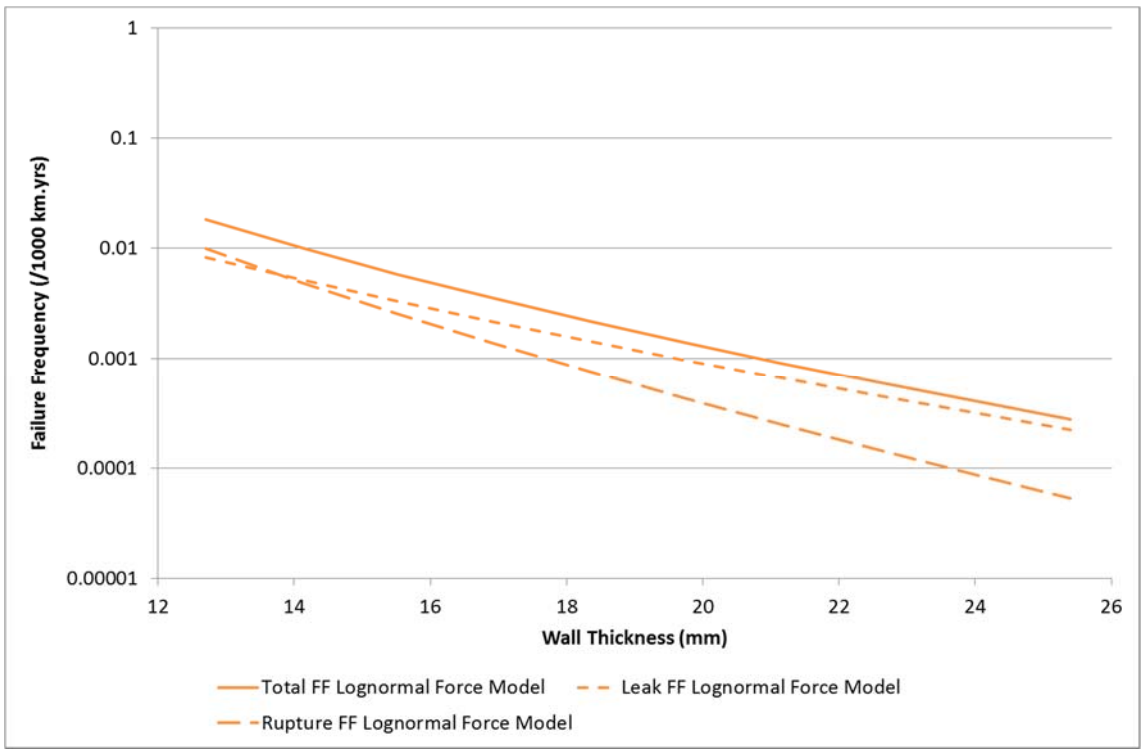

Figure A.61: Leak, Rupture and Total Failure Frequency as Calculated by the Lognormal Force Model, for Example 2

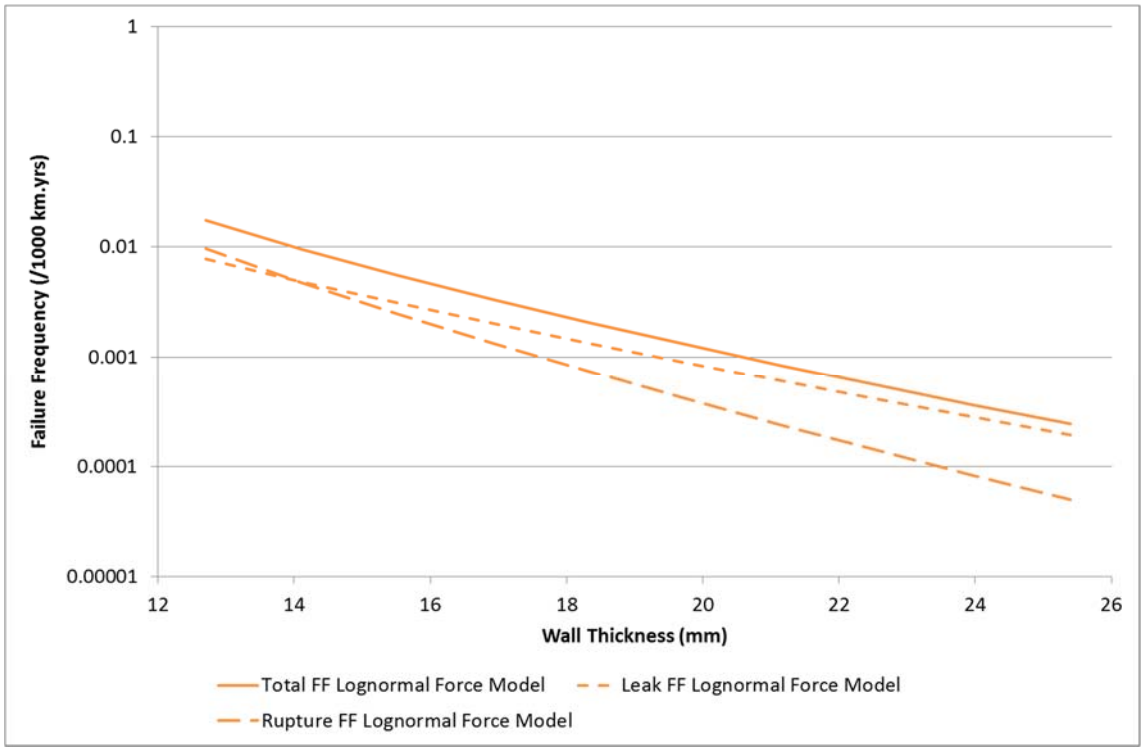

Figure A.62: Leak, Rupture and Total Failure Frequency as Calculated by the Lognormal Force Model, for Example 3

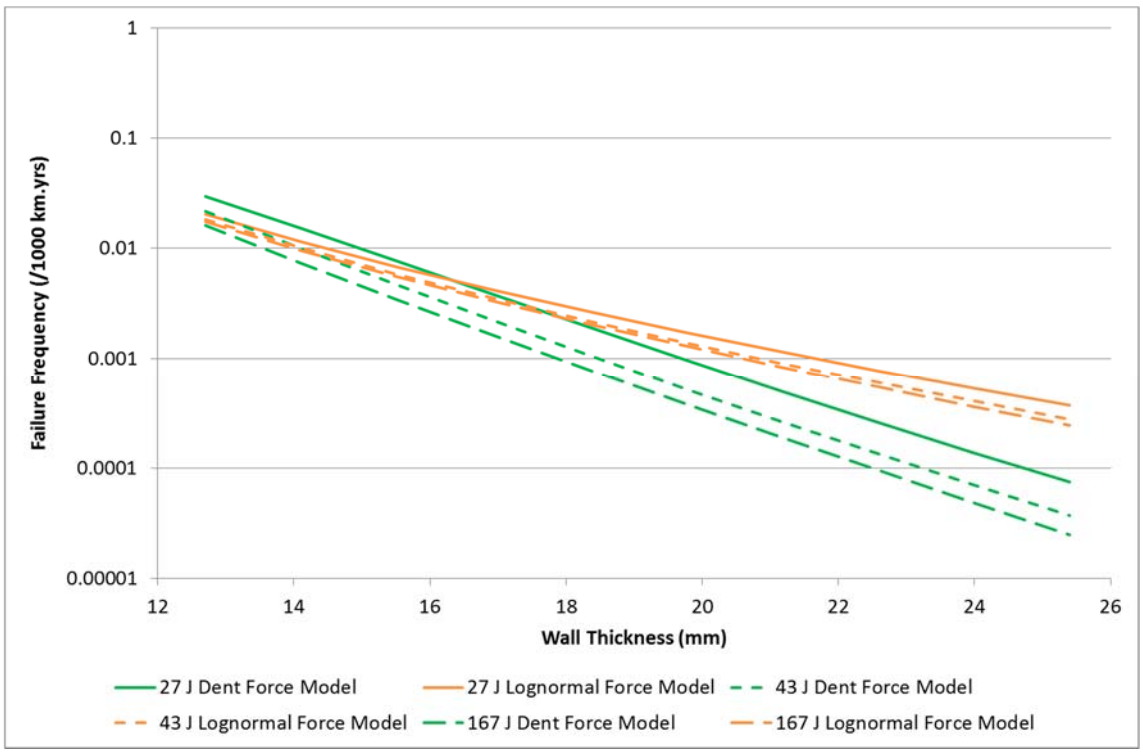

Figure A.63: Total Failure Frequency as Calculated by the Lognormal Force Model and the Dent Force Model for Examples 1, 2 and 3

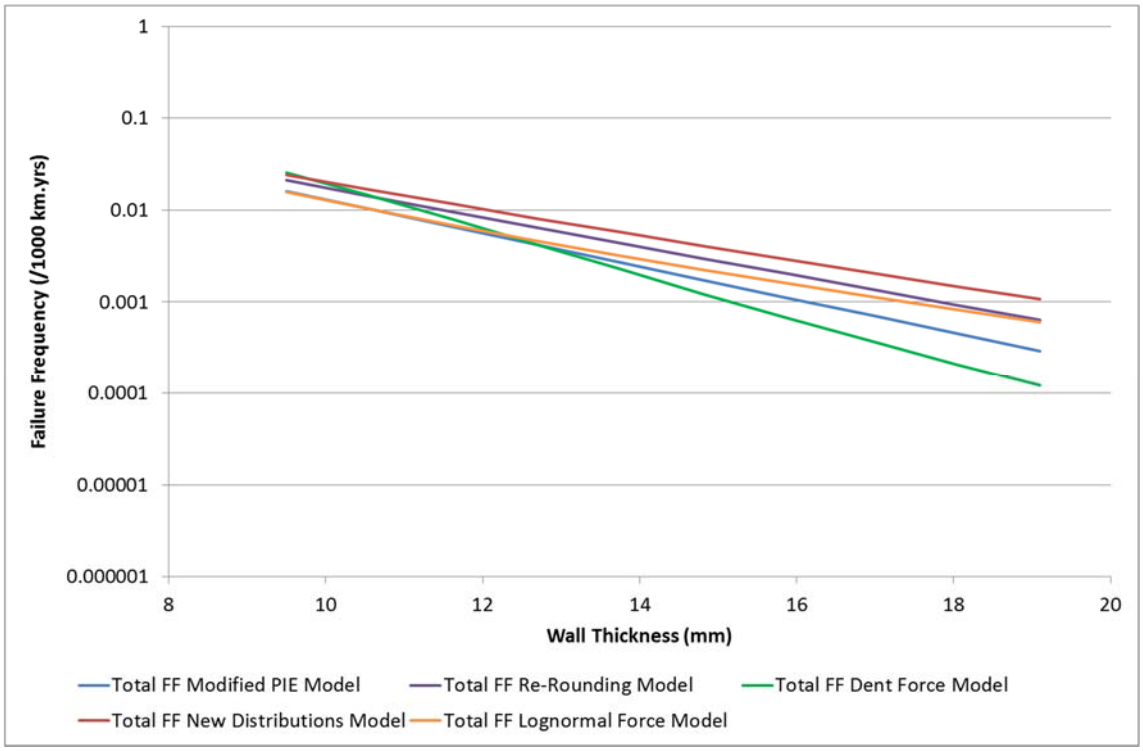

Figure A.64: Total Failure Frequency as Calculated by the Lognormal Force Model, New Distributions Model, Dent Force Model, Re-Rounding Model and the Modified PIE Model for Example 4

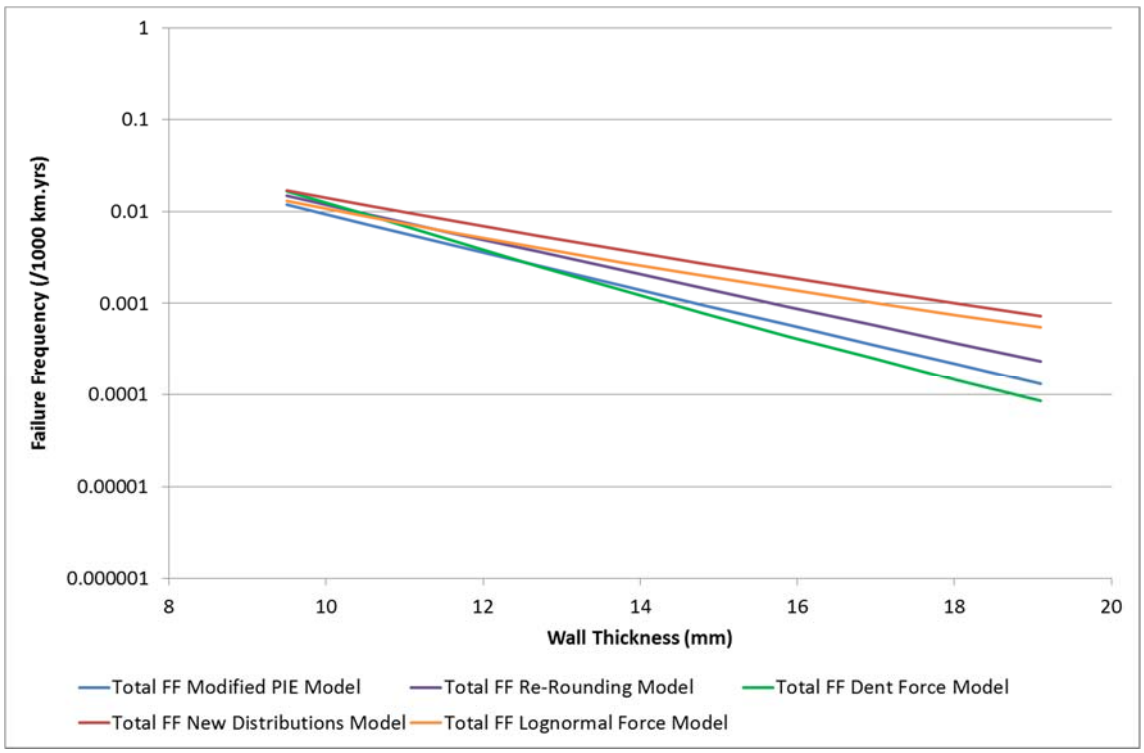

Figure A.65: Total Failure Frequency as Calculated by the Lognormal Force Model, New Distributions Model, Dent Force Model, Re-Rounding Model and the Modified PIE Model for Example 5

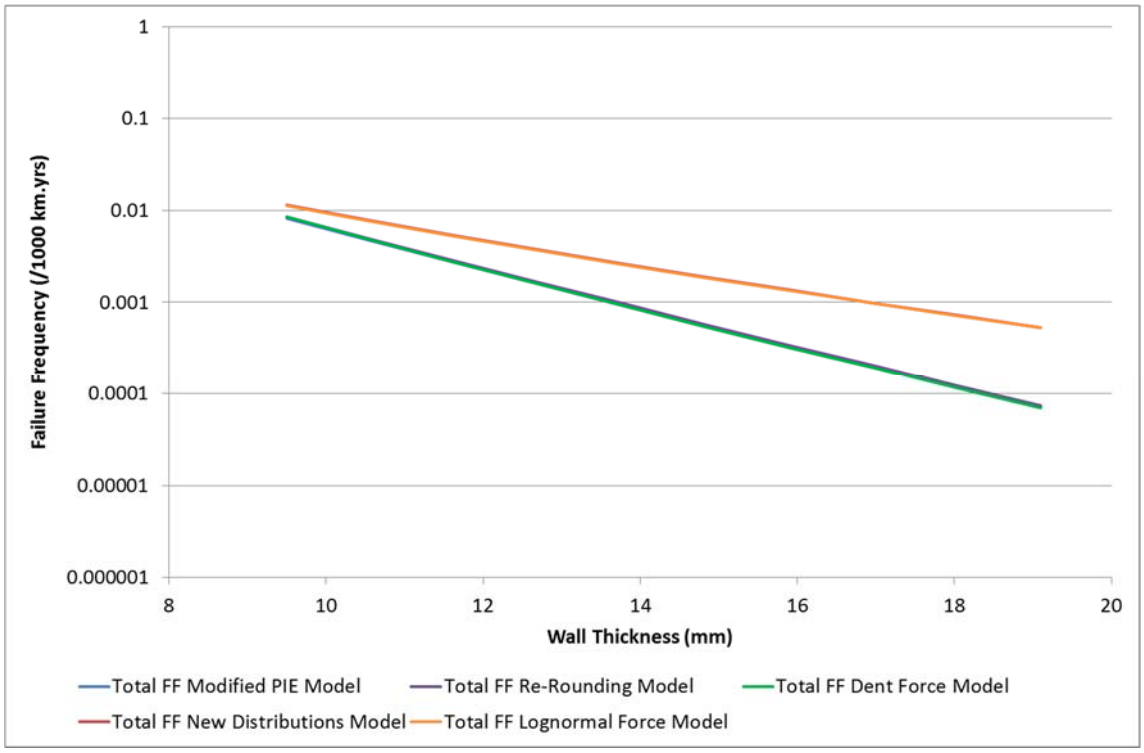

Figure A.66: Total Failure Frequency as Calculated by the Lognormal Force Model, New Distributions Model, Dent Force Model, Re-Rounding Model and the Modified PIE Model for Example 6

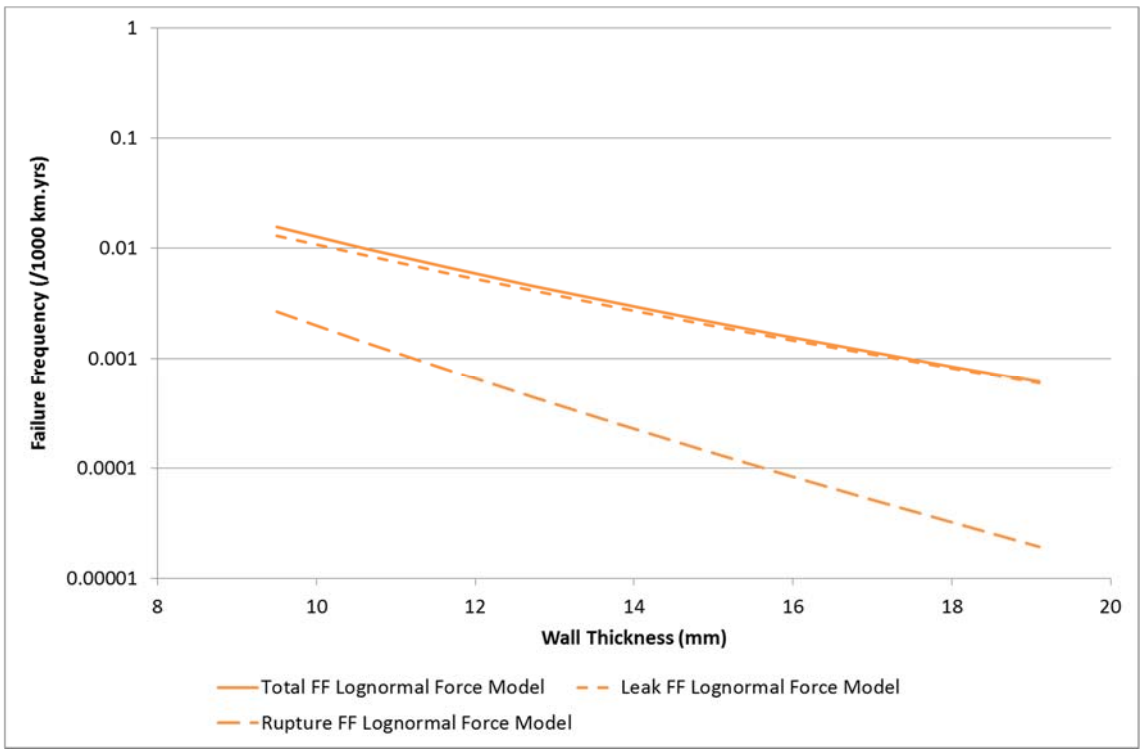

Figure A.67: Leak, Rupture and Total Failure Frequency as Calculated by the Lognormal Force Model, for Example 4

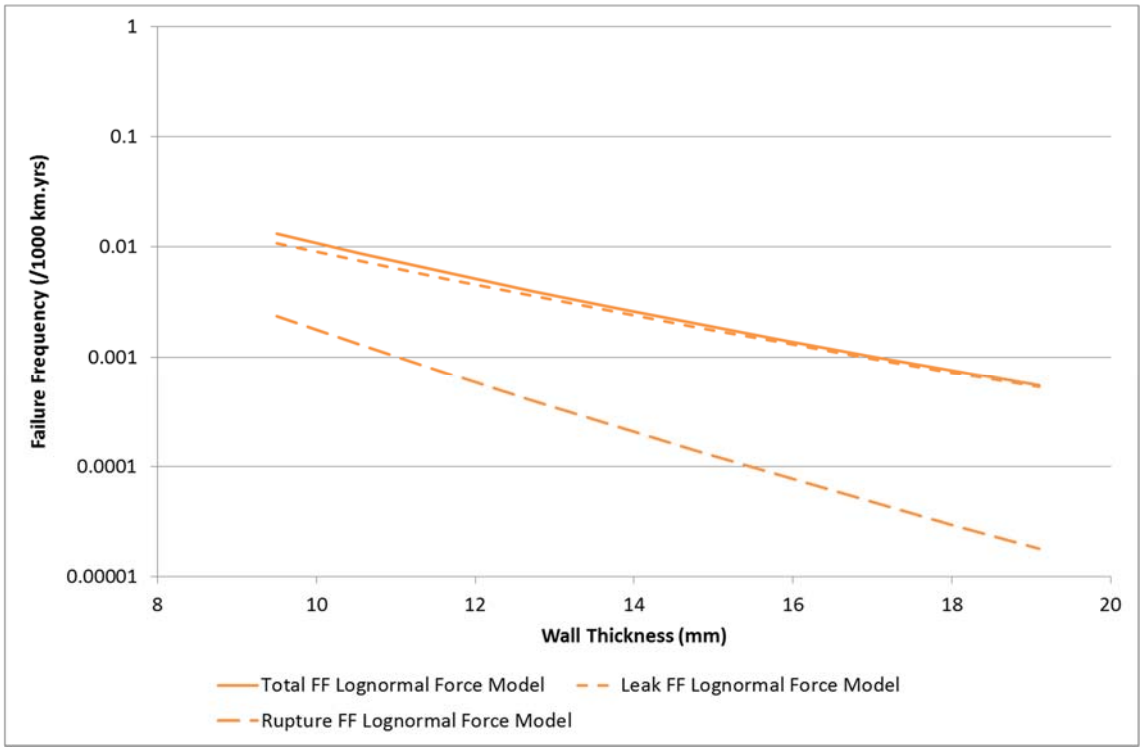

Figure A.68: Leak, Rupture and Total Failure Frequency as Calculated by the Lognormal Force Model, for Example 5

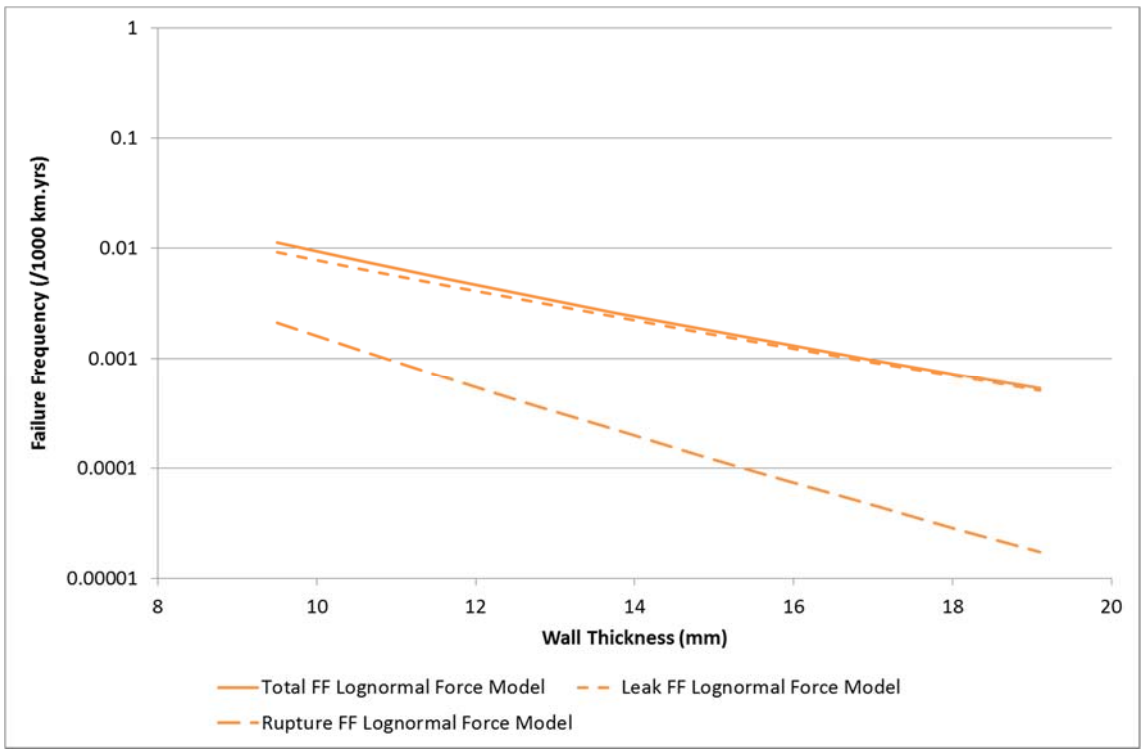

Figure A.69: Leak, Rupture and Total Failure Frequency as Calculated by the Lognormal Force Model, for Example 6

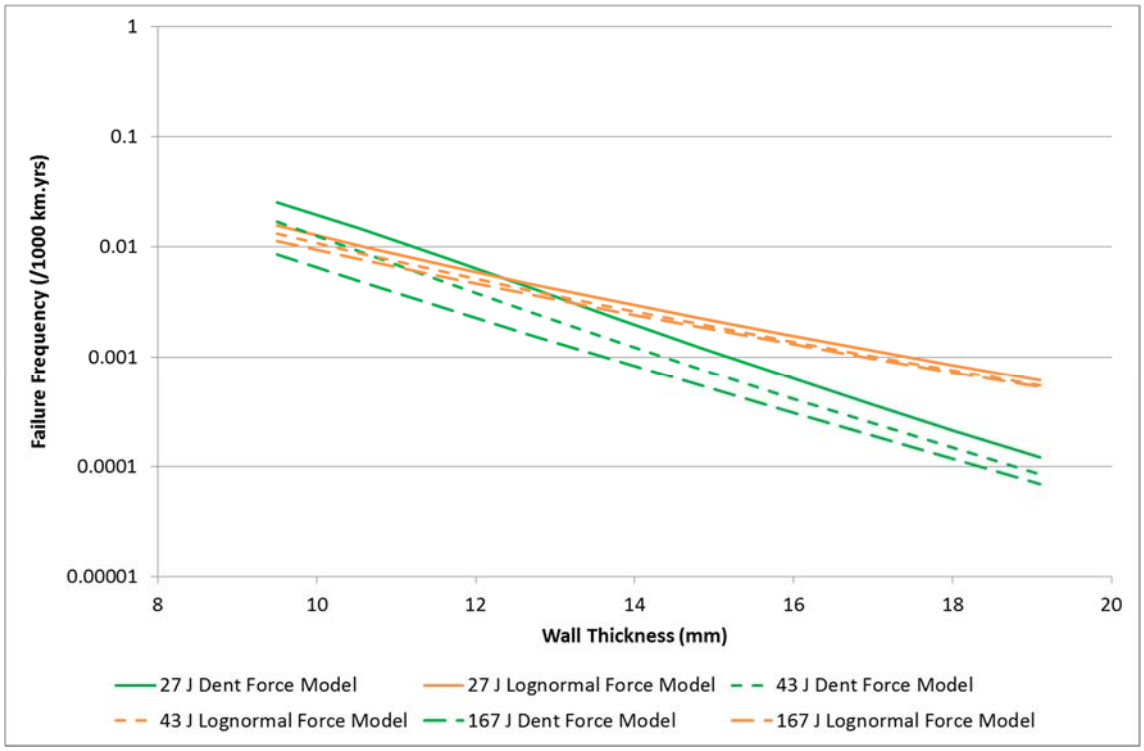

Figure A.70: Total Failure Frequency as Calculated by the Lognormal Force Model and the Dent Force Model for Examples 4, 5 and 6

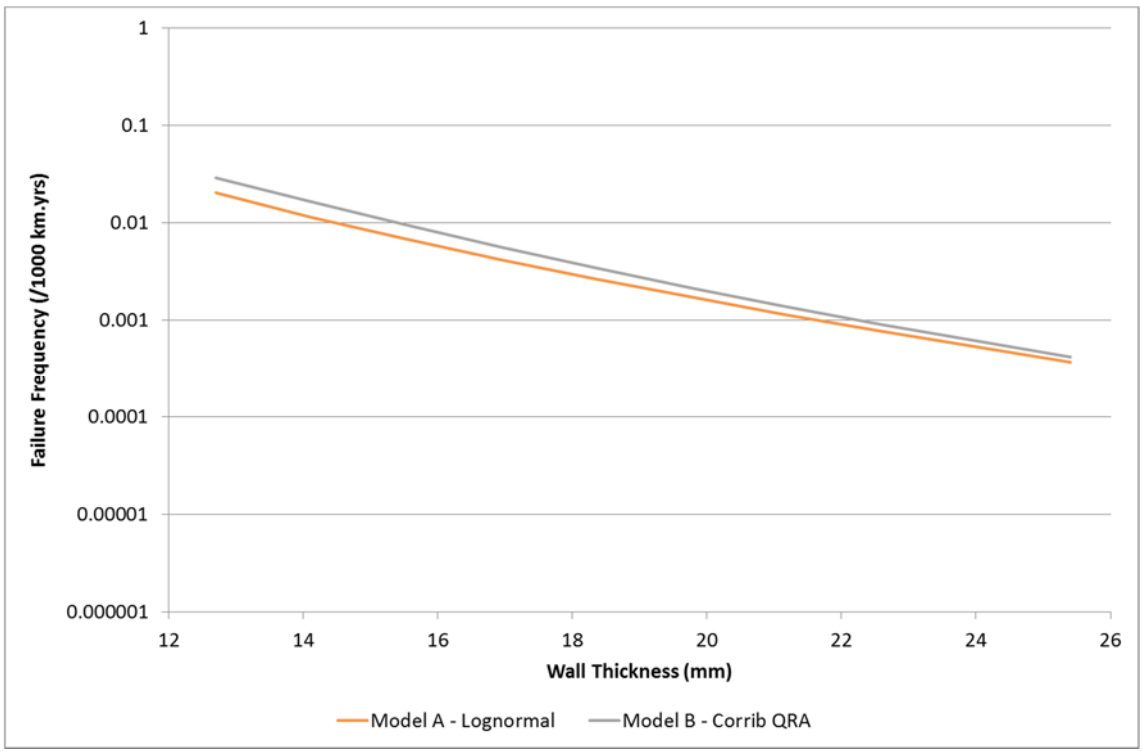

Figure A.71: Total Failure Frequency as Calculated by Model A and Model B for Example 1

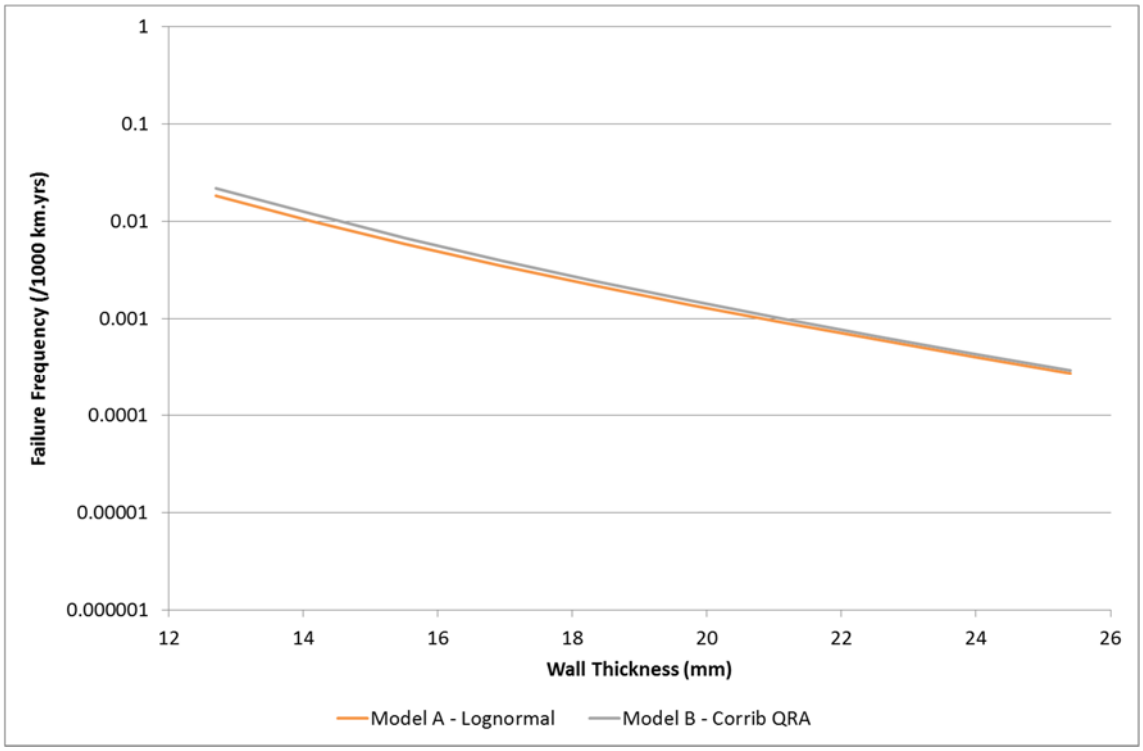

Figure A.72: Total Failure Frequency as Calculated by Model A and Model B for Example 2

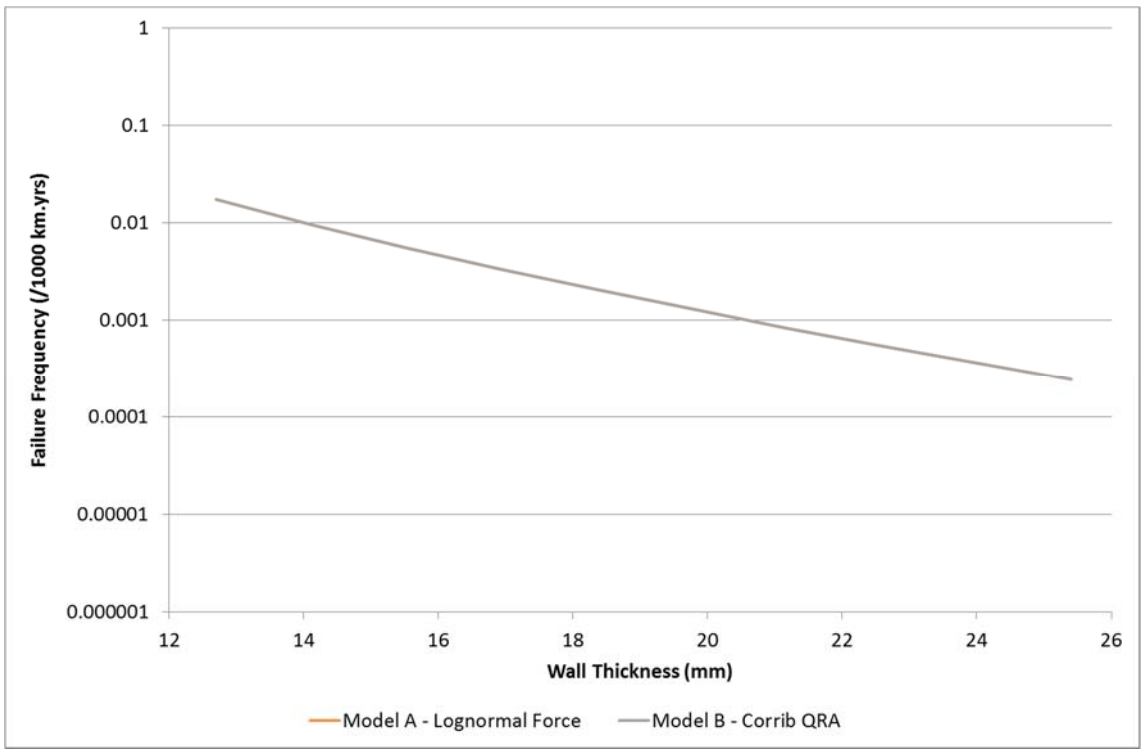

Figure A.73: Total Failure Frequency as Calculated by Model A and Model B for Example 3

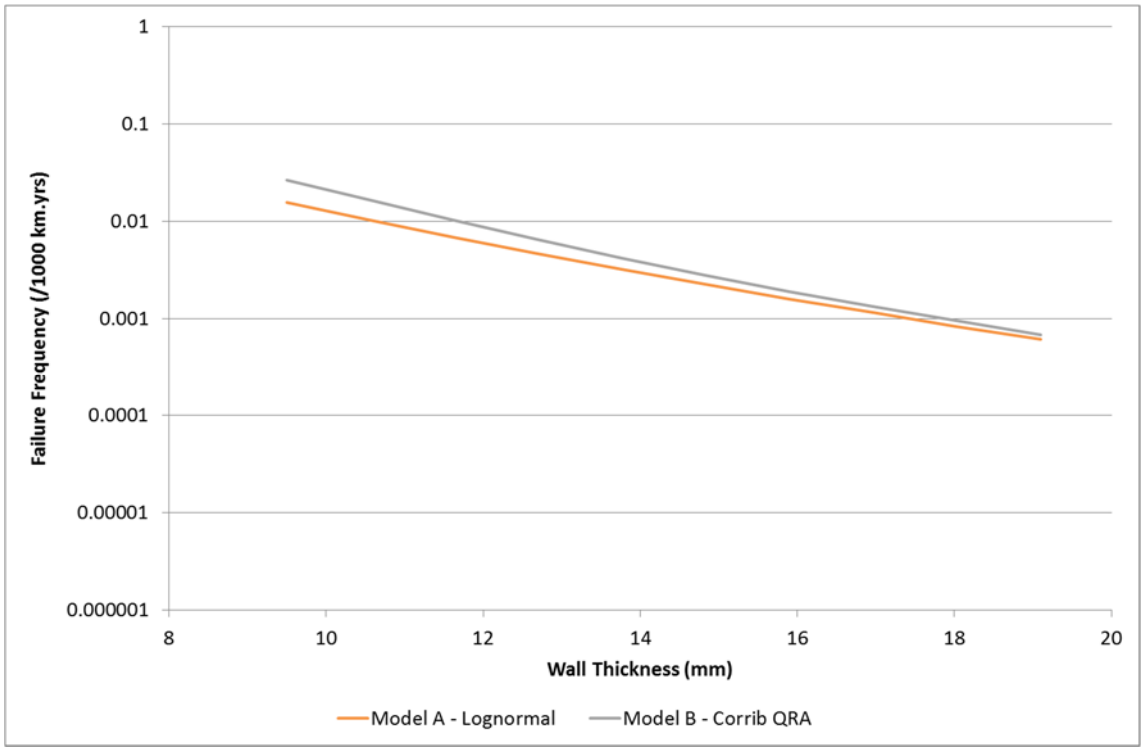

Figure A.74: Total Failure Frequency as Calculated by Model A and Model B for Example 4

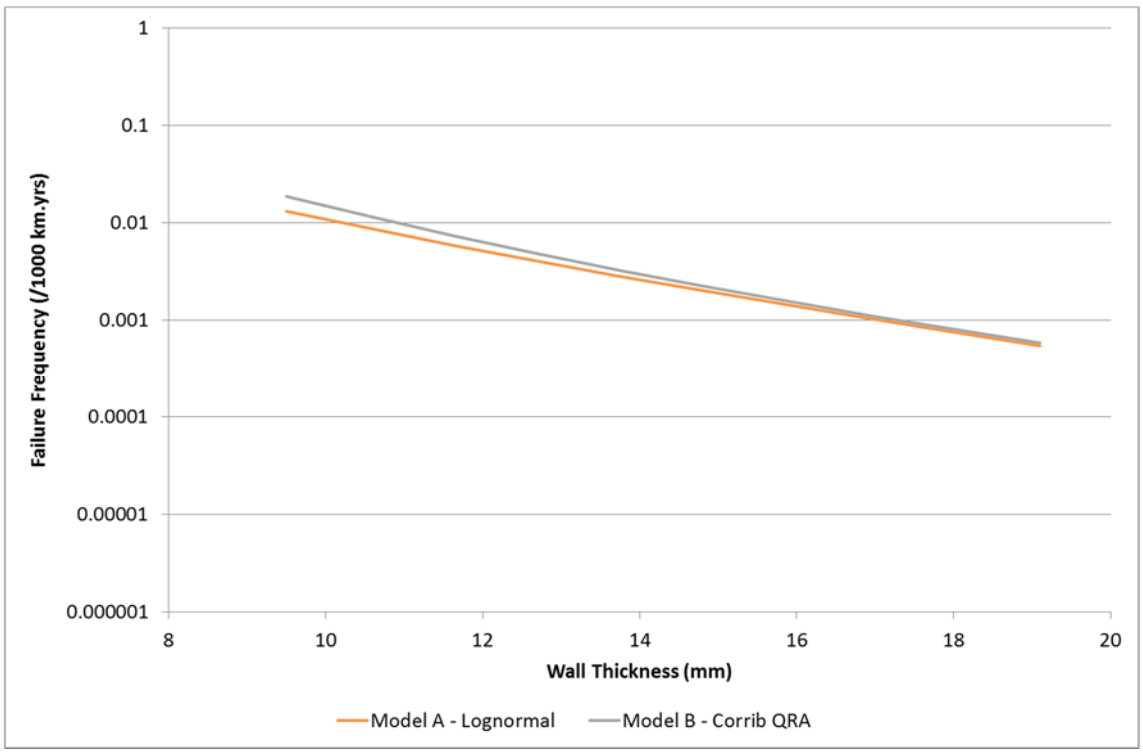

Figure A.75: Total Failure Frequency as Calculated by Model A and Model B for Example 5

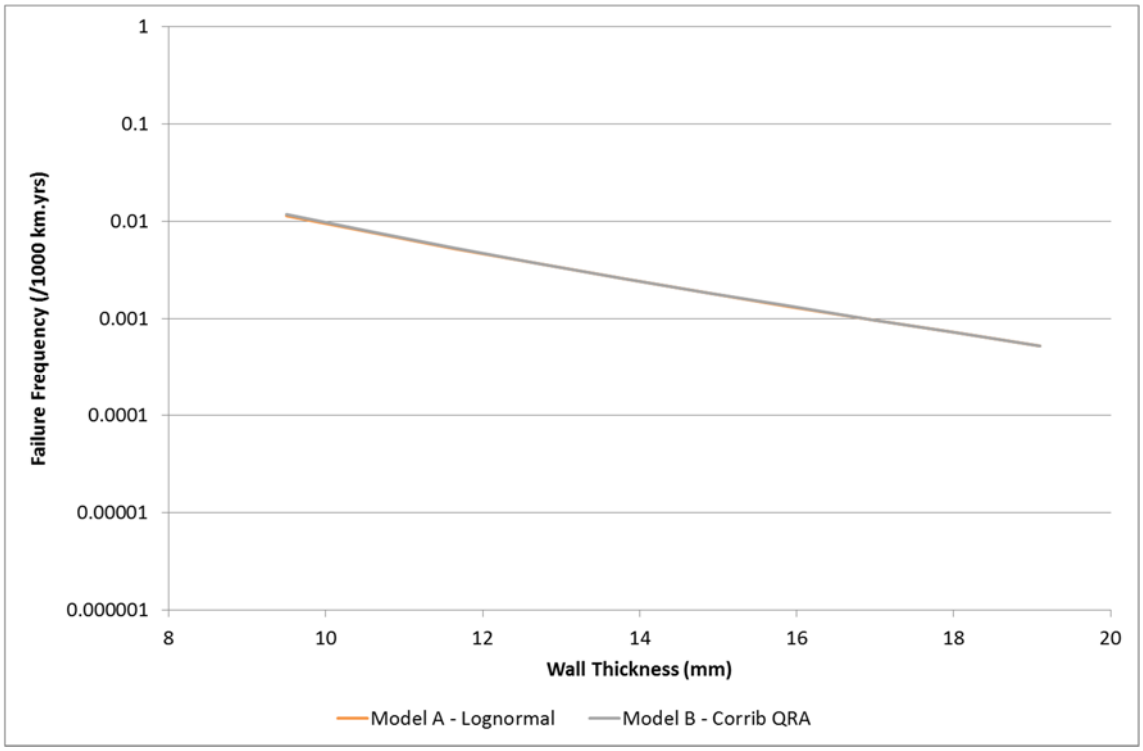

Figure A.76: Total Failure Frequency as Calculated by Model A and Model B for Example 6

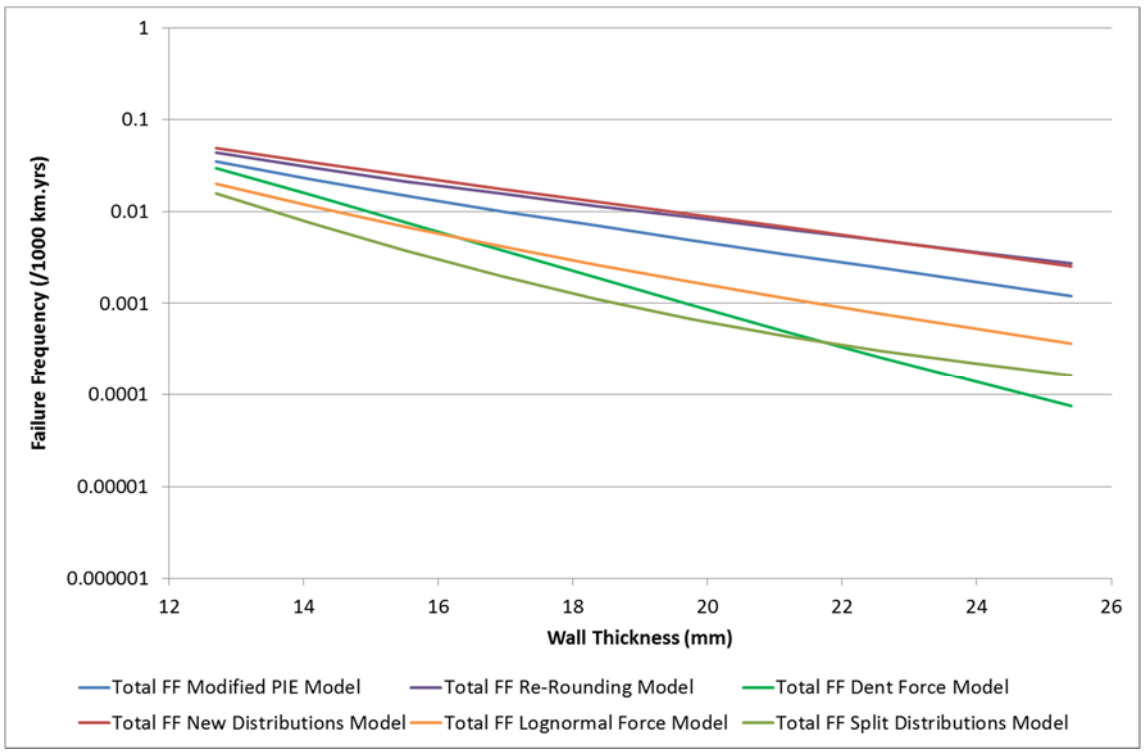

Figure A.77: Total Failure Frequency as Calculated by the Split Distributions Model, Lognormal Force Model, New Distributions Model, Dent Force Model, Re-Rounding Model and the Modified PIE Model for Example 1

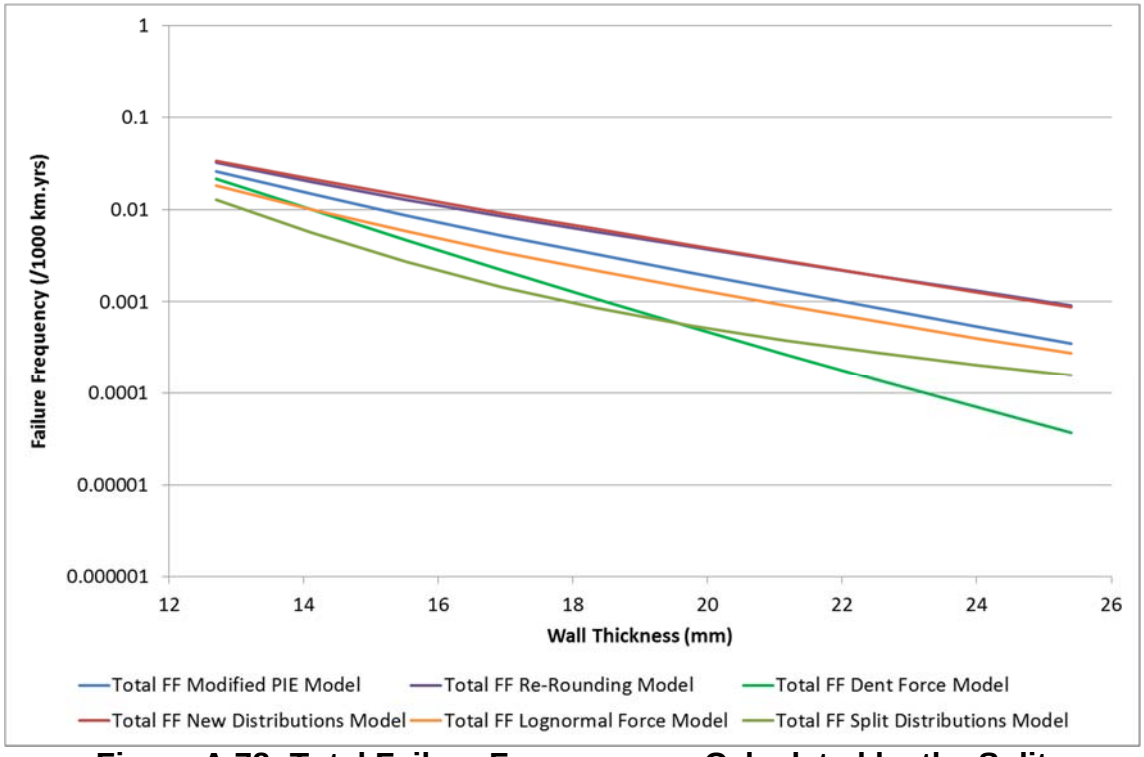

Figure A.78: Total Failure Frequency as Calculated by the Split Distributions Model, Lognormal Force Model, New Distributions Model, Dent Force Model, Re-Rounding Model and the Modified PIE Model for Example 2

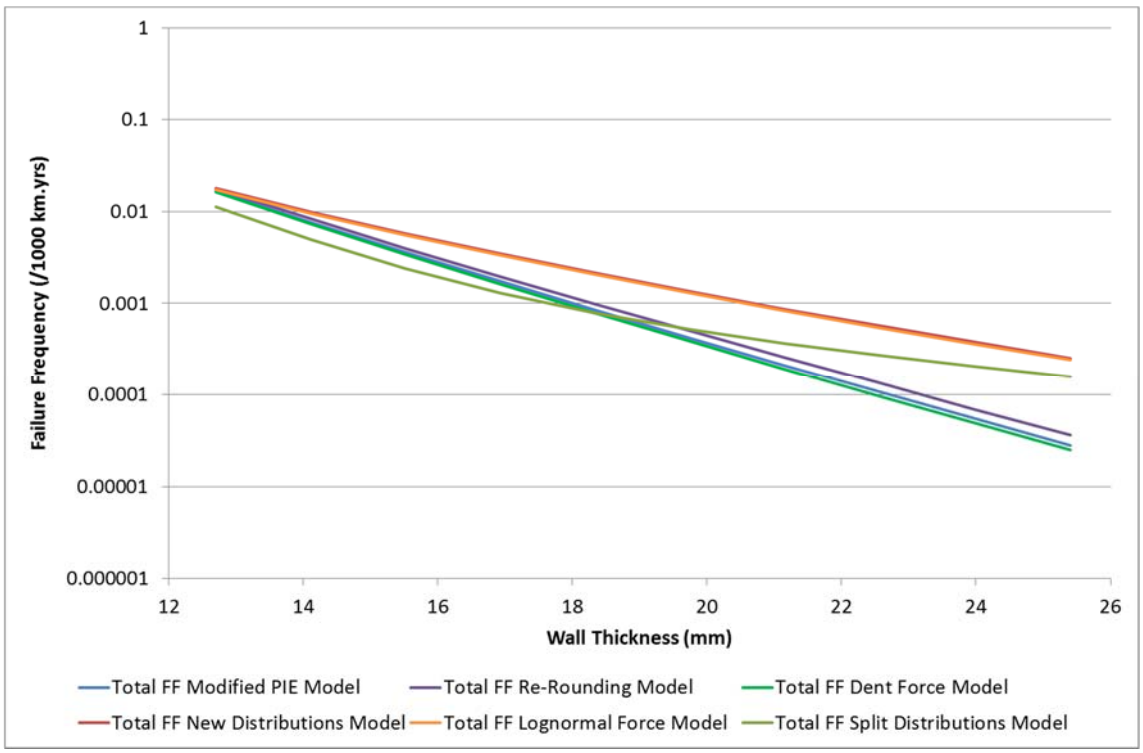

Figure A.79: Total Failure Frequency as Calculated by the Split Distributions Model, Lognormal Force Model, New Distributions Model, Dent Force Model, Re-Rounding Model and the Modified PIE Model for Example 3

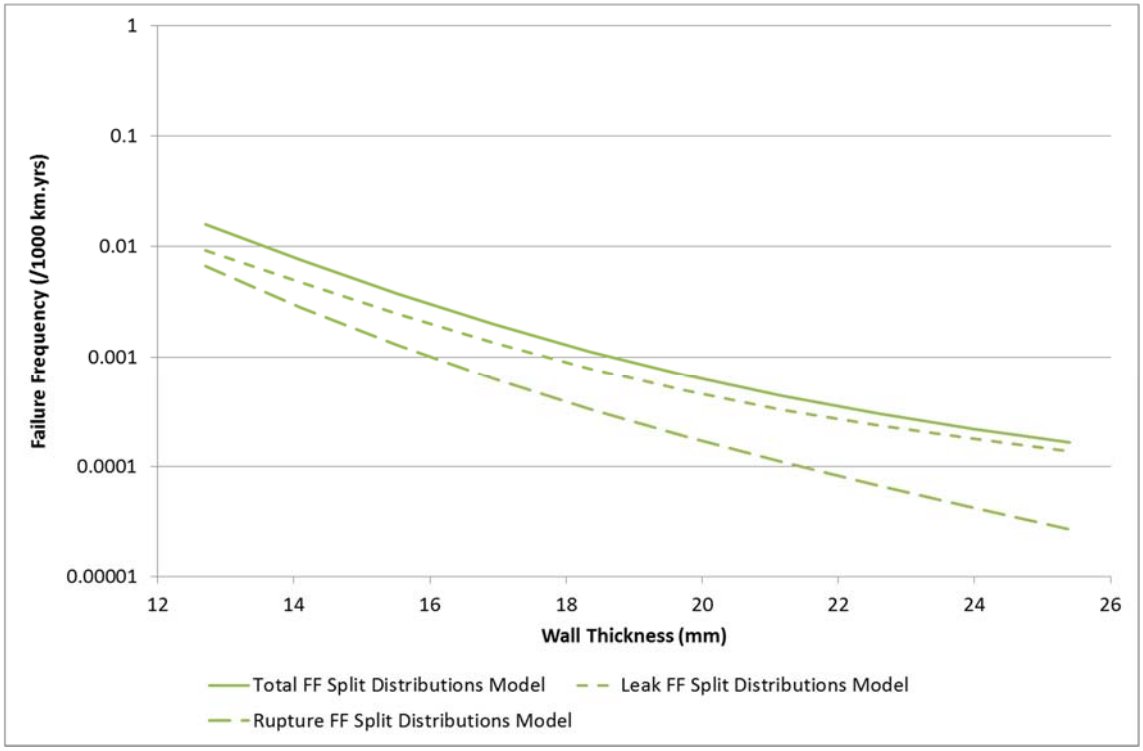

Figure A.80: Leak, Rupture and Total Failure Frequency as Calculated by the Split Distributions Model, for Example 1

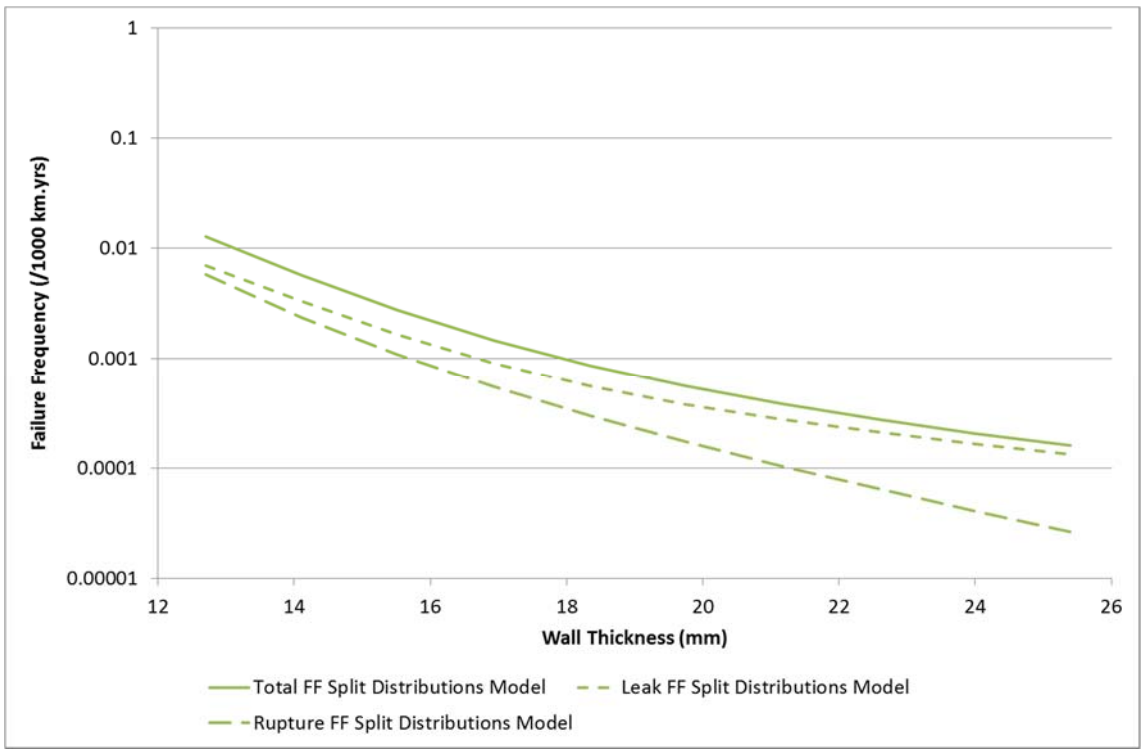

Figure A.81: Leak, Rupture and Total Failure Frequency as Calculated by the Split Distributions Model, for Example 2

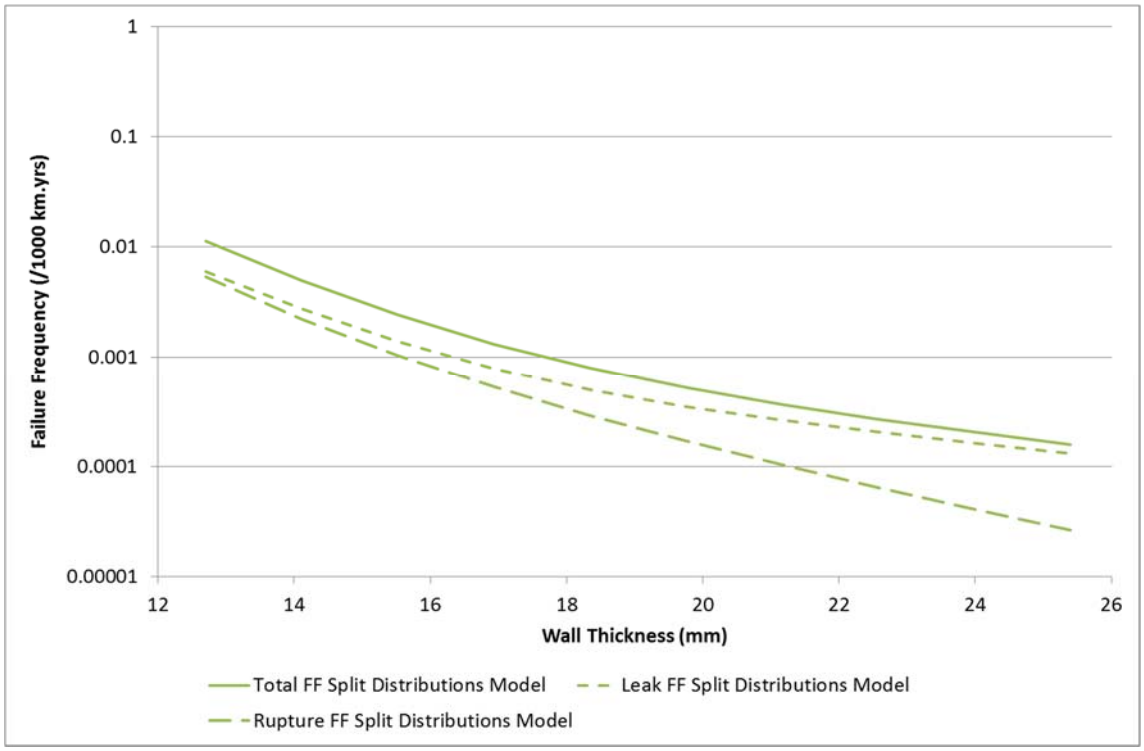

Figure A.82: Leak, Rupture and Total Failure Frequency as Calculated by the Split Distributions Model, for Example 3

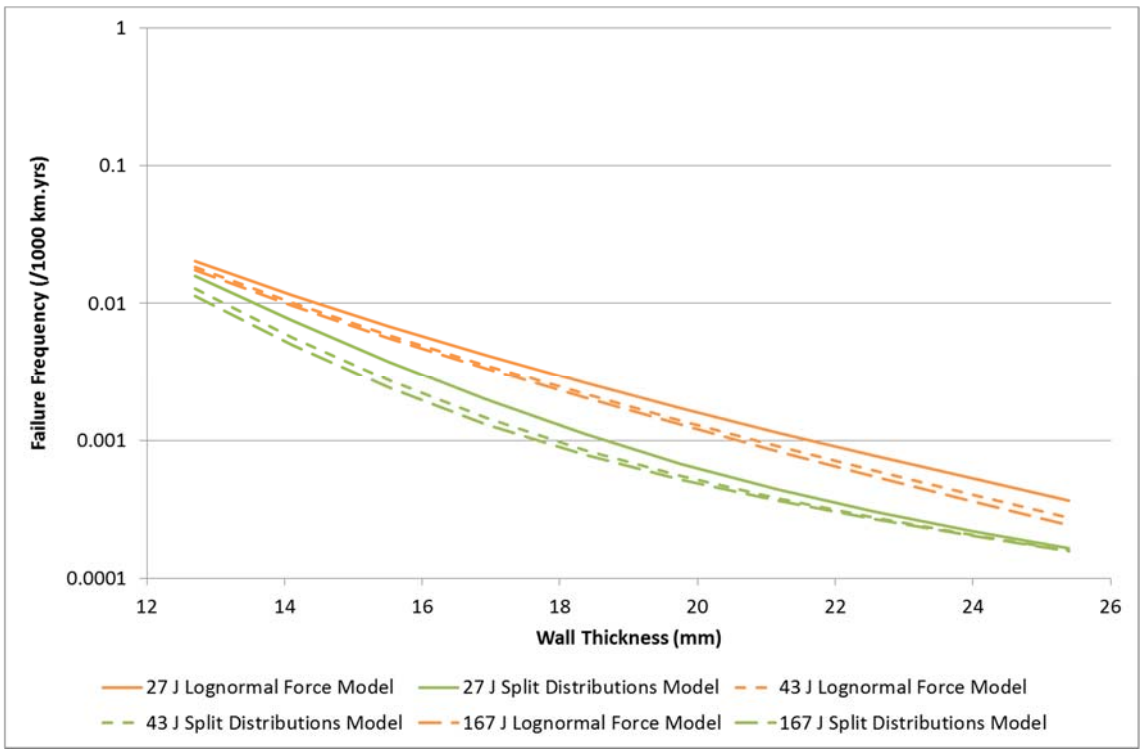

Figure A.83: Total Failure Frequency as Calculated by the Split Distributions Model and the Lognormal Force Model for Examples 1, 2 and 3

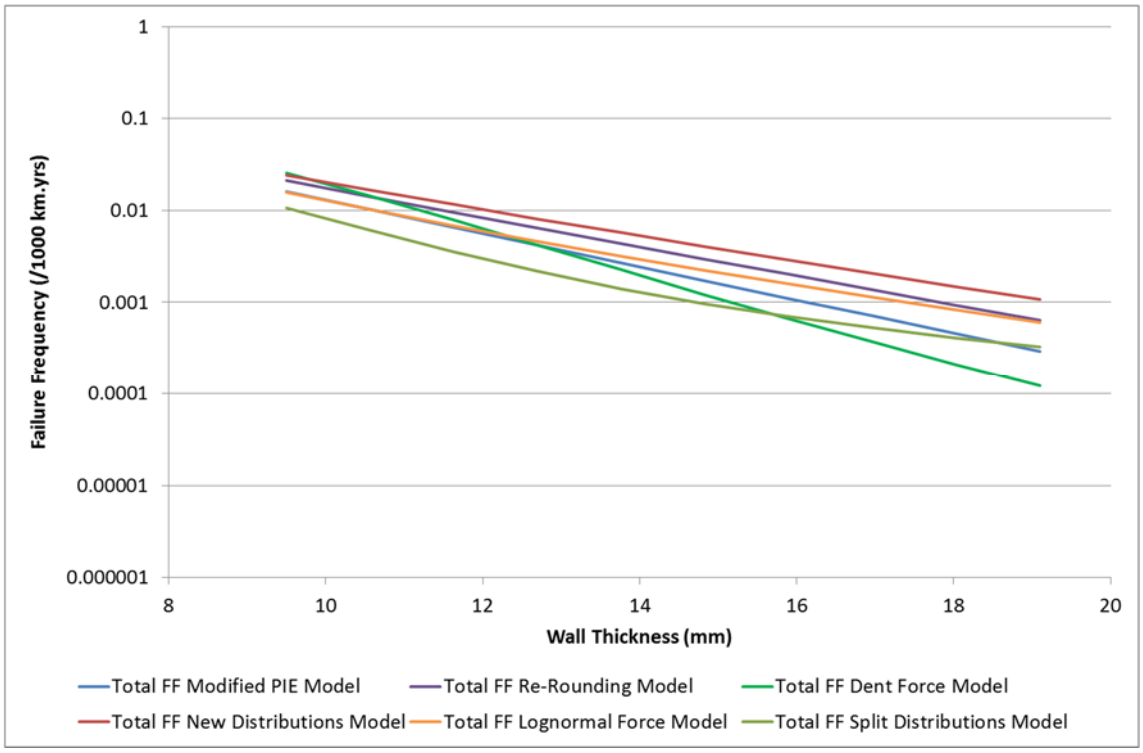

Figure A.84: Total Failure Frequency as Calculated by the Split Distributions Model, Lognormal Force Model, New Distributions Model, Dent Force Model, Re-Rounding Model and the Modified PIE Model for Example 4

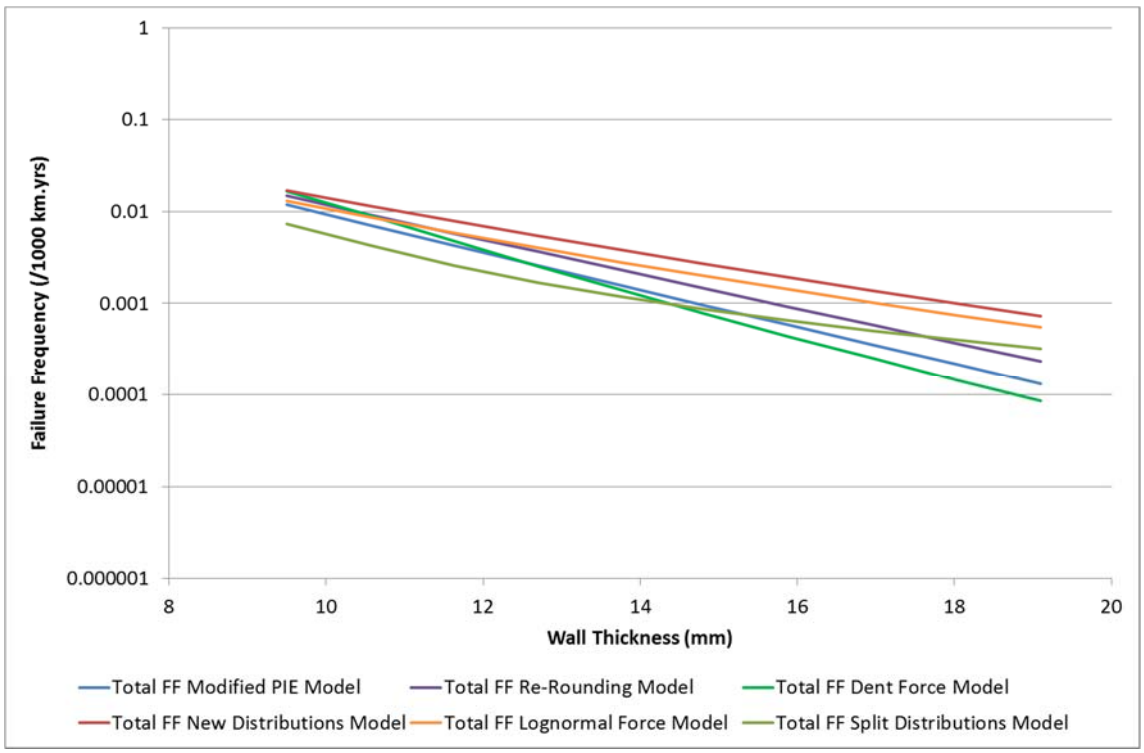

Figure A.85: Total Failure Frequency as Calculated by the Split Distributions Model, Lognormal Force Model, New Distributions Model, Dent Force Model, Re-Rounding Model and the Modified PIE Model for Example 5

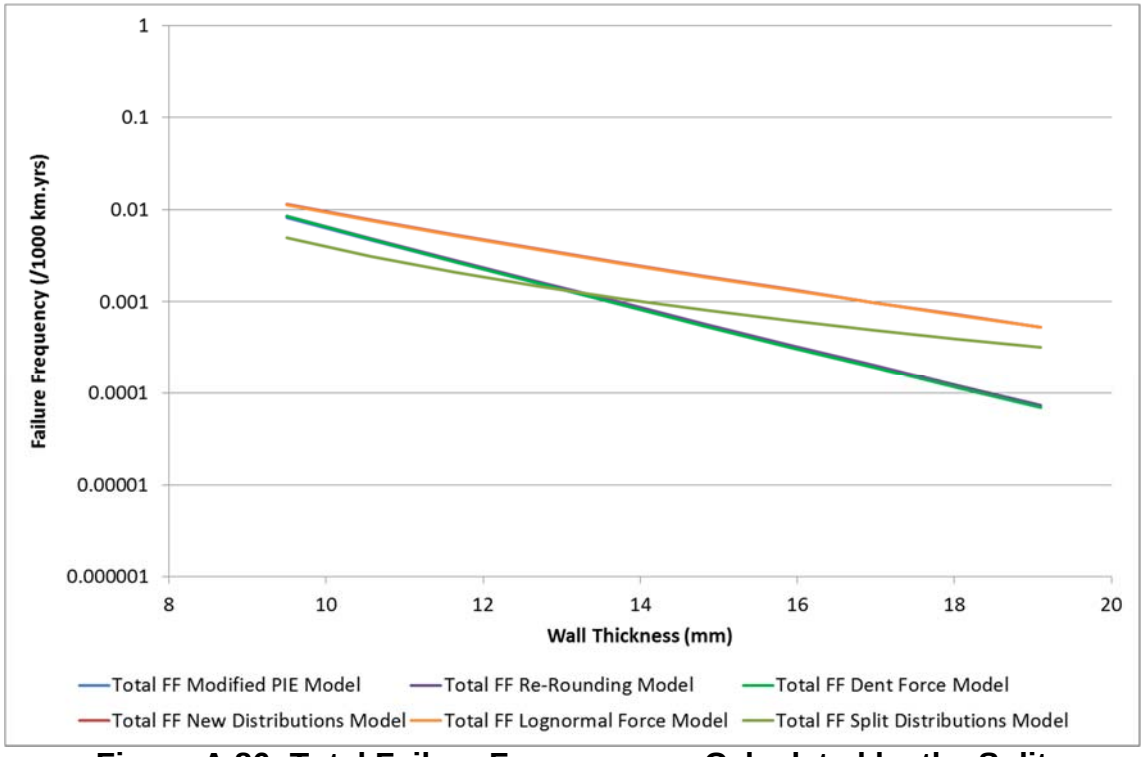

Figure A.86: Total Failure Frequency as Calculated by the Split Distributions Model, Lognormal Force Model, New Distributions Model, Dent Force Model, Re-Rounding Model and the Modified PIE Model for Example 6

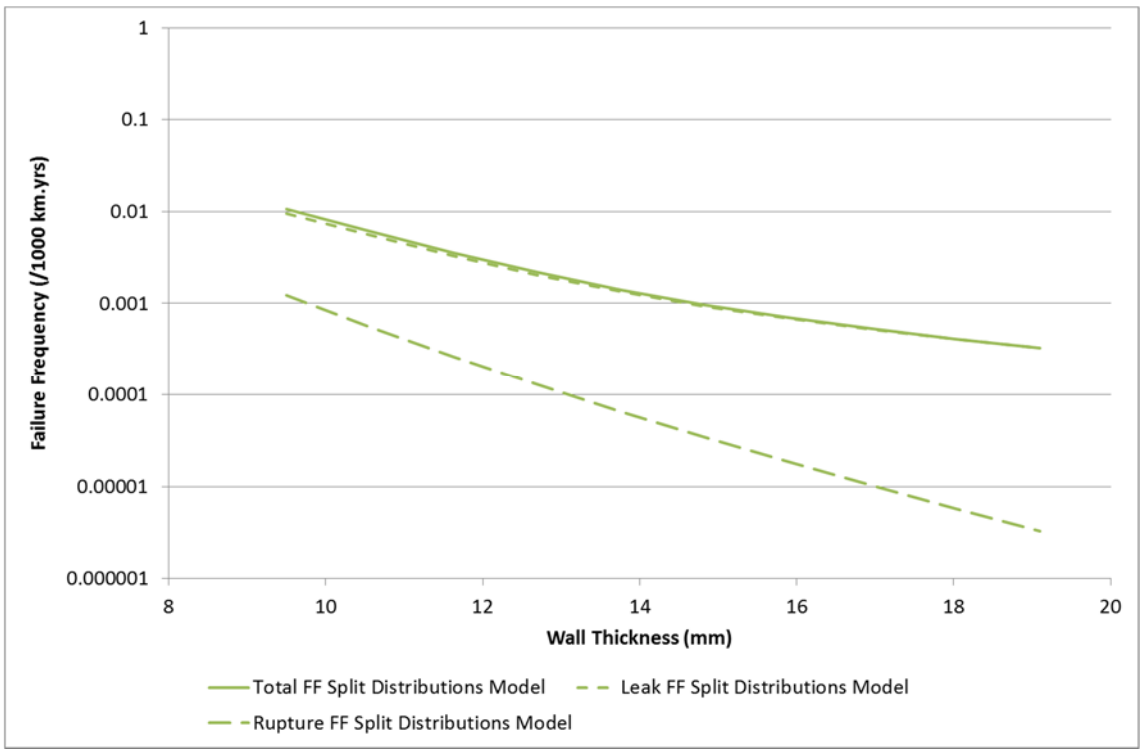

Figure A.87: Leak, Rupture and Total Failure Frequency as Calculated by the Split Distributions Model, for Example 4

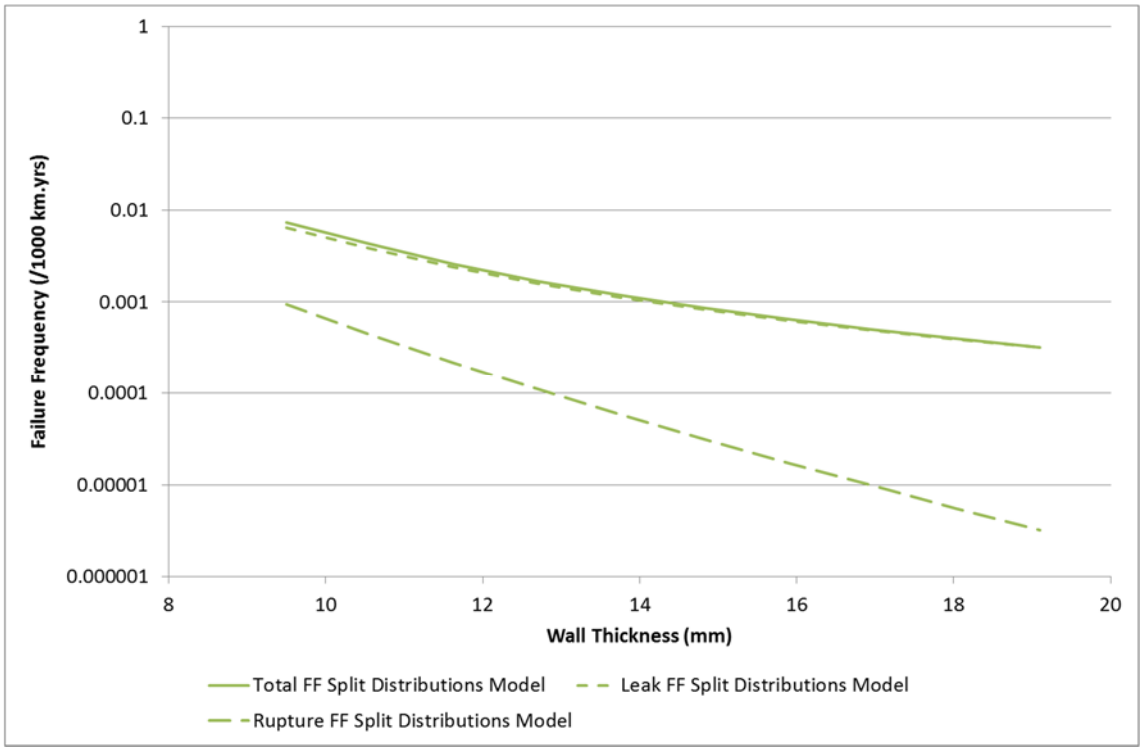

Figure A.88: Leak, Rupture and Total Failure Frequency as Calculated by the Split Distributions Model, for Example 5

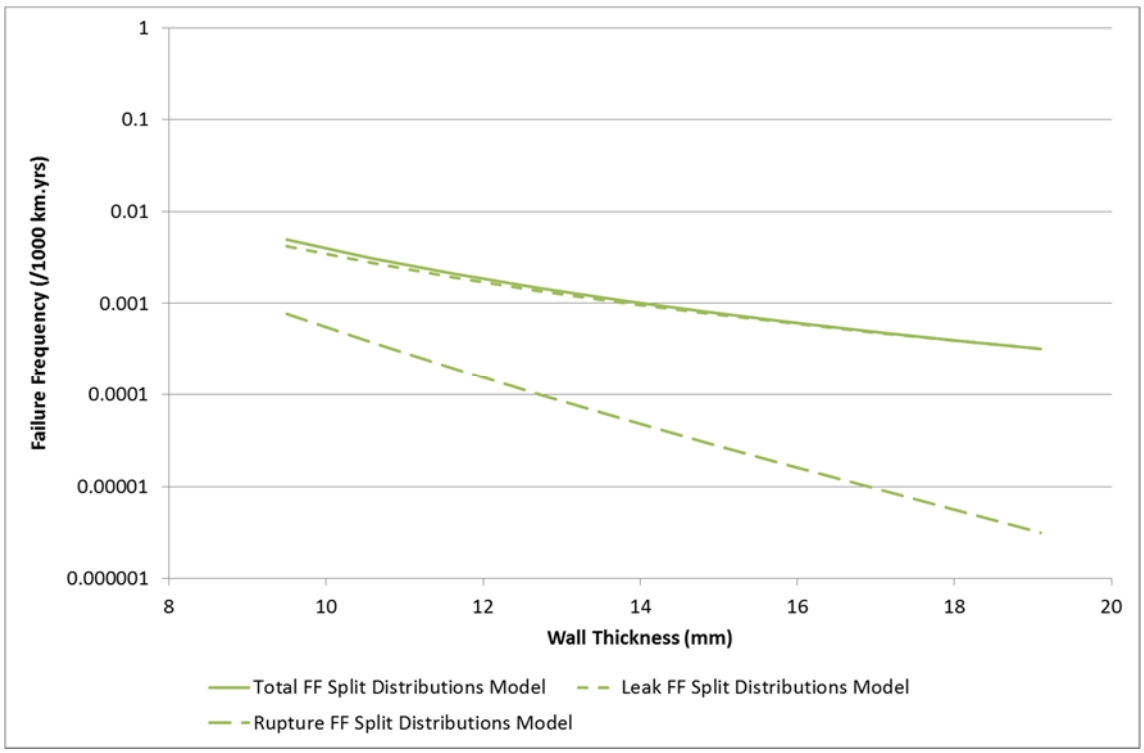

Figure A.89: Leak, Rupture and Total Failure Frequency as Calculated by the Split Distributions Model, for Example 6

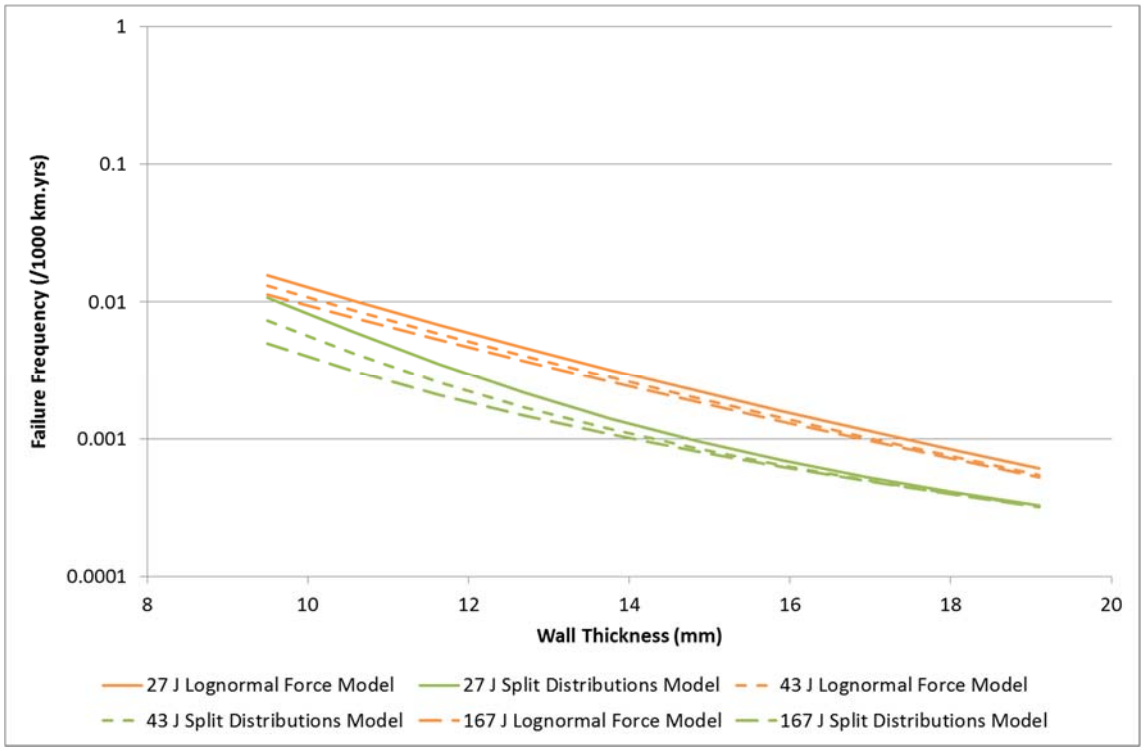

Figure A.90: Total Failure Frequency as Calculated by the Split Distributions Model and the Lognormal Force Model for Examples 4, 5 and 6

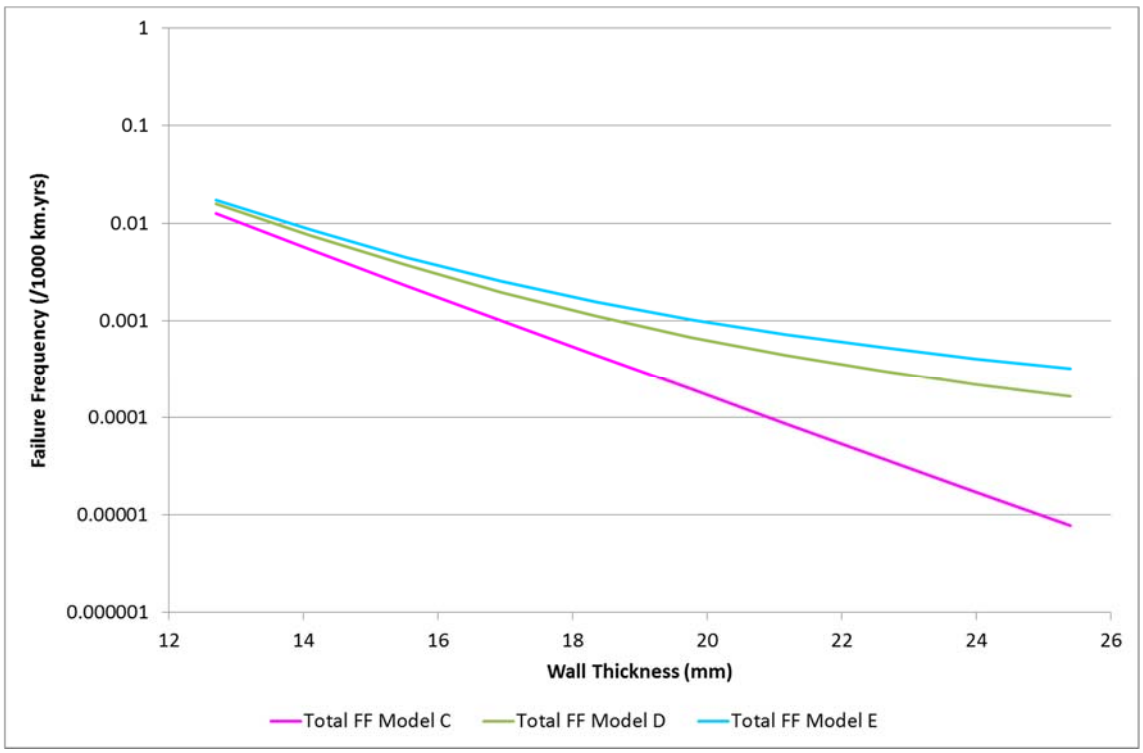

Figure A.91: Total Failure Frequency as Calculated by Model C, Model D and Model E for Example 1

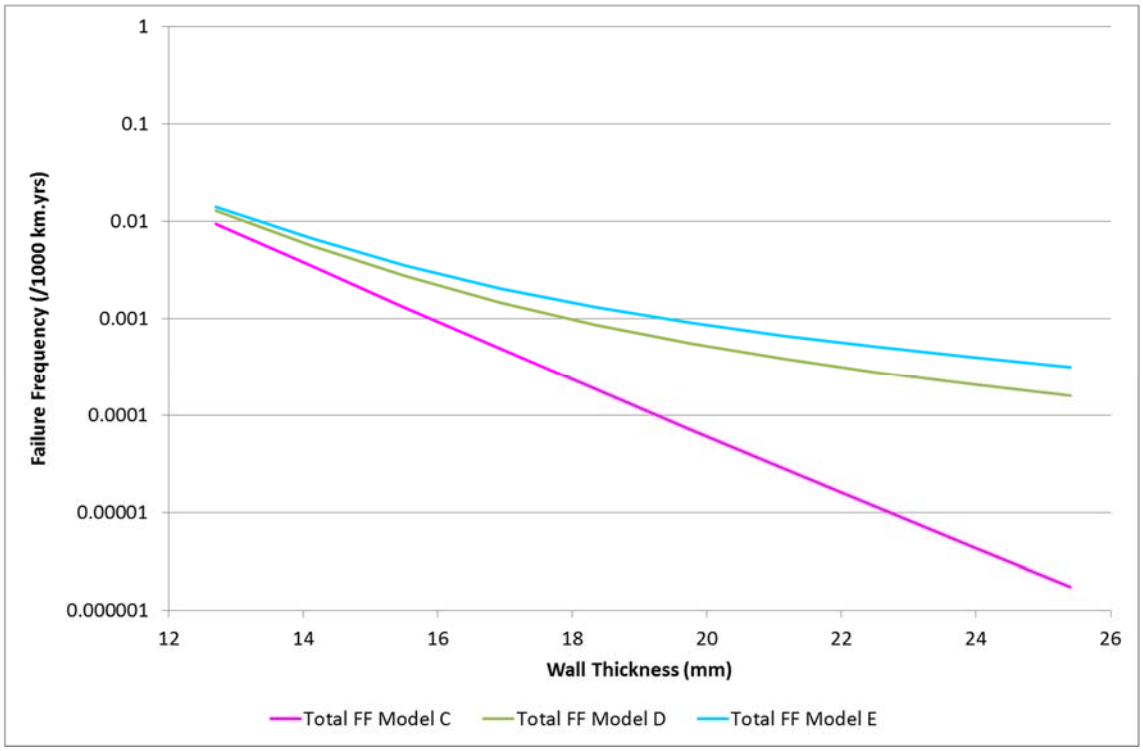

Figure A.92: Total Failure Frequency as Calculated by Model C, Model D and Model E for Example 2

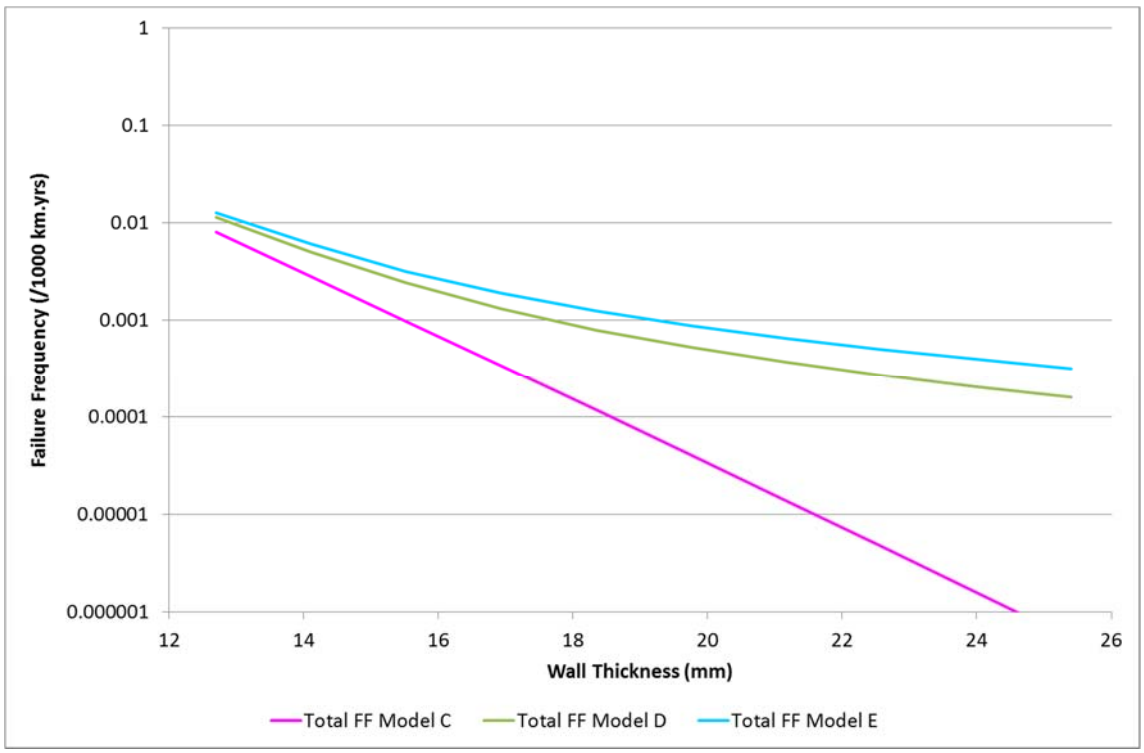

Figure A.93: Total Failure Frequency as Calculated by Model C, Model D and Model E for Example 3

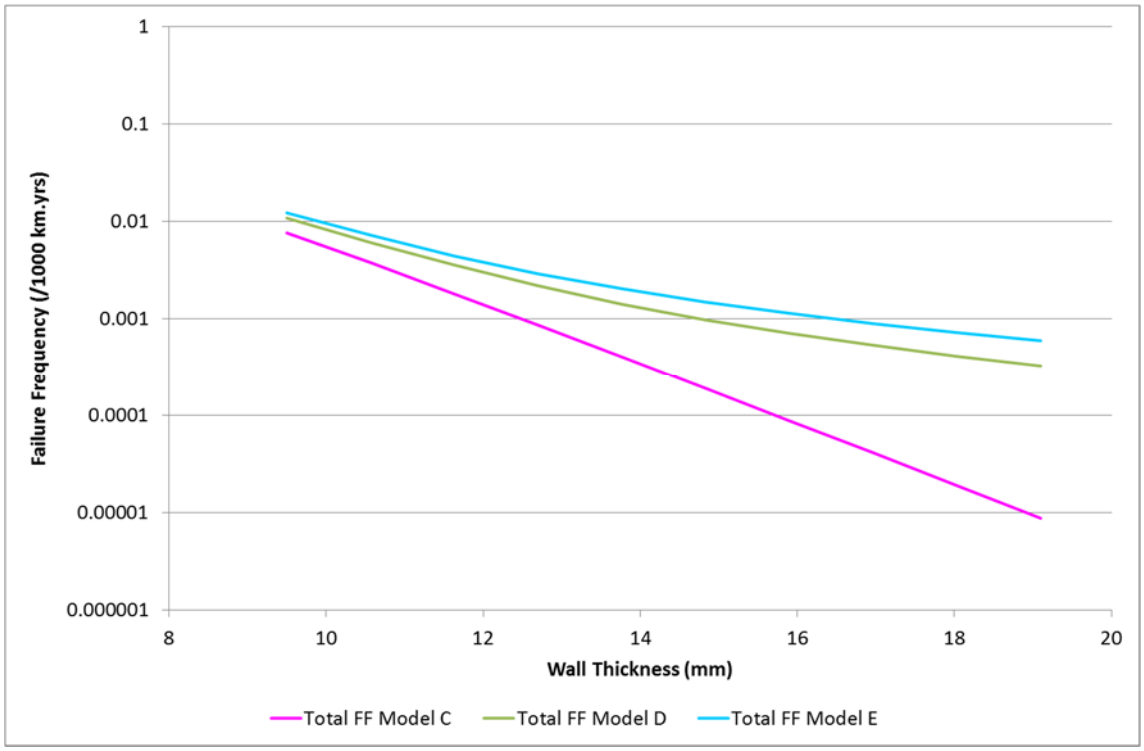

Figure A.94: Total Failure Frequency as Calculated by Model C, Model D and Model E for Example 4

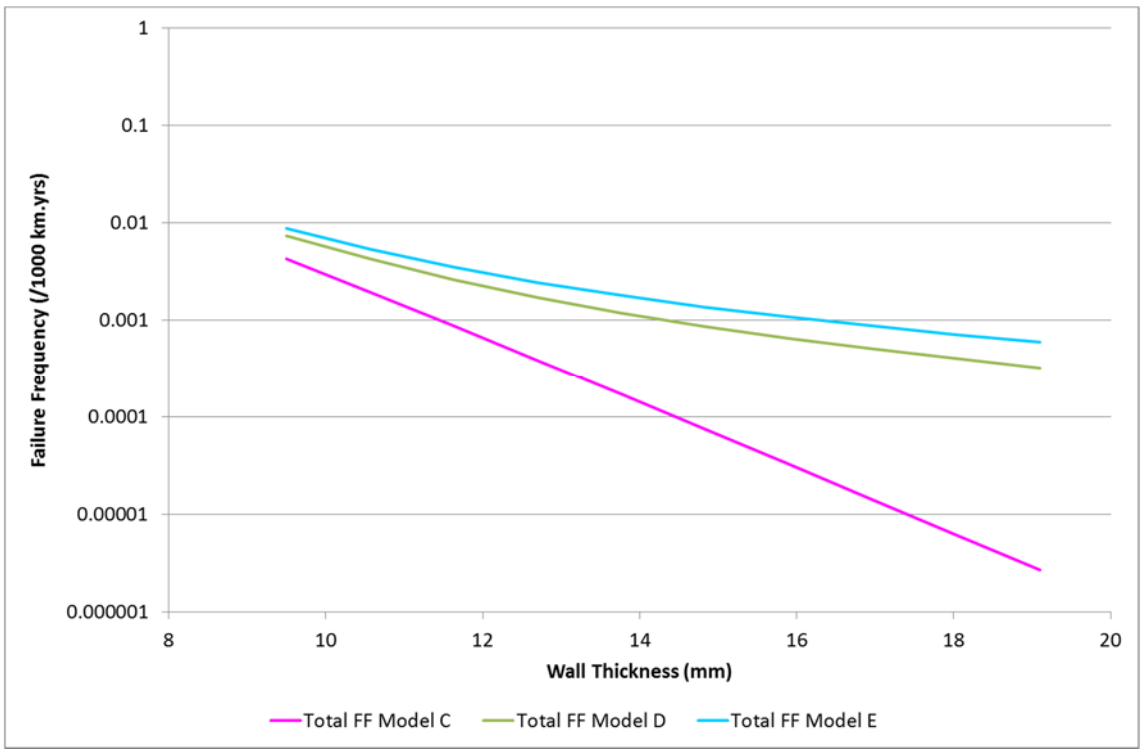

Figure A.95: Total Failure Frequency as Calculated by Model C, Model D and Model E for Example 5

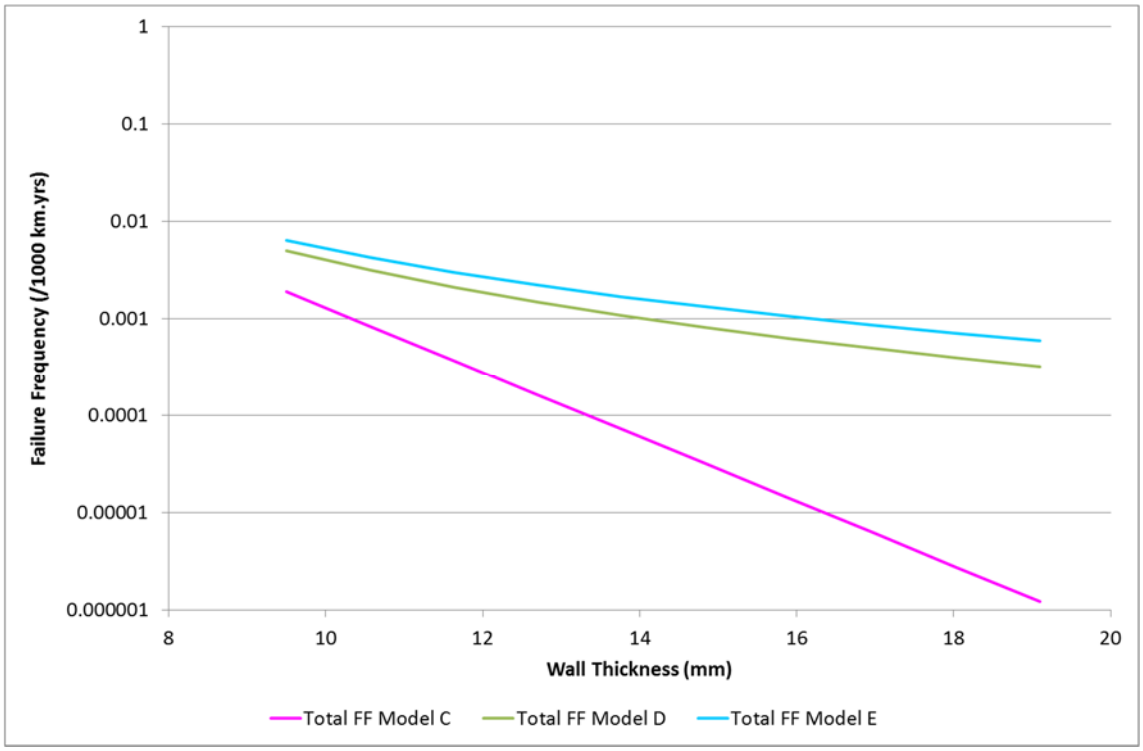

Figure A.96: Total Failure Frequency as Calculated by Model C, Model D and Model E for Example 6

Appendix B An Assessment of the 2010 UKOPA Fault Database (Review Process)

The UKOPA Fault Database gives details of all known faults discovered since 1962 associated with pipelines under the jurisdiction of UKOPA. On discovery and investigation of a fault, the pipeline operator in question completes an FR1 “Fault Data Input Form” detailing the relevant information. This form is then submitted to UKOPA for inclusion in the database. In the database, reported faults are presented as a table of records known as the “Fault Listing”. Records in the fault listing consist of 48 different fields and provide data on both the fault and the affected pipeline. The complete list of fields in the fault listing is as follows:

- Fault Number
- Pipe Outside Diameter at Fault mm
- Local Wall Thickness mm
- Fault Material Grade
- Type of Pipe Construction at Fault
- Fault Pipeline Location
- Fault Specific Location
- How Fault was Discovered
- Fault Discovery Date
- Operating Pressure at Fault
- Fault Product Supply Action
- Fault Cause
- Fault Secondary / Other Cause
- Fault External Interference Type
- Affected Component
- Fault Extent of Damage
- Fault Centre Location 0 – 360 degrees
- Fault Repair Method Used
- Cathodic Protection Status
- Protective Measures at Fault

- Type of Backfill at Fault
- Fault Depth of Cover
- External Coating Type at Fault
- Was Pipe Insulated at Fault
- Internal Coating at Fault
- Date of Previous CP Survey
- Date of Previous ILI Inspection
- Date of Previous Aerial Inspection
- Fault Additional Comments
- Fault Comments
- Number of Defects for This Fault
- Hole Area
- Hole Length
- Hole Width
- Hole Circular Position
- Amount of Product Released
- Was a Crater Formed?
- Crater Length
- Crater Width
- Crater Depth
- Crater Affected Radius m
- Was There Ignition?
- Ignition Type
- Fire Type
- Radius of Damage m
- Flame Length
- Flame Inclination
- Failure Comments

A single reported fault may contain several individual flaws, for example clusters of corrosion or the presence of multiple tooth marks from a single excavator bucket. Within the context of the database, these flaws are known as defects. A separate table, titled “Defects Associated with Faults” gives details of all the individual defects which make up the pipeline faults. Records in the table of

defects associated with faults consist of 15 different fields and include the measured dimensions of each flaw. The complete list of fields in the table of defects associated with faults is as follows:

- Defect Number
- Fault Number
- Date Discovered
- Operating Pressure
- Pipe Diameter
- Wall Thickness
- Grade
- Defect Length mm
- Defect Width mm
- Defect Depth mm
- Defect Orientation
- Defect Type
- Fault Cause
- Fault Comment
- Fault Additional Comment

The total number of faults and defects contained within the database are shown in Table B.1. Records in the table of defects associated with faults are linked to their matching record in the fault listing via the fault number which provides a unique numerical identifier for each fault. The corresponding records from each table together provide all of the known data about a single fault. It should be noted that some fault numbers appear in the fault listing but not the table of defects associated with faults, and vice versa. In these cases the information about the fault is incomplete. Table B.1 highlights the number of cases for which this occurs.

Table	Total Number of Records in Table	Number of Faults Exclusive to Table
Fault Listing	3080	200
Defects Associated with Faults	5087	11

Table B.1: Summary of Fault and Defect Numbers

The failure frequency model developed as part of this work requires the use of probability distributions for the size of pipeline damage caused by external interference. The table of defects associated with faults within the UKOPA Fault Database contains the necessary data required to derive these probability distributions. The table has therefore been analysed and filtered to produce appropriate data sets for this purpose. Descriptions of the most important fields in the table with regards to this analysis are given below. Note that the fields “Affected Component” and “Fault Extent of Damage” appear only in the fault listing and not the table of defects associated with faults. These fields are considered to provide vital information with respect to data classification and as a result have been included in the analysis.

Defect Number

In the defect number field, a record within the table of defects associated with faults is assigned a unique numerical identifier. The defect number can be used to distinguish between defect records which would otherwise be identical. The range of the defect number for the whole database is from one to 5093.

Fault Number

The fault number is also a numerical identifier and is used in the table of defects associated with faults to identify which fault a particular defect belongs to. Consequently, one or more defect records can share the same fault number. The range of the fault number is from one to 3107.

Operating Pressure

This field gives the operating pressure of the pipeline affected by the defect in barg. In considering defects caused by external interference for the purposes of this work, the information given in this field has been assumed to be the pressure at which the pipeline was operating at the time the damage occurred. It should be noted that the database contains 329 defect records for which the operating pressure is not given or has a nonsensical value, details of which are given in Table B.2:

Stated Operating Pressure Value	No. of Defects with Value
-1	212
0	114
“NULL”	3

Table B.2: Details of Nonsensical Operating Pressure Values

In the derivation of a dent force distribution for this work (section 7.1), which specifically requires the use of the operating pressure associated with a particular defect, defects with those values of operating pressures shown in Table B.2 have not been included in the procedure due to the absence of accurate data. It is noted that a stated operating pressure of “0” could suggest that the damage occurred when the line was not operating (pre-commission, during modifications etc.) rather than the omission of a value. Indeed, situations such as this are occasionally indicated by information contained within the other fields in the defect record. However, although the operating pressure value in these cases would be considered accurate, the equations used to derive dent force are not applicable to damage incidents which occur at zero pressure.

Pipe Diameter

This field gives the external diameter of the pipeline affected by the defect in millimetres. It should be noted that the database contains 31 defect records for which the pipe diameter is not given or has a nonsensical value, details of which are given in Table B.3.

Stated Pipe Diameter Value	No. of Defects with Value
6096	5
0	15
“NULL”	3
Blank	8

Table B.3: Details of Nonsensical Pipe Diameter Values

In the derivation of a dent force distribution for this work (section 7.1) which specifically requires the use of the external diameter, defects with a pipe diameter of “0”, “NULL” or blanks have not been included in the procedure due

to the absence of accurate data. None of the five defects with a pipe diameter of “6096” represent external interference damage and as a result are not considered in the analysis for this work. It could be inferred with some confidence however, that for these defects the true pipe diameter is a standard size of 609.6 mm (24”) and has been entered into the database incorrectly.

Wall Thickness

This field gives the wall thickness of the pipeline affected by the defect in millimetres. For the purposes of this work, the information given in this field has been assumed to be the local wall thickness in the region of the defect. However, based on the prevalence of standard pipe wall thickness values in this field throughout the database, it is likely that in many cases the value given is the nominal or minimum wall thickness for the pipeline. It should be noted that the database contains 62 defect records for which the wall thickness is not given or has a nonsensical value, details of which are given in Table B.4.

Stated Wall Thickness Value	No. of Defects with Value
0	45
“NULL”	9
Blank	8

Table B.4: Details of Nonsensical Wall Thickness Values

In the derivation of a dent force distribution for this work (section 7.1) which specifically requires the use of the wall thickness, defects with a missing or nonsensical wall thickness have not been included in the procedure due to the absence of accurate data.

Grade

This field gives the steel grade of the pipeline affected by the defect using the API 5L specification terminology (Anon., 2007c). For the purposes of this work, the yield and tensile strength values for the pipe material affected by the defect have been assumed on the basis of this field. The minimum values for the stated grade in the API 5L specification have been assumed in each case

(SMYS and SMUTS). It should be noted that the database contains 142 defect records for which the wall thickness is not given, details of which are given in Table B.5.

Stated Grade Value	No. of Defects
“Unknown”	115
“NULL”	19
Blank	8

Table B.5: Details of Missing Pipe Grade Values

In the derivation of a dent force distribution for this work (section 7.1) which specifically requires the use of the pipe steel yield and tensile strength, defects with a missing pipe grade have not been included in the procedure due to the absence of accurate data.

Defect Length mm

This field gives the length of the defect in millimetres. For the purposes of this work it is assumed that the value given in this field represents the extent of the defect in the axial direction. It should be noted that there are 1516 defect records for which the defect length is given as “0”. It can be inferred from other fields in the table of defects associated with faults, that the use of “0” for a defect length could indicate either; the axial length was too small to measure with available tools (for example circumferential scratches, girth weld cracks, pin holes); the investigating party believed recording a defect length was not necessary or not applicable (for example coating damage, valve leaks, severed weldolets); the defect was discovered by in-line inspection tool which did not perform sizing; or that the defect must have had a measurable length but that the data was omitted for unknown reasons. In the case of defects from the same fault, a not uncommon occurrence is for the defect with the lowest defect number (the “first” defect in the fault) to receive a non-zero defect length and for the remaining defects to have a length of “0”. This possibility is not restricted to the defect length and, when it occurs, typically affects also the defect width and defect depth fields. In these instances, the database is uncertain. An omitted length, width and depth value for a defect otherwise identical to one with non-

zero length, width and depth could suggest that its true dimensions mirror those of the sized defect (for example identical marks from adjacent excavator teeth). Alternatively, the records could suggest that the un-sized defects in the grouping were too small or superficial compared to the sized defect to warrant measurement. Based upon the above observations, it is acknowledged that a recorded length of “0” is incorrect for a large number of the 1516 defects within the database with this value. Due to the absence of any conclusive information, the defect length has been assumed as stated for this work. However, in the derivation of gouge length distributions (section 7.4), defects with a defect length of “0” have not been included in the procedure.

Defect Depth mm

This field gives the depth of the defect in millimetres. It is assumed that the value given in this field represents the depth of the defect in radial direction towards the pipe axis. For defects which are the result of metal loss on the pipe (for example gouges, corrosion) this will correspond to the depth through-wall thickness. For defects which are the result of a deformation in the pipe wall (for example dents) it is assumed the depth represents the maximum extent of the deformation, relative to the un-deformed pipe surface. It should be noted that there are 1595 defect records for which the defect depth is given as “0”. Similar observations and conclusions regarding these data can be made as to those for the defect length. Consequently, for the purposes of this work, the defect depth has been assumed as stated and defects with a defect depth of “0” have not been included in the derivation of gouge depth distributions (section 7.4). There are 136 defects in the database with a recorded defect depth in excess of the stated pipe wall thickness. For deformation-type defects, depths in excess of the wall thickness are possible due to the nature of the damage. Metal loss-type defects however, are by definition a reduction in the pipe wall thickness. It is therefore impossible for the depth of a metal loss defect to exceed the wall thickness of the pipe. The 136 defects can be categorised as shown in Table B.6:

Defects with Depth Greater Than Wall Thickness			
136			
Metal Loss		Dents	Unknown
41		90	5
Wall Thickness Zero	Wall Thickness Non-Zero		
17	24		

Table B.6: Categorisation of Defects with Depth Greater Than Wall Thickness

Of the 136 defects with a depth in excess of the wall thickness, 90 of the defects are dents and 41 are metal loss-type defects. Additionally, five of the defects are classed as either milling or weld defects. The available information for these defects is sparse and as a result the nature of the damage in these cases is unknown. The majority of the dents can be considered to have an acceptable depth measurement, given they are deformation-type defects. One dent from the 90 however has a recorded depth of 7777 mm, this depth is too large to be realistic and is therefore considered to be incorrect. From the 41 metal loss-type defects, 17 are from records where the pipe wall thickness is given as “0”. In the majority of these cases the defect depths can also be considered acceptable on the basis that the wall thickness is incorrect. Only one defect from the 17, with a depth of 38 mm, is considered to be incorrect. This defect depth is larger than the maximum pipe wall thickness in operation on all pipelines and therefore must be erroneous. 24 of the metal loss-type defects have a recorded wall thickness which is non-zero. In all of these cases the defect depth must be incorrect. Based upon information contained within the other fields in the defect records, it is evident that for some of these defects the depth measurement may be complicated by the presence of a dent occupying the same space on the pipeline (the metal loss-type defect is part of a fault which also includes a dent). It is speculated that in these cases the investigating party may have recorded a joint depth incorporating both dent and metal loss-type defect depths. Regardless of this, a realistic depth measurement cannot be obtained for any of the 24 defects. In the derivation of gouge depth distributions for this work, metal loss-type defects caused by external interference which are considered to have an unacceptable depth measurement by virtue of it exceeding the pipe wall thickness have not been included in the procedure.

Defect Type

In the defect type field the records are categorised according to the nature of the defect. There are six different types of defect recorded in the database, namely:

- Corrosion
- Crack
- Dent
- Gouge
- Mill Defect
- Weld Defect

This work is concerned exclusively with defects which are caused by external interference. The defect types caused by external interference are “Crack”, “Dent” and “Gouge”. Gouges and cracks can be classed as the aforementioned metal loss-type defects, whereas dents are deformation-type defects. It should be noted that the database contains 152 defect records for which the defect type is given as “NULL”. It can be inferred from other fields in the table of defects associated with faults that the use of “NULL” for the defect type could indicate either; the investigating party believed recording a defect type was not necessary or not applicable (for example coating faults); the defect was discovered by in-line inspection tool which did not perform the necessary identification; or that the data was omitted for unknown reasons. In approximately half of the cases, the defect type can be inferred based upon information contained within the other fields in the defect record. However, the majority of defects for which this is possible are corrosion, mill defects and weld defects. Only four defects of the 152 can be definitively identified as cracks, dents or gouges. Defects for which the defect type cannot be determined have not been included in the analysis.

Fault Cause

In the fault cause field the source of a particular fault is detailed. All defects which are part of the same fault are assigned the same fault cause. There are 11 main categories of fault cause recorded in the database, namely:

- Damage During Original Construction
- External Corrosion
- External Interference
- Girth Weld Defect
- Ground Movement
- Internal Corrosion
- Other
- Pipe Defect
- Pipe Mill Damage
- Seam Weld Defect
- Unknown

This work is concerned exclusively with defects which are caused by external interference. The fault cause field is therefore critical in distinguishing which defects should be included in the analysis. The majority of the fault cause categories are self-explanatory and cover the common causes of damage to pipelines with “Other” used for mechanisms which do not fit one of the larger categories; and “Unknown” reserved for defects for which the cause is not known. It should be noted that the database contains 33 defect records for which the fault cause is not given, details of which are given in Table B.7:

Stated Fault Cause	No. of Defects
“NULL”	32
Blank	1

Table B.7: Details of Missing Fault Cause Data

In all 33 cases the information contained within the other fields in the defect records is not sufficient to determine a definitive fault cause. The defects with

missing fault cause data can therefore be treated in the same way as defects for which the fault cause is “Unknown”.

Fault Comment

The purpose of the fault comment field is for the investigating party to indicate any additional information regarding a particular fault that they feel is important. All defects which are part of the same fault are assigned the same fault comment. This field is unlike the previous fields described in that there are no rules regarding the information it should contain. There are a large number of contributing sources to the database and therefore the information given in the fault comment shows a large degree of variation. An exhaustive list of the information the field can cover would be too large to include here, however the majority of comments can be broadly categorised as either:

- A description of the damage
- How the damage was caused
- Details of repairs carried out
- How and/or when the damage was discovered
- The location of the damage

It is not uncommon for more than one of the above to be recorded for any single fault. For the purposes of this work the fault comment can provide vital information for understanding the nature of defects and classifying them as part of the analysis. For example one defect in particular is listed with:

Defect Type	Fault Cause	Fault Comment
Gouge	External Interference	//LINES-WRONG ONE DRILLED-25MMH

Table B.8: Example Fault Comment 1

The fault comment in this case indicates that the damage was caused by a drill and therefore allows the defect to be classified in a different way to other gouges caused by external interference. This would not be possible if only the first two fields were given and would result in the defect being misclassified.

Unfortunately there is little consistency between the information recorded from one fault comment to the next, both in terms of the category of the information given; and how the information is presented within those categories. In contrast to the case shown above for example, the fault comment may only contain information already presented in other fields:

Defect Type	Fault Cause	Fault Comment
Gouge	External Interference	PIPE MISTAKEN FOR OLD RLWAY LI
Gouge	External Interference	3 SMALL GOUGES

Table B.9: Example Fault Comments 2 & 3

These comments, taken from two separate defects, are useful in the respect that they confirm and clarify data given in the fault cause and defect type fields of their respective records. However, they present no additional information about each defect. Furthermore, fault comments which give only the repair method used, the method of discovery or the location contain no relevant information as the models considered for the work are concerned only with the size and nature of damage to the pipeline:

Defect Type	Fault Cause	Fault Comment
Dent	External Interference	PERMANENT REPAIR-STOPPLE BYPASS
Gouge	External Interference	DETECTED BY PEARSON
Gouge	External Interference	Location 412730 552869

Table B.10: Example Fault Comments 4, 5 & 6

Additionally the database contains 364 defect records for which a fault comment is not given. Consequently, the usefulness of the field with regards to this work varies considerably from defect to defect.

Fault Additional Comment

The fault additional comment field is similar to the fault comment field and allows the investigating party to include further information about the fault. For example, if the fault comment field shows data relating to one of the categories

listed in the fault comment section, the fault additional comment field may be used to include data relating to another category in the list. The range of information that the field can cover and the presentation of the data is much the same as that of the fault comment field and the majority of the observations made regarding that field can also be applied to this one. Fault additional comment data therefore has the potential to be useful within the context of this work. It should be noted however, that perhaps due to its similarity to the fault comment field, the fault additional comment only rarely contains data. There are 4677 defects out of a total 5087 for which a fault additional comment is not given.

Affected Component

The purpose of the affected component field is to designate which particular element of the pipeline structure a fault is associated with. This field appears in the fault listing only and as a result all defects which are part of the same fault have been assumed to affect the same component. There are nine main categories of fault cause recorded in the database, namely:

- Bend
- Flanged Joint
- Insulation Joint
- Other
- Pig Trap
- Pipe
- Sleeve
- Tee
- Valve

The affected component categories cover the major component parts of an operating pipeline. The “Other” category is used for components which suffer faults less frequently, such stand pipes or dome ends. In the failure frequency model the probability distributions derived from the UKOPA Fault Database are used in conjunction with a limit state function, based on fracture mechanics failure models for the failure of defects in pressurised pipes. It is therefore

necessary to ensure that the distributions used in the failure frequency model are derived from data which is appropriate to the fracture mechanics failure models. The analysis is therefore concerned exclusively with defects that are located on either on the pipe or bend components. In this way the affected component field is critical in distinguishing which defects should be included in the analysis. It should be noted that the database contains 132 defect records for which the affected component is not given or cannot be determined. 13 of the 132 defects correspond to those 11 faults shown in Table B.1 for which the matching fault records in the fault listing are missing. Table B.11 summarises the data:

Stated Affected Component	No. of Defects
"NULL"	119
Associated fault does not appear in fault listing	13

Table B.11: Details of Missing Affected Component Data

The 132 defects in Table B.11 have not been included in the analysis as it is not known whether they are appropriate to the fracture mechanics failure models used in the failure frequency model.

Fault Extent of Damage

The fault extent of damage field indicates the severity of the damage associated with the fault. This field appears in the fault listing only and consequently refers to the overall severity of a fault rather than each individual defect within it. There are six main categories of damage severity recorded in the database, namely:

- Coating only
- No Loss – severe
- No Loss – Slight
- Product Loss – Fracture
- Product Loss – Leak
- Unknown

The fault extent of damage field can provide an additional layer of information to assist in understanding the nature of defects and classifying them as part of the analysis. For example, only external interference damage which has occurred to the pipe steel is considered appropriate to the fracture mechanics failure models used in the failure frequency model. This type of information is often not implied or indicated by one of the other fields, however an indication of “Coating only” damage in the fault extent of damage field can help to avoid misclassification and allow inappropriate data to be removed from the analysis. It can also be determined from this field if a fault resulted in pipeline failure. Defects caused by external interference which have failed must be treated, within the model, according to the mechanism of failure. It should be noted that the database contains 41 defect records for which the fault extent of damage is not given or cannot be determined. 13 of the 41 defects correspond to those 11 faults shown in Table B.1 for which the matching fault records in the fault listing are missing. In these cases classification of the defect must be made solely on the basis of the other fields in the defect record. Table B.12 summarises the data:

Stated Affected Component	No. of Defects
“NULL”	28
Associated fault does not appear in fault listing	13

Table B.12: Details of Missing Fault Extent of Damage Data

Classification of Defects and Uncertainty within the Database

The information required to determine the suitability of defects for inclusion in the probability distribution data sets, is contained within the fields:

- Defect Type
- Fault Cause
- Fault Comment
- Fault Additional Comment
- Affected Component
- Fault Extent of Damage

Unfortunately, the classification process is not as straightforward as simply eliminating unsuitable defects by assessing each of the above fields in turn. The data within these fields should ideally be considered as a whole for each defect. This is due to inconsistencies in the way the data has been recorded between each of the fields. For example, two separate defects have defect type, fault cause and fault comment as shown in Table B.13:

Defect Type	Fault Cause	Fault Comment
Gouge	Damage during original construction	SLIGHT SCORE/CORR. & EXT. CORR.
Corrosion	External Corrosion	GOUGE&CORR-S/F-CONSTRUCN?-OLI4

Table B.13: Defect Classification Example 1

Taking all of the information together, the two defects appear to be very similar in both cause and nature, despite having different defect types and fault causes listed. Both defects should be classified as gouges caused by construction damage with associated corrosion. It would be easy to misclassify the defects however, if either of the first two fields was considered in isolation.

The source of the inconsistencies within the database lies in the way the data is recorded and compiled. Some of the categories within each field are not mutually exclusive; for example in the defect type field, the term “Weld Defect” is non-specific and certain defects of this type could also be described as a “Crack”, “Gouge”, “Dent” or “Corrosion” depending on their nature. In terms of the fault cause, “External Corrosion” is generally used for external corrosion faults, however almost all of the other possible categories within this field can lead to the development of external corrosion provided the pipe coating is damaged and the cathodic protection (CP) system is ineffective. There is also a certain degree of crossover between the fields, for example a fault cause can be recorded as “Pipe Mill Damage”, but there also exists a defect type category of “Mill Defect”. Given these circumstances, it is clear that the way in which fault information is recorded for the database will largely be dependent on the party investigating the fault and how they interpret the FR1 fault data input form. Since the database is comprised of fault data from a large number of

independent contributing sources inconsistency between fault and defect records is not surprising.

If the above points are taken into consideration then the majority of defects within the database can be classified satisfactorily. Unfortunately however, there are a number of defects for which the data is uncertain. The issue is illustrated by the defect shown in Table B.14:

Defect Type	Fault Cause	Fault Comment
Dent	External Corrosion	2EXT.CORR,4INDENTS,GOUGE OLI4

Table B.14: Defect Classification Example 2

The fault comment for this defect indicates that corrosion was present in addition to a dent and a gouge. Dents and gouges are common forms of pipeline damage and can result from most of the categories listed in the “Fault Cause” section, apart from internal and external corrosion. Whilst corrosion is indicated to be present, recording the fault cause as “External Corrosion” in this case masks the true cause of the damage. The external corrosion is a secondary flaw which will have developed following the initial pipe damage which caused the dent and gouge. The uncertain nature of the fault cause in this case presents problems for the analysis. The fault may or may not have been caused by external interference and therefore may or may not be relevant to the current work.

The database also contains defects which contradict themselves in the data they present. In these cases, at least some of the recorded data must be incorrect. Table B.15 gives four examples:

Defect Type	Fault Cause	Fault Comment
Gouge	Other	CONSTRUCTION DAMAGE GOUGES
Mill Defect	External Interference	OLI EVERY 5 YEARS
Gouge	External Interference	PROBABLY CONSTRUCTION DAMAGE
Corrosion	External Interference	NULL

Table B.15: Defect Classification Examples 3, 4, 5, & 6

The first defect in Table B.15 has a fault cause of “Other”, however the fault comment clearly indicates construction damage as the source. The defect contains no other information regarding the fault origins so it is not clear as to why “Damage During Original Construction” was not used in this case. Either construction damage was not the cause of the fault, or the “Other” category has been used in error. The second defect in Table B.15 has a fault cause of “External Interference”, however the defect type indicates it to be a “Mill Defect”. In this case the information given in the defect type and the fault cause are mutually exclusive, the defect cannot occur as part of the milling process and be caused by external interference. For the third defect in Table B.15 the fault comment shows uncertainty regarding the source of the fault but it suggests it is probably construction damage. The fault cause field however, records the defect as being due to “External Interference”. Construction and external interference can produce very similar defects and the information in this case implies that the investigating party is not sure of the source. It is not clear however why the defect was recorded as external interference if construction damage was the more likely of the two mechanisms. The final defect in Table B.15 has a fault cause of “External Interference” and a defect type of “Corrosion”. In this case one could argue that the defect is simply analogous to those shown in Table B.13 and Table B.14 (indicating the development of external corrosion following initial pipeline damage), but with an alternative fault cause. However, given that the other fields in the defect present no further information; and that examples of defects with directly contradicting data have already been shown, being absolutely certain of this conclusion is difficult.

As previously noted this work is concerned only with defects which have been caused by external interference. The probability distributions used in the failure frequency model must be accurate representations of this damage mechanism. With regards to the above observations concerning uncertain and contradictory data, it was therefore decided that for the purposes of the analysis, only defects where an origin of external interference was certain would be included. For this purpose, defect classification has been focussed towards removing as much uncertainty as possible from the data:

- The Fault Cause field has been used as the main indicator of a defect's origin. All defects without a fault cause of "External Interference" have not been considered.
- From those defects left, a judgement has been made based on the defect type, fault comment and fault additional comment fields together as to the type of the defect and whether external interference appears to be the true cause of the damage. If another damage mechanism is suggested then the defect has not been included.
- The Affected Component field has then been used to determine if the damage occurred to the pipe or bend. If another component is indicated then the defect has not been included. Note that sometimes the defect comment field indicates the damage occurred to a component other than the pipe or bend but the Affected Component field does not. In these cases the nature of the defect is uncertain and therefore these defects have also not been included.
- Finally the Fault Extent of Damage Field has been used to determine whether the damage affected the pipe or the coating only. Defects to the coating only have not been included. Note that sometimes the defect comment field indicates the defect to be coating only and the Fault Extent of Damage Field does not. In these cases the nature of the defect is uncertain and therefore these defects have also not been included.

One final point with regards to the classification of defects for the work concerns the fault comment field. It should be noted that in some cases, the number of individual defect records grouped in the same fault is not consistent with the information given in the fault comment field for that fault. Table B.16 shows an example:

Defect Type	Fault Cause	Fault Comment
Gouge	External Interference	10 GOUGES OF WHICH 3 CRACKING
Gouge	External Interference	10 GOUGES OF WHICH 3 CRACKING
Gouge	External Interference	10 GOUGES OF WHICH 3 CRACKING
Gouge	External Interference	10 GOUGES OF WHICH 3 CRACKING
Gouge	External Interference	10 GOUGES OF WHICH 3 CRACKING

Table B.16: Defect Classification Example 7

Table B.16 shows all of the defects in the database associated with one particular fault, a total of five gouges. In this case however, the fault comment field indicates that the fault should consist of “10 GOUGES OF WHICH 3 CRACKING”. It is clear that five of the defects which should be associated with this fault have not been recorded in the database, the reason for which is unknown.

In terms of the analysis, for faults which are similar to the above example it was decided that the number of defects should be taken as the number of records in the database and any count in the fault comment field ignored. It would not be possible to introduce the additional missing data as the dimensions for these defects would not be known. The only change which could be made based on the numbers given in the fault comment is a modification to the Incident-Rate, however the Incident-Rate has not been considered as part of this work.

Analysis and Filter of the Table of Defects Associated with Faults

This section describes the analysis process through which the data sets giving the size of pipeline damage caused by external interference have been derived.

There are 5087 records in the table of defects associated with faults. Following the points on defect classification given above, 3795 of these defects are not indicated as “External Interference” by the fault cause field and can be removed from the analysis. Of the remaining 1292 defects, the defect type, fault

comment and additional fault comment fields suggest that 59 remain uncertain with regards to the true cause of the damage. These include:

- 49 defects which were potentially caused during construction
- 8 defects which are external corrosion
- 2 defects which appear to have resulted from the pipe coming into contact with an eccentric sleeve or nearby water main

Excluding the 59 defects leaves 1233 defects in the database caused by external interference. 40 of the 1233 external interference defects occurred to components other than the pipe or bend and can therefore also be removed from the analysis. The affected components include:

- 3 to dome ends
- 1 to a drain pipe
- 1 to a grout pipe
- 6 to the pipe sleeve
- 2 to the pipe sleeve coating
- 1 to a sleeve fill point
- 1 to a sleeve valve
- 2 to stand pipes
- 7 to tee pieces
- 2 to valves
- 3 to weldolets
- 1 to a weldolet dip pipe
- 2 to weldolet welds
- 1 to a pressure point
- 1 to a branch pipe
- 1 to concrete capping
- 5 for which the component is unknown

Excluding the 40 defects leaves 1193 external interference defects affecting either pipes or bends. Using a combination of the fault extent of damage and fault comment fields 109 of the 1193 defects were found to affect the pipe

coating only and can be removed from the analysis. There are therefore 1084 external interference defects directly affecting the pipe or bend material. It should be noted that of these 1084 defects:

- 12 affect pipe sections which are located within above ground installations (AGIs)
- 21 affect above ground sections of pipe

The land on which AGIs are located is under the jurisdiction of the pipeline operator. Any pipeline damage which occurs within the boundaries of an AGI is therefore not considered to be third party external interference. For this reason these defects have also been removed from the analysis. The defects affecting other above ground sections are the result of external interference; however the model is intended to calculate failure frequencies due to external interference for buried onshore pipelines. Exposed pipe sections do not benefit from the added layer of protection provided by the depth of cover for a buried line and the damage received by these sections is therefore considered to be atypical of external interference damage to buried pipelines. For this reason it was decided to remove these defects from the analysis.

Excluding the 33 defects on above ground sections of pipe leaves 1051 defects. Using a combination of the defect type, fault comment and fault additional comment fields these 1051 defects can be classified as:

- 105 dents
- 927 gouges
- 1 crack
- 18 defects for which the defect type could not be determined

To remove uncertainty from the data sets the 18 defects for which the defect type could not be determined have also been removed from the analysis. In the fracture mechanics failure models used in the failure frequency model “Gouge” and “Crack” damage are treated in the same way. For the purposes of the work, the 1 crack defect can therefore be considered as a gouge.

Based on the fault comment, fault additional comment and fault extent of damage fields within the database, the 105 dent defects and 928 gouge defects can be categorised further. Of the 105 dents:

- 5 have additional associated corrosion
- 2 are associated with drill damage
- 5 are associated with a pipeline failure
- 1 is associated with a weld

Of the 928 gouges:

- 24 have additional associated corrosion
- 19 are associated with drill damage
- 32 are associated with a pipeline failure
- 7 are associated with a pipeline failure caused by a drill
- 6 are associated with welds

Table B.17 shows a summary of the analysis of the table of defects associated with faults from the UKOPA Fault Database:

Description of damage	No. Of Defects
Not “External Interference”	3795
Uncertain Damage Mechanism	59
Damage to component other than pipe or bend	35
Damage to unknown components	5
Coating damage to pipe/bend	109
Damage to above ground section or AGI	33
Damage of unknown defect type	18
Dent to pipe/bend	92
Dent to pipe/bend with corrosion	5
Dent by drill to pipe/bend	2
Dent with failure of pipe/bend	5
Dent to weld on pipe/bend	1
Gouge to pipe/bend	840
Gouge to pipe/bend with corrosion	24
Gouge by drill to pipe/bend	19
Gouge with failure of pipe/bend	32
Gouge with failure by drill of pipe/bend	7
Gouge to weld on pipe/bend	6
Total	5087

Table B.17: Summary of Analysis of Table of Defects Associated with Faults

Appendix C A Shelter Model for Consequence Predictions Following A CO_2 Pipeline Release (Charts)

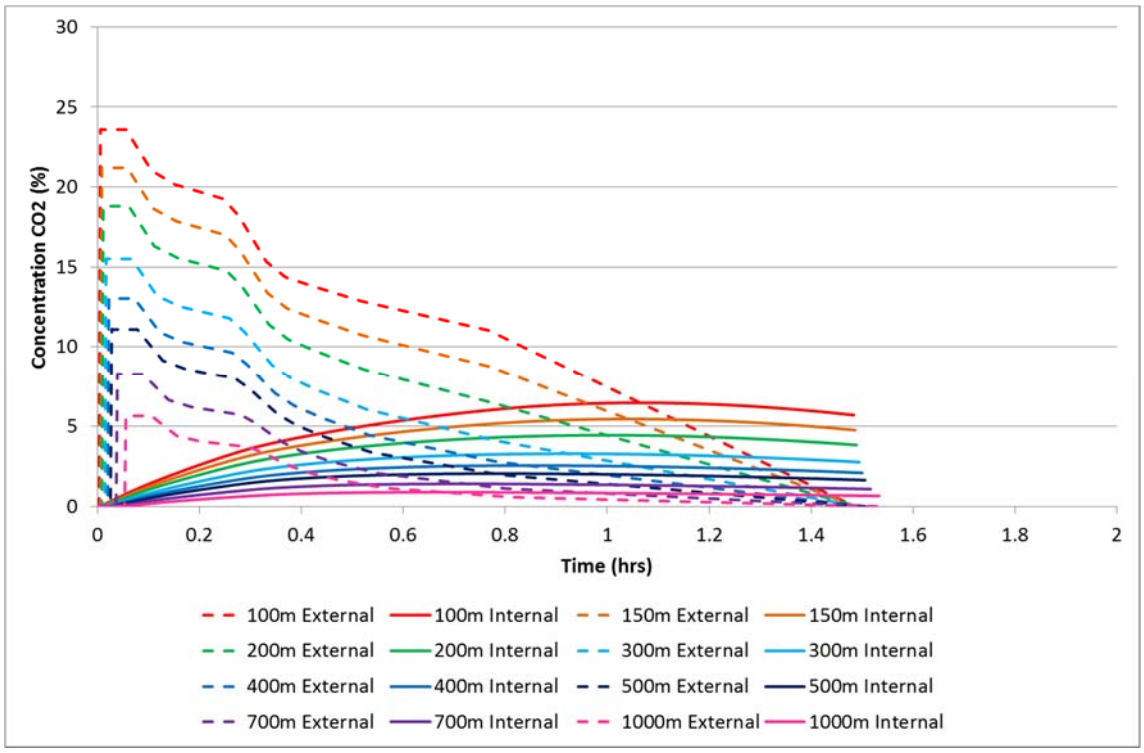

Figure C.1: Change in Mean Internal CO_2 Concentration with Time and Distance for Case 1

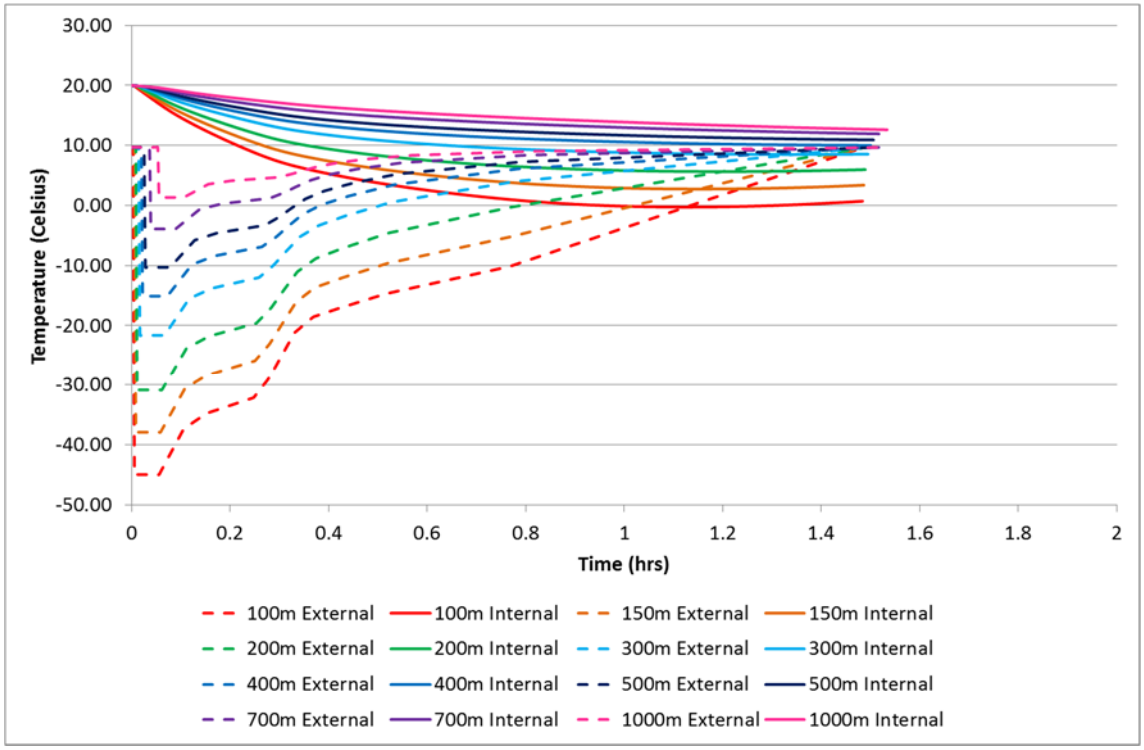

Figure C.2: Change in Internal Temperature with Time and Distance for Case 1

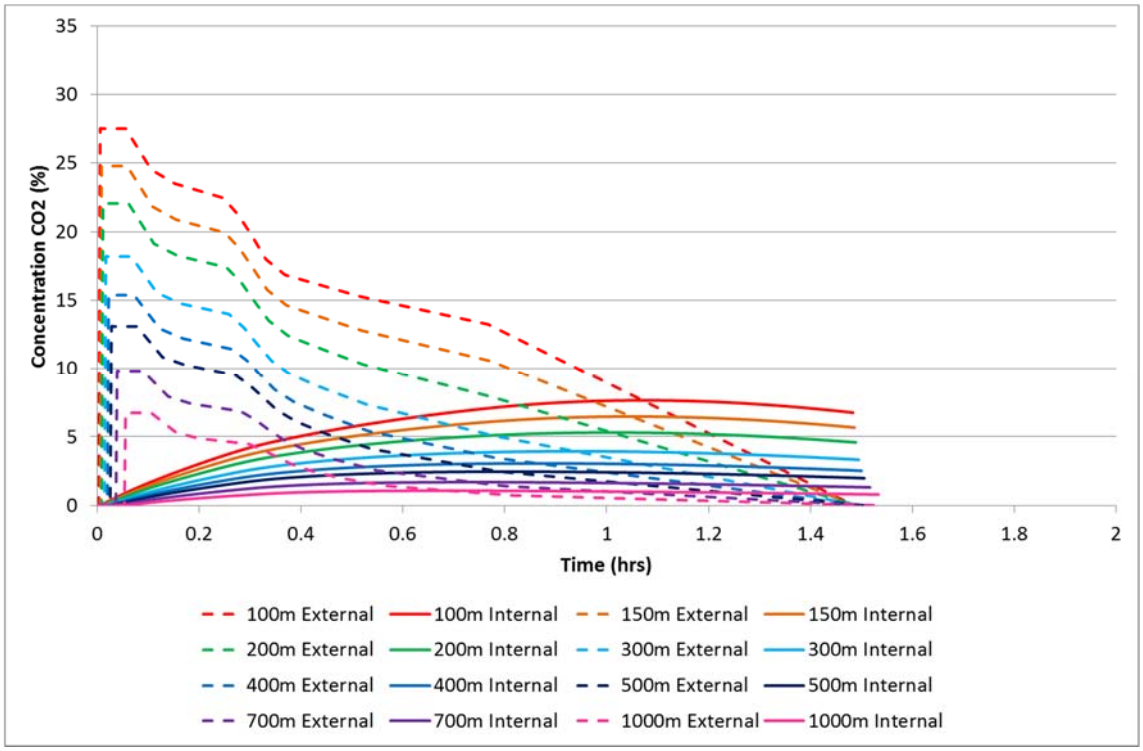

Figure C.3: Change in Equivalent Internal CO_2 Concentration with Time and Distance for Case 1

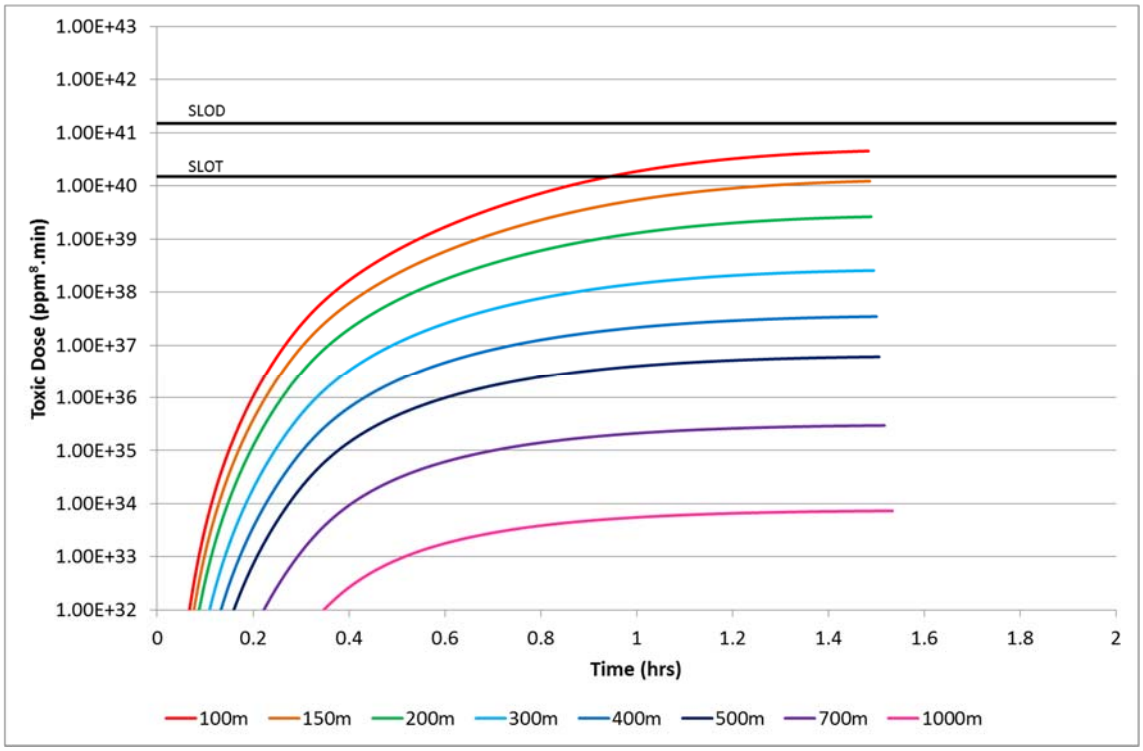

Figure C.4: Dose Received by a Building Occupant with Time and Distance for Case 1

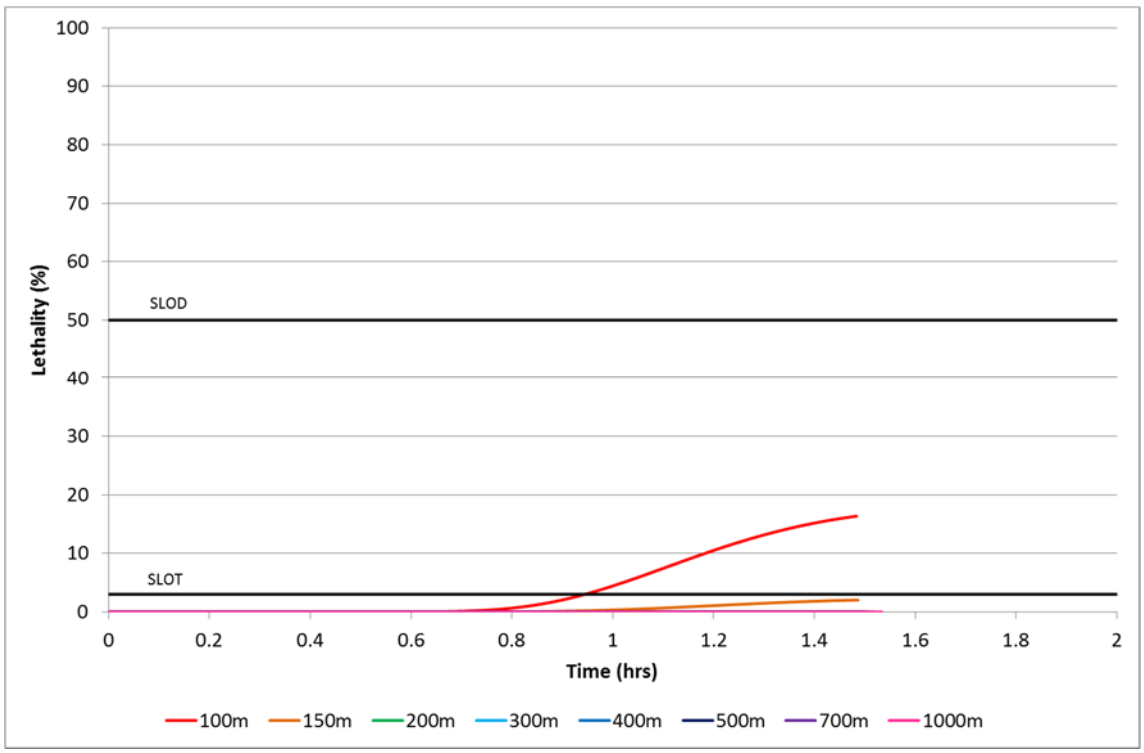

Figure C.5: Percentage Lethality for a Building Occupant with Time and Distance for Case 1

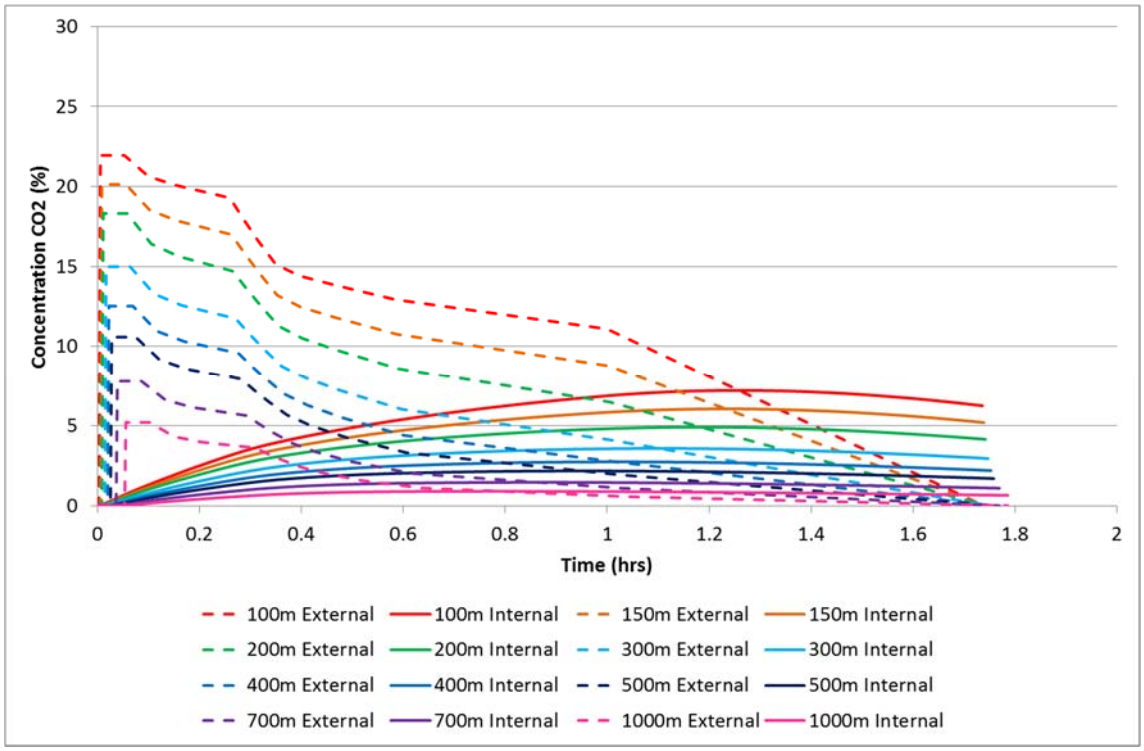

Figure C.6: Change in Mean Internal CO_2 Concentration with Time and Distance for Case 2

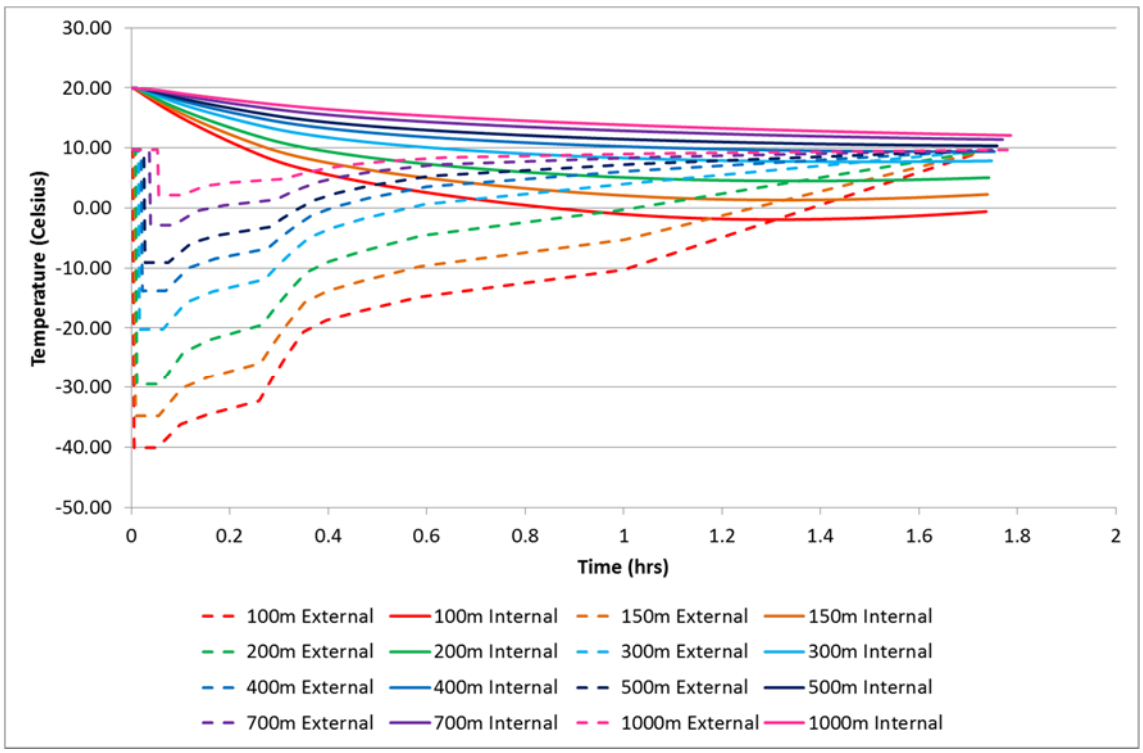

Figure C.7: Change in Internal Temperature with Time and Distance for Case 2

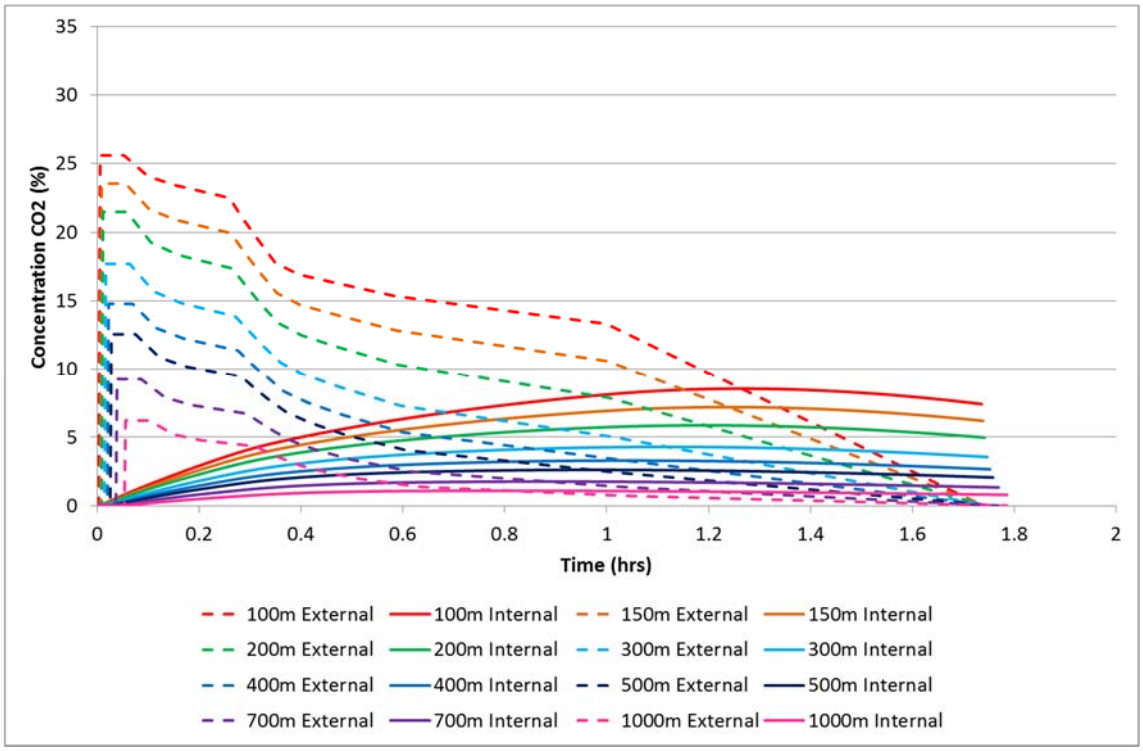

Figure C.8: Change in Equivalent Internal CO_2 Concentration with Time and Distance for Case 2

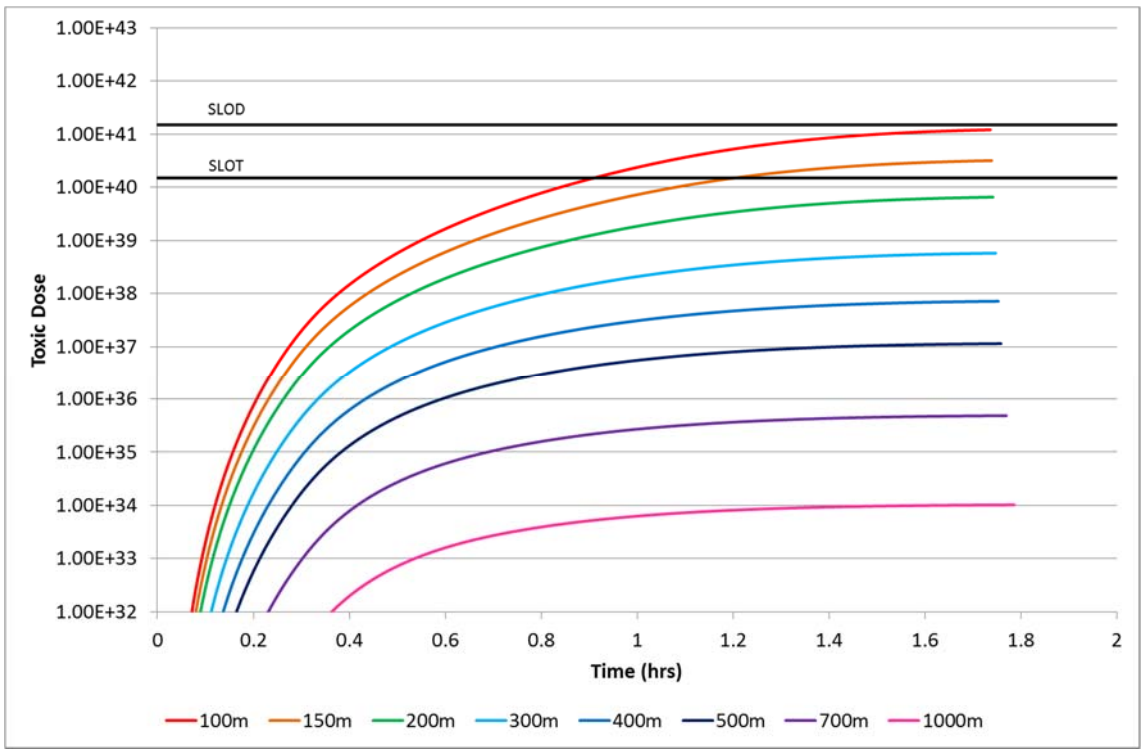

Figure C.9: Dose Received by a Building Occupant with Time and Distance for Case 2

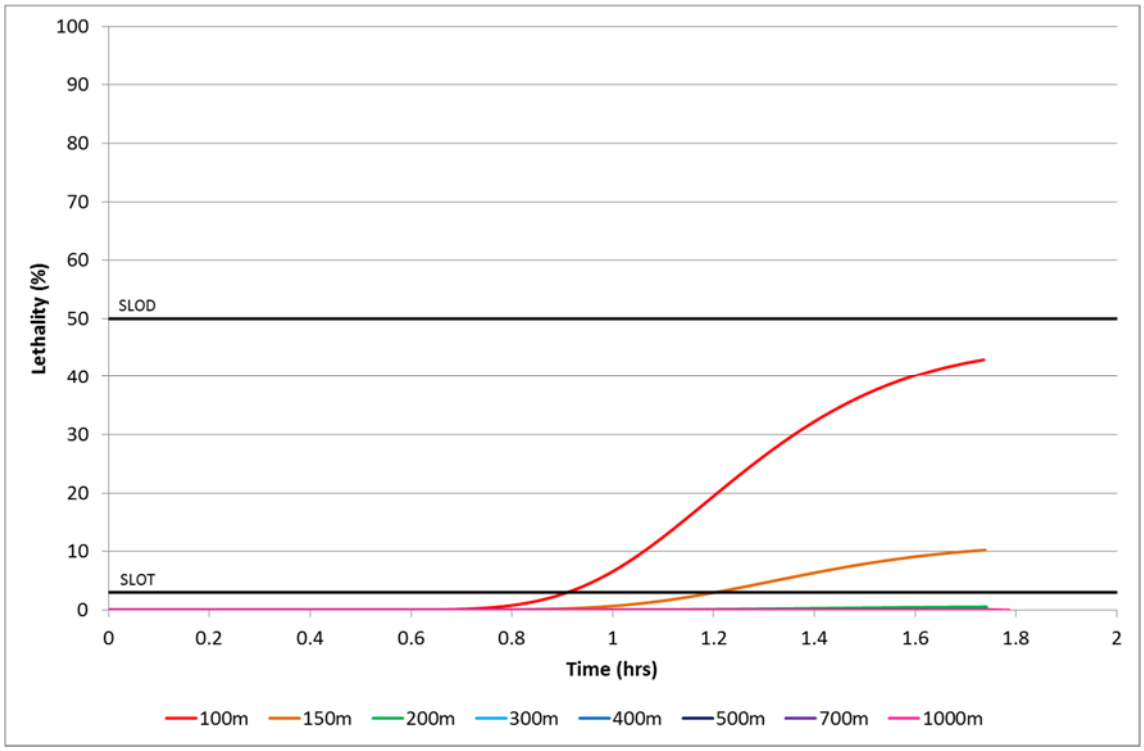

Figure C.10: Percentage Lethality for a Building Occupant with Time and Distance for Case 2

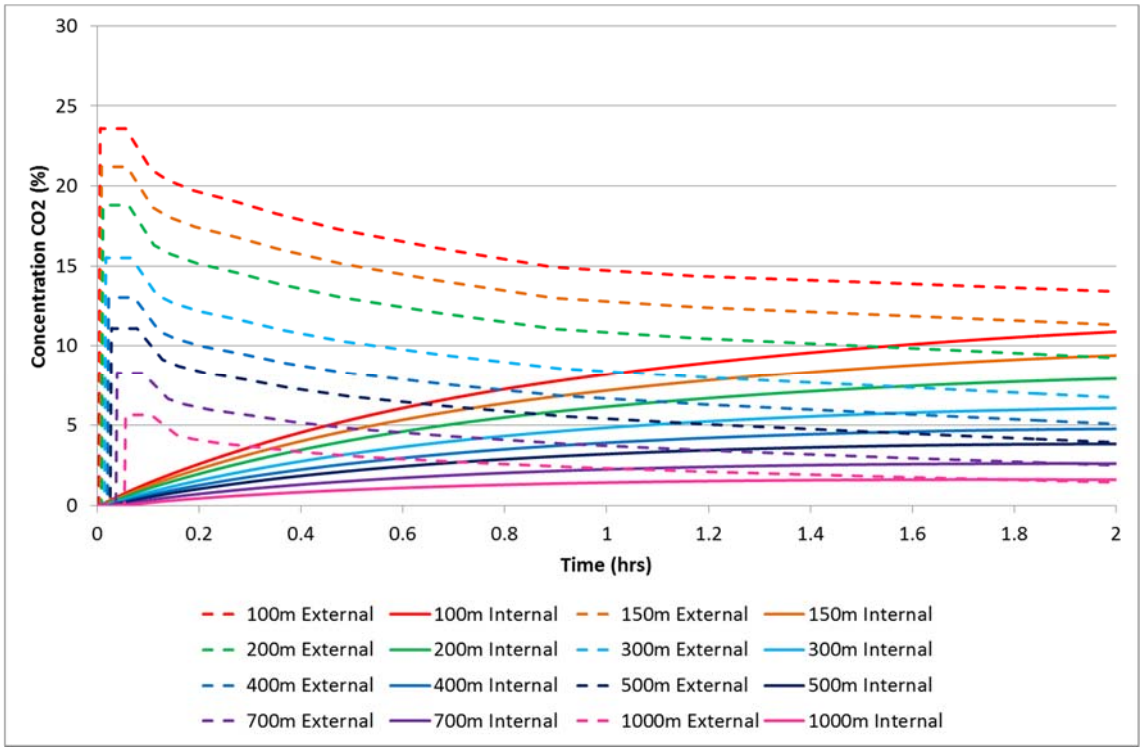

Figure C.11: Change in Mean Internal CO_2 Concentration with Time and Distance for Case 3

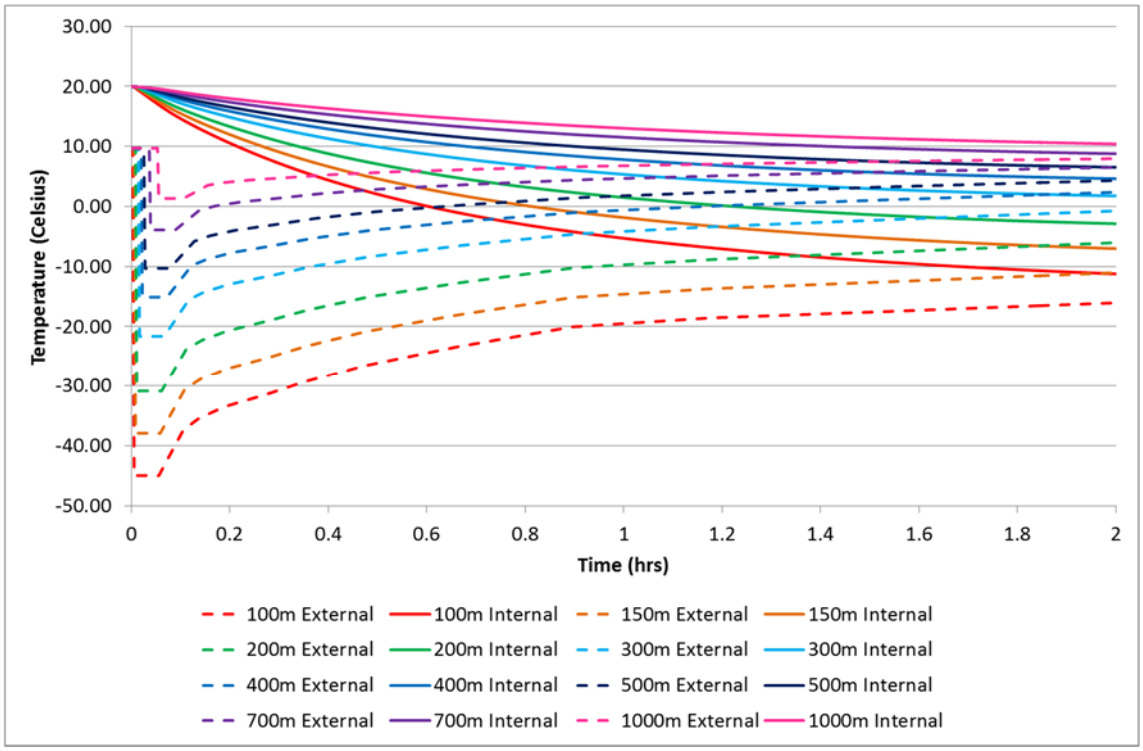

Figure C.12: Change in Internal Temperature with Time and Distance for Case 3

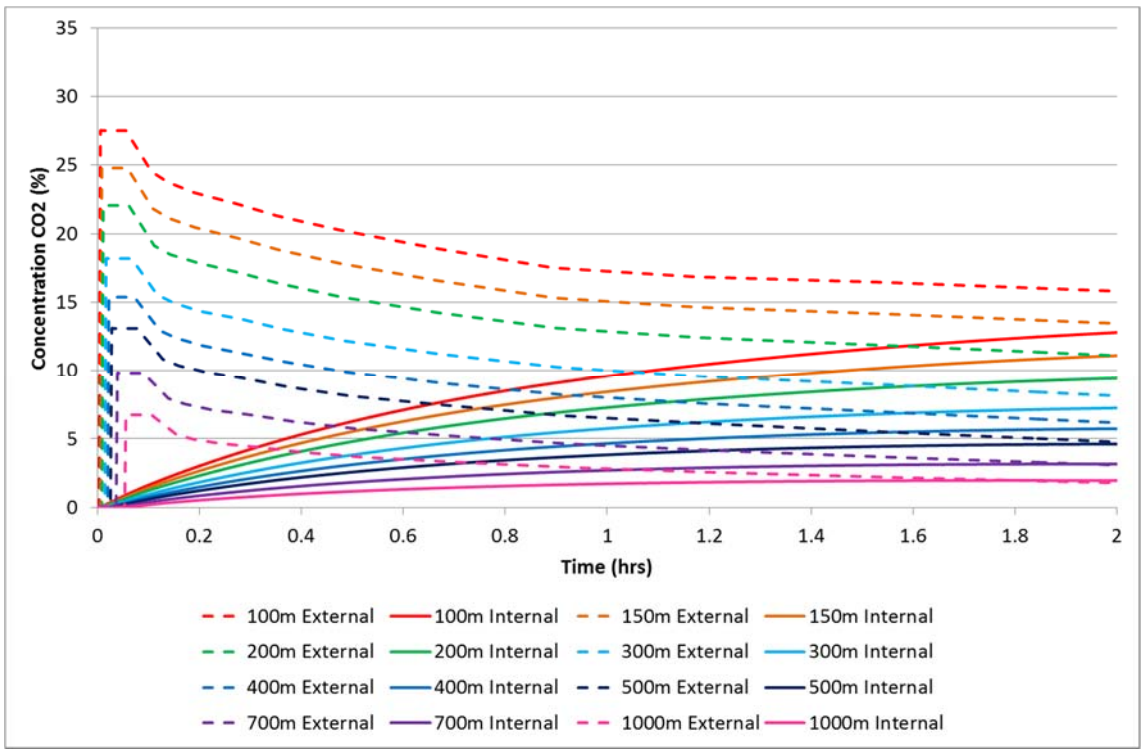

Figure C.13: Change in Equivalent Internal CO_2 Concentration with Time and Distance for Case 3

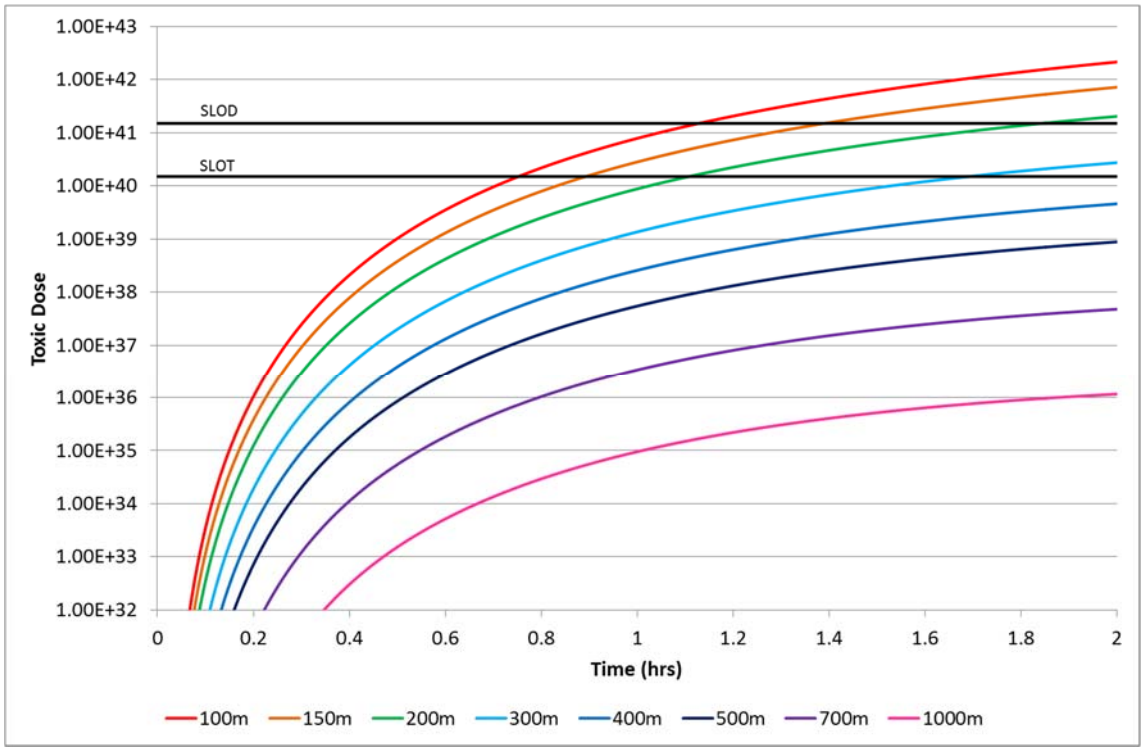

Figure C.14: Dose Received by a Building Occupant with Time and Distance for Case 3

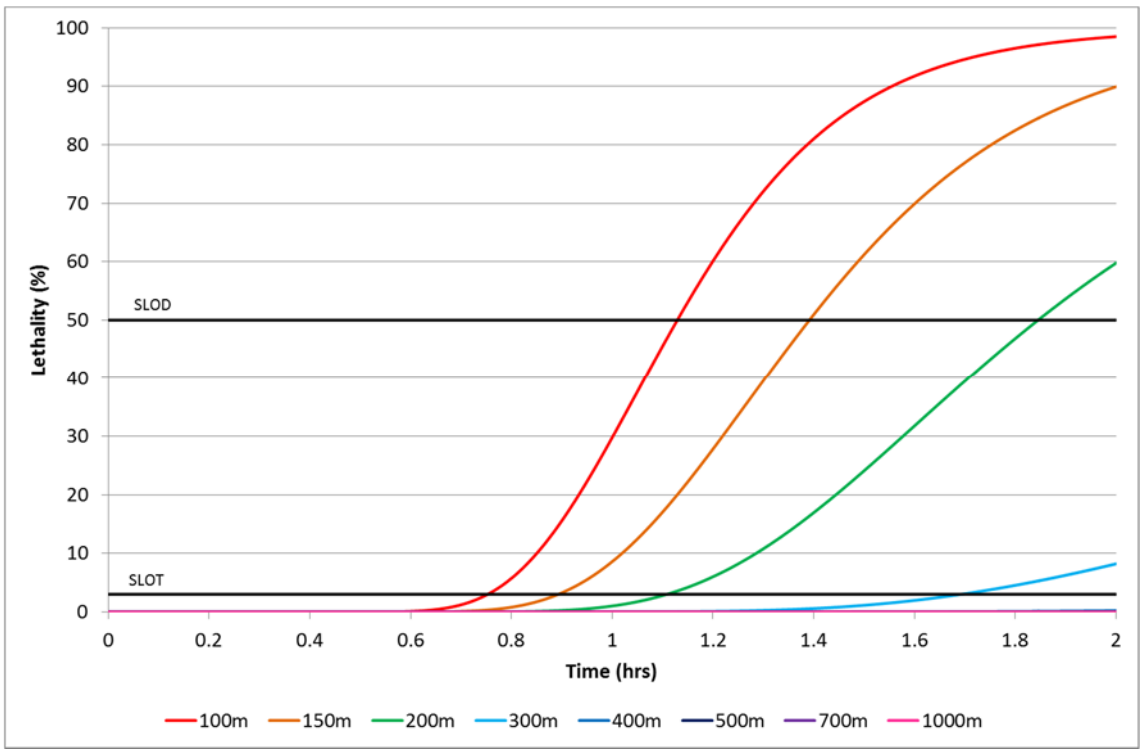

Figure C.15: Percentage Lethality for a Building Occupant with Time and Distance for Case 3

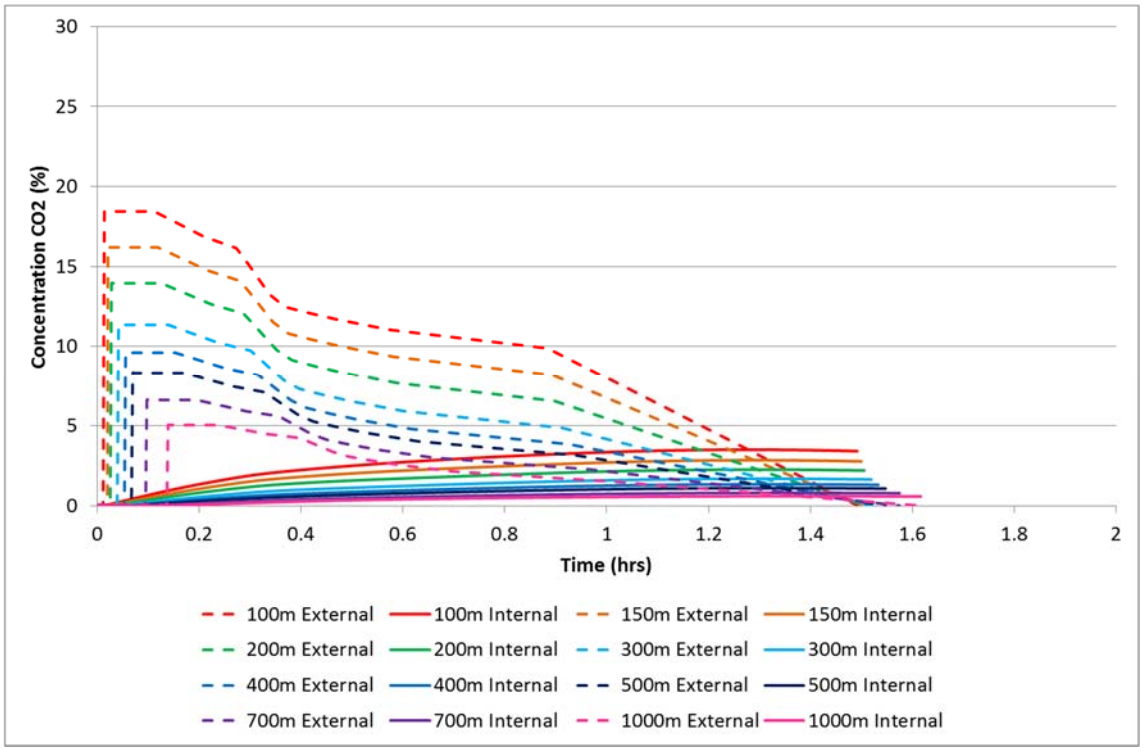

Figure C.16: Change in Mean Internal CO_2 Concentration with Time and Distance for Case 4

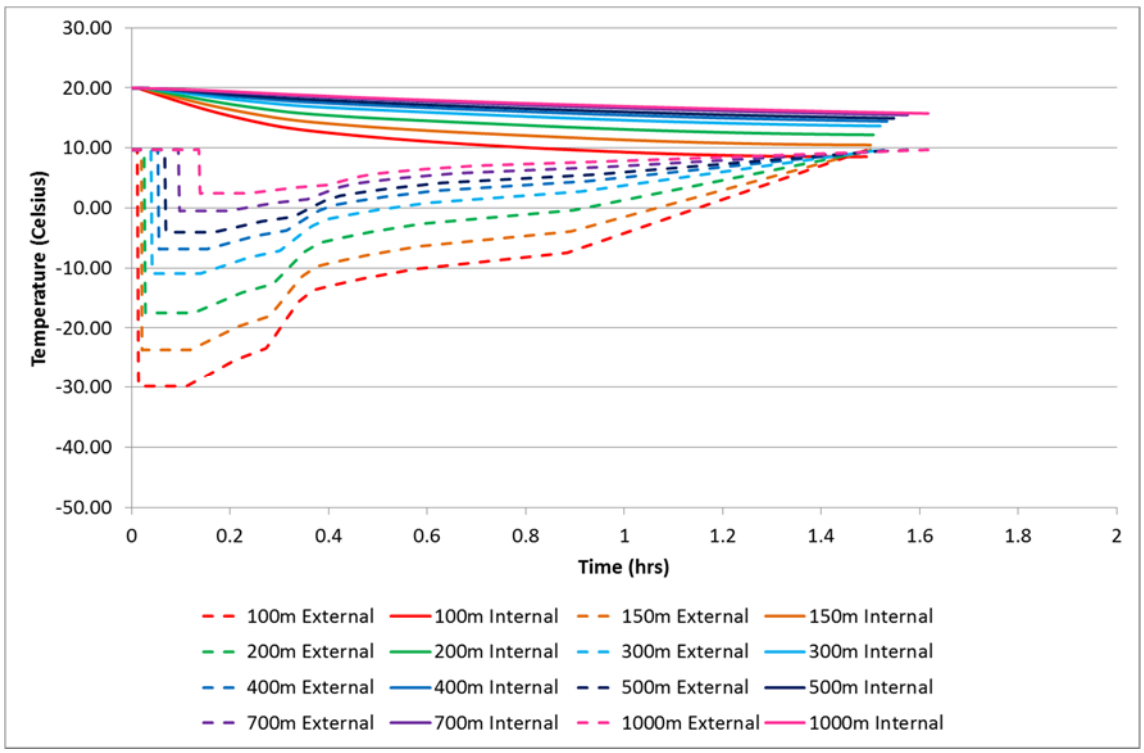

Figure C.17: Change in Internal Temperature with Time and Distance for Case 4

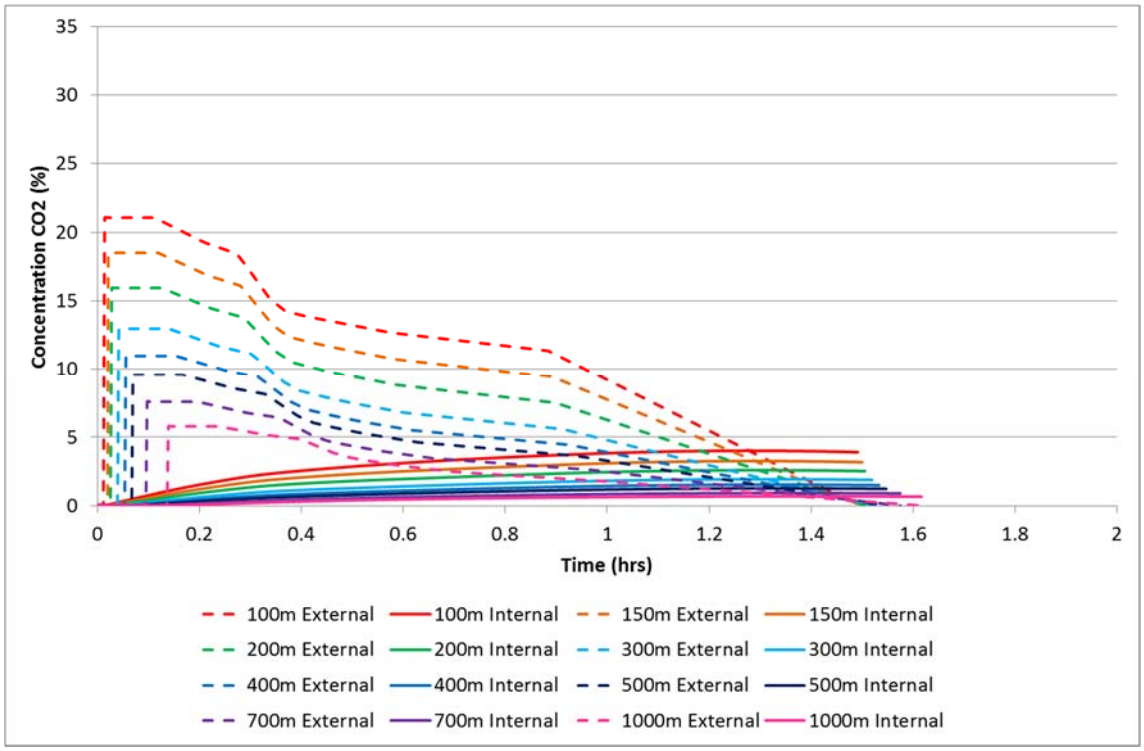

Figure C.18: Change in Equivalent Internal CO_2 Concentration with Time and Distance for Case 4

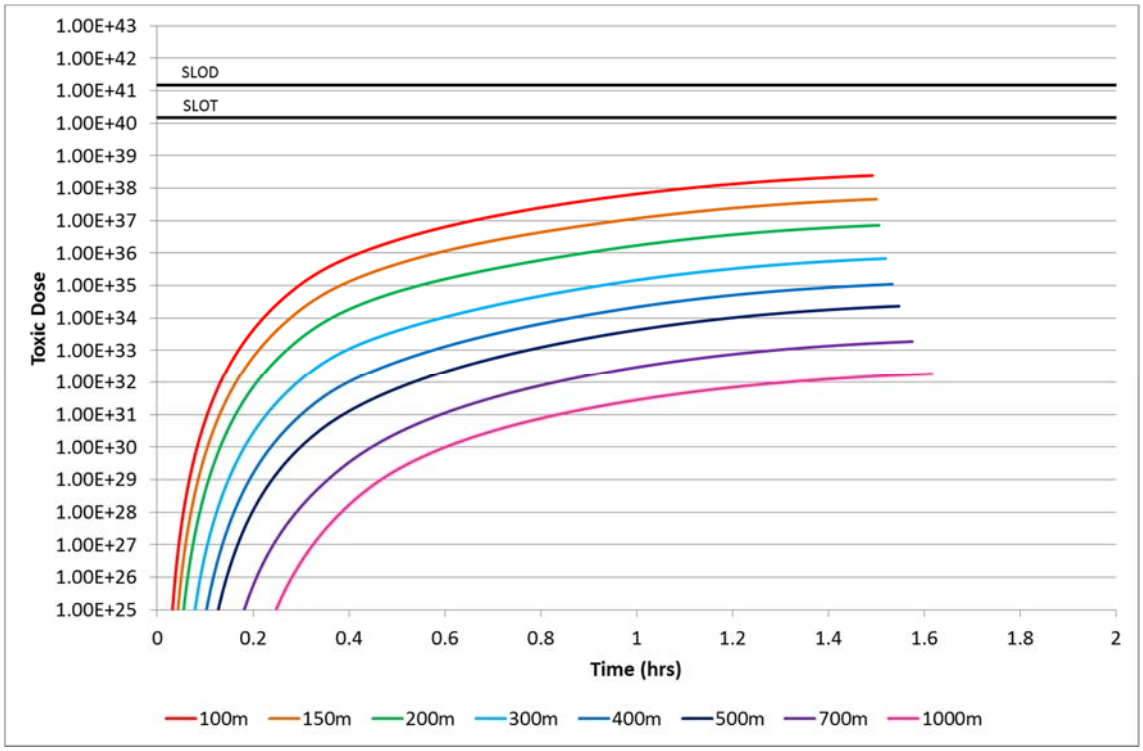

Figure C.19: Dose Received by a Building Occupant with Time and Distance for Case 4

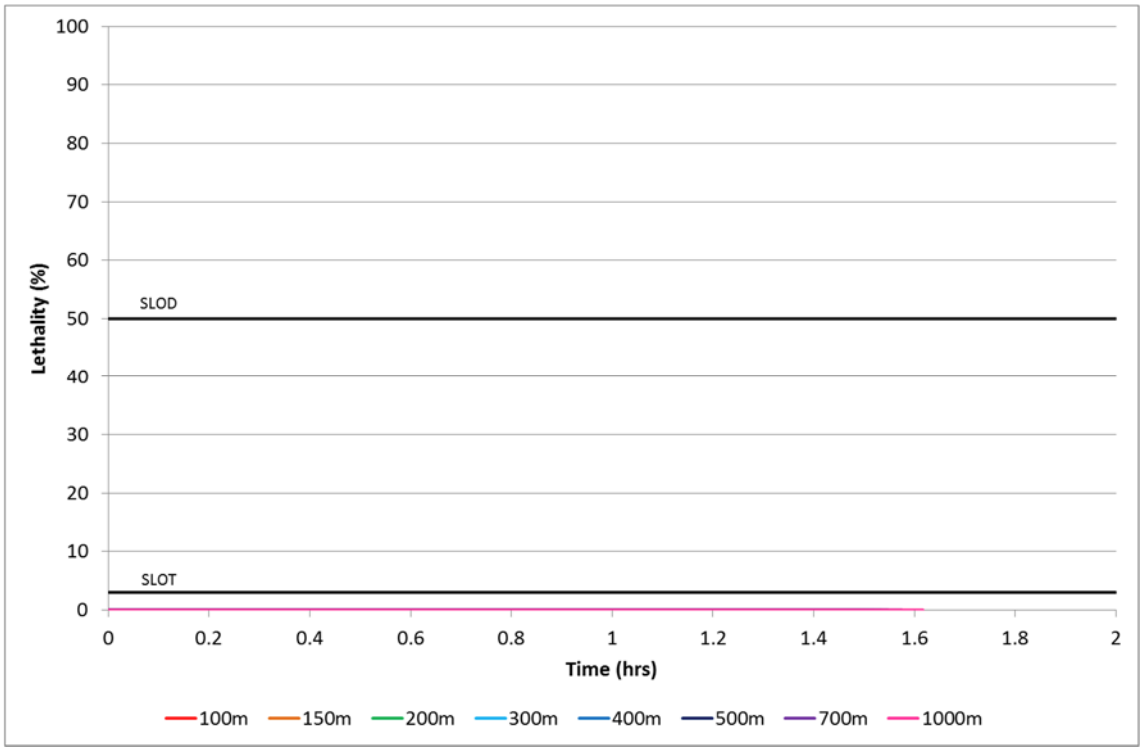

Figure C.20: Percentage Lethality for a Building Occupant with Time and Distance for Case 4

Appendix D An Escape Model for Consequence Predictions Following A CO_2 Pipeline Release (Charts)

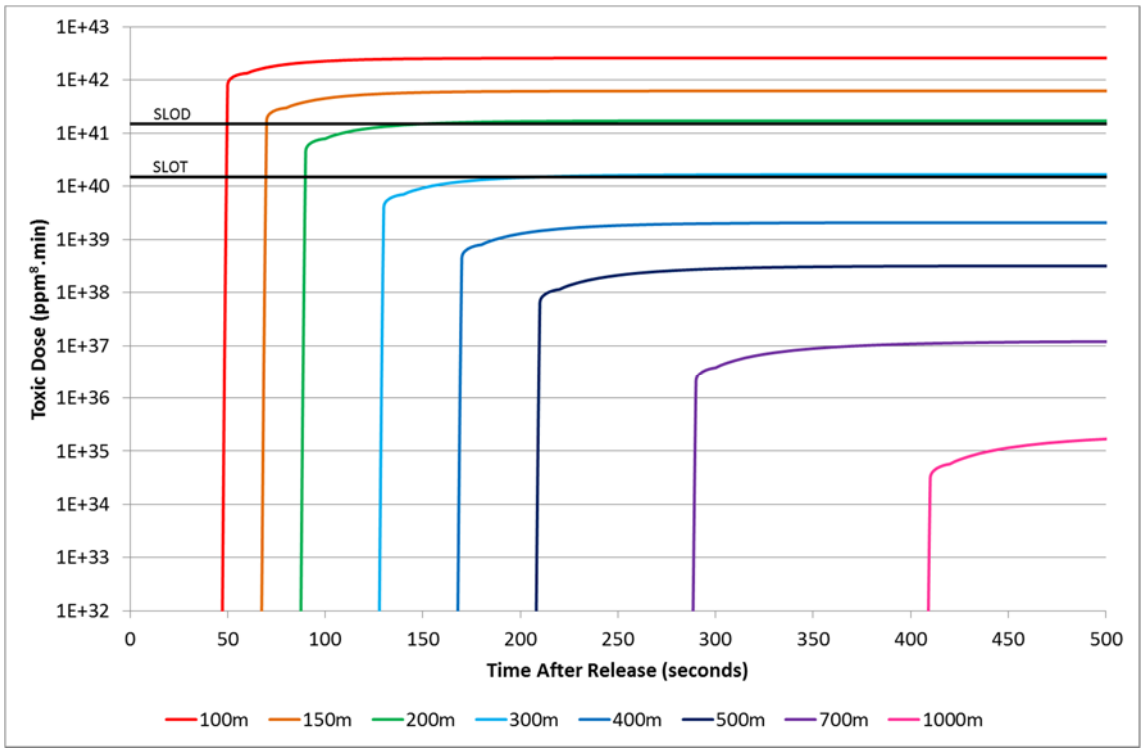

Figure D.1: Dose Received by an Escaping Individual Travelling Downwind with Time and Distance for Case 1

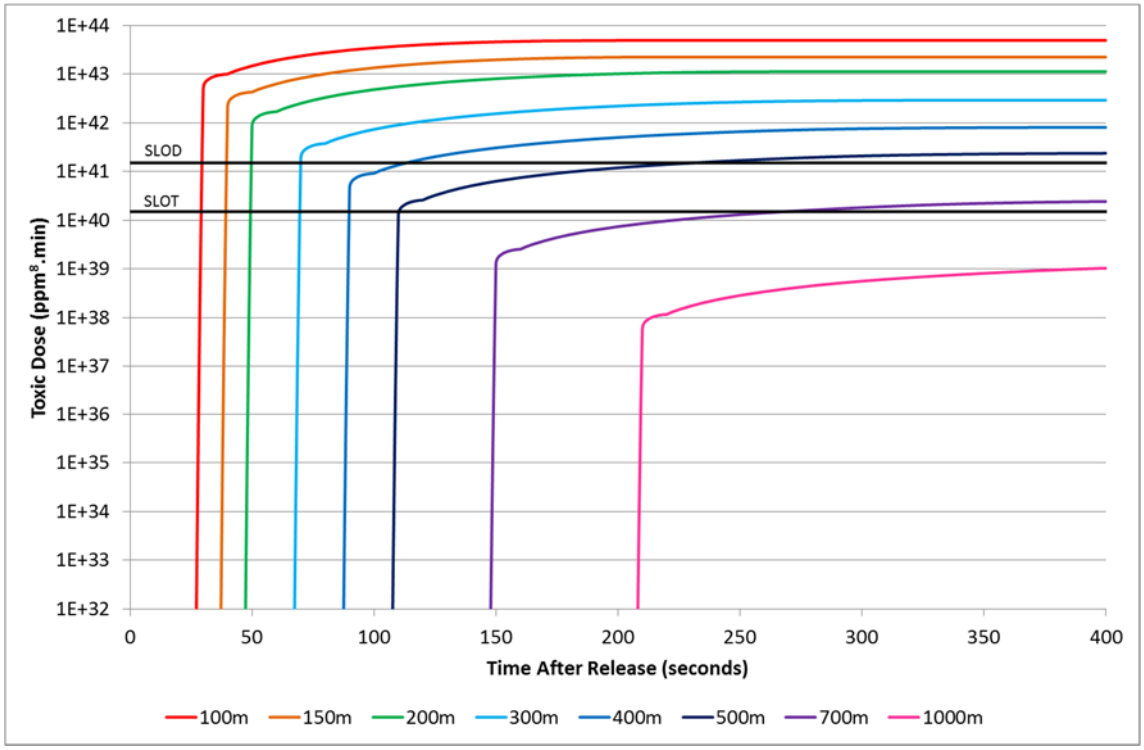

Figure D.2: Dose Received by an Escaping Individual Travelling Crosswind with Time and Distance for Case 1

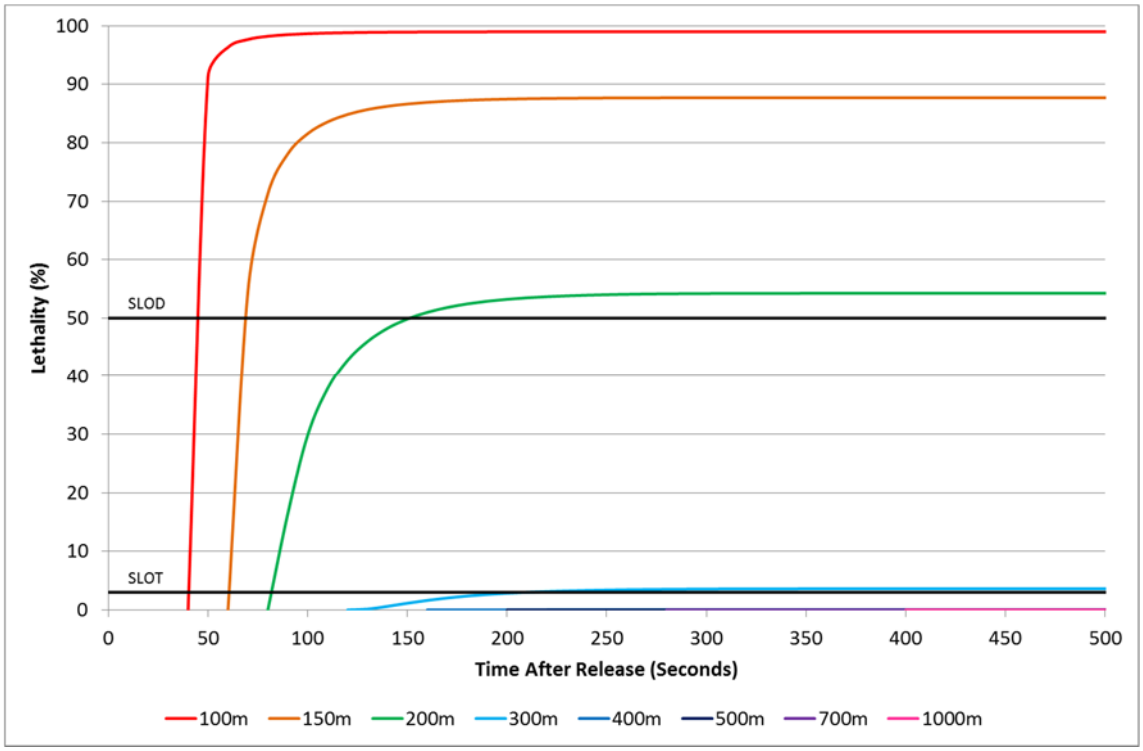

Figure D.3: Percentage Lethality for an Escaping Individual Travelling Downwind with Time and Distance for Case 1

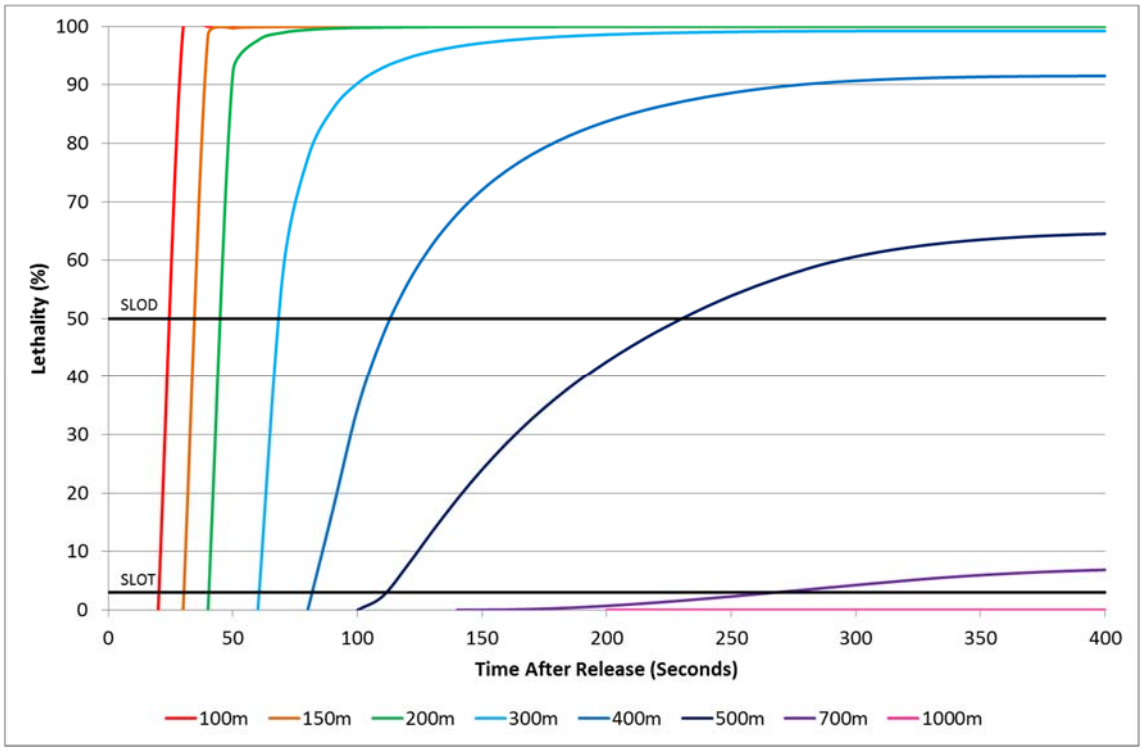

Figure D.4: Percentage Lethality for an Escaping Individual Travelling Crosswind with Time and Distance for Case 1

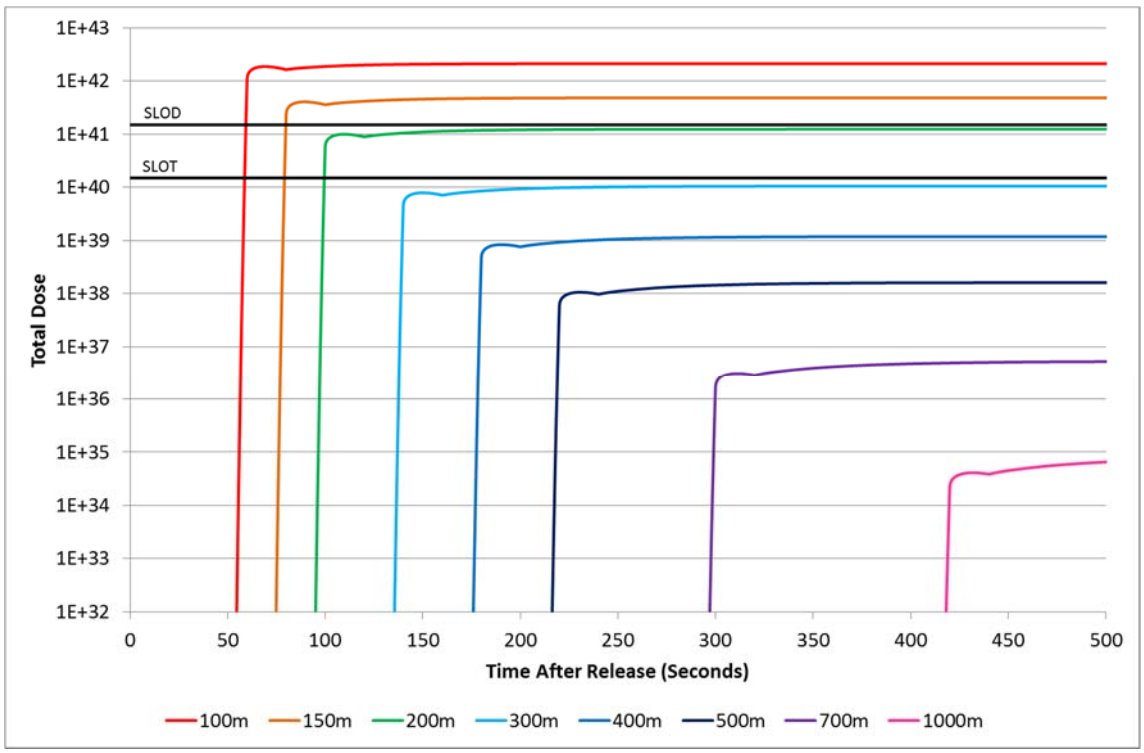

Figure D.5: Dose Received by an Escaping Individual Travelling Downwind with Time and Distance for Case 2

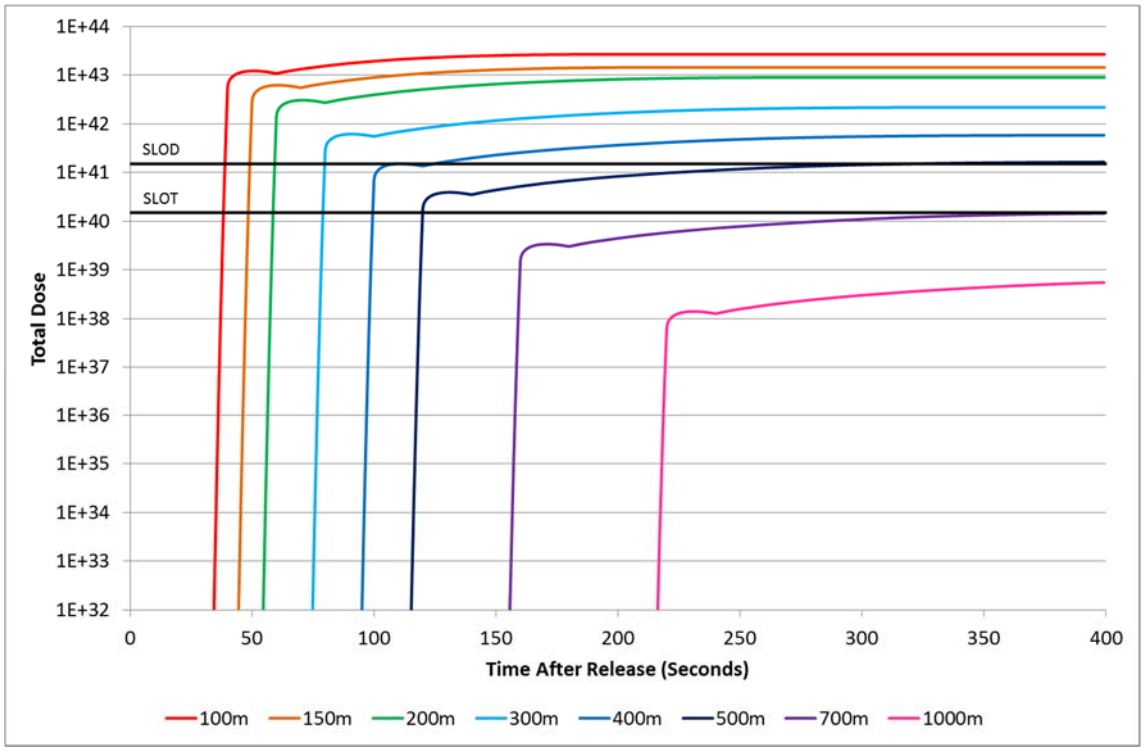

Figure D.6: Dose Received by an Escaping Individual Travelling Crosswind with Time and Distance for Case 2

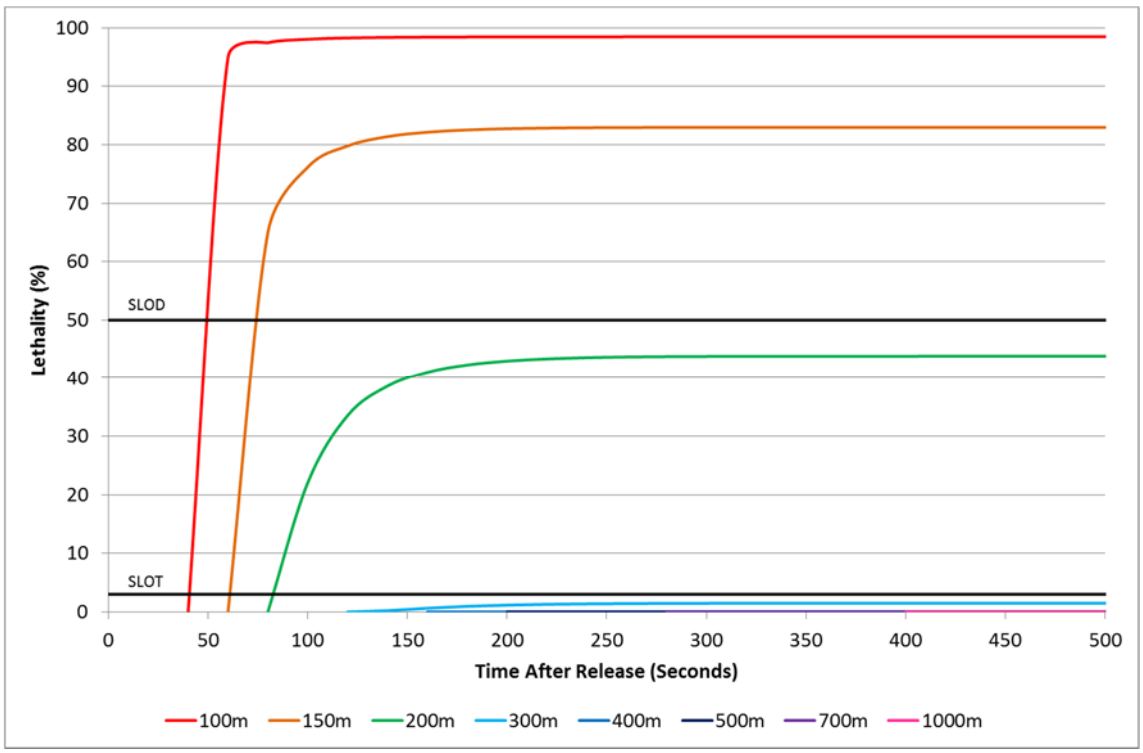

Figure D.7: Percentage Lethality for an Escaping Individual Travelling Downwind with Time and Distance for Case 2

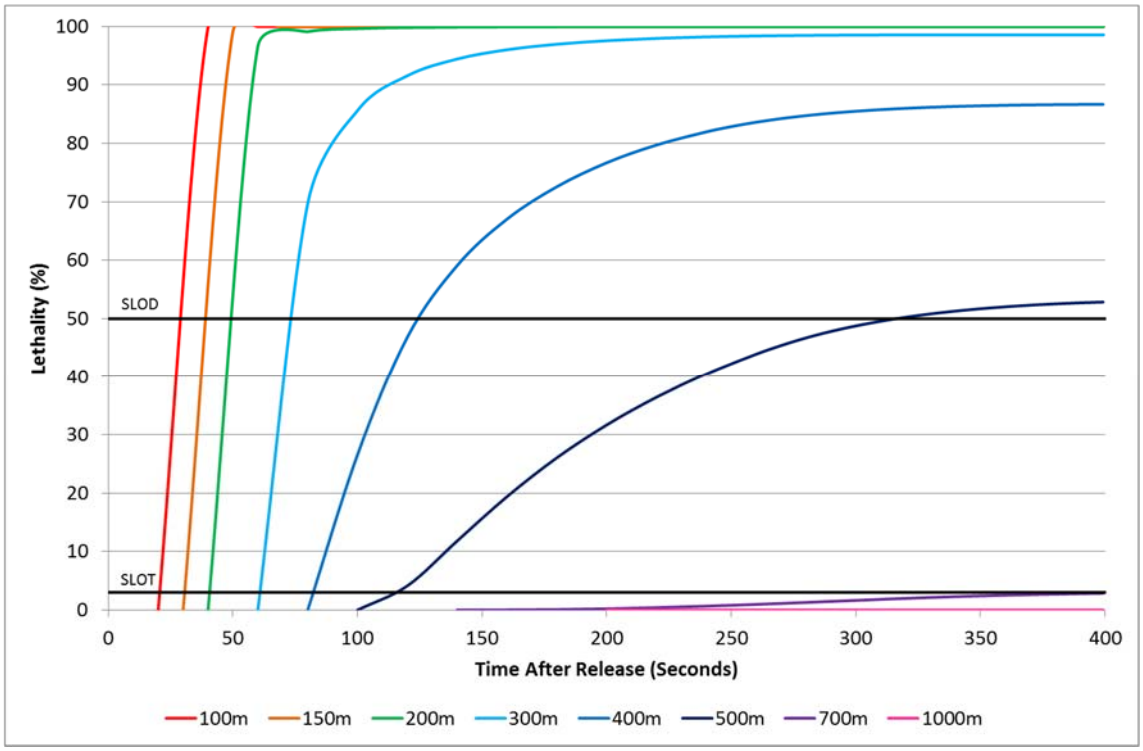

Figure D.8: Percentage Lethality for an Escaping Individual Travelling Crosswind with Time and Distance for Case 2

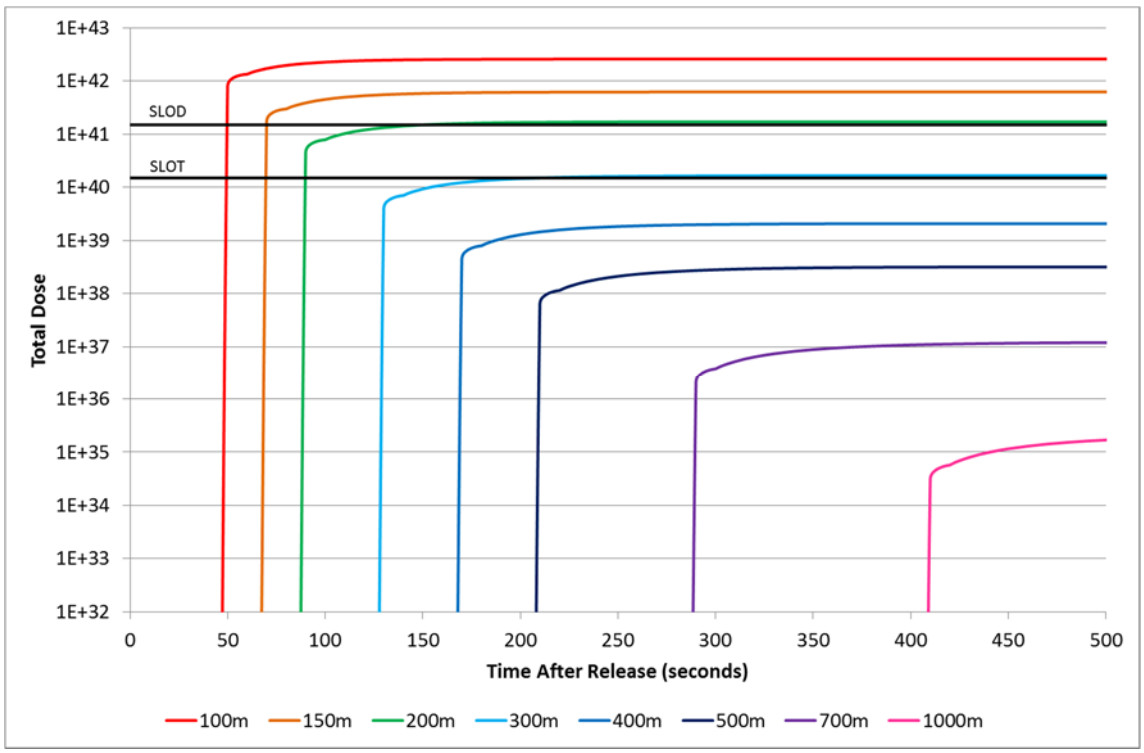

Figure D.9: Dose Received by an Escaping Individual Travelling Downwind with Time and Distance for Case 3

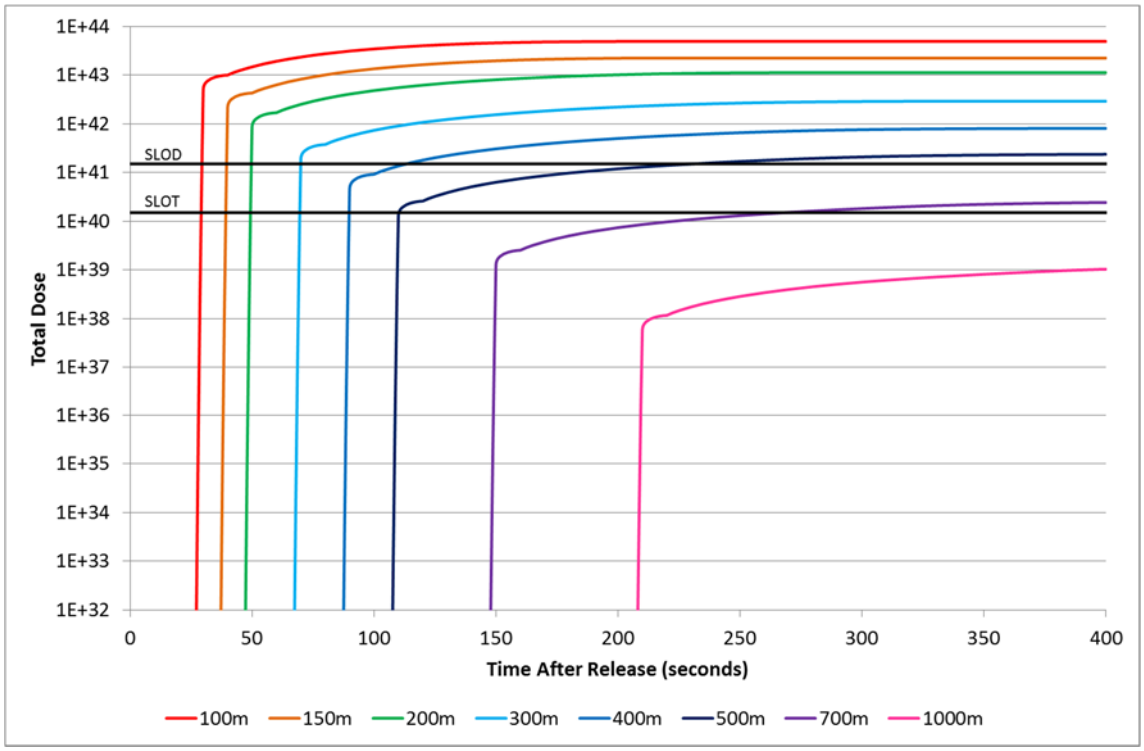

Figure D.10: Dose Received by an Escaping Individual Travelling Crosswind with Time and Distance for Case 3

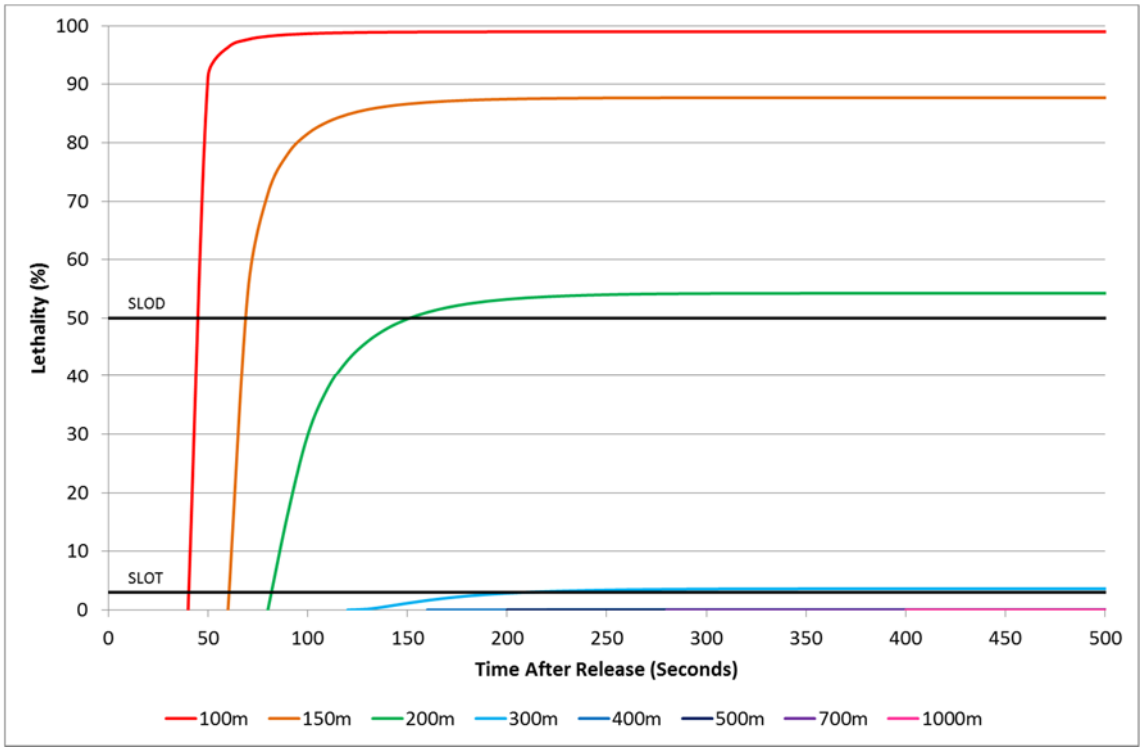

Figure D.11: Percentage Lethality for an Escaping Individual Travelling Downwind with Time and Distance for Case 3

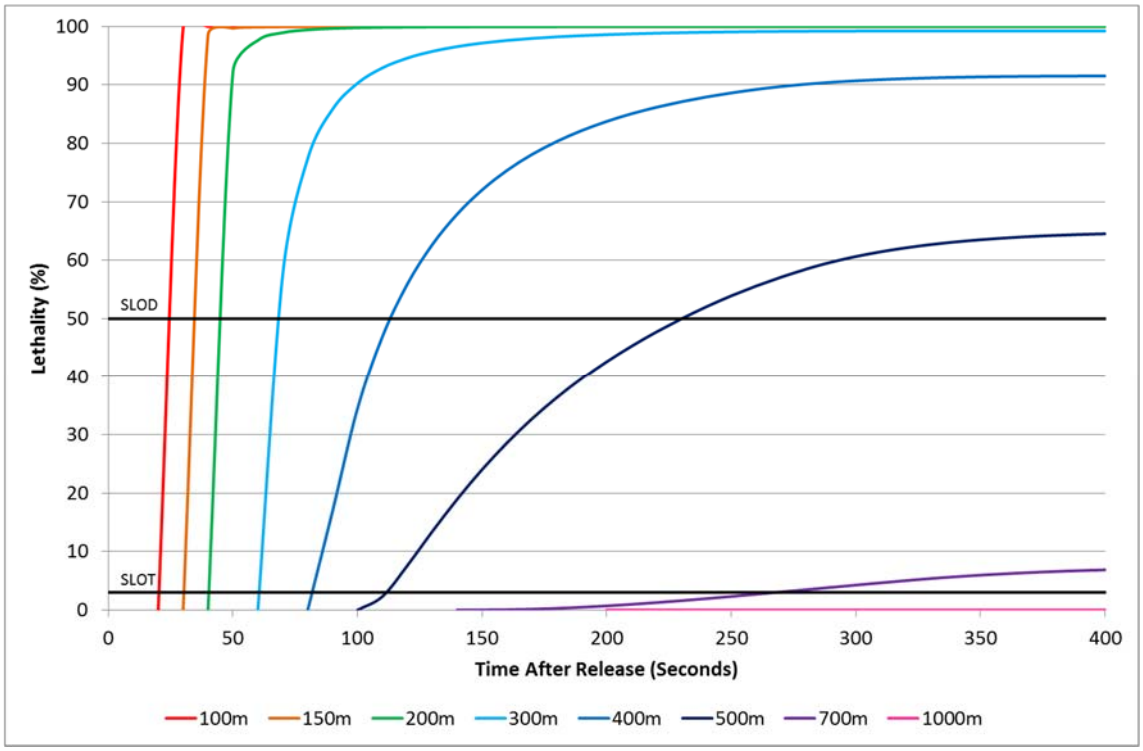

Figure D.12: Percentage Lethality for an Escaping Individual Travelling Crosswind with Time and Distance for Case 3

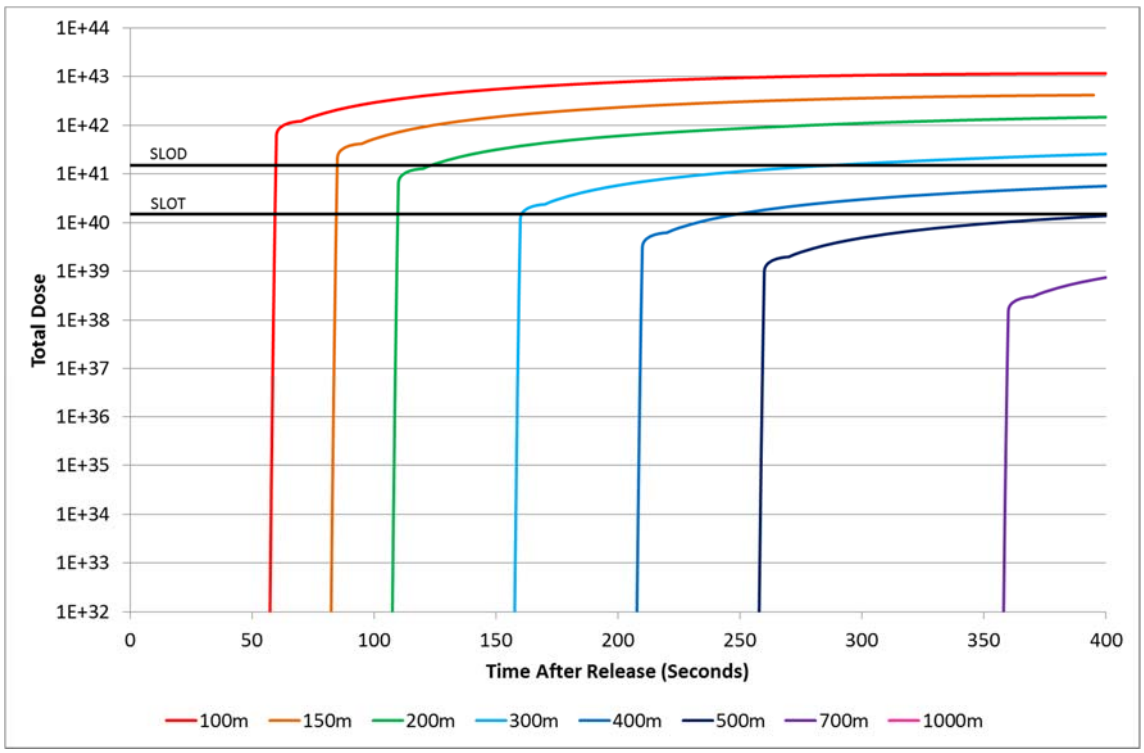

Figure D.13: Dose Received by an Escaping Individual Travelling Crosswind with Time and Distance for Case 4

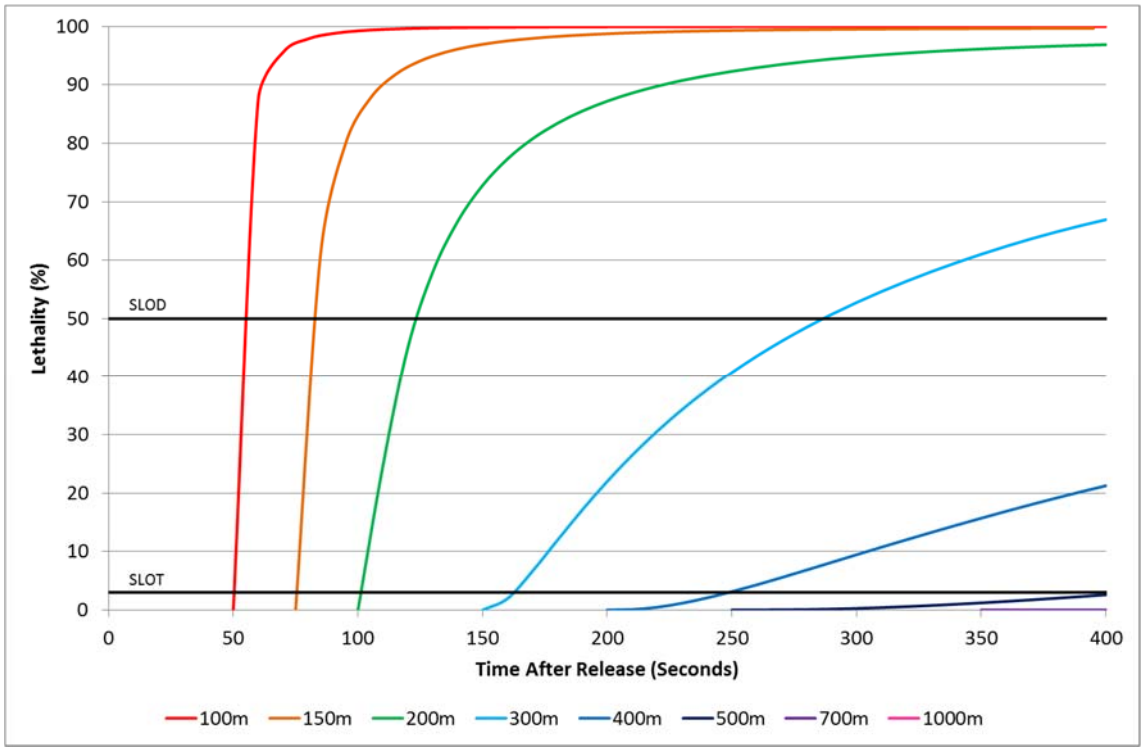

Figure D.14: Percentage Lethality for an Escaping Individual Travelling Crosswind with Time and Distance for Case 4